National Library of Canada
Canadian Theses Service
Ottawa, Canada
K1A 0N4

Bibliothèque nationale du Canada
Services des thèses canadiennes

CANADIAN THESES

THÈSES CANADIENNES

NOTICE

The quality of this microfiche is heavily dependent upon the quality of the original thesis submitted for microfilming. Every effort has been made to ensure the highest quality of reproduction possible.

If pages are missing, contact the university which granted the degree.

Some pages may have indistinct print especially if the original pages were typed with a poor typewriter ribbon or if the university sent us an inferior photocopy.

Previously copyrighted materials (journal articles, published tests, etc.) are not filmed.

Reproduction in full or in part of this film is governed by the Canadian Copyright Act, R.S.C. 1970, c. C-30.

AVIS

La qualité de cette microfiche dépend grandement de la qualité de la thèse soumise au microfilmage. Nous avons tout fait pour assurer une qualité supérieure de reproduction.

S'il manque des pages, veuillez communiquer avec l'université qui a conféré le grade.

La qualité d'impression de certaines pages peut laisser à désirer, surtout si les pages originales ont été dactylographiées à l'aide d'un ruban usé ou si l'université nous a fait parvenir une photocopie de qualité inférieure.

Les documents qui font déjà l'objet d'un droit d'auteur (articles de revue, examens publiés, etc.) ne sont pas microfilmés.

La reproduction, même partielle, de ce microfilm est soumise à la Loi canadienne sur le droit d'auteur, SRC 1970, c. C-30.

THIS DISSERTATION HAS BEEN MICROFILMED EXACTLY AS RECEIVED

LA THÈSE A ÉTÉ MICROFILMÉE TELLE QUE NOUS L'AVONS REÇUE

NL-339 (r.86/06)

Canada

THE UNIVERSITY OF ALBERTA

DEFORMATIONS AROUND ARCTIC PIPELINES

by

© PATRICK MICHAEL COLLINS

A THESIS

SUBMITTED TO THE FACULTY OF GRADUATE STUDIES AND RESEARCH

IN PARTIAL FULFILMENT OF THE REQUIREMENTS FOR THE DEGREE

OF MASTER OF SCIENCE

DEPARTMENT OF CIVIL ENGINEERING

EDMONTON, ALBERTA

SPRING OF 1987

Permission has been granted to the National Library of Canada to microfilm this thesis and to lend or sell copies of the film.

The author (copyright owner) has reserved other publication rights, and neither the thesis nor extensive extracts from it may be printed or otherwise reproduced without his/her written permission.

L'autorisation a été accordée à la Bibliothèque nationale du Canada de microfilmer cette thèse et de prêter ou de vendre des exemplaires du film.

L'auteur (titulaire du droit d'auteur) se réserve les autres droits de publication; ni la thèse ni de longs extraits de celle-ci ne doivent être imprimés ou autrement reproduits sans son autorisation écrite.

ISBN 0-315-37733-X

Canadian Geotechnical Journal

Published by
THE NATIONAL RESEARCH COUNCIL OF CANADA

Revue canadienne de géotechnique

Publiée par
LE CONSEIL NATIONAL DE RECHERCHES DU CANADA

Editor R. M. QUIGLEY Directeur scientifique

Assistant to the Editor E. MILLIKEN Adjointe au directeur scientifique

Associate Editors/Directeurs scientifiques associés

M. BOZOZUK	J. GRAHAM	D. READES
J. I. CLARK	G. LEFEBVRE	W. D. ROGGENSACK
Z. EISENSTEIN	D. R. McCREATH	P. G. SLY
M. GARNEAU	R. J. MITCHELL	R. N. YONG
	J. F. NIXON	

PUBLISHING DEPARTMENT
at the National Research Council of Canada

SERVICE DE PUBLICATION
du Conseil national de recherches du Canada

Editor-in-chief C. T. BISHOP Directeur général

Assistant Editor-in-chief P. A. REDHEAD Directeur général adjoint

Manager B. E. DREW Directrice administrative

Publishing Supervisor S. E. JENNESS Préposé de la publication

Senior Publication Officer F. M. KAVCIC Agent supérieur à la publication

Publication Officer E. ROLFE Agent à la publication

THE CANADIAN GEOTECHNICAL JOURNAL (Can. Geotech. J.) publishes papers in English or French covering the general field of soil engineering, together with papers in the related disciplines such as Geology, Soil Science, Snow and Ice Mechanics, and Rock Mechanics as they relate to civil engineering.

Manuscripts for publication should be submitted to **Dr. R. M. Quigley, Faculty of Engineering Science, The University of Western Ontario, London, Ont., Canada N6A 5B9.**

Correspondence concerning accepted manuscripts and corrected proofs should be sent to Research Journals, National Research Council of Canada, Ottawa, Canada K1A 0R6. **Telephone enquiries** should be directed to Dr. S. E. Jenness (613-993-0428).

Reprints may be purchased at the time of publication (an order form is sent out with the galley proof). All orders should be sent to the Printing Department, University of Toronto Press, 5201 Dufferin Street, Downsview, Ont., Canada M3H 5T8. Invoices relating to the reprints will be sent out by the Printer.

Instructions to Authors are published once a year, in the first issue of each volume. Copies may be obtained from the Publishing Department.

The publisher grants permission to individuals who wish to quote short excerpts and reproduce figures, tables, or photographs from articles in this journal, provided that the source of such material is fully acknowledged. As a courtesy the consent of authors of such material should be obtained.

©National Research Council of Canada 1983. World rights reserved.

Copies of articles in this journal may be made for personal or internal use, or for the personal or internal use of specific clients, in research, study, or teaching. Permission for copying beyond that permitted by Section 107 or 108 of the U.S. Copyright Law is granted by the publisher on the condition that the person or institution making the copy or copies pays a copyright fee of $1.00 (U.S.) for each copy of each article to the Copyright Clearance Center, Inc., 21 Congress Street, Salem, MA, U.S.A. 01970. The appropriate remittance should be forwarded to the Clearance Center with a copy of the first page of the article(s) that has been copied. Copies of articles published in this journal prior to 1979 may be made under similar conditions.

The above permission does not extend to other kinds of copying, such as copying for general distribution, for advertising, or promotional purposes, for creating new collective works, or for resale. For such copying, arrangements must be made with the publisher.

LA REVUE CANADIENNE DE GÉOTECHNIQUE (Can. Geotech. J.) publie des articles en français ou en anglais touchant au domaine général de la mécanique des sols ou des disciplines connexes, telles que la géologie et les sciences du sol, de la neige et des glaces, et la mécanique des roches, traitées en fonction du génie civil.

Manuscrits–Les auteurs doivent adresser leurs manuscrits à **Dr. R. M. Quigley, Faculty of Engineering Science, The University of Western Ontario, London, Ont., Canada N6A 5B9.**

La correspondance ayant trait aux manuscrits acceptés et les épreuves corrigées doivent être envoyées aux Journaux de la recherche scientifique, Conseil national de recherches du Canada, Ottawa, Canada K1A 0R6. **On peut obtenir des renseignements en téléphonant à** M. S. E. Jenness (613-993-0428).

Tirages à part–Les tirés à part peuvent être achetés au moment de la publication. Un bon de commande à cet effet accompagne les épreuves: il doit être retourné au Printing Department, University of Toronto Press, 5201 Dufferin Street, Downsview (Ont.), Canada M3H 5T8, qui se chargera de la facturation.

Recommandations aux auteurs sont publiées une fois par année dans le premier numéro de chaque volume. On peut s'en procurer une copie, sur demande, au Service de publication.

L'éditeur accorde aux particuliers la permission de citer de brefs extraits et de reproduire des figures, des tableaux ou des photos dans les articles de la revue, à la condition que la source soit indiquée explicitement. Dans ce cas, il convient, par courtoisie, d'obtenir le consentement des auteurs.

© Conseil national de recherches du Canada 1983. Tous droits réservés.

Les articles de cette revue peuvent être reproduits pour usage personnel ou interne, ou pour l'usage personnel ou interne de clients bien précis dans les domaines de la recherche ou de l'enseignement. L'éditeur accorde la permission de reproduire ces articles malgré les dispositions de la section 107 ou 108 de la Copyright Law des États-Unis à la condition que le copieur, la personne ou l'organisme, paie une redevance de 1,00 $ U.S. pour chaque copie de chaque article au Copyright Clearance Center, Inc., 21 Congress Street, Salem, MA, U.S.A. 01970. Les versements appropriés sont envoyés au Clearance Center avec une photocopie de la première page de l'article (ou des articles) reproduit. Les reproductions d'articles publiés dans cette revue avant 1979 sont soumises à des conditions semblables.

La présente permission ne s'applique pas à d'autres genres de reproduction, notamment la reproduction en vue d'une distribution générale, à des fins de publicité ou de promotion, pour la création de nouveaux travaux collectifs, ou pour la revente. Dans ces cas, il faut prendre les dispositions qui s'imposent en communiquant avec l'éditeur.

THE UNIVERSITY OF ALBERTA

RELEASE FORM

NAME OF AUTHOR PATRICK MICHAEL COLLINS

TITLE OF THESIS DEFORMATIONS AROUND ARCTIC PIPELINES

DEGREE FOR WHICH THESIS WAS PRESENTED MASTER OF SCIENCE

YEAR THIS DEGREE GRANTED SPRING OF 1987

Permission is hereby granted to THE UNIVERSITY OF ALBERTA LIBRARY to reproduce single copies of this thesis and to lend or sell such copies for private, scholarly or scientific research purposes only.

The author reserves other publication rights, and neither the thesis nor extensive extracts from it may be printed or otherwise reproduced without the author's written permission.

Patrick M. Collins

PERMANENT ADDRESS:

14 London Street

Toronto, Ontario,

Canada M6G 1M9

DATED November 14th, 1986

THE UNIVERSITY OF ALBERTA

FACULTY OF GRADUATE STUDIES AND RESEARCH

The undersigned certify that they have read, and recommend to the Faculty of Graduate Studies and Research, for acceptance, a thesis entitled *Deformations Around Arctic Pipelines* submitted by Patrick Michael Collins in partial fulfilment of the requirements for the degree of Master of Science.

.....

Supervisor

.....

.....

Dated November 14th, 1986

ABSTRACT

The recent construction activity in Canada's northern regions has primarily been a result of oil and gas exploration and development. Pipelines will be a major element of the resultant collection and distribution system, but are subject to the high deformations from thaw settlement and frost heave. This thesis examines aspects of the engineering analysis of both.

Conventional thaw analysis was examined and the need for two-dimensional thaw settlement analysis was rationalized. In contrast to conventional one-dimensional analyses, it was found that higher variabilities in thaw strain predicted significant reductions in surface settlement.

The section on frost heave summarized the thermodynamics involved and reviewed of the segregation potential (*SP*) theory heave of prediction. This work then assumed that long-term heave was primarily dependent upon *SP*, temperature gradients and pressure. An iterative procedure of modelling heave was developed to relate the *SP* concept with the results of two finite element programs in an uncoupled thermo-elastic analysis.

A simulation of the Calgary Frost Heave Test facility was performed. In addition to the upward displacement of the pipe, significant horizontal heaving stresses developed due

to the restraint against lateral displacement. This confinement resulted in higher vertical stresses and a smaller heave than that observed in the field. While these initial results predict 25% of the actual heave, the existing model predicted a credible mode of soil behaviour and is capable of performing a parametric analysis to quantify the effects of the factors controlling frost heave.

ACKNOWLEDGEMENTS

It is indeed a comfort to me to be able to say that this thesis is finished. I also find it particularly gratifying to recognise the support I received over the past five years.

Esso Resources Canada Ltd., the National Science and Engineering Research Council of Canada, and the Boreal Institute for Northern Studies at the University of Alberta all provided funding through my advisor, Dr. Norbert R. Morgenstern. Their financial support was most appreciated.

My family has been a steadfast buttress over the years, providing me with unwavering support and encouragement. Knowing that they were there strengthened my resolve on more than one occasion. They have my thanks and love.

Both Paulo Branco and Sean Maloney, my noon-hour running partners, are to be commended for their continual cajoleries which prompted me to maintain a reasonable level of fitness. Their welcome companionship was my daily breath of fresh air.

In addition to the considerable technical input from Dr. Norbert Morgenstern, I received no end of technical support from staff members in this department. I thank Dr. Dave Sego for his advice and jocular criticisms concerning the content and presentation of this material. His sincere concern for students is recognized by us all.

Dr. Dave Chan was most generous in allowing me access to his contour plotting program thereby saving me considerable work. Mr. Al Dunbar has been extremely helpful and accommodating regarding any computer-related problems. This consistency in good technical support was essential and greatly appreciated.

As with countless other graduate students from this department, I am indebted to Mr. Tom Casey for his advice and software pertaining to the presentation and preparation of this tome. His selfless contributions to this department have considerably reduced the tedium involved in producing a thesis.

Lastly, and most importantly, I wish to close with a special thanks to the perspicacious Dr. Norbert Morgenstern, without whom I would not have attempted such a thesis topic:

> This thesis has been a trial-by-fire for both of us and we have survived, although he with considerably more hair than me. I envy his eternal patience, and grant him the singular honour of being the only person in the world who could possibly be more relieved than me that this thesis has finally been completed.

May he accept that compliment, this thesis and my warmest thanks and know that I wish him the best in the years to come.

Table of Contents

Chapter		Page
1.	Introduction	1
	1.1 Thesis Organization	3
	1.2 Appendice Organization	4
2.	Pipeline Design in Thaw-Unstable Soils	8
	2.1 Design Approach	8
	2.1.1 Design Alternatives	9
	2.1.2 Aspects of Design	12
	2.2 Geothermal State-of-the-Art	12
	2.2.1 One-Dimensional Thermal Analysis	13
	2.2.2 Two-Dimensional Thermal Analysis	20
	2.2.3 Thaw with Partial Consolidation	31
	2.2.4 Other Closed-Form Solutions	37
	2.2.5 Finite Difference Method	41
	2.2.6 Finite Element Method	44
	2.3 Geotechnical Properties	49
	2.4 Soil : Pipeline Interaction	53
	2.5 Summary	61
3.	Numerical Modelling of Thaw in Permafrost	63
	3.1 Statistical Variation of the Thaw Strain Parameter	63
	3.2 Thaw Strain Variability	64
	3.3 Statistical Distribution	64
	3.4 Statistical Reduction of the Thaw Strain Parameter	67
	3.5 Simple Thaw Strain Analysis	71
	3.5.1 Thaw Strain Parameter Selection	71

3.5.2 Volumetric Strain : Bulk Modulus Relationship 72

3.5.3 Layered Analysis 72

3.5.4 Randomly Mixed A_0 Parameters 75

3.5.5 Mesh Alteration 80

3.5.6 Re-analysis of Randomly Mixed A_0 Parameters 81

3.6 Normally Consolidated Soil 84

3.6.1 Stress-Strain Relationship 86

3.6.2 Volumetric Strain : Bulk Modulus Relationship 88

3.6.3 Layered Analysis 91

3.6.4 Randomly Mixed A_0 Parameters 99

3.6.5 Disappointing Results 103

3.7 Soil with a Residual Stress 105

3.7.1 Thawing Soil and Residual Stress 106

3.7.2 e_v:K Representation of the e-$\log \sigma$ Curve 106

3.7.3 Stiffness at a Stress Below the Residual 107

3.7.4 Impracticality of a Rigorous Representation of Stiffness 109

3.7.5 Load Discretization 111

3.7.6 Soil Behaviour Beyond the Residual Stress 112

3.7.7 Freezing Reconsolidation Pressure 112

3.7.7.1 Different Materials 113

3.7.7.2 Influence of Organics 115

3.7.7.3 Homogeneity 115

3.8 Implementation of Residual Stress Theory 117

3.9 Residual Stress Results 118

3.10 Thaw Strain Variability 124

3.10.1 Settlement Reduction due to Material Variation 124

3.11 Conclusions 134

3.12 Validity of the Results 136

3.12.1 Load Discretization 136

3.12.2 Material Properties 137

3.12.3 Mesh Geometry 137

3.13 Small Deformation versus Large Deformation Analysis 137

3.13.1 Previous Experience 138

3.13.2 An Attempt at Lagrangian Analysis 141

3.14 Other Statistical Applications to Thaw Settlement 143

3.14.1 Distal Settlements as a Random Process .143

3.14.2 Graded Disorder 146

3.14.3 Three-Dimensional Considerations 147

4. The Physics of Frost Heave 148

4.1 Applicability of the Clausius-Clapeyron Equation to Freezing Soils 149

4.1.1 Differing Water Pressures 150

4.1.2 Altered Flow Rates 153

4.1.3 Micro-Thermodynamics 157

4.1.4 Cavitation 159

4.2 Implications of the General Clausius-Clapeyron Equation 163

4.2.1 Ice Lensing 166

4.2.2 Thermodynamic Stability on the Cold Side of the Ice Lens 167

4.2.3 The Thermodynamics within an Ice Lens ..169

4.3 The Segregation Potential: Theory and Practice 170

4.3.1 Deviation from the Theory 177

4.3.2 A Transition in Application 178

4.3.3 Inconsistent Application 179

4.3.4 The Use of the Thermal Gradient in the Frozen Soil 181

4.3.5 Correlating the Two Approaches 182

4.3.6 Practical Application of *SP* 183

5. Application of the Segregation Potential Theory 185

5.1 Method 185

5.2 Test NS-1 189

5.3 Test C-10 204

5.4 Modification of the Coefficient of Thermal Expansion, α, for Two-Dimensions 217

5.5 Input Parameters for the N.E.S. Simulation 222

5.5.1 Soil Parameters 222

5.5.2 Soil Stiffness 223

5.5.3 Steel Properties 225

5.6 Representation of the Pipeline 225

5.7 Surface Temperatures at N.E.S. 228

5.7.1 Soil Parameters 228

5.8 Simulation of the N.E.S. Calgary Frost Heave Test Facility 232

5.8.1 The Final Analysis 269

6. Conclusions 286

6.1 The Need for Advanced Design Methods 286

6.2 Thaw Settlement 286

6.3 Frost Heave 290

6.4 Concluding Remarks 295

Bibliography 297

Appendice A: Closed-Form Solutions and Consolidation Effects 309

Appendice B: Alternative Calculations of α 315

B.1 Example 1: Recalculate α parameter, Test NWU-2, (Nixon & Morgenstern, 1974) 315

B.2 Example 2: Recalculate α parameter, Test NWU-2 modifying L for volume change 316

B.3 Example 3: Recalculate α parameter, Test NWU-9, (Nixon & Morgenstern, 1974) after the method of Nixon & McRoberts (1973) 318

B.4 Example 4: Recalculate α parameter, Test NWU-9, assuming $W_u=0$ 320

Appendice C: Normal Distribution of A_o 322

C.1 Extraneous Events 323

Appendice D: Beta Function Analysis 325

Appendice E: Thermodynamics 340

E.1 The Thermodynamics of Co-Existing Phases 340

E.1.1 Energy 340

E.1.2 Entropy 340

E.1.3 Gibbs Free Energy: a statement of balance 341

E.1.4 Water Co-Existing with Ice 342

E.1.5 Pressure in the Ice 344

Appendice F: Konrad's Finite Difference Program (Modified) 346

Appendice G: Heave Calculations using "TRANS" 353

Appendice H: Procedure Files used with the Heave Calculations 373

Appendice I: Summary of C-10 Simulation Results 387

Appendice J: Experience with *ADINAT* 404

J.1 Comparison of ADINAT with Closed Form Methods .404

J.2 Mesh Optimization 408

J.3 The Choice of Units Affects Convergence 411

J.4 *ADINAT* and Phase Change 412

J.5 The Effect of Timestep Size on Convergence Characteristics 415

J.6 The Initialization of Temperatures for N.E.S. Simulation 418

Appendice K: Elimination of the Tension Field within the N.E.S. Mesh 424

K.1 Tension Anomaly within the Mesh 424

K.2 Restraining the Berm Horizontally 425

K.3 Reduced Void Radius 425

K.4 Altered Berm Geometry and Materials; Infilled Void 425

K.5 Degrees-of-Freedom of the Top-Right Node 426

K.6 Conceptual Simplification of the Mesh 427

K.7 Corroboration using the ADINA Program 428

K.8 The Effect of Lumped Mass 428

Appendice L: Sample Input Files 453

Appendice M: Ignoring the Different Thermal Conductivity of Ice Lenses 456

Appendice N: Glossary of Files, Programs and Procedures .458

List of Tables

Table		Page
2.1	Equivalent Latent Heat Assuming 100% Consolidation	23
2.2	Equivalent Latent Heat Assuming 80% Consolidation	33
3.1	Summary of the Preliminary Numerical Thaw Analyses	85
5.1	N.E.S. Soil Properties	224
C.1	Thaw Strain: Norman Wells Samples	322
K.1	Lumped Mass Analysis along the Right Side of the Mesh	430

List of Figures

Figure	--	Page
2.1	Deviation of Nixon's Thermal Analysis from Stefan's Solution	19
2.2	Thaw Progression - 100% Consolidation	25
2.3	Heat Flux Comparison	29
2.4	Thaw Progression - 80% Consolidation	34
2.5	Thornton's Coaxal Circles	39
2.6	Nixon, *et al*. Finite Element Model for Thaw Settlement	56
3.1	Various Forms of the Beta Distribution	66
3.2	Normal Distribution Curves	68
3.3	Variation in Bi-Linear Stress-Strain Curves	73
3.4	Comparison of Columnar and Layered Analyses	74
3.5	Mesh Configuration - 4 Node Elements	76
3.6	Numerical Instability - 4 Node Elements	77
3.7	Thaw Settlement Deformations - 4 Node Elements	79
3.8	Deformations for 8-Node Elements for Step 1	82
3.9	Final Deformations for 8-Node Elements	83
3.10	β Likelihood Distribution Functions	89
3.11	Cummulative Distribution of Thaw Strain	90
3.12	Mesh Configuration - 8 Node Elements	92
3.13	Layered Thaw-Straining Material	93
3.14	Layered Normally Consolidated Soil	94
3.15	Normally Consolidated Soil ϵ_v:K Curves	98
3.16	Element Group and Number	100
3.17	Randomly Distributed Materials	101

Figure Page

3.18 Normally Consolidated Soil with Laboratory Standard Deviation 102

3.19 Normally Consolidated Soil: 50% Standard Deviation 104

3.20 Idealized *e-log σ* Curve for a Residually Stressed Soil 108

3.21 Residual Stress *e-log σ* Curves 114

3.22 Residually Stressed Soil ϵ_v:K Curves 119

3.23 Layered Residual Stress Soil 120

3.24 Residual Stress Soil of 100% A_o Standard Deviation - Full Load 122

3.25 Residual Stress Soil of 100% A_o Standard Deviation - 9kPa Surficial Load 123

3.26 Beta Functions of Different Variances 125

3.27 Residual Stress Soil of 71% Standard Deviation - Full Load 126

3.28 Residual Stress Soil of 50% Standard Deviation - 9kPa Surficial Load 127

3.29 Residual Stress Soil of 50% Standard Deviation - Full Load 128

3.30 Residual Stress Soil of 125% Standard Deviation - 9kPa Surficial Load 129

3.31 Residual Stress Soil of 125% Standard Deviation - Full Load 130

3.32 Residual Stress Soil of 150% Standard Deviation - Full Load 131

3.33 Average Surface Settlements as a Function of Thaw Strain Variability 132

3.34 Maximum Mesh Stress as a Function of Thaw Strain Variability 133

3.35 Lagrangian Analysis of Homogeneous Material (under partial surface loading) 142

3.36 Preliminary Results of Lagrangian Analysis 144

Figure		Page
4.1	Relation between Flow Rate and Pressure Difference	154
4.2	Schematic Representation of the Ice-Water Interface	156
4.3	Hydraulic Conductivity under Melting Conditions	158
4.4	Schematic Graph of van der Waal's Equation of State	161
5.1	Flowchart of the Heave Algorithm	188
5.2	Deformations of Test NS-1 - 8 Element Mesh	191
5.3	Test of NS-1 using TRANS (Unfrozen Gradient)	195
5.4	Simulation of Test NS-1 Using Unfrozen Thermal Gradient	196
5.5	Continuation of the Simulation of Test NS-1	197
5.6	Deformations of Test NS-1 - 26 Element Mesh	198
5.7	Frost Front Progression, NS-1	199
5.8	NS-1 Thermal Gradient Progression	202
5.9	Finite Difference Prediction vs Experimental	203
5.10	Test C-10: Element, Node and Material Numbering	206
5.11	Stepped Heave Behavior, Test C-10	208
5.12	Extended Simulation of Test C-10 with Stepped Heave	209
5.13	Heave Prediction using the Frozen Soil Gradient	211
5.14	Heave Prediction using the Factored Frozen Soil Gradient	212
5.15	Test C-10 Deformed Mesh	213
5.16	Comparison of Predictive Methods	215

Figure Page

5.17 Variation of Environment Temperatures, Calgary 230

5.18 Ground Response to Varying Surface Temperatures, T= 17yr, RTOL=10^{-3} 233

5.19 Ground Response to Varying Surface Temperatures, T= 17yr, RTOL=10^{-4} 234

5.20 3yr after Applying Surface Temperatures 235

5.21 6yr after Applying Surface Temperatures 236

5.22 9yr after Applying Surface Temperatures 237

5.23 12yr after Applying Surface Temperatures 238

5.24 15yr after Applying Surface Temperatures 239

5.25 18yr after Applying Surface Temperatures 240

5.26 Spring Isotherm Distribution 241

5.27 Summer Isotherm Distribution 242

5.28 Autumn Isotherm Distribution 243

5.29 Winter Isotherm Distribution 244

5.30 Version 1 of the N.E.S. Test Facility 246

5.31 Stress Distribution within the Original Mesh 247

5.32 Incompatible Displacement Modes 249

5.33 Version 2 of the N.E.S. Test Facility 250

5.34 Stress Distribution at the Pipe - Mesh Version 2 251

5.35 Gravity Stresses and Displacements - Mesh Version 2 253

5.36 Version 3 of the N.E.S. Facility - Element Numbers 254

5.37 Element Numbers Near the Pipe (Mirror Image) 255

5.38 Version 3 of the N.E.S. Facility - Node Numbers 256

Figure		Page
5.39	Node Numbers Near the Pipe (Mirror Image)	257
5.40	Element Stresses due to Gravity	258
5.41	Gravity Stresses near the Pipe (Mirror Image)	259
5.42	Gravity Deformations	260
5.43	Gravity Deformations and Stresses near the Pipe	261
5.44	Unrealistic Stress Field - Time=8hr	263
5.45	Unrealistic Stress Field -Time=12hr	264
5.46	Unrealistic Stress Field near the Pipe (12hr)	265
5.47	Unrealistic Stress Field: Displacement Arrows	266
5.48	Stress Field with Reduced Cold Moduli	267
5.49	Displacement Field with Reduced Cold Moduli	268
5.50	Stresses and Deformations, T= 30 Days	270
5.51	Displacement Arrows, T= 30 Days	272
5.52	Temperature Distribution after 1 Month	273
5.53	Temperature Distribution after 2 Months	273
5.54	Temperature Distribution after 3 Months	274
5.55	Temperature Distribution after 4 Months	274
5.56	Temperature Distribution after 5 Months	275
5.57	Temperature Distribution after 6 Months	275
5.58	Temperature Distribution after 7 Months	276
5.59	Temperature Distribution after 8 Months	276
5.60	Temperature Distribution after 9 Months	277
5.61	Temperature Distribution after 10 Months	277
5.62	Temperature Distribution after 11 Months	278

Figure		Page
5.63	Temperature Distribution after 1 Year	278
5.64	Stresses and Displacements, T=365 Days	279
5.65	Displacement Arrows, T=365 Days	281
5.66	Displacement of Pipeline Invert	282
5.67	Variation of Segregation Potential and Thermal Gradient	283
5.68	Variation of Stress Perpendicular to the Freezing Front	284
J.1	Closed Form Solutions for Frost Front Advance in a Semi-Infinite Medium	405
J.2	Comparison of ADINAT Results with the Neumann Solution	406
J.3	Meshes Used in Optimization Study	409
J.4	Convergence Rate versus Latent Heat	413
J.5	Effect of Convergence Tolerance at Specified-Temperature Nodes	420
J.6	Monthly Fluctuation of Temperature Profiles	421
J.7	Equilibrium Iterations for Solution	422
K.1	Gravity Stresses Around the Pipeline	431
K.2	Horizontal Tension in the Top-Right Elements	432
K.3	Stresses; Center Node of Berm Fixed Horizontally	433
K.4	Gravity Stress Field for a Mesh with a Smaller Void	434
K.5	Gravity Stresses in the Vicinity of the Smaller Void	435
K.6	Gravity Stresses within the Elongated Mesh, Small Void	436
K.7	Altered Berm Configuration with the Small Void	437
K.8	Stresses Around the Small Void	438

Figure		Page
K.9	Gravity Stresses with No Void	439
K.10	Vertical Infilling of Hole	440
K.11	No Hole and an Altered Mesh at the Berm Toe	441
K.12	Stresses around Pipeline, Altered Mesh, No Hole	442
K.13	Top-Right Corner Freed and No Hole	443
K.14	Grossly Exaggerated Displacements (50×), No Hole	444
K.15	Surface Settlement Profile	445
K.16	Conceptual Simplification of the N.E.S. Mesh	446
K.17	Simplified Mesh under Gravity Loading, No Hole, No Berm	447
K.18	Simplified Mesh Under Gravity Loading, with a Hole	448
K.19	Simplified Mesh Under Gravity Loading (including Berm)	449
K.20	Check on the Original Mesh using ADINA (δ×50)	450
K.21	Original Mesh Under Surficial Loading Only	451
K.22	Disparate Contributary Areas for Lumped Gravity Analysis	452

List of Symbols

atm	atmospheres
c_f	heat capacity, frozen soil
c_u	heat capacity, unfrozen soil
d_{ff}	thickness of the frozen fringe
e_u^t	thawed undrained void ratio
e_0	initial void ratio
e_{11}	major principal strain
g	Gibb's Free Energy
h	enthalpy
h	total heave
$\dot{h}$	heave rate
h_i	heave from *in situ* freezing
h_s	heave from attracted water
h_u	suction in the unfrozen soil at the 0° isotherm
h_0	original height
$h_{80\%}$	height of soil after 80% consolidation
$h_{100\%}$	height of soil after 100% consolidation
i	hydraulic gradient
k_f	thermal conductivity, frozen soil
k_{ff}	thermal conductivity, frozen fringe
k_u	thermal conductivity, unfrozen soil
k_u	permeability, unfrozen soil
k_{ffo}	average permeability, frozen fringe, final ice lens
l	length
l_f	length, frozen soil
l_T	length, unfrozen soil & frozen fringe

l_u length, unfrozen soil

n_f n-factor for soil freezing

n_t n-factor for soil thawing

$p(z)$ probability of z

q power gained from the freezing of water

r radius

r_0 original or fixed radius

s specific entropy

s_i specific entropy, ice

s_w specific entropy, water

s standard deviation of the sample

t time

t_{hr} time, in hours

u internal energy

v volume

v_i specific volume, ice

v_w specific volume, water

v_0 velocity of attracted water at the onset of the final ice lens

w water content

w_c water content, consolidated soil

w_L water content, liquid limit

w_p water content, plastic limit

w_0 original water content

$w_{80\%}$ water content after 80% consolidation

$w_{100\%}$ water content after 100% consolidation

$\bar{x}$ mean value of the sample

A_0	thaw strain parameter (amount of strain on thawing)
C_c	compression index
C_{cr}	recompression index
C_{sr}	segregation recompression index
C_{rs}	residual stress *vs.* e_{thaw} index
CDF	cummulative distribution function
CMF	cummulative mass function
D	oedometric modulus
D_{60}	grain size diameter, for 60% passing
D_{30}	grain size diameter, for 30% passing
D_{10}	grain size diameter, for 10% passing
DZAA	depth of zero annual amplitude (of soil tempratures)
E	Young's modulus
E_i	initial tangent modulus, (Duncan, 1980)
FDM	finite difference method
FEA	finite element analysis
FI_a	freezing index for air
FI_s	freezing index for soil
G	shear modulus
G_i	specific gravity, ice
G_s	specific gravity, solids
H	height
H_w	cryogenic suction, Clausius-Clapeyron equation
H_0	height, original
I_p	Plasticity Index
J	Joules
K	Kelvin

K bulk modulus

K_L bulk modulus, loading

K_n advective heat transfer parameter (Nixon, '75)

K_T bulk modulus, tangent

K_{UNL} bulk modulus, unloading

$[K]$ stiffness matrice

L latent heat

L_f latent heat of frozen soil

L_w latent heat of water

L^* equivalent latent heat

LDF likelihood distribution function

M_s mass of solids

MAAT mean annual air temperature

MAST mean annual soil temperature

NES Northern Engineering Services (frost heave test facility)

P pressure

P β function parameter

P_b applied back-pressure

P_e external applied pressure

P_i ice pressure

P_u water pressure at the frost front

P_w water pressure

PDF probability distribution function

PMF probability mass function

Q_w β function parameter

$\dot{Q}_L$ phase change heat flux

$\dot{Q}_u$ conductive heat flux, unfrozen soil

R thaw consolidation ratio

R extent of radial thaw

RTOL *ADINAT's* convergence tolerance

S_{max} thaw-consolidation settlement, maximum

S_r Soil saturation

S_t thaw-consolidation settlement at end of thaw

SP segregation potential

SP^K Konrad's segregation potential

SP_o SP at the formation of the final ice lens, no load

Ste Stefan's number

T temperature

T_c cold step temperature

T_g ground temperature

T_s step temperature (Stefan analysis)

T_s $T_0 - T_s^*$

T_{so} T_s at the formation of the final ice lens

T_s^* segregation freezing temperature

T_{so} T_s at the onset of the final ice lens

T_w warm step temperature

T_0 freezing temperature of water, 0°C

TI_a thawing index for air

TI_s thawing index for soil

ΔT_{avg} average change in nodal temperatures for that element

∇T_f thermal gradient, frozen soil

$\overline{\nabla} T_{ff}$ thermal gradient, frozen fringe

$\overline{\nabla} T_{ff}^*$ $\overline{\nabla} T_{ff}$, obtained using $\overline{\nabla} T_f$ (after Konrad, 1980)

$\overline{\nabla T}_u$ thermal gradient, unfrozen soil

V_i volume fraction of ice

V_s volume fraction of solids

V_w volume fraction of water

$V_{w,c}$ volume fraction of water after consolidation

ΔV_c change in volume due to consolidation

ΔV_{i-w} change in volume due to phase change

W_u unfrozen fraction of water content

X thickness of the soil

α thaw penetration rate parameter

α_{obs} thaw penetration rate parameter, observed

α coefficient of thermal expansion

β beta function

γ weight density

γ_d weight density, dry

γ_f weight density, frozen

γ_b^f weight density, bulk, frozen

γ_d^c weight density, dry, consolidated

γ_d^f weight density, dry, frozen

γ_d^{th} weight density, dry, thawed

δ displacement

ϵ fraction of the pore water that freezes

ϵ_v volumetric strain

η porosity

θ temperature

κ_f thermal diffusivity, frozen soil

κ_u thermal diffusivity, unfrozen soil

ν Poisson's ratio

ρ_b^f frozen bulk density

ρ_s mass density of solids

σ' effective stress

σ'_0 residual stress

σ_{11} major principal stress

ϕ' friction angle, effective stress

Γ gamma function.

Φ water flow rate

1. Introduction

The purpose of this thesis was to examine two aspects of northern pipeline design using finite element analysis.

In brief, the finite element method is a means of numerically modelling a problem by representing the physical problem as an assemblage of discrete elements. The conditions of equilibrium are then established for each element and these are assembled into a set of simultaneous equations. These equations are solved for the unknowns. This procedure can be used for both steady-state or transient problems.

This thesis addresses two distinct, northern phenomena and can therefore be divided into two separate halves: thaw settlement and frost heave.

The purpose of the thaw settlement portion was to rationalize the reduction of predicted thaw settlement because of two-dimensional effects within the soil. Current one-dimensional analysis was seen as being too conservative. The two-dimensional approach was to take advantage of the soil's thaw strain variability in developing arching within the thawed soil.

To do this, thaw strain values from the literature were fitted to a beta distribution, from which representative values of thaw strain were selected. This variability was modelled within a two-dimensional finite element mesh as a

random assemblage of materials with these thaw strains. Gravity and surficial loads were applied and the average surface settlement was observed. Changing the variability of the thaw strain parameter caused a reduction in the average surface settlement.

The results of this analysis have far-reaching implications for pipeline design in thawing permafrost. Since pipeline design is extremely sensitive to thaw displacements, any method of reducing anticipated settlements will result in a more economical design. The approach taken here provides a means of doing so.

The second half of the thesis developed a procedure to run an uncoupled thermal and structural analysis to simulate frost heave. The novelty of this approach was the ability to model the effects of variable pressures, particularly those of the developing *in situ* heaving pressures. The model was originally designed for one-dimensional heave analysis and was later modified to handle complex two-dimensional behaviour.

The thermal analysis was done using the *ADINAT* program. This allowed for latent heat effects and a facility for including the effects of attracted water. In addition, nodal temperatures could be tied to a sinusoidal time function to simulate the varying surface temperatures. The stresses and displacements were modelled on the *SAP IV* finite element program which had a directional coefficient of thermal

expansion. This property was manipulated to simulate the heave within each element.

The initial simulations were of small, one-dimensional laboratory tests in order to refine the modelling techniques and calibrate the model. The final test was a 400-day simulation of the Northern Engineering Services' frost heave test facility in Calgary.

1.1 Thesis Organization

The thaw settlement problem is dealt with in the next two chapters. Chapter 2 is a partial literature review touching on aspects of current thaw design. Wherever warranted, a more detailed examination of particular aspects of thaw design is provided.

Chapter 3 addresses thaw settlement which is one area of particular importance to pipeline design. The current one-dimensional analysis is compared with a two-dimensional method that uses a beta distribution to represent the sampled thaw strains and the *ADINA* finite element program for the analysis.

The frost heave portion is in Chapters 4 and 5. Chapter 5 is the primary chapter, dealing specifically with the development of the numerical model of frost heave. Several issues arose while developing the model and the results of the examination of these issues are presented in Chapter 4.

Finally, the entire thesis is summarily described and commented upon , with conclusions, in Chapter 6.

1.2 Appendice Organization

The appendices to this thesis are a compromise between their inclusion in the main body of the thesis, or their omission entirely. The former obscures the main purpose of the thesis while the latter is inconsiderate of fellow researchers. As a result, enough information has been included in this work to evaluate the methods and results of the analyses. It was not practical to include all of the information generated by this analysis; however, most of it has been retained on computer tape, and is retrievable.

Appendice *A* examines the effect of thaw settlement on the rate of thawing. Appendice *B* provides four examples of thaw calculations, comparing the present method with that recommended in this thesis.

Appendice *C* lists the thaw strain values used in the analyses of Chapter *3*, and fits these values to a Normal distribution for a comparison with the beta distribution of Appendice *D*. Appendice *D* also includes programs for determining the beta distribution of the thaw strain parameter as well as programs calculating the input for the numerical analysis. Program *BETA* does this assuming normal consolidation while *BETARESID* includes the effects of residual stress.

Appendice *E* is a summary of the thermodynamics pertinent to existing theories of frost heave. While this information could be compiled from the references listed in the bibliography, it appeared prudent to retain this succint explanation, particularly when much confusion exists in the literature.

Appendice *F* is a modification of Jean-Marie Konrad's finite difference method (FDM) for calculating one-dimensional heave (Konrad, 1980). The main modification made to the program is the inclusion of pressure effects on the segregation potential (*SP*) parameter. In addition, a glossary of variables has been prefixed to the program and comments have been inserted throughout.

The *TRANS* program for calculating heaves and preparing finite element input files is in Appendice G. This is the final version which was used for the simulation of a pipe in the ground. The earlier one-dimensional version is retained on tape by this department. The *TRANS* program works in concert with a number of ancillary programs, as detailed in procedure file *LOOP* (Appendice *H*). The two finite element programs it is designed for are *SAP IV* (Bathe, *et al.* 1973) and *ADINAT* (1981 version, Bathe *et al.* 1981b). Modifications of these two programs may result in some adjustments of the format statements within *TRANS*.

Appendice *H* is a collection of flowcharts. These are provided as an outline of the file manipulations necessary

to conduct the heave calculations. The actual procedure files are dependent on the Michigan Terminal System (MTS) and are not readily transferrable to other operating systems. These files have been retained on tape for reference.

Appendice *I* is the contents of file *ARCH3* for the simulation of Test C-10. This file is a compilation of the summary spread sheets for each iteration of the heave calculation, as calculated using the one-dimensional version of the *TRANS* program. This information is provided as an aid to other researchers, who should also examine other related files (on tape) for completeness.

Appendice *J* deals with the *ADINAT* program. As the heave research progressed, many idiosyncracies of this program were found to have profound effects on the numerical results. Most were not described or alluded to in the program's user manual. To use *ADINAT* responsibly, it was necessary to determine what these idiosyncracies were, and to quantify their effect as they pertained to this work. The results of this examination are presented herein.

Appendice *K* summarizes the identification and solution to an extraneous tension field that developed in the pipeline mesh. This was a significant part of the initialization of ground conditions prior to the actual heave simulation.

Appendice *L* is a compilation of typical input files for the various computer simulations. It is not intended to be comprehensive, but rather as an aid to researchers attempting to repeat this type of analysis. Pertinent input and output (I/O) files are retained on tape by this department.

Appendice *M* examines the error in ignoring the conductivity difference between ice and frozen soil during the heave simulation.

Appendice *N* is a glossary of files, programs and procedures used in this analysis. The program listing truncates the suffix ".C" which is used to denote the compiled versions of the programs.

In addition to the chapters and appendices mentioned, there were a number of ancillary works that have not been included. These are primarily small pre- and post-processing programs that did not warrant any discussion, and the powerful graphics programs (*SAPMESH*, *ADMESH*, *ADMESH81*) that were developed for this thesis. These are retained on tape.

2. Pipeline Design in Thaw-Unstable Soils

2.1 Design Approach

With the recent increase in northern development, attention has been drawn to the performance of pipelines in thaw-unstable soils. Much concern arises from the fact that thaw-unstable soils are found throughout the arctic and cannot be avoided when selecting the route for linear structures such as pipelines. Thaw is inevitable in most cases because permafrost is susceptible to small imbalances in the thermal regime brought upon by the pipeline operation or merely by the construction activity itself.

The strength and deformation characteristics resulting from thaw are notoriously poor. However, the resulting losses of strength, stiffness and volume are not in themselves the reason for engineering interest. Instead, it is the variability of these properties within the soil mass resulting in differential settlement that is of primary concern. This differential settlement results in a variable support for the pipeline, even so far as to eliminate contact between the pipeline and zones of high thaw subsidence. In addition, overlying material tends to become supported on the structurally stiffer pipeline, significantly increasing the soil load bearing on portions of the pipeline.

Prudent route planning would avoid aligning the pipeline through regions of thermally-sensitive thaw-unstable soils. However, even if this were possible, constraints such as economics, logistics and other aspects of engineering design will likely result in sections of the route passing through unfavourable ground conditions.

2.1.1 Design Alternatives

The designer may choose to avoid burying the pipeline by using an elevated segment, as was done in the thaw-unstable regions of the Alyeska pipeline. This is much more costly because the pipeline must be self-supporting between pile supports and it requires significant design of the piles to avoid excessive settlement which would result in reduced or no support of the pipeline. In fact, thermal degradation was unavoidable under some conditions on the Alyeska project, thereby requiring heat pipes as a design option to maintain an acceptable thermal balance at some piles.

Differential settlements can be reduced by replacing some of the thaw-unstable material by thawed or thaw-stable soil. This method has the double advantage that this material will not be subject to thaw settlement and it mollifies any effects of differential settlement in the underlying sub-base. This is generally not a practical alternative for pipeline design, both because of the

economics of moving such quantities of earth and the logistics of finding large quantities of acceptable replacement material, particularly in the extensive silty fluvial deposits typical of arctic flood plains. Soil replacement techniques may be the optional design at pumping stations along the route where the thermal disturbance may be higher than average and the tolerance of settlement lower.

A variation on replacing the poor material is to install the pipeline within a berm on top of the original soil. This avoids the need to remove the underlying material and results in a higher heat flow to the surface. However, it also requires more thaw stable material than in the soil replacement design. In addition there is the additional thickness of thaw unstable material below the pipeline to contend with. Placement of the berm would also change the regional flow of water, both as an impediment to surface runoff and by reducing the hydraulic conductivity of underlying materials due to consolidation. The existance of the berm itself may raise environmental concerns.

An alternative to removing the thaw-unstable material is to thaw it before installing the pipeline. The resulting settlements, and therefore the differential settlements, occurring before pipeline placement would not affect the pipeline. This can be done by using existing disturbed and cleared rights-of-way which are generally thawed due to the

degradation of the insulating cover of vegetation. This was done in sections of the Interprovincial Pipeline Ltd. (IPL) pipeline from Norman Wells N.W.T. to Zama, Alberta (Nixon, Stuckly & Pick, 1983). The alternative of pre-clearing a right-of-way along the proposed route is also a possibility. This requires sufficient lead time to complete the clearing in the winter prior to the winter pipeline construction, with thaw occurring in the interim summer. Economically, however, the year's delay in the start of the pipeline may not be justifiable when compared to alternative placement designs.

In the particular example of the IPL pipeline, thermal disturbance due to construction activity was more deleterious than that of the anticipated operating conditions, since the oil in this pipeline was to run at close to the freezing temperature. Efforts were made to limit the depth of thaw by limiting the width of the right-of-way, in recognition of the relationship between the width of the surface disturbance to the depth of thaw.

Thaw can also be actively resisted by using circulating refrigerant lines (Wheeler, 1973). Using lengths of closed loops beneath the pipeline assures thermal symmetry and allows a closer control of flow rates and temperatures. This is an elaborate design, involving higher installation costs and the need for constant operation of the coolant lines. The cost of this alternative makes this option only

practical for extraordinary circumstances.

By far the preferable option is shallow burial in *in situ* materials. This provides a continuous support for the pipeline and a protective cover against natural or man-made hazards. There is the possibility that excessive pipe strains may develop due to differential settlements so the pipeline behavior must be predicted before opting for one of the more expensive design alternatives mentioned above.

2.1.2 Aspects of Design

There are three main aspects of pipeline design. First, geothermal prediction is necessary to determine the extent of thawing, as this will determine the volume of the soil mass that is affected. Next, the geotechnical properties of the soil itself are examined, particularly its thaw strain behavior because this will control the amount of settlement within the thawed zone. Lastly, the soil pipeline interaction is examined to see what effect the loadings have on the pipeline and what effect, if any, the resulting pipeline deformations have on the applied loads.

2.2 Geothermal State-of-the-Art

The distinguishing feature of the class of problems we are studying is that there is a moving surface within the ground at which latent heat is absorbed or released, typically with different thermal properties on either side

of this boundary. Because of non-linearity, the solution to this problem is complex and cannot be solved using any superposition methods.

2.2.1 One-Dimensional Thermal Analysis

Neumann provides a closed-form solution to the progression of a phase front into a semi-infinite region, which is initially at a constant temperature below the melting temperature, due to the application of a surficial step temperature. Nixon & McRoberts (1973) provide a graphical solution to this equation. If heat capacity is neglected, the resulting approximation to the Neumann equation assumes a steady-state temperature gradient in each of the frozen and unfrozen zones. Making the further assumption that heat flow within the frozen material is negligible, the Neumann equation collapses into the Stefan equation.

It is important to note that the standard derivation of the Neumann equation assumes no change in volume during the phase change. This assumption is rarely true but it removes the complicating effects of material contraction and expansion that generally have secondary effects on heat transfer.

Carslaw and Jaeger (1959) examine the Neumann equation and do consider the effects of volume change. For the specific case of one-dimensional freezing of water they

provide solutions for the Neumann equation when volume change is neglected and again when it is considered. In the latter case, a convection term is added to the equation of heat conduction in the liquid, which is being displaced by the expansion of freezing water. Because the water, and therefore heat, is being displaced away from the freezing front, a slightly faster rate of freezing occurs.

Back-analyses of the writers' worked examples and the requirement for dimensional similitude of their equations demonstrate that the writers have been inconsistent in their use of the latent heat term, L. In all cases they intend the use of the volumetric latent heat, $L\rho$. This latent heat is of the material being formed, an important point which will be dealt with in some detail in this work.

Nixon (1975) examines the role of the heat transfer due to the movement of water in the thawed soil. He has referred to this process as "convection", although others have labelled it as "advection". The heat conduction in the unfrozen material is modified by a convection term using the thaw-strain parameter factored by $\frac{C_w}{C_u}$, the relative heat capacities of the moving water to the unfrozen soil. Nixon does not explicitly describe what value is used for the latent heat but it is assumed the same method is used as in Nixon and McRoberts (1973). He concludes by stating that in most instances, convective heat transfer may be neglected without a significant loss in accuracy.

The Neumann equation and the simpler Stefan equation are both used to determine the α parameter which relates the depth of thaw to the square root of time

$$X = \alpha\sqrt{t} \qquad [2.1]$$

The application of either the Neumann or Stefan equation should be straight forward. However, due to the understated assumptions made in the derivation of the Neumann equation and the high thaw strain of some permafrost soils, the literature reveals an inconsistent application of the formulas. This inconsistency results when the volumetric latent heat used is not based on a unit volume of the material being formed or when the unfrozen thermal properties are not based on a moisture content representative of the unfrozen soil during thaw. Both these phenomena are a result of applying the Neumann or Stefan equations without accounting for any volume change. It must be emphasized that the implications extend beyond the inclusion of true convective heat flow, which has a negligible contribution to the thermal balance. An examination of the application of analytical heat equations to permafrost points out some of these difficulties:

Brown and Johnston (1970), in their back-calculation of thaw front advance under dykes, use the simplifying assumption that heat flow in the frozen region is negligible, but include advection effects in the thawed region. Advection is the term used to describe the heat

transfer effect due to water moving from the thaw front to the warm surface. The writers pointedly recognize that their heat source is moving towards the thaw front due to thaw settlement, and they correct their conductive heat flux for this. This was needed to increase the heat flow since they based their latent heat on the quantity of heat required to melt ice in a unit volume of the frozen soil rather than on a unit volume of the thaw-settled soil. In using their simple equation of heat balance, the two methods would result in the same answer.

Although the writers do recognize the role of volume change in reducing the dimensions of the problem, they ignore how it affects soil properties. For example, their unfrozen thermal conductivity K_u, is based upon a thawed-unconsolidated moisture content which overpredicts the moisture content thereby under estimating the thermal conductivity by 25%.

Smith (1972) in determining α values from one-dimensional thawing of soils, measured the time taken for the sample to thaw to the base. He states that the depth of thaw would be the average of the frozen and unfrozen heights but does not support his reasoning. However, if Stefan's postulate is assumed, the only reasonable height to use would be the unfrozen height since all heat flow is through the unfrozen material. This is intuitively obvious when one considers that the longest length of the heat flow

path is the height of the thawed sample.

Nixon and McRoberts (1973) in their study of factors affecting the thawing of soils examine the Neumann equation and its variations in some detail. Although the writers restrict their study to thaw-susceptible soils they include no discussion of the effect of volume change on their analyses. The latent heat calculated is correctly based on a unit volume of thawed material, however, the frozen conductivity and heat capacity are also based upon the dry density of thawed material. This leads one to conclude that the thawed values were arbitrarily chosen to calculate the input parameters to the Neumann equation. The conclusions they make are valid only for materials that are thaw-unconsolidated as no change in moisture content is allowed for in their discussion. Their resulting soil model is, however, atypical of thaw sensitive soils which are of interest primarily because of their high thaw settlements.

As an attempt to clarify the thaw-strain issue as it pertains to heat flow, the author has appended a short discussion to this work (Appendice A). To demonstrate the effect of accounting for thaw settlement and the resulting moving heat source, a set of sample calculations are presented, based on tests reported by Nixon and Morgenstern (1974) (Appendice B). First, the predicted α value is obtained using the method described by Nixon and McRoberts (1973). Next, the calculation is re-done assuming settlement

and a moving heat source. For test NWU-2, an undisturbed silt with a thaw strain of A_o= 8.3%, the Nixon and McRoberts method and the corrected latent heat method both provide excellent correlation with the observed alpha value. For test NWU-9, performed on an ice-rich material with a thaw strain of A_o= 34.5%, the two methods again provide good correlation, although some subjectivity is introduced in establishing the unfrozen water content.

It is reassuring to note that the method of Nixon & McRoberts (1973) fortuitously provides similar results to that based upon the heat equation of Carslaw & Jaeger (1959), modified for volume change. This is in spite of the fact that the thermal properties used for the unfrozen material are not representative of that material and that dimensional changes are not accounted for. This is shown in Figure 2.1 where the error involved in using Nixon's method is plotted against thaw strain for different initial moisture contents in a thawed-undrained fine-grained soil. Stefan's equation was used in the comparison and a linear function was used to describe the thermal conductivity of unfrozen fine-grained soils as a function of water content. The apparent decrease in error of high thaw strains is due to the deviation in assuming a straight-line approximation of conductivity from the actual value at low moisture contents.

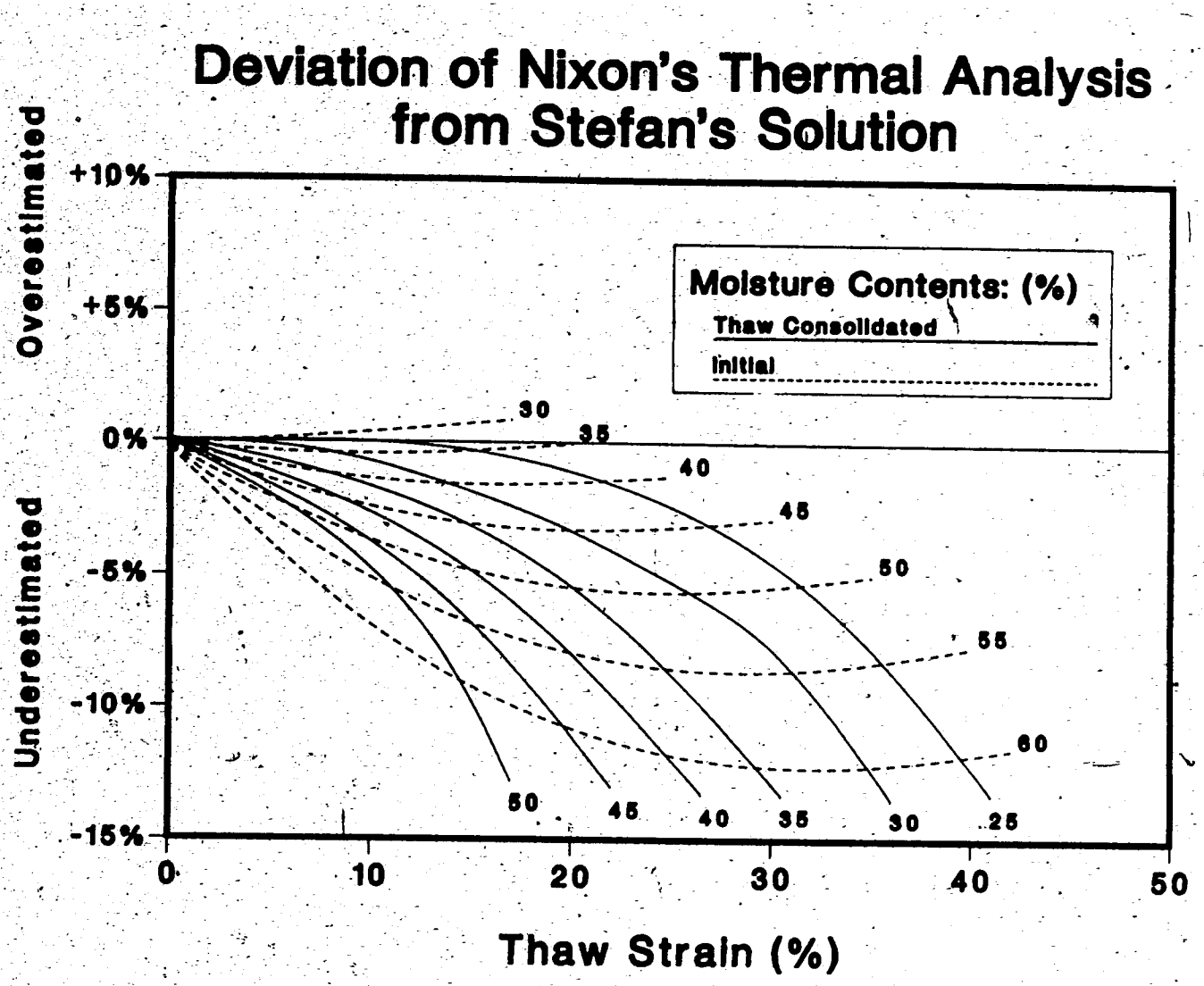

Figure 2.1 Deviation of Nixon's Thermal Analysis from Stefan's Solution

At low thaw strains and moisture contents, Nixon's method provides a fast, simple approximation to the true solution for fine-grained soils. This is due to the unique relationship between thaw strain and thermal conductivity. For higher moisture contents or thaw strains, the error involved approaches 10% and may not be acceptable.

2.2.2 Two-Dimensional Thermal Analysis

One-dimensional analyses are appropriate for most laboratory programs, however one-dimensional behavior is uncommon in practice where two- or three-dimensional behavior is the norm. Two- and three-dimensional analyses are more complex, requiring a better understanding of the processes involved and the input parameters. Often a simple one-dimensional analysis will provide a first-order approximation to the expected behavior, with subsequent modifications to the analyses improving the accuracy and precision of the answer. This can be seen in the following analyses:

Morgenstern and Nixon (1975) analyse the data collected at a warm oil pipeline facility. The testing consisted of installing a 27 m length of 61 cm diameter pipe into ice-rich permafrost. Hot oil (71°C) was circulated through the pipeline and the resulting transition of temperature settlements and pore water pressures were measured.

A previous thaw settlement analysis by Watson, *et al.* (1973a) used a correlation between the frozen bulk density and thaw strain. This reasonably predicted the total thaw settlement that the pipeline would undergo, given a simplified examination of the thawing under the pipeline.

Morgenstern and Nixon re-analyse these data using their linear thaw consolidation theory to predict not only the settlement of the pipeline, but the development of pore water pressures at the thaw front. Using the soil profile and laboratory results they determine average values of permeability, k, and the coefficient of compressibility, m_v to obtain a value for the coefficient of consolidation, c_v. This parameter is particularly important for determining the development of excess pore water pressure and settlement.

For their thermal analysis, the writers argue that, for the initial period of thawing, the thaw front would be within a diameter of the pipeline and the heat flow below the centreline would be vertical. Therefore they claim that a one-dimensional analysis would suffice as an initial approximation to the solution. They use the modified Stefan solution (Nixon & McRoberts, 1973) for the thaw depth, with a weighted average for the latent heat, L, an average Stefan number, Ste, and a thermal conductivity, k_u, based on the average consolidated moisture content. As the pipeline rests on ice and ice-rich silty soil, the thawing of the contiguous soil would result in a moving heat source.

Therefore, their results are with respect to the moving pipeline invert. Using the Stefan relationship between the thaw depth and the square root of time, the observed depth of thaw is compared with the predicted thaw, and also with a refined prediction based on a variable latent heat.

Their refined prediction diverges from observations of thaw at depth because the one-dimensional prediction of accelerating thaw in the less ice-rich material fails to account for the radial heat flow which would mitigate the thaw rate.

Upon closer examination of their determination of the α parameter relating the square root of time with thaw depth, it appears that while the writers have corrected for a moving heat source in the conduction portion of the Stefan equation, they have not modified the latent heat term. This is needed to account for the large volume of ice that has melted and was subsequently consolidated out of the soil.

To obtain the equivalent latent heats (based on thawed dimensions) the bulk frozen densities are used to calculate the water contents and dry densities, from which latent heats (based on frozen volumes) can be determined. These values of L are then factored by the height differences undergone during thaw strain to get the amount of latent heat necessary to obtain a unit volume of thawed material at w=45% in the material overlying the till (Table 2.1).

Table 2.1 Equivalent Latent Heat Assuming 100% Consolidation

Material	h_0 m	ρ_t g/cm^3	w_0 m	$\rho_d = \frac{\rho_t}{1+w_0}$ g/cm^3	$h_{100\%}$ m	$L_f = \rho_d w_0 L_w$ cal/cm^3	$L_{100\%} = L_f \frac{h_0}{h_{100\%}}$ cal/cm^3	$L_{100\%} \times h_{100\%}$ cal/cm^2
Ice	0.20	0.95	725	.115	2	66.5	665	1330
Ice with Silt	0.75	1.23	157	.479	0.33	59.8	136	4488
Silt & Ice	1.25	1.43	84	.777	0.75	52.0	87	6525
Gravel Till	0.80	2.00	21	1.653	0.80	27.6	27.6	2208
	3.00				1.90			14551

$$\bar{L}_{100\%} = \frac{14551 \text{ cal/cm}^2}{190 \text{ cm}} = 76.6 \text{ cal/cm}^3$$

When this new average value of L is used in the Stefan equation, we obtain:

$$X = \sqrt{\frac{2\ k_u\ T_s}{L}} \left[1 - \frac{Ste}{8}\right] \sqrt{t} \qquad [2.2]$$

$$= \sqrt{\frac{2 \times 0.00252 \times 71}{76.6}} \left[1 - \frac{0.66}{8}\right] \sqrt{t}$$

$$= 0.0627 \sqrt{t}\ \text{cm}/\sqrt{\text{s}}$$

$$= 0.1846 \sqrt{t}\ \text{m}/\sqrt{\text{day}}$$

Using a variable latent heat with depth, we obtain a segmented function. These plots are shown in Figure 2.2.

Watson, *et al*. (1973a) state a value of α from the field data to be 0.046 $\text{m}/\sqrt{\text{h}}$ (0.225 $\text{m}/\sqrt{\text{day}}$) and from the Stefan equation to be 0.057 $\text{m}/\sqrt{\text{h}}$ (0.279 $\text{m}/\sqrt{\text{day}}$). No calculations were shown to evaluate the assumptions they used. The relative size of their α parameter would indicate a thermal analysis similar to the subsequent analysis of Morgenstern and Nixon (1975).

If we examine the thermodynamics of one-dimensional thawing of permafrost, using the Stefan postulates of negligible heat flow in the frozen zone and negligible heat capacity effects in the thawing zone, we are left with a simple two process system: heat flux conducted through the expanding thawed zone and the resulting phase change at the frozen/unfrozen interface. Using the same premise of conservation of heat flow in two dimensions, the Stefan equation for radial heat flow in an infinite medium can be developed:

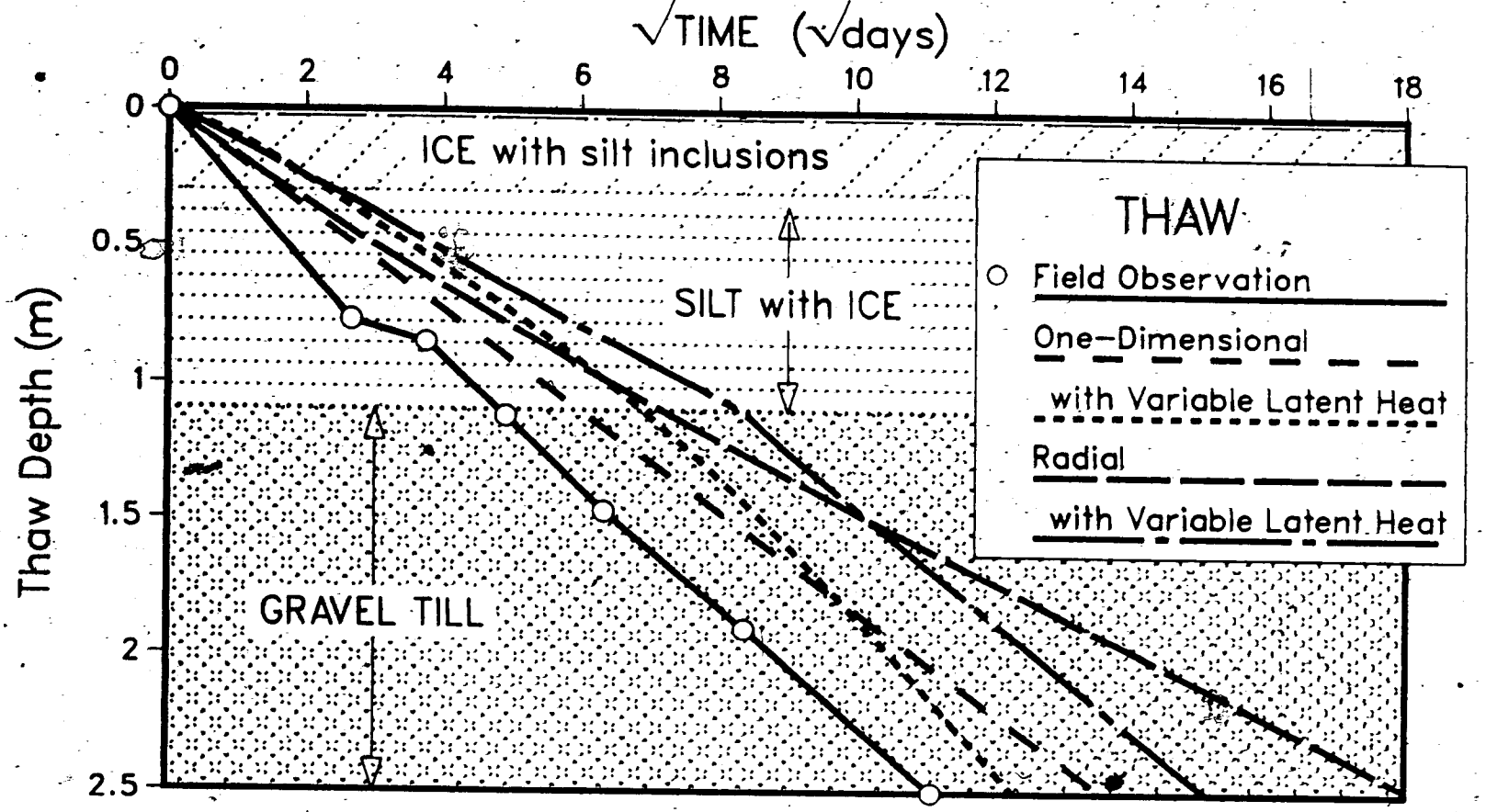

Figure 2.2 Thaw Progression – 100% Consolidation

$$T_s = \int_{r_0}^{R} \frac{d\theta}{dr}\, dr \qquad [2.3]$$

$$= \int_{r_0}^{R} \frac{\dot{Q}_k}{k_u\, 2\pi r}\, dr \qquad [2.4]$$

$$= \frac{\dot{Q}_k}{k_u\, 2\pi r} \ln\left[\frac{R}{r_0}\right] \qquad [2.5]$$

$$\therefore \dot{Q}_k = (2\pi k_u T_s)/\ln(R/r_0) \qquad [2.6]$$

(note: thaw strain unaccounted for)

$$\text{But } \dot{Q}_k = \dot{Q}_L = L\, 2\pi R \frac{dR}{dt} \qquad [2.7]$$

$$\therefore \frac{k_u T_s}{\ln(R/r_0)} = LR\frac{dR}{dt} \qquad [2.8]$$

$$\int_0^t \frac{k_u T_s}{L}\, dt = \int_{r_0}^{r} R \ln\left[\frac{R}{r_0}\right] dR \qquad [2.9]$$

$$= \int_{r_0}^{r} R \ln(R)\, dR - \int_{r_0}^{r} R \ln(r_0)\, dR$$

$$\frac{2k_u T_s}{L}\, t = r^2 \ln\frac{r}{r_0} + \frac{r_0^2 - r^2}{2} \qquad [2.10]$$

This is of the same form as that derived by Carslaw and Jaeger (1959).

Comparing the thaw depth versus root-time curve with the one-dimensional Stefan equation, we obtain good agreement initially, with greater divergence with depth as the two-dimensional effects begin to control. The resulting curve plots very close to the slope of the field data curve in the long term (Figure 2.2). It should also be noted that this analysis does not have the semi-empirical correction factor (Nixon and McRoberts 1973) which would further retard the thaw advance. However, the sharp drop in temperature

near the pipeline, due to the logarithmic radial temperature distribution, would reduce the heat capacity effect and the need for such a correction.

A simple analysis of conductive heat flux through the thawed zone indicates that the assumption of a linear temperature distribution will overestimate the amount of heat flowing through the thawed zone at an ever increasing rate:

Assuming a linear distribution, our heat flux just within the interface is:

$$\dot{Q}_{linear} = k_u \frac{\partial \theta}{\partial r} 2\pi r \qquad [2.11]$$

$$\text{But} \quad \frac{\partial \theta}{\partial r} = \frac{T_s}{r - r_o} \qquad [2.12]$$

$$\therefore \dot{Q}_{linear} = k_u * T_s \, 2\pi \frac{r}{r - r_o} \qquad [2.13]$$

For a radial heat flow analysis, we obtain a logarithmic distribution of temperature:

$$\dot{Q}_{radial} = \frac{k_u \, T_s \, 2\pi}{\ln \frac{r}{r_o}} \qquad [2.14]$$

Comparing the two, their ratio gives:

$$\frac{\dot{Q}_{linear}}{\dot{Q}_{radial}} = \frac{r}{r - r_o} \ln \frac{r}{r_o} \qquad [2.15]$$

It can be seen that close to the pipe the ratio approaches unity:

$$\text{Since } \ln(1+h) = h - \frac{h^2}{2} \ldots \qquad [2.16]$$

$$\cong h, \quad \text{as } h \to 0$$

$$\therefore \lim_{r \to r_o} \frac{\dot{Q}_{linear}}{\dot{Q}_{radial}} = 1$$

For any distance away from the pipeline, the ratio indicates an increasingly differing behavior for the two assumptions (Figure 2.3). This relationship demonstrates that even within one diameter of the pipeline, a 40% difference in heat fluxes exists.

As most of our heat during thaw is used to reduce the ground ice into water, and as very small thermal gradients generally exist on the frozen side of the frozen/unfrozen interface, the heat flow through the frozen zone is neglected. However, in the radial analysis the error accepted in using this assumption is inflated by the increased contact area at the frozen/unfrozen interface due to the expanding thaw bulb. This would allow more heat to be conducted through the frozen zone which reduces the rate of thaw. This effect cannot be seen in the available data as the test facility's hot oil was stopped for a month after 10 weeks of operation.

The frozen soil properties are necessary to predict the final extent of thawing under steady state conditions. This can be done in a transient analysis of longer duration or in

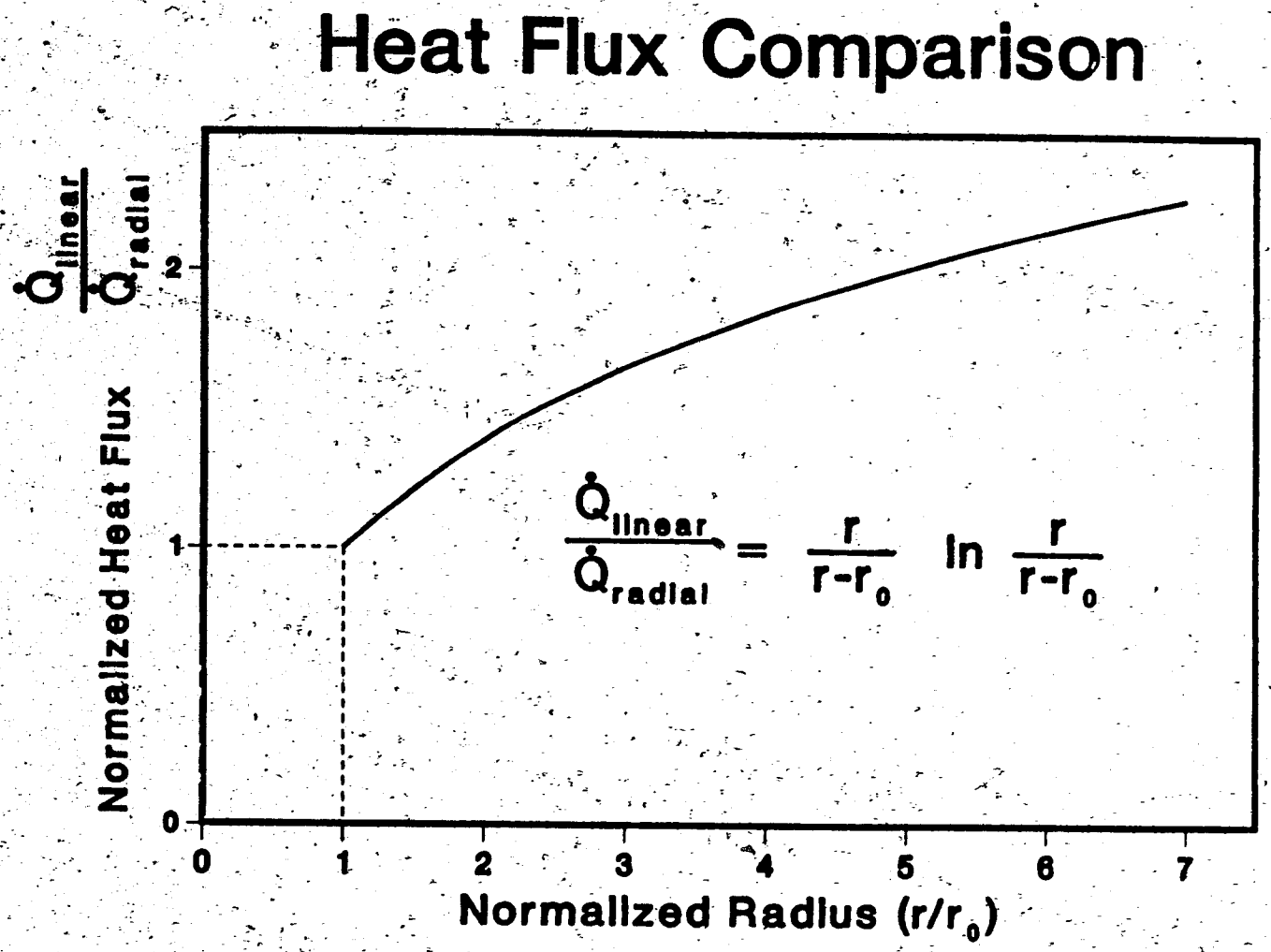

Figure 2.3 Heat Flux Comparison

a simplified static analysis where latent heat and heat capacity effects are removed from the solution.

It should be noted that the closed-form Stefan solution for radial thaw is for an unrealistic idealized situation; however, the inaccuracies are negligible for the soil below the centreline for most situations. In addition, the foregoing analysis indicates that the rate of thaw advance is better predicted in the long term using the radial analysis.

Morgenstern and Nixon (1973) conclude their paper with an analysis of the excess pore water pressures generated during the thawing. As the development of excess pore water pressures at the thaw front, and its associated flow through the soil, is analagous to the release of latent heat and heat conduction, the use of their thaw-consolidation ratio should still be valid for the radial problem. Anomalies do arise when considering the effect of a surcharge on a thaw front existing in numerous orientations with respect to the direction of loading. This is because the excess pore pressure distribution within the thawing soil is dependent upon the direction of loading and the water flow path.

It is apparent from Figure 2.2 that neither the linear Stefan nor the radial Stefan solution adequately describes the field observations. The practice of normalizing the depth of thaw to the pipeline invert has its inherent problems particularly as the soil material approaches pure

ice which would be predicted as zero depth of thaw with thaw occurring instantaneously. Correcting for a time lag in pure ice would only shift the predicted curves to the right, further from the observed curve. There is even some justification in ignoring the ice all together: Slusarchuk, *et al.* (1973) detail a sand bedding for the pipeline excavated into the ice layer.

2.2.3 Thaw with Partial Consolidation

In examining the slopes of the latter portions of all predicting curves, it is seen that they do not differ greatly from observed curves. This should give us some confidence in the applicability of a Stefan analysis in low water content materials. In the analysis of the high moisture content soil nearest the pipeline, our analyses predict a slower rate of thaw advance, as would seem reasonable with the significantly higher latent heats of the material. Instead, a far more rapid penetration is observed. This difference is not due to two-dimensional effects, as the linear Stefan solution is the least conservative of the two approaches and yet it is not the lower limit to the field curve. To examine the reason for this discrepancy, the Stefan solution parameters require scrutiny.

The thermal conductivity of the unfrozen material is relatively insensitive to moisture content at high moisture contents, as is the heat capacity. The volumetric latent heats are known to a high degree of certainty given the bulk

frozen densities. The applied step temperature is a controlled parameter. However, the calculations were done assuming completed thaw strain: this was not the case. Watson, *et al.* (1973) mention delayed settlement and the build up of pore water pressures within the thaw bulb and Morgenstern and Nixon (1973) perform an analysis to predict this excess. This effect does not change the total latent heat needed to thaw to a certain point, but instead it increases the length of the flow path of the conducted heat by an amount equivalent to the unconsolidated volume of excess pore water. In terms of the thermal equations, it reduces the effective volumetric latent heat, pro-rated to an 80% consolidated thawed volume instead of the smaller 100% consolidated thawed volume. While this would decrease the average latent heat value by approximately 10%, it would result in an increase in the slope of our lines by 5%, as shown in Table 2.2 and Figure 2.4.

In comparing the two analyses using 80% consolidation and 100% consolidation, two points are of interest. First, while the linear and radial Stefan solutions predict faster thaw penetration for the 80% consolidated material (due to the lower latent heat value), the strata are penetrated faster with the 100% consolidated analysis. This is because the total latent heat needed to thaw to a given point in the frozen soil is the same, yet the flow path through the totally consolidated material is shorter. This allows for a faster heat transfer from the pipeline to the frozen soil.

Table 2.2 Equivalent Latent Heat Assuming 80% Consolidation

Material	h_0 m	ρ_t g/cm^3	w_0 %	$w_{100\%}$ %	$w_{80\%}$ %	$L_f=\rho_d w_0 L_w$ cal/cm^3	$h_{100\%}$ m	$h_{80\%}$ m	$L_{80\%}=L_f\frac{h_0}{h_{80\%}}$ cal/cm^3	$L_{80\%}\times h_{80\%}$ cal/cm^2
Ice	0.20	0.95	725	45	81	66.5	0.02	0.056	238	1333
Ice with Silt	0.75	1.23	157	45	67	59.8	0.33	0.41	109	4469
Silt & Ice	1.25	1.43	84	45	53	52.0	0.75	0.85	76	6460
Gravel Till	0.80	2.00	21	21	21	28.0	0.80	0.80	28	2240
	3.00						1.90	2.12		14502

$$\rho_d = \frac{\rho_t}{1+w_0} \qquad \bar{L}_{80\%} = \frac{14502 \text{ cal/cm}^2}{212 \text{ cm}} = 68.4 \text{ cal/cm}^3$$

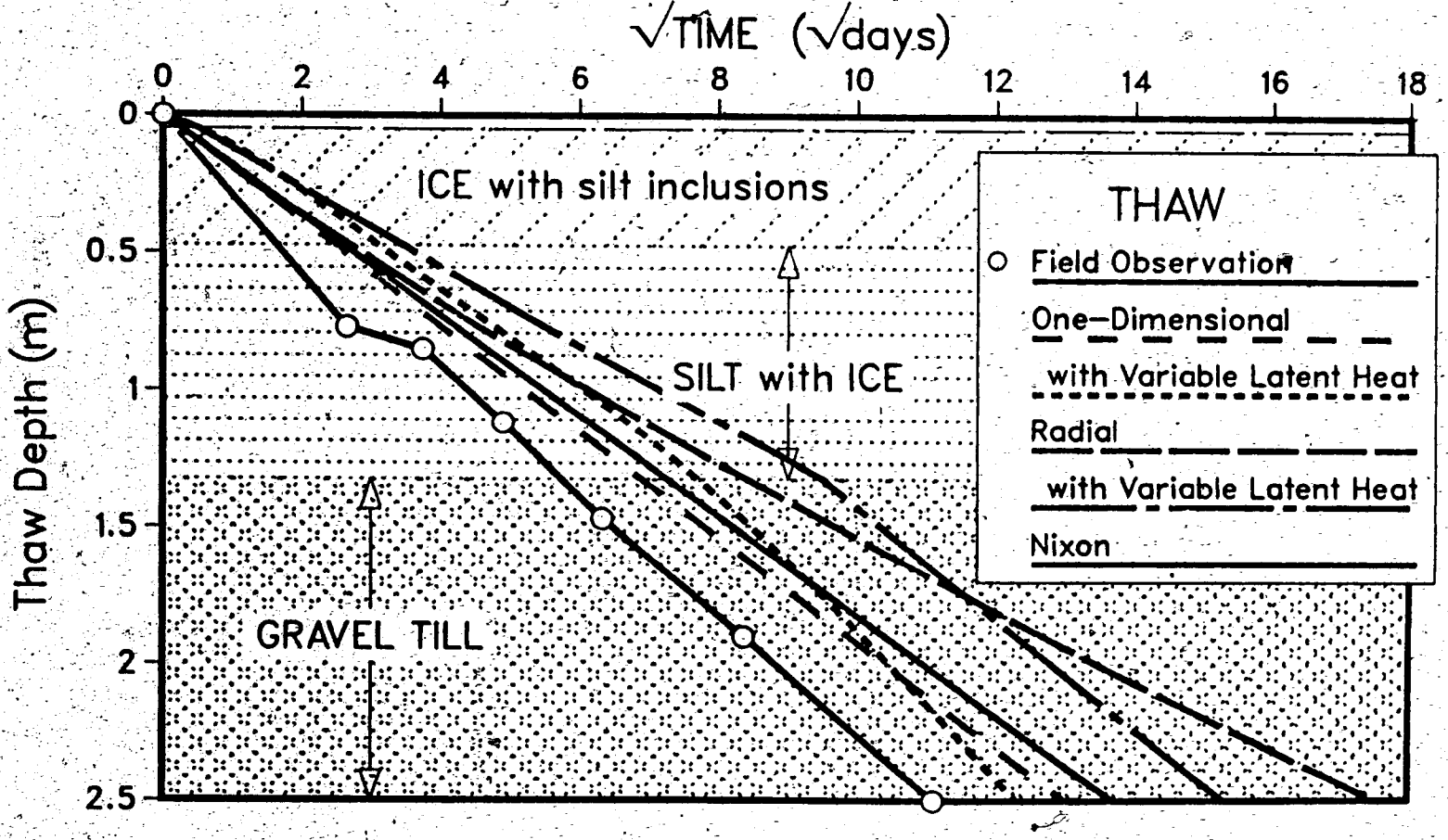

Figure 2.4 Thaw Progression – 80% Consolidation

The analyses using variable latent heats are similarly affected.

Secondly, neither the variation between linear and radial heat flow nor the difference in the degrees of consolidation have predicted the rapid thaw progression of the initial portion of the field curve. It would appear that a very rapid thaw occurred in a material that would be expected to exhibit poor thaw-front advance due to its very high moisture content. This is followed by a sharp decrease in the root-time thaw rate, without a reported change in the material being thawed, followed by a constant root-time progression of thaw. Given the material consistency, it appears that the Stefan analysis is neglecting a mode of thermal transport that is occurring during the initial stages of thaw. Heat advection, the movement of heat due to the mass transfer of excess pore water, is a possibility that deserves some consideration.

Nixon (1975) examines the contribution of advective heat transfer in thawing soils. Using his chart to assess the thaw parameter, α, we find:

$$Ste = \frac{c_u T_s}{L} \qquad [2.17]$$

$$\doteq \frac{0.71 \times 71}{68.7} = 0.73$$

Nixon's thermal convection factor,

$$K_n = \frac{c_v}{c_u} A_o \qquad [2.18]$$

$$= \frac{1.00}{0.71}\left[\frac{300 - 212}{300}\right] = 0.41 \text{ cal/°C cm s}$$

from Nixon (1975):

$$\therefore \frac{\alpha}{2\sqrt{\kappa_u}} = 0.52$$

$$\text{diffusivity, } \kappa_u = \frac{k_u}{c_u} = \frac{0.00252}{0.071} = 0.0035 \text{ cm}^2/\text{s}$$

$$\therefore \alpha = 0.52 \times 2\sqrt{0.0035}$$

$$= 0.62 \text{ mm}/\sqrt{\text{s}}$$

$$= .1825 \text{ m}/\sqrt{\text{day}}$$

As this effect deals with thaw mitigation due to the migration of heat in the excess of pore water from the thaw front, we would not expect primary convection to contribute to thawing. Its effect is seen in curve "Nixon", Figure 2.4, for the case of linear thaw.

The simplest explanation for the rapid initial thaw rate is that the ice-rich material near the surface allowed a form of thermal transport in addition to heat conduction. This is seen in Figures 2.2 and 2.4 where the one-dimensional Stefan analysis, being the liberal closed-form predictor of two-dimensional behaviour, still underestimates the thaw rate in this material. The analysis by Morgenstern and Nixon (1975) provides a closer fit to the observed thaw progression however it is based on a weighted average latent heat which would over-predict thaw rates in the ice-rich material at the surface. In addition, their analysis uses an implied relationship between thermal

conductivity and thaw settlement that is inappropriate for high thaw-settlement materials (ref. App. A). Re-evaluation of the initial data (Watson, *et al.* 1973b) may indicate the additional mode of thermal transport during the initial stages of thaw, however that study goes beyond the scope of this work.

2.2.4 Other Closed-Form Solutions

Other closed-form solutions in two-dimensions exist, particularly for the case of a circular heat source. Lunardini (1980) examines the phase change around a circular pipe within an infinite medium. He examines the effects of a number of simplifying assumptions and approximations on the radial heat flow problem. Variations that include latent heat in the calculations are also looked at. The writer concludes that the solutions provided are sufficiently accurate for engineering design. No mention is made of volume change during phase change nor of the effect of a boundary close to the pipeline.

The problem of a pipeline in a semi-infinite medium was addressed by Thornton (1976). In his thermal analysis, he astutely points out that numerical techniques have the capability of handling the complexity of freezing and thawing soil, but that this very flexibility can result in an expensive and unwieldly analysis. Instead, less exact solutions are suggested, with his paper focussing on pipelines buried in permafrost regions.

As a first approach, the steady-state condition was examined. This will provide the greatest expected extent of the thaw bulb and is analytically simpler since the latent heat of the material can be ignored. Referencing Carslaw and Jaeger (1959), and Lachenbruch (1970), he obtains a set of coaxal circles as isotherms in the solution of the Laplace equation (Figure 2.5). These offset circles describing the thaw bulb are a more exact representation of the thaw bulb around a pipeline at steady state than those the simple one-dimensional or two-dimensional solutions provide. This assumes constant temperatures at the ground and pipe surfaces.

Of more importance to heated structures with a limited design life is the rate of thaw. The Stefan solution neglects the heat capacity of the soil and as such is analagous to a moving thaw front with steady-state conditions within the thawed zone. Thus, when the damping effect of heat capacity is considered, the geometry of the thaw front is conserved because of symmetry, although a time-lag is involved. For asymmetric conditions such as a pipe in a semi-infinite medium the effect of heat capacity and latent heat is to distort the thaw bulb into a more co-axial circle form, approaching a coaxal shape in the long term (Figure 2.5).

However, Thornton's analysis only holds true for deep burial. For shallower depths, Thornton actually predicts

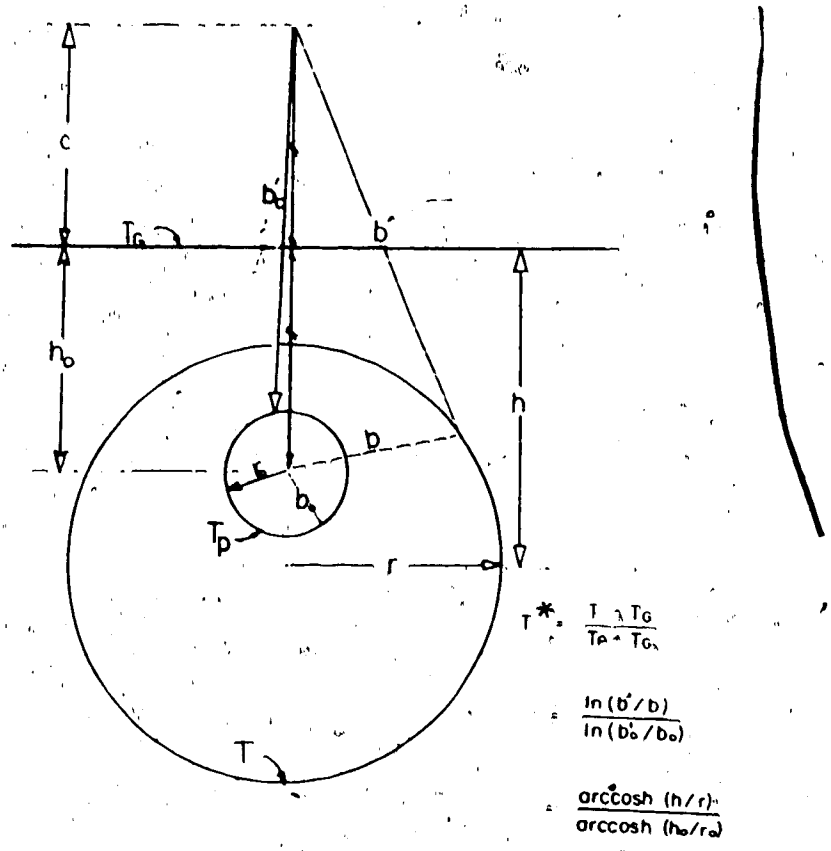

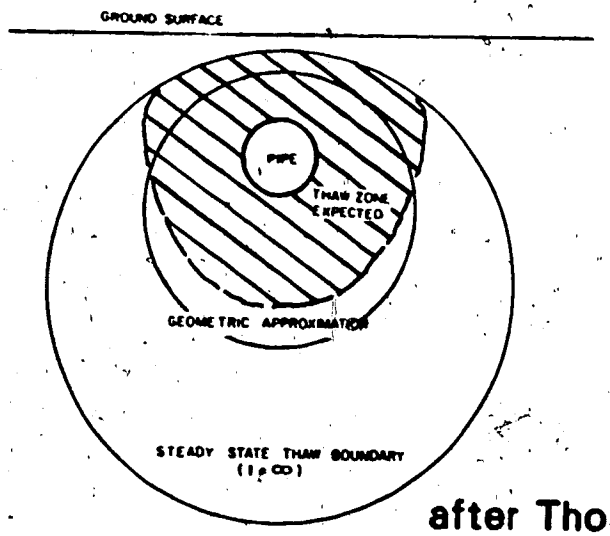

after Thornton, 1976 (modified)

Figure 2.5 Thornton's Coaxal Circles

larger thaw bulbs. This is unrealistic. A complete comparison of Thornton's method with an better method by Porkhayev is presented in Hwang (1977), in which finite element simulations are run as a check on these quasi-static solutions.

Thornton does present a useful simplifying assumption that includes the effect of sensible heat with the volumetric latent heat to come up with an "equivalent" latent heat:

$$L' = L + c_f(T_{phase} - T_{ground}) + \frac{1}{2} c_u(T_{pipe} - T_{phase}) \quad [2.19]$$

There is an implied overestimation of heat here: thermal gradients are not linear, as implied within the equation, but fall off sharply with increased distance from the pipe. This overestimation, however, is partially balanced by the unaccounted effect of heat capacity within the frozen zone. This method, however, does provide a fast check on the specific heat effects in simple heat flow formulas such as Stefan's.

The beauty of closed-form solutions lies in their accuracy and precision for the problem at hand. Unfortunately, a closed-form solution may not be available for many practical problems. In addition, the complexity of the resultant equation, however, may be that compromising assumptions are made to reduce the equation into a simpler form. Furthermore the initial conditions and applied

boundary conditions used in deriving the closed-form solution are often simplistic and are often adopted for analyses only because a closed-form solution exists for that set of conditions. Similarly, geometric configurations of closed-form solutions are often not amenable to field geometries. The obvious need for more flexibility in boundary conditions and geometries prompted the use of alternative analytical methods to solve the heat flow problem.

2.2.5 Finite Difference Method

One such method is the finite difference method, in which the case geometry is discretized into a mesh and calculations are performed to calculate values (typically temperatures) at the modes. Explicit or implicit solution schemes are used to numerically approximate the differential equations of heat flow, with implicit analyses being preferable because of their inherent stability. (This is particularly true when approaching steady-state in a transient analysis, as the time step size is limited in an explicit analysis.)

Ho, Harr and Leonards (1970) use the finite difference technique for predicting transient temperature distributions in insulated pavements. The program they develop encompasses temperature dependent thermal conductivities, latent heats and heat capacities in an explicit analysis to predict the

change in the temperature vector for a given time step. Using Newton's iterative method, this incremental temperature vector is then back-corrected to account for latent heat.

The versatility of the finite difference method can be seen in its ability to accept complex boundary conditions. Field temperature profiles can be extrapolated to determine the depth of zero annual amplitude (DZAA), which can then be used as the lower boundary temperature. The upper boundary temperature loadings can be varied to model the actual site temperature, an equivalent constant step temperature, or any anticipated temperature variation.

The conclusions drawn from the Ho, *et al*. sensitivity analysis performed in one dimension are instructive. The transient temperatures in the subgrade, below the buffering effect of the insulation, are still affected by the method of applying the surface temperatures. The constant step temperature at surface resulted in large errors when compared to measured values, while applying a varying surface temperature was very successful. This finding is to the detriment of most closed-form solutions since they generally use a constant step temperature. Nixon & McRoberts (1973) draw a similar conclusion. It was also demonstrated that a solution using an inaccurate initial temperature distribution will converge with the correct solution, but at a cost of accuracy in the initial results; therefore, a

realistic initial temperature distribution was highly recommended.

Unfortunately, the two-dimensional formulation relied on a grid of right rectangles which made the simulation of the inclined portion of the 2-D insulation quite onerous. At that time, the number of elements needed (700+) would result in several hours of computational time, so the problem was modified by transforming the inclined portion into a horizontal plane. This maintained the critical depth of cover on the insulation and the simulation was run with acceptable results.

This paper is instructive in its sensitivity analysis of some input parameters and demonstrates that some degree of simplification is necessary to overcome computational costs associated with a more rigorous pursuit of numerical fidelity. It is unfortunate that little attention was given to the effect of latent heat on the numerical stability and convergence rate of the solution. The program, as is, does not consider volume change and therefore would not be best suited for studying thaw-consolidation effects. In addition, the program was not used in high latent heat materials which would result in even lower numerical efficiencies; it is already too inefficient in handling complex geometries and materials to make it suited for application to thaw consolidation.

From this brief examination, it is obvious that this numerical method is more flexible in accepting actual geometries and boundary conditions than the closed-form analytical method. Unfortunately, with this generality we lose the accuracy and precision of the closed-form, and substitute numerical problems such as convergence requirements, time steps and the implementation of latent heat. Even with the finite difference method, however, we are limited by the formulation which requires a rectangular discretization of geometry.

2.2.6 Finite Element Method

An alternative numerical technique exists in the finite element method. This has all the advantages of the finite difference technique plus it has geometric versatility. It is, however, a much more numerically complex technique and this generally results in higher computational costs for similar analyses although factors other than computational costs will usually decide which method is preferrable, particularly as computing costs decline.

Wheeler (1973) uses a variational technique similar to that of Hwang, Murray and Brooker (1972) to solve the geothermal problem of a pipeline in permafrost. Both of these analyses have the advantage of a continuous temperature distribution over a multidimensional grid, which allows the thaw front to be fully defined, and the advantage of geometric versatility. In Wheeler's solution, the

problems of convection and thaw settlement have explicitly been neglected. His suggestion for implementing convection into the analysis consists of combining the thermal conductivity with the convection effects to make an effective thermal conductivity. Recognizing the effect of thaw subsidence on both geometry and material properties, it was recommended that a step-wise approach to altering soil properties and geometry be used.

In adapting the two-dimensional program to a pipeline problem it was found that the seasonal variation in temperature, resulting in an active layer within the soil, limits the time step size. The greater problem lies in selecting a means of imposing this temperature variation on the soil. Wheeler disregards the direct imposition of measured soil surface temperatures as being inflexible to changing surface conditions. In practice, the data required for such an analysis is usually not available, and the time and expense in obtaining such information is exorbidant. The elegant solution of modelling convection, conduction, phase change, radiation, reflection and other surface processes along with the soil analysis would involve a large set of non-linear inter- dependent equations and a high degree of modelling sophistication. This level of analysis is generally beyond the scope of the problem for engineers and many of the input parameters would be unknown. Instead, the writer has used soil surface coefficients to convert the air temperatures to soil surface temperatures. This method has

the advantage of requiring readily available air temperatures, and the soil-surface coefficients can be varied to accommodate different ground covers.

A far different approach involves determining a soil-air heat transfer coefficient with corrections for snow cover. This is an involved procedure requiring knowledge of the soil temperature profile, to back-calculate an equivalent air temperature function, and as such is not practically adaptable to most design problems.

Thermal properties are simply divided into frozen and unfrozen values. The unfrozen moisture content is addressed in modifying the latent heat term.

The pipeline simulation is initialized by cycling natural thermal conditions for the equivalent of ten years to fully develop the temperature distribution in the soil. This is an interesting development in that both the surface boundary condition and the initial temperature state are artificially determined rather than using actual field measurements, which can then be used to assess the validity of the initial imposed temperature state. The 48 inch diameter pipeline temperature was then increased from the ambient to the operating temperature in 30 days and then kept constant for the simulated 10 year period of thawing. The soil was given properties typical of thaw unstable material, with the moisture content biased conservatively. A parametric analysis was performed to examine the sensitivity

of the analysis to the parameters. This analysis however, is still sensitive to some of the underlying assumptions within the analysis.

For example, the writer finds that less thaw occurs in a silt than in a clay or sand for the same time span. This is intuitively obvious when one considers the higher thermal conductivity typical of a sand and the higher unfrozen moisture content of clays. However, implicit in the analysis is the preservation of geometry: the silts, typically ice-rich materials, could conceivably settle faster than either the sand or the clay. This would result in an effectively higher thaw rate below the pipeline.

The effect of insulation was examined as a means of lowering the heat flow rate to the soil. (The option of lowering the pipeline temperature was discounted as being atypical of pipeline operating temperatures, with the Norman Wells pipeline being a notable exception.) The analysis discovered that insulation is an effective means of controlling heat flux in cold permafrost; however, in warm permafrost the thermal balance is so delicate that even a small energy input degrades the permafrost. In such areas the use of refrigeration lines was found to be effective.

Refrigeration provides a heat sink for the heat from the pipeline and can prevent any thaw below the pipeline. Thaw alongside a pipeline is usually not of concern; in the case of sidebends or where the pipeline is adjacent a

settlement-sensitive structure, the refrigeration line placement may be altered to ensure some lateral stability. Using a pair of refrigerant lines below the pipeline enables the designer to use closed loops of refrigerants. This allows for some flexibility in the flow rates and temperatures and minimizes the differential temperature between the inflow line and the colder outflow line. Since the major refrigeration costs are associated with peak cooling rates, Wheeler examines some mitigating action such as some pipeline insulation, flow rates and refrigerant temperatures.

In conclusion, Wheeler addresses the pipeline and permafrost problem solely from a thermal viewpoint without examining the concomitant geometric and material property changes. The more critical aspects of thermal analysis are examined, most notably the difficulty in selecting an adequate surface boundary condition and a selective sensitivity analysis, including refrigeration.

Early work by practitioners used a good number of simplifying assumptions to reduce the geometry and heat equations into manageable forms. Earlier work by theoreticians addressed the more general problem of heat conduction in solids. These two extremes were brought together in the work of Tsytovich *et al.*, (1965) and Morgenstern & Nixon (1971) in the development of one-dimensional thaw-consolidation theory linking the advance of

the thaw front with soil properties in the thawed zone.

The need for two-dimensional analyses prompted the adaptation of one-dimensional theory to two-dimensional problems and further research into closed-form solutions to heat flow in solids. The difficulty in applying these two approaches to the two-dimensional problems with complex geometries, materials and conditions accelerated the development of numerical analyses, particularly the finite element method. Research in this area continues to be strong due to its flexibility and the enhanced ability of computers to handle large problems affordably.

2.3 Geotechnical Properties

Thawing permafrost soils have been divided into two groups on the basis of their performance upon thawing. Thaw-stable soils exhibit normal strength values for an unfrozen material and no detrimental settlement upon thawing. Thaw-unstable soils exhibit poor strength characteristics and large deformations upon thawing (Andersland & Anderson, 1978).

This soil classification is subjective and therefore project-specific, so the distribution of soils falling under these two headings is necessarily a function of the strength and deformation tolerances of the proposed structure. For isolated structures that are insensitive to the magnitude of settlement, the strength criterion may govern design.

However, for most linear structures such as roads, and particularly for stiffer systems such as pipelines, the bearing capacity of the thawed soil is adequate but the settlements (and the resultant differential settlements) govern design.

Although the amount of settlement is dependent upon both the extent of thawing and the soil thaw behavior, most research has been conducted on the geothermal aspects of thaw. Relatively little analytical work has been done on the soil's thaw characteristics. Early work on this topic consisted of uncontrolled thawing of permafrost in an oedometer under a seating load (Crory, 1973; Luscher & Afifi, 1973). Because there was no control over the direction of thaw during these tests and the degree of thaw or consolidation at any point was unknown, the only data obtained were the net thaw-consolidation strains. Knowing the thaw-consolidation strain values at various seating pressures, the value of thaw strain under no load could be obtained by extrapolating back to the origin. This removed the consolidation effects from the thaw strain parameter, A_o, as proposed by Tsytovich (1965) and Watson, *et al.* (1973). Nixon & Morgenstern (1974) suggested a logarithmic stress scale for high moisture-content materials, extrapolating back to the *in situ* void ratio.

The essential finding from these tests was that the thaw strain was generally much larger than the consolidation

strain. This implied a correlation between thaw strain and the amount of ice in samples. Correlations were made between thaw strain, A_o, and the dry density of the frozen soil, γ_d^f (Luscher & Afifi, 1973; Speer, *et al.*, 1973; Watson, *et al.* 1973b). Application of this one-dimensional testing of small samples to field conditions were advocated by Crory (1973) and Speer, *et al.* (1973). Both methods divide borehole profiles into homogeneous segments. The frozen dry density, ρ_d^f, of each segment can then be correlated with the thaw strain, and the summation of thaw strain times segment lengths will result in a value for the anticipated thaw settlement at that location.

There are difficulties with this approach; however, since the algorithm is insensitive to size effects of the samples. This size effect implies that non-homogeneity exists within each "homogeneous" sample. This is pointedly demonstrated in the U.S.S.R. Building Code (1960) in which correction factors are used to reduce the anticipated settlement of ice inclusions greater than 1 mm thick (Andersland & Anderson, 1978):

$$S_{ii} = \sum_{o}^{x} h_i \, r_i \qquad [2.20]$$

where, h_i = thickness of individual ice inclusions

r_i = reduction coefficient

For: $1mm < h_i \leq 30mm$ $\quad r_i = 0.4$

$30mm < h_i < 100mm$ $\quad = 0.6$

$100mm < h_i$ $= 0.8$

It is significant that thin inclusions of ice, which would presumably be discontinuous within the area of concern, are reduced by 60% while thicker slabs of ice, which would be more extensive than thinner inclusions, are only reduced by 20%. This implies that the macro-structure of the permafrost soils will also affect the magnitude of settlement.

These scale effects are treated in a statistical form by Palmer (1972) in which predictions of borehole settlements are correlated over varying distances. For arbitrary distances between boreholes, Gaussian probability distributions of settlement can be obtained from which simulations of differential settlements can be generated. This can then be reworked to provide curvature profiles. With this profile, a probability distribution of pipeline curvature can be generated. By varying the correlation distance between boreholes, several pipeline curvature distributions can be obtained for each set of pipeline specifications.

This process generates a fictitious, but realistic, set of settlements which does allow for a quantitative comparison of soil properties and design approaches.

The transient nature of thaw settlement has not been examined as part of pipeline design because it seldom, if

ever controls. To date, the common approach has been to examine the net settlements at the extent of the design thaw and to evaluate excessive curvature at that time. The time-dependent progression of thaw is not examined. While it is probable that the critical differential settlement will occur when extensive thawing has taken place, a combination of differential thaw rates, material types and thaw bulb geometry may result in the design loadings being exceeded before the design thaw has been reached. This time-wise analysis of thaw-settlement has not been implemented into pipeline design although the theory has been developed for one-dimensional thaw (Tsytovich, *et al*, 1965; Morgenstern & Nixon, 1971; and this work).

2.4 Soil : Pipeline Interaction

There are a lot of difficulties in modelling the structural system of a pipeline in thawing permafrost. If the transient nature of thaw is ignored, the problem is greatly simplified although the possibility of a critical design case is precluded. The additional simplifying assumption of modelling the three-dimensional behavior in two dimensions is also common because of the easier analysis.

The problem, reduced to a continuous structural member within a semi-infinite continuum, is still unwieldly because any displacement anywhere within the system due to loading

has an effect on all of the system. This highly interdependent system of equations can be handled by further simplification, either by disassociating segments of the system from one-another, or by modelling the continuum as discrete elements.

In the problem of a pipeline in soil, the pipeline is far more reactive to virtual displacements than the soil is because of the pipe's inherent stiffness. Since the soil continuum is relatively insensitive, the structural system can be modelled as a structural member supported by independent reaction points. The most common version of this is the Winkler beam theory in which a structural member resting on an elastic half-space is modelled as an elastic beam supported by discrete elastic springs. Hybrid methods combine Winkler beam analysis with the finite element method by representing the beam as a finite element mesh subjected to elastic-plastic soil spring loadings. Luscher, Thomas and Maple (1979) perform such an analysis on a bent pipeline in two dimensions within thaw-stable material. The pipe is subject to tie-in thermal stresses and operating stresses. While their area of interest is not pipe stresses due to thaw-consolidation, they address the key modes of loading and resistance. Nyman (1983) modifies Luscher's approach for thaw settlement by modelling the pipe in three dimensions with three-dimensional soil restraints. The elastic-perfectly plastic springs modelling the soil are given tension cut-off capabilities to represent lift-off of

the pipeline. Spring stiffness are varied to reflect the relative properties of frozen and unfrozen soil, however the Young's modulii and yield stresses of the soil springs are based on Luscher, *et al.'s* thaw-stable soil materials. These materials are not representative of the thaw-unstable soils Nyman is modelling. Nyman assumes full design thaw and models the thaw settlement below the pipe as a uniform displacement of the supporting springs below the pipe within the settlement zone.

A contemporary paper by Nixon, Stuchley and Pick (1983) details a similar design methodology for a combined thaw settlement, frost heave and bend analysis. The pipeline is modelled as a three-dimensional structure with elastic-perfectly plastic soil springs in three dimensions (Fig. 2.6). The objective of the analysis is to obtain load:displacement relationships, using the analysis to optimize on the wall thickness of the pipe for compliance to stress and strain criteria.

The writers recognize that displacement-relieved loadings, such as the reduction of support due to thaw settlement, are the critical loads since the primary loads of tie-in stresses and pressure vessel stresses are relatively fixed values. By performing sensitivity analyses of these loads on the computer model, the model itself was optimized to perform a sensitivity analysis of the pipe design parameters. The resulting computer model was then

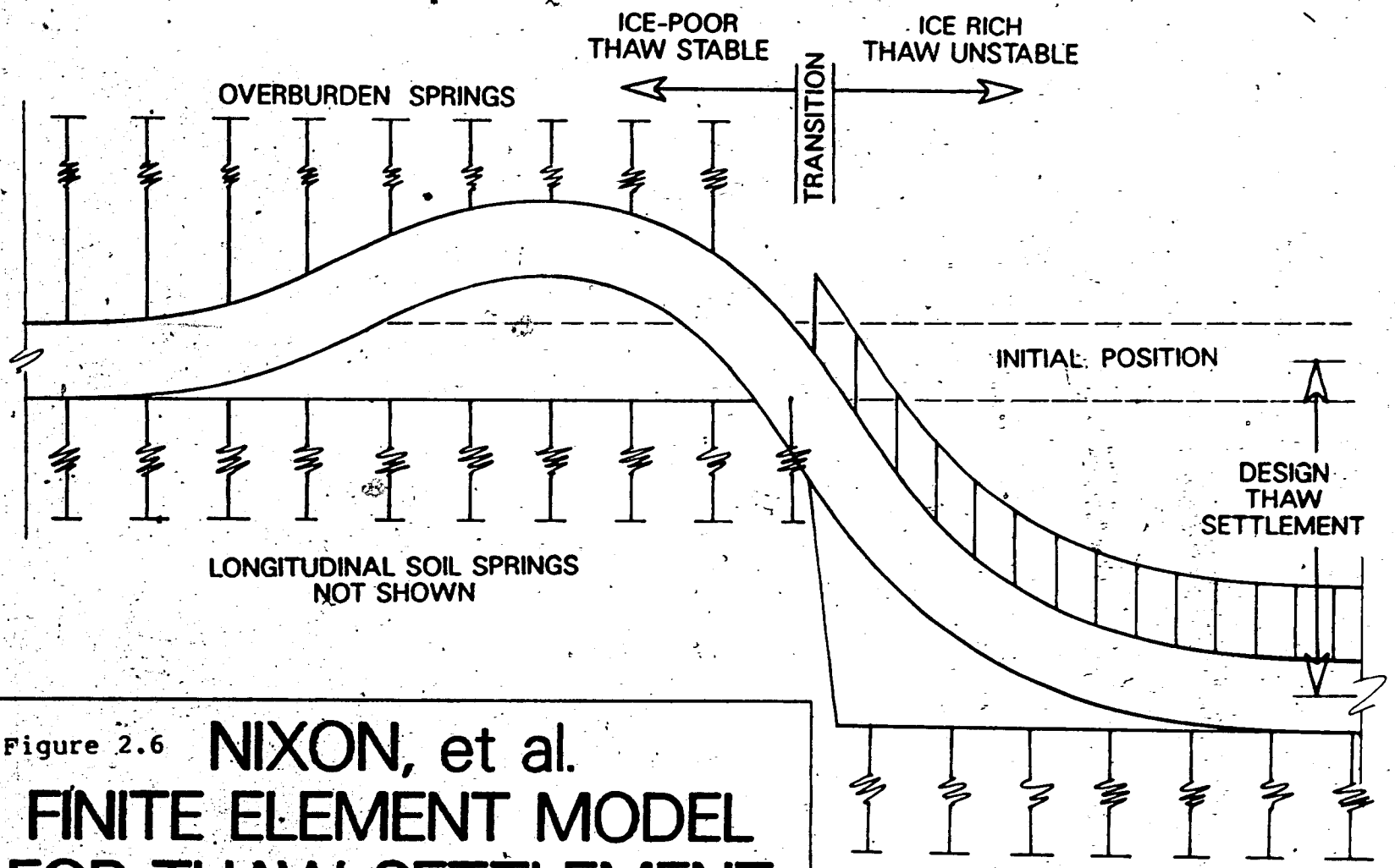

Figure 2.6 NIXON, et al.

FINITE ELEMENT MODEL FOR THAW SETTLEMENT

able to simulate design options for both frost heave and thaw settlement.

The Nixon, *et al*. analysis differs from the Nyman analysis in that the geotechnical parameters are more representative of thaw-unstable soils. In both instances, the bearing capacities and the soil loadings are adjusted to account for material variation between thaw-stable and thaw-unstable soils, and a transition zone was created in which soil properties were interpolated between the thaw-stable and thaw-unstable materials.

The Nyman analysis provides us with the general form of the relationship between allowable soil settlement against the length of the settlement zone for various depths of cover. While this emphasizes that the critical thaw span lies between a short "bridging" thaw span and a long "conforming" thaw span, it cannot be used as a design tool since it assumes that the length of the thaw settlement zone is known *a priori*. Alternatively, the Nixon, *et al*. analysis has provided a design chart, assuming the critical thaw span as determined from their analyses, which divides the proposed pipeline into segments for which design thaw settlements soil loadings and pipe wall thicknesses are specified. This type of chart can be readily applied in practice. A design chart similar to that of Nyman would be useful in ascertaining the need for remedial measures should the design thaw be exceeded.

Most analyses to date are modifications of the Winkler beam theory, using thermal analyses to determine the worst-case extent of thawing. These static analyses provide an absolute result in terms of acceptable or excessive stresses and strains, without providing an insight into the transient nature of the problem. In addition, non-linear and time-dependent material properties may cause the outcome to differ from the static case by a different redistribution of stresses. The transient analysis of thaw settlement also provides an analytically-projected sequence of significant events, such as pipe yielding, with which the credibility of the analytical model can be criticized, and improved upon if necessary.

Oddly enough, although the one-dimensional thaw consolidation theory has existed for some time (Tsytovich 1965, Morgenstern & Nixon, 1971) no one has yet directly implemented the theory into the structural analysis of thaw settlement. This could be done by using non-linear Winkler soil springs that are dependent upon the thaw-consolidation number, R, and time, t, or by uncoupling the thaw-consolidation considerations from the stress analysis and treating each spring as a permode (permafrost oedometer) with a varying surface loading. Spring stiffnesses would then be determined from the amount of thaw settlement, and the deformation properties of the thawed-consolidating soil and of the remaining frozen soil. The results of such an analysis would provide a time history of soil deformations

and pipe strains and a better simulation of the phenomenon of a pipeline in thawing permafrost.

Transient analysis capabilities have been built into the modified Winkler beam model of Row, Powell and Goodson (1983). The soil springs in their model consist of an inelastic, non-linear spring in series with a secondary creep dashpot and a primary creep parallel dashpot and spring. The inelastic spring allows no tension to develop and its stiffness is temperature-dependent to allow for seasonal variation soil properties.

The non-linear pipe behavior was modelled as a segmented three-dimensional pipe, and a thin "slice" at each end of every segment was examined for non-linear behavior. This was done by dividing each slice into sub-elements and evaluating the stress state of each sub-element using their longitudinal and hoop strains and a multi-linear stress-strain relationship. By using a summation of all the constituent sub-element stiffnesses, slice "stiffness" were assembled, relating axial strain and curvature to axial loads and bending moments. The stiffness within the elements of the segmented pipeline were obtained by interpolating between the two end stiffnesses.

The computational costs of such an analysis are high if the active material properties must be updated for every non-linear event. The method chosen by Row, *et al*. to reduce the number of updates is to allow "overshoot" tolerances for

certain parameters. This method allows threshold values, such as yielding, to be exceeded by specified amounts before updating is done. This permits a number of sub-elements to be updated at the same time. The reduction in the cost of the analysis and its effect on the outcome can be quantified by performing a sensitivity analysis on the overshoot tolerances.

The development of the analysis of a pipeline in thawing permafrost has been significant in the past decade. This is not because highly complex material non-linearity has been introduced but more so because the emphasis of design has shifted from the structural behavior of the pipeline as affected by isolated independent loads. Instead, the more recent analyses have become more sensitive to the structural performance of the soil springs and how they affect the pipe strains which are used as an indicator of the system's performance. Also, by providing flexibility for the components of the problem, the behavioral constraints of the whole system are relaxed thereby allowing the system to equilibrate along a more realistic stress path. This allows a more general mode of behavior and can be used to justify or quantify simplifying assumptions for specific analyses.

2.5 Summary

An examination of the present state of the art of pipeline analysis within thawing permafrost reveals the strengths and weaknesses of our present methods of analysis. In general, the geothermal aspects of design are well understood and corroborated with experimental results and field observations. A number of closed-form solutions exist for simple geometries and properties and the more flexible numerical approaches are allowing a more exact treatment of the problem. Consolidation effects could be accounted for in some of these analyses. Structural design aspects have evolved as well, developing from a Winkler beam approach to a hybrid finite element - Winkler beam method. In addition, both the pipe properties and the soil behaviour are now modelled in a more sophisticated manner resulting in a more realistic analysis. Improvements could be made in the way soil is modelled, by using more transient properties and by modelling the soil as a continuum.

Implicit in the improvements in geothermal and structural analyses is the fact that the principal design parameters have been adequately identified and quantified; this is not entirely true. In general, analysis proceeds from the thermal to the structural aspects. Geothermal predictions of the design thaw depth are used to determine the amount of thaw settlement which is then used as an input parameter for the structural analysis. The magnitude of the

thaw settlement determines how far the pipe must deform to maintain conformity with the soil, and as such it has a controlling effect on the pipe strains. While the geothermal and structural analyses provide realistic simulations of their respective phenomena, and draw upon rich backgrounds of research and development, the linking procedure of predicting thaw settlements is based upon extrapolation of simple one-dimension thaw strain tests. Allowing that there are difficulties with the application of one-dimensional analysis to the thaw settlement problem, particularly for ice-rich materials that exhibit the worst thaw-strain behavior, a closer examination of thaw straining within permafrost should offer some insight into design improvements. It is hoped that such an examination will allow a more rational approach to thaw strain predictions, with a reduced prediction of thaw settlement as a possible result. As any reduction in the magnitude of thaw settlement would undoubtedly reduce pipe strains, the exercise would result in less costly pipeline design.

3. Numerical Modelling of Thaw in Permafrost

3.1 Statistical Variation of the Thaw Strain Parameter

In the application of thaw-consolidation theory to field studies, the results of thaw strain tests performed on laboratory samples are extrapolated to estimate the total expected amount of thaw in the field. While one-dimensional thaw has been studied in considerable detail (Tsytovich, *et al.* 1965, Morgenstern and Nixon, 1971) it has not yet been shown that the results of small scale laboratory tests can be directly applied to predict field behaviour with accuracy. It was the purpose of this section to examine one method of extrapolating the results of laboratory test programs to do so.

A statistical approach to thaw settlement prediction was chosen. With the wide range of thaw strains obtained from a laboratory program it was felt that the ground mass behavior would be best expressed using statistical characteristics of the thaw strain. This statistical distribution was applied to a two-dimensional numerical soil model to simulate the thaw strain behaviour of non-homogeneous permafrost. One-dimensional studies are unable to explore load transfer mechanisms resulting from the spatial variability of thaw strain parameters.

3.2 Thaw Strain Variability

An opportunity to apply statistics to thaw strain properties presents itself in the paper by Speer, Watson and Rowley (1973). The writers examined the effect of ground-ice variability on thaw settlements of laboratory samples. By correlating the frozen bulk densities of laboratory samples with their respective thaw strains, the writers predicted thaw settlements at four northern sites, based on borehole profiles. Ground-ice variation across each site resulted in a variation of thaw settlements from which settlement contours were drawn.

Their prediction of thaw settlement was based upon an extrapolation of laboratory thaw strains using a weighted average of thaw strains throughout borehole profiles. This method does not consider the effect of thaw strain variability within the ground mass on the resulting thaw settlements. It is anticipated that this variability could contribute to a reduction in total and relative settlements. The ample data provides a good basis for a two-dimensional analysis using statistics.

3.3 Statistical Distribution

One distribution of interest in geotechnical engineering is the "Normal distribution". It is characterized by a symmetric bell curve with tails extending to infinity which adequately represents a population with

symmetric central tendencies. There are, however, disadvantages in using the normal distribution. First, the two tails extend to $+\infty$ and $-\infty$ regardless of the mean and standard deviation. For many applications this would not be an appreciable error. However, for geotechnical purposes values of parameters commonly vary between definite limits. The other disadvantage is that it presupposes that the population is symmetrically distributed about a central mean. For a number of geotechnical properties, this trait is highly unlikely. Thus, although the normal distribution is often used in interpretting data, it may not always be approriate. A more suitable distribution for geotechnical applications would be one that could accommodate skewness in the population and have realistic probabilities at all locations within the distribution.

Such a distribution is the beta (β) distribution which is the conjugate family of distribution for the binomial distribution. The binomial distribution is determined by the distribution of the number of absolute successes or failures on a Bernoulli trial, (which would result in a discrete distribution). The beta family is dependent on the *probability* of success or failure on any given Bernoulli trial, and as such the beta family of distribution is continuous. As probabilities lie within the range $0 \Leftrightarrow 1$, this beta distribution provides us with a continuous function within definite limits and a variety of forms (Figure 3.1).

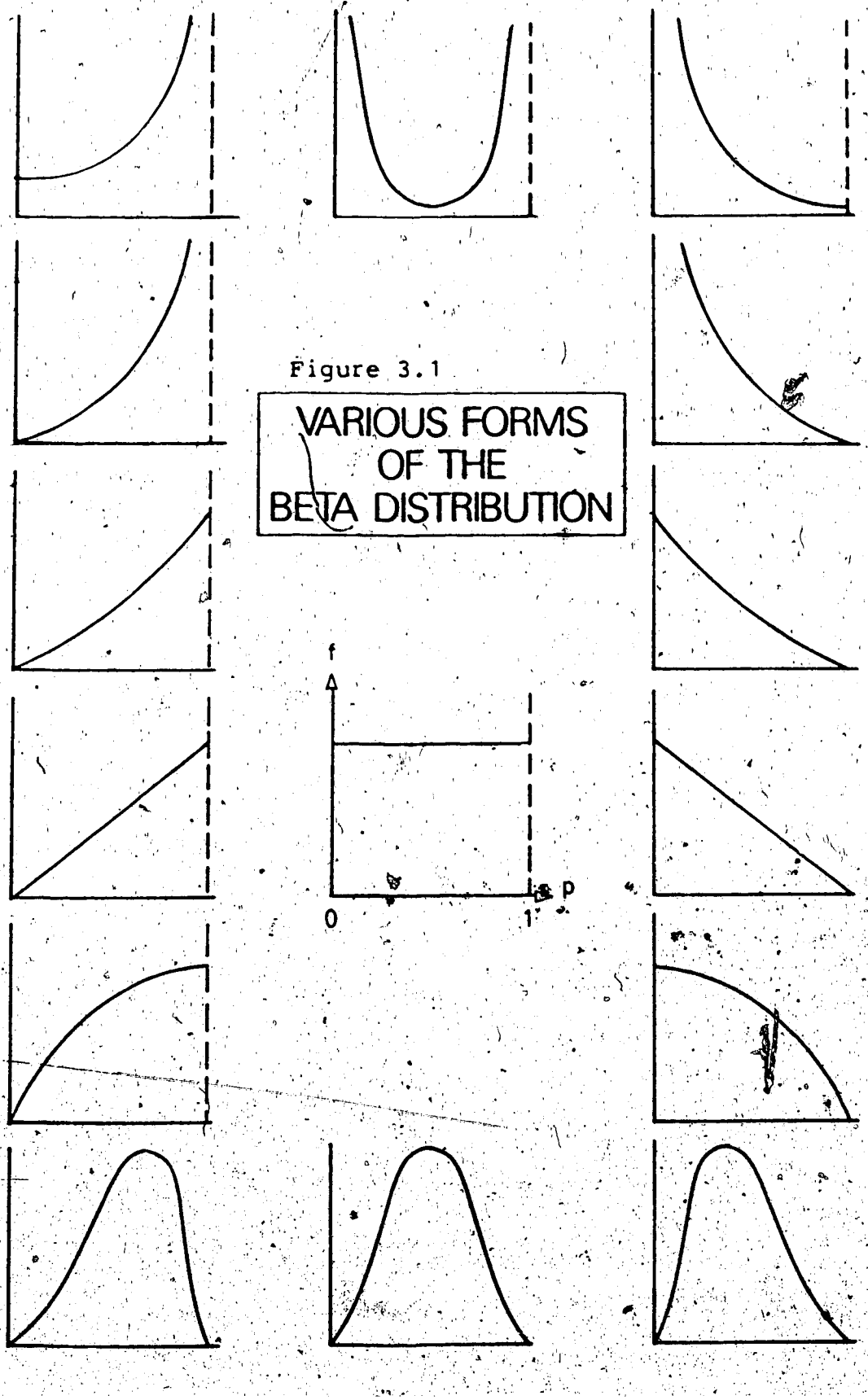

Figure 3.1

VARIOUS FORMS OF THE BETA DISTRIBUTION

3.4 Statistical Reduction of the Thaw Strain Parameter

For site 1, at Norman Wells, Speer *et al.* (1973) provide the laboratory thaw strain data and their estimates of thaw settlements in the field, assuming a 13m thaw. These were examined and compared (*viz.* Appendix C). The laboratory data were obtained from testing 10cm diameter core samples at overburden pressures and were fitted to a normal distribution curve. The estimates of settlement were normalized and expressed as strains and were also fitted to a normal distribution. Normal distributions were used because of their simplicity and to emphasize their inadmissible values below zero thaw strain.

In units of percent-settlement with respect to the original vertical dimension, the laboratory results had a mean and standard deviation of $\bar{x}$=23.414m, s=15.619m while for the estimates $\bar{x}$=6.48m, s=3.05m.

Significant conclusions can be drawn in comparing these two normal distributions (Figure 3.2). The first conclusion is that the curve of the estimates is a far more attenuated distribution than the laboratory one as can be seen from its spike-like appearance as compared to the subdued laboratory curve. This is because the field estimates are representative of a vertical average of thaw settlement properties of the thawing soil at that point. This averaging reduces the effect of extreme values. Therefore, the standard deviation is lower, resulting in a sharper peak in

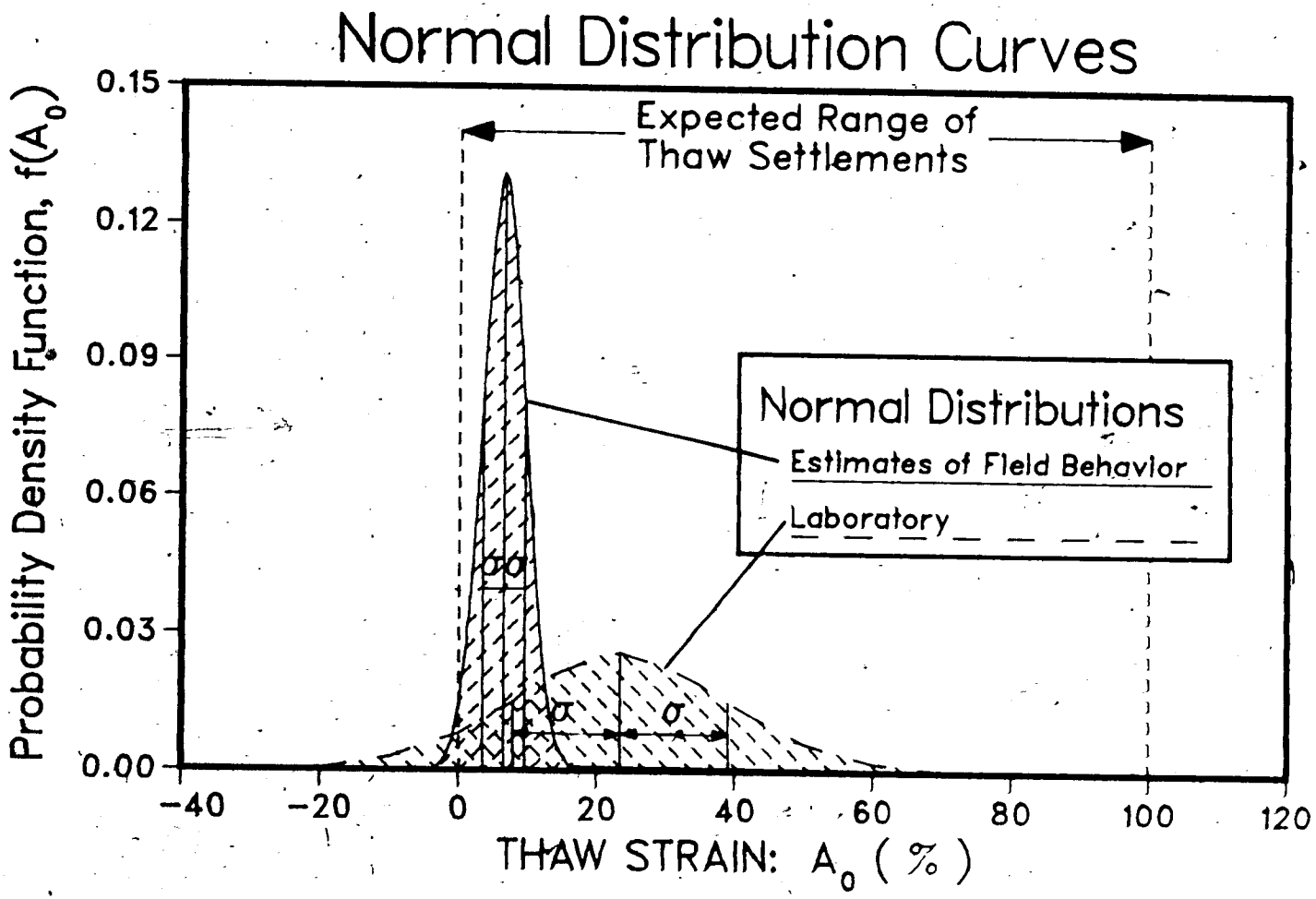

Figure 3.2 Normal Distribution Curves

the distribution.

The second conclusion is that the mean value of thaw strain is higher for the laboratory data than for the estimates. This is because Speer *et al.* (1973) have biased the data towards thaw stability in a number of ways. The total settlement was the sum of the settlements of the individual soil strata; therefore, the effect of each stratum's thaw strain would depend upon the stratum's thickness as described in the U.S.S.R. building code (Tsytovich, 1965):

$$S_t = \sum_{1}^{h_{total}} e_i \, h_i \qquad h_i = \text{layer height} \qquad [3.1]$$

where e_i is determined from the equation:

$$e_i = \frac{\gamma_d^t - \gamma_d^f}{\gamma_d^f} \qquad [3.2]$$

where: d=dry
f=frozen
t=thawed

This introduces a biasing that would account for the reduction in thaw strains for the estimate data. The laboratory testing would not then be representative of the dispersion of frozen bulk densities within the *in situ* soil. Rather, the testing schedule was biased in testing more samples at the lower densities because their high thaw strains were of particular interest.

In addition, Speer *et al.* have biased the samples with high thaw strains. Ice rich samples with frozen bulk

densities below 1.09 g/cm³ but above that of ice were given a thaw strain of 68%. The reasons for this are unclear. For a soil of density 1.09 g/cm³ this corresponds to a change in moisture content from w=312% to w=85%. This final value is well above the liquid limit for this material (w_L=[35,55]). They have also further reduced the volume change upon thawing of the denser samples. This lowers the dispersion of data points and reduces the standard deviation slightly.

An alternative factor in expecting lower thaw settlements in the *in situ* soil is alluded to in the U.S.S.R. Building Code (Eqn. [2.10]) referenced by Nixon and Ladanyi (1978): the thaw settlement due to the melting of ice inclusions thicker than 1mm is dependent upon the thickness of the inclusion. This would suggest a load transfer mechanism that diminishes with size. Such a mechanism would seem reasonable where small ice lenses are indicative of a ground ice structure within a soil, and massive ice is indicative of an extensive intrusive layer. The amount of settlement that results from thawing may well be a function of the ability of the soil to provide stress arches around weak pockets formed by the melt out of ice. The following analyses this mechanism.

3.5 Simple Thaw Strain Analysis

For the initial analysis, a simple approach was taken to the thaw strain problem. The thaw strain parameters selected were those from from the Norman Wells site (Speer *et al.*, 1973). These data were statistically reduced to a β-distribution which precluded extraneous values and allowed for any skewness in the distribution. As seen in Figure 3.10, the resultant probablility distribution function was skewed to the right, reflecting the concentration of sample densities near the thaw-stable limit. The suitability of the β-distribution to these data is evident in the close fit of the β cumulative distribution function (CDF) to the sample's CDF in Figure 3.11.

3.5.1 Thaw Strain Parameter Selection

The β-function P and Q parameters were determined and used within program *"BETAGEN"* (*viz.* App. D) to generate ten fictitious A_o values. These values would reflect the mean and variance of the β-function described by the P and Q parameters. For the purposes of this initial analysis, however, the variance was arbitrarily reduced to 40% of the laboratory data's variance to reduce the scatter in A_o values. This was done to reduce the chance of numerical instability concomitant with highly varying material stiffnesses.

3.5.2 Volumetric Strain : Bulk Modulus Relationship

These generated A_o values were then used to determine when the soil transformed from a low-stiffness to a high-stiffness material. The ten values were used to describe ten soils. Each had an initial bulk modulus of K=0.1kPa and a final K= K= 2000kPa. The transition between the two values occurred at the volumetric strain corresponding to their respective thaw strains. The Poisson's ratio was arbitrarily set at $\nu=\frac{1}{3}$. These step-wise ϵ_v:K curves resulted in the bi-linear stress-strain curves shown in Figure 3.3.

3.5.3 Layered Analysis

The first analysis used a mesh consisting of ten 1m×1m 4-node elements arranged in a column with oedometric boundary conditions. Gravity was not considered and a surficial load of 10kPa was applied incrementally in a quasi-static manner to accommodate the sharp changes in material stiffness during loading. For the initial load steps, the need for exceedingly small load increments cannot be overemphasized.

The resulting surface settlement was 2.53m (Figure 3.4, left side). This analysis was repeated for a 10m×10m grid of horizontally continuous strata with identical results (Figure 3.4).

Variation in Bi-Linear Stress-Strain Curves

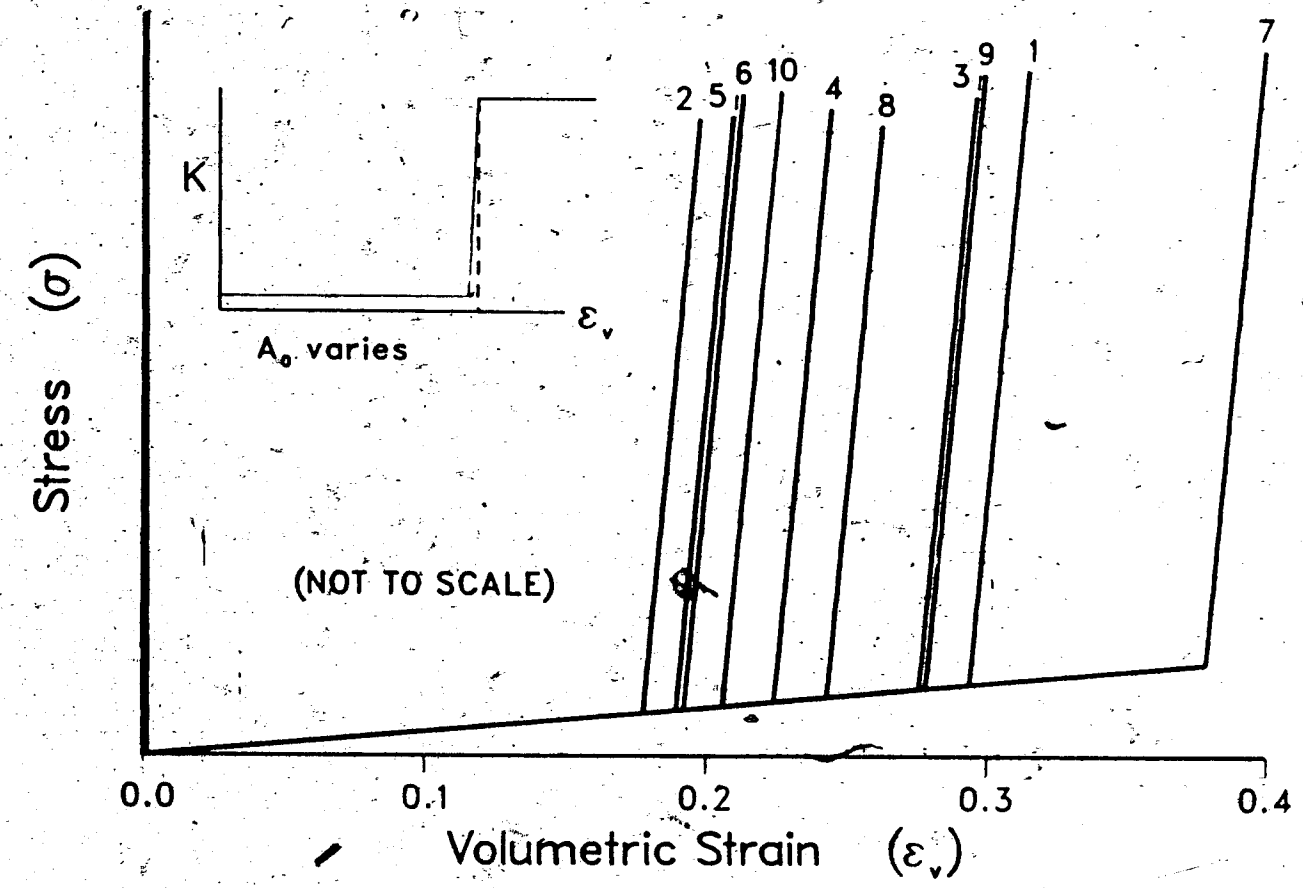

Figure 3.3 Variation in Bi-Linear Stress-Strain Curves

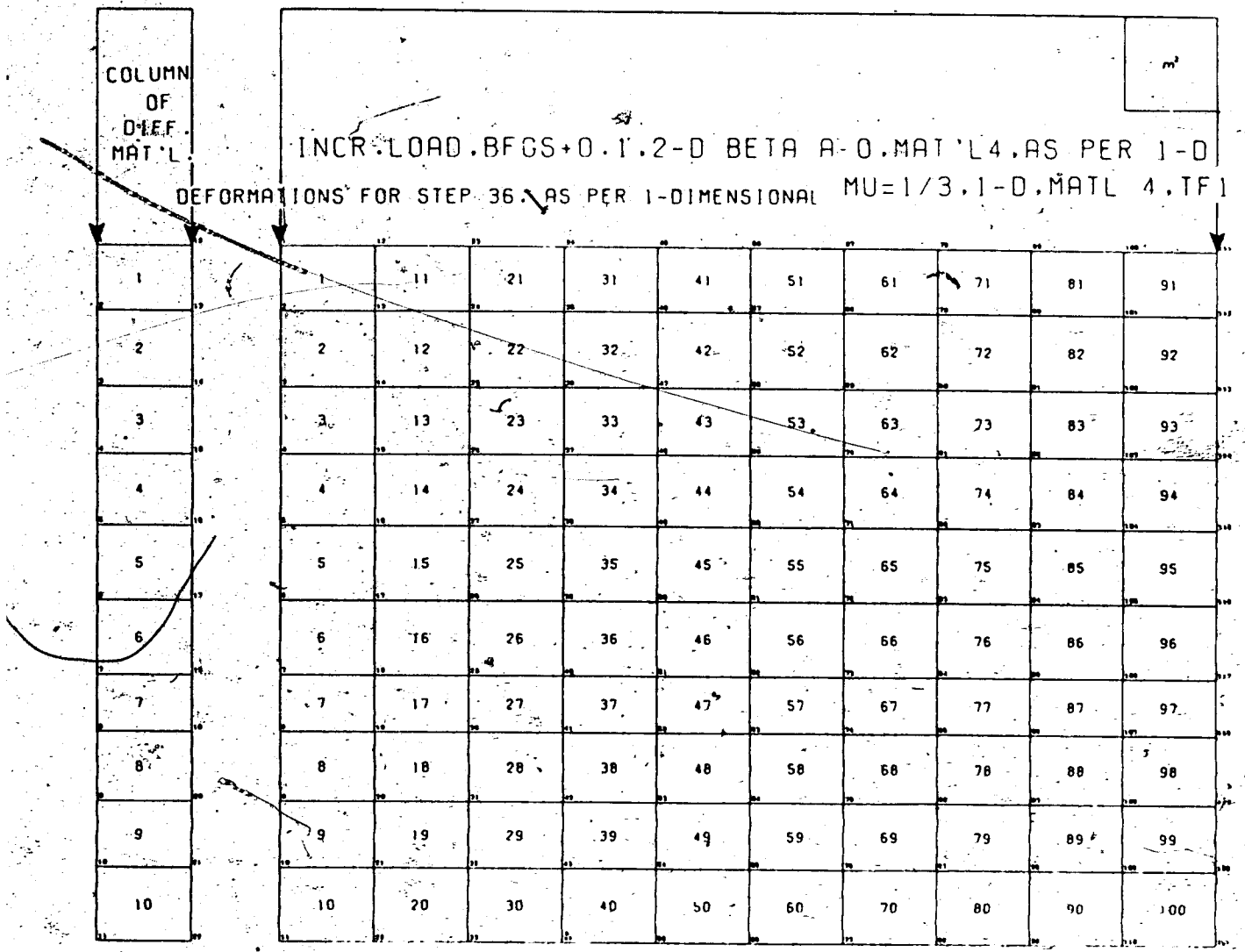

Figure 3.4 Comparison of Columnar and Layered Analyses

3.5.4 Randomly Mixed A_0 Parameters

Next, the 100 elements consisting of the ten material types were randomly distributed throughout the soil mass. To ensure impartiality, a random number generator determined the sequencing of the material models in the mesh (Figure). The same loading increment time function was used for this analysis as for the previous two analyses, with disastrous results. Some elements had deformed to such an extent that they had negative volumes. (Figure 3.6).

The 36-step time function had been specifically designed to ensure that all ten materials in the layered mesh followed their respective stress-strain curves reasonably well. Points describing the time function were obtained by calculating the ten levels of load that would deform each material through to its respective thaw strain. This procedure provided a range of loads over which all ten materials would undergo thaw strain.

This load range was discretized into 30 equal load subdivisions to ensure a very gradual application of the surficial pressure. The time function was made proportional to these loads so that as the analysis proceded the applied loads would be gradually incremented through the range of thaw strain loads. Once the total load was applied, all materials in the layered analysis were supposed to be in the stiff bulk modulus range, and the remainder of the load, which was substantial, was applied with impunity.

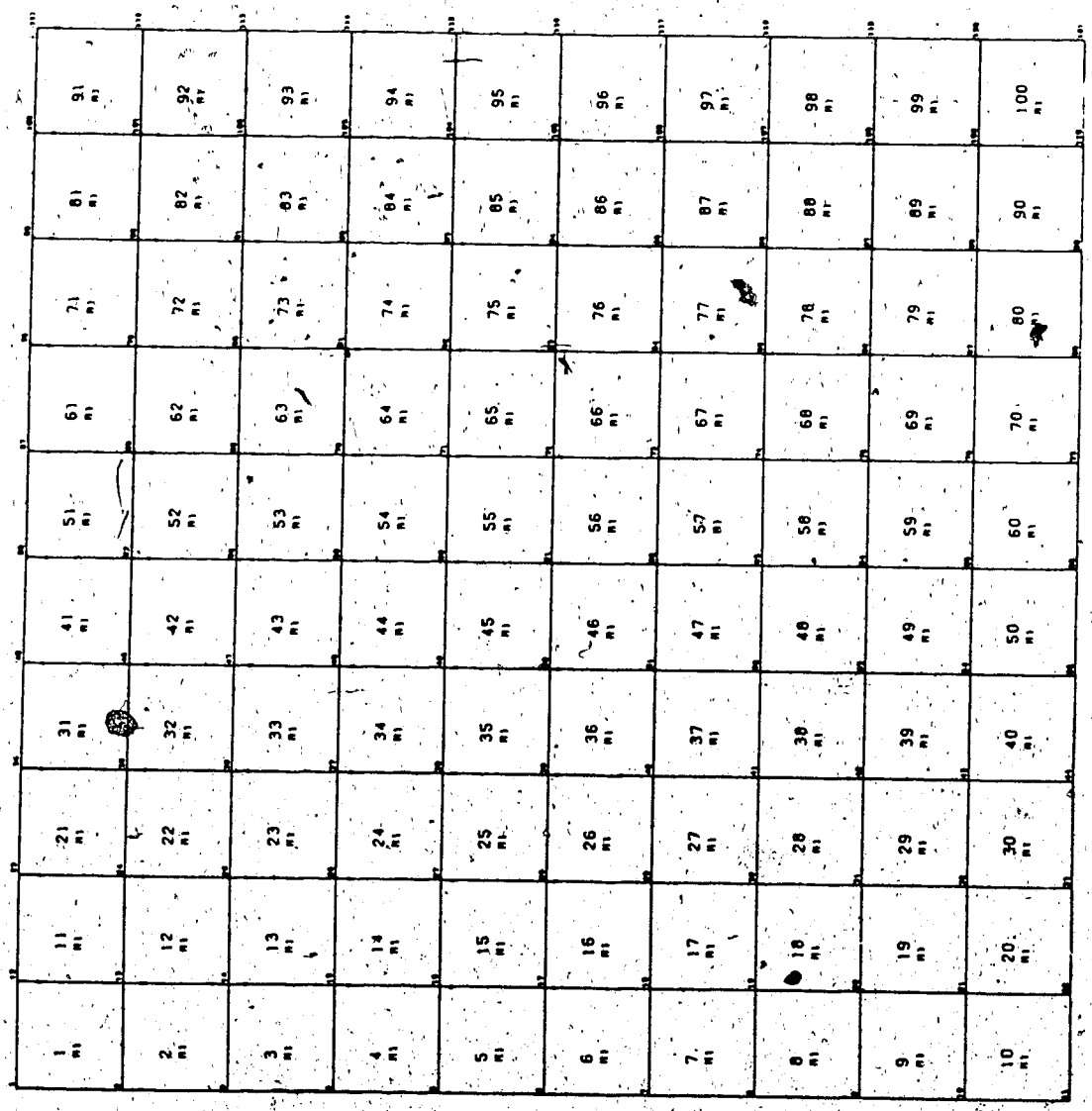

Figure 3.5 Mesh Configuration — 4 Node Elements

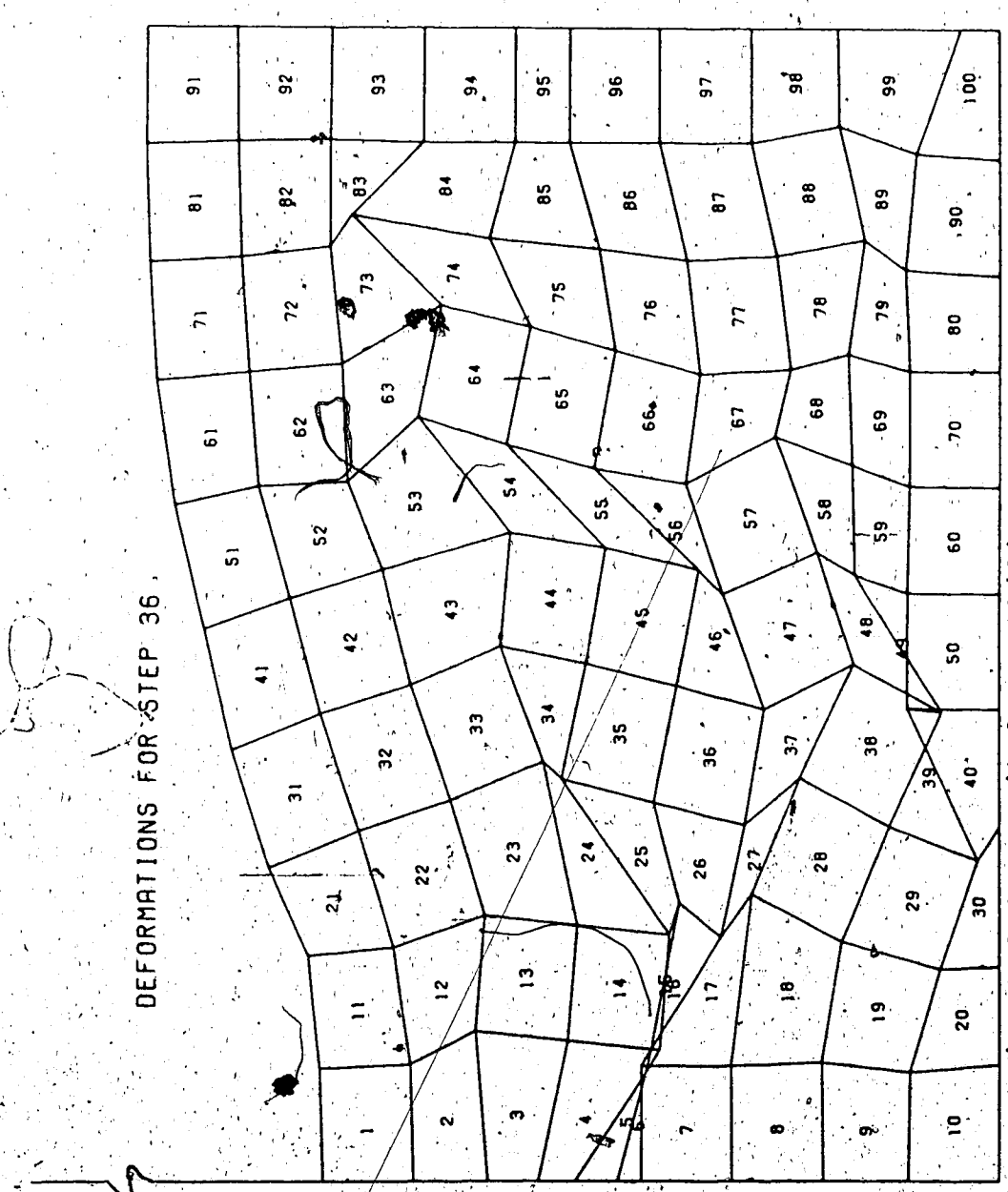

Figure 3.6 Numerical Instability - 4 Node Elements

For the randomly-distributed soil materials, however, the time function that controlled the load subdivisions did not ensure that all materials were beyond the low modulus range before significantly increasing the load, as seen in the excessive deformations in Figure 3.6. This indicated that some elements were at a lower volumetric strain than for the layered analysis at an equivalent loading. Therefore the results of this analysis were encouraging because they indicated a mode of load sharing since all elements were obviously not carrying equal portions of the load.

The solution to this problem was to extend the small load increment portion of the time function beyond the volumetric strain corresponding to the highest thaw strain. This would ensure that essentially all elements that were going to stiffen had actually done so before applying the majority of the load. Any premature load application would again result in an underestimation of the stiffness matrix of the mesh. The results of this analysis, using 81 time steps, is shown in Figure 3.7. The average surface settlement was 2.27m. This is a slight improvement over the layered prediction of 2.53m and an even smaller improvement over the expected thaw strain of 2.34m. However, the minimum value of thaw strain was 17.8%. This meant that the entire mesh would thaw strain by 17.8% before any stiffening occurred. Therefore, it was reasonable to use this minimum value as a datum for the comparison of settlement performance. With respect to this datum, the randomly

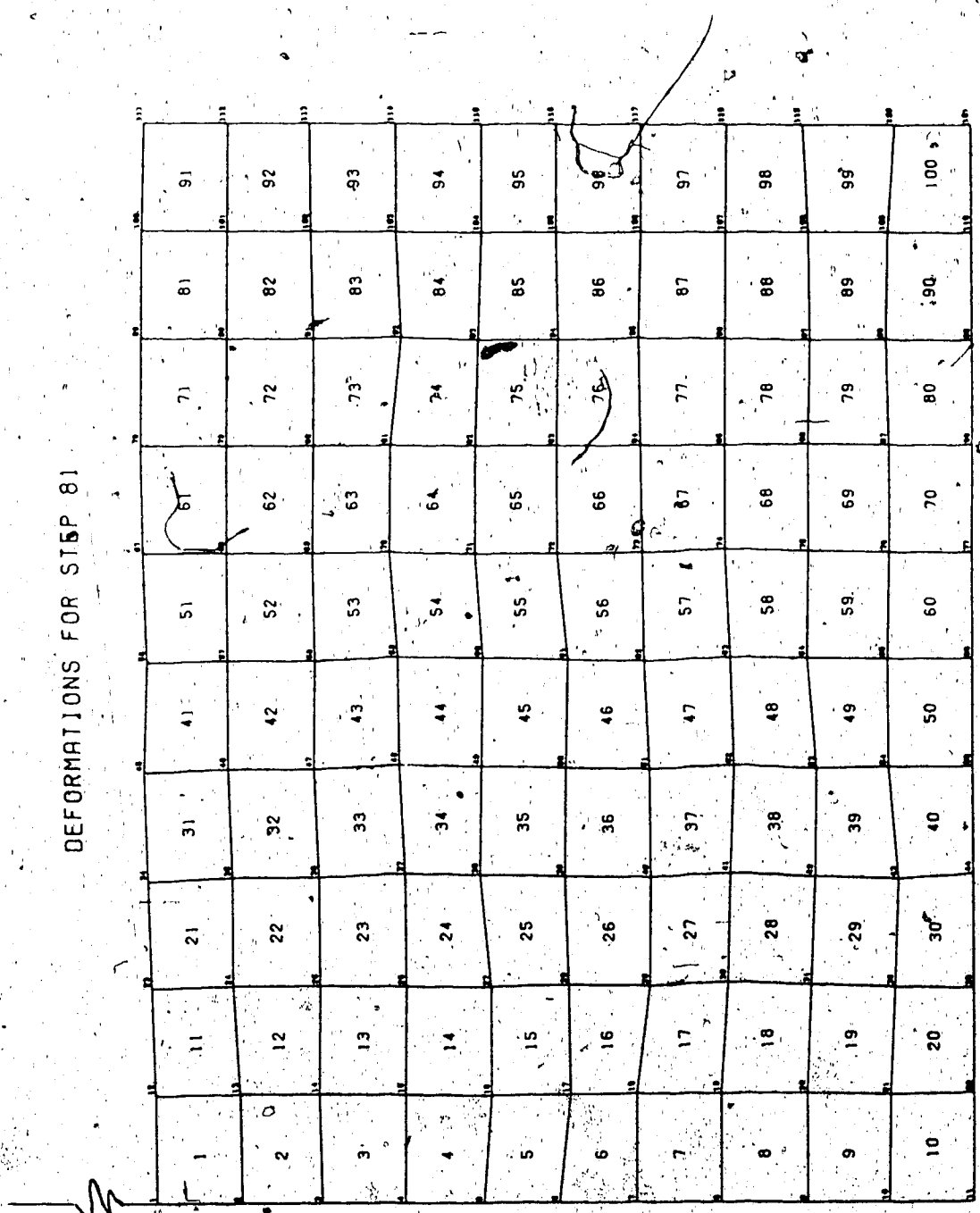

Figure 3.7 Thaw Settlement Deformations. 4 Node Elements

distributed materials resulted in 65% of the layered soil settlement, and 83% of the expected settlement of 2.34m.

3.5.5 Mesh Alteration

An examination of the stress field within the mesh revealed a high stress variation in both magnitude and orientation at the elements' four Gauss points. This was, in part, due to the in-built inflexibility of the mesh: with four nodes, the elements were restricted to linear variations in displacements between nodes. This limits the strains to a constant value between nodes. As this was far too limiting for the material variations within the mesh, the mesh was re-designed for geometric flexibility by increasing the number of nodes from four to eight. This would then allow for quadratic displacements and thus linear variations in strain within the elements. The level of Gaussian integration was increased to 3×3 integration with the redundancy for improved convergence characteristics.

An unfortunate outcome of this change was that the storage available to store the stiffness matrix was exceeded. This occurred because the previous analyses used just one element group with ten material types; however with the increased number of nodes (121 → 341) the matrix could no longer be stored as one unit by the *ADINA* program. The solution was to use ten identical element groups of ten elements each, thereby allowing the matrix to be stored in ten units. This change also allowed a clearer graphical

representation of material properties in later analyses.

3.5.6 Re-analysis of Randomly Mixed A_0 Parameters

For this run, the bulk modulus after thaw was increased to 6000kPa and the Poisson's ratio was changed to zero during thaw and 0.3333 afterwards. The load was again applied in a quasi-static manner, with the initial load designed to accommodate the minimum 1.78m deformation in one step (Figure 3.8).

The average surface settlement of 1.90m was a marked improvement over the previous analysis (Figure 3.9). This was almost entirely due to the improvement in mesh design, as the increase in moduli would result in a comparatively negligible improvement. This 1.90m settlement was 78% of the one-dimensional value, using identical soil parameters. Again, using the minimum 1.78m settlement as reference datum, this difference represented only 19% of the one-dimensional settlement.

The mechanism by which this improvement was brought about can be seen in the deformed mesh. It is clearly evident that the soil with the lowest A_0 value (material 2) remains relatively undeformed while most occurrences of the soil with the highest A_0 value are compressed. These preliminary analyses showed that improvement in settlement behaviour was possible if one considered the mixing of soils with different A_0 values. This was a significant finding, in

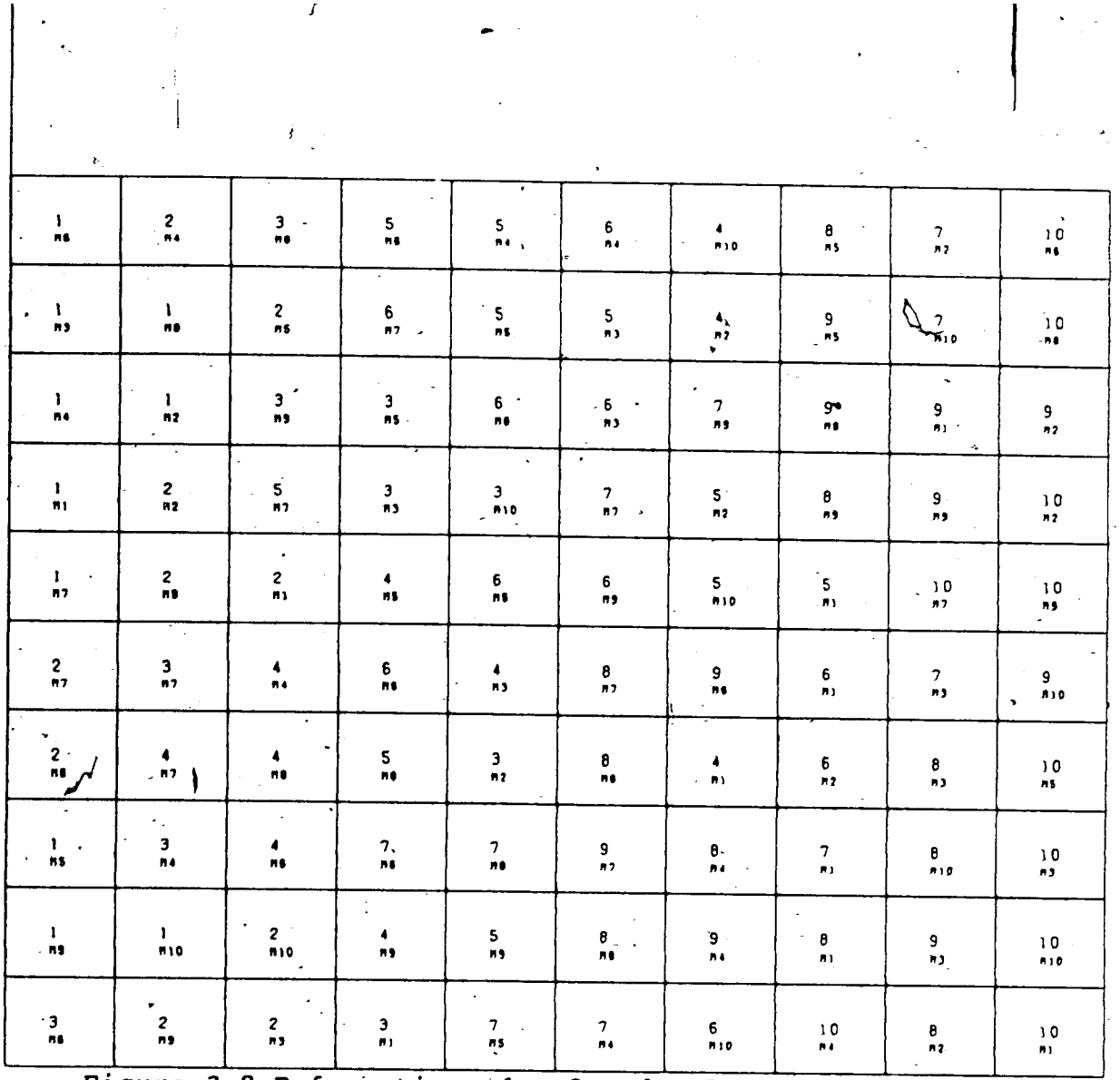

Figure 3.8 Deformations for 8-Node Elements for Step 1

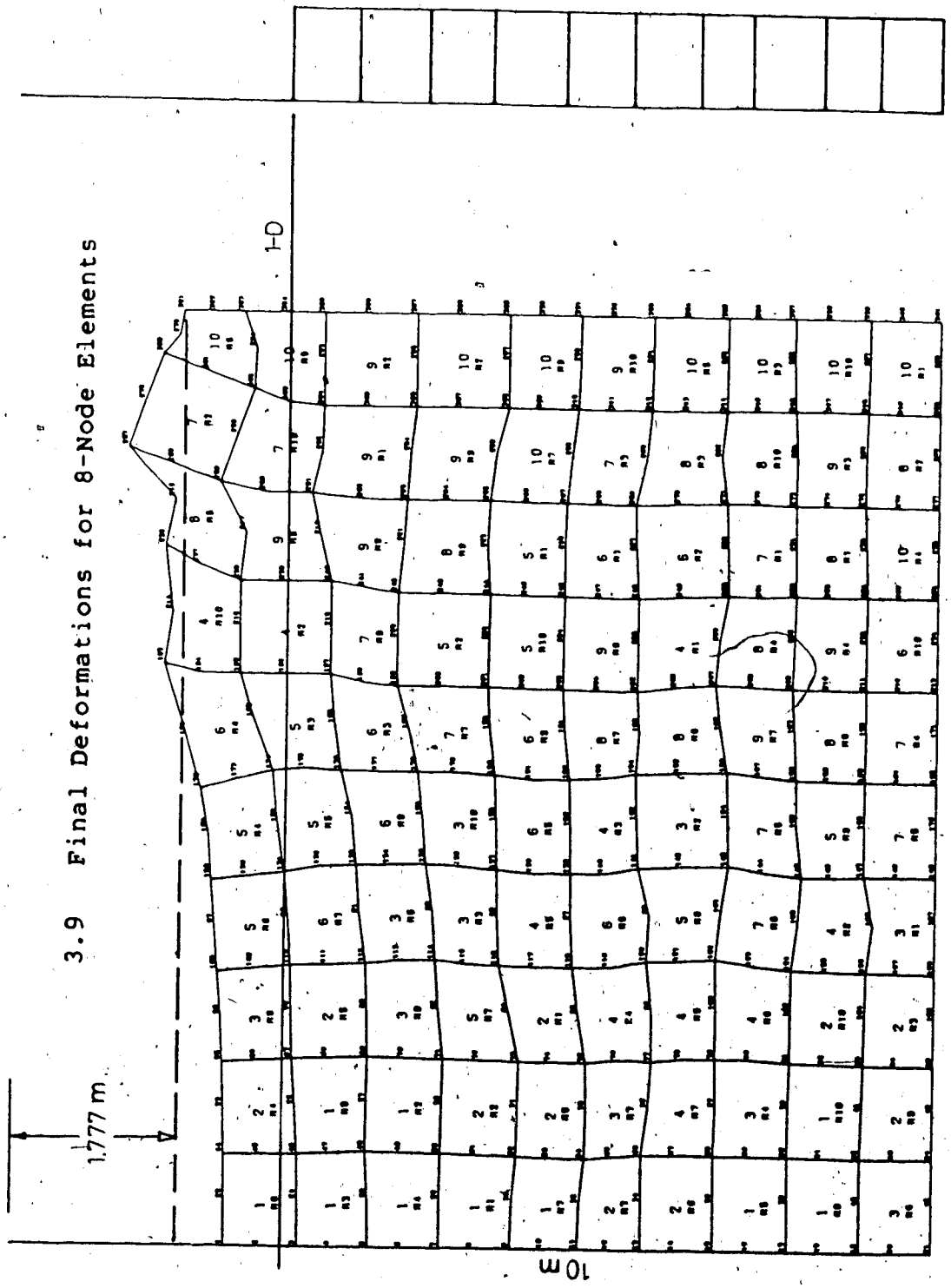

3.9 Final Deformations for 8-Node Elements

that this statistical treatment of A_o quantified a significant reduction in thaw settlement, which is the primary determinant of pipeline stresses. It was now necessary to refine the soil model to more closely reflect the soil's behaviour. (The analyses to this point have been summarized in Table 3.1.)

3.6 Normally Consolidated Soil

One possible approach to improving the soil model was to give it some strain stiffening characteristics in the post-thaw portion of the ϵ_v:K curves. This would simulate any added benefit of soil arching due to consolidation effects. In addition, the smooth, continuous ϵ_v:K curve representative of consolidation was amenable to the interpolation of element stiffnesses inherent in *ADINA's* curve description model.

The means of achieving this was to select a low stress level at which thaw strain occurred, and to allow the material to follow a consolidation curve for subsequent load increments. By choosing a conservative load of 1kPa at thaw strain, the volumetric strains up to thaw strain could also be extrapolated back along the *e-log σ'* curve to obtain an initial void ratio at zero volumetric strain. The error assumed in allowing some minimal initial stiffness was negligible.

Table 3.1 Summary of the Preliminary Numerical Thaw Analyses

FULL MESH (10mX10m) FOR BI-LINEAR STIFFNESS MATERIAL						
# Nodes per Element	Number of Time Steps	ν - pre-A_o	ν - post-A_o	K (kPa)	d (m)	Comments
4 Nodes (layered)	36	1/3	1/3	2000	2.45858	
4 Nodes	81	1/3	1/3	2000	2.27005	too flexible
8 Nodes	81	0	1/3	6000	1.90184	

SOLITARY COLUMN (10m) OF BI-LINEAR MATERIAL					
Number of Time Steps	ν		K (kPa)	δ_z (m)	Comments
	pre-A_o	post-A_o			
36	1/3	1/3	2000	2.45858	-
21	1/3	1/3	2000	3.14937	initial load too high
36	1/3	1/3	2000	2.52696	loading too coarse
10	1/3	1/3	2000	2.60654	too few time steps
10	0	1/3	2000	2.61133	too few time steps
36	0	1/3	2000	2.52311	-
36	0	1/3	2000	2.78396	initial load too high
36	0	1/3	6000	2.42518	-

3.6.1 Stress-Strain Relationship

The information needed to determine the *ADINA* input parameters were an appropriate Poisson's ratio, ν, and an *e-log* σ curve for the material. The procedure used was as follows:

Using the laboratory results for a similar material from the Inuvik test site (Watson *et al.*, 1973b), an average plasticity index of I_p=25 is obtained. From the work by Kenney, as reported by Lambe and Whitman (1969):

$$\sin \phi' = [.48, .52]$$
$$= .50 \text{ (average)}$$

where ϕ'= effective stress friction angle

After the work of Jaky, as reported by Lambe and Whitman (1969):

$$K_0 = 1 - \sin \phi' \qquad [3.3]$$
$$= 0.5$$

which is confirmed by Alpan, as reported by Lambe and Whitman (1969):

$$K_0 = 0.19 + 0.2333 \log I_p \ (\%) \qquad [3.4]$$
$$\cong 0.52$$
$$\therefore \text{use } K_0 = 0.50$$

Knowing that the value of K_0 remains relatively unchanged throughout consolidation (Lambe and Whitman, 1969) and using the stress-strain relationships for an oedometric stress state, it can be shown that the Poisson's ratio is $\nu=\frac{1}{3}$ and the oedometric modulus is $D=1.5E$. For this particular value

of ν, $D=1.5K$ where K is the bulk modulus.

The required input parameters for *ADINA*'s curve description model are the volumetric strains and corresponding loading and unloading bulk moduli, and the shear modulus: ϵ_v, K_L, K_{UNL}, and G. This information was obtained from the consolidation curve presented by Morgenstern and Nixon (1975). By relating the compression index, C_c, with the coefficients of compressibility and volume change, a_v, and m_v to the volumetric strain expressed in terms of void ratios. These calculations are performed within program "BETA" (Appendice D) and are summarized as follows:

After obtaining the ten A_o values, their corresponding bulk frozen densities (ρ_f^b) were determined using the relationship found by Speer, *et al*. (1973):

$$A_o(\%) = 73.60 - 101.8\ ln(\rho_f^b) \qquad [3.5]$$

Information about the material stiffness was obtained form an *e-log σ* curve:

$\nu=\frac{1}{3}$ $$D=\frac{\sigma_{11}}{\epsilon_{11}}=\frac{\sigma_v^{\circ}}{\epsilon_v}=1.5\ K \qquad [3.6]$$

$$K=0.667\ \frac{\sigma}{\epsilon_v} \qquad [3.7]$$

tangent modulus $$K_T=0.667\ \frac{d\sigma}{d\epsilon_v} \qquad [3.8]$$

however $$d\epsilon_v=-\frac{de}{1+e_0} \qquad [3.9]$$

$$C_c=-\frac{de}{d\ log\sigma} \qquad [3.10]$$

$$=0.270 \qquad \text{(Morgenstern and Nixon, 1975)}$$

$$d\ log\sigma=\frac{d\sigma}{\sigma\ ln\ 10}=\frac{de}{C_c} \qquad [3.11]$$

$$\therefore K_T = \frac{0.667(1+e_0)\sigma \ln 10}{C_c} \qquad [3.12]$$

$$= 5.685(1+e_0)\sigma$$

The initial void ratio e_0 was back-calculated from the frozen bulk density of each material. Bulk moduli were calculated at several arbitrary stress levels. It was conservatively assumed that thaw strain occurs at a stress of 1kPa which corresponded to a void ratio of e=1.555. With this information the entire ϵ_v:K relationship was determined, an example of which is included in Appendix D.

To obtain the relevant finite element model parameters, the laboratory values of thaw strain for the Norman Wells site (Speer *et al.*, 1973) were input into program *"SETTLE"* to obtain the statistical parameters of that site. The β-distribution P and Q parameters were then input into the program "BETA" (*viz.* App. D).

3.6.2 Volumetric Strain ; Bulk Modulus Relationship

This program used the thaw strain β parameters to generate a continuous β probability distribution function (PDF) from which 10 representative values of A_0 were calculated (Figure 3.10). The laboratory distribution was normalized to a likelihood distribution, providing the probability of occurrence of each particular thaw strain value. Using the Speer *et al.* (1973) relationship between thaw strain and bulk density, and given such basic information such as specific gravity and consolidation information, a table of soil parameters was generated. Using

Likelihood Distribution Functions

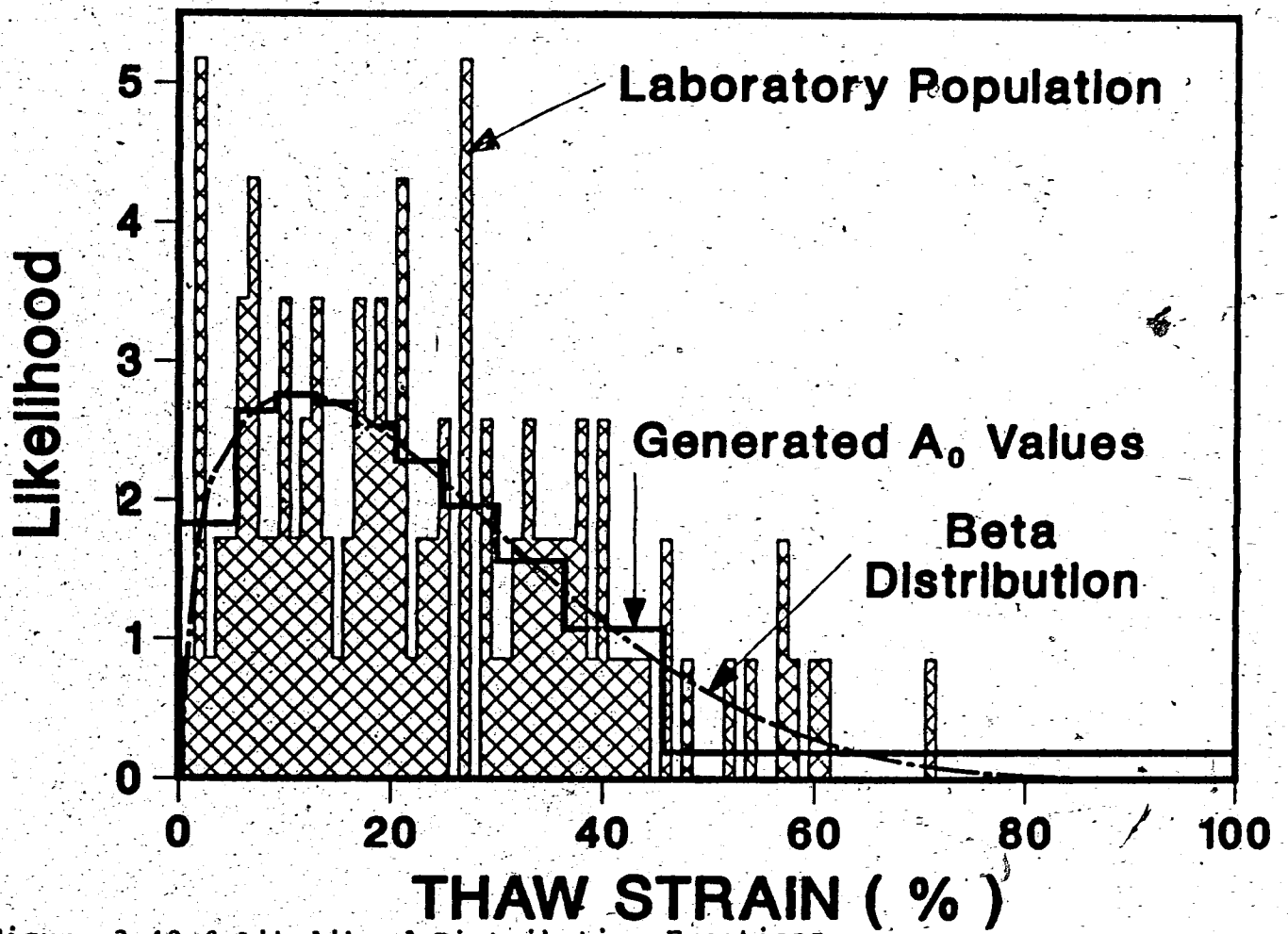

Figure 3.10 β Likelihood Distribution Functions

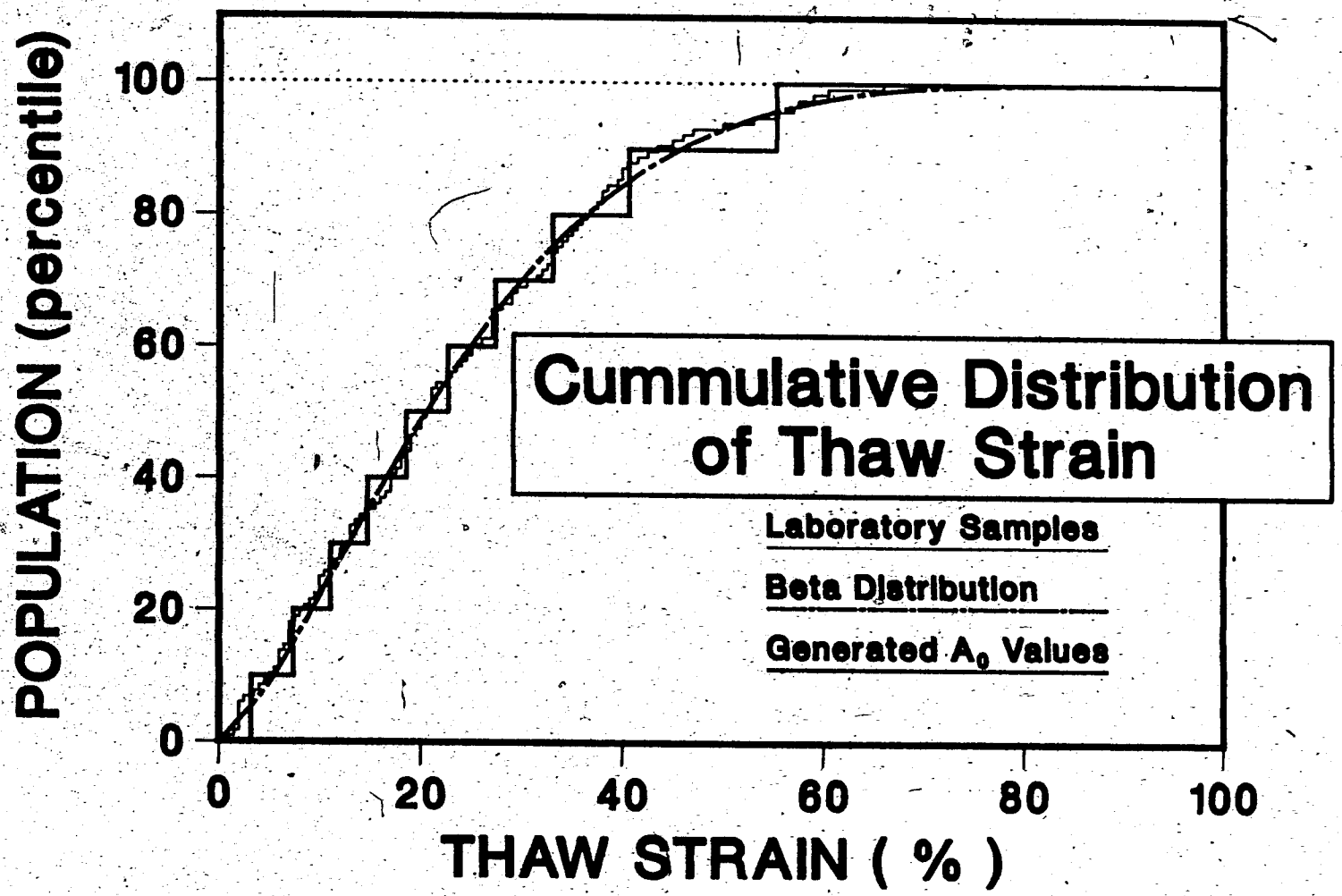

Figure 3.11 Cummulative Distribution of Thaw Strain

constituitive relationships, a set of *ADINA* input parameters could then be calculated for each of the ten representative thaw strain parameters. Arbitrary values of the bulk modulus, K, were selected from which the corresponding volumetric strains were back-calculated. The resultant ϵ_v:K curves are shown in Figure 3.15.

3.6.3 Layered Analysis

The analyses were performed with a 10m×10m mesh under plane-strain conditions. The surface is a free boundary while the three other sides allowed movement parallel to the boundary. The two bottom corners were fixed. A nominal surface load of 20kPa was applied incrementally, using very small load increments at first. This was done to prevent excessive displacements from occurring between the updating of the tangent stiffness matrix at each time step. Once sufficient volumetric straining had occurred to increase the stiffness of each element, the load increments were increased and incremental gravity loads were initiated.

The mesh is shown in Figure 3.12. The initial analysis was performed on a randomly layered soil as represented in Figure 3.13. Because of the continuous horizontal layering, the analysis is essentially one-dimensional, thereby allowing a check on the numerical procedure. The final results of this analysis are shown in Figure 3.14.

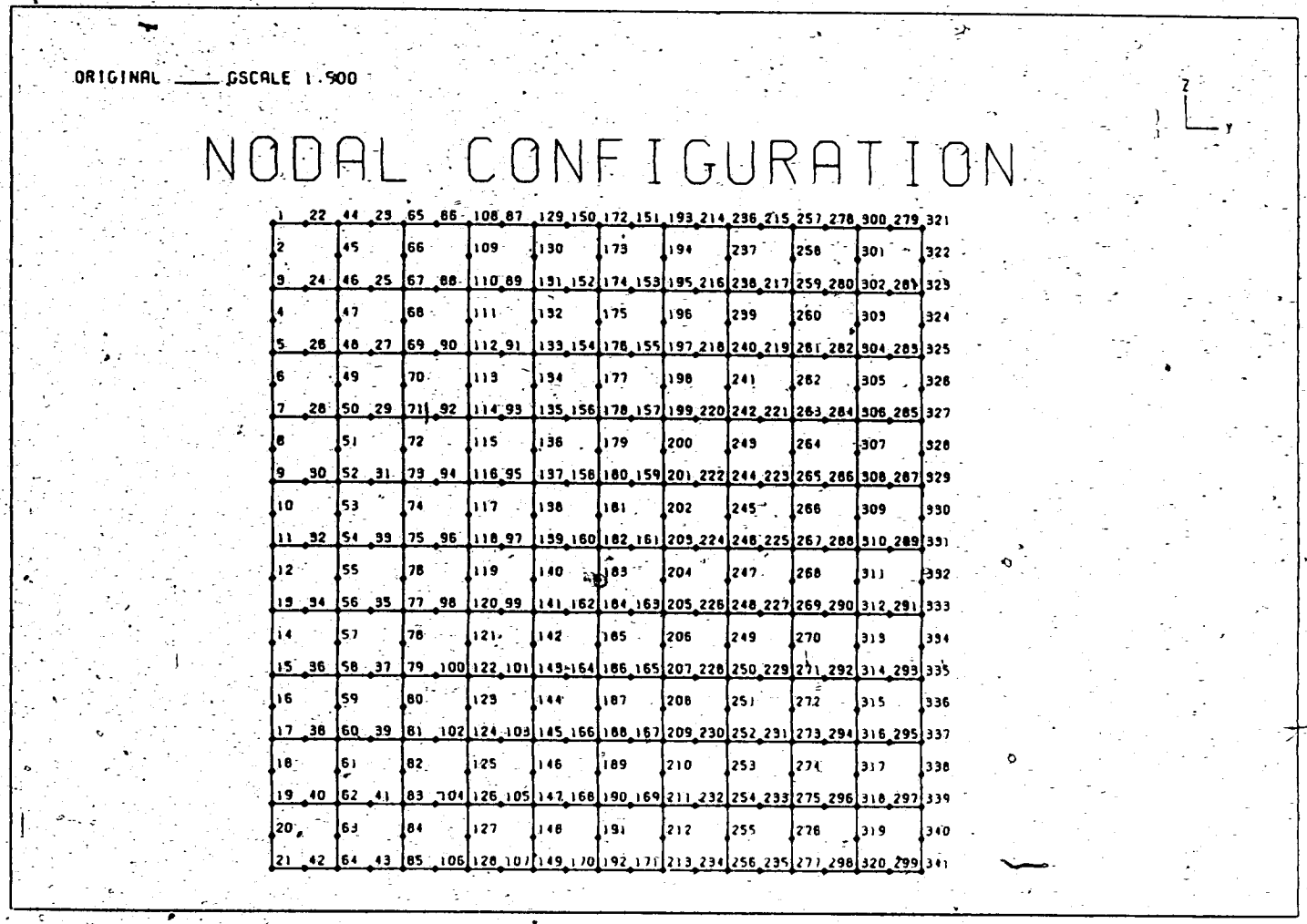

Figure 3.12 Mesh Configuration - 8 Node Elements

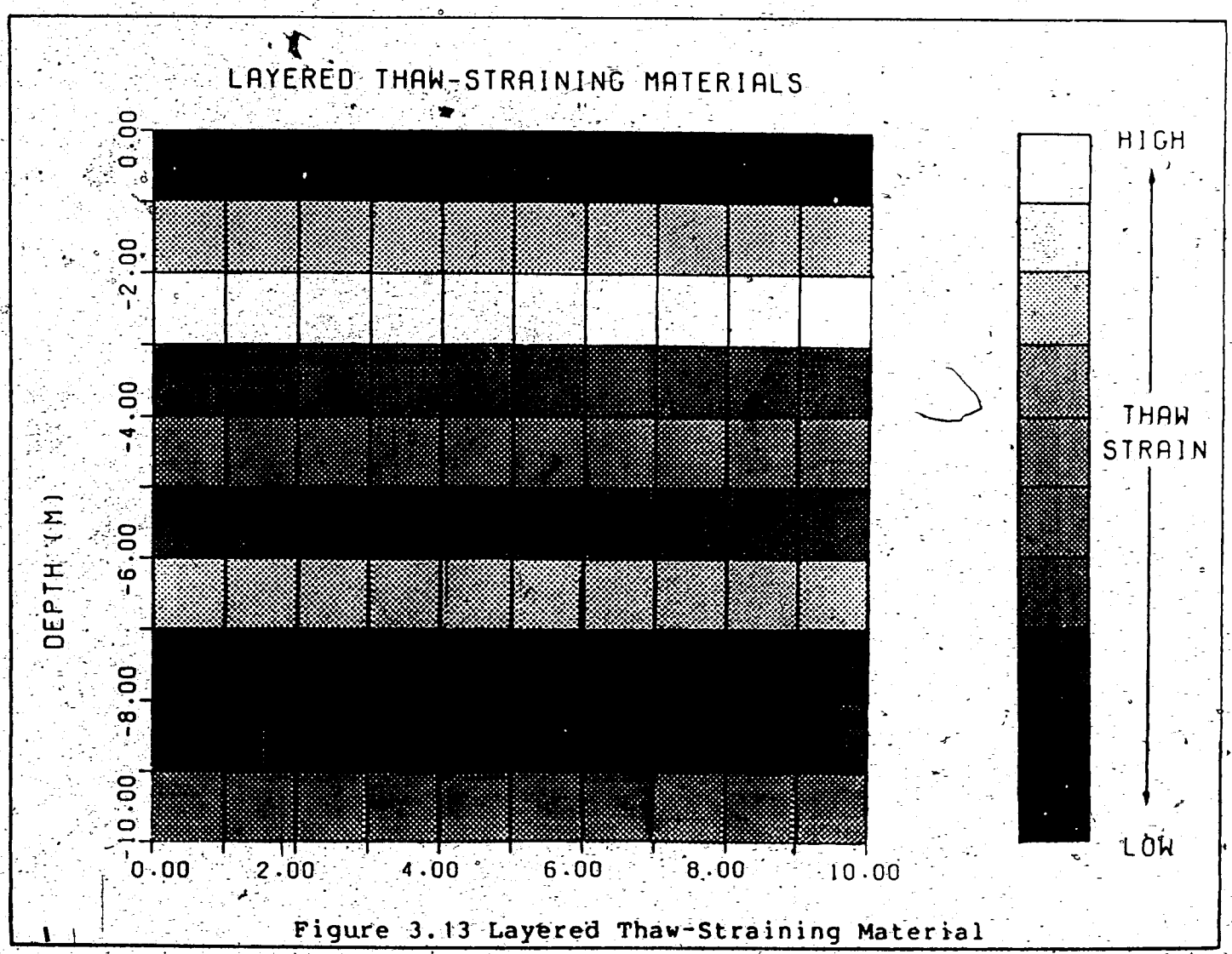

Figure 3.13 Layered Thaw-Straining Material

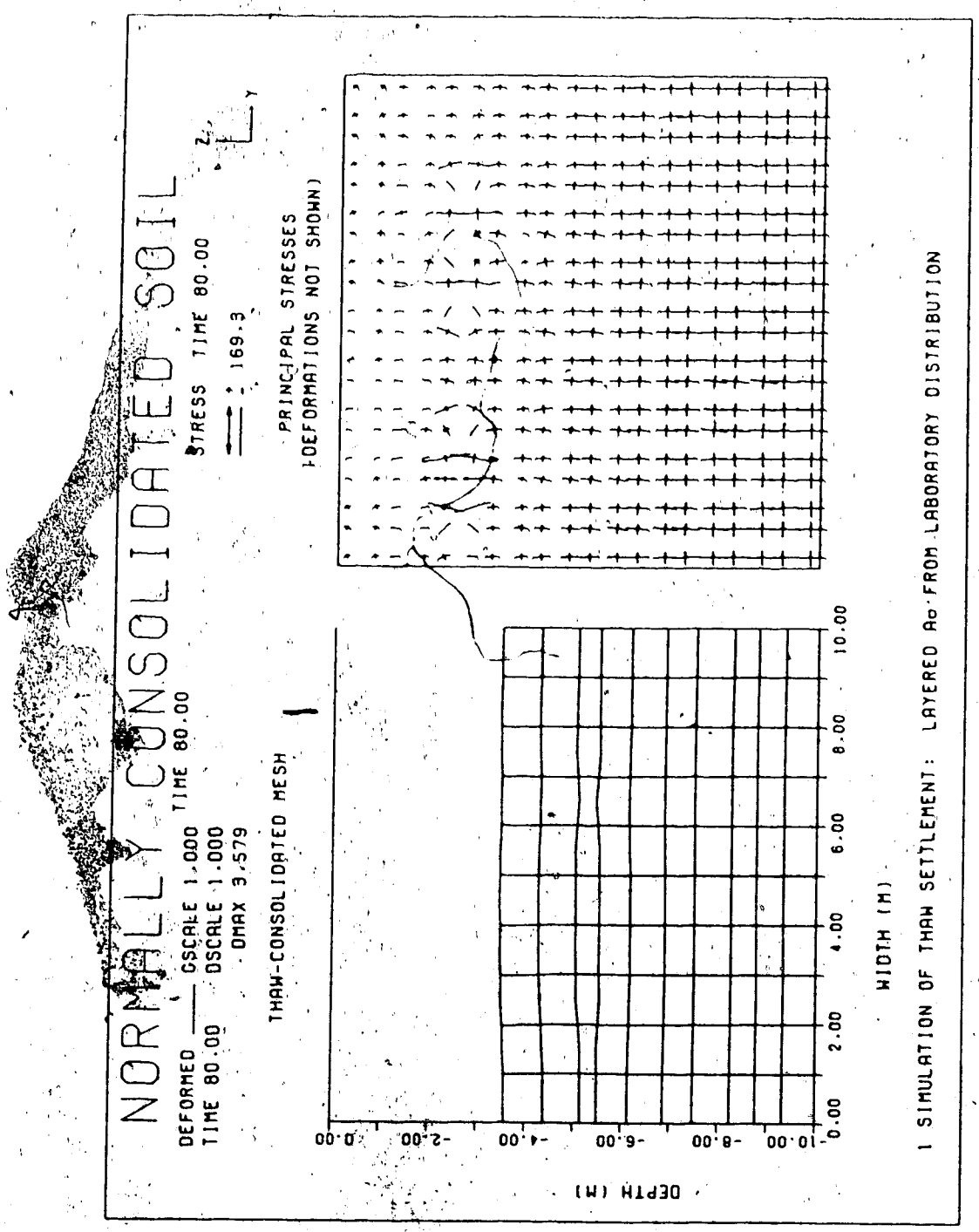

Figure 3.14 Layered Normally Consolidated Soil

Several conclusions can be drawn from this analysis. The deformed mesh exhibits the behaviour expected of a layered, consolidating material. The settlement pattern is not as regular as that in Figure 3.7 because the original analysis was performed using 4-node elements which restricted the distortion geometries. The stress field of the 8-node element mesh is similar to the closed-form stress field of oedometric conditions with the notable exception of the third layer from the top which is composed of Material 10, a high thaw-straining soil. This is likely due to the high strains and displacements that this element type had undergone during thaw straining which, with a small strain and small displacement analysis, resulted in poor results. This would be cause for concern if extensive layers of high thaw-straining soil were anticipated, however the soil is being modelled without a preferential directional bias so it is unlikely that this would occur in a mesh of randomly selected materials. Also, these softer zones, being surrounded by stiffer materials, were anticipated to make a negligible contribution to the load carrying capability of the soil. Because of this, stress aberrations resulting from high loadings were unlikely.

The second conclusion is that the final amount of settlement in this analysis exceeds, by far, the thaw settlement extrapolated from the thaw strain tests. It was found that the major contribution to this difference was from the consolidation of the thawed material due to the

20kPa surcharge and the effective weights of the assorted materials. The one-dimensional analysis by Speer, *et al.* (1973) obtained thaw strains from samples tested at overburden pressure. In this analysis it was not possible to correct each element for overburden pressures, therefore consolidation effects are in excess of A_o. This ensures a conservative bias in the results of this analysis.

Another source of error would be the problem of underestimating the tangent stiffness matrix. For each time step, the elements are given a stiffness corresponding to their ϵ_v at the beginning of the step. The elements then compress in response to the load increment for that step. Since, for each time step, the elements exhibit linear stress-strain behaviour, too large of a load increment could result in overshooting the initial soil stiffening at the thaw strain. Subsequently, imposing too large load increments would prevent the material from following the consolidation curve adequately. To minimize the overshoot effect, the time functions controlling the surficial load were designed to gradually increase the load increments, resulting in a pseudo-exponential loading curve. Once the surface load had increased to about 9kPa, by which time the elements were stiffer, the gravity loads and remainder of the surface load were added using larger load increments.

Hand calculations confirmed that consolidation effects significantly contributed to the total settlement of the

postulated soil mass. Using the material distribution shown in Figure 3.14, midpoint stresses were calculated for each layer and consolidation calculations were performed, using parameters from the e-$\log \sigma$ curve of Morgenstern & Nixon (1975).

Given the ten representative values of A_o, the anticipated strain due to unloaded thawing was 2.35m over the 10m thickness of the mesh. The hand calculations indicated an additional 1.41m of consolidation settlement, for a total of 3.76m. As a check, using an average thaw strain and an average effective stress, the total settlement was predicted as 3.81m. The difference between the two hand calculations is due to the particular sequencing of the material layers, and would change if the stratigraphy changed. Comparing the finite element approach with these results, it was found that an average total settlement of 3.51m was predicted. This was 94% of the expected value of 3.76m. This difference was probably due to the small initial value of the bulk modulus and because bulk moduli are linearly interpolated between input ϵ_v:K pairs rather than following a curve. (Figure 3.15). This generally overpredicted the bulk modulus, but qualitatively compensated for the overshoot problem.

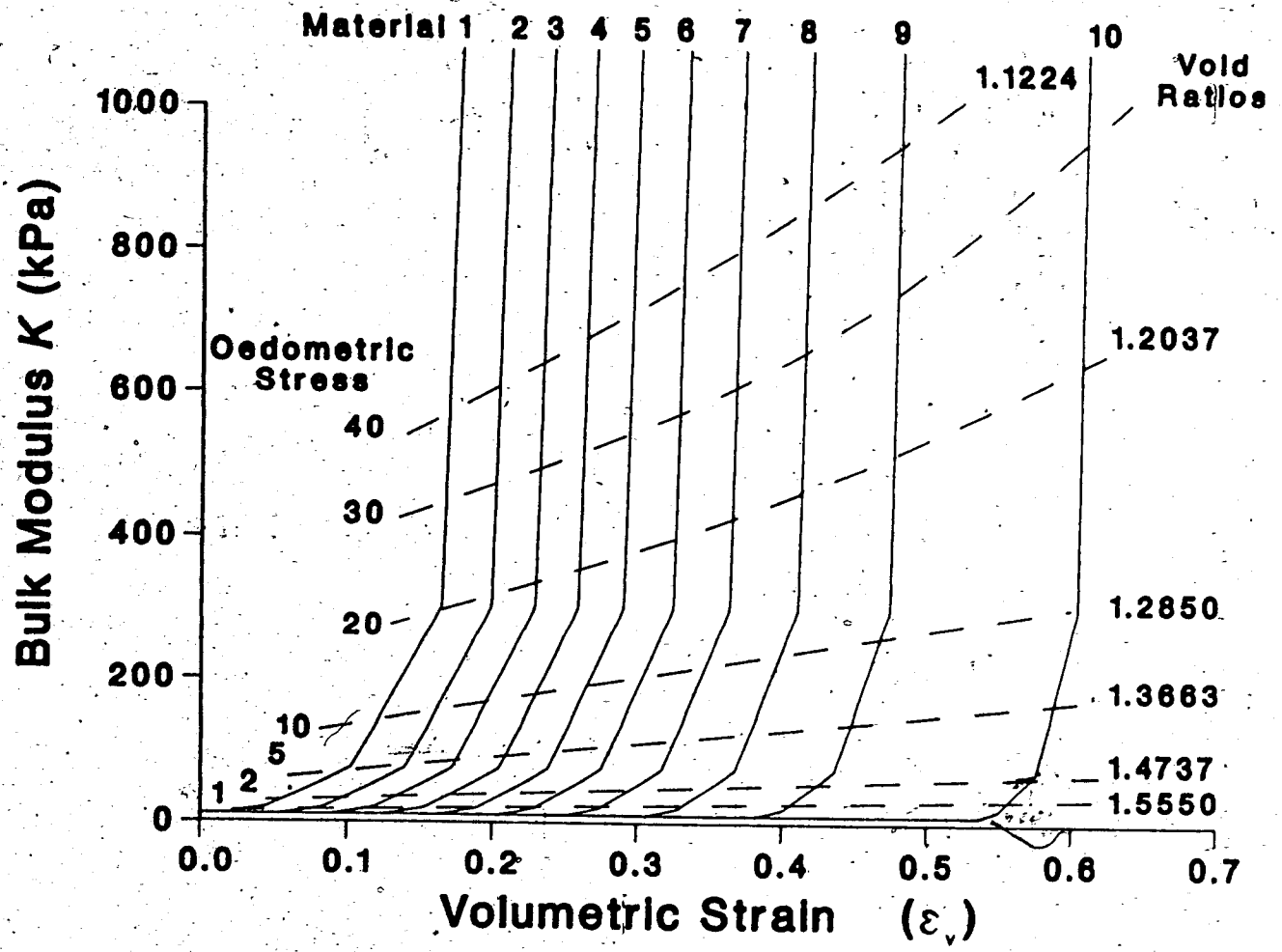
Normally Consolidated Soil ε_v:K Curves
Material 1 2 3 4 5 6 7 8 9 10
Void Ratios
1.1224
1.2037
1.2850
1.3663
1.4737
1.5550
Oedometric Stress
40
30
20
10
5
2
1
Bulk Modulus K (kPa)
1000
800
600
400
200
0
0.0
0.1
0.2
0.3
0.4
0.5
0.6
0.7
Volumetric Strain (ε_v)

Figure 3.15

3.6.4 Randomly Mixed A_0 Parameters

The next analysis was a random scrambling of the thaw strain materials throughout the mesh. The material configuration, shown in Figure 3.16, was identical to that of the earlier analysis (Figure 3.5) except that an increase in the material number now reflected an increase in the thaw strain. Therefore material 1 is the most thaw-stable and material 10 the least thaw stable. This is graphically expressed in Figure 3.17. This configuration was used for all subsequent analyses, except where noted. The 20kPa surficial loading and the gravity stresses were applied gradually, resulting in the stresses and deformations shown in Figure 3.18.

Of particular interest are the stress-free zones within the soil mesh, corresponding to the locations of the material with the highest thaw strain as seen in Figure 3.17. Adjacent to these zones are areas of high stress and directional variation. Here, the soil is compensating for the lack of support ~~from the~~ ice-rich material and is arching the load around the weaker areas. This results in stress concentrations, with the maximum stress of 246kPa being 2.4 times the highest anticipated stress assuming no stress variation. While the accuracy of this value is questionable, given the coarseness of the mesh and the high strains involved, there is no doubt that there is a significant variation in stresses.

ORIGINAL ____ GSCALE 1.500

ELEMENT GROUP AND NUMBER

6-1	4-2	8-3	6-5	4-5	4-6	10-4	5-8	2-1	6-10
3-1	8-1	5-2	7-6	5-5	3-5	2-4	5-9	10-7	8-10
4-1	2-1	9-3	5-3	8-6	3-6	9-7	8-9	1-9	2-9
1-1	2-2	7-5	3-3	10-3	7-7	2-5	9-8	9-9	2-10
7-1	8-2	1-2	5-4	5-6	9-6	10-5	1-5	7-10	9-10
7-2	7-3	4-4	6-6	3-4	7-8	6-9	1-6	3-7	10-9
6-2	7-4	8-4	6-5	2-3	6-8	1-4	2-6	3-8	5-10
5-1	4-3	6-4	6-7	8-7	7-9	4-8	1-7	10-8	3-10
9-1	10-1	10-2	9-4	9-5	8-8	4-9	1-8	3-9	10-10
6-3	9-2	3-2	1-3	5-7	4-7	10-6	4-10	2-8	1-10

Figure 3.16

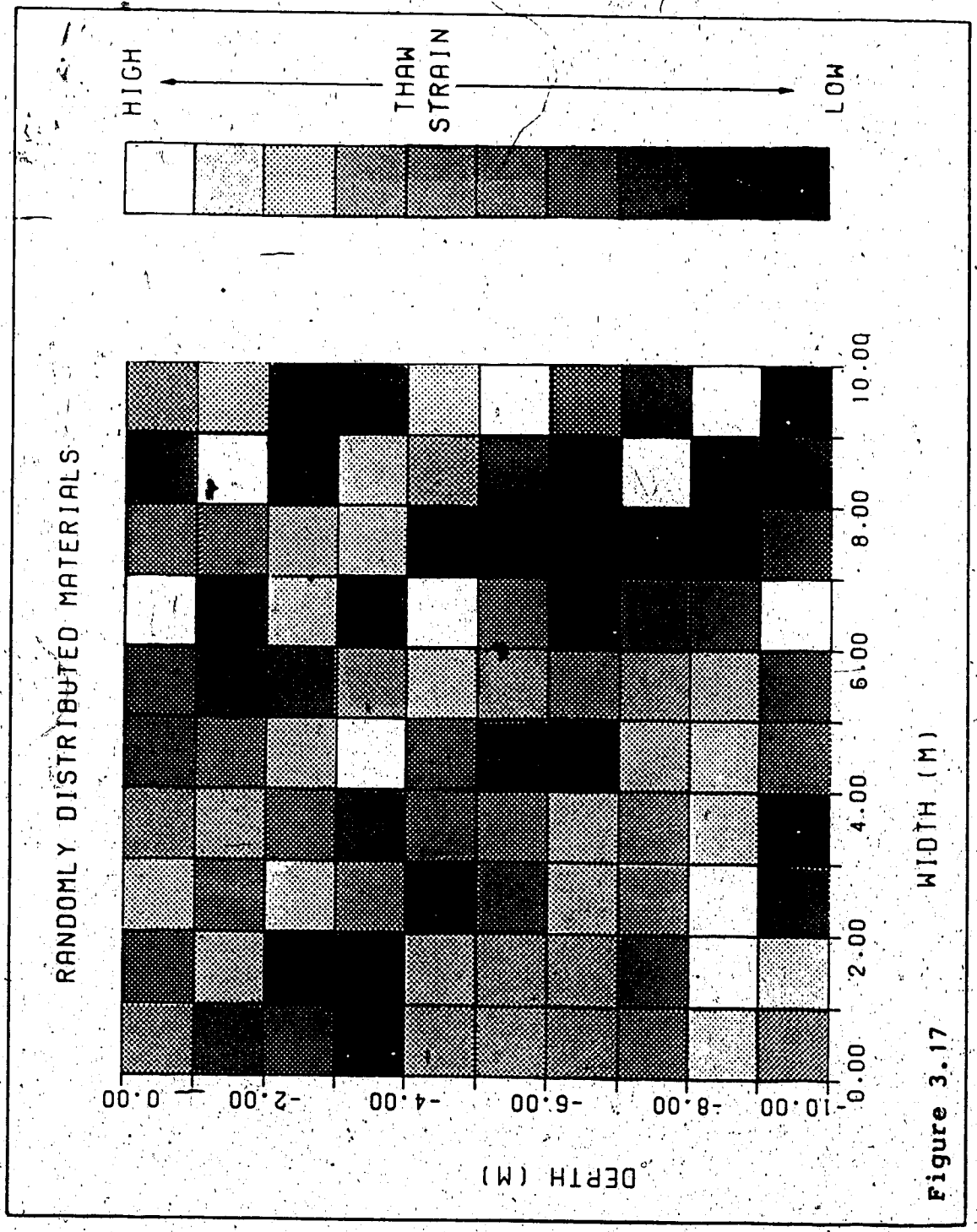
RANDOMLY DISTRIBUTED MATERIALS
HIGH
THAW STRAIN
LOW
DEPTH (M)
0.00
-2.00
-4.00
-6.00
-8.00
-10.00
0.00
2.00
4.00
6.00
8.00
10.00
WIDTH (M)

Figure 3.17

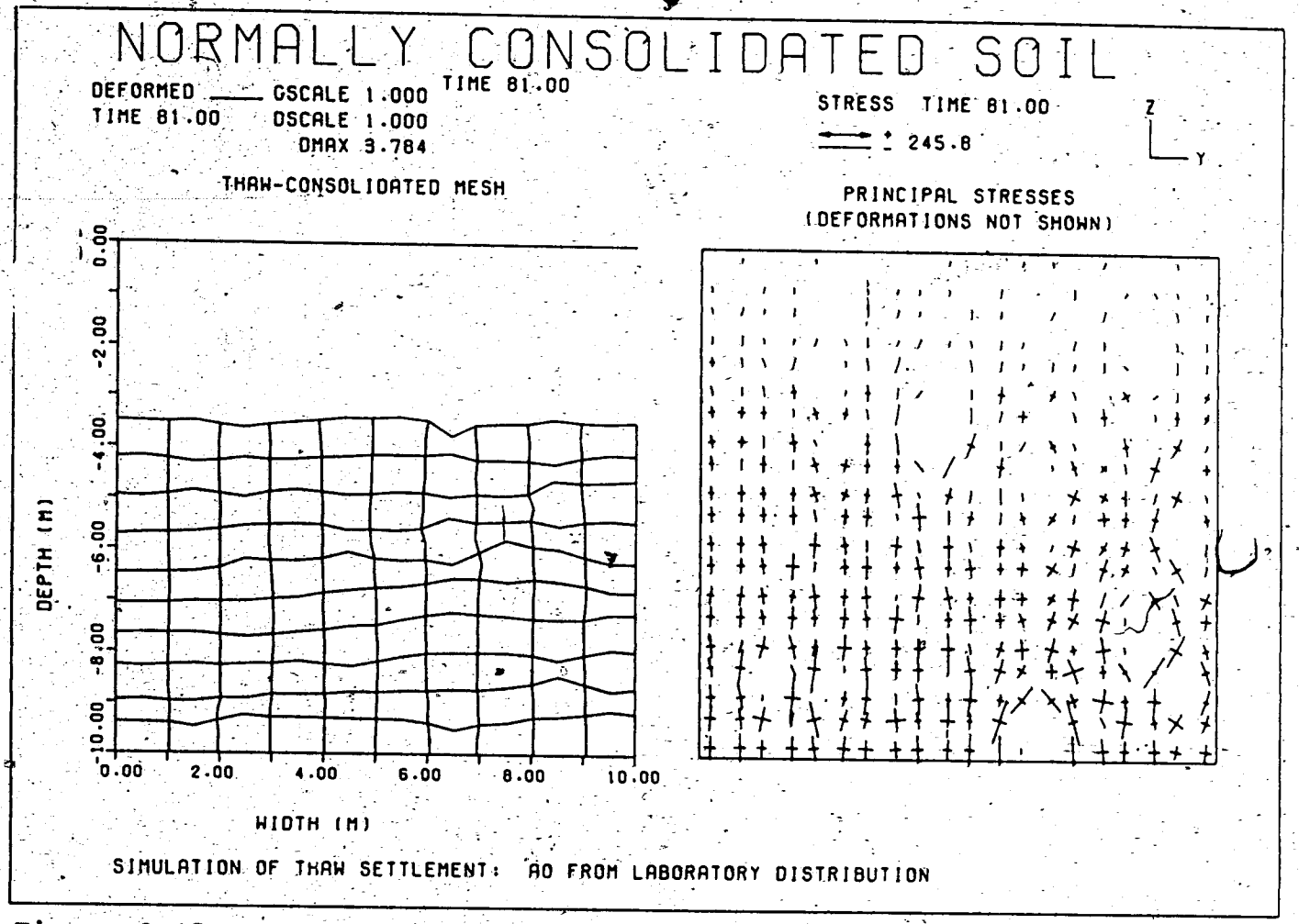

Figure 3.18 Normally Consolidated Soil with Laboratory Standard Deviation

3.6.5 Disappointing Results

What is disconcerting in this particular piece of analysis is that there is no benefit in total settlement from the random mixing of the thaw strain values. The average surface settlement of 3.511m is 92% of the 3.806m predicted using an average A_o value and normal consolidation and 100% of the 3.488m predicted in the layered finite element analysis. Given the variation in stress, and the supposition that beneficial settlement performance would result from this variation it was plausible that the increased stresses resulted in increased consolidation. This additional settlement could then negate any beneficial effects of the stress variation.

This hypothesis was examined by reducing the standard deviation of the thaw strains by 50% while maintaining the same average value (Figure 3.19). The results were encouraging: the average surface settlement was reduced to 3.50m. Associated with this improvement was a reduction of 24% in the maximum stress found in the mesh, and the stress field exhibited a more uniform development of stress with depth. This suggested that the hypothesis of improved settlement performance applied to the situation of low thaw strain variance but did not apply to high variance distributions.

This did not seem reasonable, given the general behaviour of thawing permafrost. Re-examining the results,

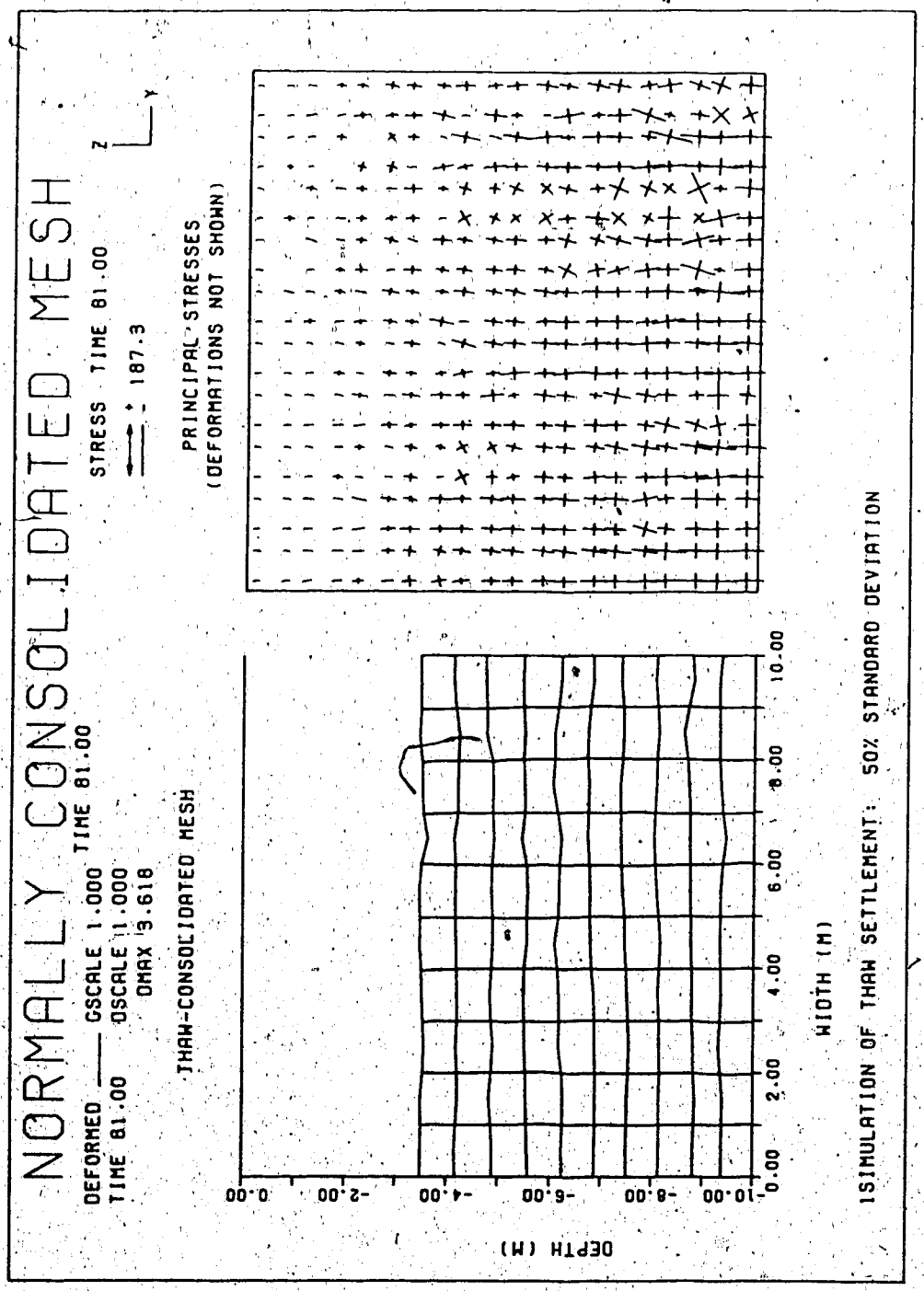

Figure 3.19 Normally Consolidated Soil: 50% Standard Deviation

it appeared that the lower variance analysis benefitted from the lack of high thaw-strain pockets which precluded higher stress concentrations. In the higher variance analysis, the low A_o materials, having higher stresses, were consolidating as a result. It was unreasonable to attribute the additional settlement to those concentrations, given the stiff behaviour of thawed ice-poor materials, yet the thaw settlement analysis did not differentiate between materials beyond the variable thaw strain parameters. Obviously the assumption of normal consolidation as a material model was untenable. This prompted the development of a refined thaw model that would encompass the concept of thaw strain variability and include improved post-thaw load:displacement behaviour.

3.7 Soil with a Residual Stress

In the genesis of the permafrost soil strata, the soil was normally consolidated prior to freezing. The existing numerical soil model, however, ignored the significant contribution of the freezing process to the overconsolidation of the soil. This contribution results from negative pore water pressures, driven by the physics of ground freezing which cause a massive normally consolidated soil to differentiate into distinct ice lenses and soil peds (Nixon & Morgenstern, 1973). Since the soil peds are, therefore, at a lower void ratio than the original unfrozen soil, they are overconsolidated, and would exhibit improved

deformation characteristics.

3.7.1 Thawing Soil and Residual Stress

After undrained thawing, some of the segregated water is reabsorbed into the soil peds. This reabsorption largely occurs adjacent to the macropores left by the melt-out of the segregated ice. Some material will then be at a higher moisture content thereby reducing the effective stress contribution to the soil's load bearing capacity. This initial effective stress, σ', in the thawed undrained soil is referred to as the "residual stress", σ'_0 (Nixon & Morgenstern, 1973). When this thawed soil is allowed to drain, returning to its effective stress prior to freezing, it is at a lower void ratio because of the overconsolidation effects of freezing. As a result, the recompression curve during thaw-consolidation is of a far stiffer material than the original normally consolidated soil. Both of these factors result in reduced volumetric strains upon thaw-consolidation.

3.7.2 ϵ_v:K Representation of the *e-log* σ Curve

In modelling a normally consolidated soil the ϵ_v:K relationship was based on a linear *e-log* σ curve. This represented the thawed permafrost as a continually stiffenning material. A soil with residual stress, in contrast, exhibits variable stiffnesses depending on its position on its *e-log* σ curve. Therefore in order to

implement the concepts of residual stress into the numerical soil model, it was first necessary to determine the entire stress-strain relationship of the material over the expected stress range of the problem. As this would involve consolidation effects and much of the required data was obtained by consolidation testing, the *e-log σ* curve best describes this relationship.

Upon thawing, the permafrost soil undergoes thaw strain under no load. On the *e-log σ* curve, this can be represented as a change in void ratio under negligible load (segment *A*, Figure 3.20). The next known point is the residual stress. Applied stresses above the required stress, stiffness may be deduced from the thaw-recompression curve (segment *B*, Figure 3.20). Some judgement is needed, however, to assess the soil stiffness at stresses after thawing but below the residual stress, as represented by Segment *B*, in Figure 3.20.

3.7.3 Stiffness at a Stress Below the Residual

Given that an undrained saturated sample loaded to the residual stress has, by definition, zero pore water pressure, then an applied stress of less than the residual stress would result in negative pore water pressures within the sample. With the low compressibility of the water fraction (ϵ_v=0.0046%/atm) essentially no volume change would occur as negative pore water pressures developed. These pressures would restrain the elastic expression of the soil structure and therefore maintain the effective stress state

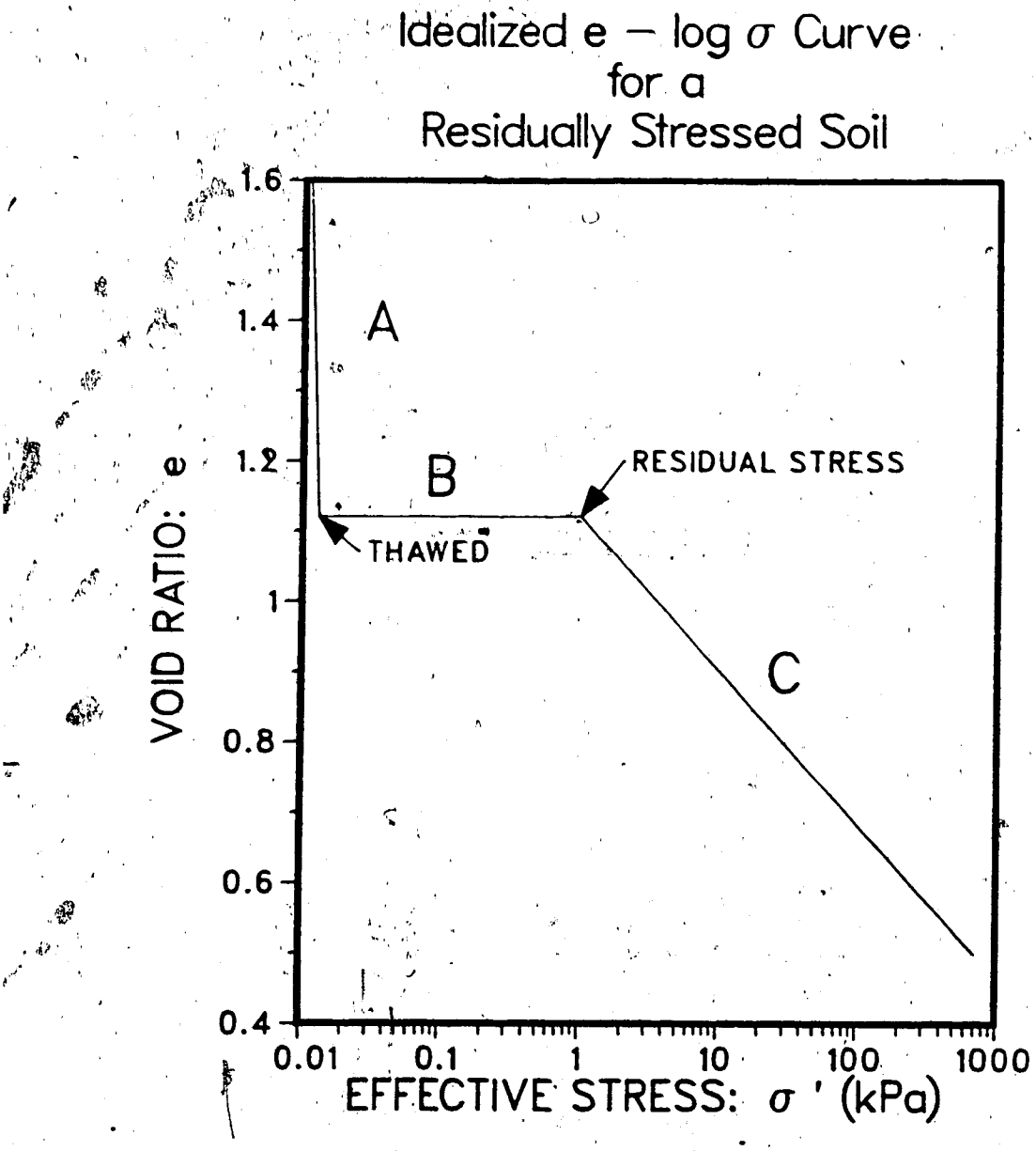
Idealized e – log σ Curve
for a
Residually Stressed Soil
VOID RATIO: e
1.6
1.4
1.2
1
0.8
0.6
0.4
A
B
C
RESIDUAL STRESS
THAWED
0.01
0.1
1
10
100
1000
EFFECTIVE STRESS: σ ' (kPa)

Figure 3.20

of the soil. This soil model predicts the upper limit of stiffness for the soil.

However, this upper limit may not be practically attained for the following reasons. First, thaw strain assumes drained conditions. For the ice-rich samples, there is certainly an excess of water thereby preventing the development of negative pore pressures. The soil would therefore rebound elastically with unloading from the residual stress state.

For thaw stable soils where no excess water exists after thaw, there is the question of the degree of saturation within the sample. Gas bubbles can be found in permafrost samples and are due to the exclusion of soluble air in water or due to the *in situ* decomposition of organic material (Roggensack, 1977). Because of bubbles within the sample, no significant negative water pressures could exist without developing cavitation. With pore water pressures at the cavitation pressure the soil would rebound with marginally stiffer behaviour than the case with water flow into the sample.

3.7.4 Impracticality of a Rigorous Representation of Stiffness

While the realities of applied stresses below the residual stress are such that a large difference in stiffness would occur solely dependent upon the development

of negative pore water pressures, the practicalities are such that the differences are moot. In this numerical analysis it is imperative that element stresses be developed that correspond with the volumetric strains rather than have a rigorous representation of the stress-strain curve. This is because of the highly variable ϵ_v:K relationship peculiar to thawing permafrost where the initial negligible modulus up to the thaw strain is followed by an extremely stiff modulus. The sample develops this residual stress over a relatively small volumetric strain increment. This is followed by a change in the modulus as the sample begins recompression consolidation. Thereafter, the sample stiffens gradually as consolidation proceeds.

The single most important difficulty with a material model like this is ensuring that the numerical model approximates the ϵ_v:K close enough to utilize the beneficial stiffness of the soil between the conditions of thaw strain and residual stress (Segment *B*, Fig. 3.20). With this stiffness, internal stresses are developed in the elements which oppose the external surficial and gravity loads. If the full value of the "residual stiffness" is not used, the elements do not develop the necessary internal stresses and must then deform further to do so, exhibiting a more flexible behavior than that predicted by the ϵ_v:K curve.

The reason that the "residual stiffness" may not be fully utilized lies in the numerical procedure associated

with the *ADINA* curve description model. The technique uses the current volumetric strain, ϵ_v, to determine what K value to use for the next time step. A meticulous analysis would require a discetization of the applied load that would re-evaluate the tangent stiffness at every change in bulk modulus. By allowing a less onerous loading criterion and increasing the load increments, the stiffness is inexact and deformations are overestimated in strain-stiffenning material and underestimated in strain-softenning material.

3.7.5 Load Discretization

The danger in using larger load increments with a modulus curve with a pronounced peak, is that the volumetric strains corresponding to the peak may be bypassed. This is especially a problem with thaw strain given the negligible initial stiffness of the material. This problem is analogous to the numerical solution to a latent heat problem modelled using a variable specific heat capacity.

For the study of thaw assuming a normally consolidated soil, exponential ϵ_v:K relations were linearized to be input into the *ADINA* curve description model as shown in Fig. 3.15. With the revised residual stress model, however, the flexibility of linearizing curves is much reduced since four of the six (ϵ_v:K) input pairs must be used to describe the thaw strain and residual stress portions of the curve. Fortunately, the anticipated effective stress for any one

element is of the same order of magnitude as the residual stress for most of the soils. As a result, not much extrapolation of the ϵ_v:K curve was necessary beyond the residual stress.

3.7.6 Soil Behaviour Beyond the Residual Stress

To obtain a soil stiffness at stresses above σ'_0, the e-$\log \sigma$ behaviour of the soil must be known.

From the residual stress, an increase in load will reduce the void ratio along the thaw-recompression curve (Figure 3.21), similar to a consolidation recompression curve which recompression curve defines the e-$\log \sigma$ behaviour of a uniformly overconsolidated material. In contrast, the thaw-recompression curve defines the behaviour of a non-homogeneous material comprised of highly overconsolidated soil peds and re-saturated soil adjacent to the relic macropores. Thus the thawed soil behaviour is highly dependent on the soil's freezing history, so the thaw-recompression index would be best determined experimentally.

3.7.7 Freezing Reconsolidation Pressure

The e-$\log \sigma$ curve of thaw recompression would be expected to converge with the virgin compression line at higher stresses since segregation consolidation is just a special case of over-consolidation. What is found in the

literature, however, is a material behaviour of a stiff material at a much higher void ratio than expected. If we examine the e-$\log \sigma$ curves for residual stress specimens (Roggensack, 1977) and superimpose the remoulded virgin compression line of a material at the same site. (Nixon & Morgenstern, 1973) it is obvious that the e-$\log \sigma$ curves are consistent yet extend beyond the expected region of soil behaviour defined by the virgin compression curve (Figure 3.21). This results in the unusual situation of having a soil with overconsolidated stiffness at a void ratio higher than that of the virgin remoulded material.

3.7.7.1 Different Materials

There are three possible explanations for such behaviour. The first is that the material used for the virgin remoulded compression differred in kind from the field samples. This is possible given the 8km separation of the two sites. The pro-glacial geomorphology of the region, however, should have resulted in extensive, fairly uniform fine-grained strata which should exhibit similar compression characteristics throughout the region. This is further supported by the consistent compression behaviour over the full depth of the soil, even over the progression of facies from the highly plastic silty clays of depth to the low plasticity clays and silts nearer the surface. The reported clay and silt fractions at the Norman Wells CAGPL (Nixon & Morgenstern, 1973) are consistent with the grain size

e - log σ' Curves for Residual Stress Test Specimens, Borehole NW2
(modified after Roggensack, 1977)

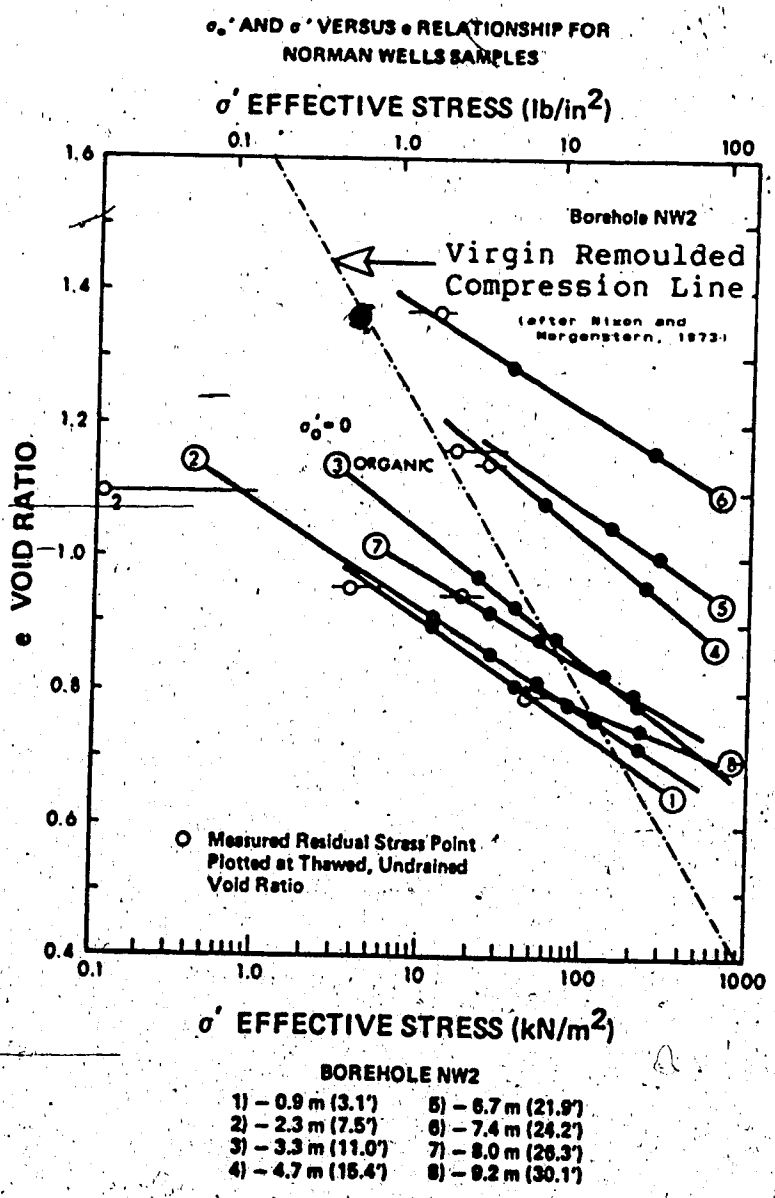

Figure 3.21 Residual Stress *e-log σ* Curves

curves of the material from the top 5m at the Norman Wells MVPL site (Roggensack, 1977). Given that the material would seem to be very similar, and that the virgin remoulded compression line is well within the *e-log σ* data points, other factors may have contributed to this discrepancy.

3.7.7.2 Influence of Organics

One distinguishing feature of this material as compared to "typical" soils is the high organic content of the soil. Nixon and Morgenstern (1973) found an organic content of 6 to 10% and Roggensack (personal communication) found up to 15% to 20% by weight of organics in the form of decomposed material and, more importantly, in the form of undecomposed leaves, sticks, twigs and roots. Given the strength of undecomposed organics their porosity, a higher void ratio should be expected. It is unlikely that samples with high contents of undecomposed organics were used in the correlations tests as the inclusion of organics in the samples would affect the results. Insufficient data prevents a quantitative analysis of the results.

3.7.7.3 Homogeneity

There is another possible cause for the higher stiffnesses at higher void ratios than the virgin remoulded compression curve. This stems from questioning the assumption of homogeneity of the sample which is the

usual premise of consolidation tests. In the standard consolidation test, a nominally homogeneous sample is loaded under drained conditions, becoming another, denser, homogeneous material. Even under unloading and reloading the material remains homogeneous. In the case of consolidation followed by a freeze-thaw cycle under undrained conditions the sample will undergo structural change. If the freezing is "instantaneous", resulting in a massive sample with no internal variation in moisture content, the resultant thaw strain at the consolidation load would be expected to be minimized. However, a freezing process that resulted in a highly non-homogeneous material of segregated ice and overconsolidated soil peds would be expected to undergo a larger thaw strain because of the meltout of the segregated ice.

After thaw-straining, the formerly segregated material should behave stiffer than a uniform material at the same void ratio due to the "intergranular" effect of the soil peds. The degree of sample stiffening will depend upon the connectivity of the soil peds, as this will affect the load carrying ability of the soil peds. Given a continuous layer of softer material in a relic macropore, for example, the segregated material would exhibit softer behaviour than a uniform material at the same void ratio. This would continue until sufficient consolidation had occurred to mobilize the greater

bearing capacity of the soil ped network. At increased loads the stiffening effect of the soil peds would be less significant due to the realignment of the soil peds and the general stiffening of the surrounding matrix. The re-adjustment of the soil peds within the matrix may result in a net decrease in void ratio, which would be observed as a sharp increase in the slope of the compression curve.

The results presented by Nixon & Morgenstern (1973) and of Roggensack (1977) are for the working range of pressures normally associated with thawing permafrost. As such, the range of applied stresses is narrow. It would be of benefit to examine thaw-consolidation behaviour at higher stresses to see if the segregation-recompression curve behaved as a recompression curve and rejoined the virgin remoulded compression line, or if a structural softenning were observed, as might be expected given the soil model described above.

3.8 Implementation of Residual Stress Theory

The following algorithm was used to determine input parameters for the residual stress portion of this study. The β-function was used to generate ten A_o values for the numerical analysis. These thaw strains were correlated with frozen bulk density, ρ_b^f, using the relationship developed by Speer, *et al.* (1973). Knowing the thaw strain and frozen

bulk density, and assuming a density of solid particles, ρ_s, all other soil parameters can be calculated. The thawed undrained void ratio, e_u^t, was used to predict the residual stress, σ_0', using the relationship for Norman Wells silt at 5m to 12m depth (Roggensack, 1977).

The residual stress was implemented into the ϵ_v:K curves in two ways. For thaw strains below a 5% volumetric strain, the residual stress was developed by using a high initial modulus so that under oedometric conditions the residual stress would exist at the volumetric strain corresponding to the thaw strain. For thaw strains exceeding 5% volumetric strain, the high step modulus was used within the 5% volumetric strain immediately preceeding the thaw strain. For post thaw strain behaviour, all elastic parameters were calculated from segregation-recompression curves similar to those in Figure 3.21. From these, the slope of the compression line beyond the residual stress or the "segregation-recompression coefficient", C_{sr}=0.16 was determined. All these calculations and the resultant β-distributions and *ADINA* input parameters were calculated in program *BETARESID* (*viz.* Appendice D).

3.9 Residual Stress Results

The layered soil problem was re-analysed using the residual soil concept (Figure 3.23). The resulting thaw settlement of 2.341m is remarkably close to that anticipated by an extrapolation of one-dimensional analysis. The

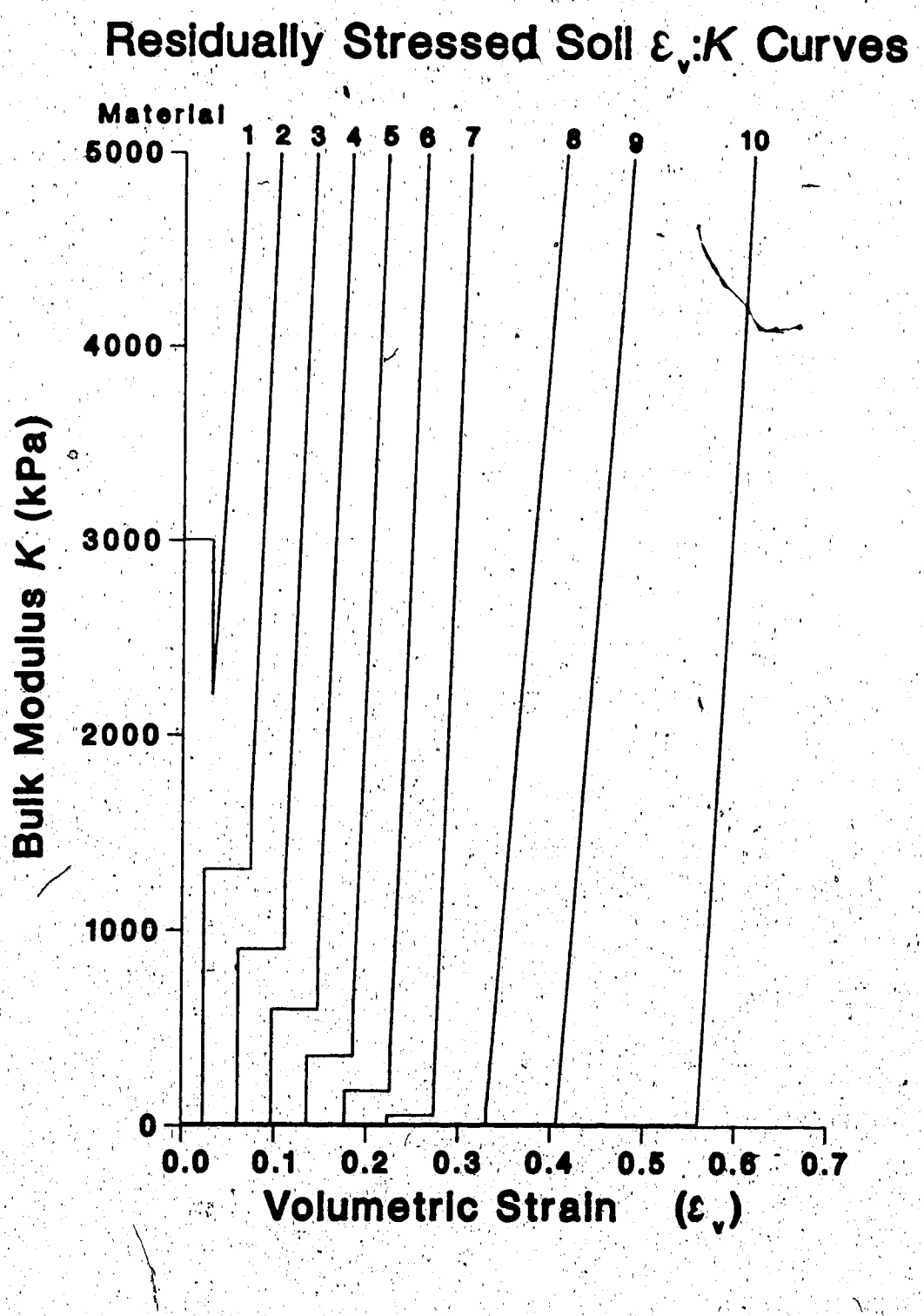
Residually Stressed Soil ε_v:K Curves
Material
1
2
3
4
5
6
7
8
9
10
5000
4000
3000
2000
1000
0
Bulk Modulus K (kPa)
0.0
0.1
0.2
0.3
0.4
0.5
0.6
0.7
Volumetric Strain (ε_v)

Figure 3.22

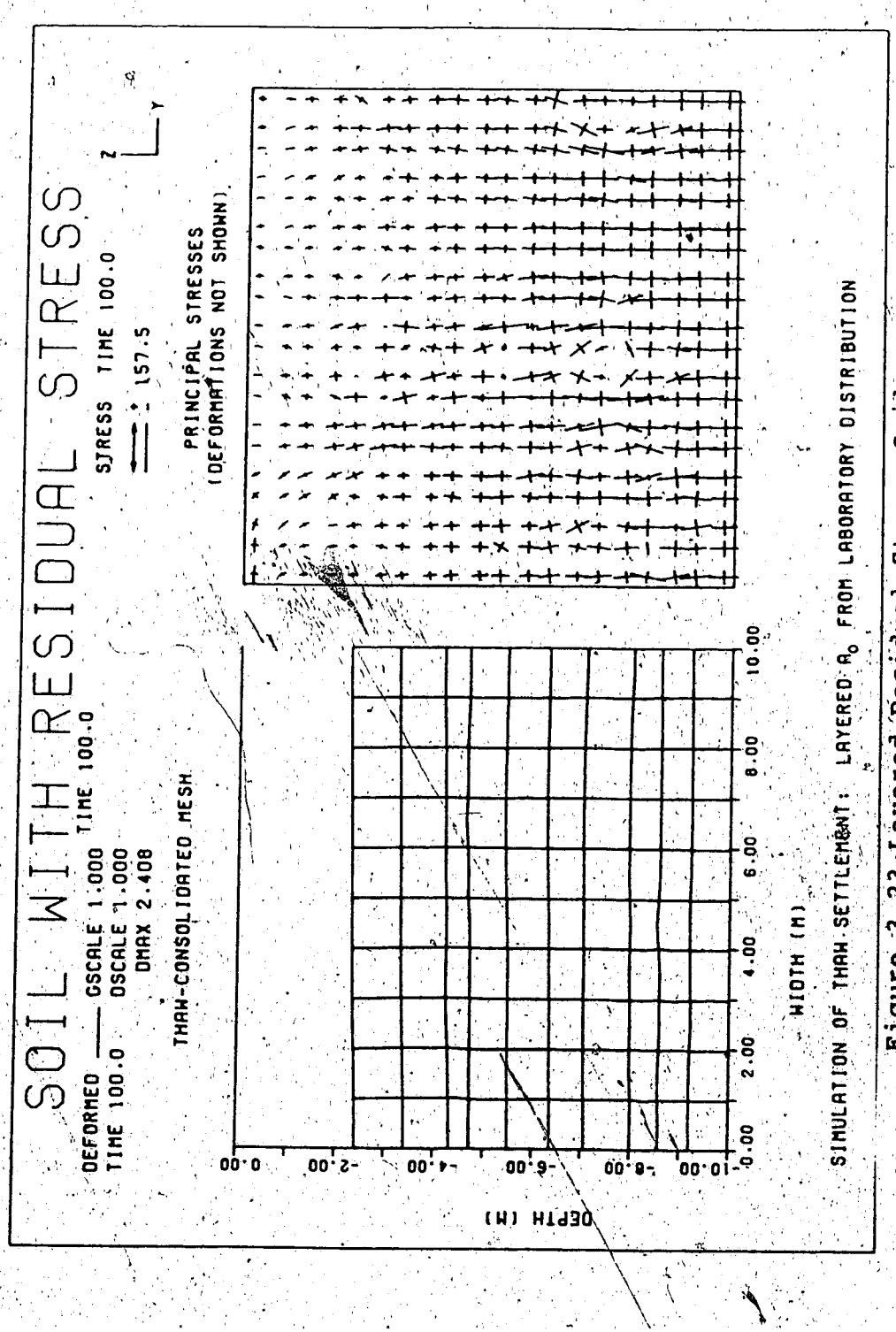

Figure 3.23 Layered Residual Stress Soil

settlements are relatively consistent throughout the mesh but the stress field exhibits some perturbations. This disturbance in the stress field is probably due to the combination of highly varying material stiffnesses and cummulative numerical imprecisions over the 100 time steps. The number of time steps was increased to accommodate the newer, more variable ϵ_v:K curves.

Mixing the materials randomly as shown in Figure 3.17 and applying loads (using 80 time steps) the settlement results were better than the layered analysis. The average surface settlement of 2.152m was 93% of the layered analysis and a significant improvement over the 3.511m predicted using the normally consolidated soil model (Figure 3.24).

The mechanism by which this improvement occurs is very clearly shown in Figure 3.25. At this point, no gravity loads have been applied and the surficial load has only increased to 1.4kPa. (The smaller stresses were not plotted for the sake of clarity.) A definite development of shear stresses was actually re-directing load onto the stiffer materials, in particular the column of stiff materials in the lower-right of the mesh. (*ref.* Figure 3.17). This significant contribution of the stiffer materials to mitigating settlements prompted this study of the effects of material variability on thaw settlement.

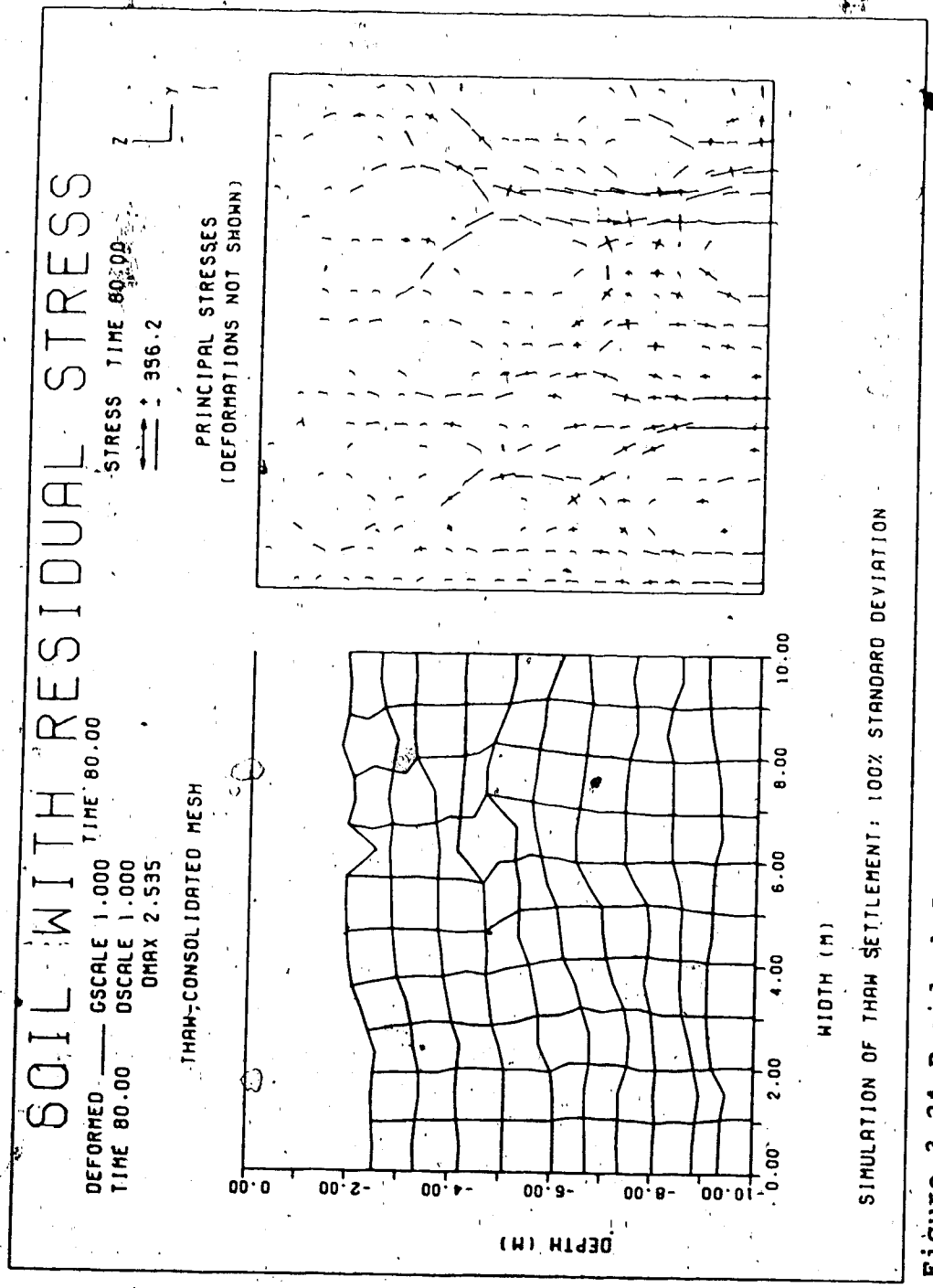

Figure 3.24 Residual Stress Soil of 100% A_o Standard Deviation - Full Load

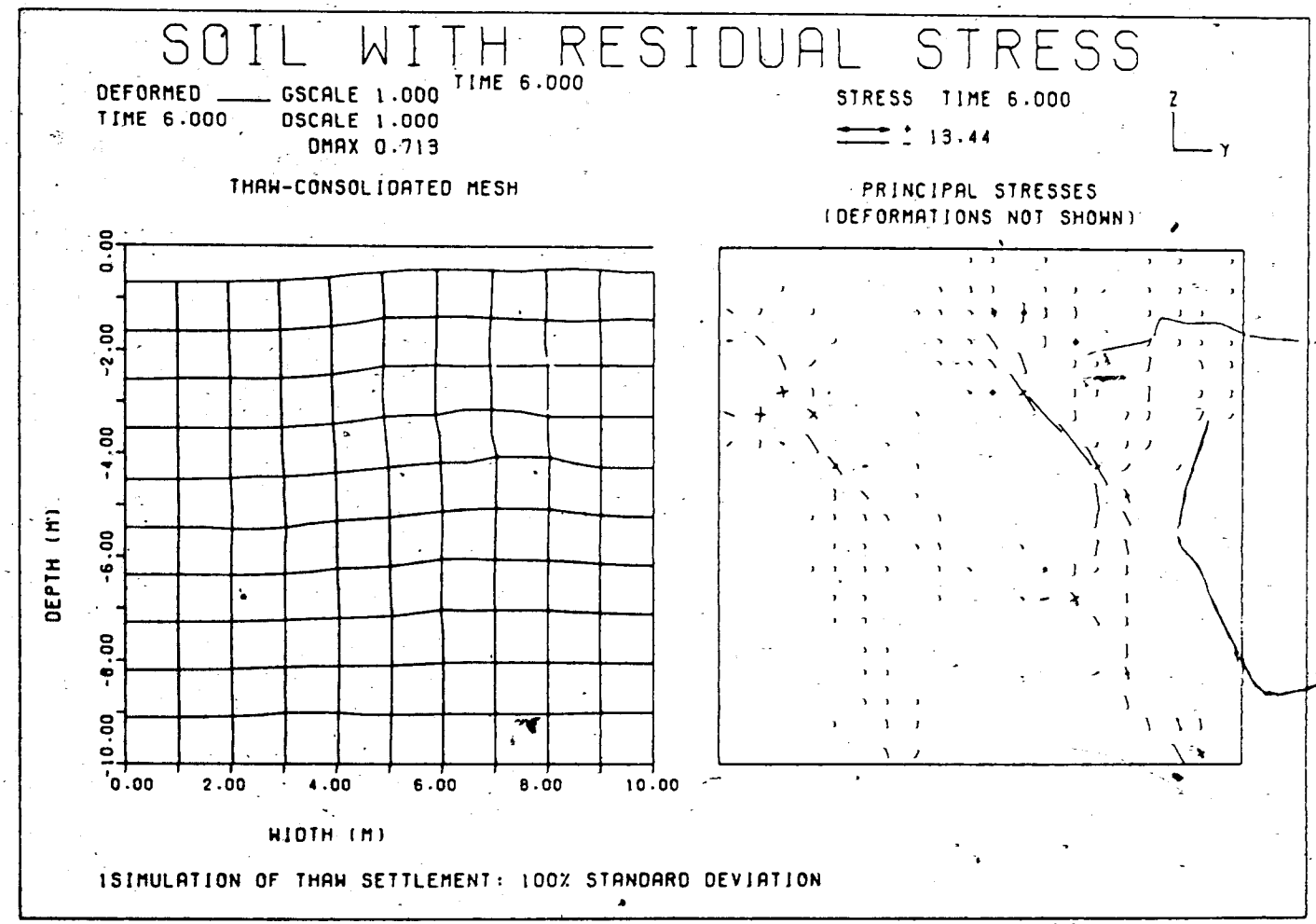

Figure 3.25 Residual Stress Soil of 100% A_o Standard Deviation - 9kPa Surficial Load

3.10 Thaw Strain Variability

The initial step in this series of analyses was to determine thaw strain distributions of different variances, yet maintain the average A_o value for comparison with the one-dimensional approach. By varying the standard deviation of the A_o distribution, and using the richness of the β-function, the PDF's for a number of arbitrary distributions were obtained (Figure 3.26). For each of these distributions, A_o values were generated and input as residual stress soils into the *ADINA* program. The results of these analyses are shown in Figures 3.27 through 3.32.

3.10.1 Settlement Reduction due to Material Variation

There are definite trends present in the results. The most significant result is the reduction of surface settlement with increased A_o variance (Figure 3.33). This was expected to be a result of improved soil arching ability and this is corroborated by the marked increase in maximum mesh stress as summarized in Figure 3.34. For comparison, the results of the analyses for the normally consolidated soil model have also been plotted. Re-examining Figures 3.27 through 3.32, it is also evident that an increase in variance also results in a more irregular surface profile, higher element distortions and significant variations in stress orientations and magnitudes.

While the improvements are due to material differences, there is also the effect of the Eulerian assumptions of

Beta Functions of Different Variances

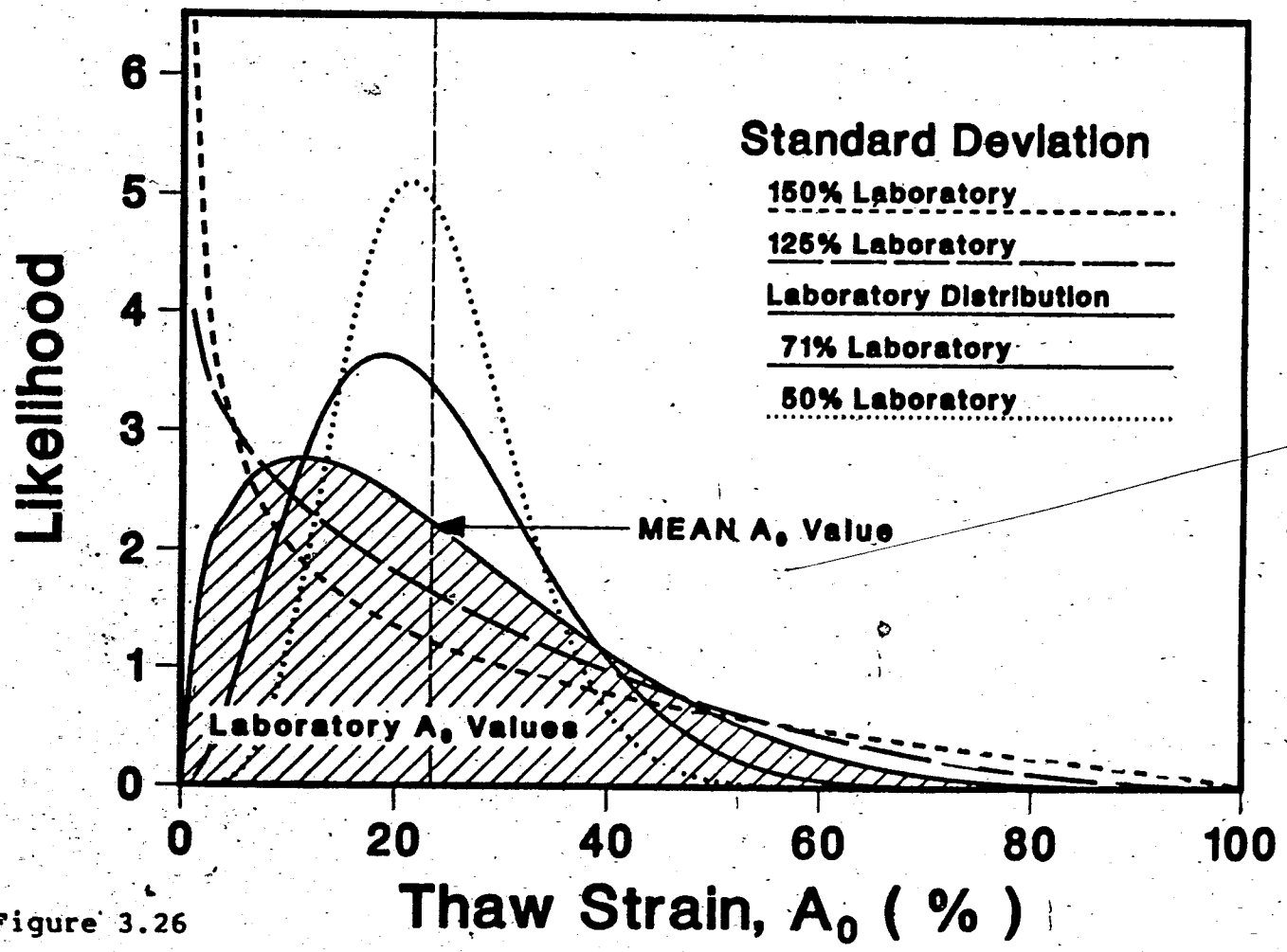

Figure 3.26

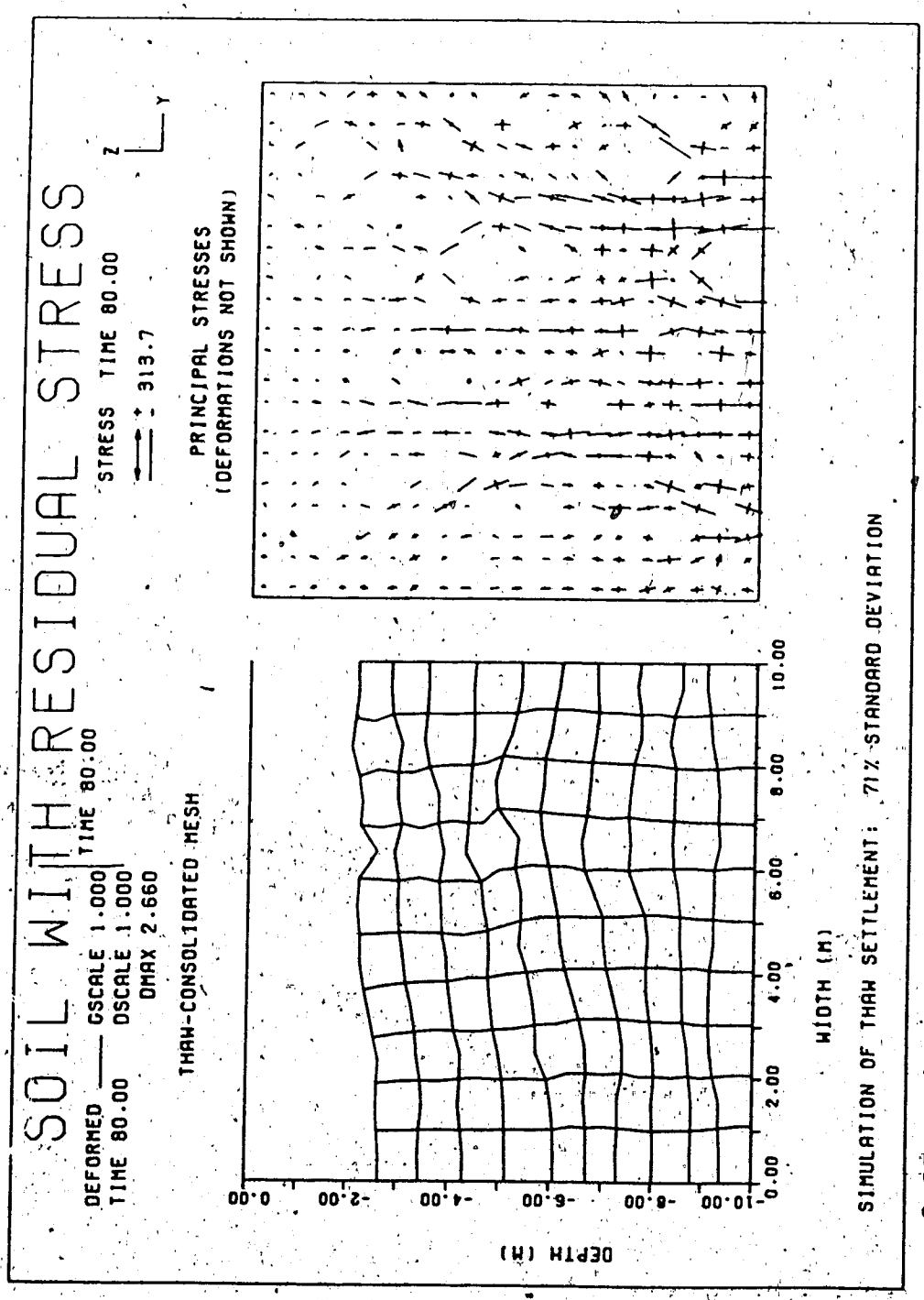

Figure 3.27 Residual Stress Soil of 71% Standard Deviation - 9kPa Surficial Load

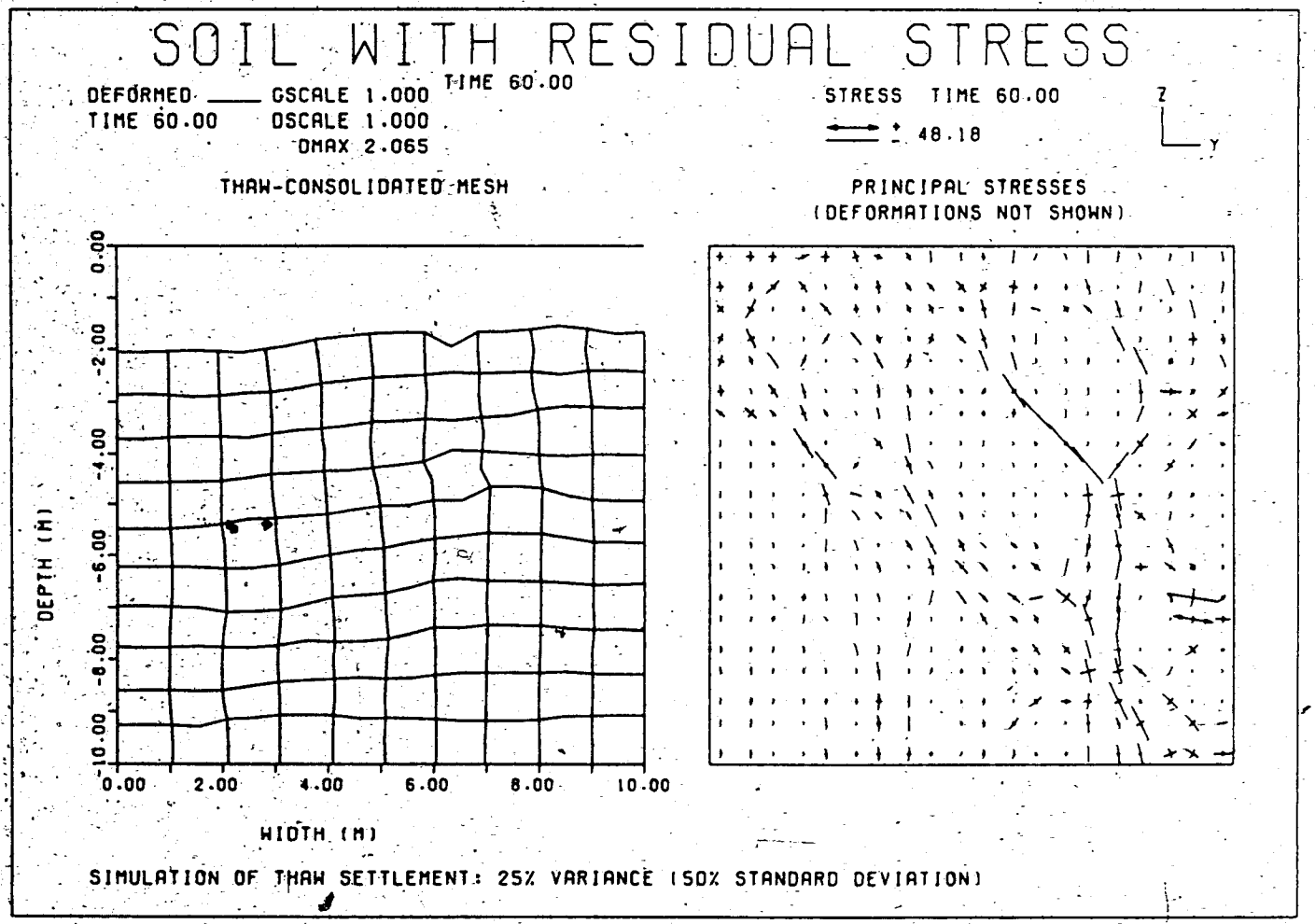

Figure 3.28 Residual Stress Soil of 50% Standard Deviation - 9kPa Surficial Load

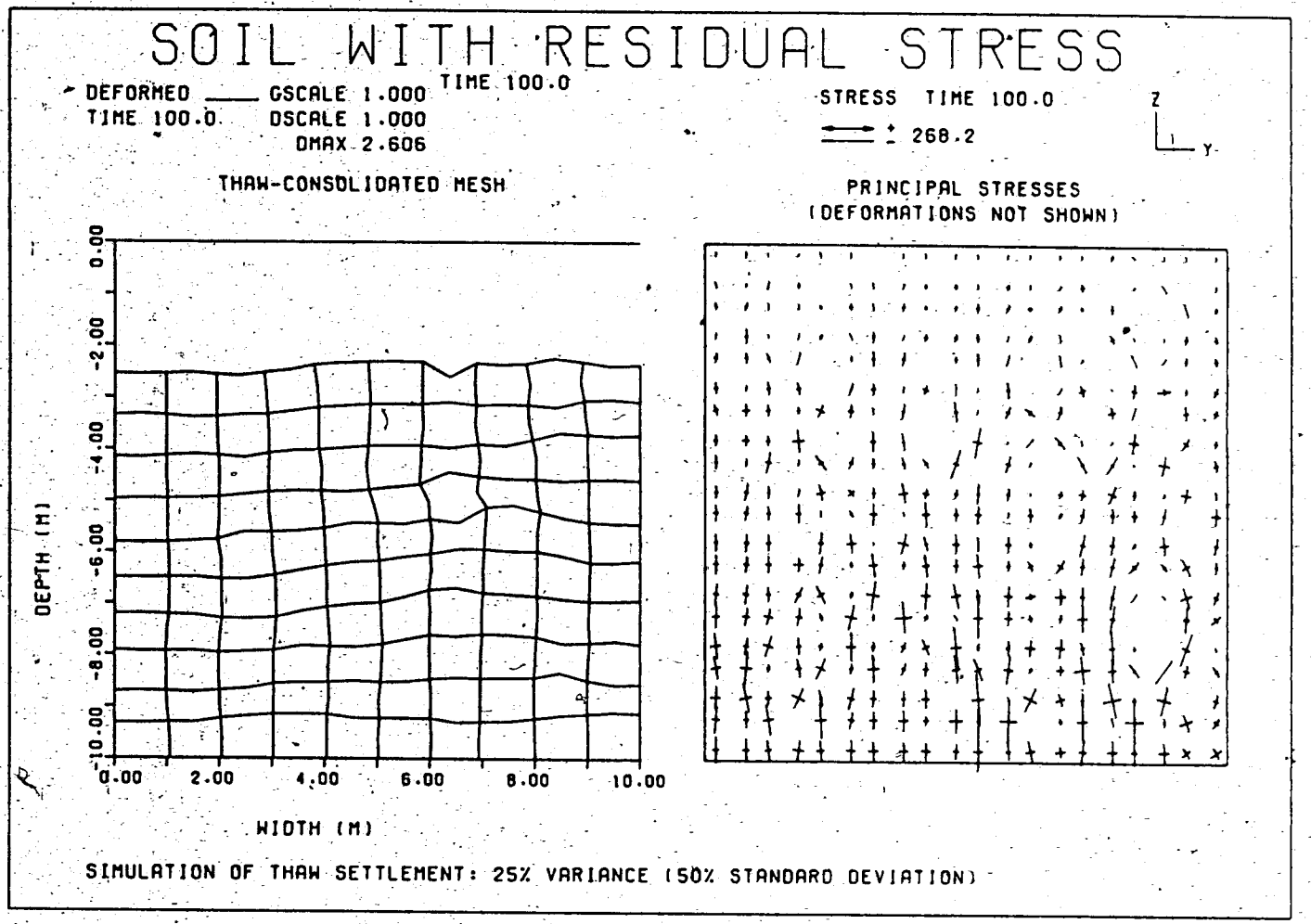

Figure 3.29 Residual Stress Soil of 50% Standard Deviation - Full Load

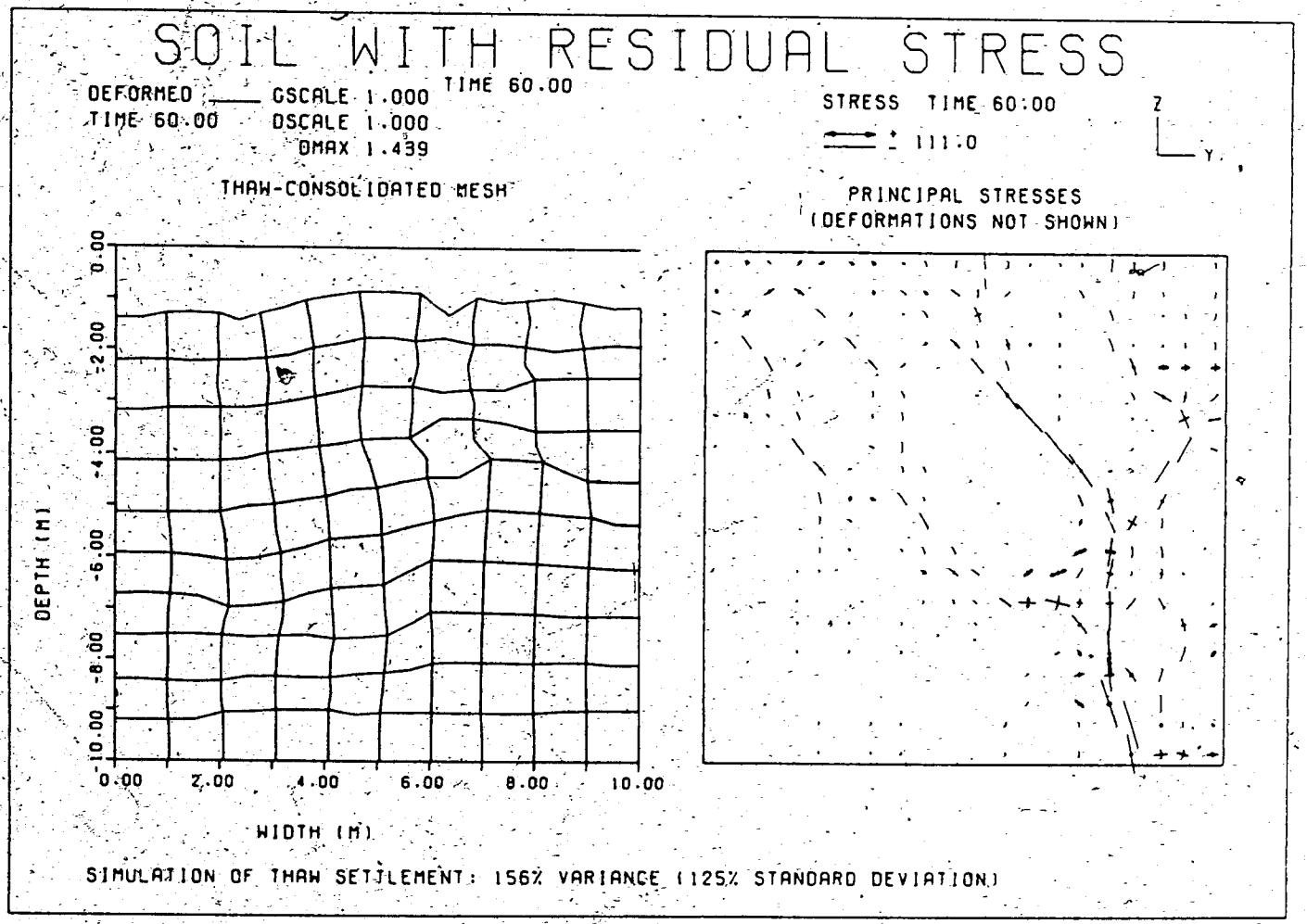

Figure 3.30 Residual Stress Soil of 125% Standard Deviation - 9kPa Surficial Load

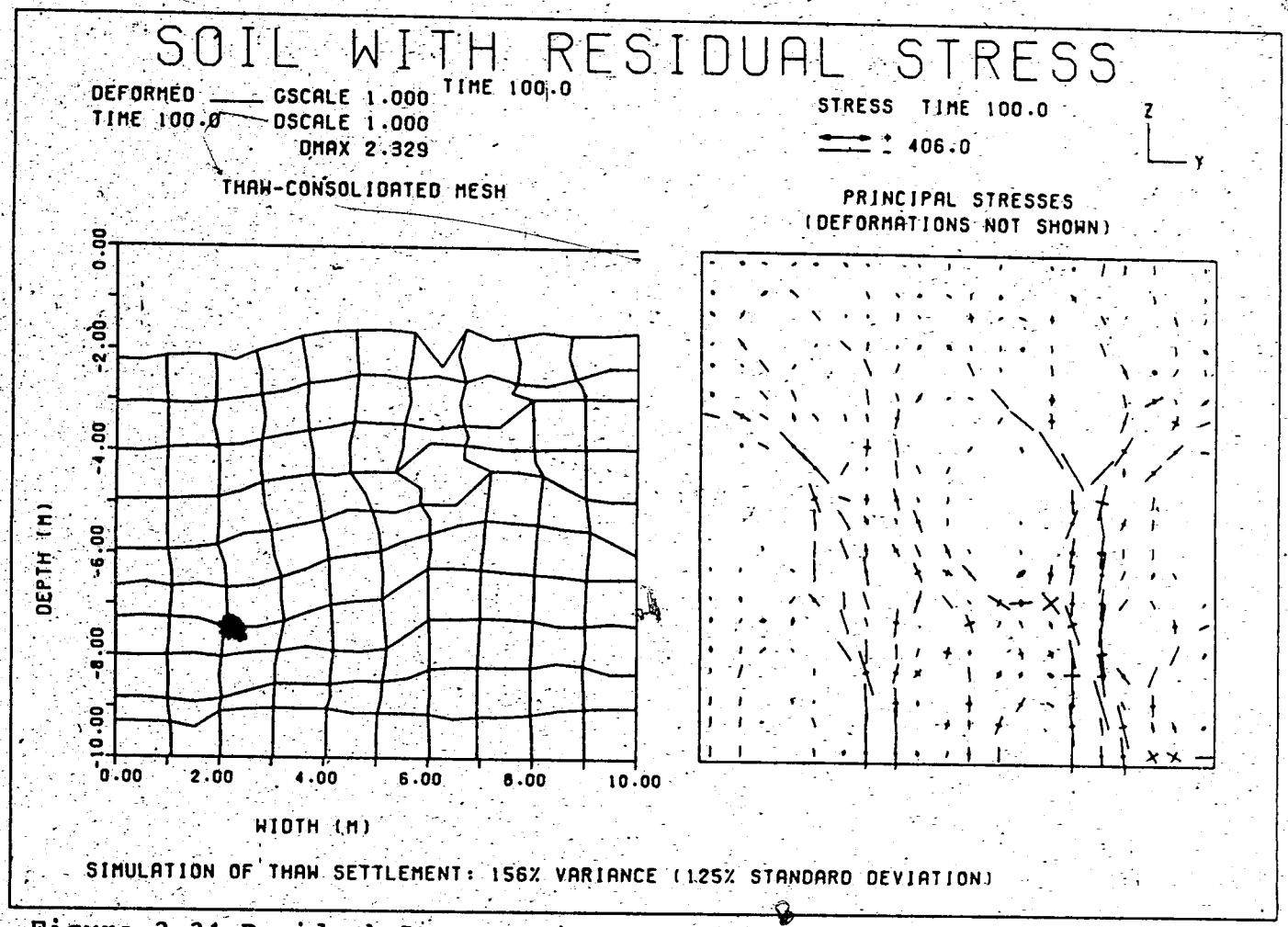

Figure 3.31 Residual Stress Soil of 125% Standard Deviation - Full Load

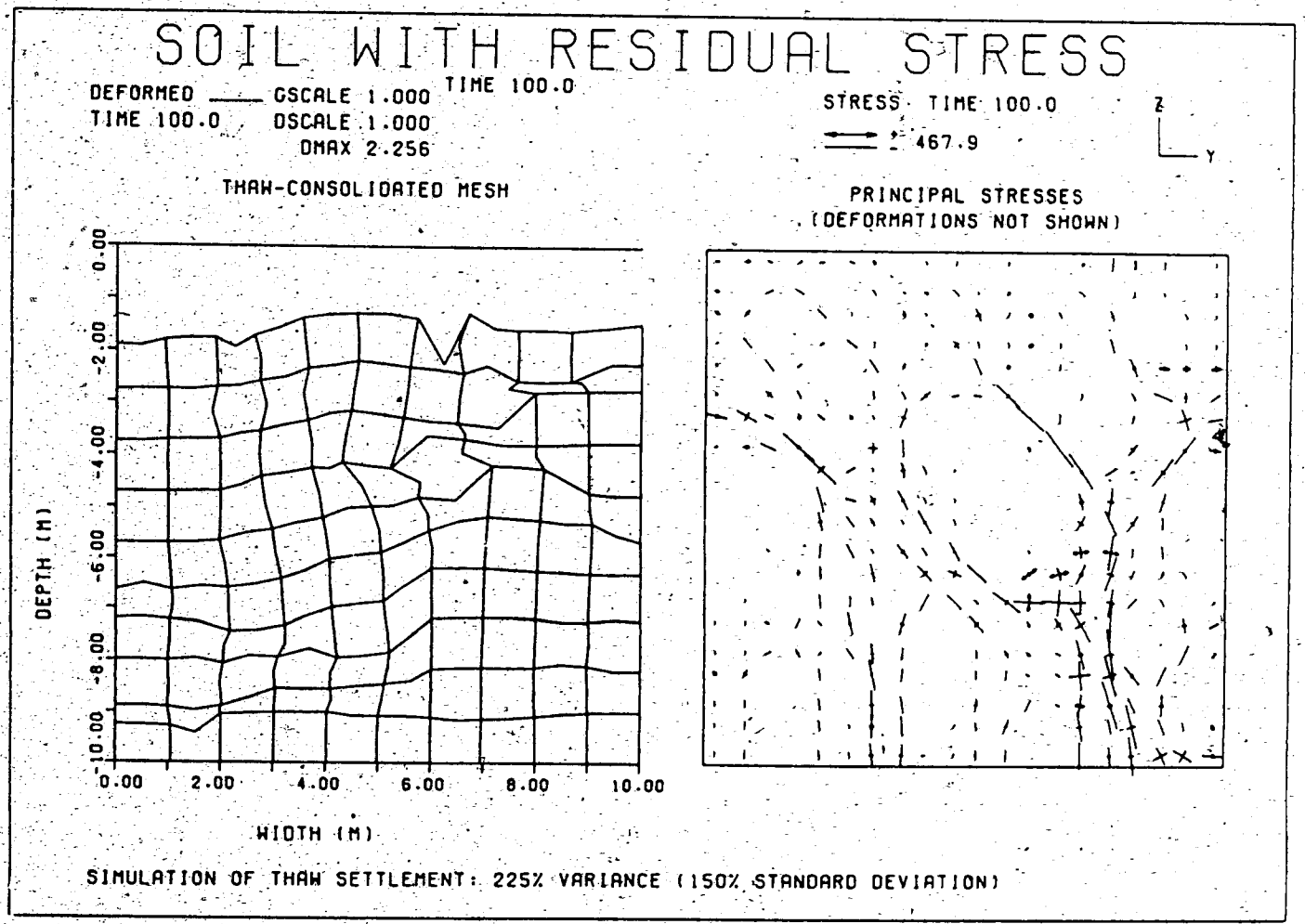

Figure 3.32 Residual Stress Soil of 150% Standard Deviation - Full Load

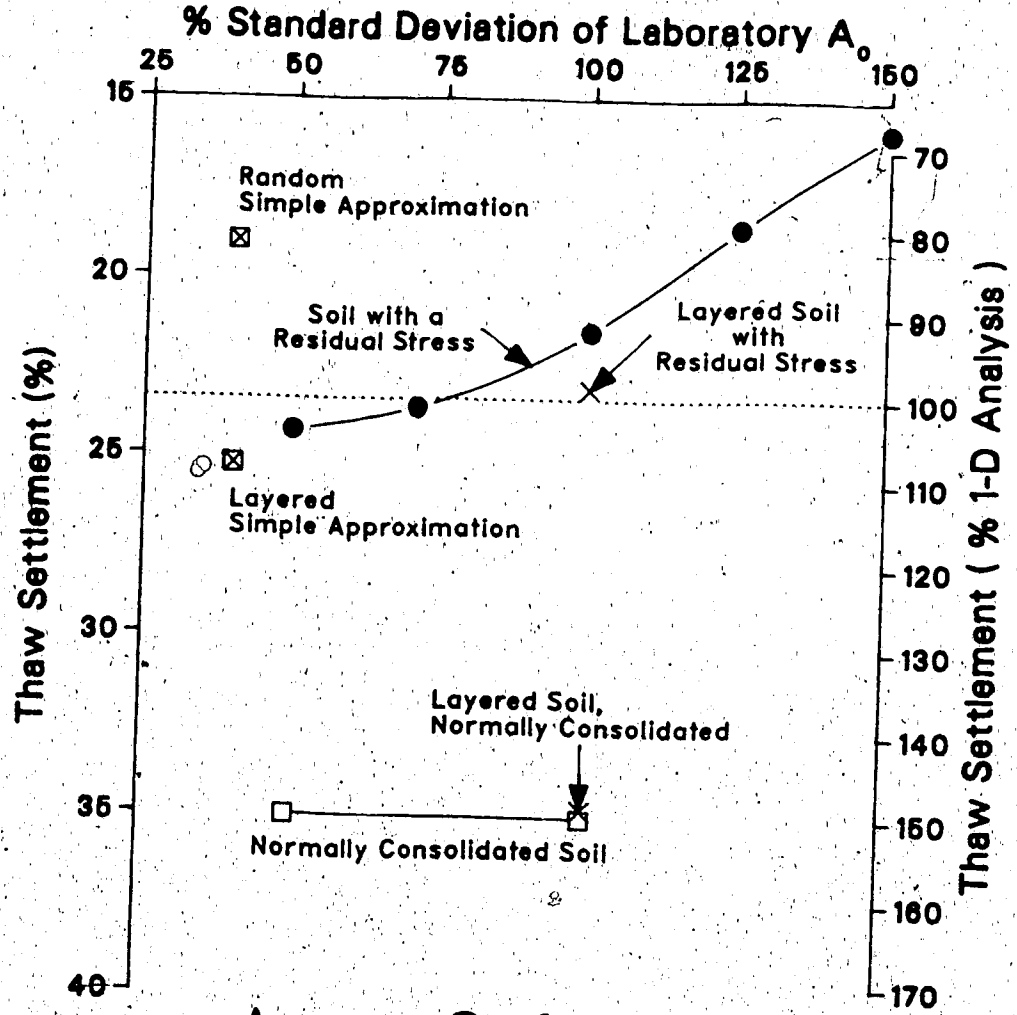

Average Surface Settlement
as a
Function of Thaw Strain Variability

Figure 3.33

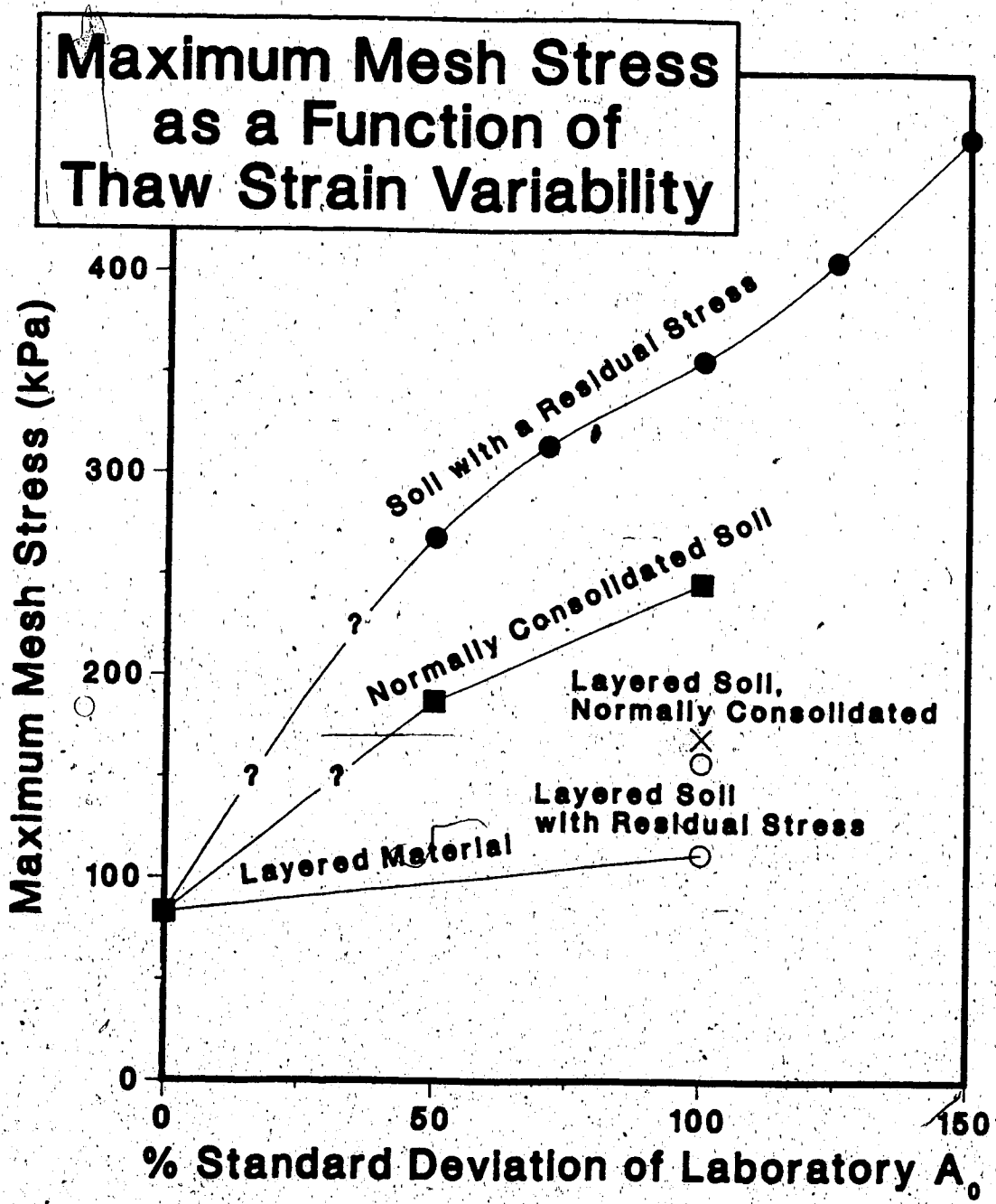
Maximum Mesh Stress as a Function of Thaw Strain Variability
Maximum Mesh Stress (kPa)
400
300
200
100
0
0
50
100
150
% Standard Deviation of Laboratory A_0
Soil with a Residual Stress
Normally Consolidated Soil
Layered Soil, Normally Consolidated
Layered Soil with Residual Stress
Layered Material
?
?
?

Figure 3.34

small strains and small displacements. It is difficult to quantify the numerical effect without performing total or updated Lagrangian analyses. Unfortunately, the updated Lagrangian formulation within *ADINA* was incompatible with the curve description model and the total Lagrangian analysis was excessively unstable and provided numerically inconsistent results.

3.11 Conclusions

The premise that a variation in the thaw strain parameter can result in improved settlement behaviour when considered in two dimensions was examined, and the results are very promising. This reduction in surface settlements with increased A_0 variance extends beyond the predictive capability of the one-dimensional analyses used currently in practice. Because the design of strain-sensitive structures such as pipelines is largely controlled by the predicted settlement behaviour of the ground mass, any improvement in the soil description results in considerable savings. This is particularly the case for capital-intensive projects such as pipelines.

The beta distribution was found to be a highly recommended means of representing the thaw strain data. With its limited range, combined with its richness of form, the beta function naturally lends itself to other geotechnical applications.

Assuming that the soil was a normally-consolidating material obviated the fact that each material would have an initial stiffness that was not negligible. Representing the soil as a material with residual stress provided the necessary means of stiffenning the material without excessive strain deformations. In retrospect, the initial analysis assuming a bi-linear stress-strain relationship was not inappropriate for a first-order analysis.

It has been shown that the results are primarily a function of the A_0 variance, with material properties and numerical effects having a secondary influence. An attempt was made to quantify the effects of the small strain and displacements by performing a Lagrangian analysis with little success. Preliminary results, however, indicated that the Lagrangian analysis would predict an even larger reduction in settlements as a result of the A_0 variance. This would agree with the findings of others (Hwang, *et al.*, 1971; Bathe, *et al.*, 1975; Carter, *et al.*, 1979; Chen and Davidson, 1977) and would be consistent with a behavioural appreciation of soil arching.

The number of nodes per element had a significant effect on the results. Although the elements could be made even more complex, it is unlikely that any further improvement would be gained. Instead, some consideration should be given to the further discretization of the mesh, so that each block of material would be made of four or nine

elements. This would provide some measure of convergence for the mesh. This was not done due to time limitations and because the assumption of discrete blocks of different A_0 material is, in itself, an approximation.

3.12 Validity of the Results

With any numerical analysis the results must be carefully scrutinized and compared to closed-form solutions whenever possible. This ensures that the precision of numerical results is not confused with their accuracy, and it develops confidence in interpolating between solutions with corroborated results.

3.12.1 Load Discretization

The results of the preliminary numerical analyses, (Table 3.1) show the effect of load discretization on displacement behaviour. This effect is particularly important when using the curve description model because applied loads affect the displacements which, in turn, determine the volumetric strains controlling the subsequent stiffness matrix. The results show that refinement of the loading increment will provide a closer representation of the exact stress-strain relationship as described by the ϵ_v:K parameters. This effect would become less pronounced as the change in moduli was smaller or occurred gradually. Load discretization was refined to prevent any substantial cummulative error.

3.12.2 Material Properties

Varying the material parameters had less effect on the overall performance of the mesh than did the various loading schedules. Using a variable Poisson's ratio of $\nu=0$ for thawing and $\nu=0.3333$ afterwards only increased settlements by *1%* to *3%*. Tripling the bulk modulus from $K=2000kPa$ to $K=6000kPa$ only reduced the average surface settlement by *4%*. In comparing the runs assuming a normally consolidated material with those assuming residual stress, the marked difference in settlements shows that some account must be taken of the beneficial post-thaw stiffness of the permafrost.

3.12.3 Mesh Geometry

The geometric constraints imposed by the choice of elements are significant. Comparing the difference in settlement predictions using 4-node and 8-node elements, a *17%* improvement was observed. It should be noted that both the ν and the K differed for this comparison; however, based on the mesh's relative insensitivity to reasonable variations in these parameters the major contribution was from the numerical effects.

3.13 Small Deformation versus Large Deformation Analysis

This analysis was done using the assumption of small strains and deformations. This was carried out in order to use the simpler finite element formulation within *ADINA*

since preliminary runs using large deformation (Lagrangian) analysis proved to be unstable. Simulations of one-dimensional consolidation using small strain analysis also were quite satisfactory. However, it remained to be seen if the results of the subsequent analyses could be relied upon, both qualitatively and quantitatively.

The large deformations of thaw straining results in geometric non-linearity. This will influence the analysis' equilibrium equations and strain:displacement equations and there is a gross distortion of the elements. The equilibrium equations are affected because the formulations change, introducing second order effects such as buckling for an axial compression number. The strain:displacement equations must be altered to account for the redirection of forces e.g. when a beam exhibits catenary characteristics after significant bowing. Finally, the distortion resulting from the large deformations can result in substantial changes in area. Bathe, *et al.*, (1975) cite an additional 50% deformation using large deformation analysis of a rubber sheet with a hole in it under axial entension. Conversely, unconfined compression should produce reduced deformations due to an increase in area.

3.13.1 Previous Experience

Despite the simplistic approach in using small deformation analysis for the thaw strain problem, other writers' experiences were encouraging. Hwang, *et al.* (1971),

used small deformation finite element methods to study plane strain consolidation problems. They predicted transient pore pressures and effective stresses to obtain settlements and degrees of consolidation. Notably, they found an excellent correlation with the closed-form solution to the problem of a strip footing on a consolidating stratum. This involved varying two-dimensional stresses and deformations as does the variable thaw strain analysis. Carter, *et al.* (1979), examine the consolidation of an elasto-plastic soil subject to finite deformations. The writers show that small strain analysis of a footing on a consolidating elasto-plastic stratum shows results similar to the large strain analysis until the collapse loads are approached at approximately 15% of the mesh depth. For a purely elastic soil, less agreeable results were obtained, assuming a constant shear modulus throughout the consolidation. The poorest results were for high load/low modulus cases beyond the range of the thaw strain analyses. Also, this analysis was for a loaded footing that resulted in significant differential settlements and accompanying shear distortions, rather than an extensive surface pressure, as is the case for this work.

Chen and Davidson (1977) study the static response of homogeneous clay with elasto-plastic behaviour with yield capability. After developing their finite element formation for large deformation analysis the writers provide the results of four analyses, comparing the large deformation analysis with the small deformation analysis. For an elastic

material under oedometric strain conditions, the large deformation analysis showed improved soil behaviour with increased strain. This is because this analysis can approximate the logarithmic strain due to the strain-shortening of the material, whereas the small deformation analysis cannot and thereby conservatively underpredicts the system's stiffness. Similarly, for a footing on a soil stratum, deformations of comparative stresses are smaller for the large deformation analysis therefore the system is stiffer. In addition, the stress predicted by the small deformation analysis approach a maximum while the large deformation analysis predicts a continuing ~~rise in~~ stresses. Again, the small deformation analysis provided the conservative result.

The exception to this pattern was the analysis of a 30ft vertical cut slope in which the crest settled 5ft and the toe bulged 2.3ft. In this case the small deformation analysis gave higher stresses and exhibited stiffer behaviour. The writers astutely point out that the slope analysis studies a weakening effect and not a strengthening one as for the previous two analyses.

The thaw strain analyses of this work are generally of a strengthening phenomenon. This is not only due to the strain-stiffening ϵ_v:K properties assigned to the various materials, but because the structural behaviour of random thaw-straining soils is an improvement over the averaging

techniques used to date. The results of these small deformation analyses of thaw strain should provide a conservative lower limit to the exact behaviour of the soils. An exception to this may be made for highly variable A_o soils where thaw straining may result in high shear strains. The soil should then exhibit strain softening behaviour, such as that proposed by Nixon, *et al*. (1983). This would begin to homogenize the stress and deformation fields and lessen the benefits of high A_o variance. In the limit, an increase in variance may actually increase thaw settlements by isolating stiff materials within a matrice of ~~less st~~iff materials and by increasing the shear stresses within the soil. However, it would be highly unlikely that a material of this nature would be modelled with this type of analysis.

3.13.2 An Attempt at Lagrangian Analysis

Previous finite element runs were used to quantify the small deformation-large deformation discrepancy. The material ϵ_v:K curve used for the analysis was that of material type 4 of the residual stress analysis since its thaw strain was close to the average thaw strain. After applying no gravity loads and a surficial pressure of 0.6kPa over 30 time steps, the Lagrangian (large deformation) analysis was discontinued due to the spurious results (Figure 3.35). This was in spite of the tightened energy convergence tolerance in *ADINA*.

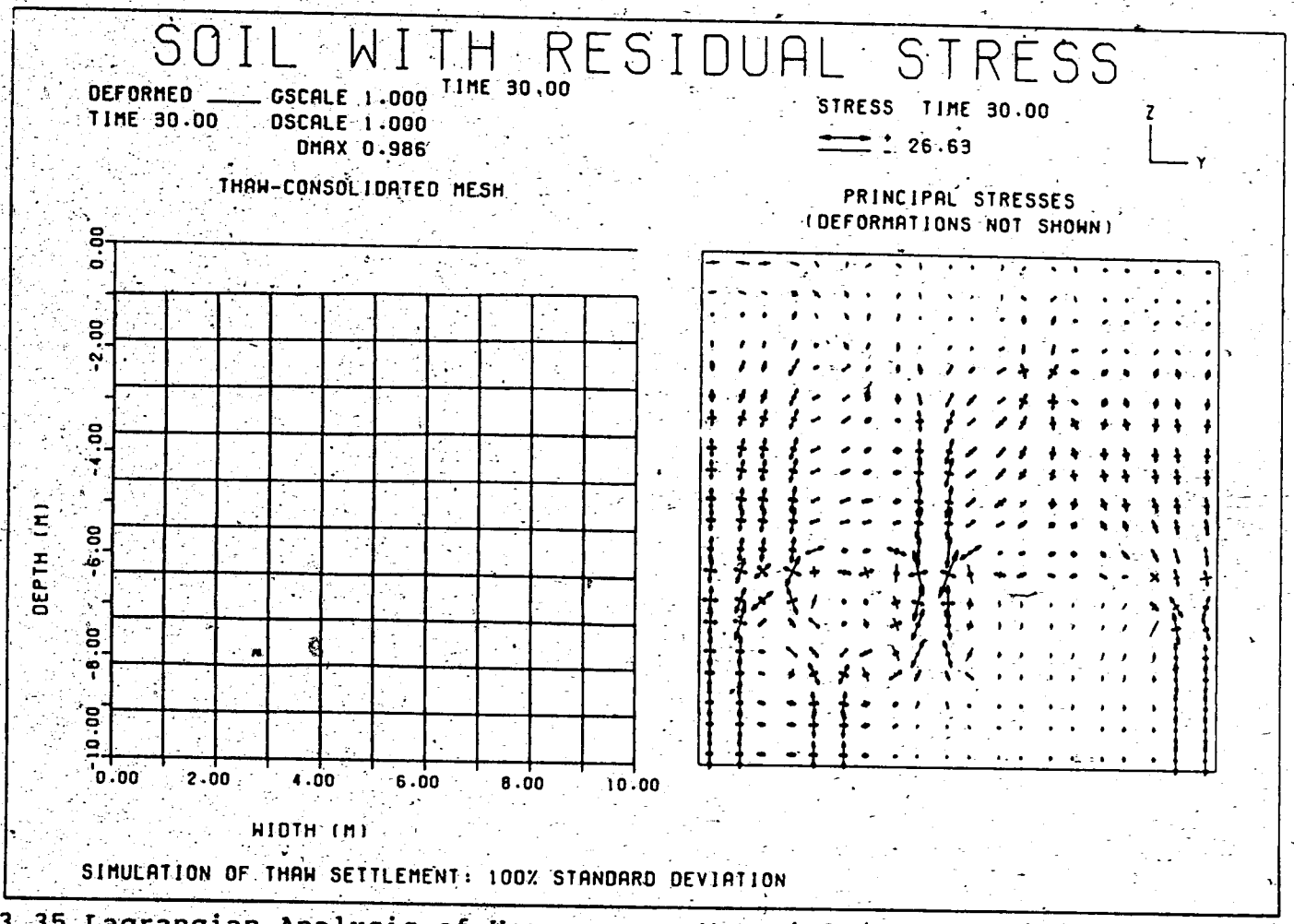

Figure 3.35 Lagrangian Analysis of Homogeneous Material (under partial surface loading)

The Lagrangian analysis was rerun for the laboratory distribution of A_o. The results, (Figure 3.36) are very encouraging. After incrementally applying a uniform surficial pressure of 0.603kPa over 50 time steps, the analysis shows improved arching behaviour over the small deformation analysis, with stresses in the stiffest elements being twelve times the surficial stress. This improvement is due to the true arching effects achieved through the Lagrangian formulation's inclusion of strain deformations. The analysis became unstable at the sixtieth step due to high stresses in stiff elements adjacent to soft elements. The examination of the Lagrangian analysis was discontinued.

3.14 Other Statistical Applications to Thaw Settlement

3.14.1 Distal Settlements as a Random Process

Palmer (1972) investigated an application of statistics to the settlement of pipelines on thawing permafrost. The use of statistics was justified because of the impracticality of undertaking a detailed field study for the entire route of a pipeline. Instead, statistics were used to predict the frequency of exceeding a pipeline's design strain.

This was done in two ways. The first method assumed that settlement was a random process which could be modelled with a normal *PDF*. An auto-correlation could then be performed, relating the settlement at any given point with

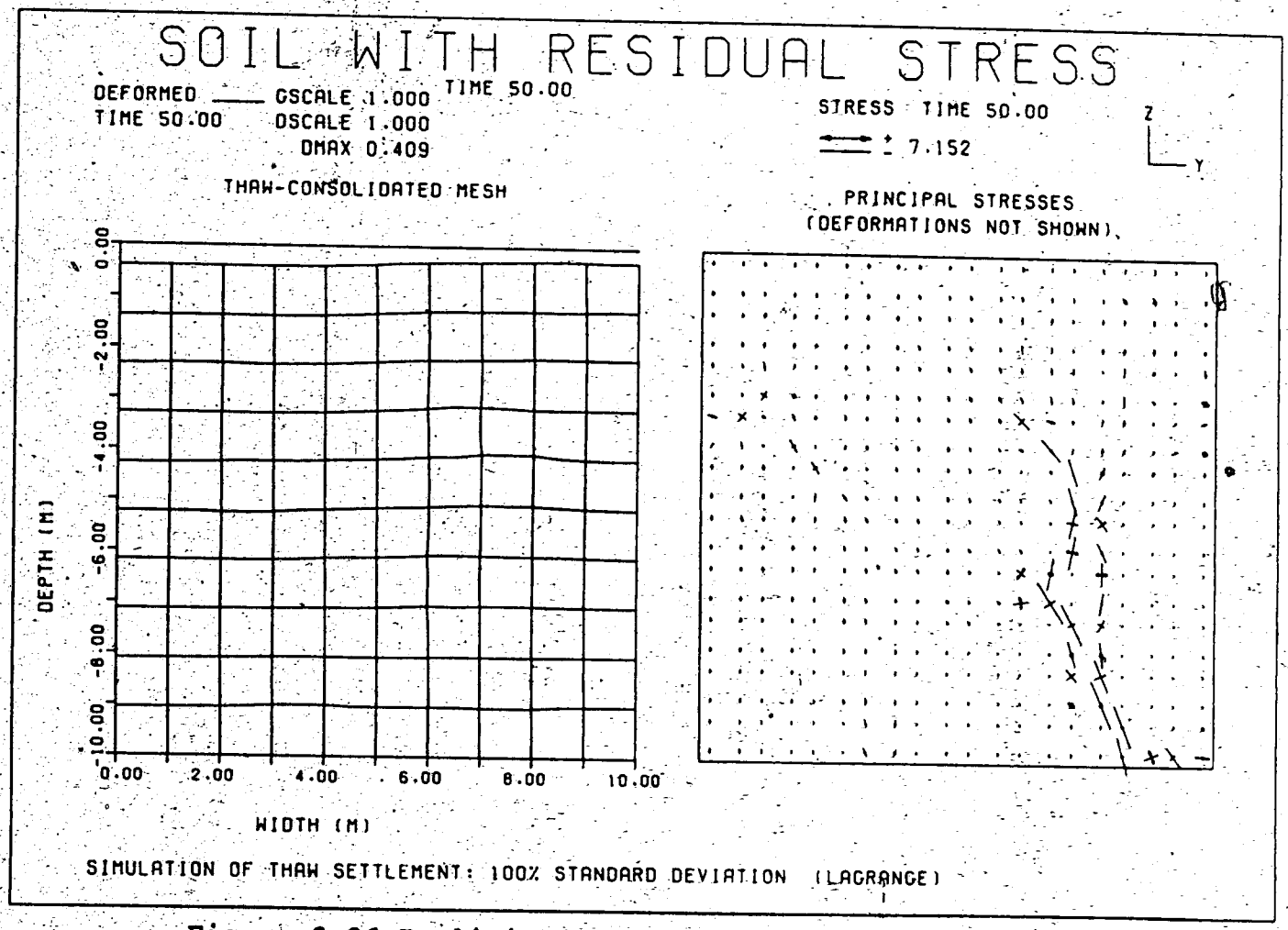

Figure 3.36 Preliminary Results of Lagrangian Analysis

contiguous settlements. Ultimately, this determined the number of peaks, in a given distance, for which the design curvature was exceeded. The difficulties with this approach were the problems faced in obtaining enough data to determine the density function, and in assuming a normal distribution which was questionable given that 30% of the locations had no thaw settlement.

The second method was a simulation of a random process, comparable with the thaw settlement study conducted in this study. A cummulative distribution of the data was used to generate a random sequence of settlements representing a "typical", although fictitious, thaw profile. Assuming a perfectly flexible pipeline, the number of occurrences of excessive strain over a given distance could then be determined. A finite element beam theory analysis was conducted on these sensitive areas to evaluate the effects of pipe bridging, ground stiffness modulus and axial thrust on the expected pipe strains.

This paper is instructive in two ways. First, it confirms the viability of using a fictitious situation generated from a distribution of real data. Secondly, it draws attention to the correlation of thaw settlements. This recognises the fact that settlements at two neighbouring locations are similar whereas a distant location could have any value of settlement. This is intuitively obvious, and the beginnings of such behaviour can be seen in the thaw

profiles of the finite element meshes (Figures 3.24, 3.27, 3.29, 3.31 and 3.32). This variation in surface settlements could be correlated with the variation in A_0; however, an extended mesh would have been required to obtain sufficient settlement data.

Palmer attributes the differing thaw settlements to changes in the amount of ground ice in the thawed soil (assuming a uniform thaw depth). His analysis does not consider the macrostructure of permafrost, a feature created by the soil's depositional environment and the thermodynamic genesis of the permafrost condition. Permafrost soils of concern are predominantly silts and clays. The depositional environment of these fine-grained soils commonly results in discontinuous sub-horizontal strata of interbedded materials. In addition, the advance of the freezing front upon exposure of these beds to surficial freezing temperatures would result in horizontal layering of ice. This preferred orientation of ice is due to the horizontal continuity of thermal conductivities within each strata and due to the presence of sub-horizontal isotherms. The result is a soil mass of permafrost with layers of soil, ice and ice-rich soil having a preferential horizontal alignment.

3.14.2 Graded Disorder

This structuring within the soil was not modelled in this study. A refinement of this analysis would be to attempt to simulate the general layering pattern within the

permafrost. A related study by Kröner (1980) examined the direction of crystals in polycrystalline aggregates and found that a "graded disorder" existed due to the perferential direction of crystal growth. The varying lengths and widths of different phases of metal were considered in a statistical manner in order to develop effective directional elastic moduli. This microscopic anisotropy accounted for differing macroscopic material behavior. This same procedure could be applied to thaw settlement if the appropriate material properties and the spatial distributions of the homogeneous bands were known.

3.14.3 Three-Dimensional Considerations

In conclusion, it should be noted that this solution has only considered a two-dimensional approach. Thus, the occurrence of softer pockets within the two-dimensional grid created a significant amount of settlement. There is a far smaller probability of such a pocket extending into three dimensions, therefore the collective stiffness of the system would be less variable.

The effect of the third dimension would be significant in the case where there is a wide range of material stiffnesses. As the stiffness variance reduces, the bolstering effect of the stiffer members does not add that much to the collective stiffness since the less stiff members will still carry significant load.

4. The Physics of Frost Heave

Previous studies of frost heave in soils recognized the dependence of frost heave on the rate of freezing, availability of water, applied loads and the grain size of the soil. As a result of extensive empirical studies, a number of index tests for frost susceptibility were developed.

However, these tests have limited applicability because they are restricted to design problems comparable to the original empirical tests that often cannot be reasonably extrapolated. Moreover, when these empirical relations could be applied, other constraints can restrict the solution to less conservative solutions, generally requiring a level of precision beyond the capability of these tests. This situation demands a deeper understanding of frost heave mechanics, and therefore an appreciation of the controlling physics behind the phenomenological behaviour of the process.

The critical aspect of frost heave is the attraction of water to the frost front, where it freezes, displacing the frozen soil in the process. The resultant deformations, stresses and moisture migration are of importance to engineers, as they effect the behaviour of adjacent structures and the thawing performance of the soil. In addition, although rarely of concern, problems can arise from changes in the structure of the soil due to freezing in

a closed system (Jones, 1986).

Experimental and analytical work by a number of researchers has identified the driving forces behind frost heave as the physics at the ice/water interface within the freezing soil. A clear understanding of these forces demands a basic familiarity with the controlling thermodynamics. While many authors have used thermodymnamics in the interpretation of their laboratory work and others have embraced it in their analytical models of frost heave, the treatment of the subject itself has been confusing. As a point of clarification, this author has presented some of the basic concepts in this work (App. E).

4.1 Applicability of the Clausius-Clapeyron Equation to Freezing Soils

The Clausius-Clapeyron Equation has been applied to soil freezing within a constant volume with drainage (Hoekstra, 1969). Hoekstra showed that the pressures developed during freezing of an enclosed soil originate at the ice lens and found that the temperature dependence of pressure is a function of a soil's ablilty to form an ice lens below 0°C. This relationship between the temperature at the base of the ice lens and the corresponding pressure was experimentally determined to be $\frac{dP_i}{dT} = -10.4$ atm/K. This predicts an increase in ice pressure with a freezing point depression.

Unfortunately, Hoekstra objected to the use of equilibrium thermodynamics in a system with a temperature gradient, and questioned the applicability of using:

$$dP_i = \frac{-L}{v_i T_0} dT \qquad [4.1]$$
$$= -11.4 \text{ atm/K}$$

in interpreting the results. This was because the equation assumes that $dP_w=0$. He maintained that this was not the case because the base of the ice lens is separated from the soil particles by a thin film of water which must also be under the same stress as the ice. However, Hoekstra has not explained why there was no water flow under such a pressure differential nor has he considered that, at the scale of the film, other forces may affect the thermodynamics, such as the structuring of water due to surface adsorption (Anayan, 1973; Aguirre-Puente, *et al*. 1973; Derjaguin & Churaev, 1986). In addition, in re-evaluating Hoekstra's laboratory results, a much better fit to the theoretical slope of 11.1 atm/K was found when the best-fit line was forced through the origin, as would be reasonable. This further supported the use of thermodynamics in interpreting soil freezing.

4.1.1 Differing Water Pressures

The various forms of the Clapeyron equation provide extremely powerful analytical tools for examining the dynamics of freezing. Biermans, *et al*. (1978) investigated just one aspect of this in varying the dP_w term, however they provide sufficient data to draw further conclusions.

Their experimental set-up consisted of a column of ice hydraulically connected through a porous filter to a supercooled pressurized water reservoir. Three filters were used, each with millions of columnar pores with diameters ranging from *1μm* to *6μm*. The whole system was immersed in a sub-zero temperature bath to ensure isothermal conditions.

With the column of ice maintained at atmospheric pressure, the bath temperature and water pressure were varied. At any given temperature an equilibrium water pressure was found, above which resulted in ice accretion and heave. In contrast, lower pressures resulted in melting of the ice column. In a plot of the system's temperature T_s *versus* the pressure difference between the ice and water, (P_i-P_w), a slope of 12.07 atm/K was obtained, as predicted by the Kelvin equation, and described by the writers. As a point of clarification, the ice pressure, P_i is statically equivalent to the pressure in the thin film of water between the ice and the filter. Thus, the (P_i-P_w) term is actually equivalent to the dP_w in the Kelvin equation. After evaluating the authors' analysis of the melting ice column, it is not certain that this was clear to them. Since all the ice in the system is maintained at one atmosphere the dP_i term is zero.

The writers maintained the temperature in the range of -0.01°C to -0.06°C, below which the water in the filter froze and ice propagated throughout the supercooled water

reservoir. Supercooled water exists because the initiation of spontaneous ice growth requires the creation of an ice-water interface. This interface has a surface tension which creates a pressure difference between the two phases due to the geometries involved. Approximating the initiating ice as a sphere, thereby minimizing its specific area, the pressure difference between the ice and water can be expressed as (Williams, 1968):

$$P_i - P_w = \frac{2\sigma_{iw}}{r_c} \qquad [4.2]$$

where σ_{iw} = surface tension of the ice/water interface

= 30.5 dyn/cm = 30.5×10^{-6} kPa·m

r_c = radius of the ice/water interface

A sphere of radius $r<r_c$ would not be stable because of the higher pressure in the ice. A sphere of radius $r>r_c$ would quickly propagate, however since the required surface energy varies with the square of the radius, this would not happen spontaneously. The above equation can be combined with the Kelvin equation to relate supercooling to the critical radius

$$\frac{2\sigma_{iw}}{r_c} = \frac{L\,T_s}{v_w T_0} \qquad [4.3]$$

$$r_c T_s = \frac{2\sigma_{iw} v_w T_0}{L} \qquad [4.4]$$

$$= \frac{2\times30.5\cdot10^{-6}\ \text{kPa}\cdot\text{m}}{1121\ \text{kPa/K}}$$

$$= 0.0544\ \mu\text{m}\cdot\text{K}$$

For the specified supercooling in the range of 0.01°C to 0.06°C, this corresponds to diameters ranging from 1.8μm to

11μm, which is essentially the same as the range of filter pore diameters used in the experiments. For a temperature below the the critical radius temperature for a given filter, ice would be able to propagate through the filter as a column with a domed interface. As the ice entered the water reservoir the dP_i term would no longer be zero but would equal dP_w. The thermodynamics would then be described by the Clapeyron equation for fusion, which would require 133 atmospheres for every degree of freezing point depression. As this was not available, ice and water would not co-exist so the system would freeze solidly.

The writers also studied dynamic equilibrium by altering the water pressure from the equilibrium pressure and measuring flow rates to and from the ice column. For a fixed bath temperature, flow rates were proportional to the increase in P_w above the equilibrium water pressure. For a water pressure below the equilibrium pressure, water was released from the base of the ice column. The flow rate during melting, however, was significantly reduced for each of the four temperatures as shown in Figures 4.1. Biermans, *et al*. claimed that the reason for the discrepancy was not clear.

4.1.2 Altered Flow Rates

Thermodynamics can also explain this discrepancy, in terms of the Kelvin equation and the roughness of the base of the ice lens. Biermans, *et al*. have assumed a flat base

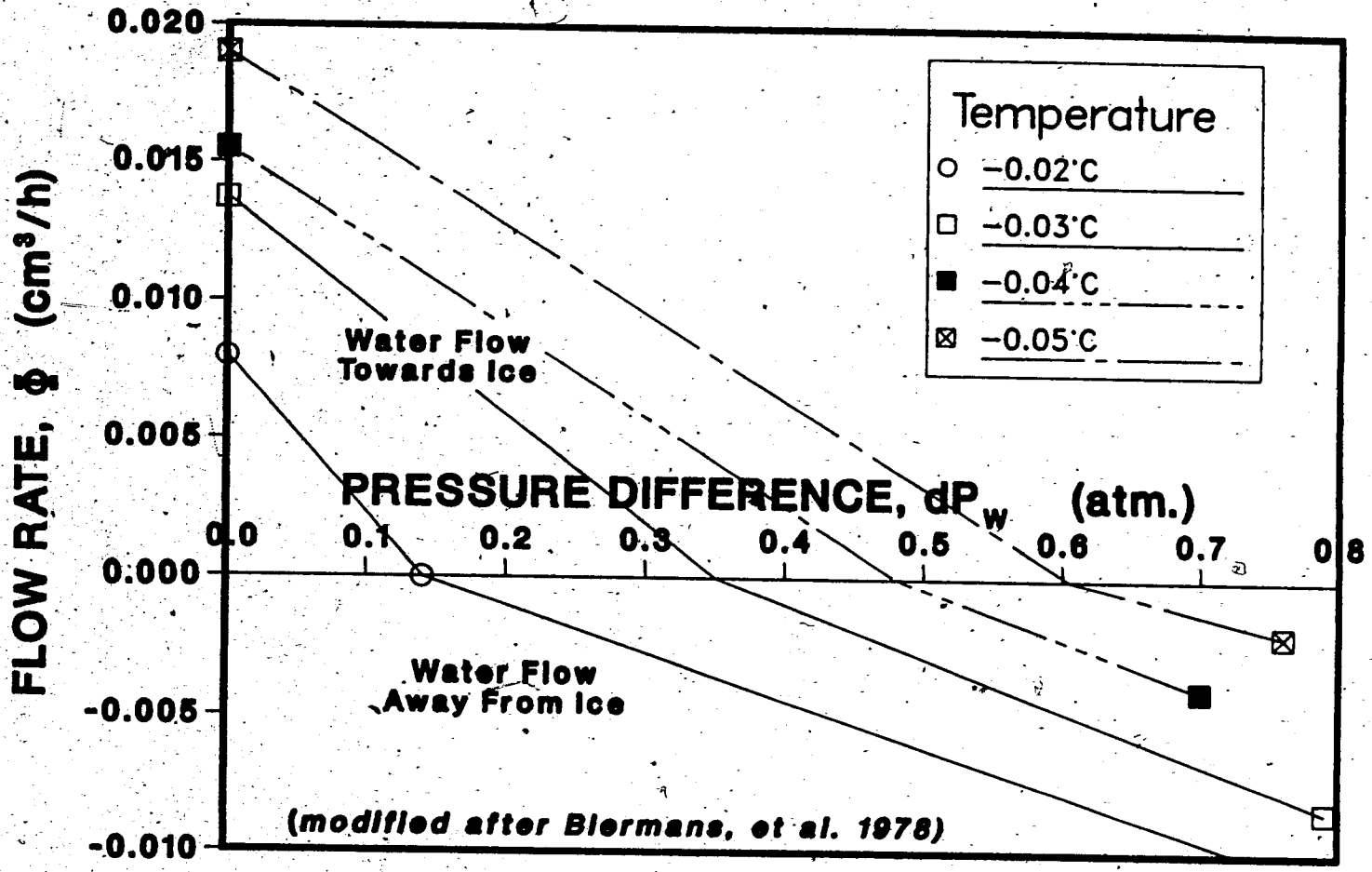

FLOW RATE versus PRESSURE DIFFERENCE

Figure 4.1 Relation between Flow Rate and Pressure Difference

for their ice column, although the base would more probably be nearly flat above the glass surface and dimpled down into the water at the pores (Figure 4.2a). For the equilibrium configuration, the radius of curvature of the dimple would equal the critical radius as discussed previously. This would ensure a uniform ice pressure at the ice/water interface. During ice melting the dimple radius would have to be slightly smaller than the equilibrium radius in order to remain at a marginally higher energy state than the adjacent flat ice under atmospheric pressure.

The reduction of the reservoir pressure, P_w, increases the pressure difference term in Equation [4.2]. For equilibrium, the radius of the interface, r_c, must decrease to a new stable radius. The Kelvin equation, however, demands that this reduction in radius be accompanied by an increase in the amount of supercooling. Since the Biermans, *et al.*, experiment was maintained at a constant temperature, this resulted in a localized decrease in temperature at the interface. This established a temperature gradient between the warmer bulk water and the interface, creating a heat flux within the system and causing melting at the interface. The resultant flow rates away from the interface were found to be linear functions of the pressure imbalance, as shown in Figure [4.1].

In this melting process the dimple radius would be slightly smaller than the critical radius, thereby allowing

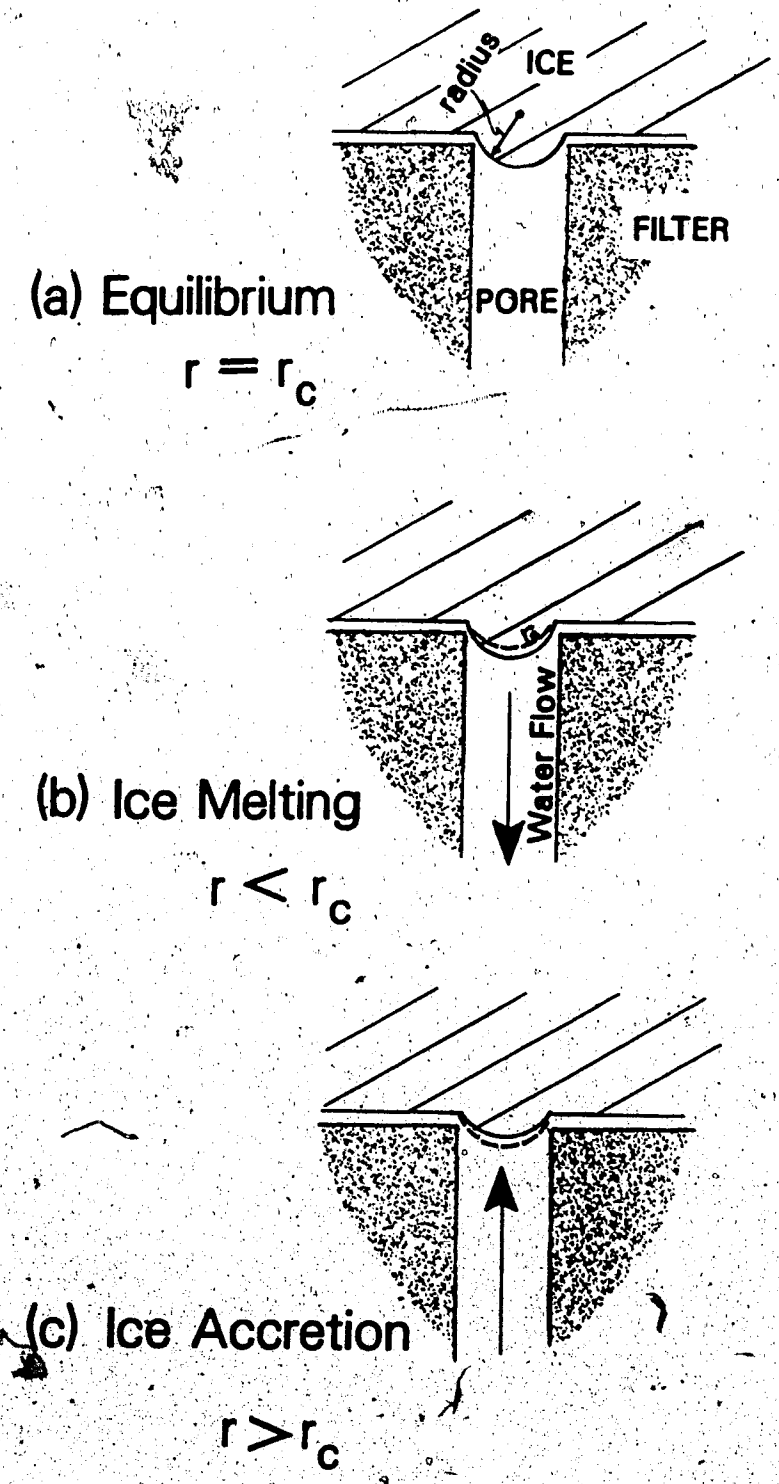

Figure 4.2 Schematic Representation of the Ice-Water Interface

the dimple to intrude further into the pores and by doing so, further obstructing the water flow. The water next to the flat sections of the ice, which represents 80% to 90% of the ice surface area, would have more difficulty in flowing through the pores. The support for this hypothesis is seen in Figure 4.3 which plots the critical radius, r_c, and the corresponding temperature depression, T_s as functions of the water flow rate over the hydraulic head. It is reassuring to note that the flow rate intercepts the temperature and radius axes at the values also predicted for ice progression through the filter pores towards the water reservoir (Figure 4.3). This is based on a pore diameter of 1μm, which is consistent with the filter's high porosity yet low water conductance (~ permeability), and its higher capability of supercooling (-0.05°C) under isobaric conditions.

The thickness of the interfacial film may also be affecting the water flow, as Biermans, *et al.* suspected. This was also discussed in Aguirre-Puente *et al.'s* (1973) paper in which the film would also be a function of temperature. It is impossible to assess the relative importance of these two effects without further laboratory results.

4.1.3 Micro-Thermodynamics

A similar theoretical examination of the micro-thermodynamics of frost heaving was done by Aguirre-Puente, *et al.* (1973). Their model predates a

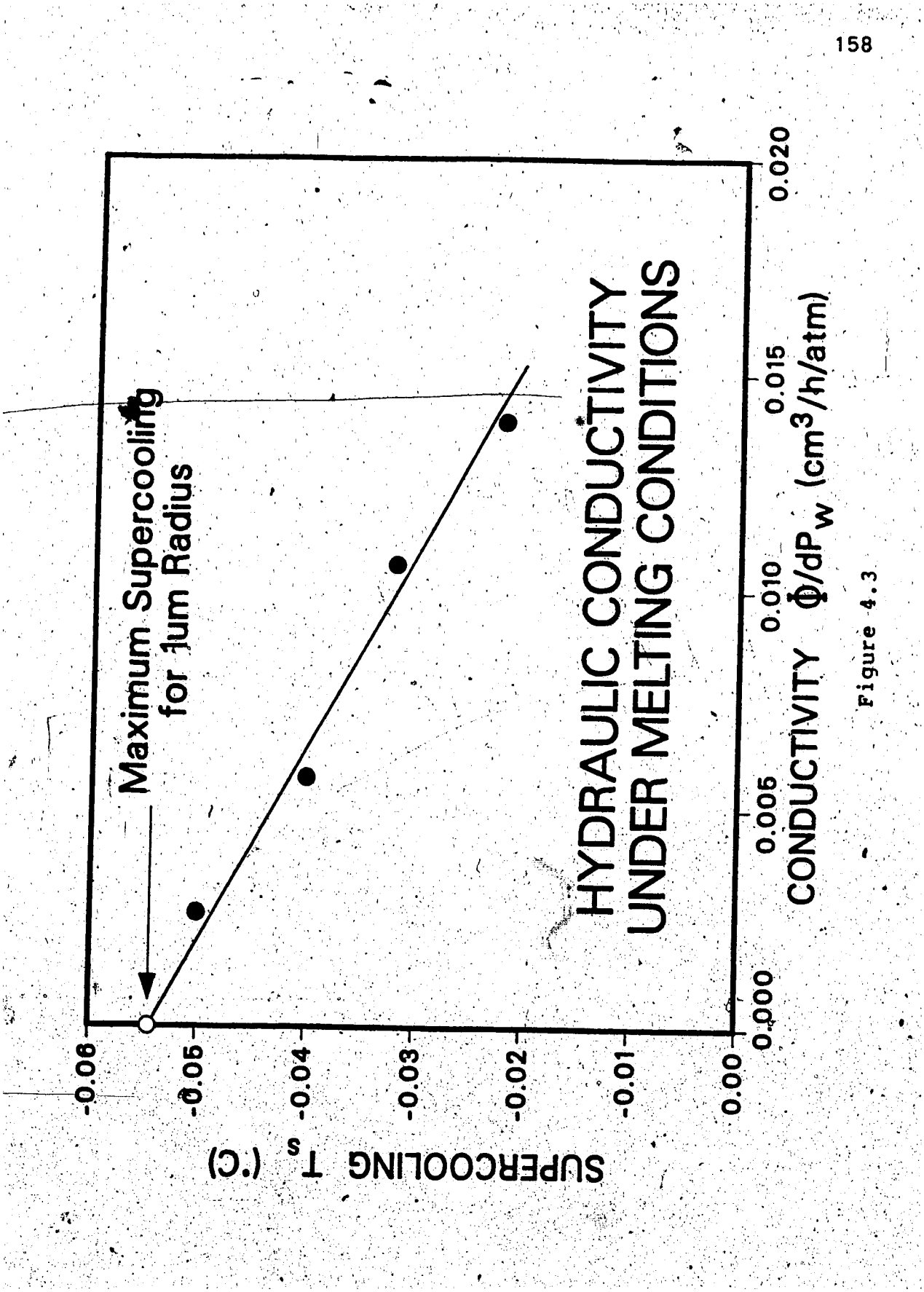
HYDRAULIC CONDUCTIVITY
UNDER MELTING CONDITIONS
Maximum Supercooling
for 1um Radius
SUPERCOOLING T_s (°C)
-0.06
-0.05
-0.04
-0.03
-0.02
-0.01
0.00
0.000
0.005
0.010
0.015
0.020
CONDUCTIVITY Φ/dP_w ($cm^3/h/atm$)

Figure 4.3

similar experimental model by Biermans, *et al.* (1978), except that they also draw attention to the effect of the adsorbed water between the ice phase and the solid substrate. Their concept of the chemical potential of the attached water, also expressed by Ananyan (1973), helps to explain the dichotomy raised by Hoekstra (1969). Hoekstra questioned having a statically pressurized water film, hydraulically connected to an unpressurized reservoir, without having any water flow. Their work suggests that water cannot flow away from the adsorbed water film without reducing its thickness which would only be possible with a commensurate drop in temperature or an increase in the ice pressure.

A further interpretation of the physics surrounding frost heave was presented by Derjaguin and Churaev (1986) in which the Biermans, *et al.* (1978) work was cited. Their analytical analysis considered the effect of the adsorbed water on the system entropy, however an unmeasured parameter in their analysis precluded a quantitative corroboration with Biermans, *et al.*'s experimental results.

4.1.4 Cavitation

It is significant that the development of the suction at the freezing front can extend into the negative pressure range (Konrad and Morgenstern, 1980). Conventional gas mechanics would indicate a minimum pressure of P_v, the water's vapour pressure, in the presence of liquid water.

For phase transition between a liquid and a gas, conventional wisdom maintains that there exists a two-phase region within a bell-shaped curve, in which both phases coexist. Outside this region, the pressure:specific volume *P:v* relationship can be determined experimentally. Within this region, a constant *P* expansion of liquid to vapour is determined by the fixed entry and exit points, interpolating on the mole fractions of each phase.

However, it is possible to have a metastable phase in which liquid is superheated or where the vapour is supercooled. It is actually possible to overexpand or "superheat" the liquid phase with the negative pressure being due to the tensile strength of the water (i.e. not surface tension effects). Pressures of -270 *bar* have been attained by placing a capillary in a centrifuge; conversely, by heating water at 1 *bar* a temperature of 270°C has been achieved (Rowlinson, 1969; van Stralen, 1979; Cole, 1979).

In an isothermal system, a superheated liquid is obtained by lowering the pressure. In order to initiate a vapour bubble a small number of contiguous molecules must have energies exceeding the "energy of activation" (Cole, 1979). Without this, a bubble does not form even if within the two phase region. Instead, the liquid proceeds to drop in pressure along a path that is not the most stable, but is metastable as long as $\left[\frac{\partial P}{\partial v}\right]_T < 0$. As the liquid spinodal is reached (Figure 4.4) the liquid is unconditionally unstable

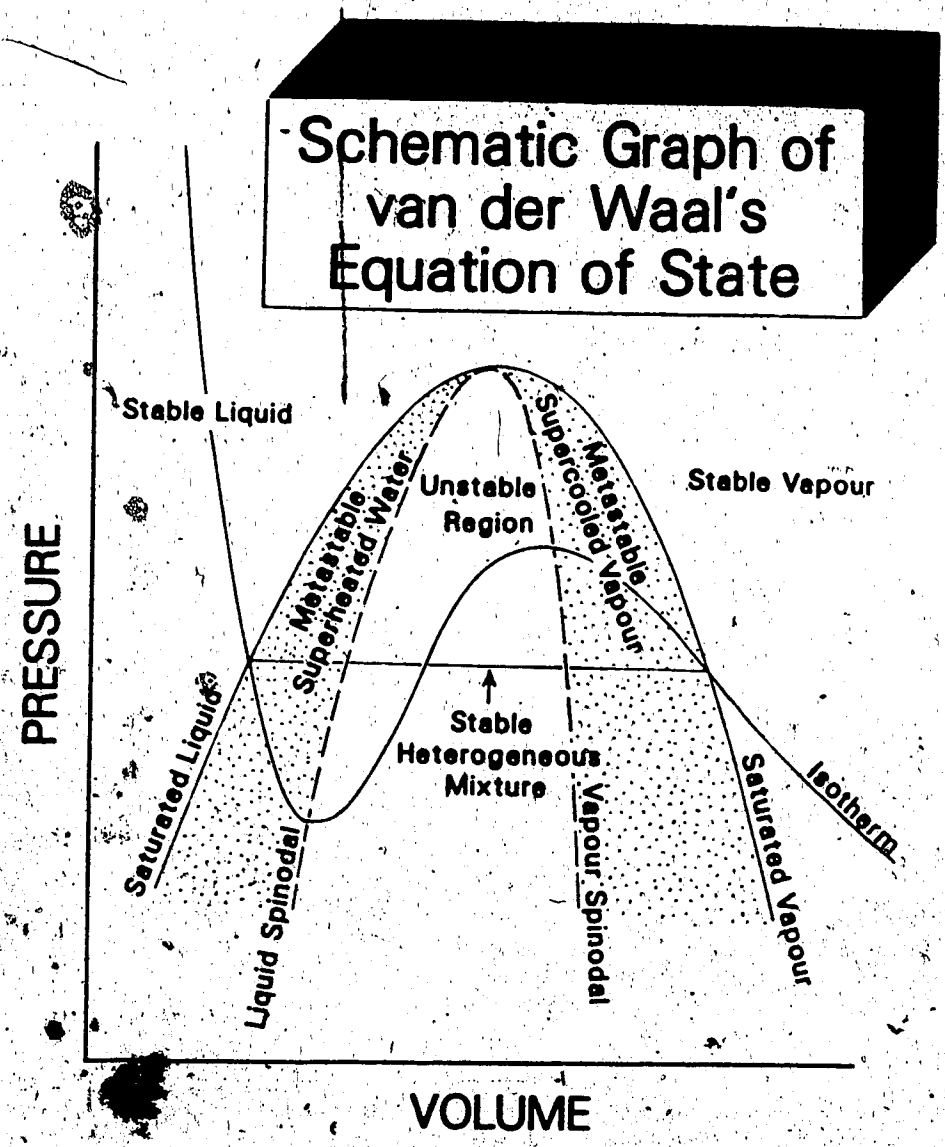
Schematic Graph of van der Waal's Equation of State
Stable Liquid
Metastable Superheated Water
Unstable Region
Supercooled Vapour
Metastable
Stable Vapour
PRESSURE
Saturated Liquid
Liquid Spinodal
Stable Heterogeneous Mixture
Vapour Spinodal
Saturated Vapour
Isotherm
VOLUME

Figure 4.4

and bubble nucleation occurs. Using the method prescribed by Cole (1979) this would occur at a pressure of -290 *MPa* for water at 0°C. Moderate decreases in temperature result in considerate decreases in pressure. Using conventional interface theory, assuming a spherical bubble within bulk water and an air/water surface tension of 75.64×10^{-6} *kPa m* (Daniels and Alberty, 1975) a bubble of 100Å radius would result in a liquid/gas differential pressure of 15 *MPa*. A bubble of such size would have difficulty forming in the thin interfacial films.

The argument may be presented that spontaneous nucleation of vapour bubbles is unnecessary because of the existence of pre-existing bubbles within the freezing soil (Gilpin, 1982). Gas bubbles have been found in natural permafrost (Roggensack, 1977) and attributed to gas exsolution from the saturated pore water as pure water freezes (Glen, 1974; Roggensack, 1977; Gilpin, 1982) or from the products of reaction from the decomposition of organic inclusions (Roggensack, 1977).

However, neither seeded nor spontaneous cavitation appears to occur in freezing soils. There is no physical evidence of extensive cavitation bubbles, nor is there a marked change in frozen soil permeability at any temperature that may correspond with a cavitation pressure. It would appear that the specific physics associated with the water film between the ice and solids precludes the development

and propagation of vapour bubbles.

4.2 Implications of the General Clausius-Clapeyron Equation

The general form of the Clausius-Clapeyron equation (Eq'n. [E.28]) relates a freezing temperature depression to pressure changes in ice and in water. Facets of this relationship have been proven by experimenters, and the physics used in a number of frost heave theories. The physics depends on the co-existence of two phases of the same substance.

The co-existence of the ice and water phases depends on pore water. Pore water can exist in pure ice because of the high surface energy of inter-granular boundaries. With an ice/water surface energy of 3.3×10^{-4} N/m (J/m^2) and an ice/ice surface energy of 6.5×10^{-4} N/m it is favourable to have water channels wherever three ice grains meet (Glen, 1974). Thus a system of interconnecting channels exists within polycrystalline ice.

If one allows that a continuous network of interconnecting channels exists within the frozen soil, then extremely high suction must also develop within the pore water. This is essentially the position taken by some authors (Blanchard and Fremond 1982, 1984). They extrapolate the effects of this pressure differential and anticipate a redistribution of water within the frozen soil towards the coldest regions, where the suction is highest.

However, this is contrary to the conditions found *in situ* and from laboratory results. It does not reflect the distribution of ground ice in natural soils, in which massive deposits of ice can be found at depth (Johnston, 1981). Furthermore, it does not predict the formation of ice lenses near the frost front as is common during experimental frost heave studies.

Part of this discrepancy may be explained by the properties of the ice in the lens. Within this ice there are movements of grain boundaries so as to reduce the net amount of surface energy (Glen, 1974). This is most dramatically demonstrated in the experimental work of Biermans, *et al.* (1978) in which the seeded polycrystalline column of ice eventually graded into a unicrystalline column of ice. This column was most probably parallel to the ice's "c-axis" which is normal to the hexagonal structure of ice. Radd and Oertle (1973) conducted polarized light studies on experimentally grown ice lenses and found the grain size to be large. Interestingly, they observed movement of clay particles through the ice lens against the thermal flux as the pressure in the confined sample increased (due to freezing). This occurred through visible channels in the ice which they speculated to be dislocation vacancy flows. These voids filled with ice as the particles passed. The authors noted that the ice lens clarified in time, preventing further particle movement. This indicated that a restructuring of the ice was occurring.

Konrad and Morgenstern (1980, 1981) have also used the Clausius-Clapeyron equation in their frost heave predictions, reducing the physics and mathematics down to a material-specific "segregation potential" parameter, *SP*. This value, factored by the temperature gradient, predicts an approach velocity for attracted water. The driving force within their approach is the pressure difference between the suction at the ice lens, as predicted from the Clausius-Clapeyron equation, and the water pressure in the unfrozen soil, as determined from Darcy's law. The authors circumvent the difficulty of water flow through the frozen soil by discounting it, claiming that the frozen soil has a very low permeability and that distinct ice lenses are effective barriers to water flow. Their theory is effective for engineering design but does not explain the long-term stability of ground ice features under the high hydraulic gradient induced by the temperature gradient. Gilpin (1982) made a similar observation in his paper in which he examined some aspects of the segregation potential for adaptation to numerical modelling.

The key issue missing from these frost heave theories is that the hydraulic gradient, as determined from the Clausius-Clapeyron equation, is a necessary but not a sufficient determinator of the approach velocity of water. Williams and Fremond rigidly apply the Clausius-Clapeyron equation and obtain an erroneous model. Konrad and Morgenstern and Gilpin avoid the issue by negating water

flow in the frozen soil and by retricting themselves to short term problems (in a geomorphological time frame). Neither approach addresses the energetics of the water film at the ice/solid interface nor how this film's existence can explain aspects of frost heave behaviour beyond the ice lens phenomenon.

The existence of this ice/solid interface is reflected in the unfrozen water contents of soils by which the water content is expressed in terms of the amount of solids present. It is significant that it is solely dependent on the solids and is independent of the amount of bulk water available. This unfrozen water content decreases with colder temperatures, similar to the theoretical model of Aguirre-Puente, *et al.* (1973). By extrapolating their theory, any water flow into, or out of, this film would require the freezing or thawing of the adjacent ice surface to regain the equilibrium unfrozen water content at any given temperature.

4.2.1 Ice Lensing

Thus, the hydraulic gradient, established by the physics behind the Clausius-Clapeyron equation, attracts water to the base of the ice lens through increasingly constrictive interface films. This increases the thickness of the films above their equilibrium thickness so the excess freezes onto the ice surfaces. The latent heat released during freezing is conducted through the frozen soil. When

the heat flux within the frozen soil exceeds the latent heat rate, the frost front advances, freezing some pore water as well. This increases the length of the frozen soil thereby reducing its conductance. As a result, the rate of frost penetration diminishes.

In the limit, the arrival rate of water, with its latent heat, plus the conducted and convected heats, will approximate the heat flux in the frozen soil. At this point, the final ice lens will be formed. Eventually the heaving begins to diminish because the increasingly longer heat flow path through the frozen materials reduces the capacity of the system to conduct the latent heat released at the ice/water interface. The water films throughout the frozen fringe slowly collapse to their equilibrium thicknesses and heaving stops. Heat flow continues but only due to conductance through the frozen and unfrozen materials.

4.2.2 Thermodynamic Stability on the Cold Side of the Ice Lens

On the cold side of an ice lens the temperature gradient is towards the lens rather than away from it. The suction in the frozen soil is therefore greater away from the lens. This has led some authors (Blanchard and Fremond 1982, 1984) to conclude that water flow will necessarily be towards the cold source. This would certainly be the case where an excess of unfrozen water exists. In experimental work performed on closed-system samples of frozen soil,

Mageau (1978) found an accumulation of ice rich soil and pure ice at the cold platen, as had other workers. It is unlikely that this deposition is due to vapour diffusion, as speculated, but rather to the suction created by the imposed thermal gradient. This would be more reasonable given the author's description of the ice as being clear, massive, and with soil inclusions. This water would originate from the water film between the ice and solids, which would have increased in size as the sample warmed from the cold room temperature (-10°C) to the platens' testing temperatures (-4.2°, 0°). With the imposed temperature gradient, water would move towards the cold platen until the equilibrium thicknesses of films were attained.

This redistribution of water within the frozen soil could not be expected to continue unabated. Instead, a suction gradient would develop in parallel with the temperature gradient. This suction gradient would be in equilibrium with the thicknesses of the interfacial water films. The Biermans, *et al.* (1978) experiment, under isothermal conditions, was a limited example of this process. In addition, their work was further simplified because ice existed at one pressure whereas the pore ice within a frozen soil under a temperature gradient may be at various pressures, due to the suction in the water and surface tension effects. The essential point here is that the experiment confirmed the no-flow condition existing under a hydraulic gradient.

4.2.3 The Thermodynamics within an Ice Lens

Much discussion has centered about the phase composition of ice lenses occurring both in laboratory test and in the field. This interest arises from a desire to know the permeability of these lenses as this will affect the amount, accumulation rate and the distribution of ice within a freezing soil.

If one allows that a continuous network of interconnecting channels exists within the ice lens and the frozen soil, then extremely high suctions must also develop within the pore water within these channels. In general, however, water flow within the frozen soil is low due to the constrictive and tortuous flow path through these channels. This is particularly true at lower temperatures (Williams and Burt, 1974) and the presence of an ice lens further impedes water flow (Mageau and Morgenstern, 1980). Ice lenses formed within a soil are essentially impermeable (Mageau and Morgenstern 1980, Konrad and Morgenstern 1980). This is seen in the effects of long-term frost heave in which ice accumulates at the current frost front, with little moisture redistribution within the frozen soil.

It is interesting to note that the insertion of a pre-made ice lens into a frozen soil test sample still permitted significant moisture redistribution in the frozen soil above the lens (Mageau, 1978). In addition, traces of tritium-doped water were found to travel from the unfrozen

soil into the frozen soil above the manufactured lens. Mageau attributed this to contamination of the moisture sample.

It is unlikely, however, that such a lens adequately represents the tight crystallographic order of a natural ice lens and therefore the lens permitted some water flow. Grain boundaries in the artificial lens would result in a more permeable material, allowing water to pass through to the colder side. No details were given concerning the manufacture of this lens so it is reasonable to assume that it was made from a polycrystalline sample of ice. This assumption is supported by photographs of the artificial lens in which the surface of the colder side had decayed into a porous material. This was because the ice crystals with high surface energies melted out. The water was redistributed within the adjacent frozen soil.

Walker (1986) provides an interesting article in which some pertinent ice properties are introduced. Included are some simple methods of examining ice to determine its crystalline make-up and orientation.

4.3 The Segregation Potential: Theory and Practice

As with other engineering topics, it is not necessary to include all aspects of physics in the development of a workable frost heave model. Often the complete physics are not known, and their inclusion may be needlessly exact if

only one or two aspects control the behaviour of the model. Such is the case in frost heave and the derivation of the segregation potential (Konrad & Morgenstern, 1980).

The derivation first requires an examination of the physical model representing the freezing soil. For simplicity, the one dimensional case shall be used.

The model assumes an unfrozen column of soil with radially adiabatic boundaries so that all heat flow is vertical. A warm step temperature is applied to the base and a cold step temperature is applied to the top, causing frost to penetrate into the soil. Water is allowed to enter at the base of the column as freezing progresses. Heaving and freezing continue to occur until the system comes to dynamic equilibrium.

For continuity of heat flow, assuming a unit cross-sectional area and a finite time interval, the heat flow through the frozen soil must equal the heat flow in the unfrozen soil plus the heat released by phase change. This phase change heat includes that of the *in situ* water and that of the water attracted to the freezing front. The thermodynamic equations for the one-dimensional frost heave model have been detailed in Konrad and Morgenstern (1980). This model assumes that all heat transfer is due to heat conduction and the release of the latent heat of freezing. No account is taken of the heat transfer due to advection as water flows through the unfrozen soil to the freezing front.

However, the error introduced is negligible, particularly for the small water velocities and unfrozen thermal gradients involved (Nixon, 1975). No account is taken of convective heat due to the relative displacements of the frozen and unfrozen soils. Again, this is seen as a negligible tertiary effect. Water is attracted to the frost front because of the suction developed at the phase interface according to the thermodynamic requirements of equilibrium.

Konrad and Morgenstern (1980) applied the Clausius-Clapeyron equation to this physical model of soil freezing. Ice crystals nucleate at the centre of voids at the zero-degree isotherm and the soil is considered completely frozen at the segregation freezing temperature.

The region of partially frozen soil between these two extremes is referred to as the frozen fringe. The exact phase compositions within this region are not well defined, and this poses a problem for a rigorous examination of the physics within. The writers circumvent this problem by using the easily obtained or calculated values for the extremities and using an average value for the prediction of behaviour. This approach has the practical benefit of dispensing with tediously precise measurements on the scale of the frozen fringe. Instead, the water pressure at T_s was calculated using the Kelvin equation, the water pressure at T_0 was calculated from the water intake velocity and the unfrozen

soil's length and permeability. The length of the fringe was determined from T_s and the thermal gradient in the frozen fringe. In summary, the average frozen fringe permeability is:

$$\bar{k}_{ffo} = \frac{v_o}{i} = \frac{\Delta l}{\Delta h} v_o \qquad [4.5]$$

$$= \frac{d_{ff}}{H_w - h_u} v_p \qquad [4.6]$$

$$= \frac{\left| \frac{T_{so}}{\bar{\nabla} T_{ff}} \right| v_o}{\left| \frac{L}{v_w T_0} T_{so} \right| - \frac{v_0 l_u}{k_u}} \qquad [4.7]$$

the subscript "$_0$" referring to the conditions at the formation of the final ice lens.

For all frozen fringes in a given material the average temperatures should be identical, as should be the unfrozen water contents. For the same pressure at the 0° isotherm, $\bar{k}_{ffo}$ should also be the same.

Under any given thermal conditions, then, for a material with a defined $\bar{k}_{ffo}$, the approach velocity of the water can be determined from the thermal gradient of the frozen fringe as follows:

from [k=lv/h], $v_0 = \frac{\Delta H}{\Delta L} \bar{k}_{ffo}$ [4.8]

$$= \frac{H_w - h_u}{T_{so}} \bar{\nabla} T_{ff} \bar{k}_{ffo} \qquad [4.9]$$

$$= \left[\frac{H_w - h_u}{T_{so}} \bar{k}_{ffo} \right] \bar{\nabla} T_{ff} \qquad [4.10]$$

$$= SP \, \bar{\nabla} T_{ff} \qquad [4.11]$$

where SP is the "segregation potential" of the soil. This equation presupposes the value of T_{so} however Konrad and

Morgenstern (1980) show that K_{ffo} is relatively insensitive to practical variations in T_{so} . More significant is SP's dependance on h_{uf}, the suction in the unfrozen soil, and corrections can be made for this. However, it should be remembered that in many field problems the secondary permeability of the soil would prevent high suctions from developing. Closed systems, such as pingo formation, would require such a correction.

The thermal gradient of the frozen fringe, $\overline{\nabla}T_{ff}$, is not measured but can be extrapolated from the adjacent gradient. Konrad (1980) has used the thermal gradient in the frozen soil ($\overline{\nabla}T_f$) for this. However, it is evident from the derivation of SP that the unfrozen gradient should be used. Using the definitive conditions during formation of the final ice lens as an example, it is evident that the unfrozen gradient can be factored by the fringe/unfrozen thermal conductivity ratio to obtain the frozen fringe gradient. Conversely, the use of the frozen gradient would include latent heat effects from the growing ice lens, which would preclude a similar derivation of $\overline{\nabla}T_{ff}$. Heave can still be related to the frozen thermal gradient provided that the SP values are consistent with it, as will be demonstrated in this chapter.

While the use of $\overline{\nabla}T_f$ may be justified from a practical stance, given that it is usually easier to determine for field conditions than either $\overline{\nabla}T_u$ or $\overline{\nabla}T_{ff}$, it is disconcerting

to note that Konrad has been inconsistent in his choice of gradients.

Konrad and Morgenstern (1980) explicitly described the thermal gradient to be

$$\nabla T = \frac{T_u + |T_{so}|}{l_T} \qquad [4.12]$$

$$= \frac{T_u}{l_u} \qquad [4.13]$$

where the frozen fringe gradient was compared to the unfrozen gradient. Konrad (1980) in his doctoral theses develops the theory based on the Clausius-Clapeyron equation which is dependent upon the temperature depression from the 0° isotherm to the base of the final ice lens. However, in his finite difference program for one-dimensional analyses, Konrad uses $\nabla T_{ff} = \nabla T_f \frac{k_f}{k_{ff}}$ which implies pure conduction across the fringe/frozen interface with no contribution from the latent heat of the growing ice lens. His program has been appended, with numerous explanatory comments added for completeness (Appendice F).

In addition, both the simple frost heave calculation and the calculations for frost heave beneath a chilled pipe (Konrad, 1980) use the cold gradient, ∇T_f.

Konrad (1980) has developed this approach in his doctoral thesis but adopts a different approach in interpreting his laboratory results. Rather than use the frozen fringe gradient, or an equivalent based on the unfrozen soil's thermal gradient, he has used the frozen

soil's thermal gradient to predict the approach velocity of water. This was not stated explicitly within the text, but is implicit in the finite difference program appendended to his work. Consequently the *SP* values obtained from his testing program are with respect to this frozen gradient. This affects the segregation equations as follows:

$$\bar{\nabla}T_f = \frac{T_c}{l_f} \qquad [4.14]$$

$$\bar{\nabla}T_{ff}^{*} = \frac{k_f}{k_{ff}}\bar{\nabla}T_f \qquad [4.15]$$

$$v^{*} = SP^{*}\,\bar{\nabla}T_{ff}^{*} \qquad [4.16]$$

The power gain from the latent heat of the *in situ* and attracted water is:

$$q = k_f\,\bar{\nabla}T_f - k_u\bar{\nabla}T_u \qquad [4.17]$$

Knowing v^{*}, the frost front velocity can be calculated:

$$q - v^{*}L = \epsilon\eta L\,\frac{dx}{dt} \qquad [4.18]$$

where ϵ = the fraction of the pore water that freezes

η = the porosity

Examining the power balance at the frozen/frozen fringe interface:

$$k_f\bar{\nabla}T_f = k_u\bar{\nabla}T_u + v^{*}L + \epsilon\eta L\,\frac{dx}{dt} \qquad [4.19]$$

The problem with this development is that by using $\bar{\nabla}T_{ff} = \frac{k_f}{k_{ff}}\,\bar{\nabla}T_f$ the power gain from the latent heat of the attracted water is ignored. This assumption would overestimate $\bar{\nabla}T_{ff}$ especially for higher approach velocities. An analysis of laboratory results, using the measured velocity and the derivation of $\bar{\nabla}T_{ff}^{*}$ would underestimate the value of *SP*.

4.3.1 Deviation from the Theory

This departure from the theory as developed using the Clausius-Clapeyron equation may be traced to the thesis of a contemporary of Konrad's, Mageau (1978). In his thesis, Mageau also takes two conflicting stances. From his experimental work, he concludes that the driving suction pressures are initiated in the frozen fringe and that the governing factors for the water intake rate are also determined there. This contrasts with an earlier statement in which he claims $\overline{\nabla T}_f$ would be a controlling factor on the rate of heave during the formation of the final ice lens.

This contrast is expressed algebraically in Mageau's simplified upper-bound heave rate calculation (Mageau, 1978: Eq'n. 5.6)

$$\frac{h}{t} = \frac{k_{ff}\overline{\nabla T}_{ff} - k_u\overline{\nabla T}_u}{L} \qquad [4.20]$$

This implies that the ice lens is forming between the unfrozen soil and the frozen fringe which is clearly not the case. Mageau continues, stating that for a field situation the gradient within the fringe should be close to the frozen gradient. Mageau was not able to substantiate this with his experimental results which, in fact, showed a higher gradient in the fringe than in the frozen soil. He attributed this to boundary effects. He did not consider the differing conductivities of the two materials which would have a larger-order effect.

Konrad (1980) has continued in this vein by stating that Mageau found the frozen soil above the warmest ice lens had little to no effect on the heave rate, and yet Konrad used the frozen gradient in all predictive calculations. Certainly for the bulk of his experimental data there appears to be a uniform thermal gradient throughout the sample at the formation of the final ice lens. However, this condition cannot hold true for the sample throughout the test and other authors have detected a noticeable break in the temperature profile at the phase change temperature (Palmer, 1967; Gupta, 1971; Ishizaki and Nishio, 1985). Konrad implicitly recognizes that a break exists as evidenced in the diagram of an idealized temperature profile in Konrad and Morgenstern (1980).

4.3.2 A Transition in Application

As a result, subsequent papers reflect this uncertainty and undergo a transition from using a thermal gradient based on an unfrozen gradient to that of the frozen gradient. Konrad and Morgenstern (1981) explicitly reject the use of the frozen gradient in favour of the the unfrozen gradient and detail its calculation, with examples. In a subsequent paper, Konrad and Morgenstern (1982a) made reference to the thermal gradient at the frost front, but provided no details.

The paper by Konrad and Morgenstern (1982b) marked the turning point in approaches because it was the first

occurrence of the use of the frozen gradient in the water velocity calculation. Paradoxically, the results tabulated for the "C" series of tests (Konrad and Morgenstern 1982b: Table 1) are temperature gradients obtained from warm-side temperatures (Konrad, 1980). This can bee seen in their Figure 4 which shows the results of Test C6, although the reader is cautioned to refer to Konrad (1980, Fig. E.5) for the correct dimensioning of the sample.

4.3.3 Inconsistent Application

Other authors using the segregation potential approach to frost heave prediction have not explicitly described what gradient is being used at the frost front. Nixon (1982) provided measured temperature profiles below a chilled pipeline which, surprisingly, show no break in the curvature at the 0° isotherm. Thus, the gradients on the warm and cold sides of the frost front would be identical. Nixon stated that the gradient changes rapidly in the first day or two, which implies that the frozen gradient was used. This is substantiated by a later work (Nixon, 1986) in which a two-dimensional finite difference analysis was performed. The thermal gradient was calculated by fitting a quadratic through three adjacent points in the mesh, two of which were at temperatures below freezing, and taking the slope of the quadratic at the 0° isotherm.

In the interim, Konrad and Morgenstern (1984) have provided a method of predicting heave below a chilled

pipeline in which they explicitly use the frozen gradient.

The misunderstanding surrounding the temperature gradient is most pointedly demonstrated in a collection of papers presented at the same symposium in which a number of different approaches were used. Akagawa, *et al.* (1985), in referencing only the early papers of Konrad and Morgenstern (1980,1981,1982a) used the unfrozen thermal gradient for their interpretation of laboratory results. Knutsson, *et al.* (1985) used the gradient at the frozen fringe as extrapolated from the nearest two thermocouple readings. As they referenced Konrad and Morgenstern (1982b) it is assumed that they extrapolated from the frozen side. Ishizaki and Nishio (1985) used a frozen fringe gradient equivalent to their frozen gradient for their analysis. They observed a marked difference between the frozen and unfrozen gradients so their results are definitely affected by their interpretation of the segregation potential theory.

Evidently there is confusion or a lack of understanding of the physics regarding frost heave. Equally evident is the fact that the present method of using the frozen thermal gradient provides acceptable long-term results. This can be explained by examining the thermal balance during the formation of the final ice lens: assuming that the approach velocity of the attracted water is constant, there is a unique relationship between the approach velocity and either the frozen or unfrozen gradient.

4.3.4 The Use of the Thermal Gradient in the Frozen Soil

There is a practical reason for using the frozen fringe thermal gradient as determined with the frozen thermal gradient ($\overline{\nabla T}^{\bullet}_{ff}$) instead of a more exacting determination of $\overline{\nabla T}_{ff}$. The determination of $\overline{\nabla T}_{ff}$ requires a knowledge of the thermal conductivities of the frozen fringe and the unfrozen soil, the gradient in the unfrozen soil and the inclusion of latent heat of the *in situ* water. As Konrad's analysis requires a knowledge of thermal conductivities, and as the *in situ* latent heat is less important as steady state is approached, the main difference between the two approaches is in the determination of the thermal gradients adjacent to the frozen fringe.

In Konrad's analysis the frozen thermal gradient is calculated from $\frac{T_c}{l_f}$. In most practical problems, T_c is known to a high degree of certainty because the cold source is either man-made or easily monitored. The distance l_f is readily determined from thermistor readings and will be accurate, given the low step temperature and high frozen thermal gradients of most field problems. The more exacting solution, in constrast, requires more knowledge of the thermal environment of the unfrozen soil. Here, the thermal gradient must be calculated from an assumed environmental temperature, T_v, over an assumed length, l_u. Boundary conditions must be established that will simulate the thermal regime in the physical problem. With such small

unfrozen thermal gradients, secondary effects begin to control the solution such as the "drawdown" of soil temperatures adjacent to the freezing front due to the heat capacity of the soil. This increases the thermal gradient adjacent to the frozen fringe which makes it difficult to determine through field measurements or to model numerically.

4.3.5 Correlating the Two Approaches

Nevertheless, if the segregation potential is to be universally applied, there must be a means of manipulating the value of *SP* so that it can be used with the value of $\overline{v}T_{ff}$ as derived from either method. Allowing that the approach velocity of the water would be identical, regardless of the method used:

$v=v^K$ where 'K' denotes parameters obtained using the $\overline{v}T_f$ according to Konrad's thesis (1980)

$$\therefore SP\ \overline{v}T_{ff} = SP^K \overline{v}T_{ff}^K \qquad [4.21]$$

from Konrad's F.D.M.,

$$\overline{v}T_{ff} = \overline{v}T_f \frac{k_f}{k_{ff}} \qquad [4.22]$$

$$\therefore SP\overline{v}T_{ff} = SP^K \overline{v}T_f \frac{k_f}{k_{ff}} \qquad [4.23]$$

$$= \frac{SP^K}{k_{ff}} \left[k_u \overline{v}T_u + v^K L + e\eta L \frac{dx}{dt} \right] \qquad [4.24]$$

$$\text{Let } r = \frac{SP^K}{k_{ff}} \times \left[\frac{J}{mm^3}\right] \text{ (dimensionless)} \qquad [4.25]$$

$$a_1 = k_u \overline{v}T_u \times \left[\frac{mm^3}{J}\right] \qquad [4.26]$$

$$a_2 = v^* L \times \left[\frac{mm^3}{J}\right]$$

$$= \frac{SP^K}{k_{ff}} k_f \bar{v}T_f \times \left[\frac{mm^3}{J}\right] \qquad [4.27]$$

$$a_3 = \epsilon\eta L\frac{dx}{dt} \times \left[\frac{mm^3}{J}\right] \qquad [4.28]$$

$$\therefore SP\ \bar{v}T_{ff} = r[a_1 + ra_2 + a_3] \qquad [4.29]$$

$$= r[a_1 + r(a_1+ra_2+a_3) + a_3]$$

$$= (a_1+a_3)(r+r^2+r^3+\ldots+r^{n-1}) + a_2r^n$$

$$= (a_1+a_3)(r^0+r^1+r^2+\ldots+r^{n-1}) + a_2r^n - (a_1+a_3)$$

$$= \frac{a_1+a_3}{1-r} + a_2r^n - (a_1+a_3) \qquad \text{for } |r|<1$$

$$\lim_{n\to 0} SP\bar{v}T_{ff} = (a_1+a_3)\frac{r}{1-r} \qquad [4.30]$$

$$= (k_u\bar{v}T_u + \epsilon\eta L\frac{dx}{dt})\frac{r}{1-r}$$

$$= k_{ff}\bar{v}T_{ff}\frac{r}{1-r}$$

$$\therefore SP = \frac{SP^K}{1 - [SP^K/k_{ff}][J/mm^3]} \qquad [4.31]$$

This provides a value of SP to be used with the true $\bar{v}T_{ff}$ for the formation of the final ice lens. It would be less dependable for a progressing frost front because the value of k_{ff} would be highly variable and difficult to determine, and both thermal gradients would be changing.

4.3.6 Practical Application of SP

The segregation potential is a soil property relating the attraction of water to the freezing front due to a thermal imbalance in the soil. As demonstrated in this chapter and in E, this is a result of the suction developed due to a depression of the freezing temperature with co-existing phases. While the physics of the process requires the temperature gradient in the frozen fringe, which has been likened to that of the unfrozen soil, some

applications of the theory have used the SP theory with the thermal gradient of the frozen soil.

This, however, does not affect the usefulness of the SP theory. Due to the interrelationship of the thermal gradients and the amount of phase change at the phase interface, it is possible to use either the frozen or the unfrozen thermal gradient provided that the SP has been determined using the same gradient. Researchers should be well aware that both methods are currently being used.

5. Application of the Segregation Potential Theory

5.1 Method

The dependence of the frost heave rate on pressure has been well documented, as has the build-up of heaving stresses within a confined freezing soil with drained conditions (Hoekstra 1969; Penner & Ueda 1978; Konrad 1980). Thus the degree of restraint of a freezing soil will affect the rate of heave and ultimately the magnitude of heave for any soil. Heaving tests performed under different applied loads have verified this (Konrad, 1980).

This pressure dependence has broader implications within a soil continuum. The relationship between heaving and pressure attenuates the build-up of high heaving stresses in a soil. Localized highly stressed regions at the frost front have a reduced heave rate while other, less stressed regions, experience comparatively higher heave rates. The net result of this differential heaving within a region of non-homogeneous stress is a reduction in the variation of deformation and stresses within the soil.

In the case of a chilled pipeline inducing soil freezing, this reduction in stress variation results in reduced pipe curvature and consequently in lower pipe strains. Prediction of the complex interaction of a cold pipeline with the surrounding soil should result in an improvement in the expected performance of the pipeline. The

economic benefits of this are self-evident.

No analysis to date has fully embraced the continuum approach because of the complexity of the problem. The interdependency of the thermal and structural aspects, and their variation in time, requires formidable computational capacity and no existing computer program can handle this specific problem.

The approach taken in this research was to combine existing software in an uncoupled thermo-elastic analysis. Thus, the thermal and structural aspects of the problem were isolated. The stress field was determined in a static analysis and the temperature field was determined in a transient analysis for a specified time increment. The results were used within an appropriate frost heave model to predict incremental heaves within the continuum. These in turn were used in generating revised input for the thermal and structural analyses programs. By iterating with this procedure the frost heave behaviour of a continuum could be predicted.

The finite element method was chosen for both the thermal and structural analyses. This method allows for non-homogeneity and variable material properties and allows a variety of shapes and sizes which allows complex problems to be modelled. Existing general-purpose finite element programs provided choice in how phenomena could be modelled and thereby the flexibility required to develop the

interconnecting software that would perform the heave calculations.

The thermal analyses were undertaken with the program *ADINAT* (Bathe 1981b) which had the ability to model latent heat effects and to include the effects of attracted water. The program was also similar in structure to *ADINA* thereby reducing the time needed for user familiarization.

The structural analyses required a means of simulating a directional heave, which could be done by modelling it as a directional thermal expansion. The only available program with such a facility was the *SAP IV* program. Its orthotropic thermo-elastic model could be manipulated to develop heaving stresses and deformations in the soil.

Using the stresses, temperature, and temperature gradients, the location, magnitude and direction of heaves for each time step were determined using the segregation potential theory (Konrad and Morgenstern, 1981). These heaves were reduced to modified coefficients of thermal expansion and latent heat surcharges, and re-introduced to the finite element programs as input using the program "TRANS" and the procedure file "LOOP" (Appendices G and H).

While the primary objective of this study was to model heave in a simple fashion by using a constant *SP* and the algorithm described above, it was apparent that a number of problems had to be solved in order to do so. These problems

Figure 5.1 Flowchart of the Heave Algorithm

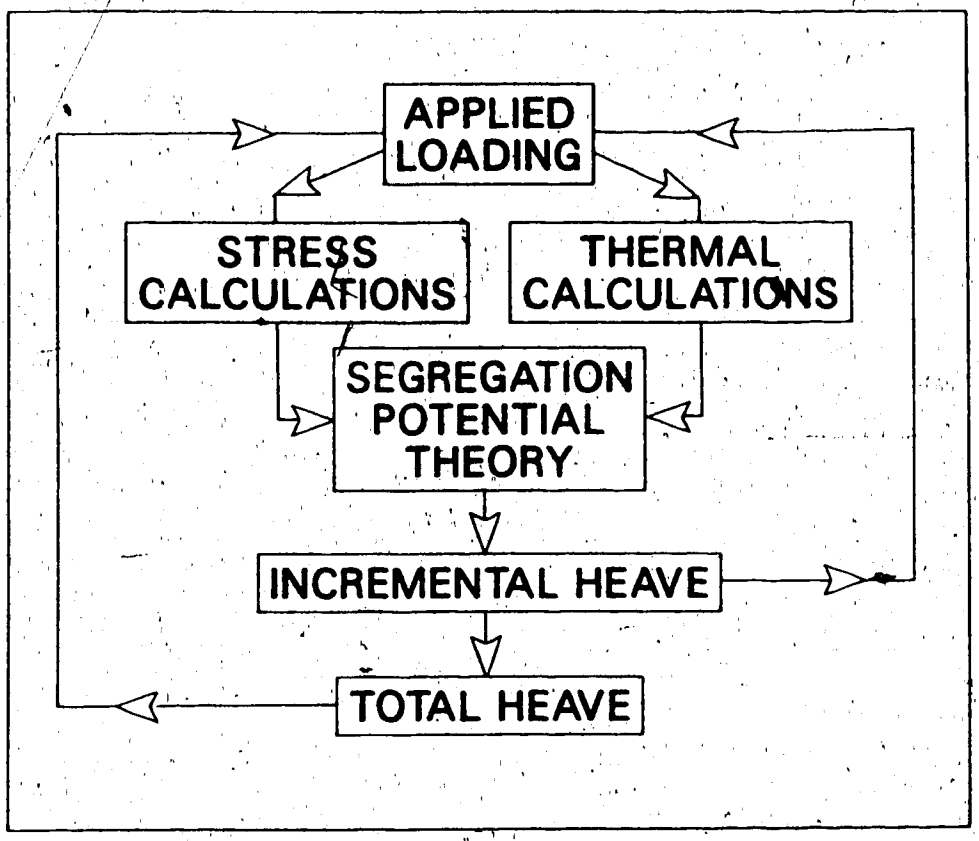

are divided into four areas: modelling assumptions, numerical idiosyncracies, data interpretation and file management. The modelling assumptions relates to the physics of frost heave while the latter three deal with obtaining, presenting and manipulating the relevant data. Often, these latter areas controlled the accuracy and precision of the simulation and as such warranted a closer examination. Discussion of the results of these examinations have been included as appendices and are referred to where appropriate.

5.2 Test NS-1

The final version of program *TRANS* was an elaboration of a simpler version designed to model Test *NS-1*. This test was chosen as the test case because of its simplicity, it being essentially one-dimensional and having no complex boundary conditions.

The test consisted of a 10.4cm column of unfrozen silt, initially at a temperature of +1.0°C. At the beginning of the test, a -3.4°C surface temperature was applied to one end while a +1.1°C temperature was applied to the other. The warm end was hydraulically connected to a water source. As the test proceeded, the frost front penetrated the soil and created ice lenses, particularly later in the test. The freezing continued until the frozen and unfrozen gradients were in equilibrium (Konrad, 1980).

For the numerical analysis, the soil was initially represented as a column of elements. Input decks were prepared for the *SAP IV* and *ADINAT* programs to model the stress and temperature behaviour of the soil. The *TRANS* program was developed in which heave was calculated for those elements adjacent to the frost front. This was done by calculating which element was freezing, taking its average vertical stress and unfrozen temperature gradient, and applying the segregation potential theory (Konrad and Morgenstern, 1980) to obtain an approach velocity for the attracted water.

Given this velocity and the time increment, a height of attracted water was known, which together with the *in situ* pore water, provided a means of calculating the incremental heave. Knowing the vertical height and temperature of the heaving element, a coefficient of thermal expansion could be calculated which would result in a representative heave in the next time step (assuming no restraining boundary conditions).

The initial simulation of test *NS-1* was composed of eight elements stacked into a column. All elements had four modes and increased in size with depth. Two-dimensional elements were used for this one-dimensional analysis in anticipation of future two-dimensional meshes.

The platen temperatures (-3.4°C, +1.1°C) were applied and the frost front advance was observed. Figure 5.2 shows the mesh deformations over time. Poor frost front prediction prompted an examination of the underlying causes (viz. App. J) which proved to be the effect of lumping the latent heat at the nodes, and the mesh geometry. The mesh was subsequently redesigned and further discretized to ensure an even distribution of latent heat throughout. The simulation of *NS-1* was continued.

The next results provided a more consistent frost progression into the soil. The heave for the first 5.5 hours is shown in Figure 5.3. The curves undulate slightly because of the inherent discretization in the mesh and the time

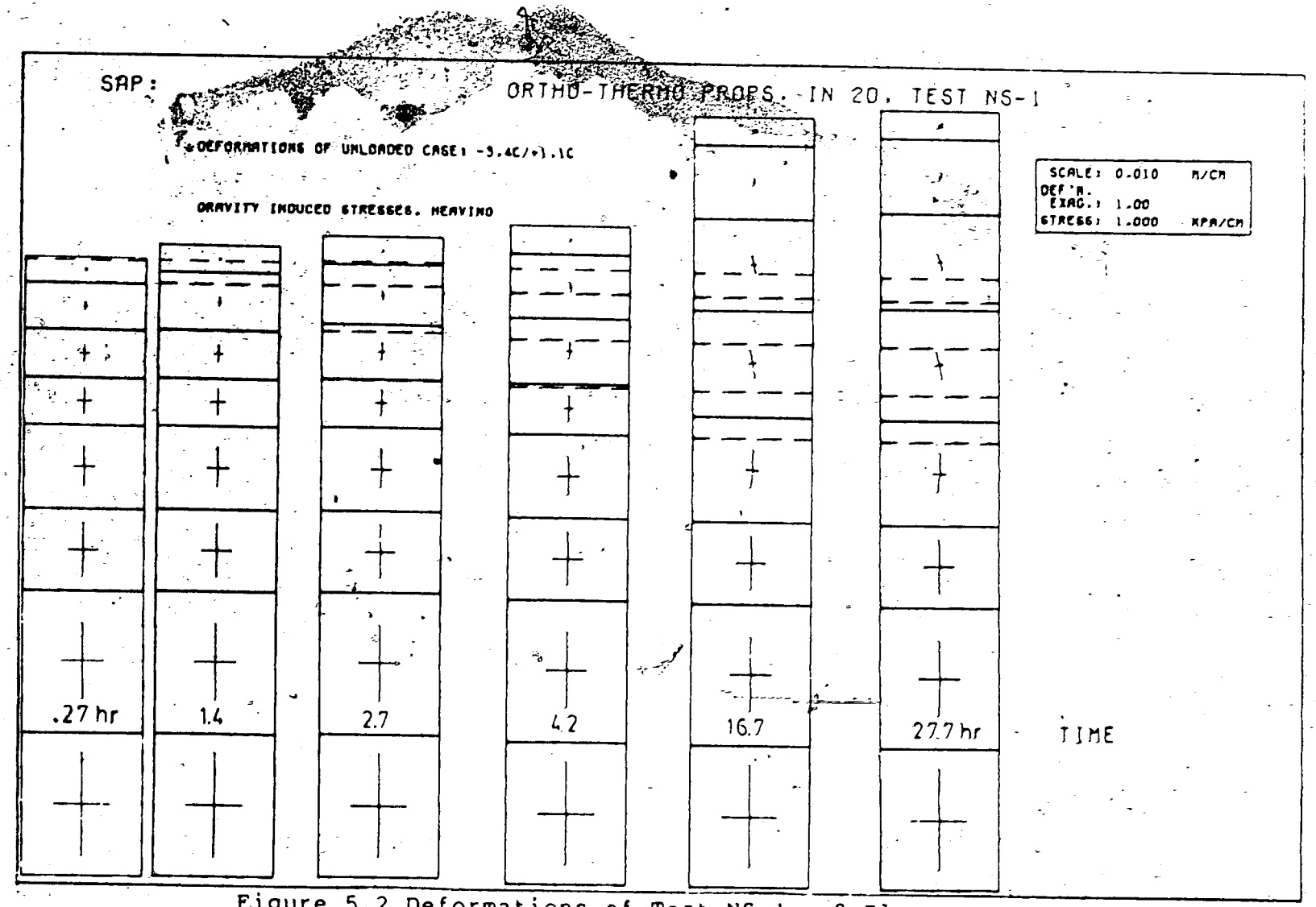

Figure 5.2 Deformations of Test NS-1 - 8 Element Mesh -

function. The curve representing the introduced water, as determined by the segregation potential, SP, and the thermal gradient in the frozen fringe, ∇T_{ff}, shows a very high heave for the first time step. This is because the temperature drawdown curve, on the warm side of the frost front, was very pronounced after the initial application of the cold step temperature. The temperature immediately fell from the initial temperature of +1.1°C to the freezing temperature. The SP value used with this high temperature gradient was held constant at SP_o without any modification for the rate of cooling of the frozen fringe. The result was a high heave for the first time step. This use of a constant SP introduced a significant error for the initial stages of freezing when the frost penetration rate prevents an accumulation of introduced water, however it had little effect on the long-term behaviour.

While the results of this short-term simulation displayed the anticipated tapering-off of heave with time, the magnitude of heave calculated was double that of Konrad's finite difference method. An examination of the finite element results attributed this to the *in situ* portion of the heave which implied that the frost front was progressing too rapidly. This finding was confirmed by comparing the temperature profile with the experimental results.

This rapid advance was not unexpected because the thermal effect of the attracted water had not yet been introduced into the *TRANS* program. The frost front, however, was advancing far more rapidly than even the Neumann solution predicted. An examination of *ADINAT* revealed a weakness within the *ADINAT* program in that it was incapable of correctly calculating the latent heat associated with a nodal temperature when using a phase change range (App. J). As a result, *TRANS* required modification. It was also adjusted to account for the latent heat of the attracted water by calculating an equivalent concentrated heat flux for the next time step. This flux was applied to the heaving element at its colder nodes.

The numerical model had all the essential capabilities to model frost heave. Using a constant SP_0 of $92 \cdot 10^{-5} mm^2/s \cdot C$, the heaving process for test *NS-1* was again modelled. A disappointing underestimation of segregational (introduced) heave was attributed to the choice of *SP* value, so the analysis was re-run using an *SP* of $170 \cdot 10^{-5} mm^2/s \cdot C$. The improved magnitudes of heave (Fig. 5.4), corresponding with the measured experimental values of heave, would indicate that the heave was being modelled accurately. The undulations in the total heave curve, which are far less pronounced in the introduced heave, are due to the irregular advance of the frost front due to discretization of the mesh. However, the latter portions of the two heave curves displayed a scallopped concave shape which indicated a heave

rat[redacted]hat was accelerating rather than decelerating. This was contrary to the expected heave behaviour and to Konrad's reported finite difference results.

To ensure that this observed aberration was not a temporary numerical problem, the analysis was restored from time=34 hours and continued until a time of 98 hours. The deformed mesh is shown in Figure 5.6. The predicted heave behaviour deviated significantly from that expected, both in magnitude and curvature (Figure 5.5). The portion of heave attributed to the freezing of *in situ* water is shown as the difference between the two curves and it agreed well with the experimental values. The heave due to the attracted portion, therefore, was solely responsible for the discrepancy.

An examination of the frost front progression for the analysis using *SP* values of $92 \cdot 10^{-5}$ and $170 \cdot 10^{-5} mm^2/s \cdot C$ showed that the thermal aspects of the problem were being modelled correctly. By deduction, the frozen and unfrozen thermal gradients were also correct since the location of the frost front and the geometry of the the sample were stable. At a time of 30 hours the rate of heave was calculated to cross-check the numerical results:

$$\dot{h} = 1.09\ \bar{v} \qquad [5.1]$$

$$\cong 1.09\ SP \cdot \bar{\nabla} T_u$$

$$= 1.09 \times 170 \cdot 10^{-5}\ mm^2/s \cdot C \times \frac{(+1.1 - -0.1)°C}{36mm}$$

$$= 13.3\ mm/hr$$

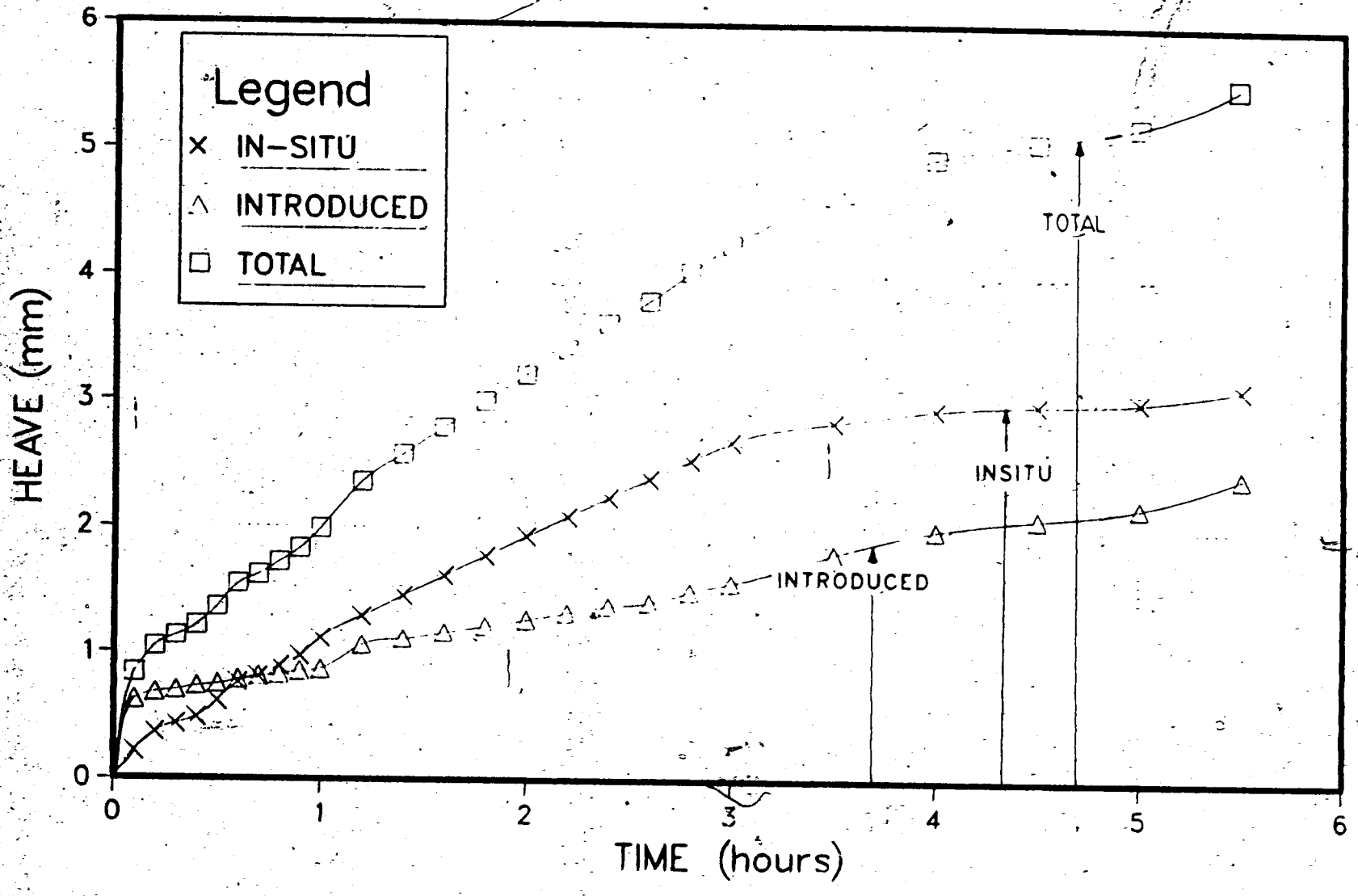

Figure 5.3 Test of NS-1 using TRANS (Unfrozen Gradient)

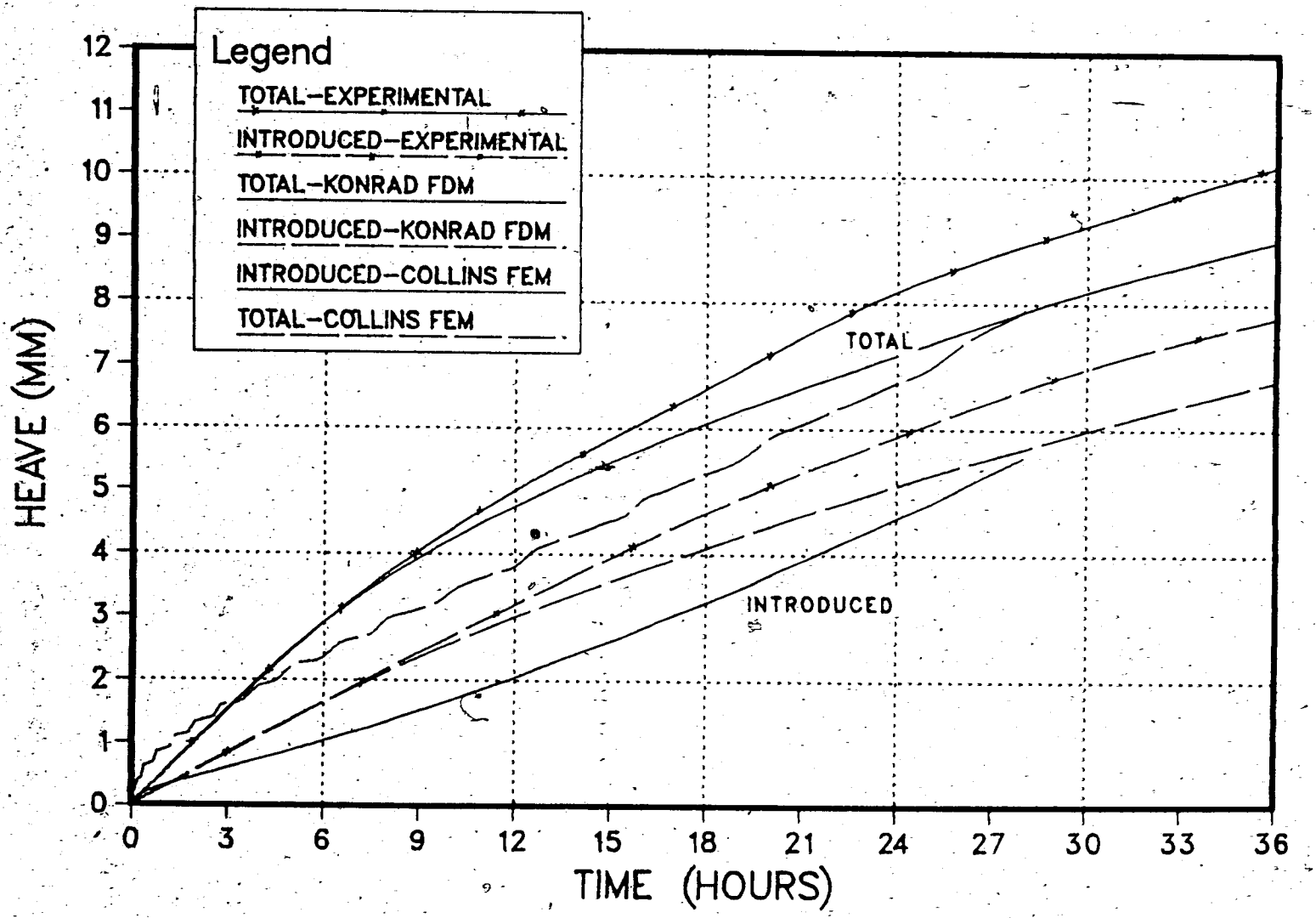

Figure 5.4 Simulation of Test NS-1 Using Unfrozen Thermal Gradient

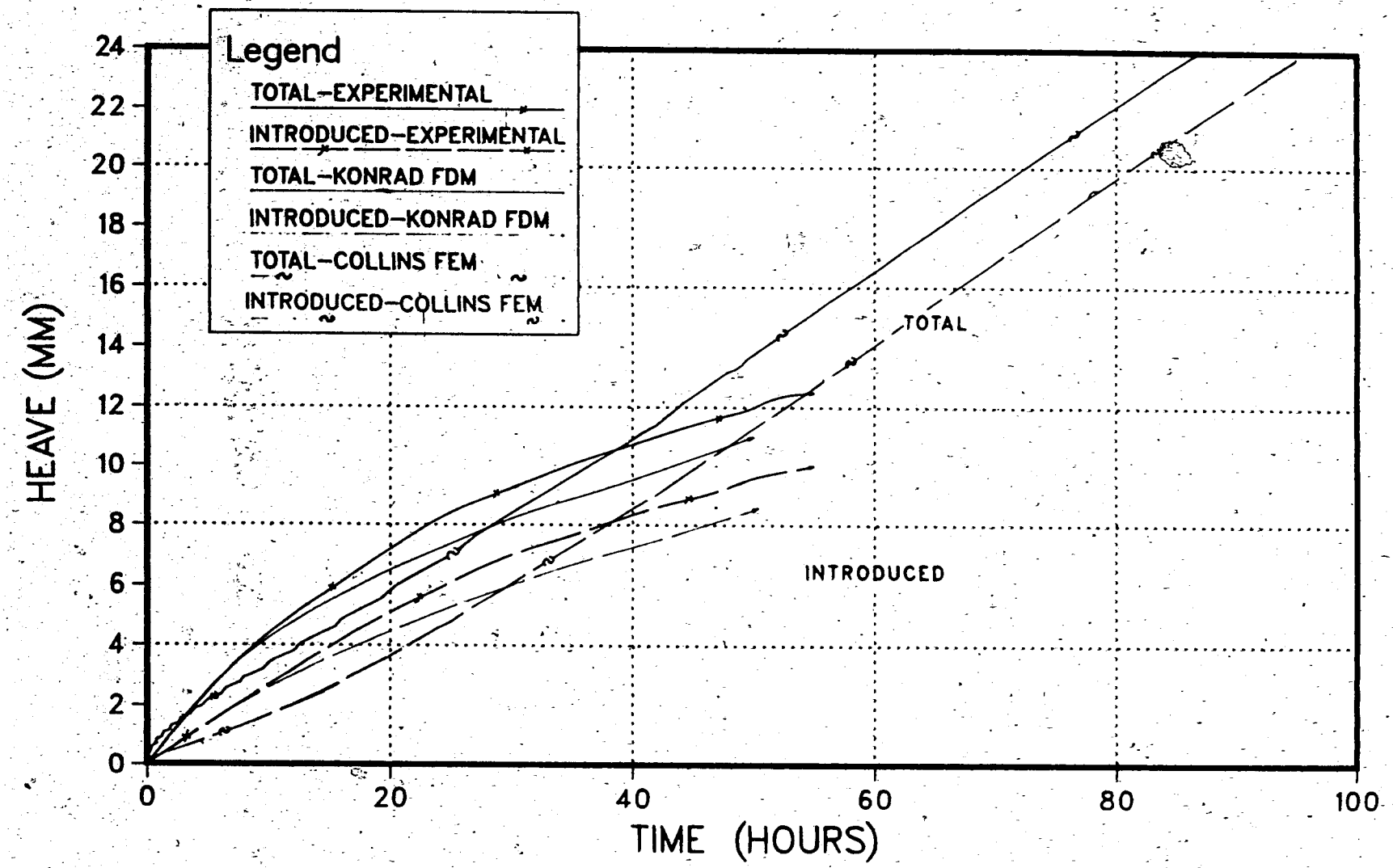

Figure 5.5 Continuation of the Simulation of Test NS-1

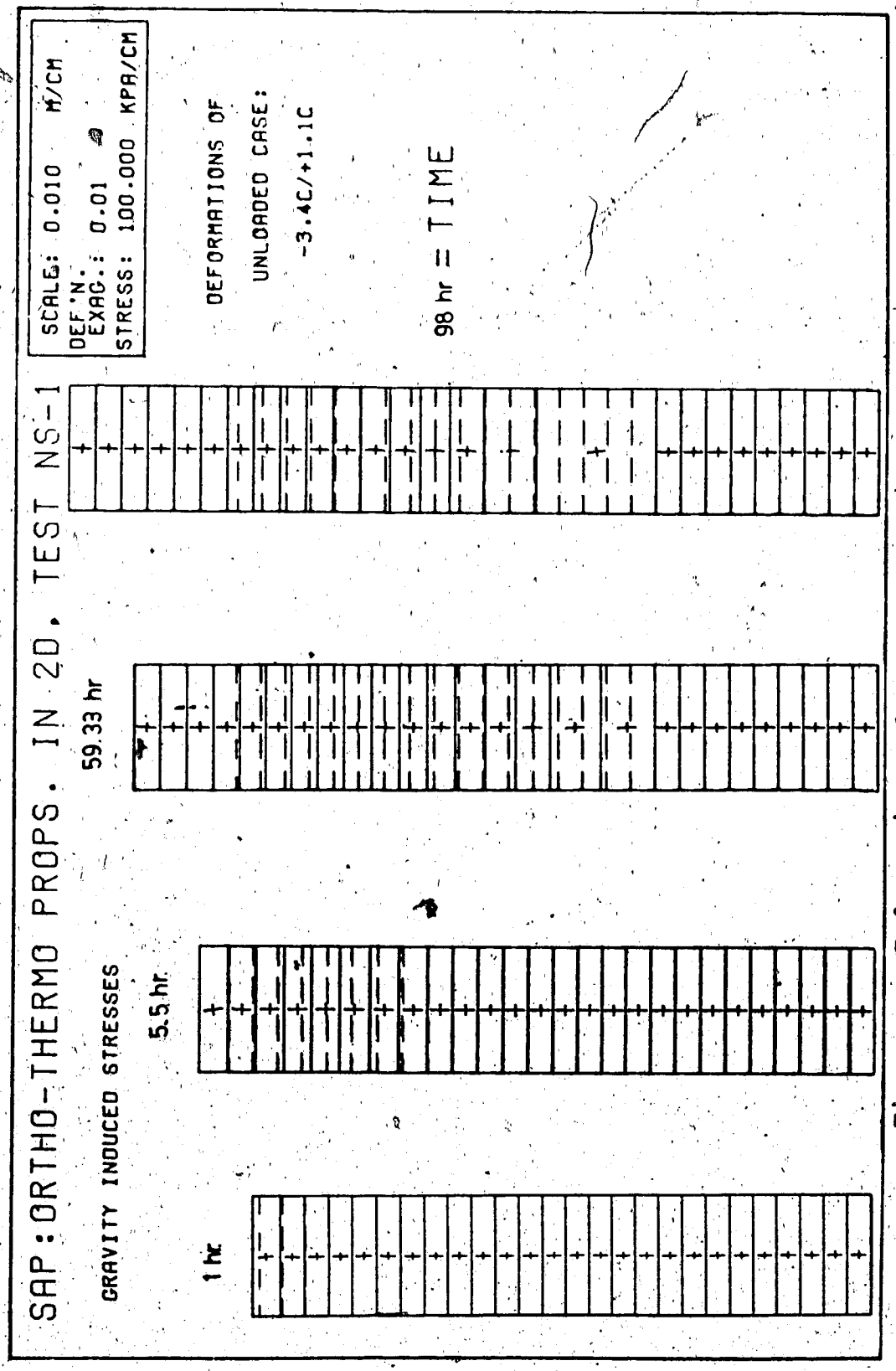

Figure 5.6 Deformations of Test NS-1 - 26 Element Mesh

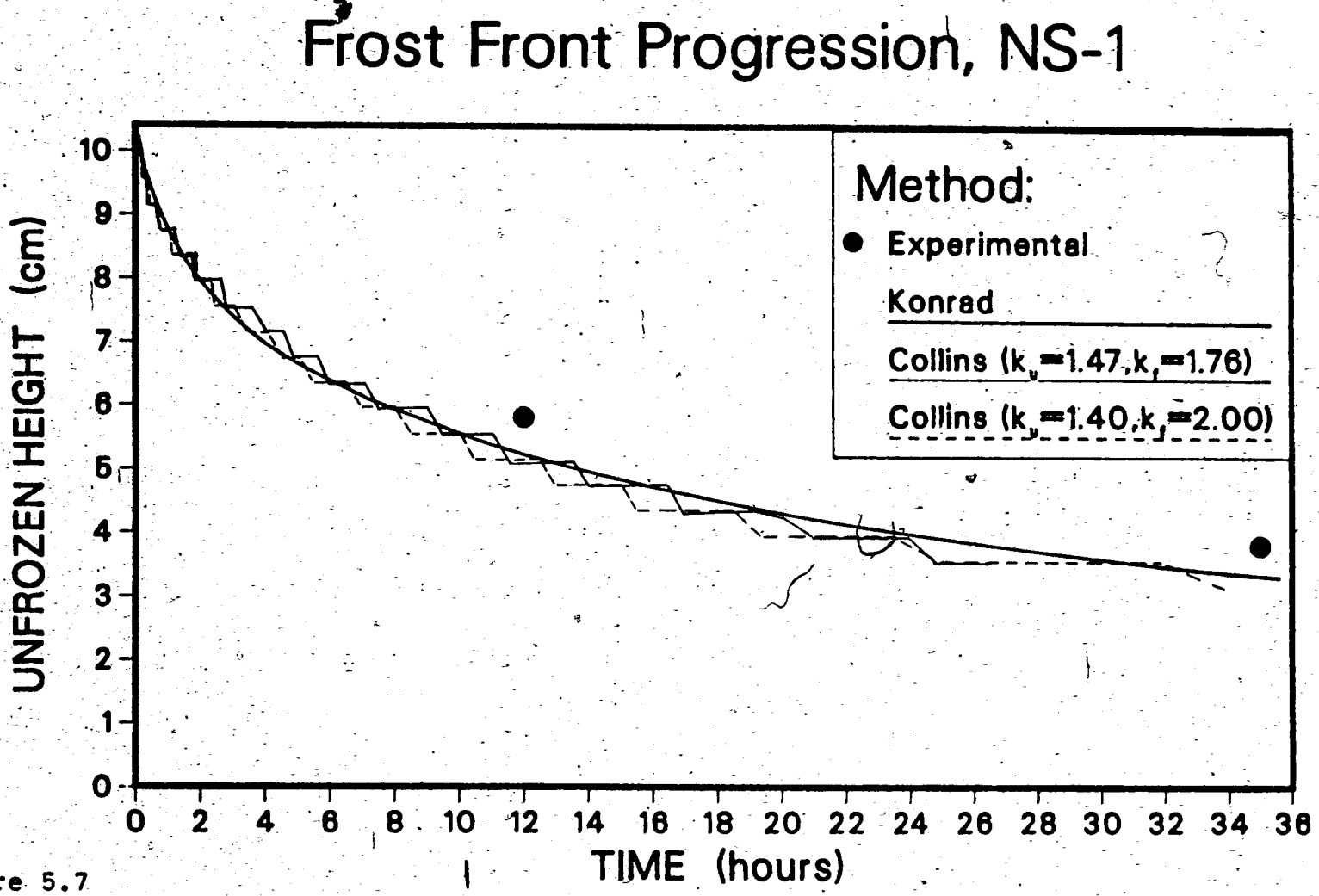
Frost Front Progression, NS-1
UNFROZEN HEIGHT (cm)
TIME (hours)
Method:
Experimental
Konrad
Collins (k_u=1.47, k_f=1.76)
Collins (k_u=1.40, k_f=2.00)
0
1
2
3
4
5
6
7
8
9
10
0
2
4
6
8
10
12
14
16
18
20
22
24
26
28
30
32
34
36

Figure 5.7

By taking the slope of the tangent of the introduced heave curve, the heave rate was found to be $\dot{h} \cong 13$ mm/hr. This confirmed the numerical result, as did similar calculations at other times. An examination of the underlying assumptions in the analysis was warranted in order to determine the cause for the discrepancy.

The use of a constant *SP* for the analysis exaggerated the heave rate for the first few hours. In the long term this assumption becomes more realistic and remains valid until steady-state thermal conditions are approached. No adjustment of the constant *SP* value would result in an improved representation of the heave trend.

An advancing frost front shortens the length of the unfrozen soil thereby increasing the unfrozen thermal gradient with time. A plot of the change in temperature gradients with time is shown in Figure 5.8. The unfrozen gradient reaches a maximum at steady-state. The product of this constant *SP* and the unfrozen thermal gradient (factored by a conductivity coefficient to obtain the frozen fringe gradient) is the introduced water velocity. The segregational heave rate calculated from this should increase with time as confirmed by this numerical analysis due to the increasing unfrozen thermal gradient. In contrast, the observed behaviour and Konrad's finite difference prediction show a heave rate that diminishes with time. Obviously, a fundamental difference in the

interpretation of the segregation potential theory was responsible for the markedly different results.

Konrad, in his finite difference method for the prediction of one-dimensional frost heave, uses a frozen fringe thermal gradient based on the frozen thermal gradient. The implications of this were presented in the previous chapter. It was found that Konrad determined the segregation potential in terms of the frozen thermal gradient instead of the unfrozen thermal gradient. In addition, Konrad's program was deciphered and re-coded to provide an independent check on the numerical model (Appendice F).

Konrad's program was run using input parameters identical to those used in this analysis which were selected and calculated from values presented in Konrad (1980). Excellent correlation with the previously predicted heaves verified these parameters and the re-coded program. By altering the frozen/unfrozen conductivity ratio, and setting the value of *SP* to a constant, the relative effects of these changes could be quantified.

Most significantly, Figure 5.9 shows how the constant *SP* heave curves parallel the experimental curves after ten hours of freezing. The most significant error occurs just after the application of the cold source and diminishes thereafter. For long-term prediction of heave, this error would only represent a small portion of the total heave and

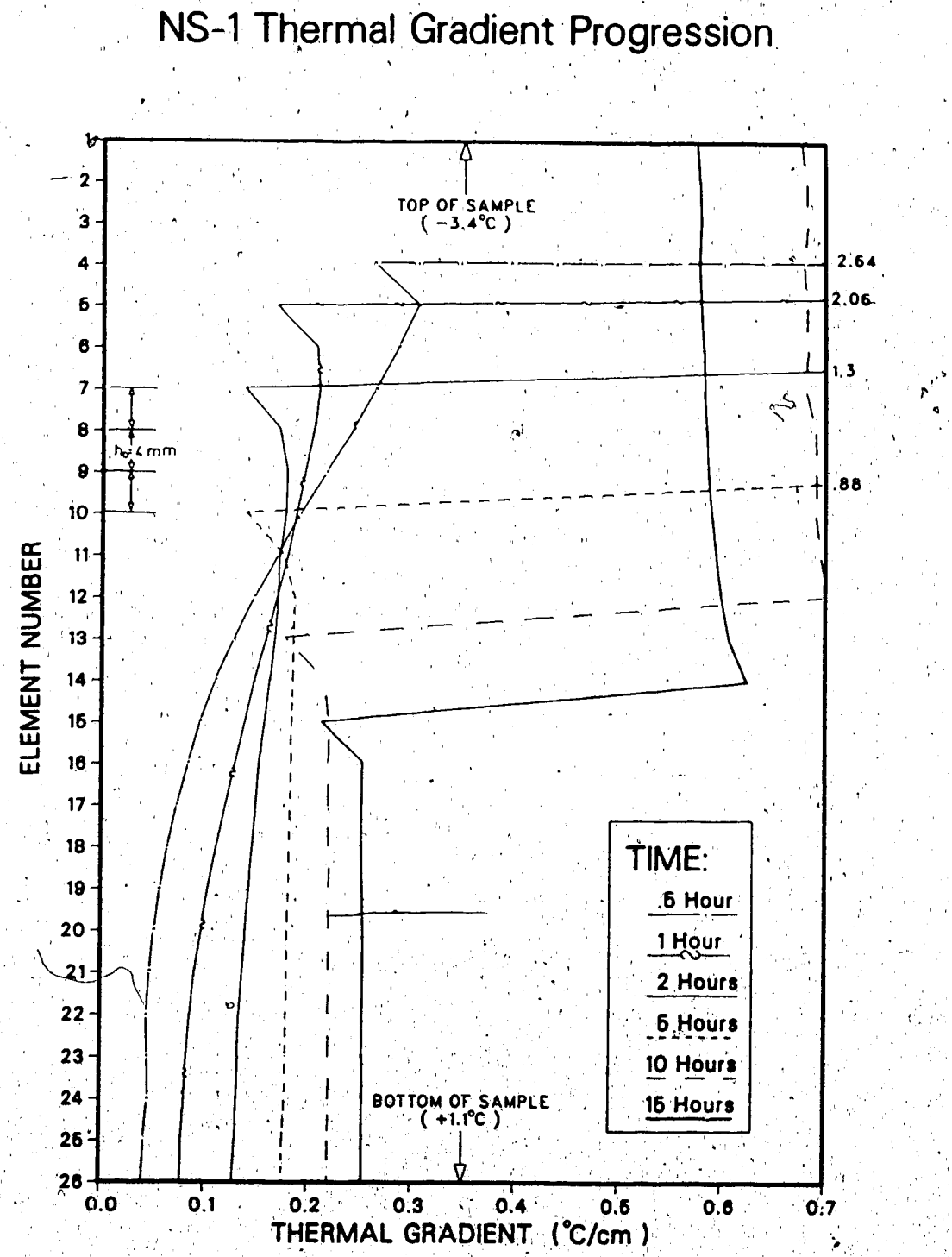

Figure 5.8 NS-1 Thermal Gradient Progression

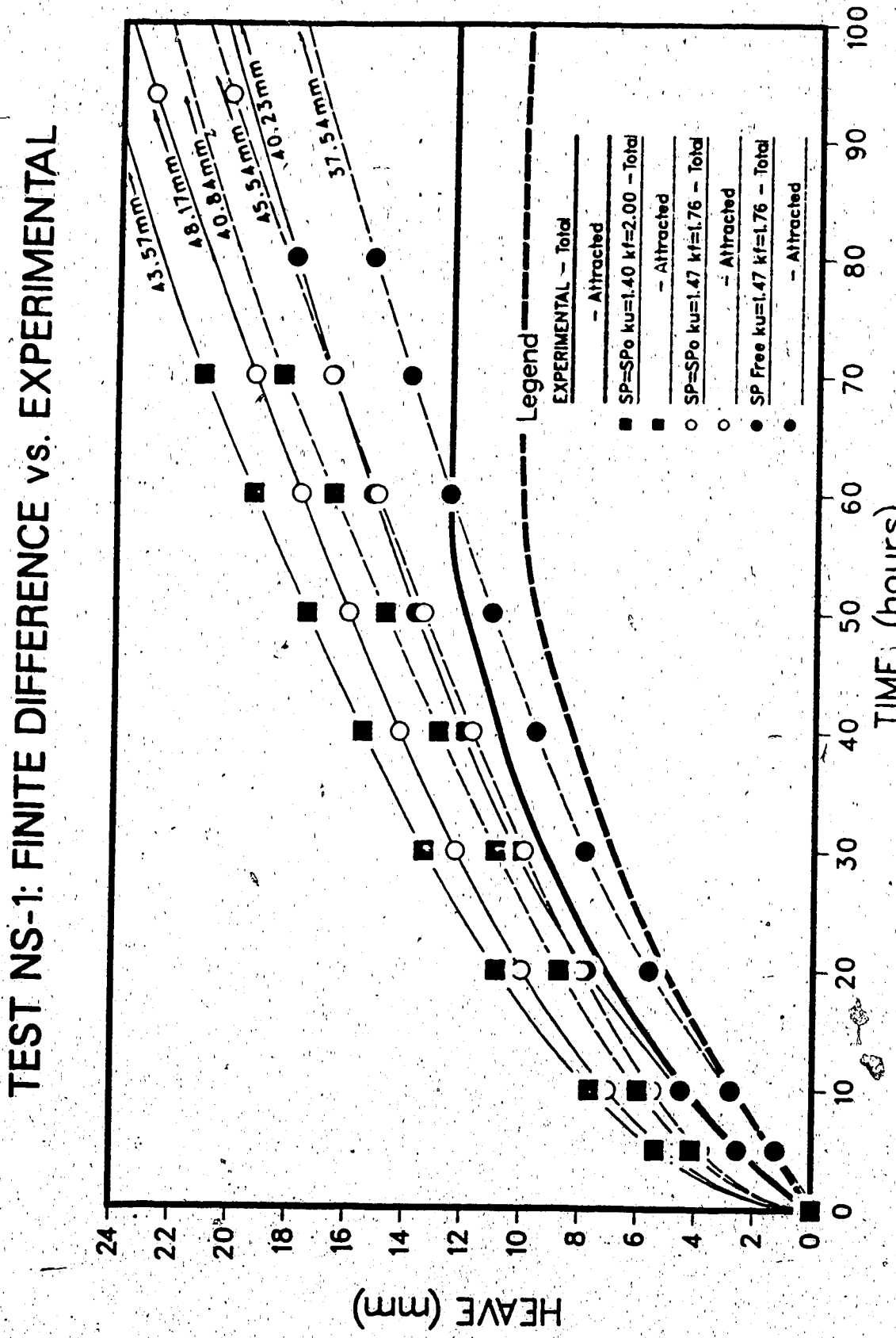

Figure 5.9 Finite Difference Prediction vs Experimental

could be discounted in most engineering applications.

Preliminary calculations indicated that test *NS-1* could be modelled using the modifications to the finite element programs. Essentially, this was a conversion of the heave calculations so that the frozen fringe gradient was based on $\overline{\nabla}T_f$ instead of $\overline{\nabla}T_u$. A stress-dependent *SP* facility was also incorporated into the *TRANS* program to handle the interdependency of stress and segregational heave. Moreover, the segregation potential subroutine within Konrad's finite difference model was modified in a similar manner by reducing the calculated *SP* value for pressure. This provided an independent check on the finite element results.

5.3 Test C-10

The ultimate objective of this research was to develop a method of modelling frost heave involving complex geometry and stress development. Therefore, the logical extension of the simulation of an unloaded one-dimensional problem (Test NS-1) was one involving an applied load. Test C-10 was arbitrarily selected as the test case for this study. Sample C-10 was comparable in dimension to NS-1 but had a 100 kPa surcharge and platen temperatures of -4.7°/+1.8°.

To account for the pressure effects, subroutine *SPTL* within program *TRANS* was modified to reduce the *SP* value as a function of the stress normal to the freezing front. An

interpolation routine was designed to model the SP-T_e relationship (Konrad, 1980; Fig. 6.6) but was later changed to the simpler logarithmic relationship (Konrad, 1980; Tab. 9.1/9.2). An SP value of 92×10^{-5} mm^2/s·C was used as it implicitly recognized the development of suction within the soil. The pressure effects reduced this to $SP=35\times10^{-5}$ mm^2/s·C which agreed well with both the value at the formation of the final ice lens (Konrad, 1980; Table 6.1) and with Konrad's finite difference method program when modified for pressure effects.

The mesh used in this analysis (Figure 5.10) shows the node, element and material numbers. The stress field is represented by principal stress crosses. Prior to this analysis, the top element thickness was reduced to 0.15cm to minimize the effect of specifying a nodal temperature while using a lumped latent heat analysis. The numbering and stresses remained unchanged.

The simulation of C-10 was halted at 215 hours while the sample was still heaving to examine the interim results.

The curves in Figure 5.11 are similar to those of NS-1 up to 135 hours. The introduced heave exhibits a rapid rise at the onset of freezing followed by a long period of an almost constant heave rate. The marginal reduction in the heave rate over this period is due to the reduced frozen thermal gradient created by the additional flow path through the accumulating ice. The curve representing total heave

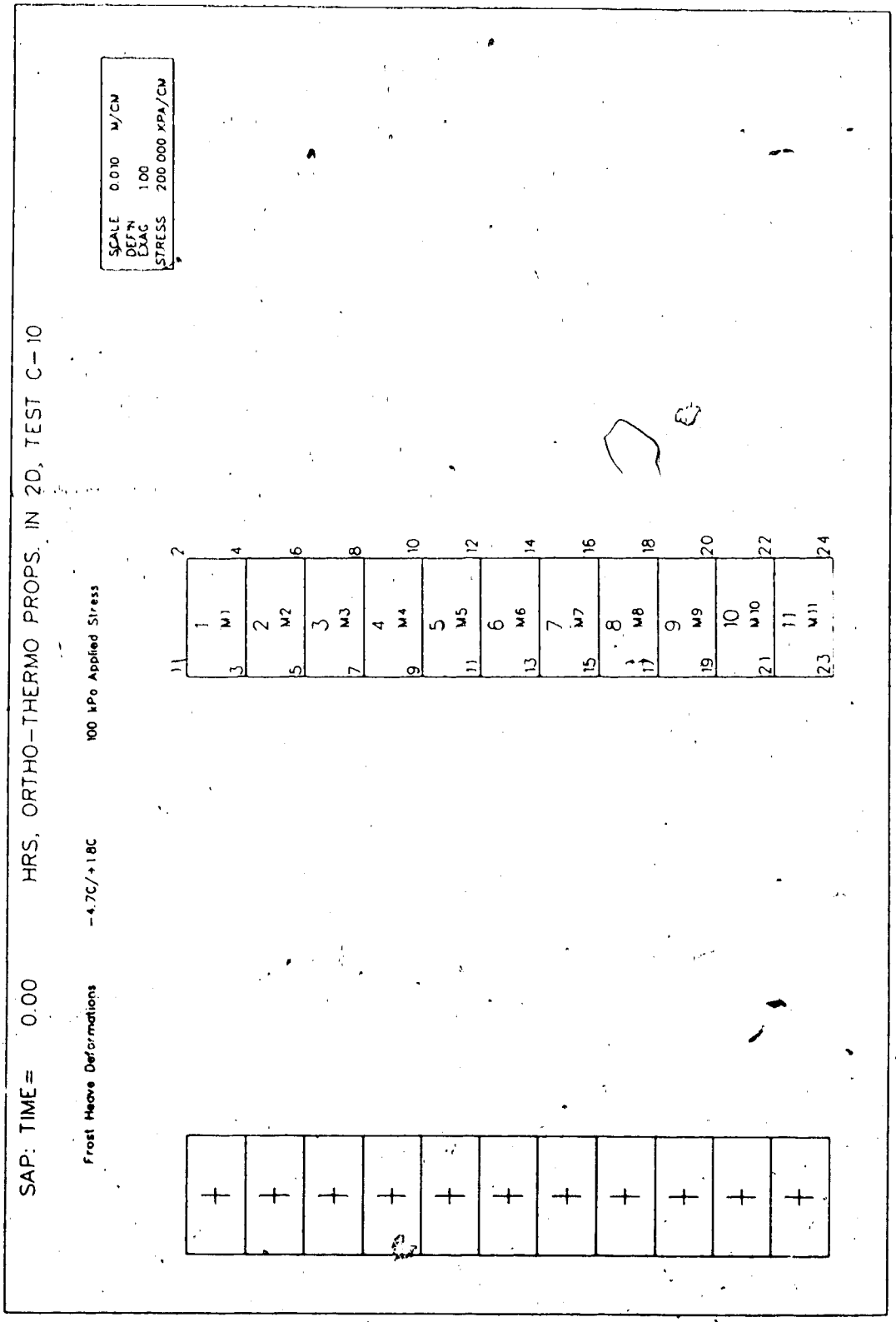

Figure 5.10 Test C-10: Element, Node and Material Numbering

wavers during the initial freezing because of the discretized representation of the sample.

After 135 hours, however, the simulation displayed stepped heave, alternating every time step. The reason for this was an oscillation of the frost front, due to the discretization, and because the heat flux due to conduction in the unfrozen soil plus the segregational latent heat exceeded the flux in the frozen soil. This resulted in a partial thaw-back of the frost front which triggered a no-heave response for the subsequent time step. During that next time step, without the latent heat of the attracted water, the frost front advanced, thereby instigating heave for the next step. This process continued without change up to 800 hours, with an increase in heave step size when the time step also increased.

Konrad avoided this difficulty by relating his *SP* values to the rate of cooling of the frozen fringe. As the rate slowed, the segregation potential was reduced. This resulted in a gradual reduction in the segregation heave. In addition Konrad performed a rough heat balance check in his FDM program that reduced the velocity of the attracted water in response to the onset of steady-state thermal conditions.

It was not practical in this analysis to modify the *SP* value to account for the frost front advance. Due to the lumping of latent and specific heats within the *ADINAT* program, the frost front advances in surges. The heat fluxes

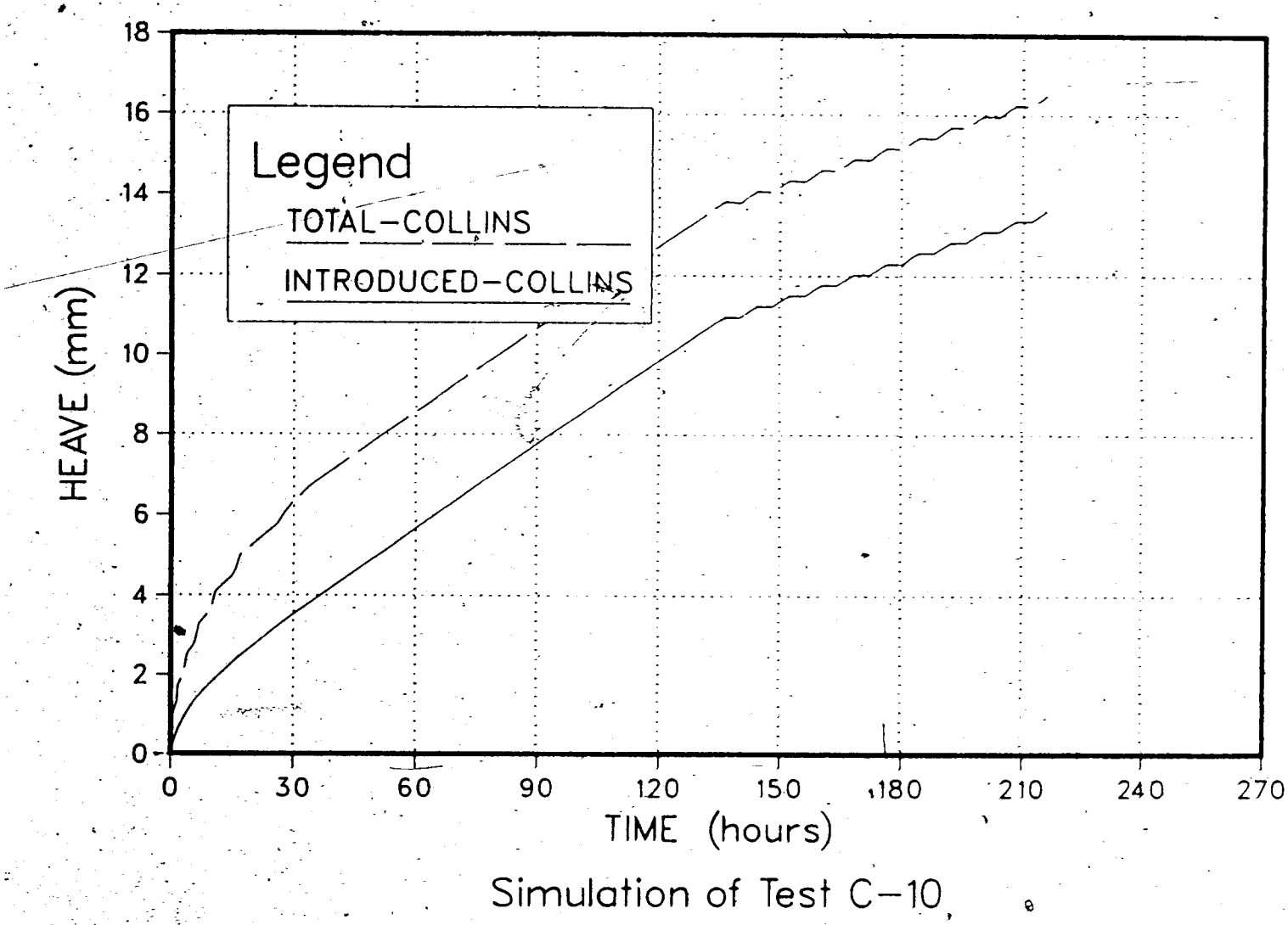

Figure 5.11 Stepped Heave Behavior, Test C-10

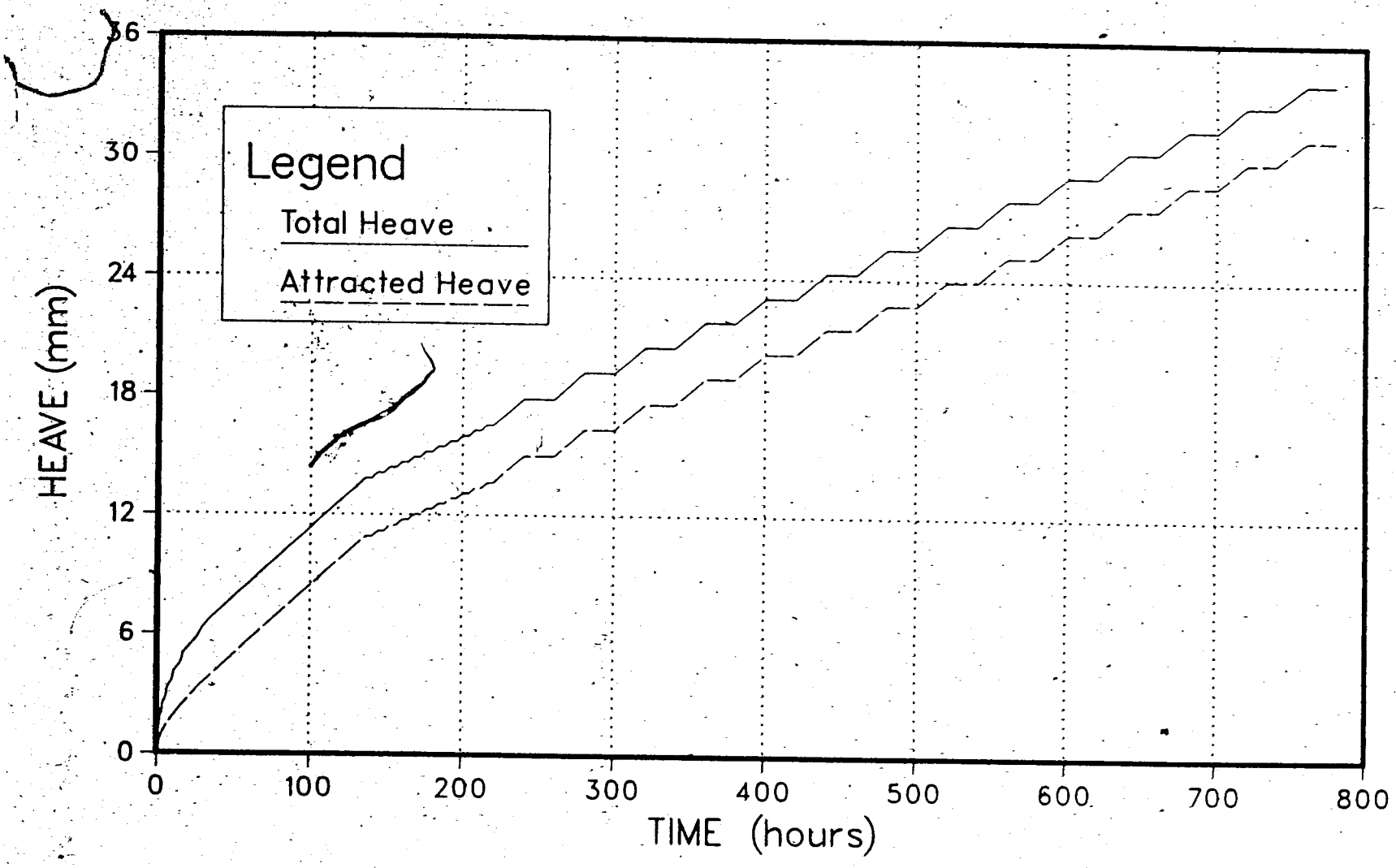

Figure 5.12 Extended Simulation of Test C-10 with Stepped Heave

on either side of the heaving element proved more reliable and consistent for calculations so an algorithm was inserted into *TRANS* to search elements adjacent to the frost front for appropriate fluxes. This modification resulted in a smooth, although sudden, cessation of heave (Figure 5.13). A slight reduction in the heave rate is seen just prior to steady state conditions and is not as gradual as Konrad's FDM due to the use of a constant *SP*. The analysis was continued up to a time of 150 hours to ensure that steady state had been reached.

This analysis was performed using $\overline{\nabla}T_f$ and $SP=92\times10^{-5}$ $mm^2/s\cdot C$. In keeping with Konrad's determination of the thermal gradient, $\overline{\nabla}T_f$ was subsequently factored by a ratio of thermal conductivities to obtain a value for the frozen fringe gradient, $\overline{\nabla}T_{ff}$. This was used in the subsequent analysis which developed the deformed mesh shown in Figure 5.15.

When the results of this analysis, Figure 5.14, are compared with Figure 5.13, three observations can be made. Firstly, the rate of heave was greater for the latter test due to the use of the larger thermal gradient, $\overline{\nabla}T_{ff}$. Secondly, steady state was attained earlier when using the frozen gradient instead of the frozen fringe gradient. This was entirely due to the inhibiting effect that attracted water had on the frost front advance: more of the frozen soil's heat flux was used in conducting away the latent heat

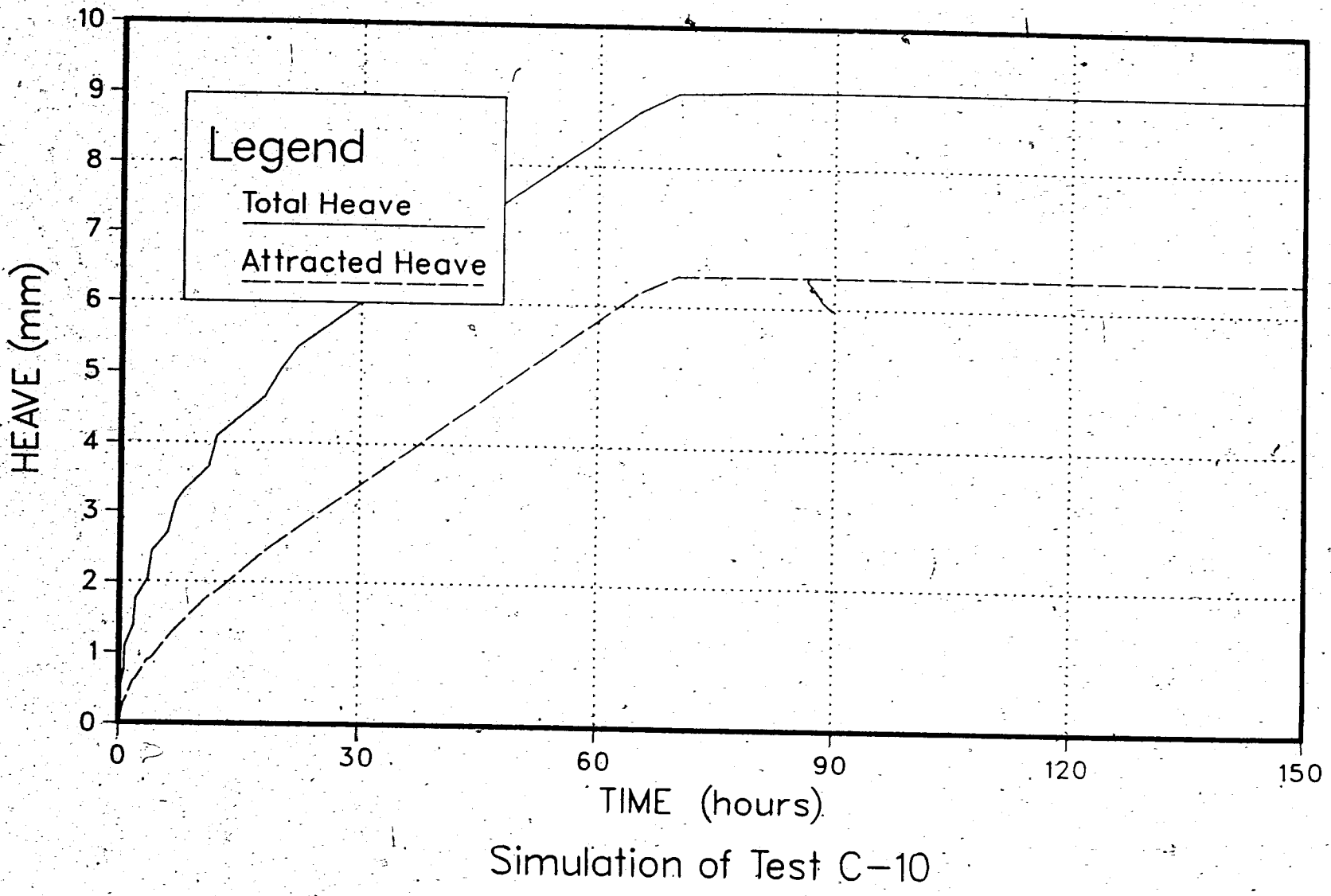

Figure 5.13 Heave Prediction using the Frozen Soil Gradient

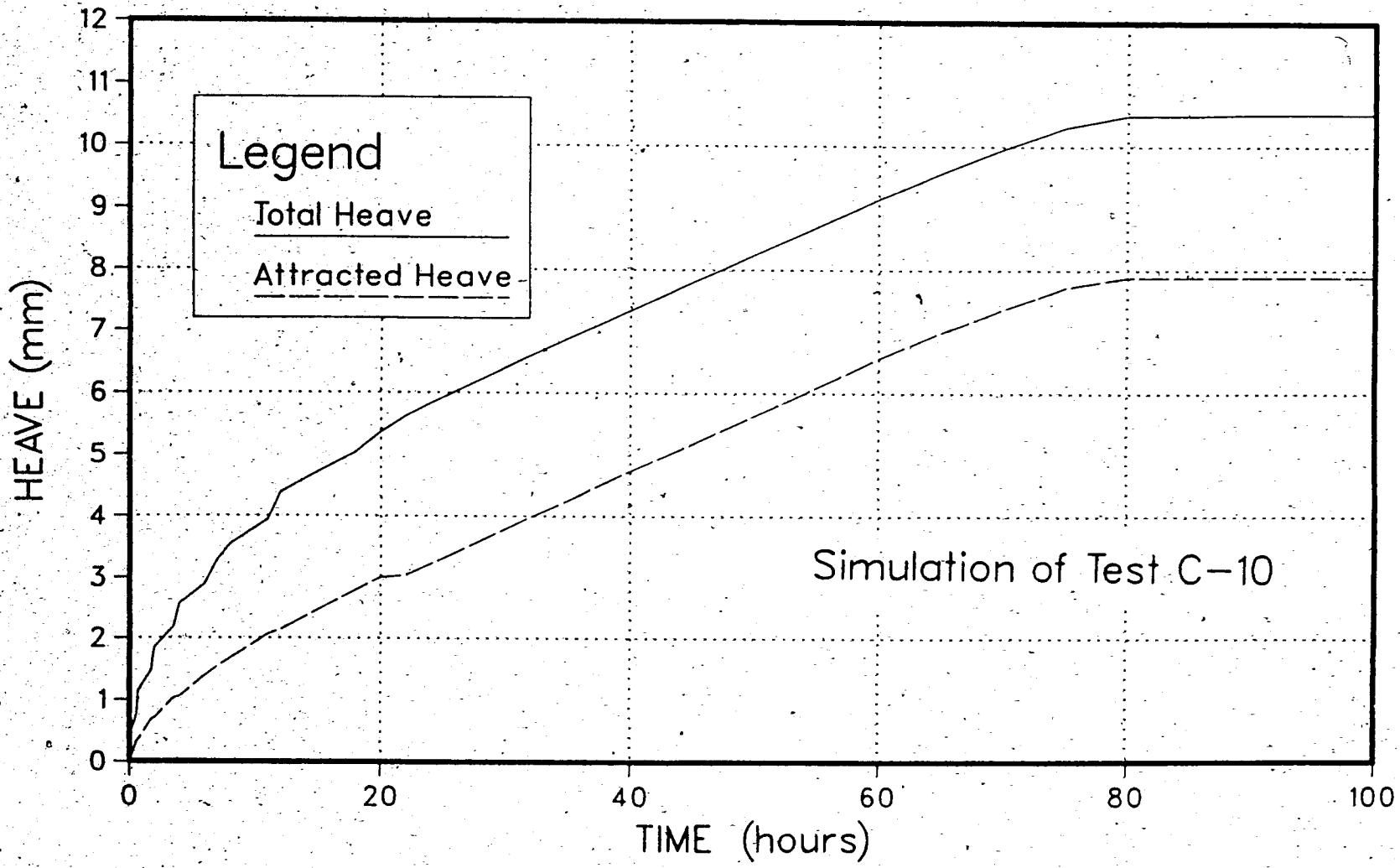

Figure 5.14 Heave Prediction using the Factored Frozen Soil Gradient

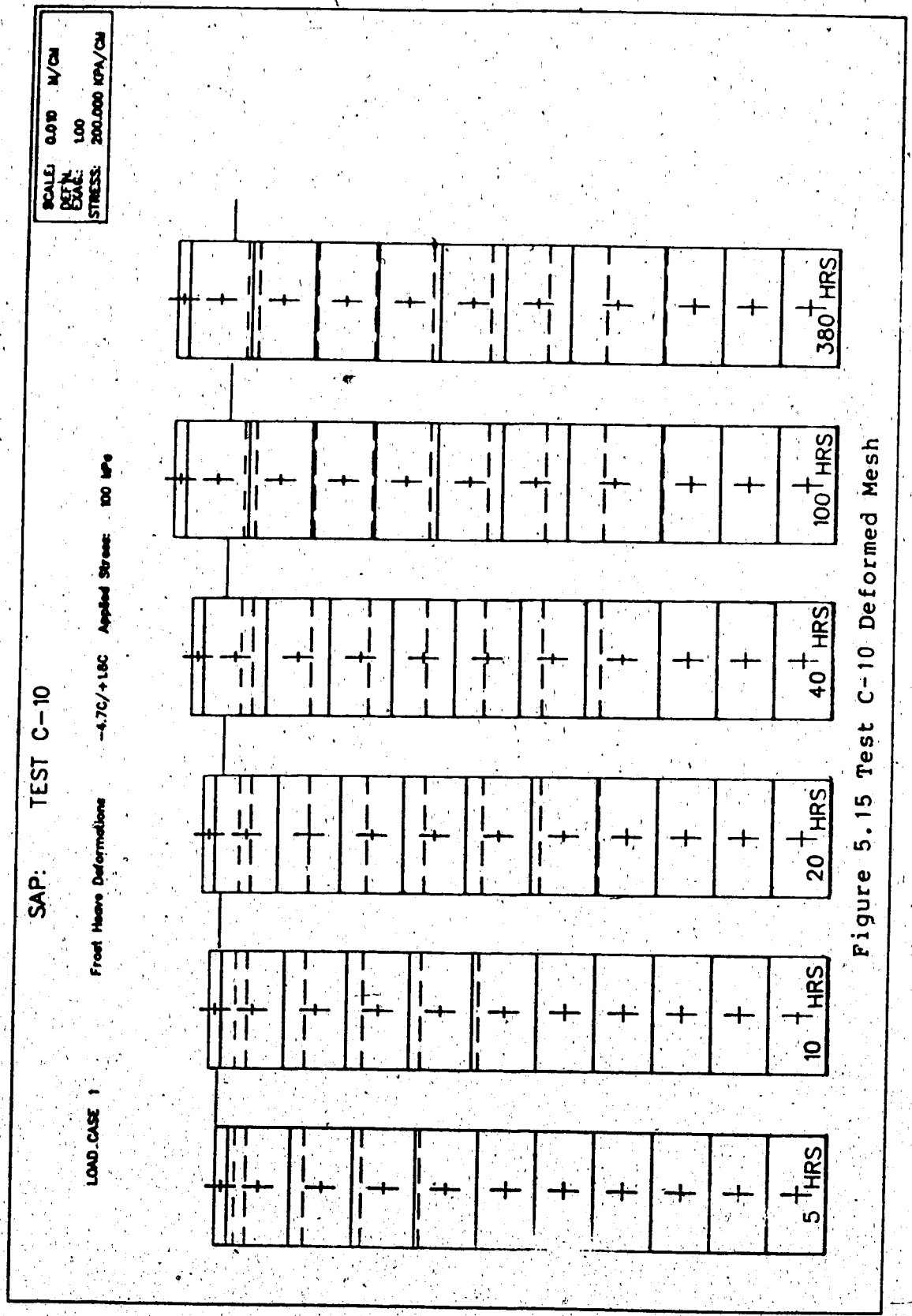

Figure 5.15 Test C-10 Deformed Mesh

of the attracted water, leaving less for the freezing of *in situ* water. Thirdly, the segregational heave remained constant for one time step at a time of 20 hours. The *ADINAT* results at that time had predicted an unusually low gradient because the frost front had just advanced forward, resulting in a temperature lag in the frozen nodes. This type of numerical error could not be prevented without developing a complex correcting algorithm. This small error was a result of the combination of the small element size and rapid frost front advance and would only occur at the beginning of freezing. In addition, by reducing the heave, it partially corrected for the conservative assumption of $SP=SP_o$ for the initial portion of the test.

Figure 5.16 compares the results of this analysis with both the experimental and that of Konrad's FDM modified for pressure effects. The results of the finite element procedure are in agreement with the experimental results both in final magnitude and curvature. Konrad (1980, Fig. E.9) reports an initial water expulsion, followed by intake as noted by other authors (McRoberts and Morgenstern, 1975). In this analysis, this phenomenon is not modelled but the resultant overestimation of attracted water is compensated by the shorter heaving duration of the simulation.

The reason for the shorter heaving period in the simulation is not clear. Insufficient experimental data prevented a comparison of the segregational heaves. The

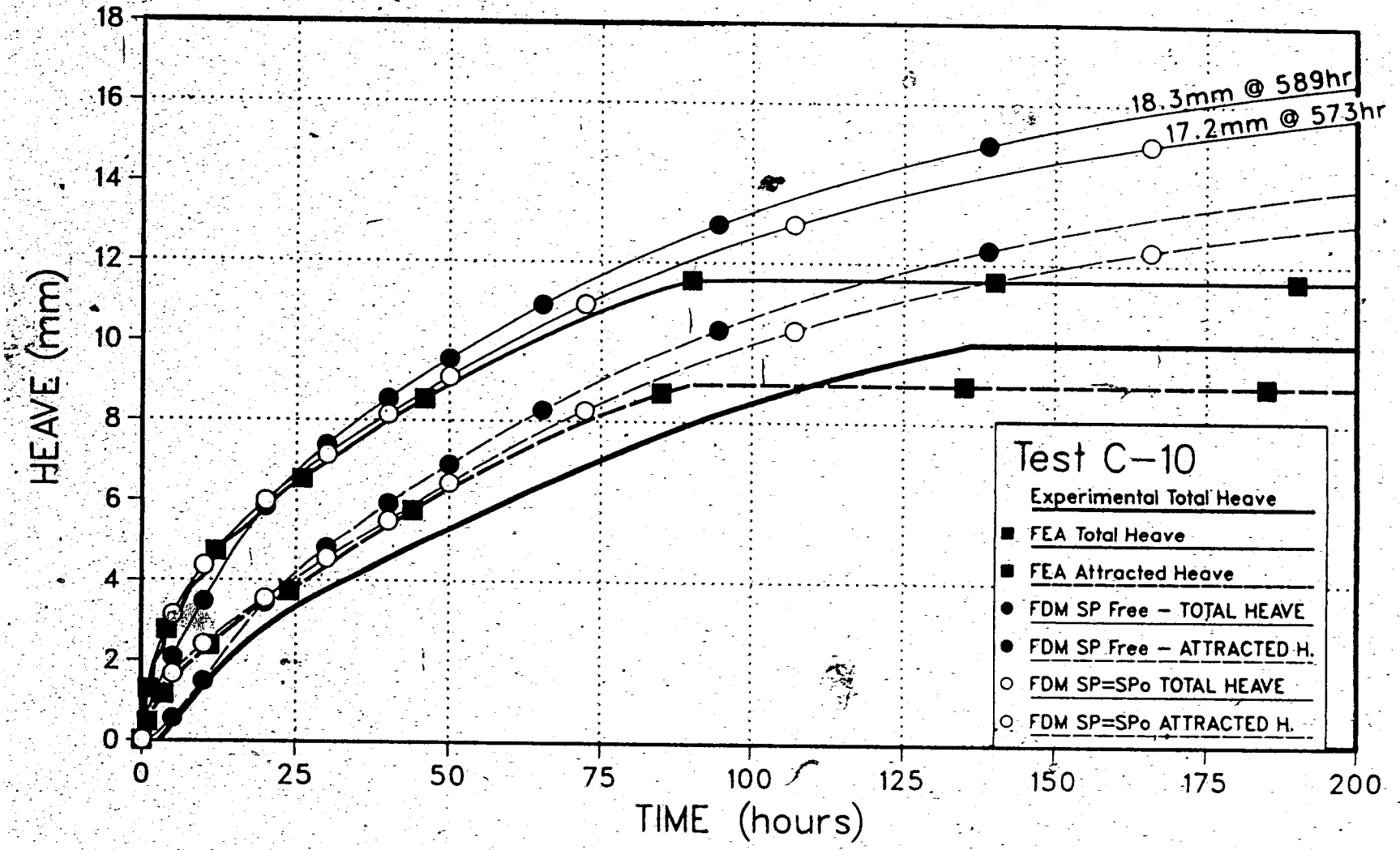

Figure 5.16 Comparison of Predictive Methods

differences could be due to the assumption of an instantaneous application of the -4.7°C surface temperature in the numerical analysis as opposed to the experiment's thermal loading, in which the surface would drop from the sample's initial temperature.

Konrad's FDM program was run twice, once with the internally calculated *SP* values and once with a constant *SP*. In both runs the segregation potentials were corrected for pressure effects. Their total and attracted heaves are shown in Figure 5.16 and are significantly greater than those of the experiment or the finite element simulation. The marked increase in heaves occurs during Konrad's retreating frost front phase when the water velocity is reduced. It is evident from statements within Konrad's program that the prediction of this condition is delayed since the ratio of conductivities (k_f/k_{ff}), used in the main body of the program was omitted from the power balance equations. This underestimates the thermal gradient in the frozen fringe and thus the retarding effect of the arriving latent heat. In addition Konrad assumes that the net heat flux between the frozen and unfrozen soil will necessarily be used in freezing attracted water. However, it is apparent from his experimental work that a warming of the segregation freezing temperature occurs that results in a thin margin of frozen soil between the base of the ice lens and the 0° isotherm at steady-state (Konrad 1980; Fig. E.9). This would have a significant effect on the sample's thermal dimensions and on

the driving physics of the Clausius-Clapeyron equation.

In comparing the two FDM results, the analysis using the internally-determined *SP* predicted the higher heave. This was because most *SP* values for the first 30 hours were significantly higher than the fixed value used in the second analysis. Both analyses predicted an ultimate heave of h≅18 mm and displayed identical heave rates during the formation of the final ice lens.

In conclusion, it is evident that the finite element procedure provides the superior prediction of heave for the loaded sample. A close examination of the results of this analysis reveals a marginal increase in heave (0.008 mm) between 90 and 130 hours, with no change up to 400 hours (Appendice I). This was due to minor adjustments of the thermal gradients and indicates a minute advance of the frost front into the unfrozen soil is occurring.

5.4 Modification of the Coefficient of Thermal Expansion, α, for Two-Dimensions

The simulation of frost heaving in a one-dimensional mesh was ~~relatively~~ simple to implement especially since the heat flow was parallel to one of the elements' axes. In the previous analyses (tests NS-1 and C-10) heave was simulated by manipulating the directional coefficients of thermal expansion available with *SAP IV* two-dimensional quadrilateral elements. The coefficient of thermal

expansion, α, was set to zero for two of the three orthogonal directions and the third was set equal to the vertical heave for the element divided by the change in average temperature and the height of the element parallel to the heave:

$$\alpha_{vertical} = \frac{D_{vertical}}{H_{vertical}\Delta T_{avg}} \qquad [5.2]$$

The *SAP IV* program then reversed this procedure to calculate volumetric distortions. In some cases these distortions would be totally or partially restrained thus developing element stresses. These stresses were then used in concert with thermal gradients and Konrad's segregation potential theory to obtain incremental heaves for a given time increment. This entire procedure was repeated for each time increment.

For true two-dimensional heaving, a number of new difficulties arose. First, the direction of heaving could no longer be arbitrarily set *a priori*. Certainly the rational approach would be to anticipate the direction of heat flow and align the elements accordingly; however, this would only be an approximate measure and any stringent geometric constraints would unnecessarily restrict the adaptability of the program. Instead, the problem was approached on the basis that a simple effective numerically-complete method was needed to provide an acceptable answer for any reasonable mesh configuration.

One difficulty in using a coefficient of thermal expansion to model heave in two dimensions is the assumption that the heave distortion is distributed evenly through the entire element. For rectangular elements with heat flow parallel to an axis, modelling the formation of a thin incremental layer of ice as a macroscopic property of the whole element is an excellent simplification of the physics involved. However for irregular elements or skewed heat flow the numerical model distorts the element as if it were spatially elongated parallel to the heat flow rather than by inserting a thin slice of ice material, at the 0° isotherm, perpendicular to the flow. A rational mesh configuration that aligns element axes parallel to the anticipated heave would minimize the effect of this approximation.

One of the new difficulties arising from the two-dimensional analysis was the varying direction of heat flow. This was due to the changes in the applied heat sources or to a reorientation of heat flow as freezing and heaving progressed. A book-keeping method then became necessary to record and update the directions of heave for each element.

The calculation of α also assumed that the accumulated heave is unidirectional and not multi-directional as would truly be the case for a directional heat flow that changes orientation during the heaving process. A rigorous approach to heaving would require complex equations to describe the distorted geometry of heaved elements. This complexity would

not have been justified in light of the level of precision of other portions of this analysis. In fact *ADINAT*, by lumping the latent heat at the nodes, simplified the heave problem by stabilizing the orientation of heat flow within elements resulting in a nearly uni-directional heave.

Three approaches to implementing the heave accumulation were considered. The first was to resolve the incremental heaves from each time step into perpendicular and normal components. A file containing each element's initial heave vector was updated with subsequent heave components parallel and perpendicular to it. This approach was discarded because volumetric distortions associated with a directional heave are less than or equal to the distortions calculated using the components of heave. The second approach developed the concept of an expanding heave surface to record the accumulating heaves. This was found to be too cumbersome to easily implement.

The last approach was to use vector addition to increment heave. The magnitude and direction of the resultant would be used in determining the single directional coefficient of thermal expansion, with all heave components resolved into absolute values to prevent any cancellation of heave as a result of a change in direction. This method had the advantage of being numerically simple but was restrictive in limiting heave to only one direction with no perpendicular components. No difficulty was

anticipated with this method since the direction of heat flow throughout the mesh remained fairly constant, particularly with the lumped latent heats and heat capacities. In addition, abrupt change in the heat flow direction would likely be attributable to the lumping and would not be a function of the physical model. The smoothening effect of using this method was preferable to limiting the heave direction to the initial direction.

A series of *SAP IV* runs confirmed that thermal distortions of elements with a single effective α value would result in an elongation of the element in the prescribed direction.

Once an element was determined to be freezing, thereby attracting water to the freezing front, it was necessary to know how much water was being attracted each time step. In a one-dimensional analysis the flow rate is multiplied by the time increment to obtain a directional incremental heave which could be used directly with the element height to calculate an alpha factor.

In a two-dimensional analysis heave could be resolved into components which would determine both the magnitude and direction of the element heave. Using this value in Equation 5.2 presented difficulties as the element "height" would no longer be applicable: the elements being non-rectangular and with heat flow skewed to the elements' axes. A method would be necessary to obtain an equivalent height parallel to the

heat flow in order to calculate the pertinent α factor.

The "average" length of the heaving element parallel to the heat flow was chosen to represent the element "height". This length would vary depending on the location within the element so the evaluation points had to be chosen to minimize any bias. The four gauss points were arbitrarily selected, and the edge-to-edge lengths through these points, parallel to the heat flux, were used to calculate the average height for the element.

This entire procedure was complex and resulted in inconsistent results: isolated elements occasionally developed odd stresses. A major modification was made to subroutine *COEFF* within *TRANS* to express α in terms of a volumetric expansion instead of a linear elongation. Thus, the calculation only required the span of the frost front within the heaving element, greatly simplifying the procedure.

5.5 Input Parameters for the N.E.S. Simulation

5.5.1 Soil Parameters

The thermal properies used in the N.E.S. analysis were obtained from Konrad and Morgenstern (1984) and verified with values calculated from data given by L.E.C. Engineering Ltd. (1984). For the calculations it was assumed that 10% of the water in the frozen soil did not freeze. The thermal

conductivity of the frozen fringe, k_{ff}, was assumed to be between the frozen and unfrozen values in the same proportion as for Test NS-1 (Konrad, 1980). All pertinent values soil properties are listed in Table 5.2.

5.5.2 Soil Stiffness

There was no published value for the soil stiffness at this site. Values were obtained by correlating soil indices with those of Duncan, *et al.* (1980) for which stiffnesses could be calculated. The material with indices similar to those of Calgary Silt was the Birch Dam Shell Sandy Silt (ML-3B) for which the initial tangent modulus was

$$E_i = 270 \times 101.35\text{kPa} \left[\frac{\sigma_3}{101.325\text{kPa}}\right]^{.38} \qquad [5.3]$$

Assuming K_o conditions and a Poisson's ratio of ν=0.33, the initial soil modulus was related to the overburden pressure. Using Konrad and Morgenstern's (1984) estimate of pressure at the pipeline invert as P_o=11kPa, this corresponded to a modulus of E_i=9MPa. Alternatively, assuming an overburden pressure of 2m, a value of E_i=27.7MPa was obtained. Both values lie within the range of moduli used by Nixon *et al.* (1983a) of E_i=[6.9,69.0]MPa. They reported maximum displacements and strains from the lower end of this range. For this reason a low modulus of 8.5MPa was used for the unfrozen soil.

The analysis had originally been designed to use a temperature-dependent modulus as available within *SAP IV*.

Table 5.2 N.E.S. Soil Properties

Porosity	ν = 0.38
Saturation	S_r = 1.00
Specific Gravity	G_s = 2.65
Weight Density, dry	γ_d = 16.12 kN/m^3
Weight Density, saturated	γ_{sat} = 19.85 kN/m^3
Water content	w = 0.231
Thermal Conductivity, Frozen	k_f = 1.8 W/m·K
Thermal Conductivity, Fringe	k_{ff} = 1.54 W/m·K
Thermal Conductivity, Unfrozen	k_u = 1.5 W/m·K
Specific Heat Capacity, Frozen	c_f = 2.109 MJ/m^3
Specific Heat Capacity, Unfrozen	c_u = 2.823 MJ/m^3
Volumetric Latent Heat (90%)	L = 114.23 MJ/m^3
Liquid Limit	w_L = 24 to 31%
Plastic Limit	w_P = 14 to 18%
Grain Size	D_{60} = 0.0200mm
	D_{30} = 0.0050mm
	D_{10} < 0.0001mm

Johnston (1981) reports the relationship between E and the temperature below freezing as

$$E = 400\ (1+3.5\theta)\text{MPa} \qquad \theta \text{ in } °C \qquad [5.4]$$

This equation predicts a significant increase in stiffness as the soil gets colder. This increases the stiffness of the frozen soil around a chilled pipeline thereby strengthening the soil:pipe composite (Davison, *et al.* 1978). It was unfortunate that this approach was necessarily abandoned, as discussed later in this chapter.

This simplification would tend to reduce localized stress concentrations due to heaving and therefore result in a higher variation of heave at the frost front. Conversely, the lower *E* compensates for creep effects which would result in a lower effective modulus in the long term.

5.5.3 Steel Properties

Steel properties are relatively constant, with the exception of the yield stress which was not important in this analysis because only hoop bending stresses would be developed. Longitudinal bending would be the more critical mode of flexure for heave. The steel properties selected were E=200 GPa G=83 GPa and ν=0.3. Beam theory was used in determining the section modulus for the beam elements representing the pipe cross-section.

5.6 Representation of the Pipeline

In a two-dimensional analysis of a cross-section of a pipeline buried within a soil, the shape and stiffness of the pipeline must allow stress transfer around the void of the interior pipeline and be responsive to asymmetric loading of the perimeter of the pipeline. The support from the pipe was needed since preliminary results, confirmed by hand calculations, predicted excessive pipeline deformations due to the exclusion of the hoop bending stiffness.

In this analysis, the rigidity of the steel pipe comes from the flexural stiffness of the pipe thickness in the plane of the analysis, and the rotational fixity of the pipe at the centreline boundary of symmetry. This structural system is under zero stress from the interior of the pipe, with gravity, soil heaving and soil arching loads on the exterior of the pipe. In a more elaborate analysis, the zero-stress state within the pipe could be replaced with a

transiently varying pressure loading due to fluctuations in operating pressures of the fluid within the pipeline.

Out of the plane of the analysis we have a plane-strain stress state. In the case of a welded pipeline, we have a monolithic structure with essentially no material or sectional variation so a plane strain condition exists. It is possible to modify the elastic constants of a material in plane stress to simulate the displacement behavior in plane strain. In the case of steel with ν=0.30 and E=200 GPa,

$$\epsilon_{11}=\sigma_{11}\times 4.55\cdot 10^{-9}/\text{kPa} \qquad [5.5]$$

$$\epsilon_{22}=\sigma_{22}\times 1.95\cdot 10^{-9}/\text{kPa} \qquad [5.6]$$

Using these parameters, the analysis was performed using beams displaying plane strain behaviour.

Initially, thin elements adjacent to the void were used to represent the pipe. For the initial run these two-dimensional elements were given steel properties, but soil behaviour, since the four-noded quadrilateral elements with 2×2 gaussion integration could not model bending. An attempt was made to use incompatible displacement modes to represent constant bending moments within the elements (Bathe, 1982) with poor results (Fig. 5.32).

As a result, a series of simple beam tests were run on the *SAP IV* program to evaluate the different ways of modelling beam behaviour. The criteria for comparison were the nodal displacements and rotations as those would be affecting the contiguous soil. Beam stresses were not

considered since they would have no direct effect on the soil and would be simplistic. Pipe stresses would be predicted more precisely using mesh substructuring with a hybrid method (Row *et al.*, 1983).

The tests were performed on plate and shell elements, two and three-dimensional elements and beam elements using plane stress, plane strain and equivalent plane strain conditions. The latter was performed using plane stress boundary conditions with modified E and ν as discussed previously.

In summary, the plate and shell elements predicted satisfactory rotations and displacements but required out-of-plane nodes for the analysis. Two- and three-dimensional elements with eight nodes per face performed well when the load was distributed to all the midspan nodes and 3×3 integration was used. This approach would have required more nodes to simulate the pipe which would have unnecessarily complicated the analysis, and the requirement for an even distribution of load to the nodes was unrealistic.

The analysis was finally performed using beam elements within the *SAP IV* program. This method was initially discarded when preliminary results were poor. However, subsequent runs traced the poor behaviour to the nodal degrees-of-freedom specification. It was necessary to release some unrelated, redundant degrees-of-freedom to

obtain the desired results.

5.7 Surface Temperatures at N.E.S.

5.7.1 Soil Parameters

The environmental thermal conditions at the N.E.S. Calgary site were represented as a modified sinusoidal temperature curve applied to the soil surface. This gradual change in temperature allowed a better representation of the seasonal variation in temperature. From the 10 year thermistor data (L.E.C., 1984) the average maximum and minimum ground temperatures at a 3m depth were found to be 9.9°C and 4.0°C with little variation. This agreed with Konrad and Morgenstern's (1984) average ground temperature of +6.5°C. Any applied surface temperature should be able to reproduce this temperature behaviour in the soil.

The surface temperatures were modelled as a sinusoidal air temperature curve, modified by surface "*n*-factors" (Anderson and Andersland, 1978). Using the Normal Ambient Air Temperatures at Calgary International Airport, the variation in air temperature could be expressed as:

$$\theta = +2.5 + 14.5 \sin\left[\frac{t_{hr}-720}{1395.15}\right]_{radians} \qquad [5.7]$$

The air temperature equalled the mean air temperature at t=720 hr, assuming t=0 on March 20, 1974 when the chilled gas circulation began. Freezing temperatures existed up to day 20 and after day 203 of each year. By integrating, the

freezing and thawing indices for air are TI_a = 2119°days and FI_a = 1206°days. Indices for this soil are obtained by factoring the air temperatures by the *n*-factors for gravel, as determined by the U.S. Department of the Army (n_f = 0.9, n_t = 1.5 to 2.0). By back-calculating from an assumed mean annual soil temperature of MAST=+6.5°C, the *n*-factor for thaw was determined to be n_t=1.63. The air and surface temperatures over a three year period are shown in Figure 5.17.

An initial series of *ADINAT* runs were done to initialize the soil temperature regime due to the effect of the seasonal variation in soil surface temperature. The mesh with the 1.2m diameter hole was used, with the specified surface temperatures applied to all nodes at the 0.0m level. The inclusion of the hole did affect the temperature in that region, but not significantly.

ADINAT uses lumped latent heats and heat capacities. Therefore by prescribing nodal temperatures at the surface we essentially remove a portion of the latent heat and heat capacity from the analysis. This reduces the buffering effect of these factors on temperature changes, particularly at the surface where the annual variations in temperature are greatest. The 0.2m thick "skin" layer at the surface was used to mitigate this effect by reducing the volume of material lumped at the surface nodes. The high aspect ratio (length to width) of these elements was acceptable, given

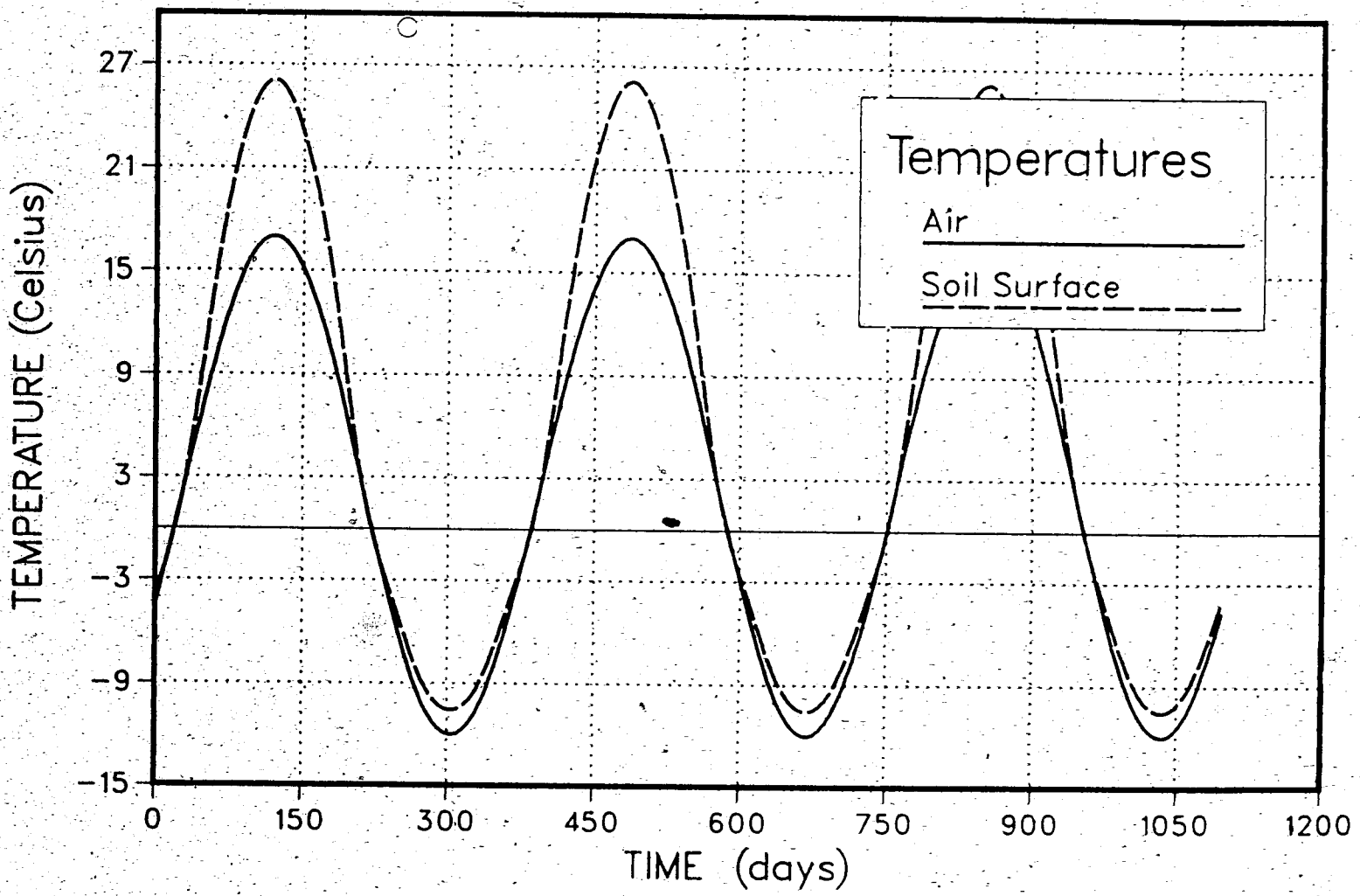

Figure 5.17 Variation of Environment Temperatures, Calgary

that the heat flux at surface would be predominantly vertical, and therefore parallel to the element axes.

The varying temperatures at the soil surface were discretized into temperatures at one-month intervals over a period of 40 months and inserted into *ADINAT* as a time function. All nodal temperatures at the soil surface were servile to this function and oscillated as the the transient analysis progressed. This simulated the seasonal fluctuation in temperature. For the initial conditions, the entire mesh was set to +6.5°C, with soil properties obtained from Konrad and Morgenstern (1984) and L.E.C. Engineering Ltd. (1984). Appropriate latent heats and heat capacities were calculated assuming soil saturation and 90% of *in situ* water freezing.

The analysis simulated the downward progression of surface temperatures for a peiod of 3 years, calculated monthly. Subsequent 3 year periods were analyzed by using the final output temperatures of the previous run as initial temperatures, and restarting the analysis. *ADINAT's* restart option using file 57 was not used because it would have required a sinusoidal time function several years long.

There were difficulties in obtaining reasonable temperatures in the analysis. These could be traced to the latent heat algorithm *ADINA* uses, and a more detailed explanation is provided in Appendice J. The convergence tolerance, RTOL, had a controlling effect on the acceptability of results. This can be seen in Figures 5.18

and 5.19 where two runs, begun with identical initial conditions at year 15, had significantly different surface temperatures by the autumn of year 17 because of a magnitude difference in RTOL. This figure is of the worst case, with significantly better behaviour at other times. Unfortunately, the analysis using RTOL = 10^{-3} also predicted some smearing of the phase change instead of a unique, definite frost front. This rendered this particular analysis useless for the segregation potential theory, so it was abandoned in favor of the tighter convergence tolerance of 10^{-4}.

The progression of the varying surface temperatures into the initially isothermal +6.5°C soil is seen in Figures 5.20 through 5.25. The final temperatures are cooler than the average 6.5°C reported by Konrad and Morgenstern (1984) however these represent the early spring temperatures, and were used as the initial temperatures for the N.E.S. frost heave simulation. The seasonal variation in temperatures is better represented by Figures 5.26 to 5.29.

5.8 Simulation of the N.E.S. Calgary Frost Heave Test Facility

The Northern Engineering Services Co. Ltd. (N.E.S.) conducted a frost heave project for Canadian Arctic Gas Study Ltd. This facility is described in Konrad and Morgenstern (1984) and was basically a 1.20m dia. pipeline at an invert of 2.0m. Some variations on this normal section

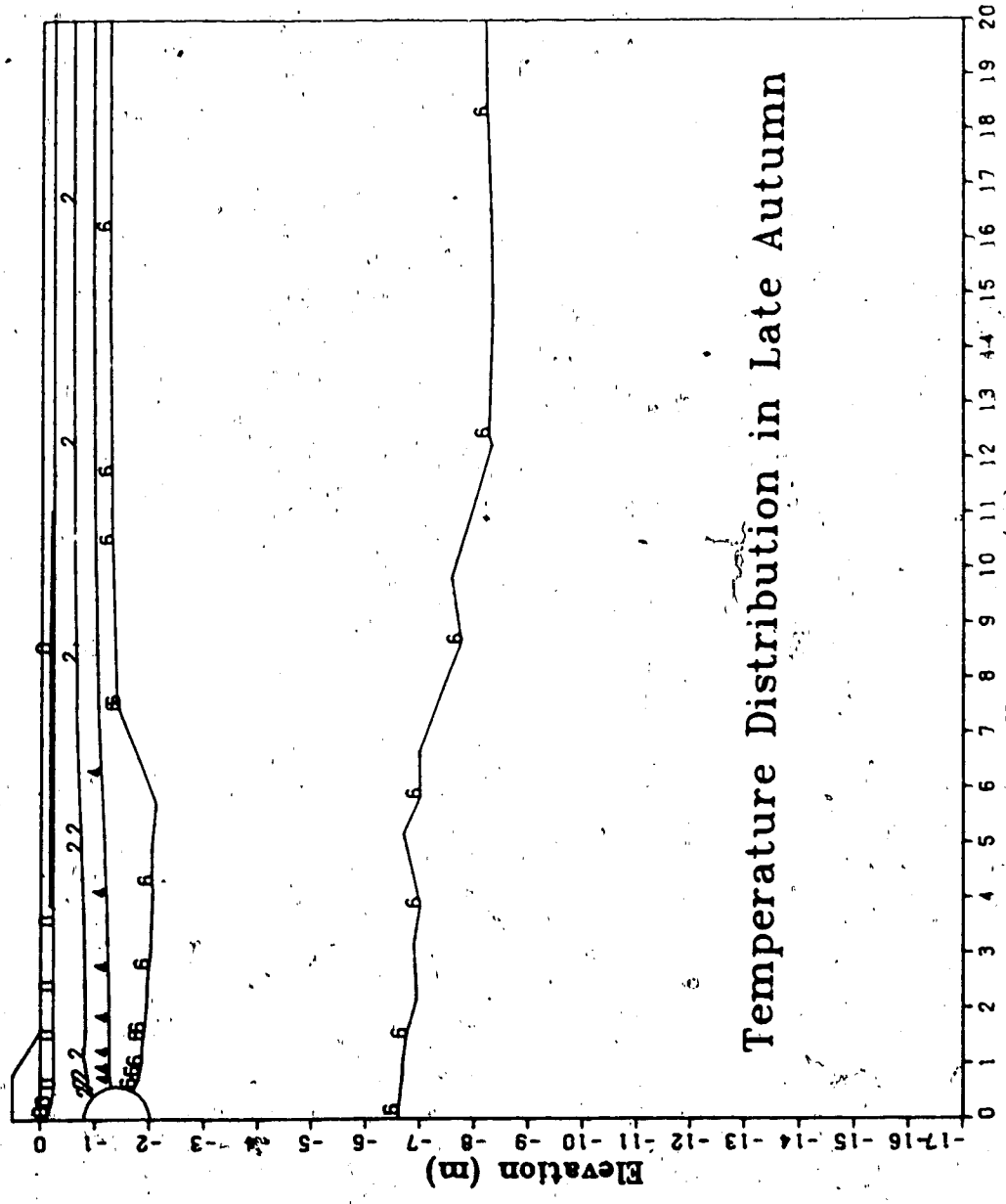

Figure 5.18 Ground Response to Varying Surface Temperatures, T= 17yr, RTOL=10^{-3}

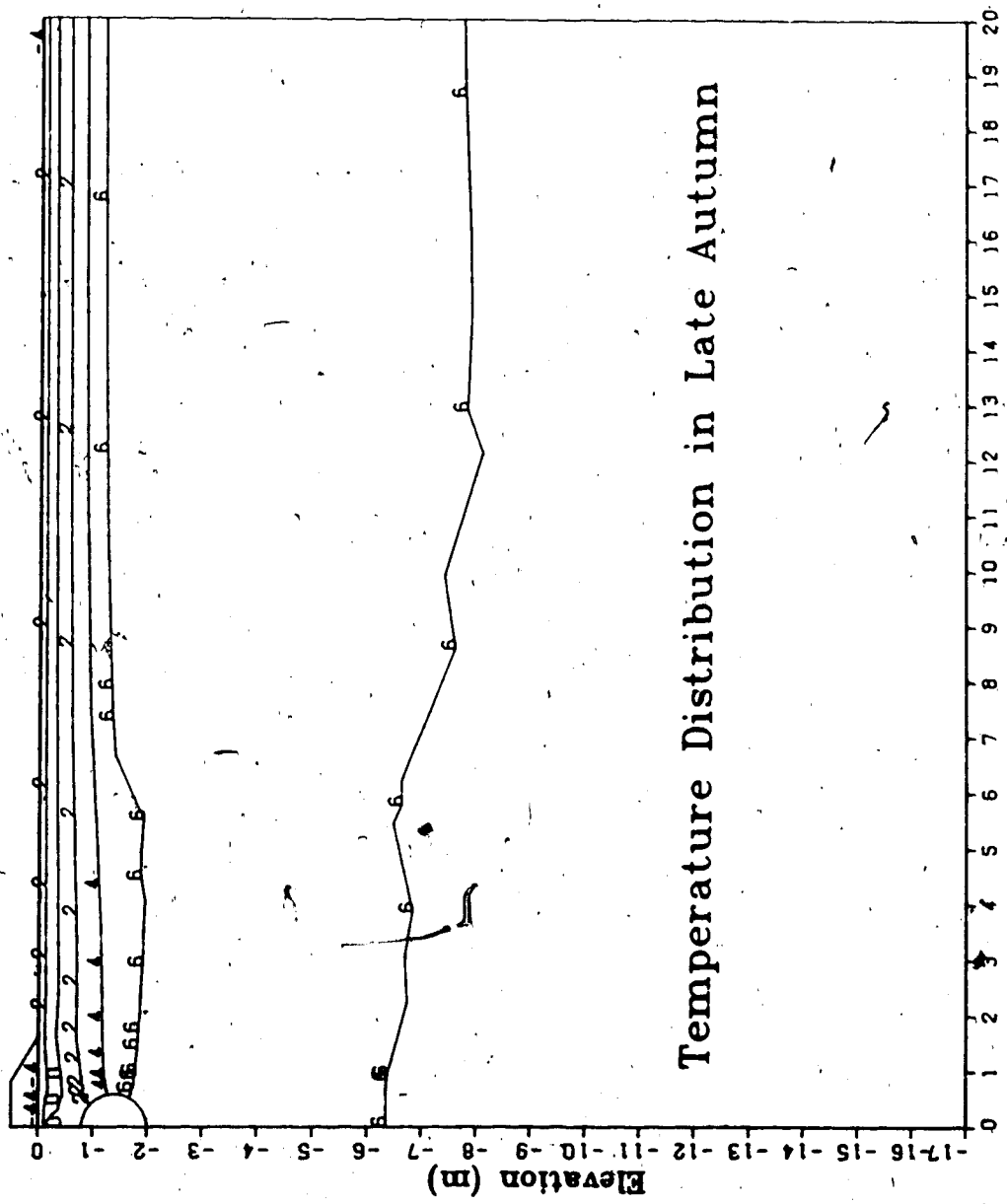

Figure 5.19 Ground Response to Varying Surface Temperatures, T= 17yr, RTOL=10^{-4}

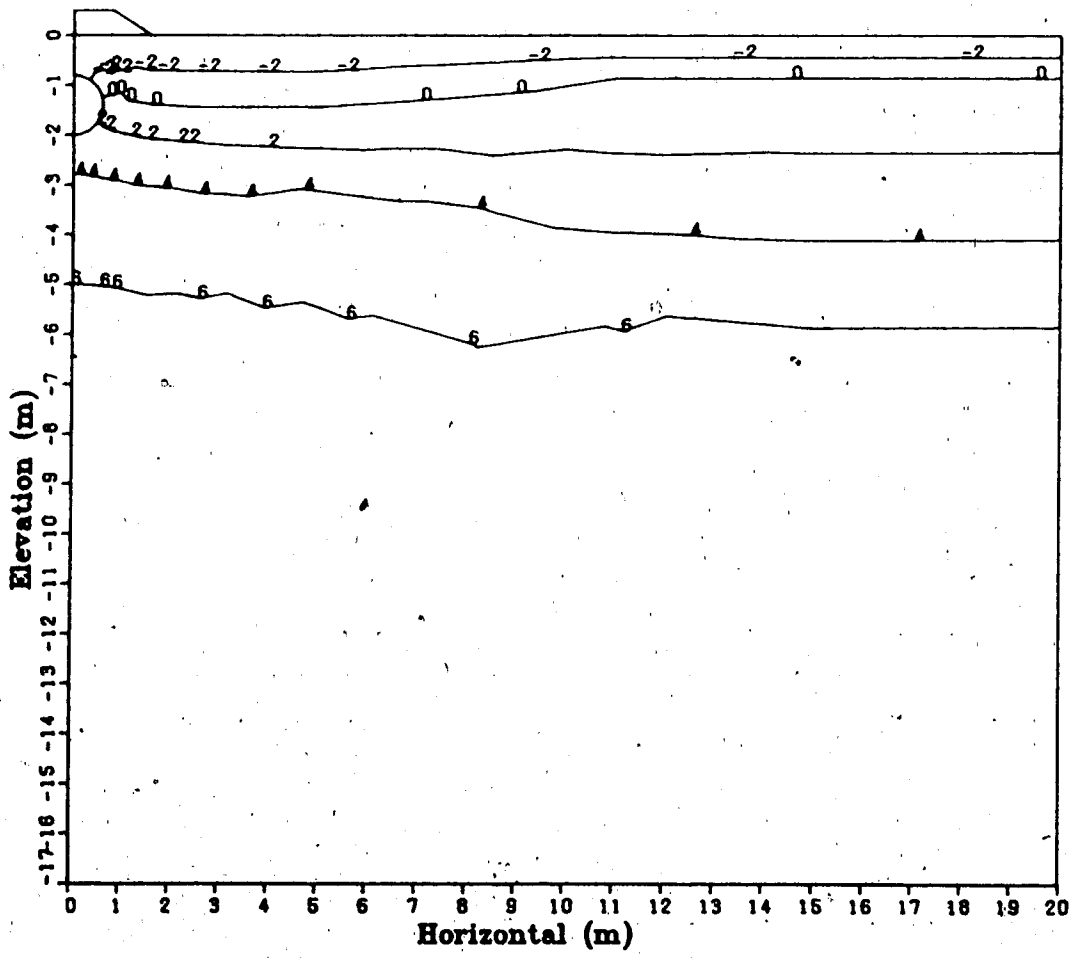

Figure 5.20 3yr after Applying Surface Temperatures

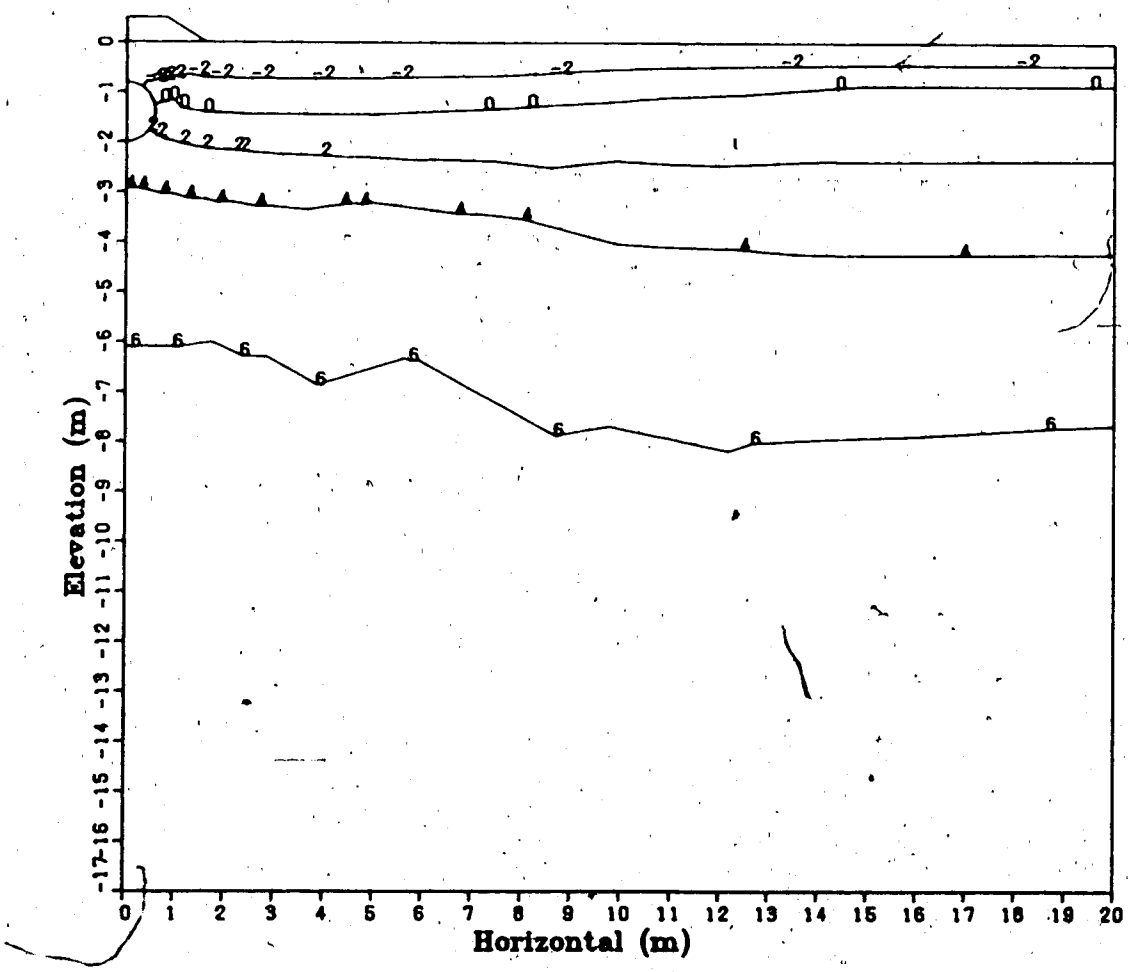

Figure 5.21 6yr after Applying Surface Temperatures

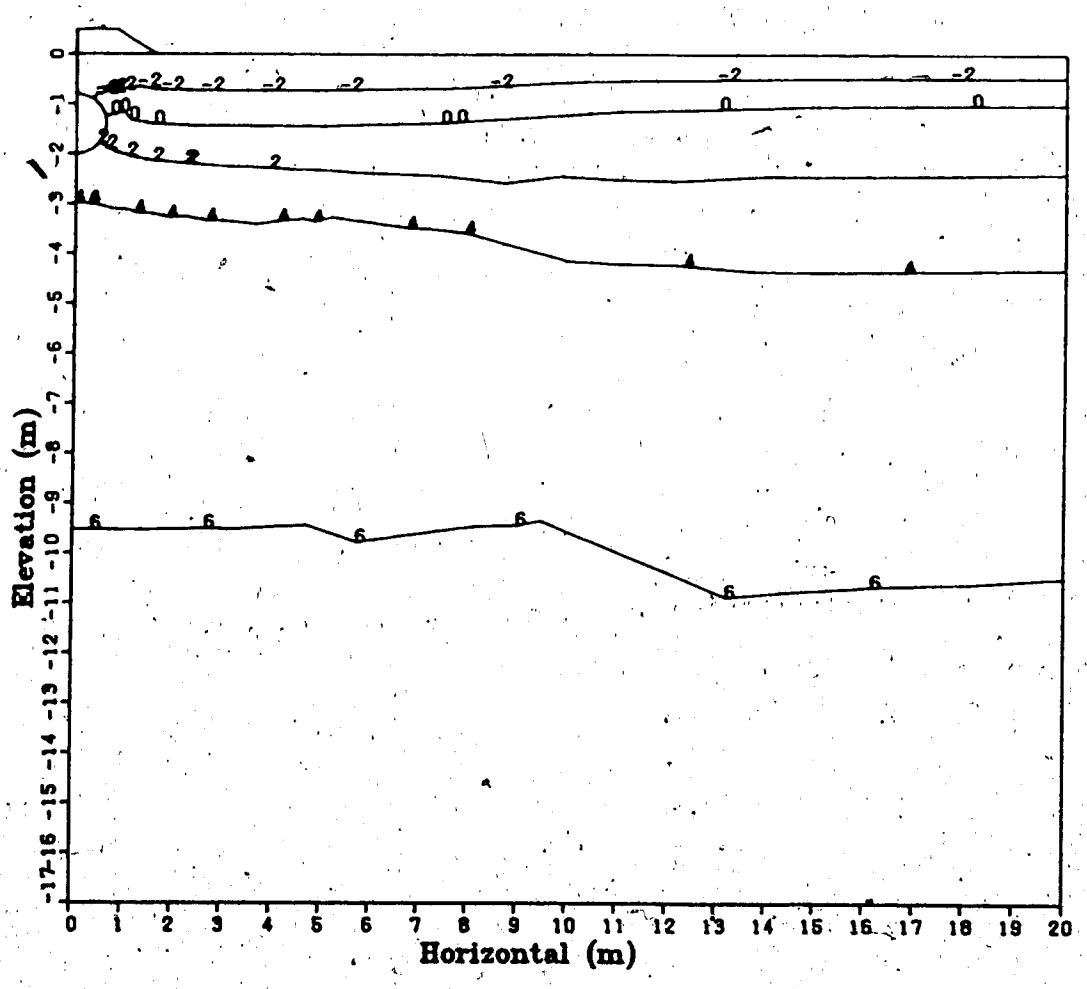

Figure 5.22 9yr after Applying Surface Temperatures

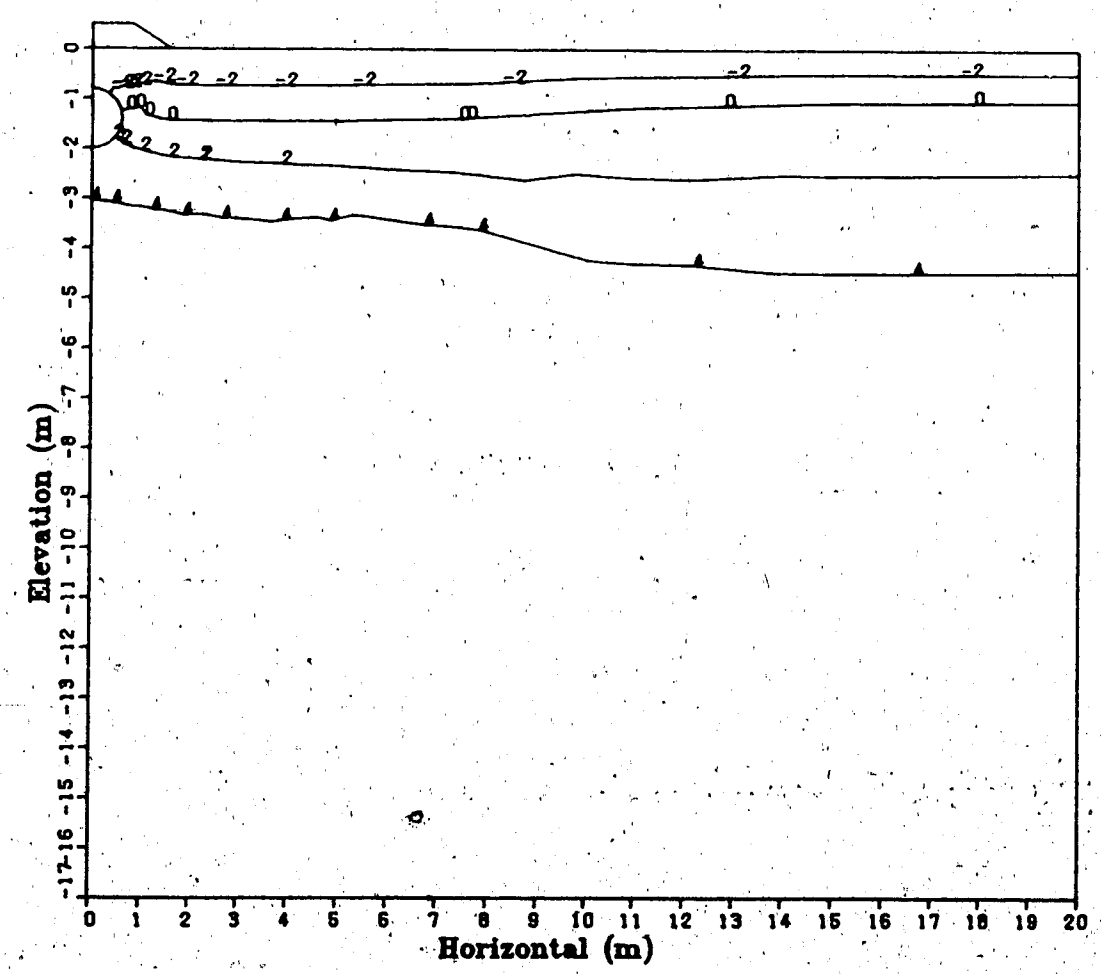

Figure 5.23 12yr after Applying Surface Temperatures

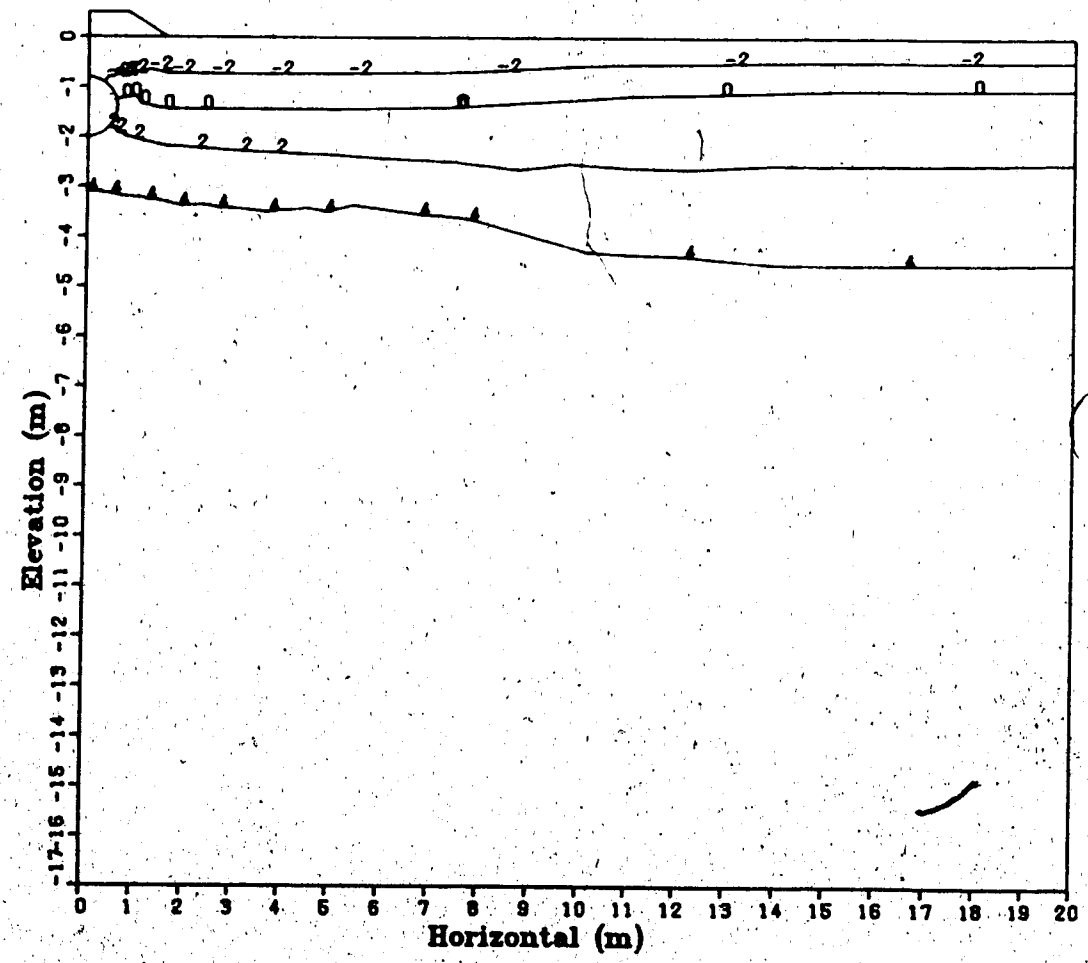

Figure 5.24 15yr after Applying Surface Temperatures

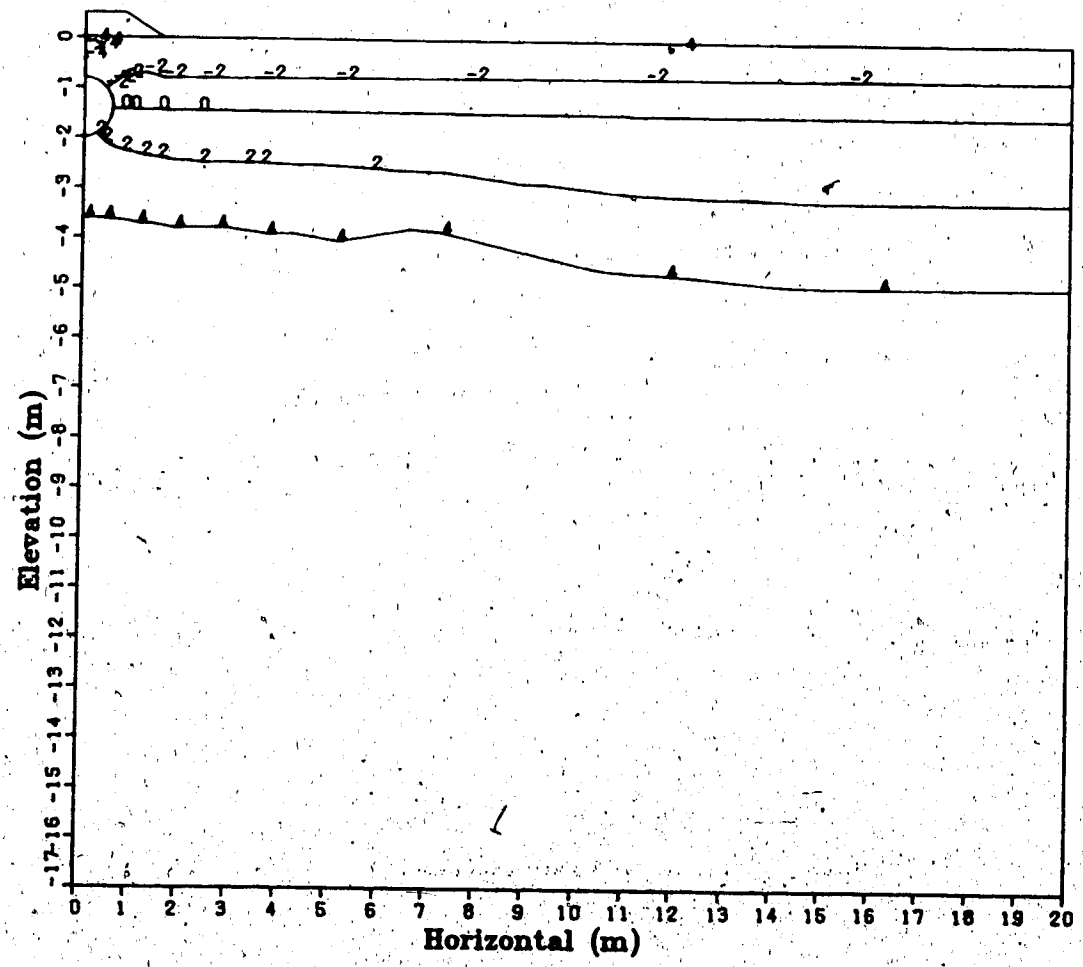

Figure 5.25 18yr after Applying Surface Temperatures

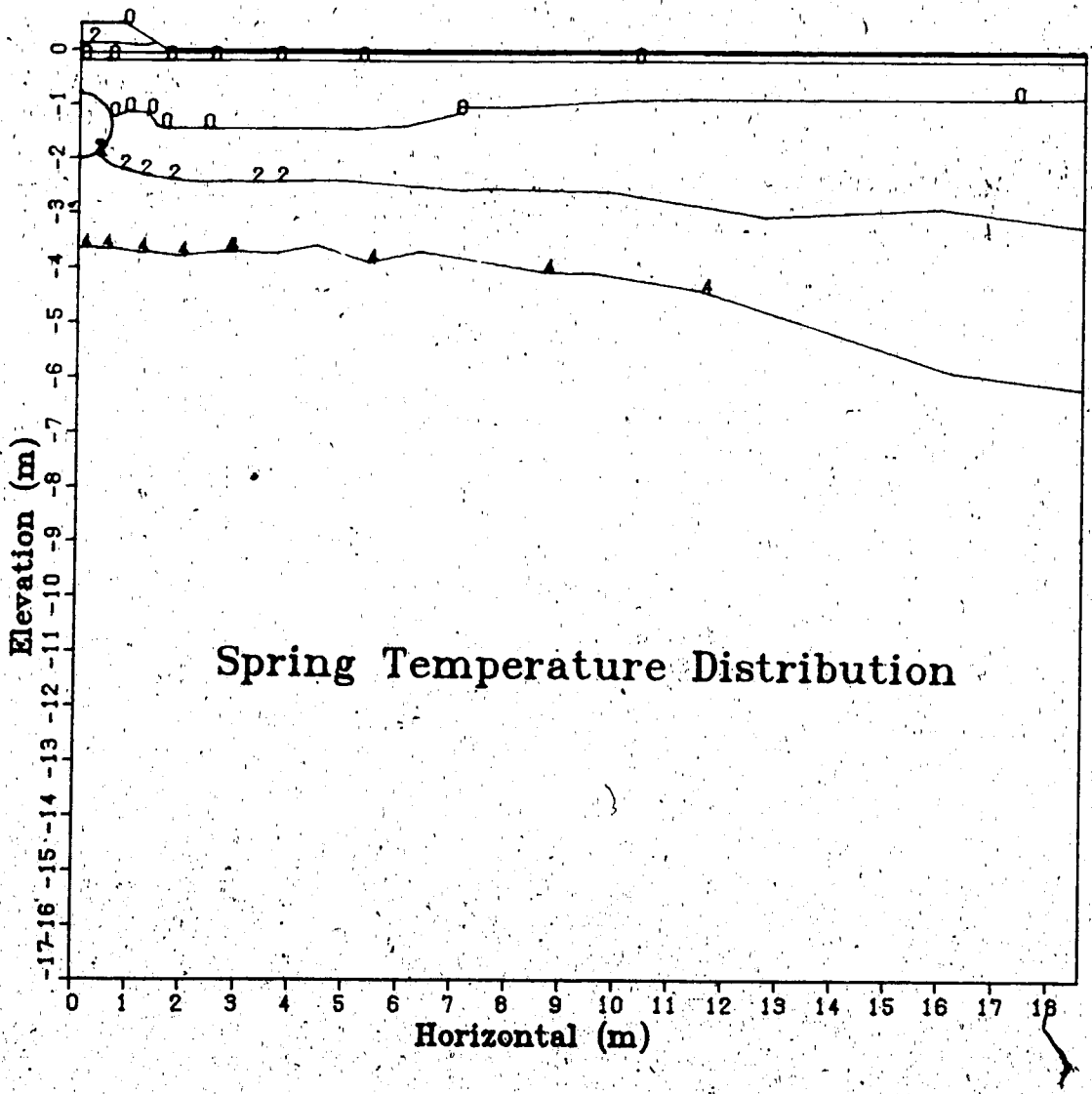

Figure 5.26 Spring Isotherm Distribution

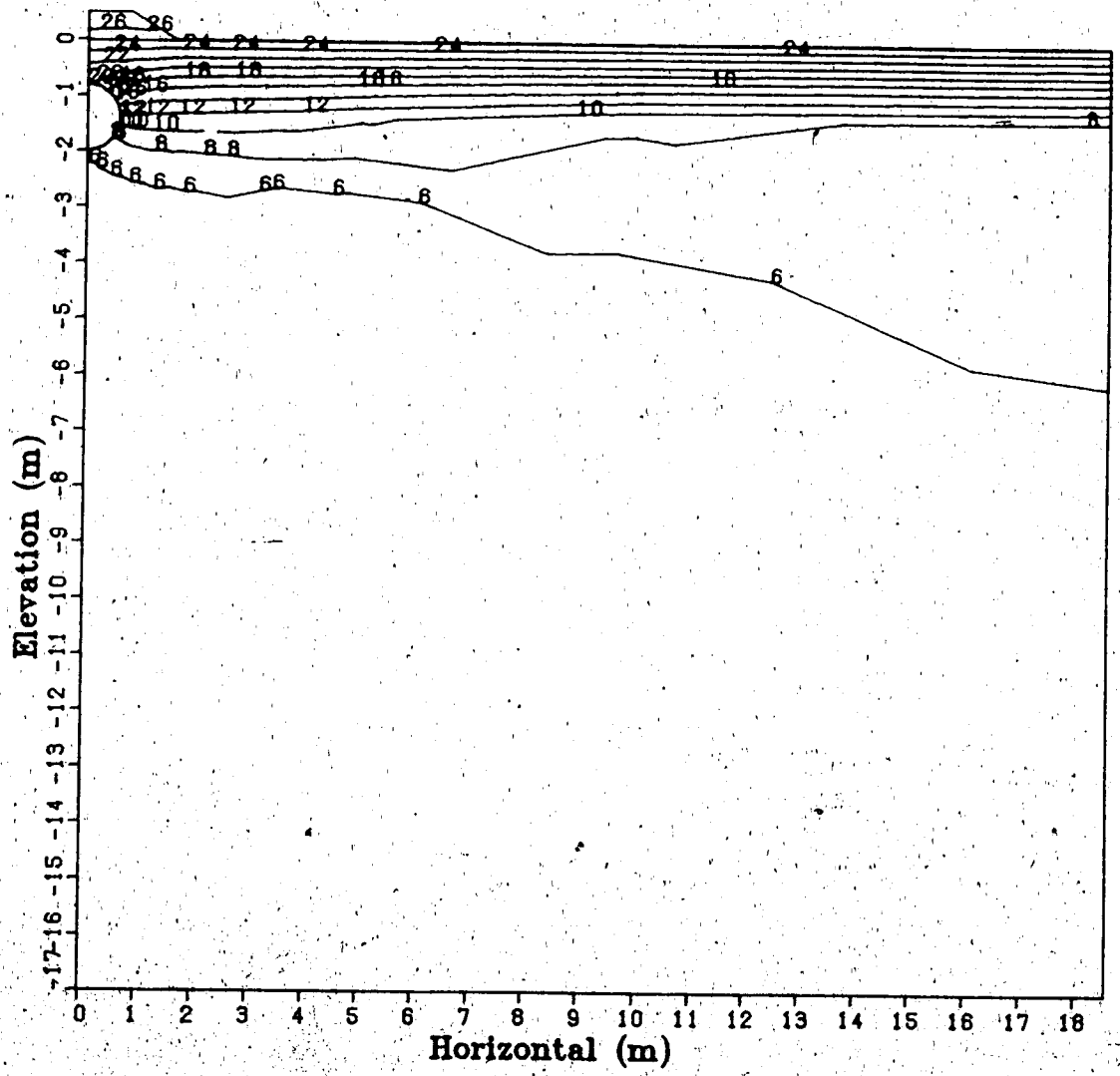

Summer Temperature Distribution

Figure 5.27 Summer Isotherm Distribution

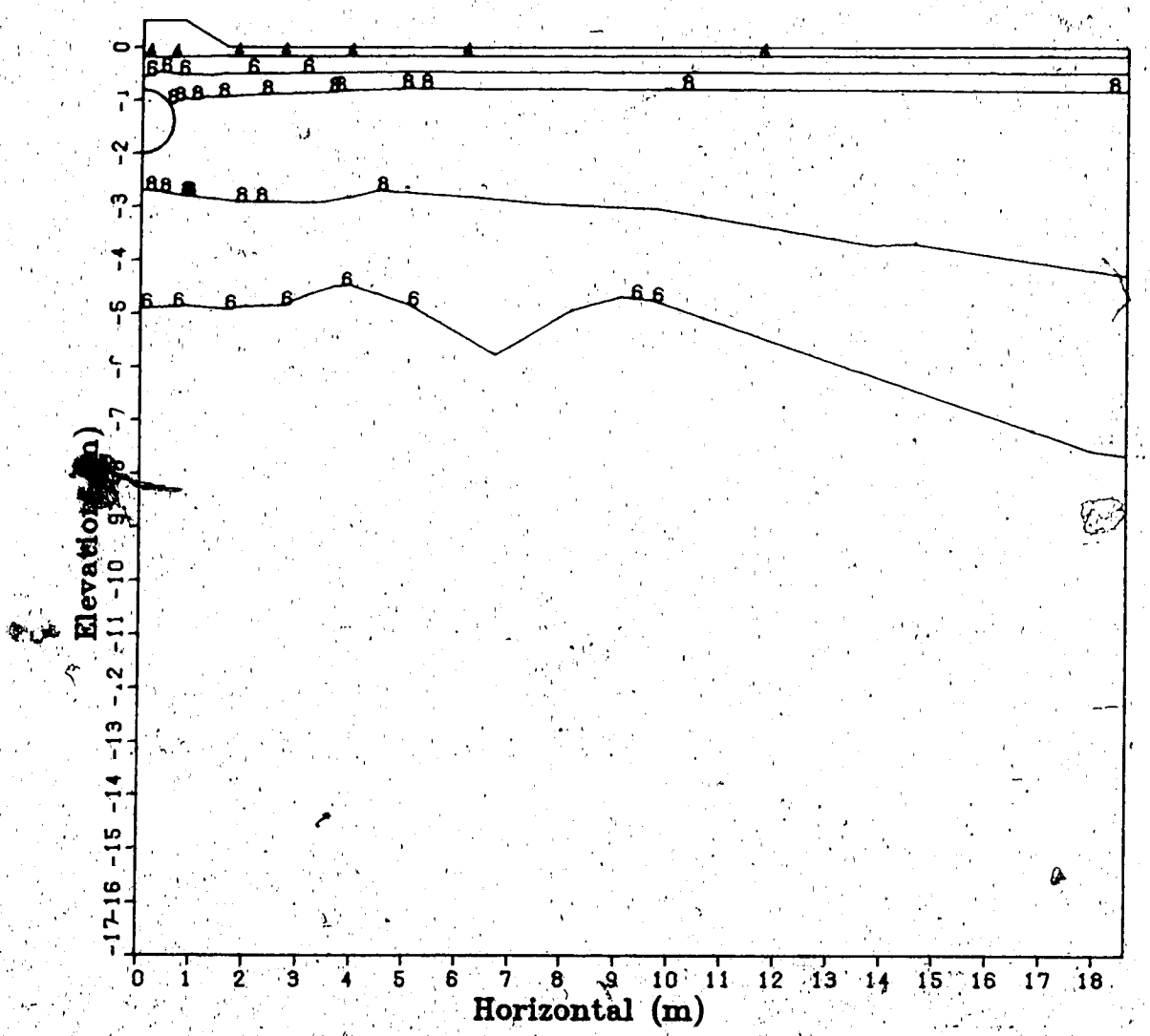

Autumn Temperature Distribution

Figure 5.28 Autumn Isotherm Distribution

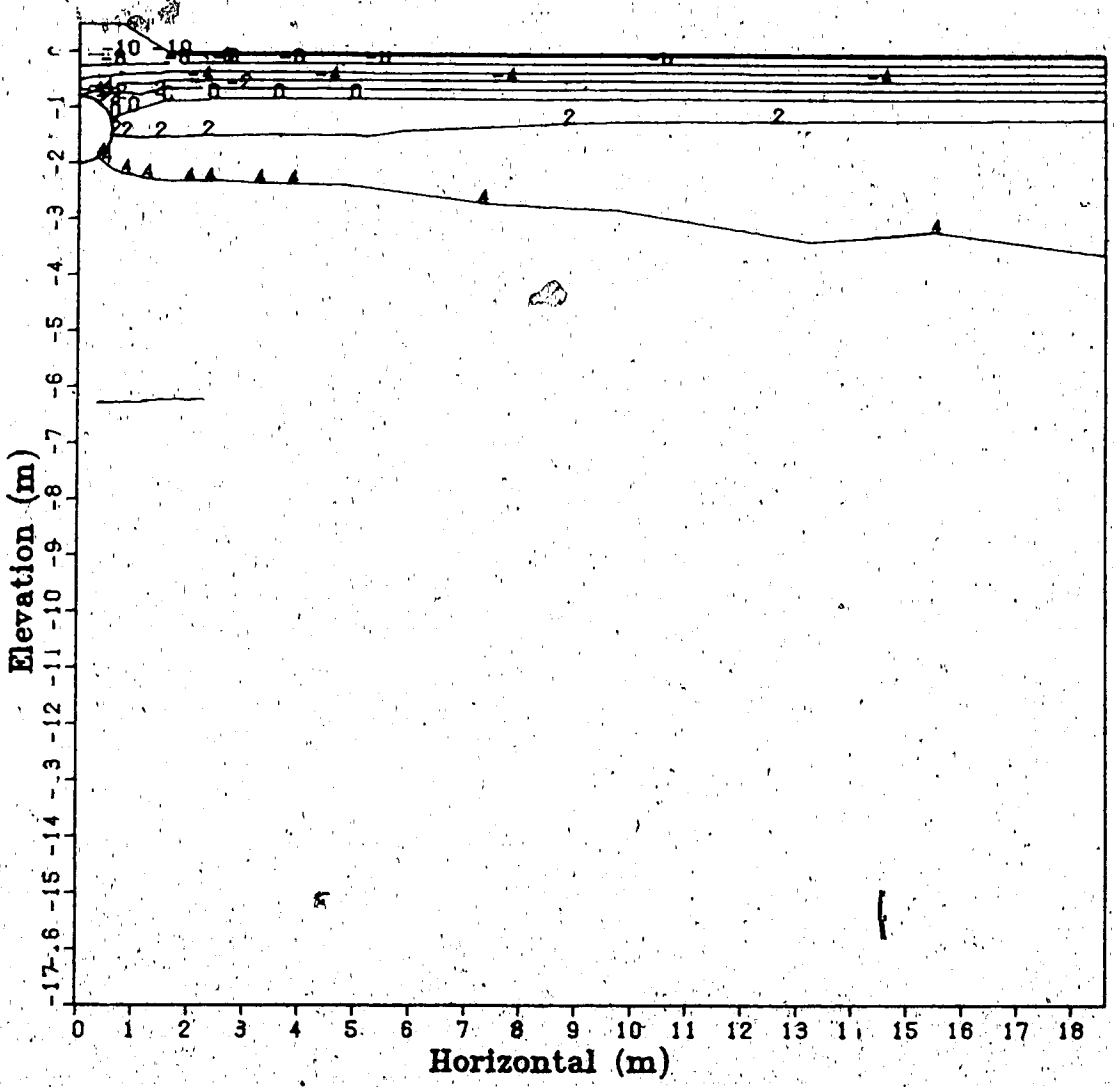

Winter Temperature Distribution

Figure 5.29 Winter Isotherm Distribution

examined the effects of deeper burial, a restraining assembly and subgrade material.

It was anticipated that the initial finite element mesh, which would be used in both *ADINAT* and *SAP IV*, would require modifications. As such, the first version was a simple centerline-symmetric mech consisting of 54 elements. The pipe was represented by a thin ring of two-dimensional quadrilateral elements, which were given steel properties. The mesh (Fig. 5.30) is plotted with its mirror image. The stress field is represented by principal stress crosses at the elements' centroids, with arrowheads indicating tension. The stress field exhibits the classical rotation of principal strsses around a void, with some deviation due to the effects of shallow burial and gravity.

The mesh was redrawn using proportional stress crosses (Fig. 5.31). The elements representing the steel pipe have significantly higher stresses than the surrounding soil. This is not surprising since the inclusion of a stiff member within a continuum and subsequent gravity loading results in a concentration of stress within that member.

The variation in stress direction within the pipe elements would not have been of concern had the thrust line remained within the elements. Figure 5.30 indicated that this was not the case, and it was anticipated that the non-homogeneous heave around the perimeter of the pipe would result in higher stress deviations, which would induce

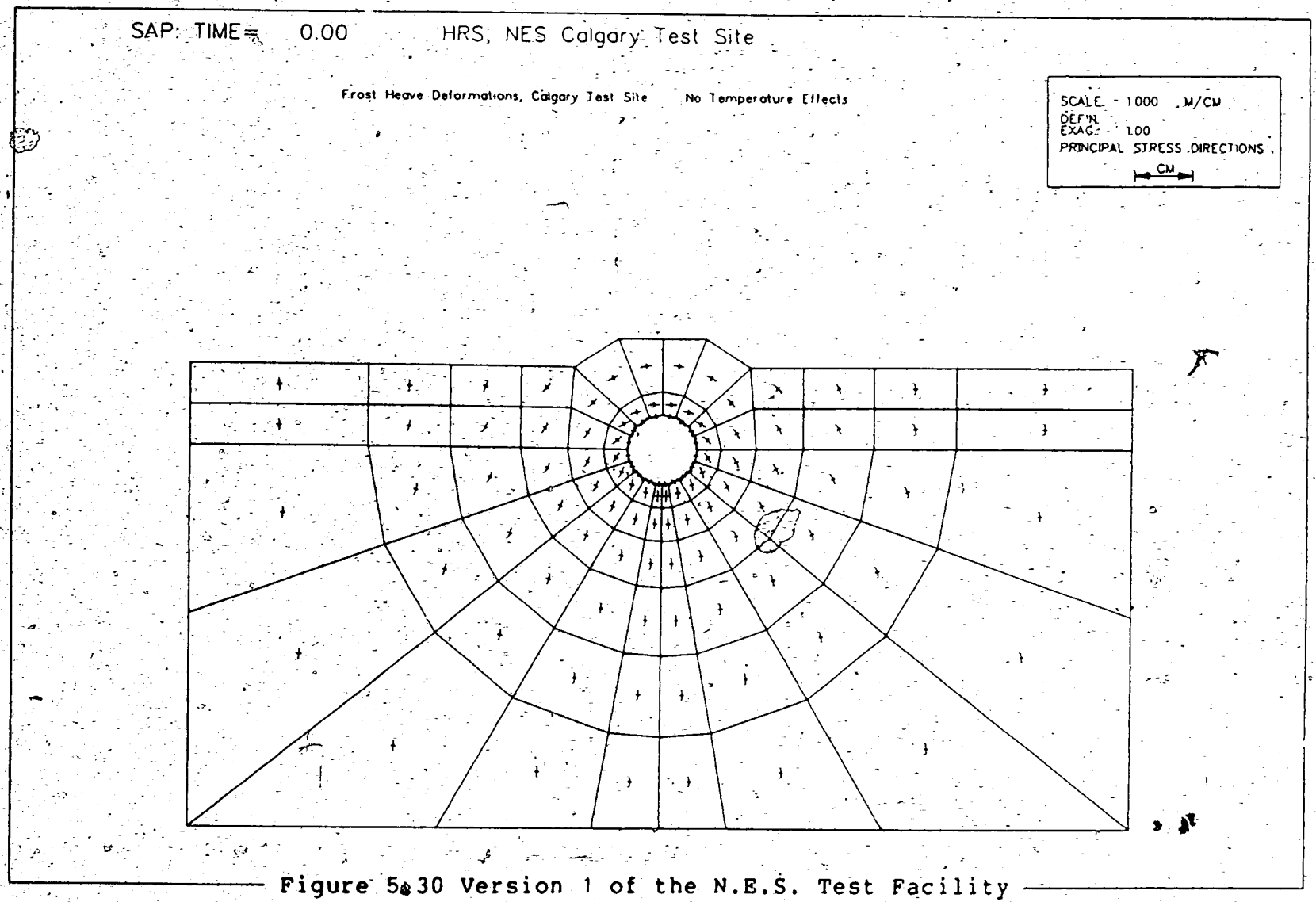

Figure 5.30 Version 1 of the N.E.S. Test Facility

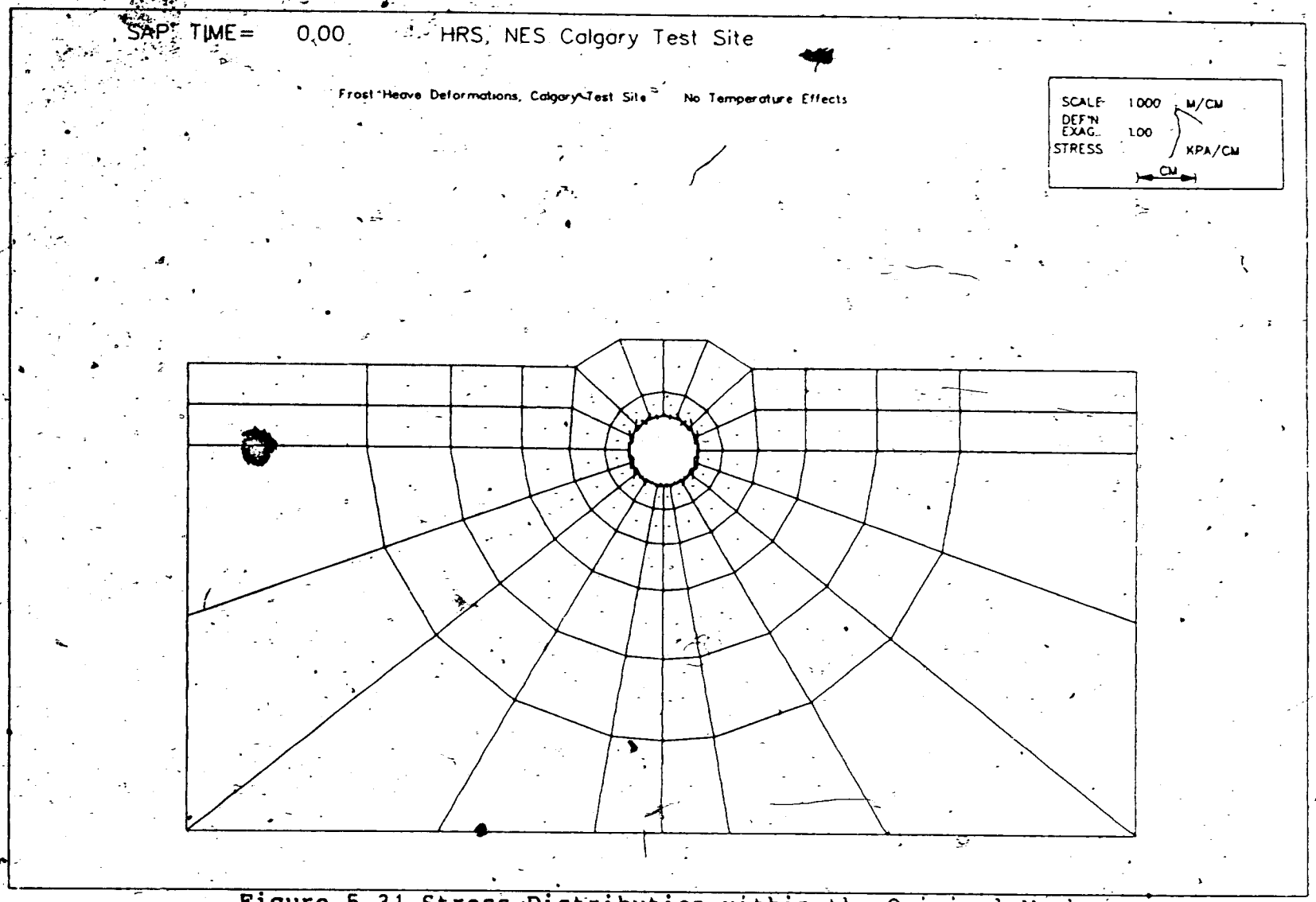

Figure 5.31 Stress Distribution within the Original Mesh

bending moments in the pipe.

The simple two-dimensional quadrilateral elements were incapable of modelling bending behaviour. Incompatible displacement modes were used in the elements representing the pipe to accommodate a constant bending moment within each element, with poor results (Figure 5.32). The predicted pipe stresses were unrelated to any reasonable expectation of pipe stresses, so an alternate method of representing the pipe was needed.

The present mesh had predicted a reasonable distrbution of stress within the continuum, with minimal boundary influences. However, the mesh was inadequate for thermal calculations. Konrad and Morgenstern (1984) report a zero heat flux at a depth of 15m which was well beyond the base of the existing mesh. The layer of elements at the soil surface varied in thickness which would result in a varying frost front penetration rate across the mesh. This was remedied by adding a thin layer at the surface to equalize and minimize the frost front advance due to the specified surface tmperature. Finally, the berm was isolated as three elements. This permitted the berm's addition or removal by varying its stiffness and weight density.

These modifications resulted in the mesh shown in Fig. 5.33. The principal strsses are drawn to scale and the mesh is plotted with its mirror image, for completeness. Figure 5.34 details the stress field at the pipe, with the steel

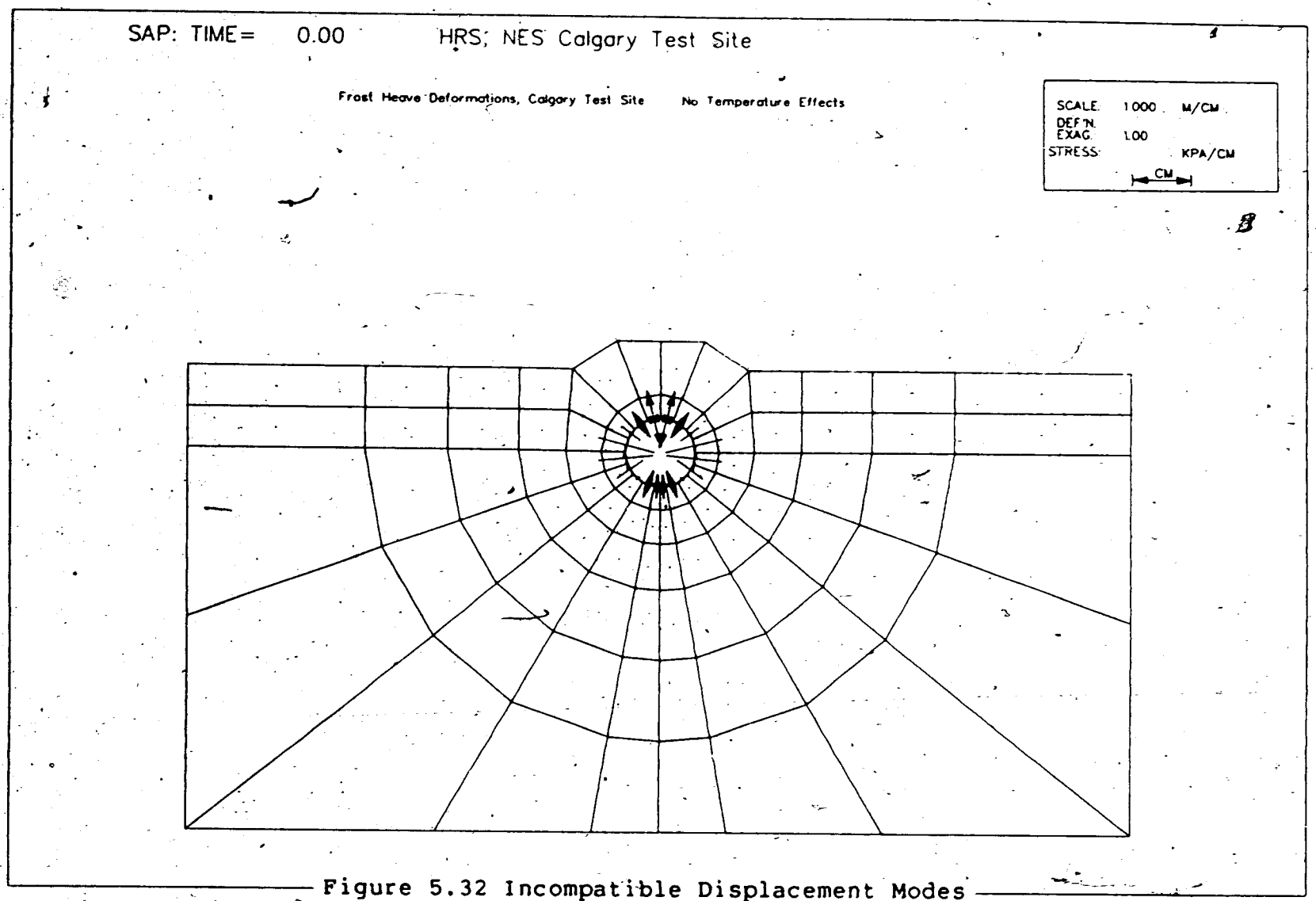

Figure 5.32 Incompatible Displacement Modes

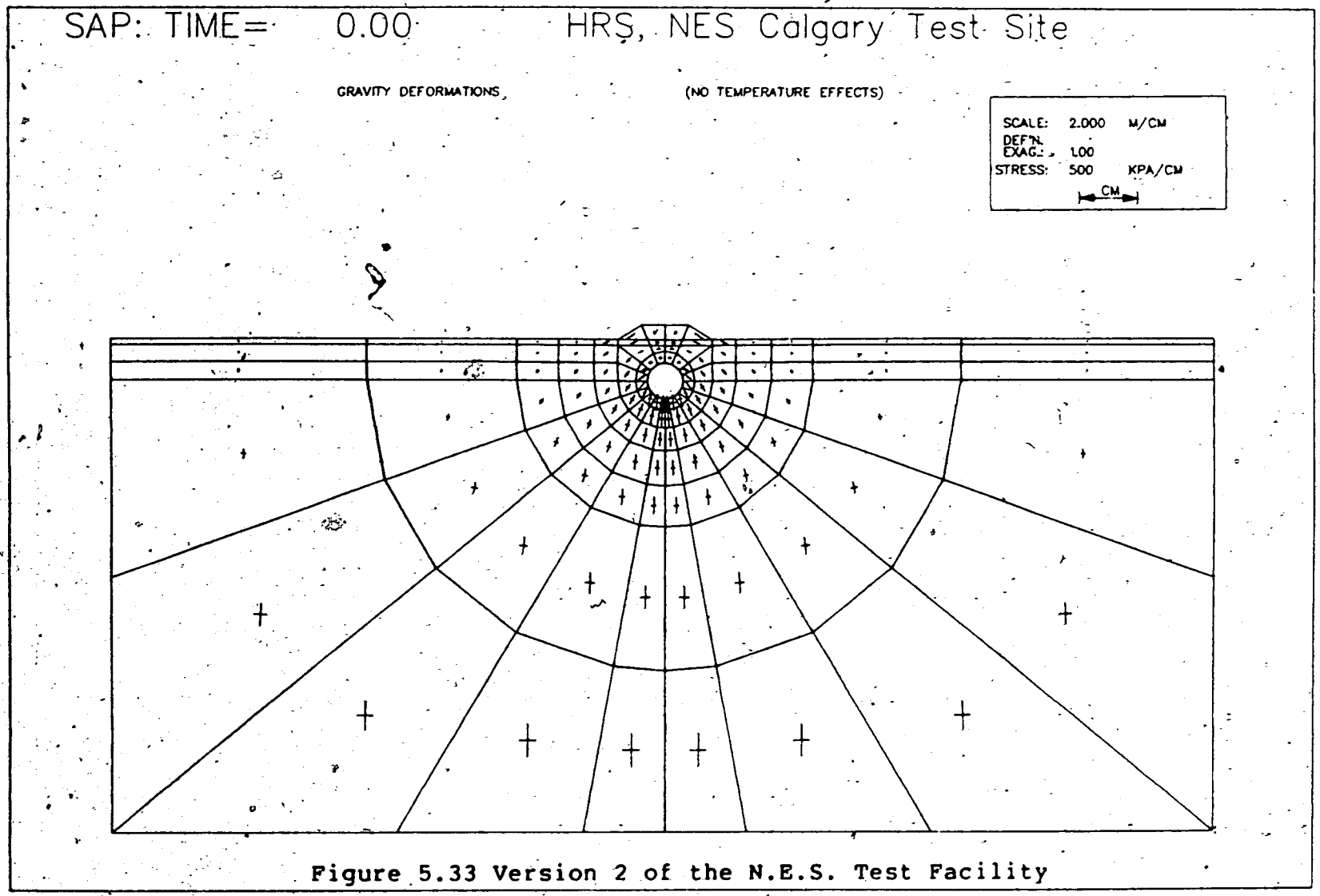

Figure 5.33 Version 2 of the N.E.S. Test Facility

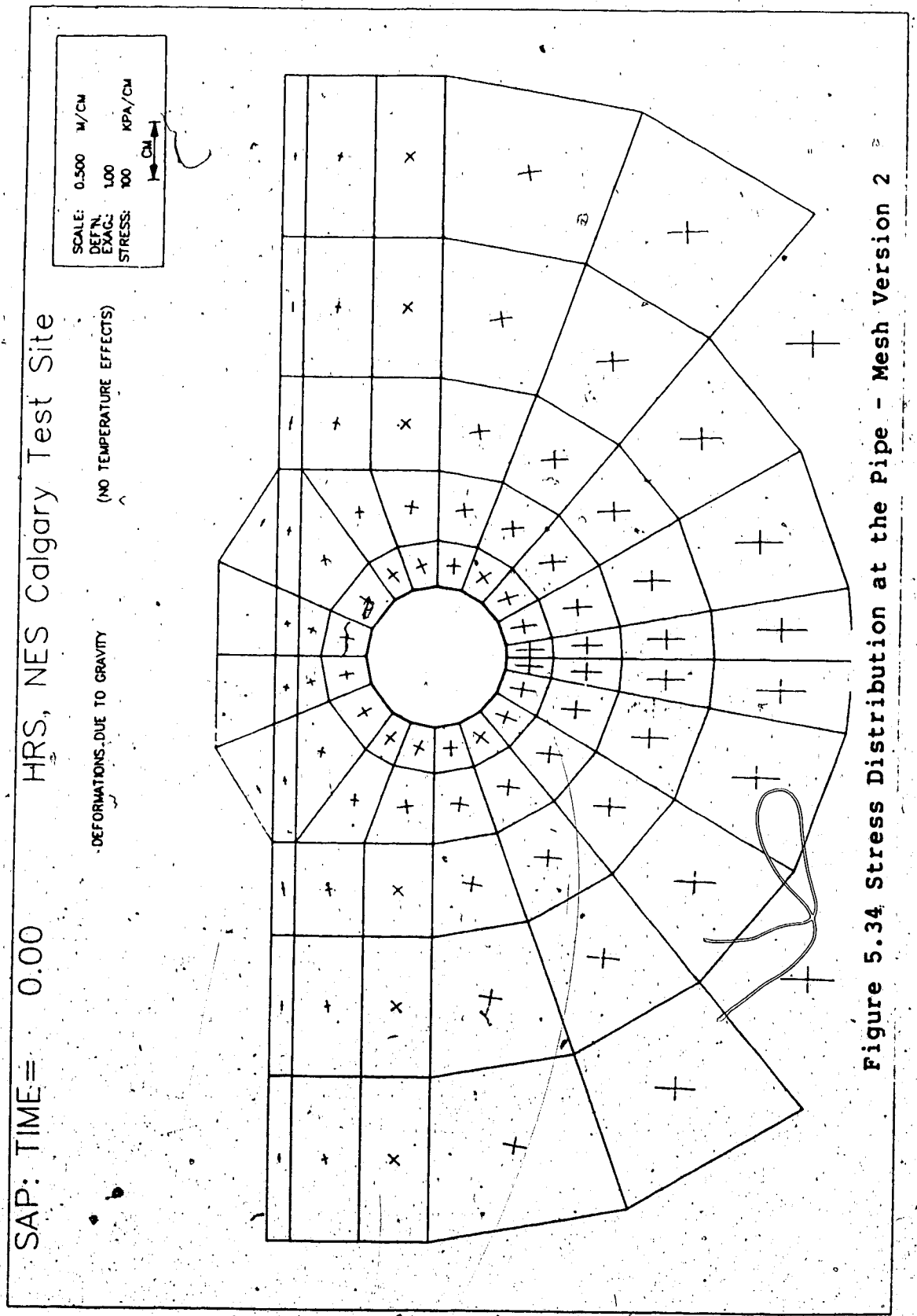

Figure 5.34 Stress Distribution at the Pipe - Mesh Version 2

pipe's stresses not plotted for reasons of clarity, as they were much higher than those of the adjacent soil. Figure 5.35 shows the original configuration with dashed lines, and the deformed mesh with solid lines. The displacement pattern was satisfactory, although the vertical displacements below the invert appeared to be higher than for those at a similar depth elsewhere. In addition, there were unexpected horizontal thrusts at the surface elements at the berm toe. Examination of the entire mesh revealed an unexpected tension field in the upper right-hand corner which prompted a series of *SAP IV* runs, summarized graphically in Appendice K, to discover the cause. It was eventually traced to the combination of the lumped gravity analysis and the large irregularly-sized elements along the base. This prompted a major re-evaluation of the mesh (App. K) resulting in a third and final version (Figures 5.36 to 5.39). The mesh was improved by creating a smaller element in the bottom right corner of the mesh and included ten beam elements to represent the pipe.

The stress field under gravity loading is shown in Figures 5.40 and 5.41. Gone are the unusual compressive stresses above the pipe, however some tension has developed above it due to soil arching and the restraint offerred by the buried pipe. The displacement behaviour is an improvement on the previous mesh's (Fig. 5.42 and 5.43).

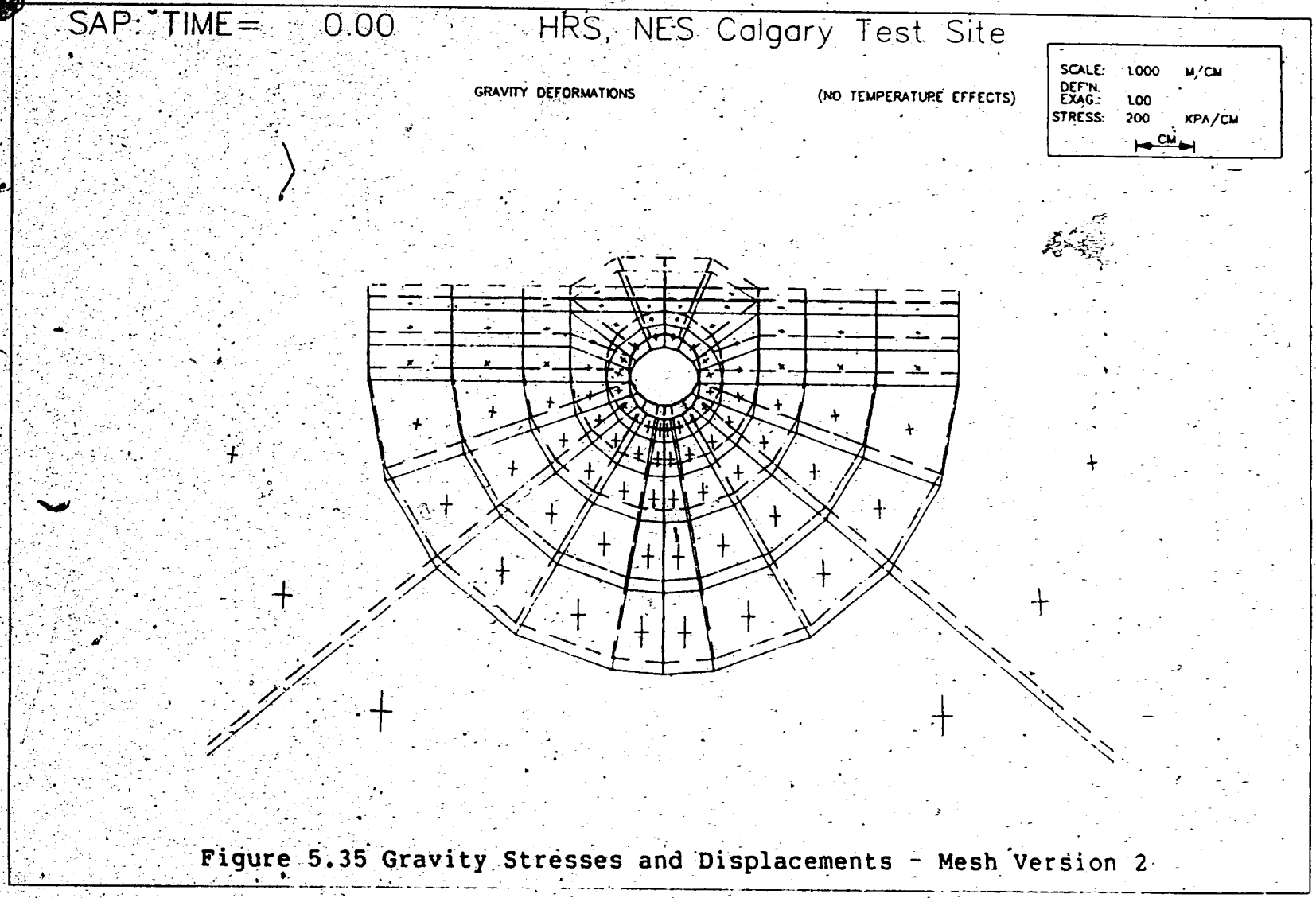

Figure 5.35 Gravity Stresses and Displacements - Mesh Version 2

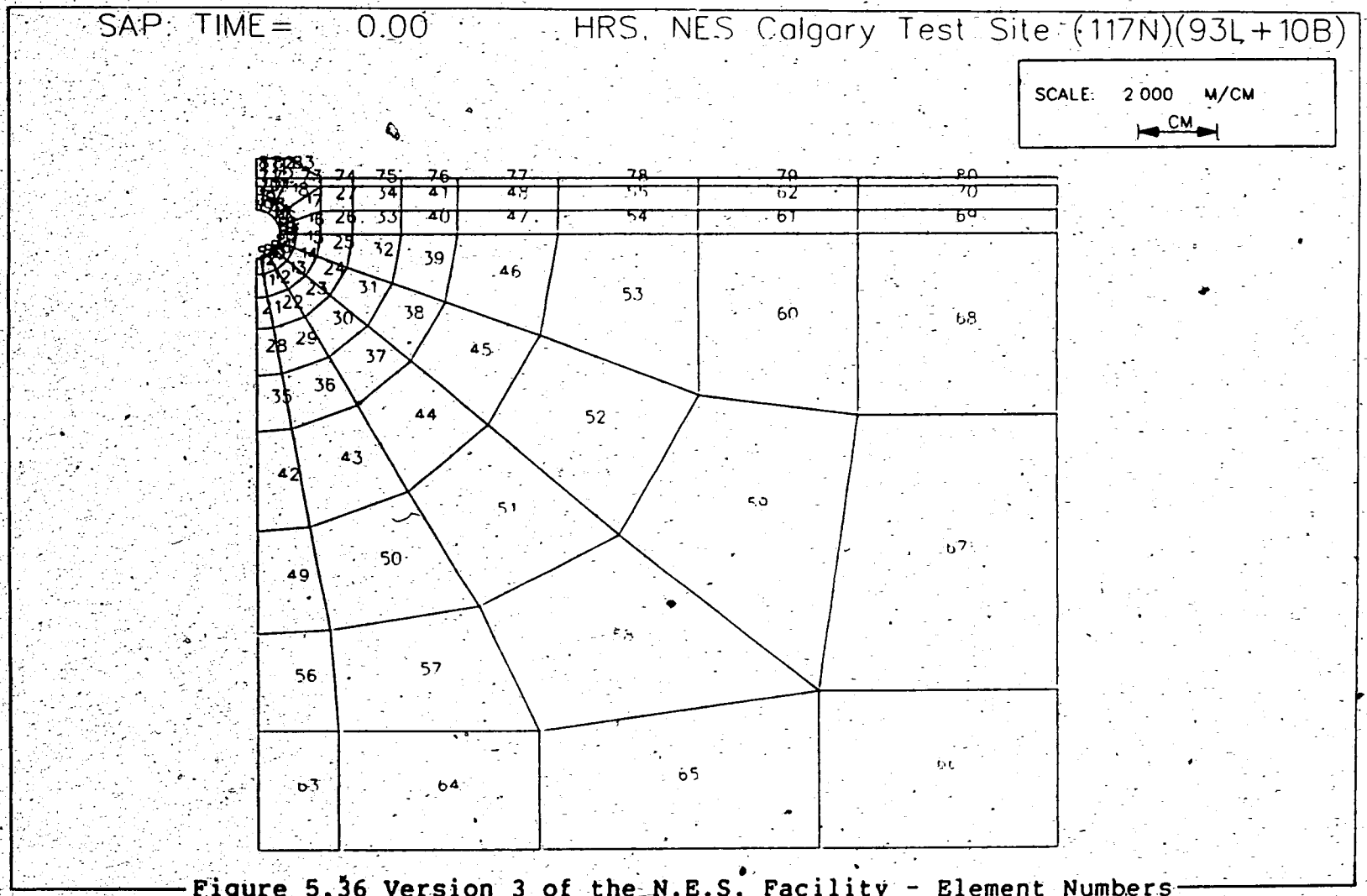

Figure 5.36 Version 3 of the N.E.S. Facility - Element Numbers

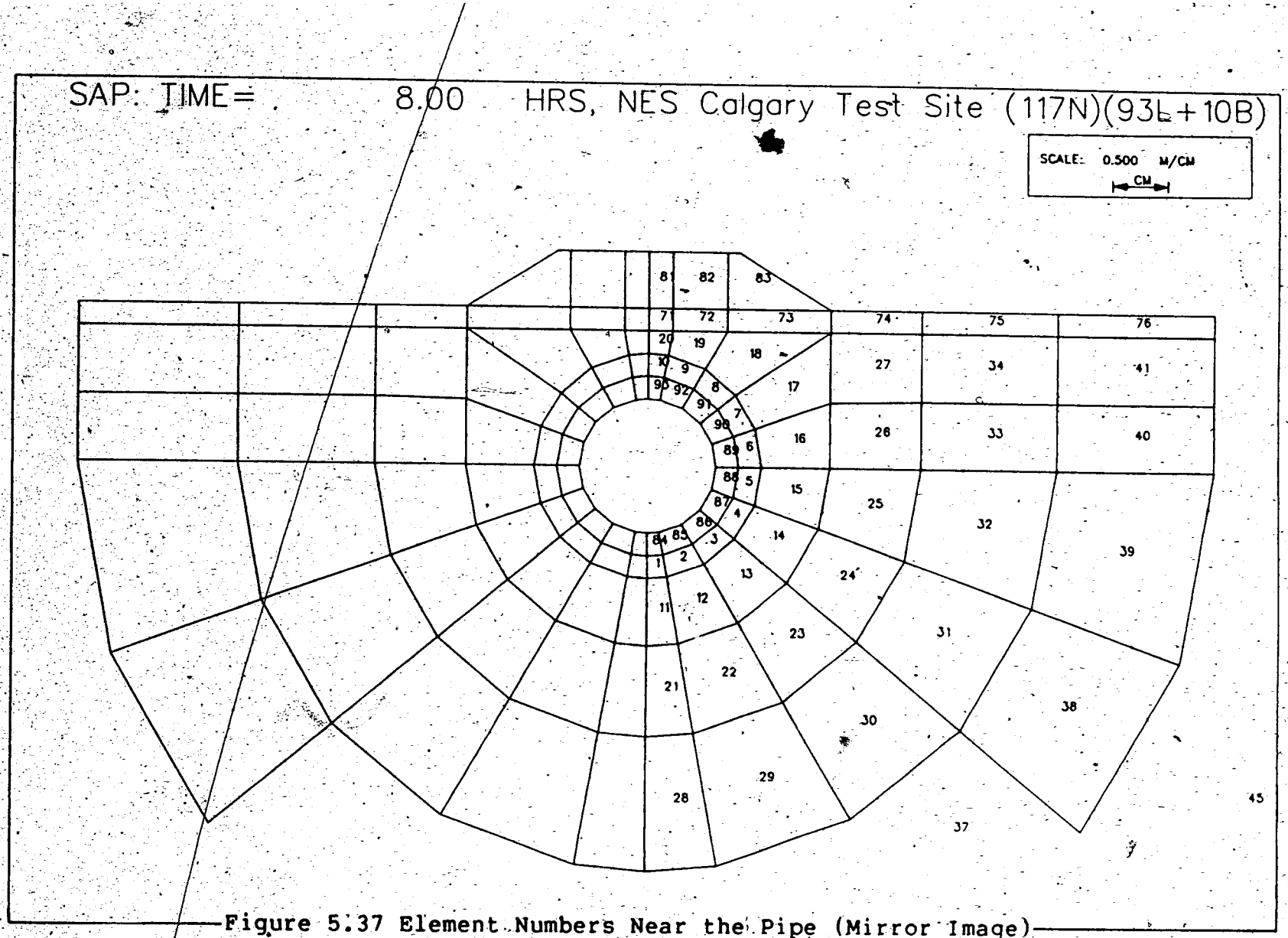

Figure 5.37 Element Numbers Near the Pipe (Mirror Image)

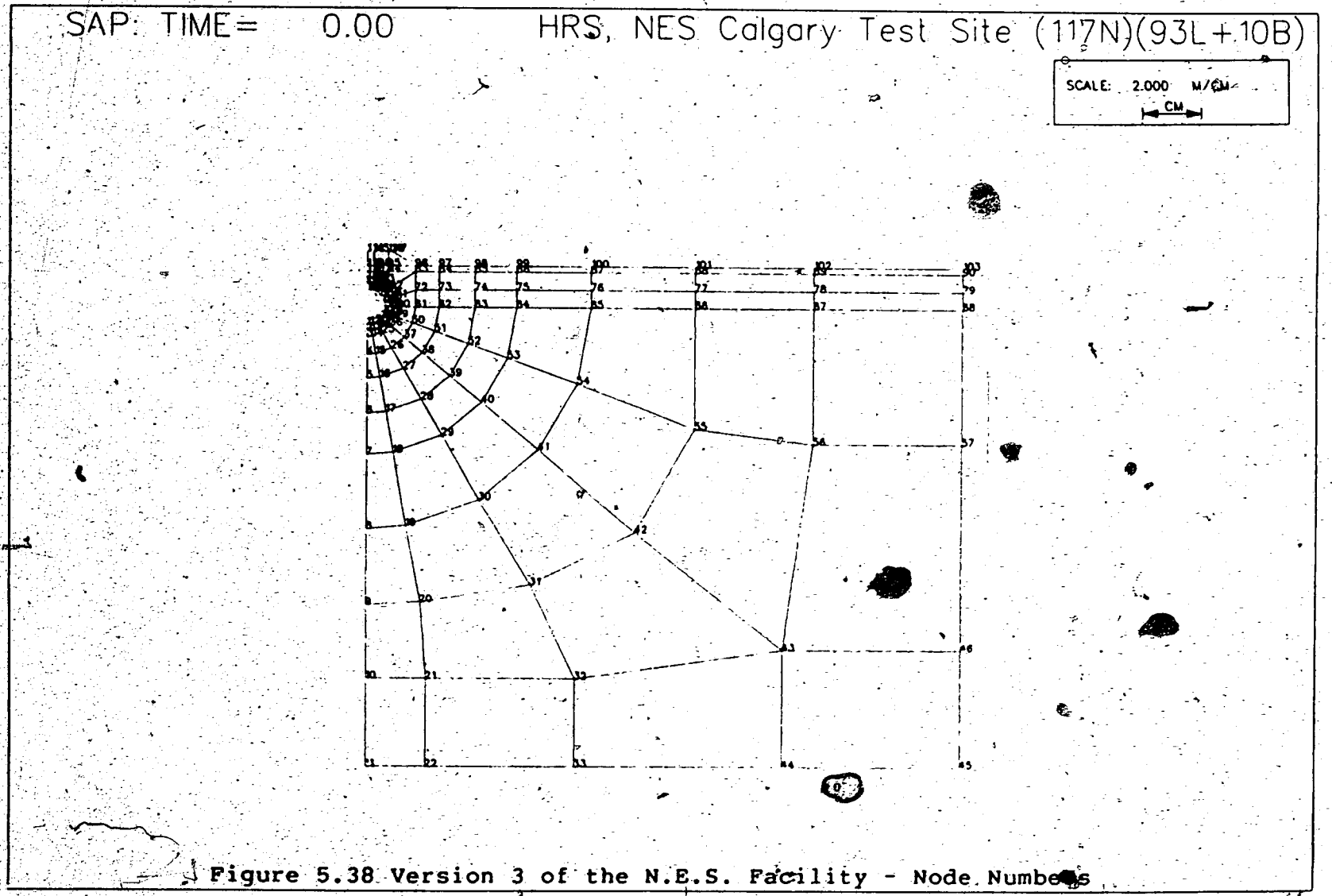

Figure 5.38 Version 3 of the N.E.S. Facility - Node Numbers

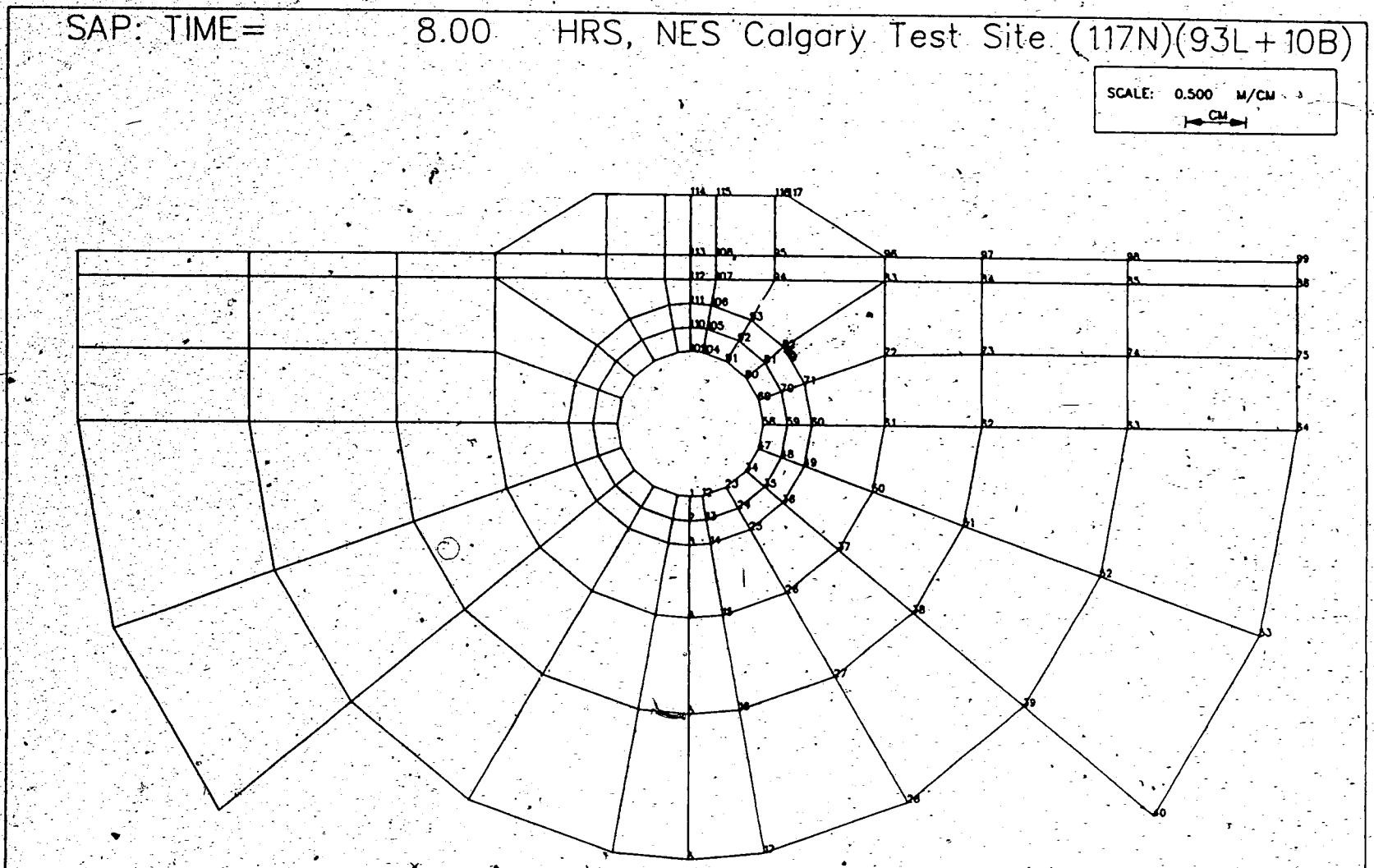

Figure 5.39 Node Numbers Near the Pipe (Mirror Image)

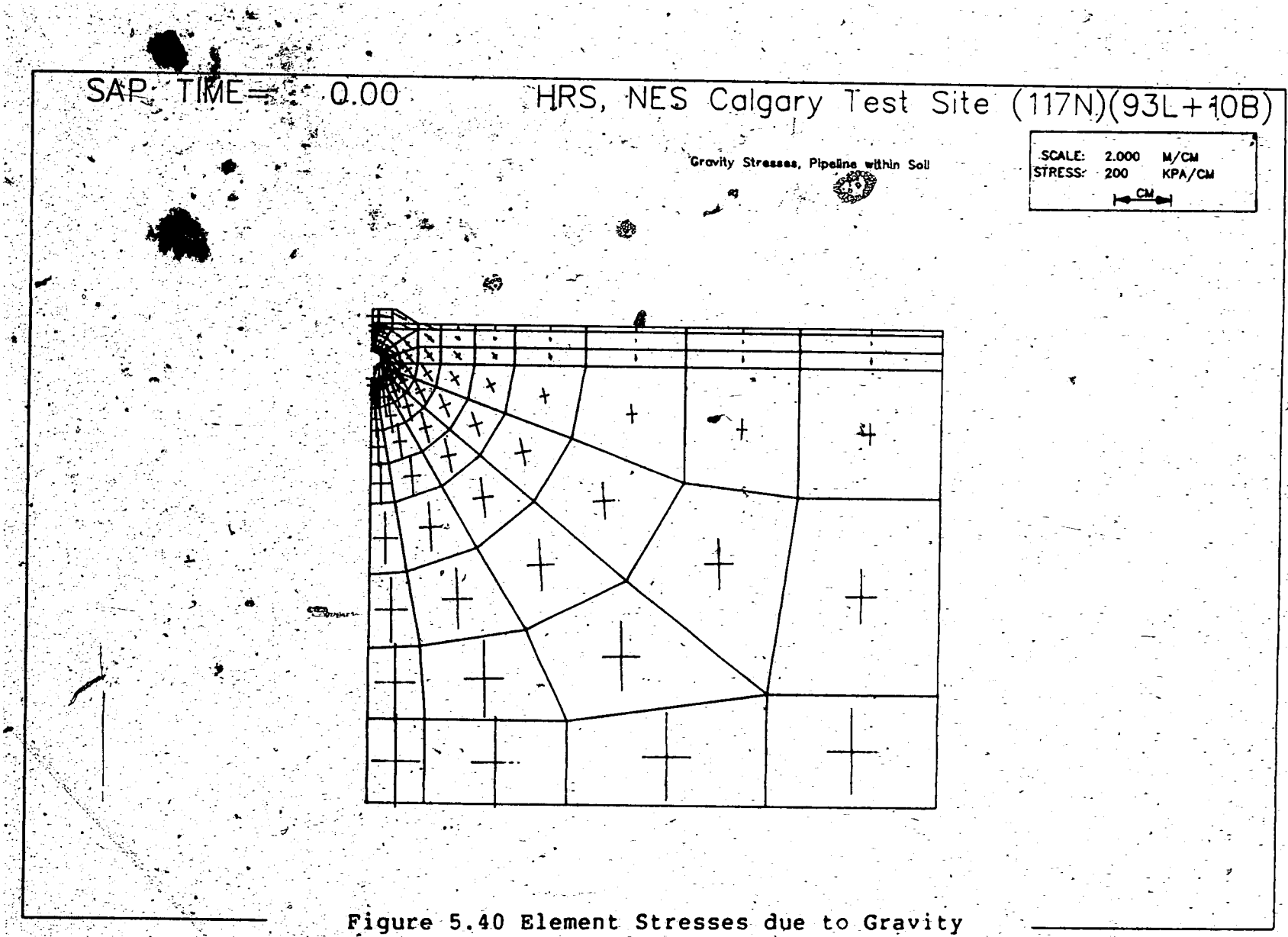

Figure 5.40 Element Stresses due to Gravity

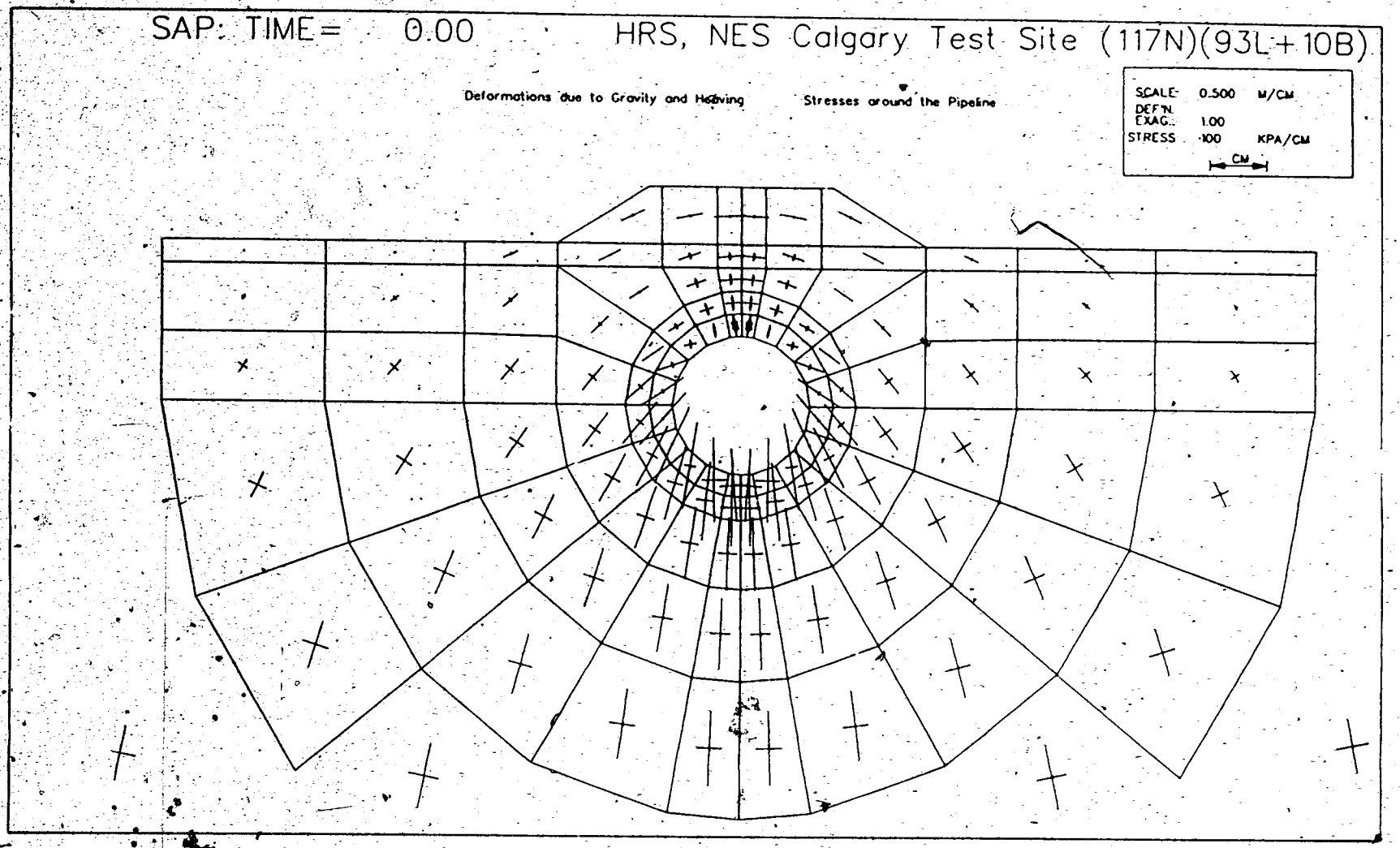

Figure 5.41 Gravity Stresses near the Pipe (Mirror Image)

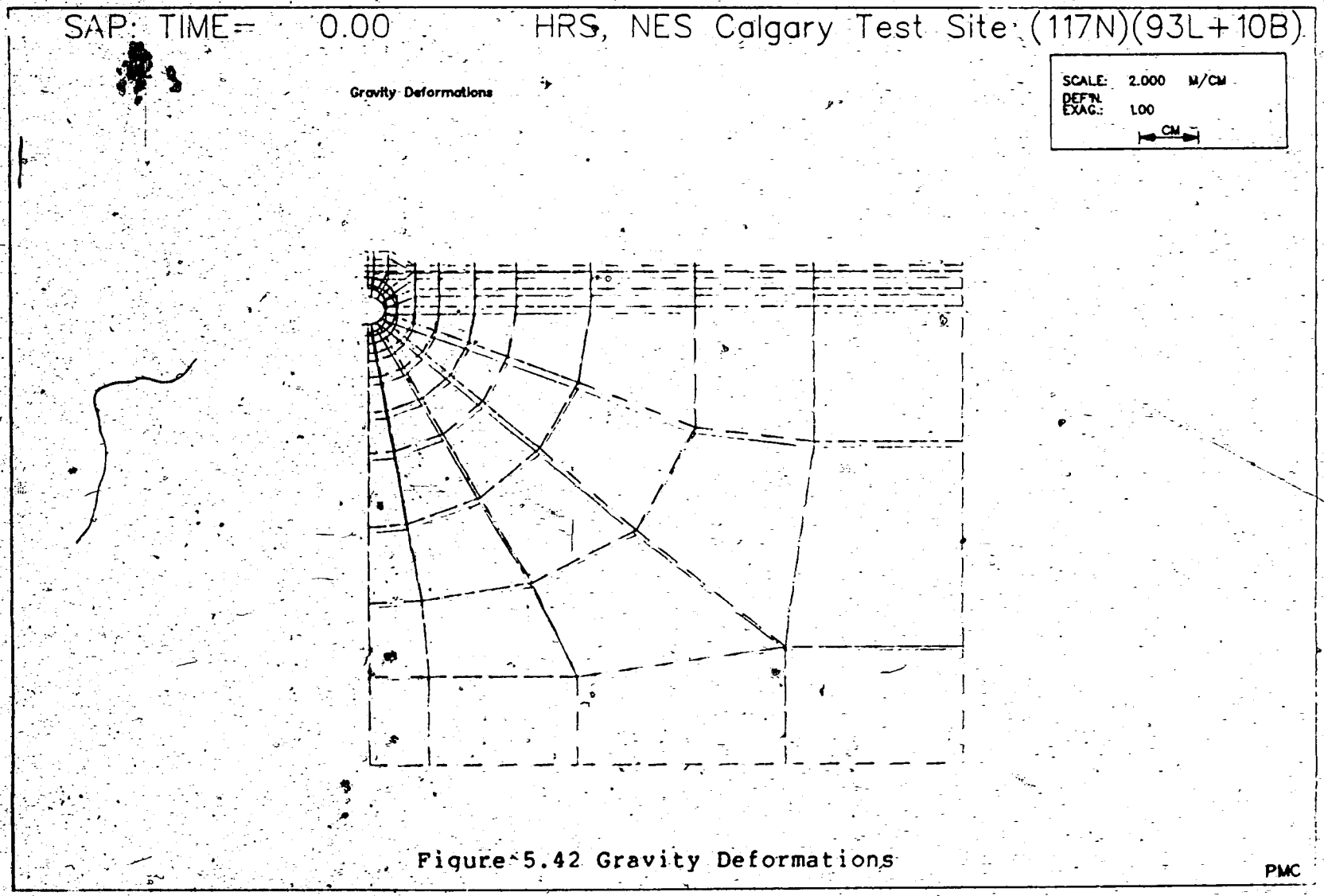

Figure 5.42 Gravity Deformations

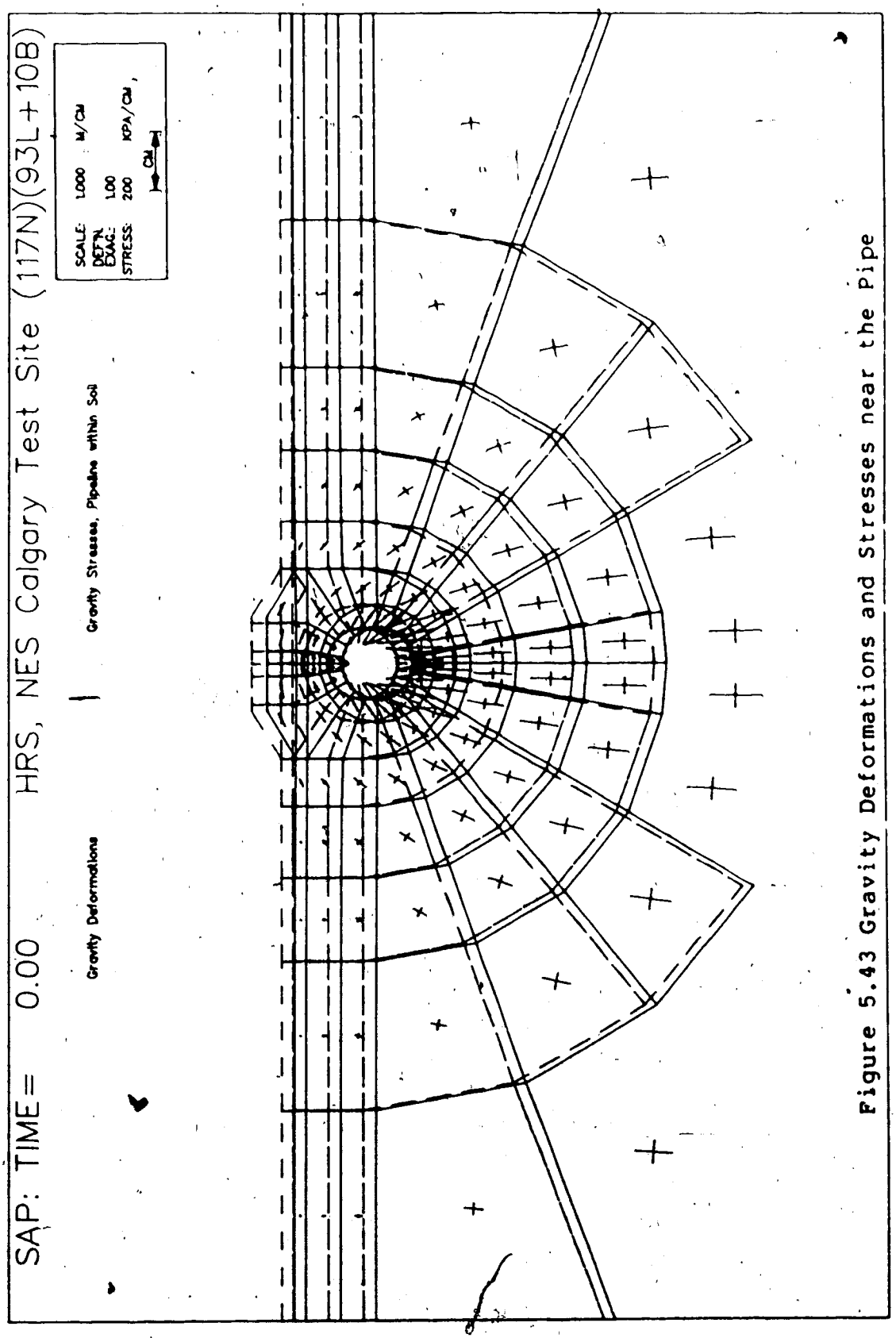

Figure 5.43 Gravity Deformations and Stresses near the Pipe

The frost heave simulation was begun using the *SAP IV* and *ADINAT* programs for finite element results and the *TRANS* program for heave effects. The actual sequencing is detailed in Appendix H. The simulation was performed in segments so that interim results could be evaluated.

Unreasonable stresses appeared early in the analysis. By time t=8hr large tension and compression forces had developed above the pipeline (Fig. 5.44). Gravity stresses were inconsequential in comparison. To completely remove the effect of the berm, the analysis was restarted using a flexible, weightless berm. The results were examined at t=12hr. Because there was no improvement in the stress field, and because the bulk of the activity centered around the pipe, this indicated that the heaves were the cause of the exteraneous stresses (Fig. 5.45, 5.46). Certainly the displacement vectors shown in Figure 5.47 indicated that the pipe was being pulled up by these overlying stresses.

The tension was obviously due to the implementation of heaves as an α factor and not due to arching effects from heaving because a high compression layer existed above the tension layer capping the pipe. Since the heaving stresses depended on the α value and the stiffness matrix $[K]$, the moduli of the cold soil was reduced by a factor of ten and the analysis was restarted.

The much reduced stresses and displacements (Fig. 5.48, 5.49) confirmed that an incompatibility existed between the

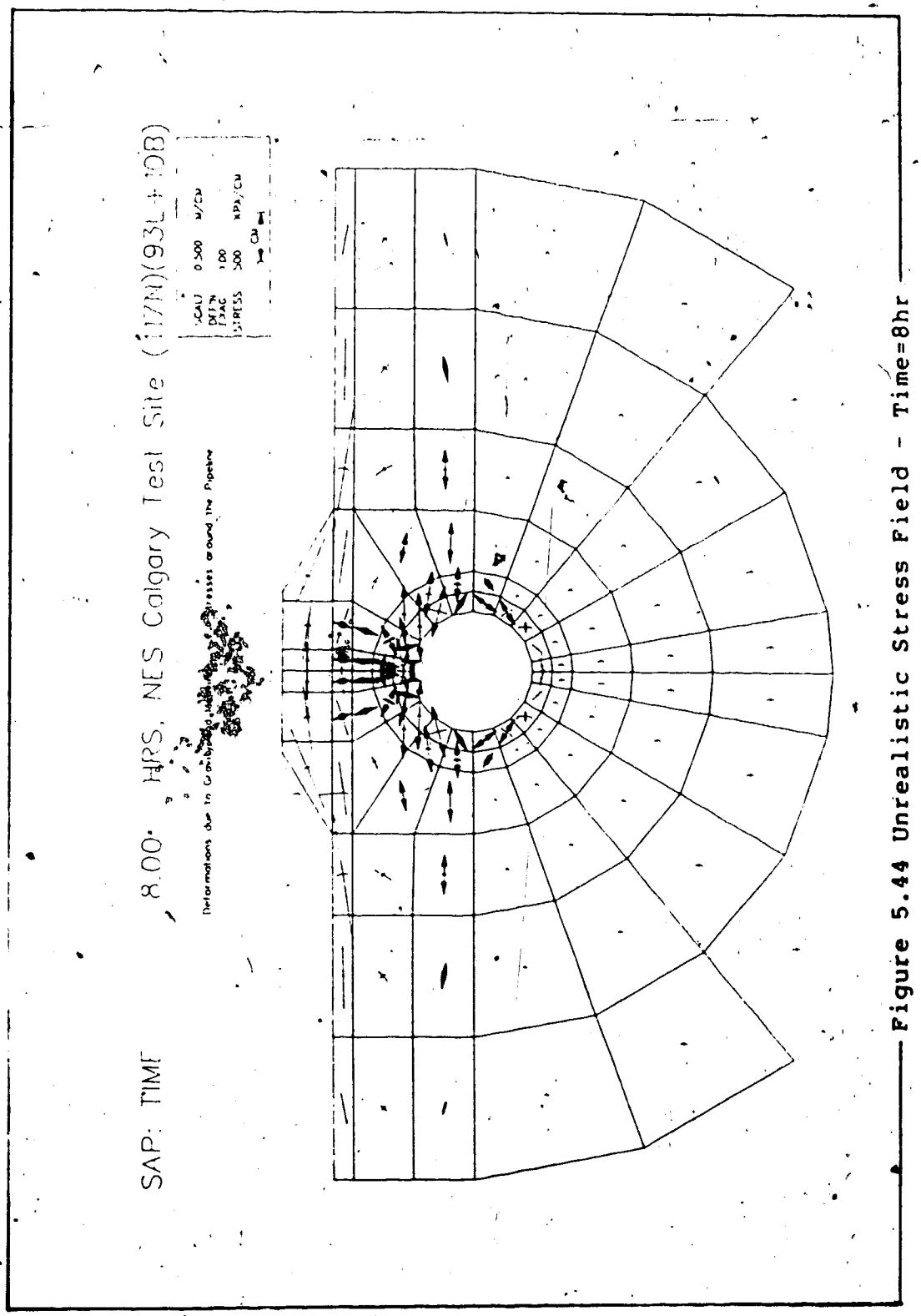

Figure 5.44 Unrealistic Stress Field - Time=8hr

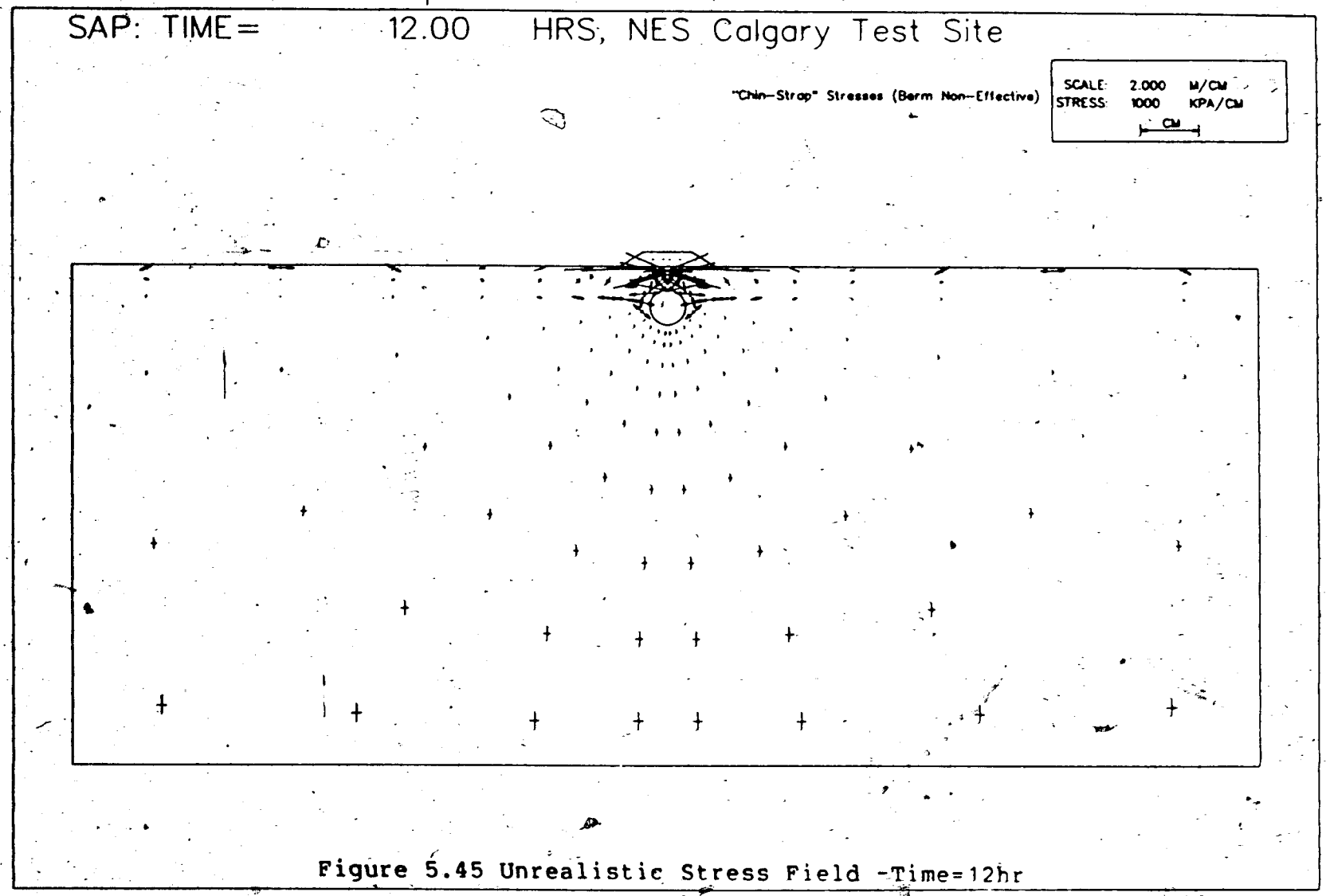

Figure 5.45 Unrealistic Stress Field -Time=12hr

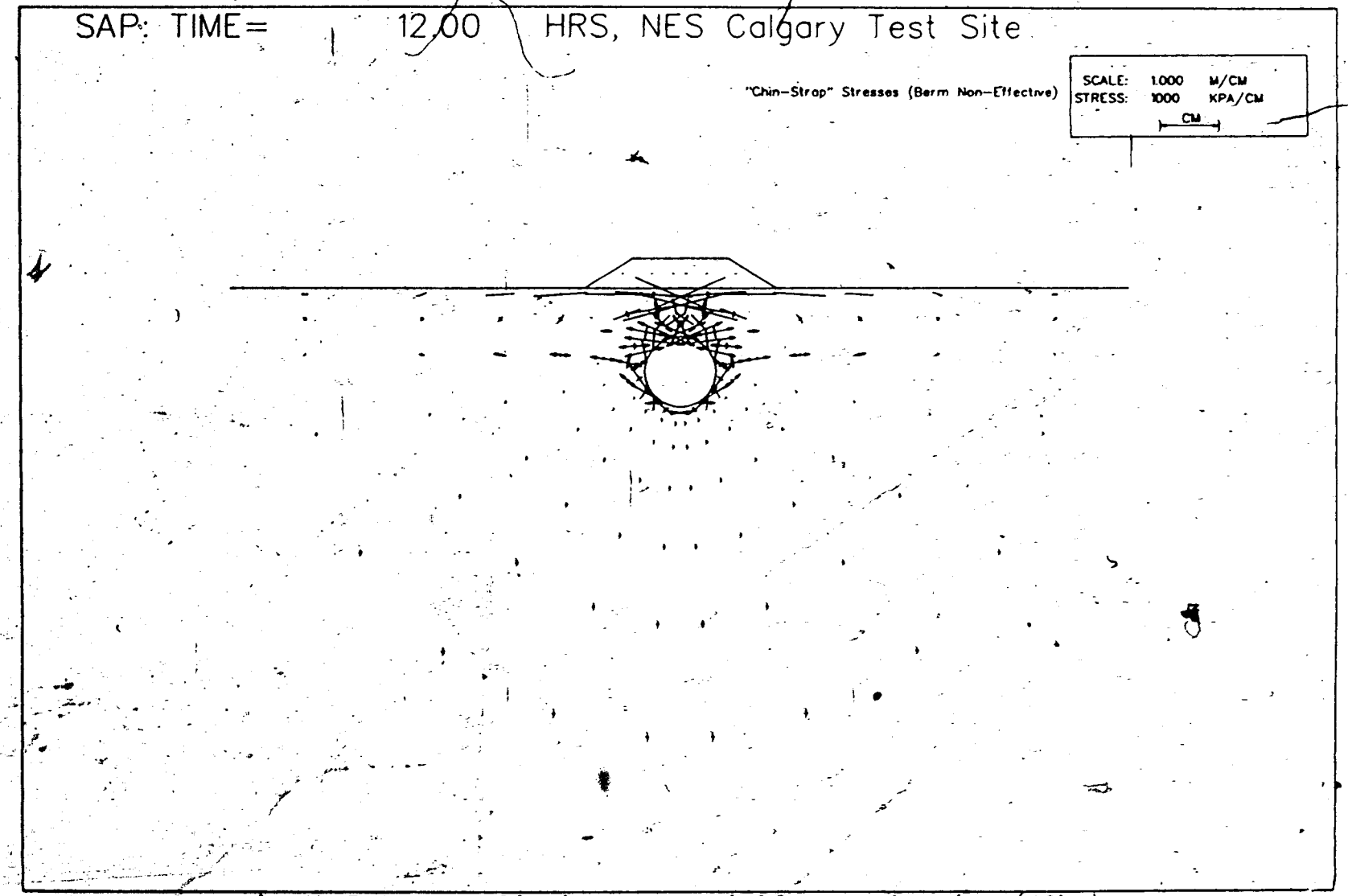

Figure 5.46 Unrealistic Stress Field near the Pipe (12hr)

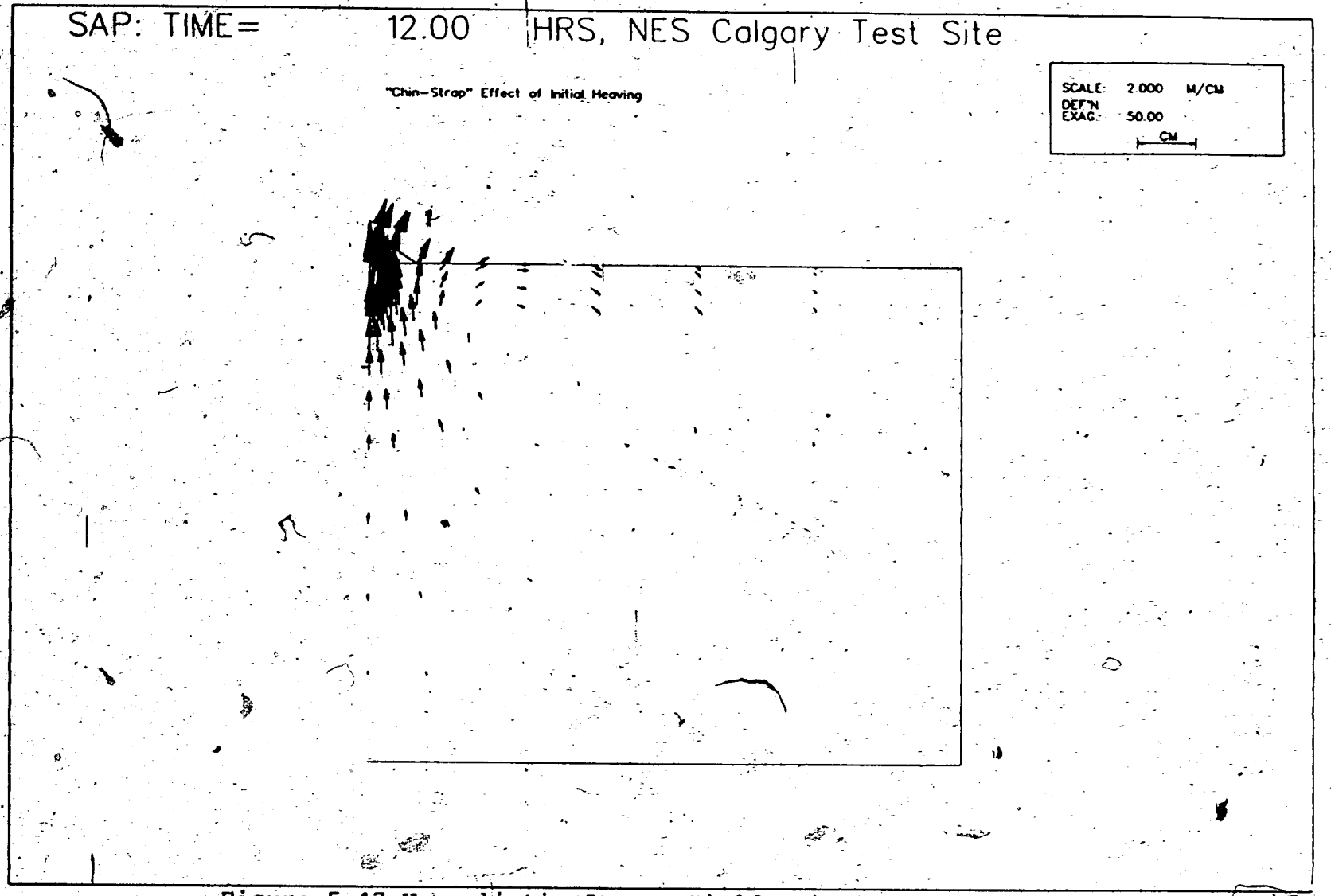

Figure 5.47 Unrealistic Stress Field: Displacement Arrows

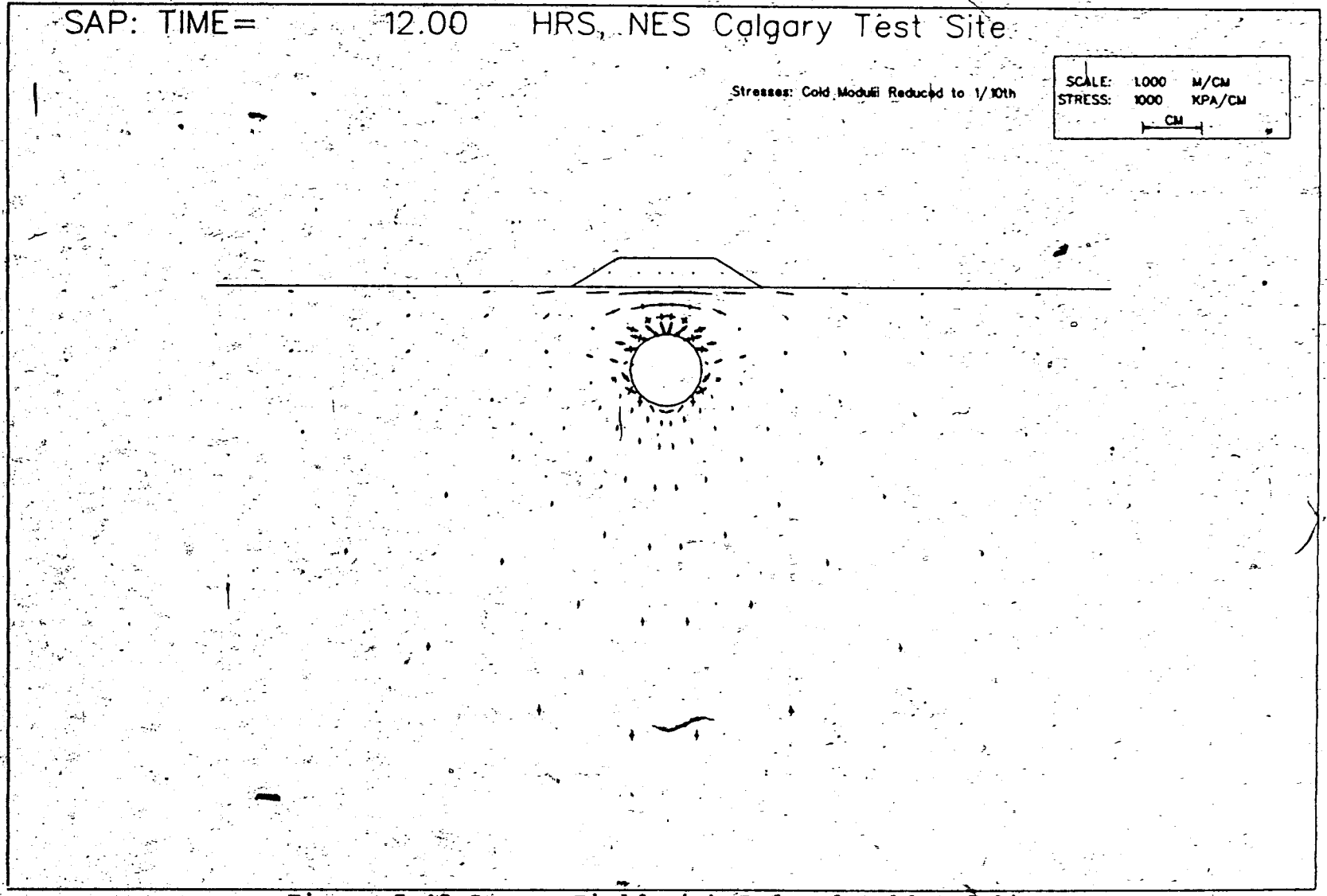

Figure 5.48 Stress Field with Reduced Cold Moduli

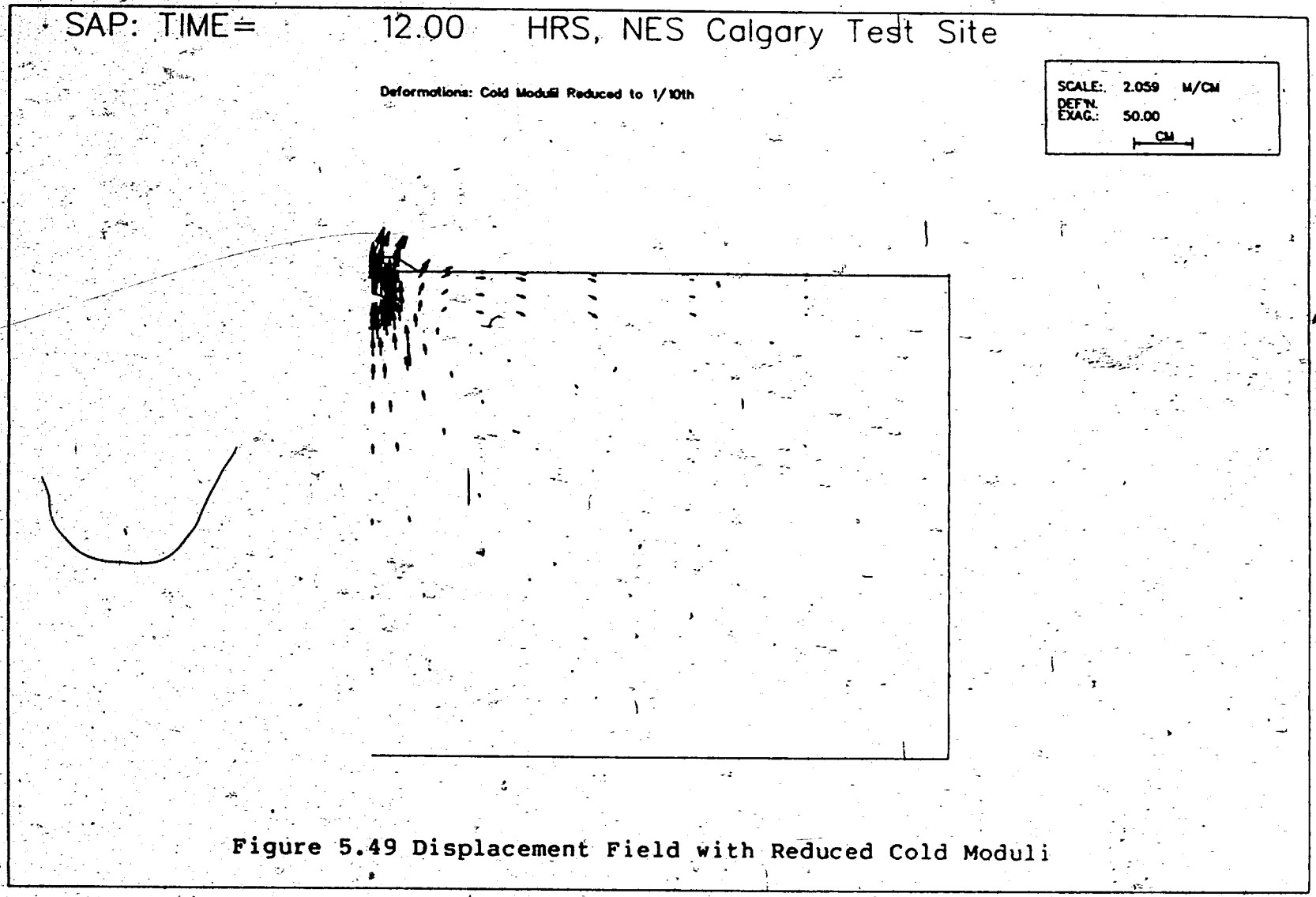

Figure 5.49 Displacement Field with Reduced Cold Moduli

a values for heave and the stiffness matrix $[K]$. The concept of a variable modulus was rejected because the strain energy resulting from imposing a cummulative heave onto a cooling (therefore stiffening) material was not representative of the strain energy within the soil. Thus, the previous displacements resulting from heave could not be reproduced, using the current stiffness matrice [K], without developing higher stresses. No viable alternative solution was available, other than to use a constant material stiffness of E=8500kPa.

5.8.1 The Final Analysis

Using constant E and ν, the analysis was restarted. A tension problem within the berm had been anticipated, so the top centerline node was freed. This allowed a crack to develop in the berm, as this would be the more realistic than tension development.

The displaced mesh with stresses (Fig. 5.50) shows the heaved pipeline at time t=30 days. Initial gravity displacements have been subtracted from the final displacements to emphasize the heaves. (A deformation exaggeration of 10 was used.)

The elements immediately below the pipe have distorted vertically, as have elements on both sides of the pipe. Significant pressures were developing below the pipe in response to the two-dimensional frost front and the

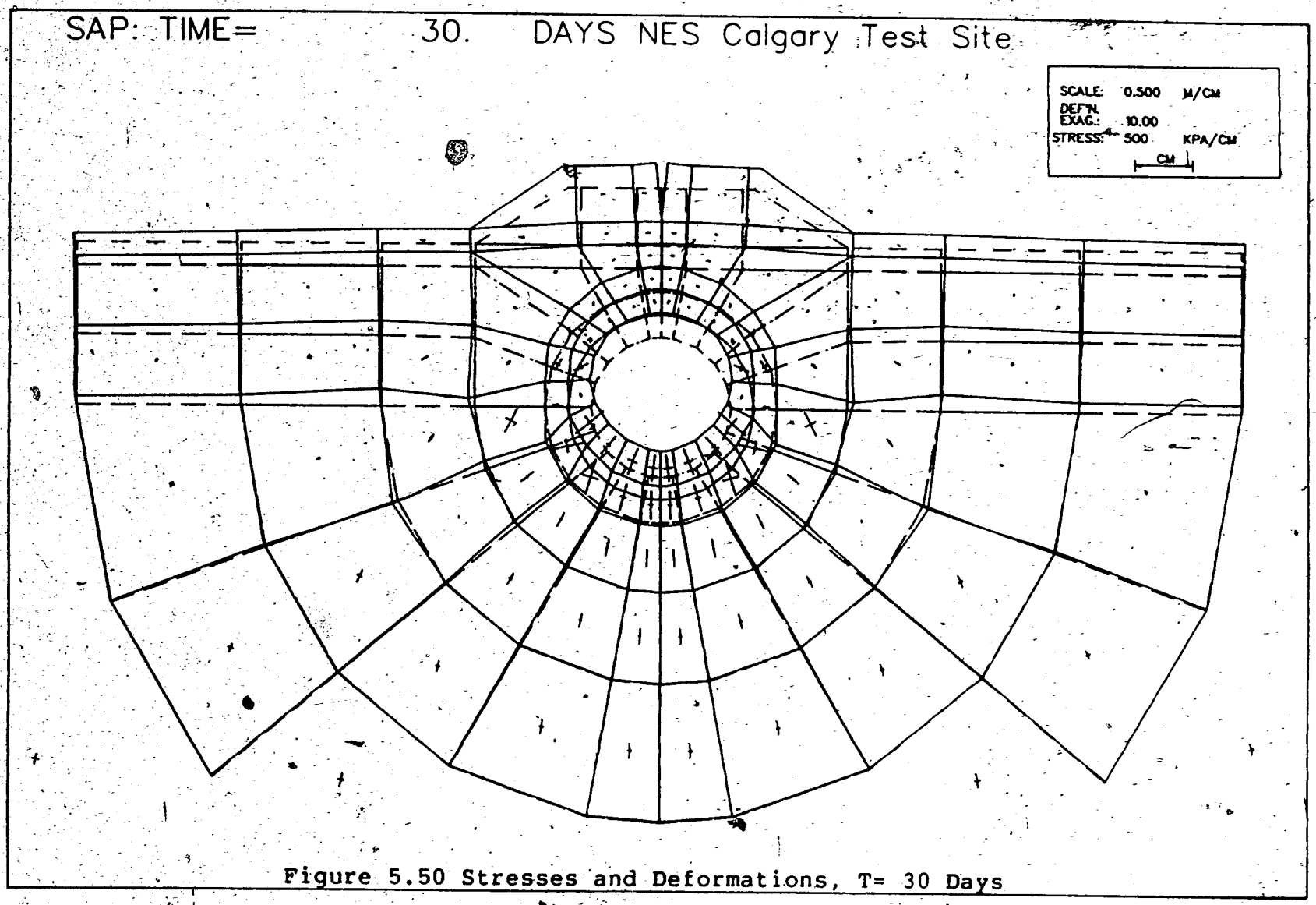

Figure 5.50 Stresses and Deformations, T= 30 Days

confinement. Heaving had caused the berm to deform and crack, as expected. The berm had been rendered non-effective until time t=400 days when the field berm was applied. The heave displacements are seen in Figure 5.51.

The analysis was restarted from t=30 days until t=400 days. The monthly variation of temperature in response to the applied surface temperature, pipeline temperature and latent heat effects are shown in Figures 5.52 to 5.63.

One year after the chilled gas began circulating, the stresses and deformations had developed to those shown in Figure 5.64. Again, there had been significant stress development below the pipe. It is of interest to note that the principal stresses were beginning to rotate into the horizontal plane due to the lateral restraint and the horizontal heave. The pipe cross-section had remained circular because the circumferential stress variation was small in comparison to the moment capacity of the pipe wall.

Tension had developed above the pipe because cracking was not allowed in the soil below the berm. This tension would not exist in the field due to the poor compaction of backfill material and creep effects. These element tensions could be reduced by stopping the iterative procedure when tension began to develop and freeing an additional node at the centreline. This "unzipping" of the mesh above the pipe would result in the propagation of a crack as the heaving process displaced the overlying material upwards and

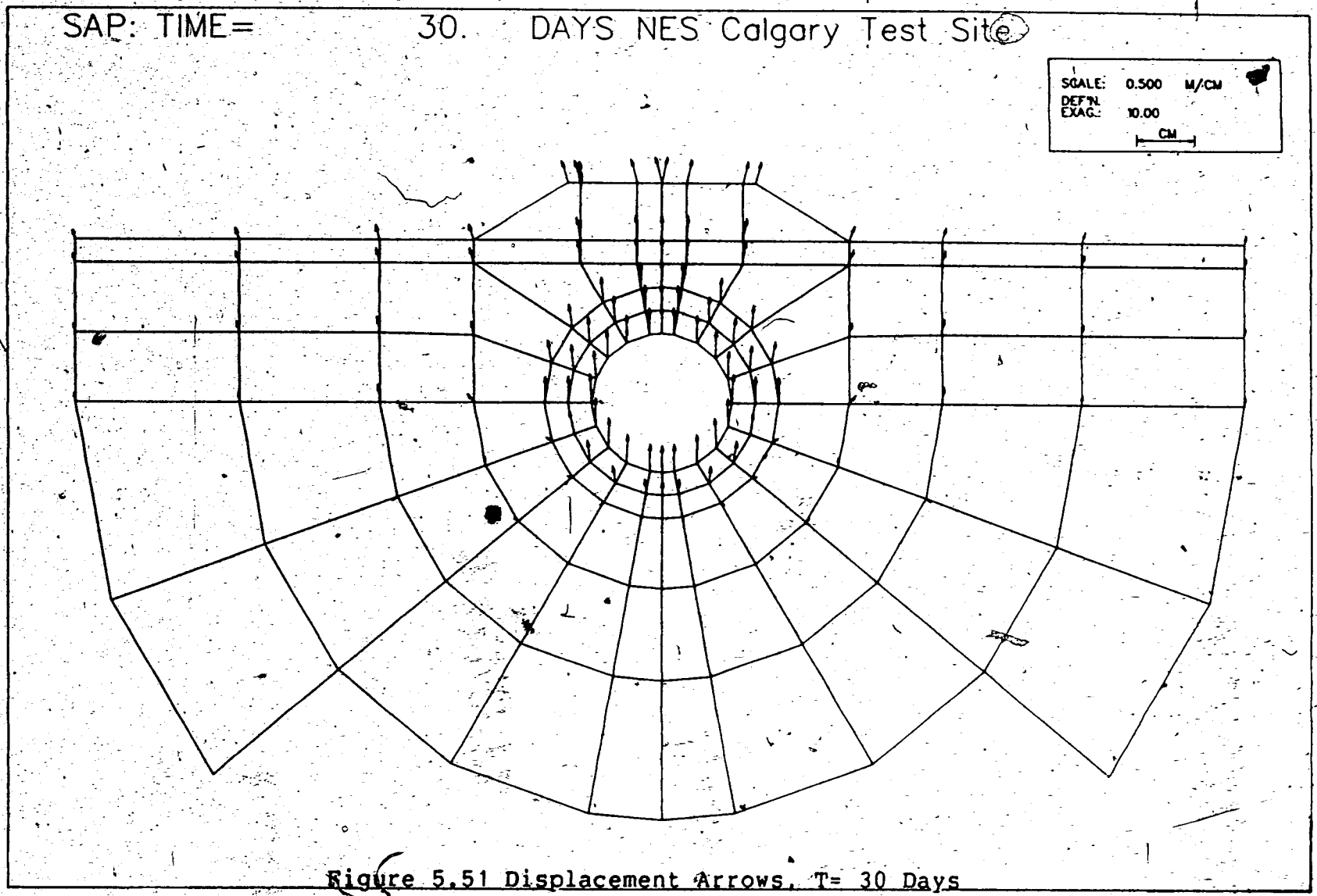

Figure 5.51 Displacement Arrows, T= 30 Days

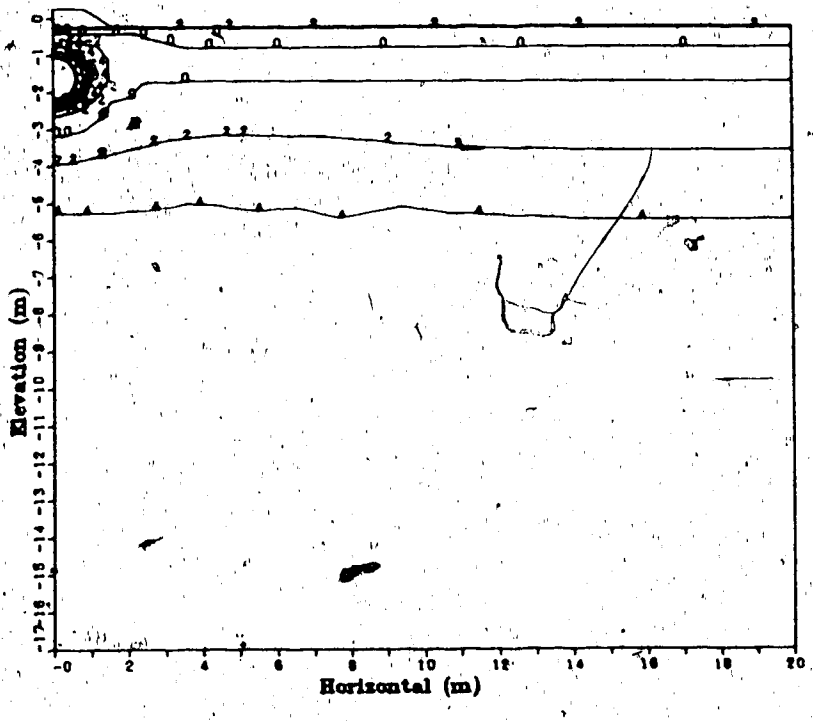

Figure 5.52 Temperature Distribution after 1 Month

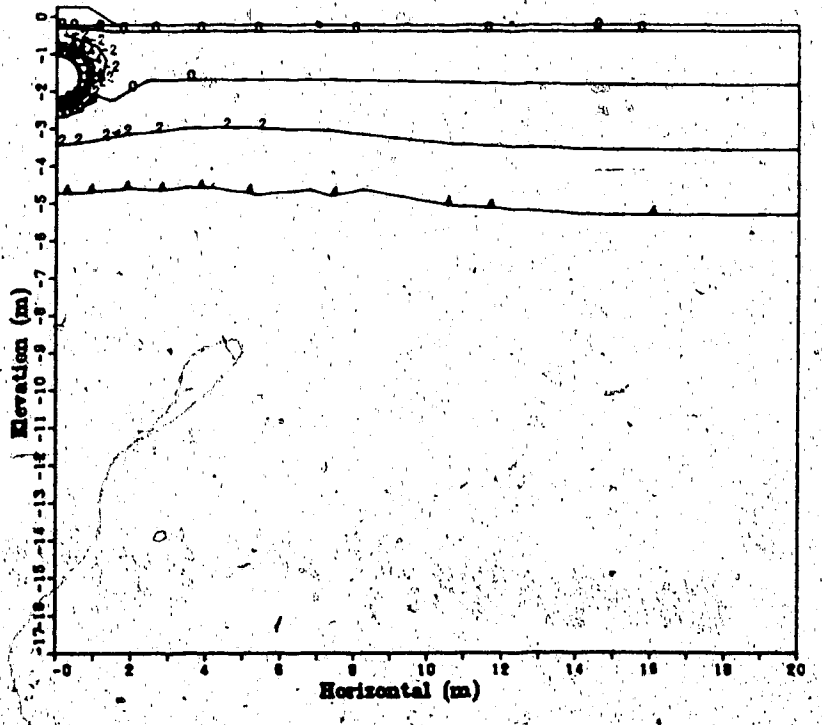

Figure 5.53 Temperature Distribution after 2 Months

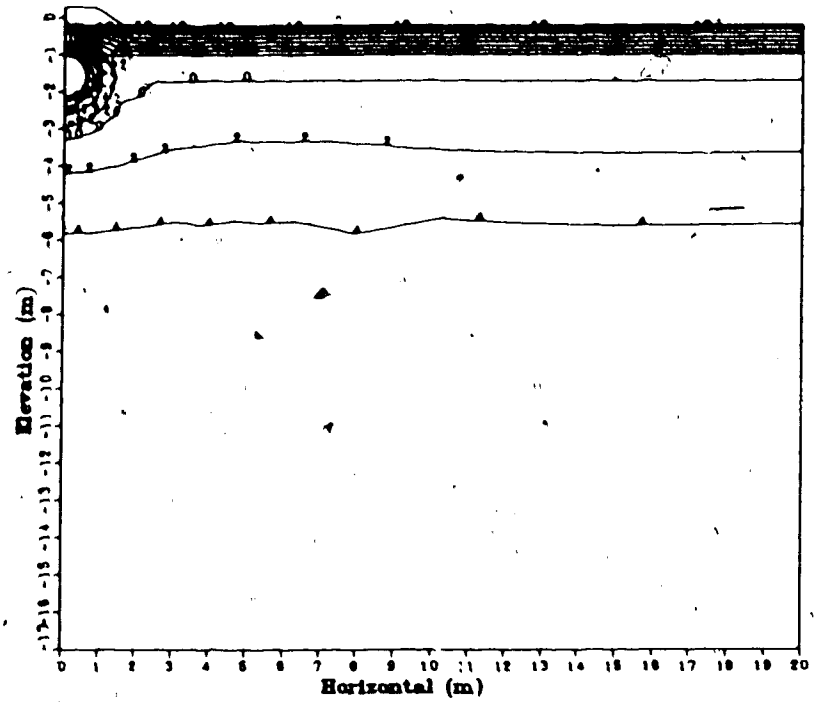

Figure 5.54 Temperature Distribution after 3 Months

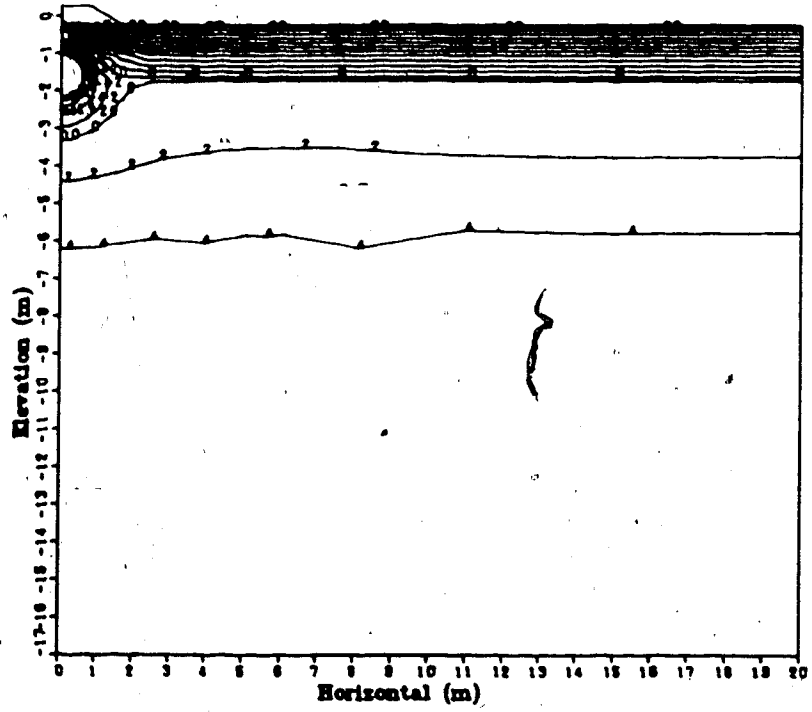

Figure 5.55 Temperature Distribution after 4 Months

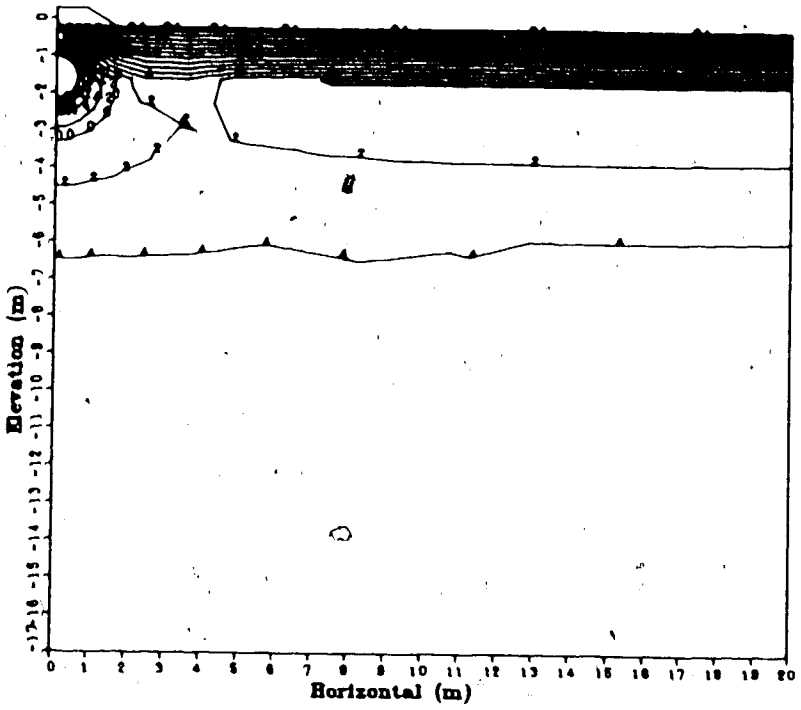

Figure 5.56 Temperature Distribution after 5 Months

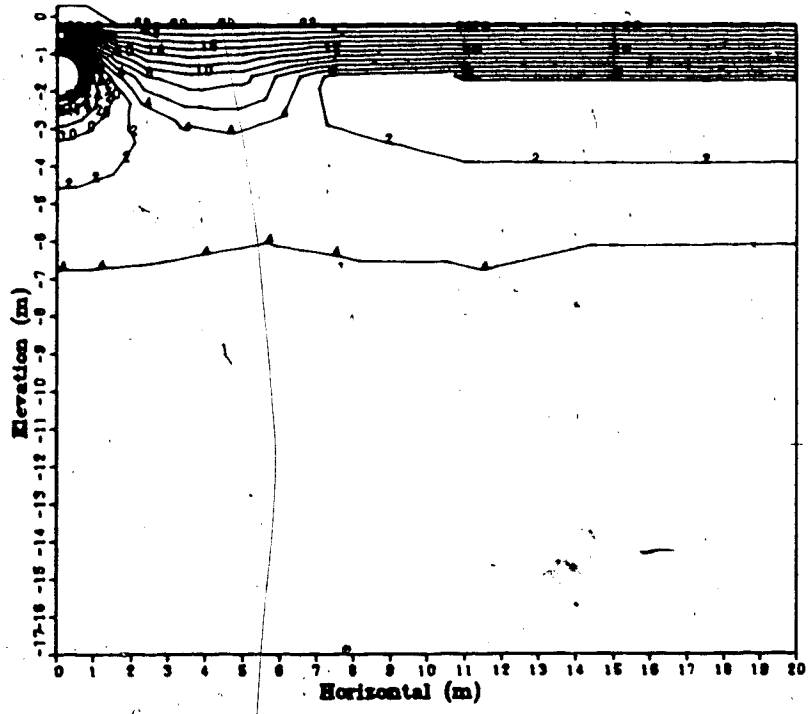

Figure 5.57 Temperature Distribution after 6 Months

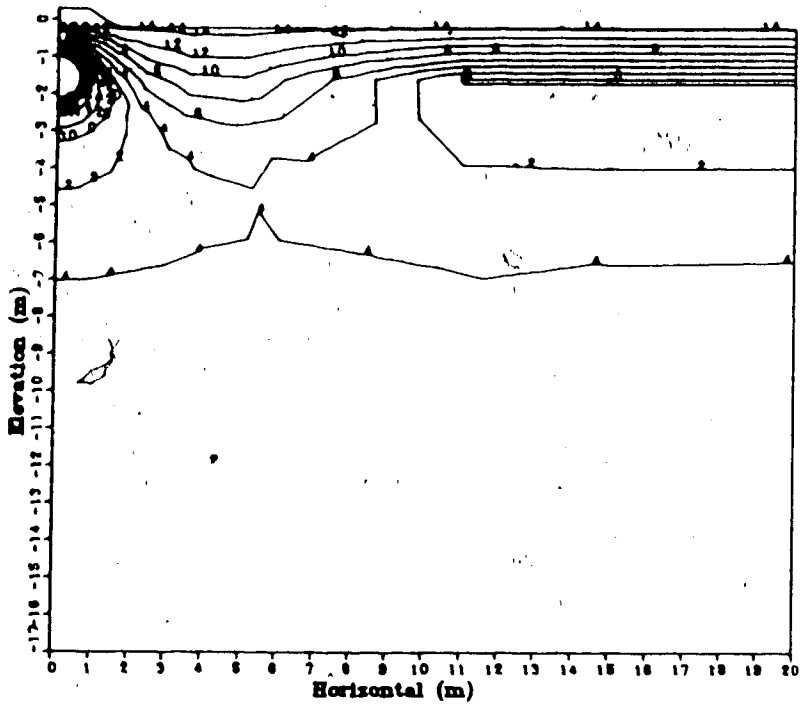

Figure 5.58 Temperature Distribution after 7 Months

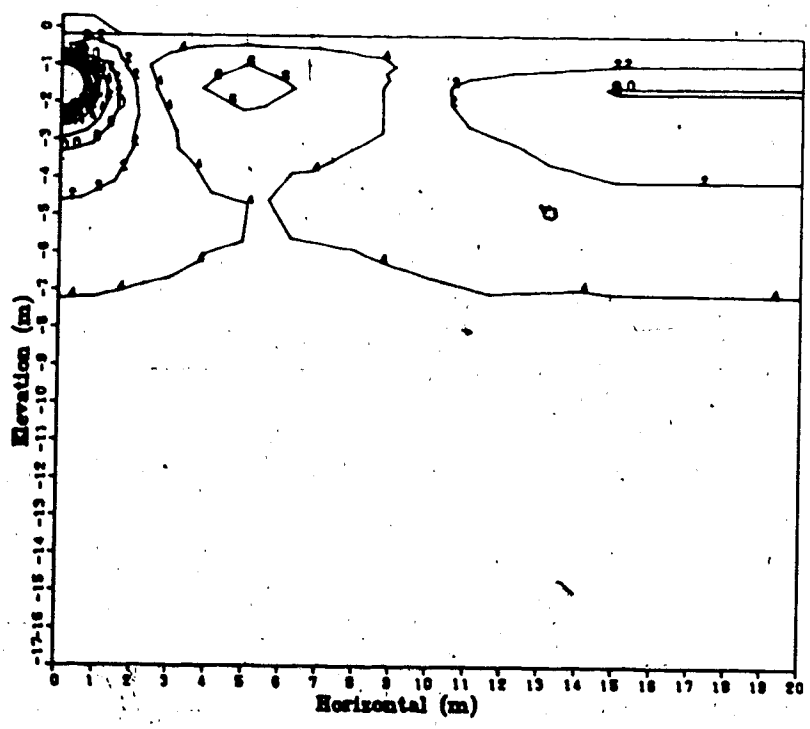

Figure 5.59 Temperature Distribution after 8 Months

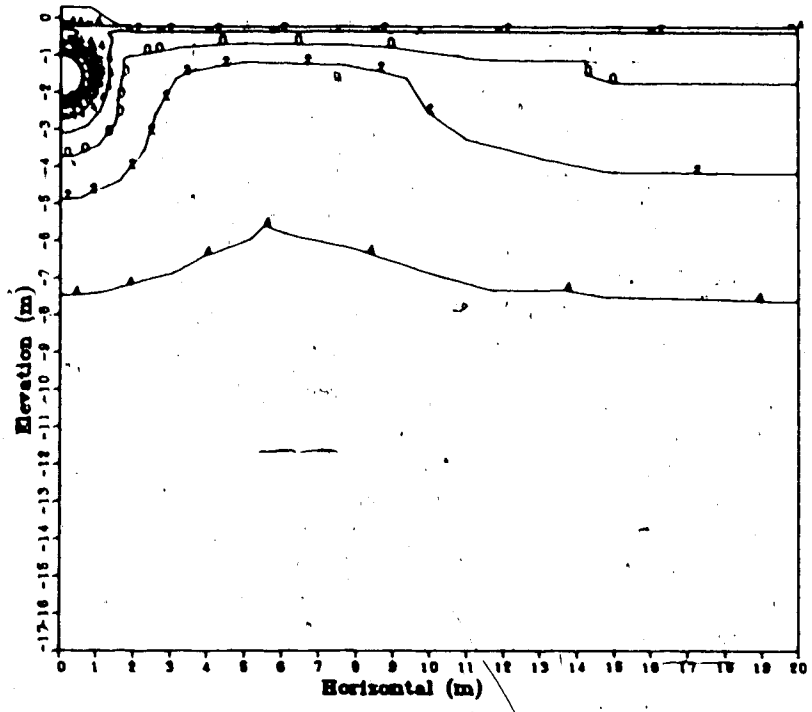

Figure 5.60 Temperature Distribution after 9 Months

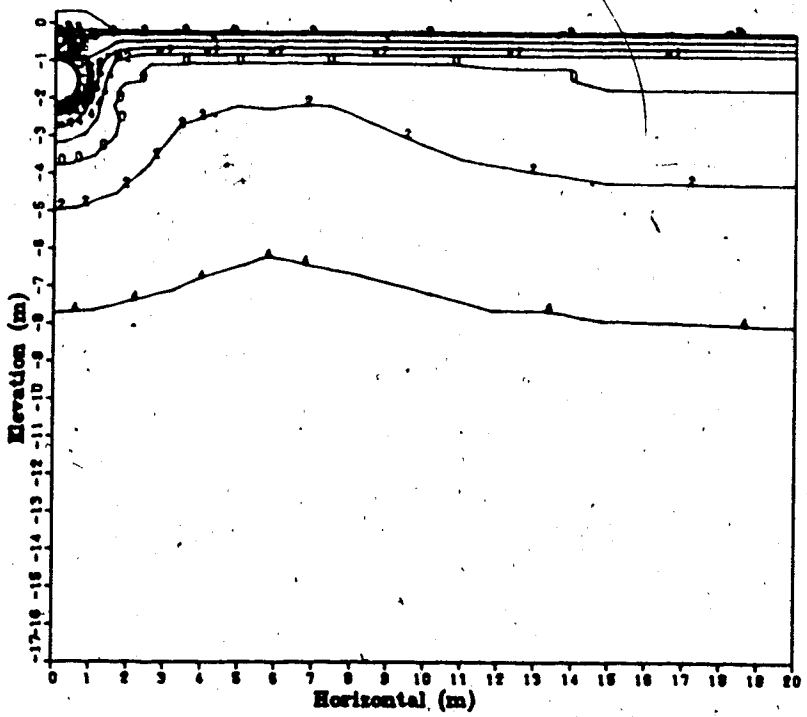

Figure 5.61 Temperature Distribution after 10 Months

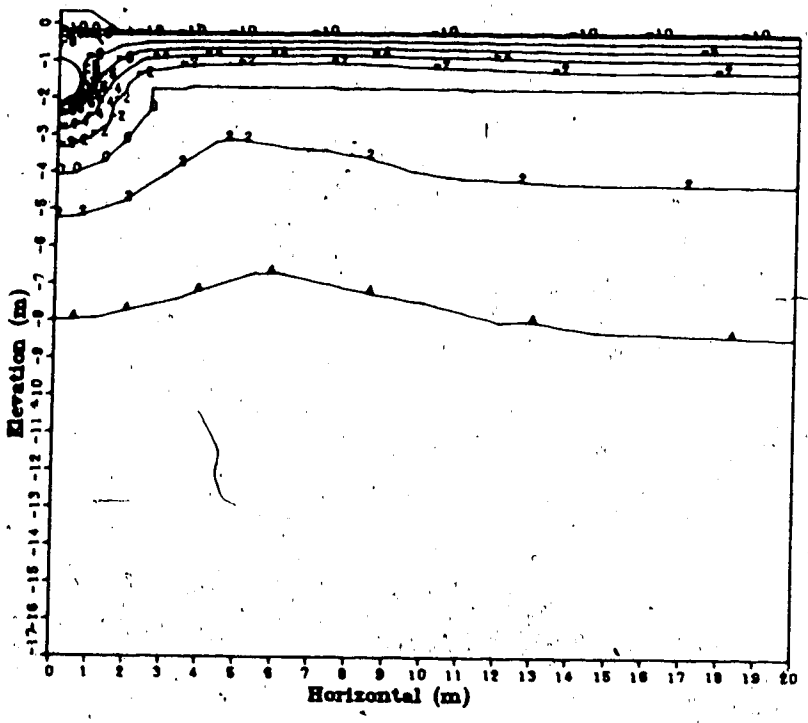

Figure 5.62 Temperature Distribution after 11 Months

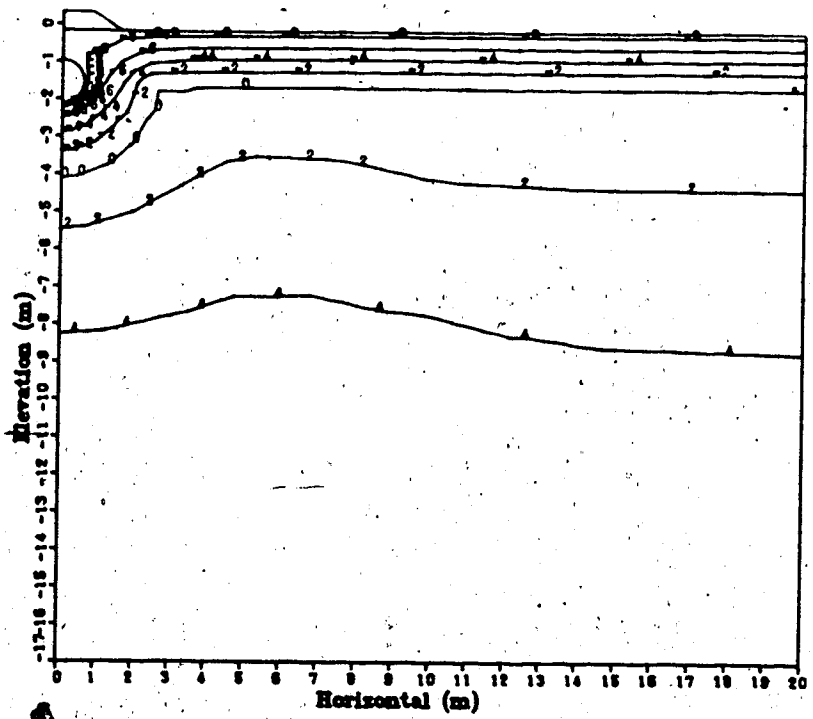

Figure 5.63 Temperature Distribution after 1 Year

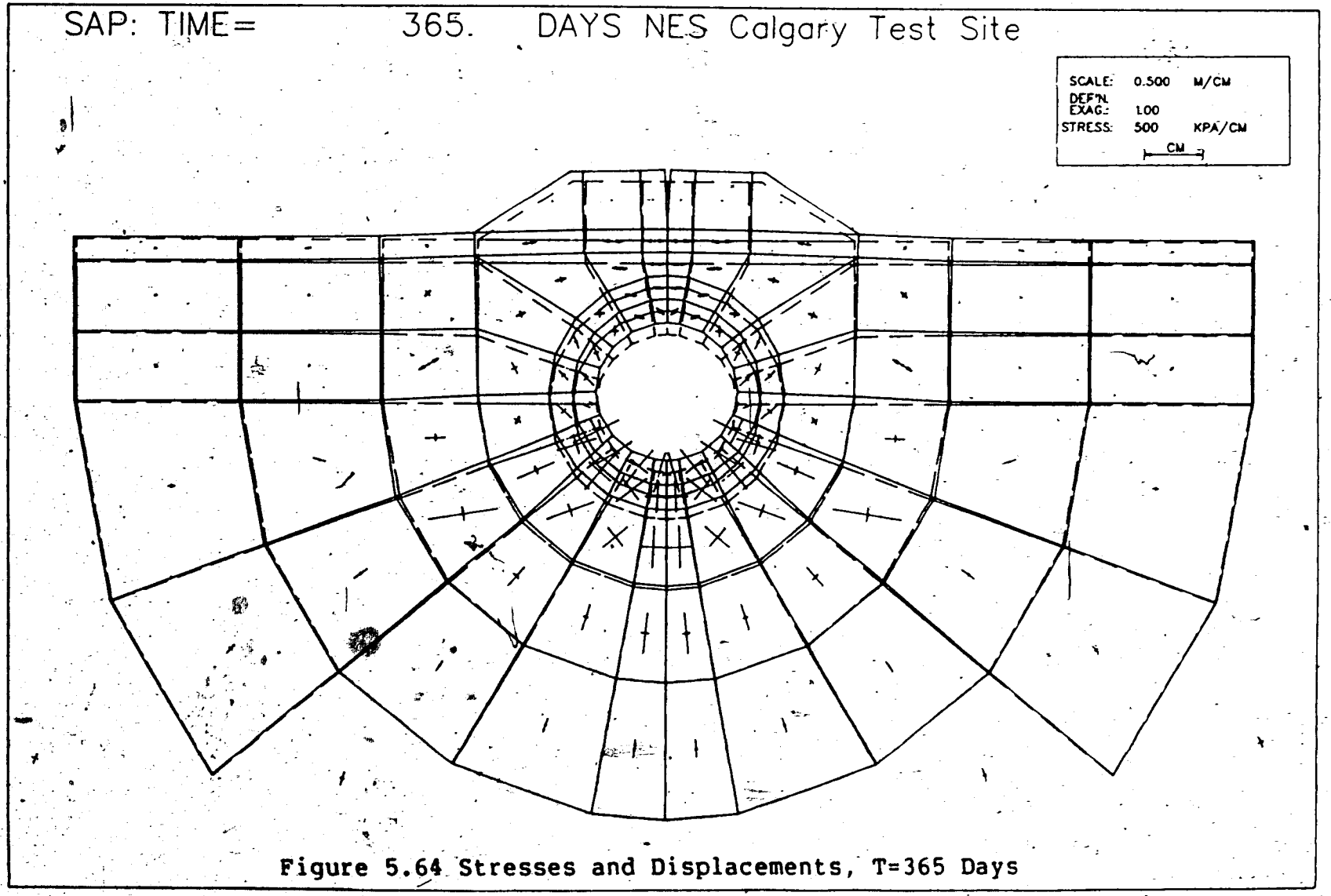

Figure 5.64 Stresses and Displacements, T=365 Days

outwards. Such behaviour may already be seen in Figure 5.65.

The comparison of the finite element results with observed field behaviour is made on the basis of the vertical displacement of the pipeline invert (Fig. 5.66). After one year of operation the finite element approach, based on a SP_o=230 $\cdot 10^{-5}$ mm^2/s$\cdot$C was only 25% of the observed heave. Finite difference predictions (Konrad and Morgenstern, 1984) are closer to the observed behaviqur. The difference was traced to the segregation potential actually used in the heave calculations. Due to the pressure effects, the finite element method predicted SP values of $SP<20 \cdot 10^{-5}$ mm^2/s$\cdot$C for most of the test, with stresses of about 400kPa. (Figures 5.67 and 5.68). In contrast, the finite difference approach used a pressure of 54kPa at the freezing front which corresponded to $SP=140 \cdot 10^{-5}$ mm^2/s$\cdot$C.

The issue is whether Figure 5.64 is a good representation of the stress field around the pipeline. Certainly the tension field above the pipe is questionable, however the major tensile stress is horizontal and should not greatly affect the compression beneath he pipe.

The high horizontal stresses developing below the pipe invert increase the confinement of the subgrade soil. This fosters the development of high vertical stress beneath the pipe due to arching stresses superimposed on the heaving stresses. Assuming that a 1.5m ditcher was used in excavating for the 1.2m pipe it is reasonable to assume poor

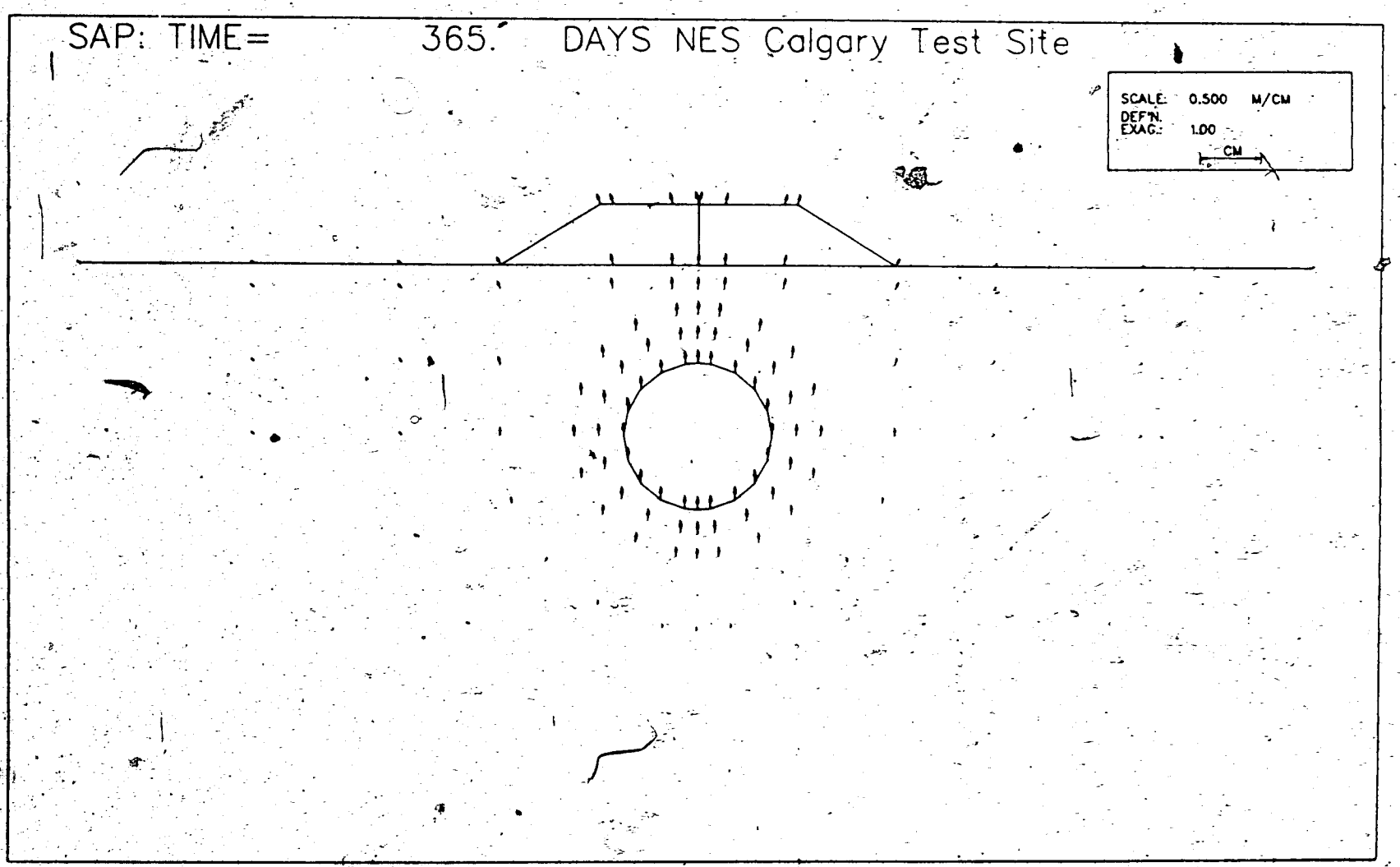

Figure 5.65 Displacement Arrows, T=365 Days

Figure 5.66 Displacement of Pipeline Invert

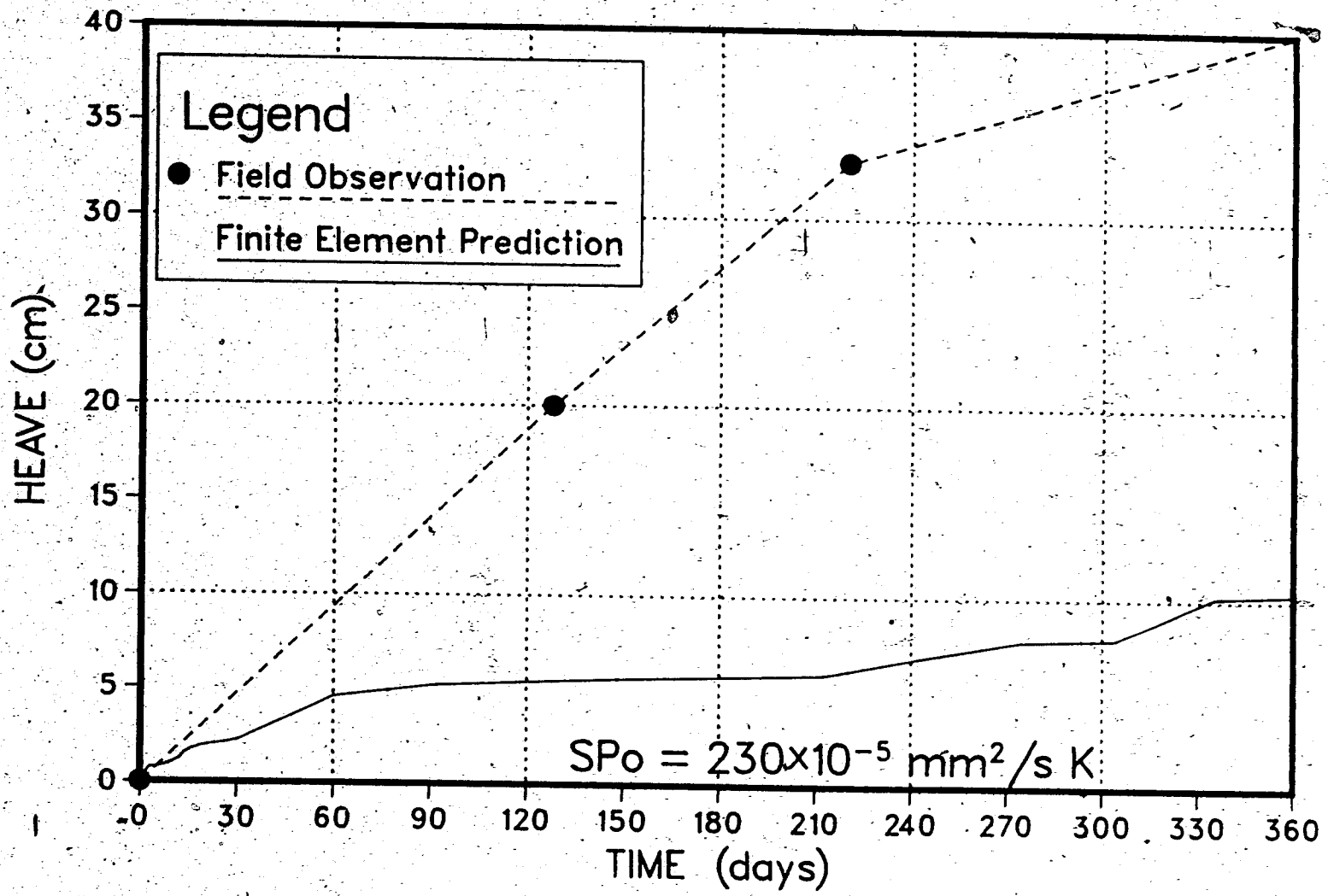

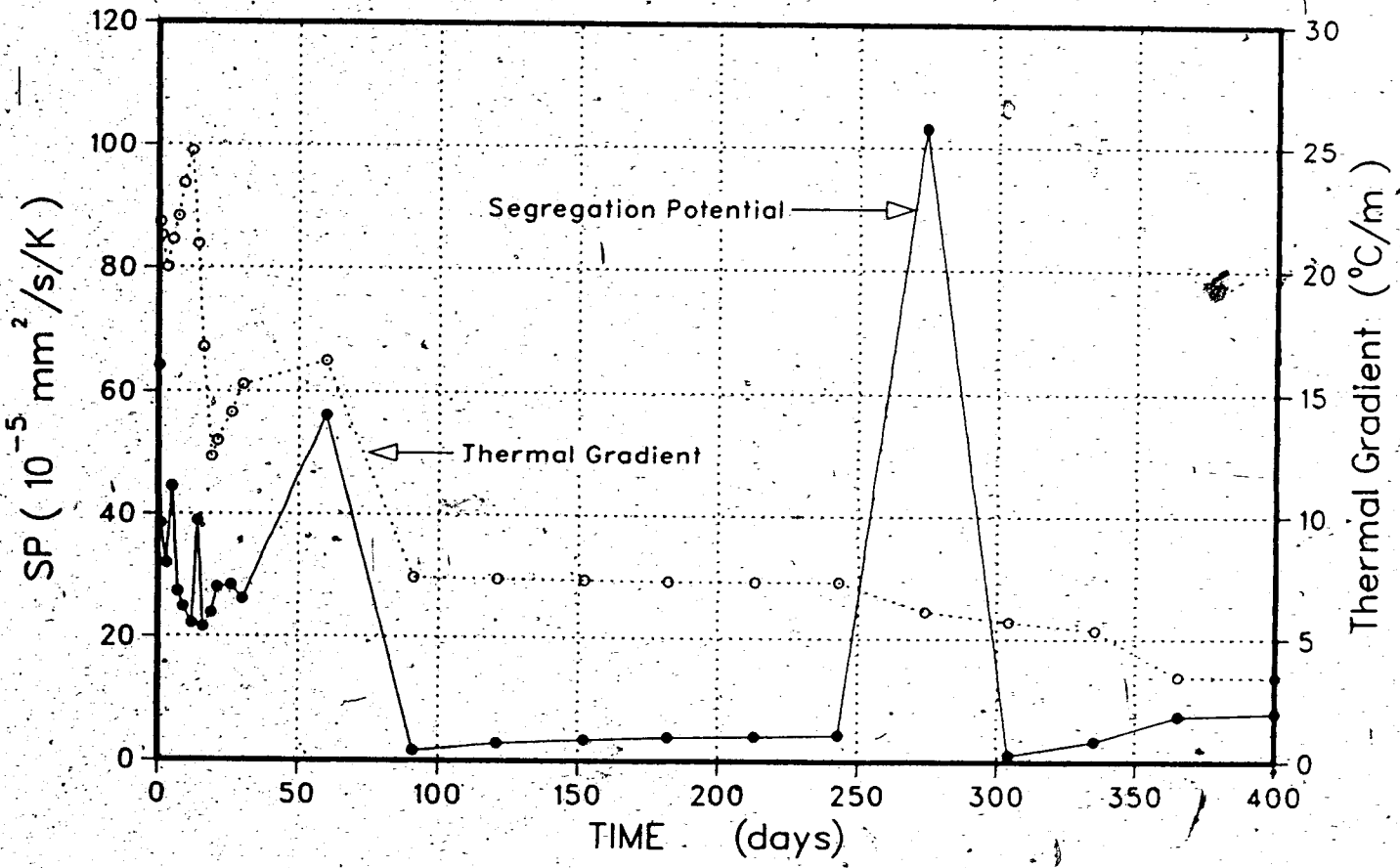

Variation of Segregation Potential and Thermal Gradient

Figure 5.67

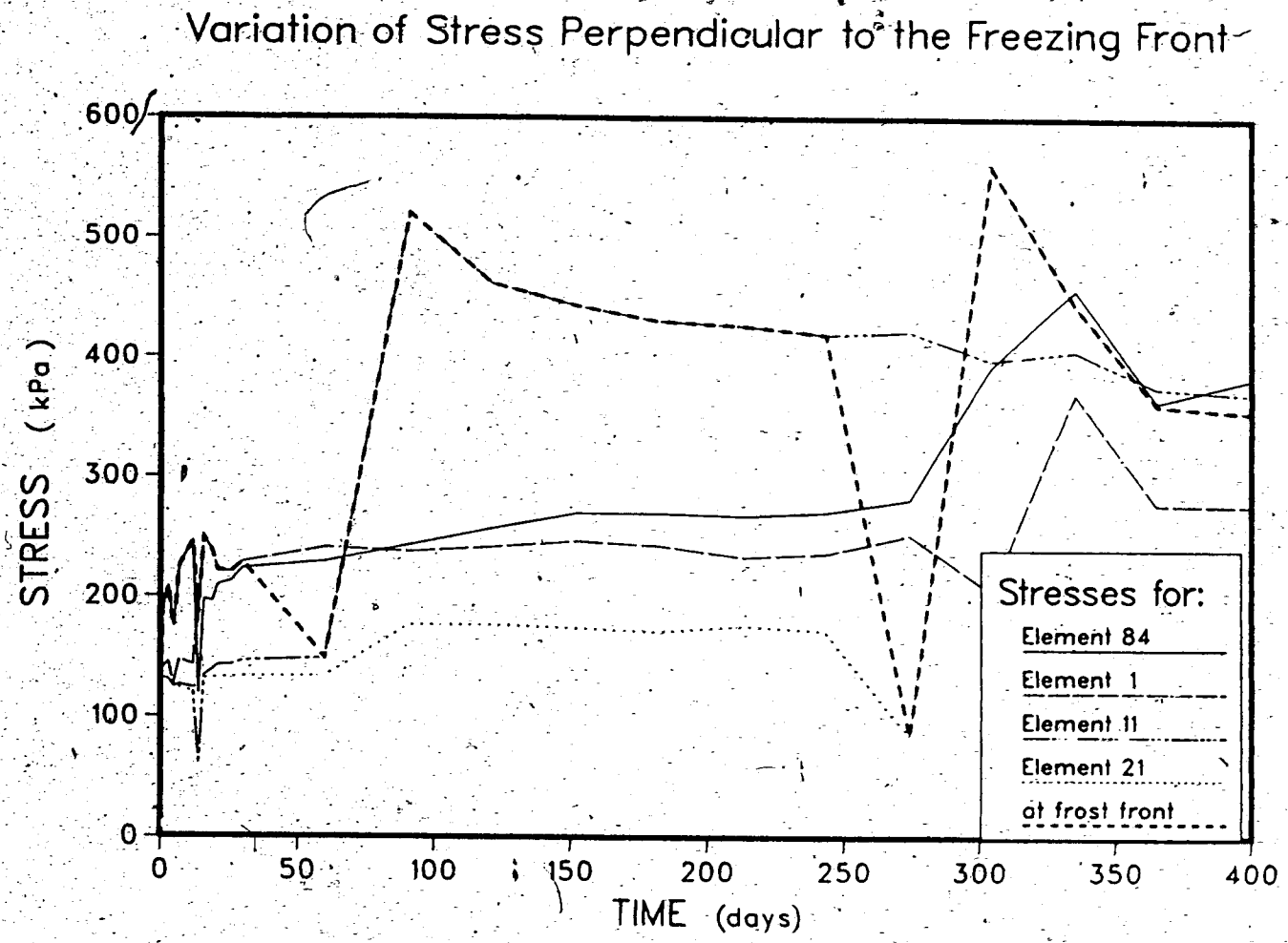

Figure 5.68 Variation of Stress Perpendicular to the Freezing Front

compaction of the soil backfill at the springline. This would inhibit the development of these high lateral stresses, resulting in reduction in the vertical stress at the frost front below the pipe.

Creep effects have not been implemented in this analysis, other than to use a constant E, and this would tend to reduce deviatoric stresses.

In summary, any modest reduction of the stress beneath the pipe would result in significant increases in heave rates. A re-analysis of this test implementing these stress modifiers should result in a closer simulation of the field behaviour.

6. Conclusions

6.1 The Need for Advanced Design Methods

This work recognizes the complexity of design in permafrost conditions, requiring consideration of geothermal, geotechnical and structural aspects of pipeline design. Often these aspects are interdependent thereby complicating design considerably.

To date, the use of simplifying assumptions has resulted in adequate design for most problems. However, when the complexities of the problem preclude simplification, or when the economics of large-scale projects warrant a refined analysis, other design methods are justified. Numerical methods and particularly finite element analyses are one means of simulating the complexities of materials, geometries and operating conditions of a more detailed design. Finite element methods have been, and will continue to be, a major growth area in engineering research due to the favourable economics and capabilities of computer analyses.

6.2 Thaw Settlement

Thaw settlement was initially examined from a geothermal viewpoint. It was found that the Neumann and Stefan equations are adequate for all one-dimensional and axi-symmetric phase change problems in thaw-stable

materials. For simple irregular geometries, some quasi-stable solutions are available (*viz.* Hwang, 1977). More complex geometries must be handled with some form of numerical approach.

The geothermal effects on consolidation have been addressed (Tsytovich, 1965; Morgenstern & Nixon, 1971) but the effect of the degree of consolidation on the geothermal problem has not been examined in detail, with the exception of Brown and Johnston (1970) and this work. The effect of the degree of consolidation on the thaw rate is to decrease the length of the heat flow path. For thaw stable materials this is inconsequential, but for thaw straining material this can alter thaw rates. Morover, the effect of true convection, i.e. the relative displacement of the frozen mass with respect to the heat source, has often not been correctly addressed. Carslaw and Jaeger (1959) is an exemplary exception.

The concept of thaw strain has been addressed assuming both a linear and a logarithmic extrapolation of pressure to find the thaw strain, A_o (Tsytovich 1965; Morgenstern & Nixon 1974). The results of these one-dimensional tests, performed on small samples, have been extrapolated on and been applied to two- and three-dimensional thaw settlement design problems. This approach is seen as being overly conservative and some corrections have been recommended in practice.

This work supports the approach that a rational reduction of thaw settlement can be justified due to two-dimensional thaw strain behaviour. Pipeline design studies have identified thaw settlement as the key parameter controlling pipeline wall thickness (Nyman, 1983; Nixon *et al.*, 1983). Thus, this reduction in the design settlement is seen as a contributing factor in reducing pipeline construction costs.

To support this argument, the thaw strain data obtained from A_o tests (Speer *et al.*, 1973) were fitted to a beta (β) distribution. This distribution was found to be superior to the Normal distribution and should be applied to other geotechnical parameters. The β-distribution was used to generate ten typical A_o values for the analysis.

These ten material types were randomly distributed within a 10m×10m mesh in the finite element program *SAP IV*. A volumetric strain : bulk modulus curve was used to describe the stress:strain properties of each material. Gravity and surficial loads were applied and deformations were observed. The initial soil model consisted of a stepped volumetric strain *versus* bulk modulus (ϵ_v:K) curve. This resulted in a bi-linear stress:strain curve for each material, with the K increased at their respective A_o values. The results were encouraging but it was felt that the model was simplistic and warranted improvement.

The next soil model, based on a normally consolidated soil, was too deformable. This resulted in excessive settlements. Intuitively, small A_o materials would have some inherent stiffness upon thawing and the existing model failed to embrace this.

The concept of a residual stress in thawed permafrost (Roggensack, 1977) was used to increase the post-thaw stiffness of the low A_o materials. Residual stresses were implemented using stepped bulk moduli on the ϵ_v:K curves so that the appropriate residual stress would be developed at a strain of A_o.

The initial success of this last model was that it adequately reproduced the conventional one-dimensional results when the ten A_o materials were layered, yet predicted a reduction in thaw settlement when the materials were randomly arranged. This demonstrated that design thaw settements in two dimensions could be reduced due to A_o variability.

A number of tests were performed, using the value of the original β-distribution but altering the distribution's standard deviation. While the one-dimensional analysis would predict no change, this study predicted a significant improvement in settlement behaviour with an increase in the A_o variance. The graphical representation of the stress field indicated that a high degree of soil arching was occurring, with more load being carried by the stiffer

elements.

The logical extension to this study would be to alter the mean value of the A_o values. It is expected that the variance would have less effect for materials with very low or very high A_o values. For the low A_o materials, a high variance would result in many very stiff materials and few weaker ones. The whole soil mesh would be so stiff that the relative stiffness of isolated elements of weak material would be unimportant. For the opposite case of a high A_o, high-variance distribution, the structurally isolated stiff elements would not add to the stiffness of the entire soil mesh. The optimum arching effect would be exhibited in a thaw unstable soil with a high A_o variance such that the stiffer elements would just be able to maintain contact and bridge around weak pockets.

Anisotropy could be examined by distorting the elements or, preferably, by further discretizing the mesh for a refined analysis of any directional bias. This concept of a graded disorder, rather than a perfectly random disorder of a material property, has been applied to other materials (Kröner, 1980) and is suited to permafrost showing layering.

6.3 Frost Heave.

The second half of this thesis developed a frost heave model for two-dimensions, utilizing the pressure dependency of heave. This model was an important application of

Konrad's segregation potential theory because it allowed for heave mitigation due to heave-induced pressures. Other predictive methods (Konrad and Morgenstern 1984; Nixon 1986) used a single constant reduction of *SP* due to pressure effects at the onset of their simulation. This simplification of heave's dependency on pressure, however, could not simulate the development of *in situ* heaving pressures.

This development of *in situ* heaving pressures has significant design implications. First, the pressure effects will result in reduced heave rates, and ultimately in reduced displacements for a given design life. As the associated pipe curvature will be less severe, pipe sections can be lighter. Secondly, the pressure-dependent heave will reduce the variation of ~~stress~~s along the pipeline which should reduce localized bending stresses. Previous analyses by other authors are incapable of modelling this effect. Thirdly, the reduction in segregational heave, due to pressure effects, will generally result in less total heave. This is because the reduced water velocity to the freezing front allows more freezing of *in situ* material. Thus, the geometry of steady state thermal conditions would be attained sooner, thereby reducing the time available for heaving.

The approach taken in this work was to develop a model capable of simulating some heaving tests (Konrad, 1980) with

the inclusion of pressure effects. Subsequent modifications were made to enable two-dimensional modelling. As an independent check, Konrad's finite difference method (FDM) program was revived and altered to include pressure effects.

For the frost heave analyses, the finite difference method was found to be inexpensive and fast; however, it was limited to one-dimensional and axisymmetric problems. While thermal analyses of frost heave could be conducted on more irregular geometries (Nixon, 1986), the effect of heave on *SP* could not be modelled. The finite element method with available software provided the flexibility needed to model the interaction of stress and temperature.

The results of the heaving tests simulations were quite acceptable. Most of the errors in heave magnitude were due to the overestimation of *SP* during the initial rapid frost penetration. The model was not modified to compensate for this since it would be a negligible effect in long-term heaving.

Significantly, the finite element model provided a better prediction of freezing after the peak heave rate was attained. This post-peak reduction in the predicted heave was due to the stabilizing warm and cold fluxes that prevented all of the predicted heave from occurring because of insufficient cooling power. In Konrad's finite difference program the assumption is made that the ultimate ice lens thickness can be determined from a conductive heat balance

equation that assumes the lens grows until its resistance stabilizes the freezing front. This appears to be overly conservative as it negates any further freezing of *in situ* soil on the warm side of the lens as seen in samples after testing.

The finite element method calculates the difference in heat fluxes in the frozen and unfrozen materials and applies this as a latent heat load. The frozen fringe is not expected to thaw back at the end of freezing as this would be impossible in this exothermic process of soil freezing. As a result, the frost front appears to marginally advance into the unfrozen soil, precipitating thermal equilibrium.

The excellent results of the C-10 simulation were followed by a number of program modifications that allowed the simulation of true two-dimensional heave. As the analysis was totally dependent upon the finite element results, it was first necessary to obtain reasonable stress and temperature behaviour from the mesh. The necessity of having confidence in these initial conditions cannot be over-estimated since the heave calculations would be extrapolating from these known conditions. Moreover, this initial examination of *ADINAT* and *SAP IV* revealed some program idiosyncracies that would have had significant effects on the results had they not been detected.

The simulation of the frost heave test facility in Calgary was disappointing only because the magnitude of the

heave was underestimated. In all other respects, the model behaved as expected by reducing the segregation potential for each individual element experiencing heave.

It is very significant that the model predicted lower segregation potentials due to heave-induced stresses. Thus, the model identifies and quantifies a self-mollifying property of heave: high heave rates will be moderated by the development of heave pressures.

The predicted development of high horizontal stresses, due to the restrained freezing of the soil, is a phenomenon that may not be fully mobilized in the field. This could be due to construction techniques that result in loose backfill and an accompanying lower soil modulus. Thus, high stresses may not be able to develop before extensive heaving has occurred.

Alternatively, this model may be demonstrating that this frost heave model is incomplete and requires further modification for creep effects or tension cracking. The existing model, however, will allow a sensitivity analysis of the input parameters to quantify their relative importance.

6.4 Concluding Remarks

While the intent of this thesis was to examine two permafrost phenomena using numerical techniques it became pointedly obvious that no intelligent analysis was possible without a supporting structure of interpretive and manipulative procedures.

The single most important component of this was the graphical representation of data and output. Although originally intended as a means of presenting results, the graphics became a means of interactively designing and modifying the model. Without the development of the *ADMESH*, *ADMESH81* and *SAPMESH* programs and the later aquisition of *ADINAPLOT* and **TELL-A-GRAPH*, this thesis would never have been completed. No finite element program is complete without a compatible plotting program.

Almost as important were the procedural routines used to manipulate files automatically. It would not have been possible to do this by hand with any reasonable accuracy or speed. This includes operations directly involved with the heave calculations as well as those of an ancillary nature used for mounting tapes, compiling programs, printing, searching and other common or repetitive operations.

The files containing these procedures have not been appended because they are incidental to the underlying frost heave physics. However those pertaining to file manipulation for the heave calculations have been retained on tape with

the geotechnical section of this department, Some flow charts have been appended to this thesis as a basic outline of the algorithms involved (App. H).

Bibliography

Abramowitz, M. and Stegun, I. A., editors. 1964. **Handbook of Mathematical Functions with Formulas, Graphs, and Mathematical Tables (Illus.)**. Dover.

Adkins, C.J. 1983. **Equilibrium Thermodynamics**. 3rd ed. Cambridge University Press.

Aguirre-Puente, J., Vignes, M., and Viaud, P. 1973. Study of the Structural Changes in Soils During Freezing. Permafrost: USSR Contribution to the Second International Conference on Permafrost, Yakutsk, National Academy Science, Washington, D.C. , pp. 315-323.

Ahmed, S. and McMickle, R.W. 1981a. Using Geotechnical Engineering In Pipeline Design, Construction Part 2. Pipeline & Gas Journal, March, 208, No. 3. pp. 63-66.

Ahmed, S. and McMickle, R.W. 1981b. Using Geotechnical Engineering In Pipeline Design, Construction Part 3, Pipeline & Gas Journal, May, 208 No. 6. pp. 66-78.

Akagawa, S., Yamamoto, Y. and Hashimoto, S. 1985. Frost heave characteristics and scale effect of stationary frost heave. Fourth Int'l. Symp. on Ground Freezing. Sapporo, Japan. August 5-7. pp. 137-143.

Alberta Gas Trunk Line (Canada) Ltd. 1976. Alaska Highway - Pipeline Project Application, Volume 2: Supporting Exhibits, Part 4 - Financial, Part 5 - Public Interest (before the National Energy Board), November, Calgary, Alberta

Ananyan, A. A. 1973. Nature of Water in Very Fine-grained Deposits and its Crystallization Characteristics. Permafrost: USSR Contribution to the Second International Conference on Permafrost, Yakutsk, National Academy Science, Washington, D.C. pp. 283-286. (translation, National Academy of Science, 1978)

Andersland, O.B. and Anderson, D.M., eds. 1978. **Geotechnical Engineering for Cold Regions**. McGraw-Hill Book Co. 566pp.

Anderson, D.M. and Morgenstern, N.R. 1973. Physics, Chemistry, and Mechanics of Frozen Ground: A Review. Permafrost: The North American Contribution to the Second International Conference on Permafrost, Yakutsk. National Academy Science, Washington, D.C.. pp. 257-288.

Arvidson, W.D. ans Morgenstern, N.R. 1977. Water flow induced by soil freezing. Canadian Geotechnical Journal 14 pp. 237-245.

Bathe, K.J., Wilson, E.L. and Peterson, F.E. 1973. **SAP IV A Structural Analysis Program for Static and Dynamic Response of Linear Systems**, U.C.L.A. Berkeley, June (revised 1974)

Bathe, K.J., Ramm, E., and Wilson, E.L. 1975. Finite Element Formulations for Large Deformation Dynamic Analysis. International Journal for Numerical Methods in Engineering 9. pp. 353-386.

Bathe, K.J. 1977. Static and Dynamic Geometric and Material Nonlinear Analysis Using ADINA. Report 82448-2. Acoustics and Vibration Lab., Mechanical Engineering Dept., M.I.T. (revised)

Bathe, K.J. 1981a. ADINA - A Finite Element Program for Automatic Dynamic Incremental Nonlinear Analysis. Report 82448-1. Acoustics and Vibration Lab., Mechanical Engineering Dept., M.I.T. Sept. 1975 (rev. 1978, 1981)

Bathe, K.J. 1981b. ADINAT - A Finite Element Program for Automatic Dynamic Incremental Nonlinear Analysis of Temperatures. Report 82448-1. Acoustics and Vibration Lab., Mechanical Engineering Dept., M.I.T. Sept. 1975 (rev. 1978, 1981)

Bathe, K.J. 1982. **Finite Element Procedures in Engineering Analysis**. Prentice-Hall, New Jersey. 735pp.

Biermans, M.B.G.M., Dijkema, K.M. and De Vries, D.A. 1978. Water Movement in Porous Media towards an Ice Front, Journal of Hydrology 37 pp. 137-148,Elsevier Scientific Publishing Co., Amersterdam.

Blanchard, D. and Frémond, M. 1985. Soils frost heaving and thaw settlement. Fourth Int'l. Symp. on Ground Freezing. Sapporo, Japan. August 5-7.. pp 209216.

Blank, L. 1980. **Statistical Procedures for Engineering, Management, and Science**. McGraw-Hill Book Company.

Bock, G.R. 1979. Arctic Winter Construction and Cost Estimating of the North Slope Fuel Gas Pipeline, Pipelines in Adverse Environments, a State of the Art; Vol.II, Proceedings of the ASCE Pipeline Division Specialty Conference, January 1979; pp. 511-520.

Bolz, R.E. and Tuve, G.L., eds. 1973. **CRC Handbook of tables for Applied Engineering Science**. 2nd ed. CRC Press, Inc. Boca Ratón, Florida. 1166 pg.

Bowles, J.E. 1977. **Foundation Analysis and Design**, 2nd ed., McGraw-Hill Book Company. 750 pp.

Brooker, Elmer W. and Ireland, H.O. 1965. Earth Pressures at Rest Related to Stress History: Canadian Geotechnical Journal 2 pp. 1-14.

Brown, W.G. and Johnston, G.H. 1970. Dikes on permafrost: predicting thaw and settlement. Canadian Geotechnical Journal 7 pp. 364-371.

Brown, R.J. 1979. Engineering Innovation for Arctic Conditions, Pipelines in Adverse Environments, a State of the Art; Vol.II,Proceedings of the ASCE Pipeline Division Specialty Conference, January 1979, pp. 418-429.

Canadian Arctic Gas Pipeline Limited. 1974. LOCATION, DESIGN AND CAPACITY OF FACILITIES SECTION 8 AND CONNECTING PIPELINE FACILITIES SECTION 9 an Exhibit in Support of Applications to the Department of Indian and Northern Development of the Government of Canada for authorization to Use Land and to the National Energy Board of Canada for a Certificate of Public Convenience and Necessity Authorizing the Construction of Pipeline Facilities

Cameron, J.J. 1977. Buried Utilites in Permafrost Regions; Utilities Delivery in Arctic Regions; Economic and Technical Review Report EPS 3-WP-77-1. Environmental Protection Service Environment Canada. January, 596 pp.

Carslaw, H.S., and Jaeger, J.C. 1959. **Conduction of Heat in Solids.** 2nd ed. Oxford University Press, London, 510 pp.

Carter,J.P., Booker,J.R. and Small,J.C. 1979. The Analysis of Finite Elasto-Plastic Consolidation. International Journal for Numerical and Analytical Methods in Geomechanics 3, pp. 107-129.

Chen, W.F. and Davidson, H.L. 1977. Large Deformation Response of Clay to Loads. Finite Elements in Non-Linear Mechanics, proc. Int'l. Conf. F. E. Non-Linear Solids and Structural Mechanics. pp. 487-511.

Cole, R. 1979. Homogeneous and Heterogeneous Nucleation. **Boiling Phenomena: Physicochemical and Engineering Fundamentals and Applicatiions**, 1, pp. 71-88. ed. S. van Stralen and R. Cole. Hemisphere Publishing Co., Washington D.C., 443 pp.+app.

Crory, F.E. 1973. Settlement Associated with the Thawing of Permafrost. Permafrost: The North American Contribution

to the Second International Conference on Permafrost, Yakutsk. National Academy Science, Washington, D.C., pp. 599-607

Daniels, F. and Alberty, R.A. 1975. Physical Chemistry. 4th ed. John Wiley & Sons, Inc., Toronto, 671 pp.

Davison, B.E., Nottingham, D., Rooney, J.W., and Vita, C.L. 1979. Chilled Pipeline Frost Heave Mitigation Concepts, Pipelines in Adverse Environments, a State of the Art. I, Proceedings of the ASCE Pipeline Division Specialty Conference, January 1979, January. pp. 294-306.

Derjaguin, B.V., and Churaev, N.V. 1986. Flow of Nonfreezing Water Interlayers and Frost Heaving. Cold Regions Science and Technology 12 pp. 57-66.

Duncan, J.M., Byrne, P., Wong, K.S. and Mabry, P. 1980. Strength, Stress-Strain and Bulk Modulus Parameters for Finite Element Analyses of Stresses and Movements in Soil Masses. Report No. UCB/GT/80-01 . College of Engineering, University of Berkeley, California. 70pp.+app.

Foothills Pipe Lines (Yukon) Ltd. 1976. Application before the National Energy Board and to the Department of Indian Affairs and Northern Development, Volume 1 - Facilities, Section A - Location, Section B - Design & Capacity

Fukuda, M. 1985. Heat flow measurements in freezing soils with various freezing front advancing rates. Fourth Int'l. Symp. on Ground Freezing. Sapporo, Japan. August 5-7. pp. 445-452.

Gilpin, R.R. 1982. A frost heave interface condition for use in numerical modelling. Fourth Canadian Permafrost Conference. pp. 459-465.

Glen, J.W. 1974. The Physics of Ice C.R.E.L.L. Monograph II-C2a. Hanover, New Hampshire. 86pp.

Gray, E. 1979. Super Pipe: the Artic Pipeline- World's Greatest Fiasco?. Griffin House, Toronto, 262 pp.

Gupta, J.P. 1971. Moisture Migration and Heat Transfer in Wet Sand During Freezing Ph.D. thesis, Dept. Chem. Eng'g., University of Pennsylvania. 135pp.

Hale, D. 1979. Frost Heave Tests Underway For Alaska Gas Pipeline. Pipeline & Gas Journal. September. pp. 24-26.

Ho, D.M., Harr, M.E. and Leonards, G.A. 1970. Transient temperature distribution in insulated pavements -

predictions vs. observations. Canadian Geotechnical Journal 7 pp. 275--284.

Hoekstra, P. 1969. Water Movement and Freezing Pressures. Soil Science Soc. of Amer. 33 pp. 512-518.

Huck, R.W. 1979. Arctic Pipeline Construction - An Overview, Pipelines in Adverse Environments, a State of the Art; I, Proceedings of the ASCE Pipeline Division Specialty Conference, January 1979, pp. 51-62.

Hwang, C.T., Morgenstern, N.R. and Murray, D.W. 1971. On Solutions of Plane Strain Consolidation Problems by Finite Element Methods. Canadian Geotechnical Journal 8 pp. 109-118

Hwang, C.T., Murray, D.W. and Brooker, E.W. 1972. A Thermal Analysis for Structures on Permafrost. Canadian Geotechnical Journal 9 pp. 33-46

Hwang, C.T. 1977. On quasi-static solutions for buries pipes in permafrost. Canadian Geotechnical Journal 14 pp. 180-192

Ishizachi, T. and Nishio, N. 1985. Experimental study of final ice lens growth in partially frozen saturated soil. Fourth Int'l. Symp. on Ground Freezing. Sapporo, Japan. August 5-7. pp. 71-78.

Johnston, G.H., ed. 1981. **Permafrost Engineering Design and Construction.** John Wiley & Sons. 540pp.

Jones, C.W. 1986. Closed-system freezing of soil in earth dams and canals. Canadian Geotechnical Journal23 pp. 1-8

Jumikis, A.R. 1977. **Thermal Geotechnics.** Rutgers University Press. New Brunswick, New Jersey. 372 pp.

Kiselev, V.F., Kvlividze, V.I., and Kursayev, A.B. 1973, Surface Phenomena at the Ice-Gas and Ice-Solid Interfaces. Permafrost: USSR Contribution to the Second International Conference on Permafrost, Yakutsk, National Academy Science, Washington, D.C. pp. 339-341. (transl. from the Russian, National Academy of Science, 1978)

Knutsson, S., Domaschuk, L., and Chandler, N. 1985. Analysis of large scale laboratory and in situ frost heave tests. Fourth Int'l. Symp. on Ground Freezing. Sapporo, Japan. August 5-7. pp. 65-70.

Konrad, J.-M. 1980. **Frost Heave Mechanics.** Ph.D. thesis, University of Alberta. Edmonton.

Konrad, J.-M. and Morgenstern, N.R. 1980. A mechanistic theory of ice lens formation in fine-grained soils. Canadian Geotechnical Journal 17 pp. 473-486.

Konrad, J.-M. and Morgenstern, N.R. 1981. The segregation potential of a freezing soil. Canadian Geotechnical Journal 18 pp. 482-491.

Konrad, J.-M. and Morgenstern, N.R. 1982a. Prediction of frost heave in the laboratory during transient freezing. Canadian Geotechnical Journal 19 pp. 250-259.

Konrad, J.-M. and Morgenstern, N.R. 1982b. Effects of applied pressure on freezing soils. Canadian Geotechnical Journal 19 pp. 494-505.

Konrad, J.-M. and Morgenstern, N.R. 1984. Frost heave prediction of chilled pipelines buried in unfrozen soils. Canadian Geotechnical Journal 21 pp. 100-115.

Kovacs, A.and Morey, R.M. 1979. Remote Detection of Massive Ice in Permafrost along the Alyeska Pipeline and the Pump Station Feeder Gas Pipeline, Pipelines in Adverse Environments, a State of the Art; Vol.I, Proceedings of the ASCE Pipeline Division Specialty Conference, January 1979. pp. 268-279.

Kröner, E. 1980. Graded and Perfect Disorder in Random Media Elasticity. Journal of the Engineering Mechanics Division of ASCE 5. pp. 889-914.

Lambe, T.W. and Whitman, R.V. 1969. **Soil Mechanics.** John Wiley & Sons, Toronto. 553 pp.

LaValle, I.H. 1970. **An Introduction to Probablility, Decision, and Inference.** Holt, Reinhart and Winston, Inc. 767 pp.

L.E.C. Engineering Ltd. 1984. Analysis of Data from the Calgary Frost Heave Test Facility. Earth Sciences Branch, Dept. of Energy, Mines & Resources. Ottawa.

Loch, J.P.G. 1978. Thermodynamic Equilibrium between Ice and Water in Porous Media. Soil Science 126, pp. 77-80.

Lunardini, V.J. 1980. **Phase Change Around a Circular Pipe.** CRREL Report 80-27. U.S. Army Cold Regions Research and Engineering Laboratory. Hanover, N.H. 26pp.

Luscher, U. and Affifi, S.S. 1973. Thaw Consolidation of Alaskan Silts and Granular Soils, Permafrost: The North American Contribution to the Second International Conference on Permafrost, Yakutsk. National Academy Science, Washington, D.C., pp. 325-334.

Luscher, U. 1977. Geotechnical Aspects of the Trans-Alaska Pipeline System. Proc., Ninth Int'l. Conf. on Soil Mechanics and Foundation Engineering. Case History Volume, pp. 83-106.

Luscher, U., Thomas, H.P. and Maple, J.J. 1979. Pipe-Soil Interaction, Trans-Alaska Pipeline. Volume II - Pipelines In Adverse Environments - A State of the Art. Proc. of the ASCE Pipeline Division Specialty Conference, New Orleans, January 15-17., pp. 486-502

Mageau, D.W. 1978. **Moisture Migration in Frozen Soil.** MSc. thesis. University of Alberta, Edmonton. 160pp.

Mann,Jr., L. 1970. **Applied Engineering Statistics for Practicing Engineers.** Barnes & Noble, Inc., New York, 175 pp.

Marks, A. 1980. **Handbook of Oceanic Pipeline Computations.** PennWell Publishing Co., Tulsa, 524 pp.

McRoberts, E.C. 1975. Field Observations of Thawing in Soils. Canadian Geotechnical Journal 12 pp. 126-130.

McRoberts, E.C. and Morgenstern, N.R. 1975. Pore Water Expulsion during Freezing. Canadian Geotechnical Journal 12 pp. 130-141.

Mikhailov, G.D. and G.P. Bredyuk. 1966. Shear Strength of Clayey Ground During Thawing (According to Laboratory and Field Study) , Materials of the 8th All-Union Interdepartmental Conference on Geocryology (Cryopedology), U.S.S.R. Academy of Sciences, Sibrian Department, Cryopedology Institute, No. 5, pp. 51-60, transl. U.S. Joint Publications Research Service for U.S. Army C.R.R.E.L., reproduced by National Technical Information Service, Springfield Va.

Miller, R.D. 1972. Freezing and Heaving of Saturated and Unsaturated Soils. Highway Research Record 393. pp. 1-11

Mohan, A. and Lovell, C.W. 1979. Heat Flow Around Pipes Buried in Cold Ground, Pipelines in Adverse Environments, a State of the Art; Vol.I, Proceedings of the ASCE Pipeline Division Specialty Conference, January 1979; pp. 79-102.

Morgenstern, N.R. and Nixon, J.F. 1971. One-dimensional Consolidation of Thawing Soils. Canadian Geotechnical Journal 8 pp. 558-565.

Morgenstern, N.R. and Smith, Laurence B. 1973. Thaw-Consolidation Tests on Remoulded Clays. Canadian

Geotechnical Journal 10 pp. 25-40.

Morgenstern, N.R. and Nixon, J.F. 1975. An Analysis of the Performance of a Warm-oil Pipeline in Permafrost, Inuvik, N.W.T. Canadian Geotechnical Journal 12, pp. 199-208.

Morgenstern, N.R. 1977. Ground Behavior Due to Freezing and Thawing; Utilities Delivery in Arctic Regions; Economic and Technical Review Report EPS 3-WP-77-1. Environmental Protection Service, Environment Canada; January 1977, 596 pp.

Nguyen, V.V., Pinder, G.F. and Botha, J.F. 1981. Phenomenological Interpretation of the Thereodynamics of Steam-Water Systems Using Catastrophe Theory. J. of Non-Linear Thermodynamics. 6 pp. 285-294. Verlag Walter de Gruyer & Co., N.Y.

Nixon, J.F. 1973. **The Consolidation of Thawing Soils.** Ph.D. thesis, University of Alberta. Edmonton.

Nixon, J.F. 1973. Thaw-Consolidation of Some Layered Systems. Canadian Geotechnical Journal 10 pp. 617-631.

Nixon, J.F. and McRoberts, E.C. 1973. A Study of Some Factors Affecting the Thawing of Frozen Soils. Canadian Geotechnical Journal 10 pp. 439-452

Nixon, J.F. and Morgenstern, N.R. 1973. The Residual Stress in Thawing Soils. Canadian Geotechnical Journal 10, pp. 571-580

Nixon, J.F. and Morgenstern, N.R. 1974. Thaw-Consolidation Tests on Undisturbed Fine-grained Permafrost. Canadian Geotechnical Journal, 11 pp. 202-214

Nixon, J.F. 1975. The Role of Convective Heat Transfer in the Thawing of Frozen Soils. Canadian Geotechnical Journal 12 pp. 425-429.

Nixon, J.F. and Ladanyi, B. 1978. Thaw Consolidation. **Geotechnical Engineering for Cold Regions.** Chapter 4. Andersland, O.B. and Anderson, D.M., eds. McGraw-Hill Book Company. 566pp.

Nixon, J.F. 1982. Field frost heave predictions using the segregation potential concept. Canadian Geotechnical Journal 19 pp. 526-529.

Nixon, J.F., Morgenstern, N.R. and Reesor, S.N. 1983a. Frost heave - pipeline interaction using continuum mechanics. Canadian Geotechnical Journal 20 pp.251-261.

Nixon, J.F., Stuchly, J. and Pick, A.R. 1983b. Design of Norman Wells Pipeline for Frost Heave and Thaw Settlement. Second Int'l. Offshore Mechanics and Arctic Engineering Symp., Amer. Soc. Mech. Eng'g., Houston. pp. 69-76.

Nixon, J.F. 1986. Pipeline Frost Heave Predictions Using a 2-D Thermal Model. Draught paper, ASCE Conference on Research on Transportation in Cold Regions. Boston, October.

Nyman, Kenneth J. 1983. Thaw Settlement Analysis For Buried Pipelines in Permafrost. Proceedings of the Conference on Pipelines In Adverse Environments II. Pipeline Division of the American Society for Civil Engineers, San Diego, November., pp. 300-325

Oriard, L.L. and Tart, R.G.,Jr. 1979. Controlled Trench Blasting in Frozen Ground, Pipelines in Adverse Environments, a State of the Art; Vol. I, Proceedings of the ASCE Pipeline Division Specialty Conference, January 1979; pp. 63-78.

Palmer, A.C. 1967. Ice Lensing, Thermal Diffusion and Water Migration in Freezing Soils. Journal of Glaciology 6, #47, pp. 681-694.

Palmer, A.C. 1972. Settlement of Pipeline on Thawing Permafrost. Transportation Engineering Journal of ASCE. 98 Paper 9090, pp. 477-511.

Palmer, A.C. ed. 1981. Offshore Oil and Gas Pipeline Technology, Oyez Intelligence Reports: a series of structured reports on aspects of business, law, management and technology, Oyez Publishing Limited, London, 137 pp.

Pendarvis, R.C. 1979. Cold Region Pipeline Construction, Volume II - Pipelines In Adverse Environments - A State of the Art. Proc. of the ASCE Pipeline Division Specialty Conference, New Orleans, January 15-17.; pp. 481-485.

Penner, E. and Walton, T. 1978. Effects of temperature and pressure on frost heaving. Ground Freezing, proc. of the First Int'l. Symp. on Ground Freezing. Bochum, W. Germany, March 8-10. Engineering Geology 13 (1979). pp. 29-39.

Penner, E. and Ueda, T. 1978. A Soil Frost-susceptibility Test and basis for Interpretting Heaving Rates. Third International Conference on Permafrost, Edmonton, Alberta, July 10-13. pp 722-727.

Phukan, A. 1979. Geotechnical Engineering Applications to the Chilled Gas Pipeline Design in Cold Regions, Pipelines in Adverse Environments, a State of the Art; Vol.I, Proceedings of the ASCE Pipeline Division Specialty Conference, January 1979; pp. 157-168, publ. ASCE N.Y.

Radd, F.S. and Oertle, D.H. 1973. Experimental Pressure Studies of Frost Heave Mechanisms and the Growth-Fusion Behavior of Ice. Permafrost: The North American Contribution to the Second International Conference on Permafrost, Yakutsk. National Academy Science, Washington, D.C.. pp. 377-384.

Reynolds, Wm.C. and Perkins, H.C. 1977. **Engineering Thermodynamics**. 2nd ed. McGraw Hill Book Co., N.Y.; 690 pp.

Revie, R.W. and Staff of the Physical Metallurgy Research Laboratories, Canada Centre for Mineral and Energy Technology, Dept. E.M.R. 1980. Line Pipe Research in the Canadian Federal Government, Pipeline and Energy Plant Piping: Design and Technology, Proceedings of an International Pipeline and Energy Plant Piping Fabrication in the 80's, Welding Institute of Canada, November, Calgary pp. 21-30, Pergamon of Canada Ltd., Toronto 374 pp.

Roggensack, W.D. 1977. **Geotechnical Properties of Fine-Grained Permafrost Soils**. Ph.D. thesis, University of Alberta. Edmonton.

Rolphe, W.D. III and Bathe, K.J. 1982. An Effecient Algorithm for Analysis of Nonlinear Heat Transfer with Phase Changes. International Journal for Numerical Methods in Engineering 18, pp. 119-134.

Row,D., Powell, G.H., Goodson, M. 1983. Finite Element Techniques for Pipelines Subjected to Extreme Loads. Proceedings of the Conference on Pipelines In Adverse Environments II. Pipeline Division of the American Society for Civil Engineers, San Diego, November., pp. 474-485.

Rowley, R.K., Watson, G.H., Wilson, T.M. and Auld, R.G. 1973. Performance of a 48-in. Warm-oil Pipeline Supported on Permafrost. Canadian Geotechnical Journal 10 pp. 282-303.

Shephard, M.S. and Gallagher, R.H., eds. 1979. Finite Element Grid Optimization. Presented at the Third Nat'l. Cong. on Pressure Vessels and Piping. ASME. June 24-29, San Francisco.n Francisco.">

Simon, Leslie E. 1945. **An Engineer's Manual of Statistical Methods**. John Wiley & Sons, Inc., New York.

Slusarchuk, W.A., Watson, G.H. and Speer, T.L. 1973. Instrumentation Around a Warm Oil Pipeline Buried in Permafrost. Canadian Geotechnical Journal 10, pp. 227-245.

Smith, L.B. 1972. **Thaw-Consolidation Tests on Remoulded Clays**. M.Sc. thesis. University of Alberta. Edmonton. 157 pp.

Smith, M.W., Dallimore, S.R. and Kettle, R.J. 1985. Observations and prediction of frost heave of an experimental pipeline. Fourth Int'l. Symp. on Ground Freezing. Sapporo, Japan. August 5-7. pp 297-304.

Speer, T.L., Watson, G.H., and Rowley,R.K. 1973. Effects of Ground-Ice Variability and Resulting Thaw Settlements on Buried Warm-Oil Pipelines. Permafrost: The North American Contribution to the Second International Conference on Permafrost, Yakutsk. National Academy Science, Washington, D.C., pp. 746-752

Sykes, J.F., Lennox, W.C., and Unny, T.E. 1974a. Two-Dimensional Heated Pipeline in Permafrost, Journal of the Geotechnical Engineering Division, American Society for Civil Engineers 100, No. GT11, Proc. Paper 10956, November, pp. 1203-1214.

Sykes, J.F., Lennox, W.C., and Charlwood, R.G. 1974b. Finite Element Permafrost Thaw Settlement Model. Journal of the Geotechnical Engineering Division, American Society for Civil Engineers 100, No. GT11, Proc. Paper 10957, November, pp. 1185-1201.

Terzaghi, Karl. 1943. **Theoretical Soil Mechanics**. John Wiley & Sons, Inc., New York, 510 pp.

Thornton, D.E. 1976, Steady-state and quasi-static thermal results for bare and insulated pipes in permafrost, Canadian Geotechnical Journal 13, pp. 161-171.

Trahair, N.S. 1977. **The Behaviour and Design of Steel Structures**. John Wiley & Sons, Inc., New York, 320 pp.

Tsytovich, N.A., Zaretsky, Yu K., Grigoryea, V.G., and Ter-Martirosyan, Z.G. 1965. Consolidation of Thawing Soils, 6th Int'l. Conf. Soil Mech. & Foundation Eng'g. 1, pp. 390-394.

van Stralen, S. 1979. Survey of Boiling Phenomena. **Boiling Phenomena: Physicochemical and Engineering Fundamentals and Applicatiions**, 1, pp. 1-14. ed. S. van Stralen and

R. Cole. Hemisphere Publishing Co., Washington D.C., 443 pp.+app.

Walker, J. 1986. The Amateur Scientist. Scientific American. Vol. 225, No. 1, July. pp.114-119.

Watson, G.H., Rowley,R.K. and Slusarchuk, W.A. 1973a. Performance of a Warm-Oil Pipeline Buried in Permafrost. Permafrost: The North American Contribution to the Second International Conference on Permafrost, Yakutsk. National Academy Science, Washington, D.C., pp. 759-766.

Watson, G.H., Slusarchuk, W.A. and Rowley,R.K. 1973b. Determination of Some Frozen and Thawed Properties of Permafrost Soils. Canadian Geotechnical Journal, 10, pp. 592-606.

Weast, R.C., ed. 1972. **Handbook of Chemistry and Physics.** 53rd ed. The Chemical Rubber Company. Boca Raton, Florida. 2335 pp.

Wheeler, J.A. 1973. Simulation of heat transfer from a warm pipeline buried in permafrost, presented at the 74th National Meeting of the American Institute of Chemical Engineers, New Orleans, La., March.

Williams, P.J. 1968. The Nature of Freezing Soil and its Field Behaviour. Properties and Behaviour of Freezing Soils. Norwegian Geotechnical Institute Publ. No. 72. Oslo.

Williams, P.J. and Burt, P.T. 1974. Measurement of Hydraulic Conductivity of Frozen Soils. Canadian Geotechnical Journal 11 pp. 647-650.

Williams, P.J. 1979. **Pipelines and Permafrost: physical geography and development in the circumpolar North Topics in Applied Geography.** Longman Inc., New York

Winkler, R.L. 1972. **An Introdustion to Bayesian Inference and Decision.** Holt, Rinehart and Winston, Inc. 563 pp.

Winkler, R.L. and Hays, Wm. L. 1975. **Statistics: Probability, Inference, and Decision.** 2nd ed. Holt, Rinehart and Winston, Inc.

Zienkiewicz, O.C. 1977. **The Finite Element Method.** 3rd ed. McGraw-Hill Book Company (UK) Ltd. 787pp.

**********>

Appendice A: Closed-Form Solutions and Consolidation Effects

The most complex problems of thermal imbalance analyses are based upon simple principles and are best examined using simple models; an examination of the Stefan assumptions in one dimension best illustrates the effect of thaw-settlement on the thawing of permafrost.

The Stefan equation assumes that heat is conducted through the thawed soil to be absorbed at the moving thaw front. No heat capacity effects are considered and conduction through the frozen soil is negligible. The frozen soil is initially at the phase change temperature. Assuming a unit cross-sectional area, and applying a surficial step temperature, T_s, at time t=0, we obtain the heat flux through the unfrozen soil:

$$\dot{Q}_k = \frac{k_u \, T_s}{l_u} \qquad [A.1]$$

where $\dot{Q}_k$= conductive heat flux

k_u= thermal conductivity in the unfrozen soil

T_s= applied step temperature

l_u= length of heat flow path (height of thawed material)

The absorption rate of heat for phase change is a product of the volumetric latent heat of the soil and the rate at which the thaw front advances:

$$\dot{Q}_L = L_f \frac{dl_f}{dt} \qquad [A.2]$$

where $\dot{Q}_L$ = Latent Heat absorption rate

L_f = Volumetric latent heat of the frozen soil

$-\frac{\partial l_f}{\partial t}$ = thaw front velocity into the frozen soil

The equation of heat balance is

$$\dot{Q}_k = \dot{Q}_L$$

$$\frac{k_u T_s}{l_u} = L_f \frac{dl_f}{dt} \qquad [A.3]$$

$$k_u T_s dt = L_f l_u \, dl_f \qquad [A.4]$$

For a thaw stable soil,

$$dl_f = dl_u = dl, \qquad L_f = L_u = L$$

$$\therefore k_u T_s \, dt = L \times l \, dl$$

$$\int_0^t k_u T_s \, dt = \int_0^x L \, l \, dl$$

$$X = \sqrt{\frac{2k_u T_s}{L}} \sqrt{t} \qquad [A.5]$$

and the Stefan equation is recovered. However, for thaw unstable soils:

$$dl_u = (1 - A_o) dl_f \qquad [num]$$

where A_o is the thaw strain parameter

$$\therefore k_u T_s dt = L_f l_u dl_f$$

$$= L_f l_u \frac{dl_u}{1-A_o}$$

$$X_u = \sqrt{\frac{2k_u T_s (1-A_o)}{L_f}} \sqrt{t} \qquad [A.6]$$

(= depth from thawed surface)

This can also be done by using $L_u = \frac{L_f}{1-A_o}$ which represents the latent heat required to form a unit volume of thawed material. This simplifies the calculations by putting all dimensions in terms of the thawed-consolidated dimensions:

$$X_u = \sqrt{\frac{2k_u T_u}{L_u}}\sqrt{t} \qquad [A.7]$$

This latter method is consistent with Carslaw & Jaeger (1959) in which they specify the volumetric latent heat in terms of the material being formed.

In examining Equation [A.6] it is apparent that a high thaw strain parameter will result in a slower rate of thaw front penetration. This is intuitively obvious when remembering that this equation is with respect to the thawed surface which is settling towards the thaw front. In terms of the original frozen dimensions, the rate of thaw becomes:

$$X_f = \frac{X_u}{1-A_o} \qquad [A.8]$$

$$= \sqrt{\frac{2k_u T_s}{(1-A_o)L_f}}\sqrt{t} \qquad [A.9]$$

which represents an accelerated rate of thaw relative to the case with no volume change. This is due to the thaw strain causing the heat source to move towards the thaw front, thereby decreasing the length of the heat flow path, which increases the heat flux to the thaw front.

Modifications to Equation [A.7] can also be made to account for the effects of consolidation. This is done by adjusting the values of k_u and L_u because of the decrease in moisture content and the resulting dimensional shortening. The degree of consolidation is controlled by the thaw consolidation ratio (Morgenstern and Nixon, 1971) which is proportional to the thaw parameter, α. The rate of thaw, α, is also dependent upon the ongoing consolidation so a value of α consistent with the degree of consolidation can be obtained iteratively.

Adopting the Neumann equation for volume change is more involved since the equation uses more parameters that are dependent upon the state of the soil. It differs from the Stefan equation in that heat flow within the frozen soil is included, as are all heat capacity effects. Carslaw and Jaeger (1959) provide a derivation of the Neumann equation for the progression of a freezing front into water. Nixon (1975) provides a similar equation for the thawing of permafrost with thaw strain, neglecting any effects from the frozen soil. In applying his equation to examine the effects of thaw strain, however, it appears that Nixon has not used the strain-corrected value of volumetric latent heat.

Nixon (1973) in his doctoral thesis on the consolidation of thawing soils provides two sample solutions to the Neumann equation. The hypothetical soil considered is typical of thaw unstable soil, with a moisture content of

w=40% and a thaw strain of A_o=25%. Back-calculating the value of L shows that the volumetric latent heat of the frozen material was used instead of the latent heat needed to form a unit volume of the thaw-consolidated material. This reduces the L term by 33%.

By not considering the significance of this effect, the writer erroneously concludes that the effects of large strains in the thawing zone may be completely ignored if depth is measured from the applied surface temperature. To corroborate this statement, Nixon cites the earlier work of Brown and Johnston (1970) in which excellent correlation is found to exist between the calculated thaw penetration and field observations for a material with 30% thaw strain. Brown and Johnston, however, are reporting thaw with respect to the original surface. What Nixon failed to discern was that the writers, in performing their calculations with respect to the original foundation surface, recognised the effect of the moving heat source on the thermal balance. They introduce a significant correction to the rate of heat conduction through the unfrozen material which is equivalent to the latent heat correction in a Stefan analysis. This correction is missing from the Nixon analyses (1973, 1975).

The complete treatment of the advance of a thaw front into thaw-settling soil would include the equivalent volumetric latent heat effects of the unfrozen material, the convection effect of the frozen soil moving relative to the

thaw surface due to thaw straining, the convection effect of the dissipation of excess pore water pressures in the unfrozen zone, and the thermal conductivities and heat capacities in both the frozen and the unfrozen soils. Generally, the thermal gradients and mass velocities are small enough to disregard any convection effects (Carslaw and Jaeger, 1957; Nixon, 1975). In the unfrozen soil, the excess pore water pressures vary non-linearly from a maximum at the thaw boundary to zero at the surface, resulting in a non-linear moisture content profile.

The unfrozen thermal conductivity and heat capacity also vary with moisture content so that the effective conductivity and thermal capacity would be averages determined using integrals of their respective functions of moisture content. These variations in thermal properties generally centre on the thermal property corresponding to that of the average moisture content. Over the range of moisture contents existing in the thawed soil, then, the difference is generally small enough to be disregarded. Using an average moisture content to obtain thermal properties for the unfrozen soil is sufficient for most engineering purposes.

Appendice B: Alternative Calculations of α

B.1 Example 1: Recalculate α parameter, Test NWU-2, (Nixon & Morgenstern, 1974)

after the method of Nixon & McRoberts (1973)

Given: $w = 0.36$ = water content

$T_g = -5.0°C$ = initial ground temperature

$T_s = 21.1°C$ = applied step temperature

$W_u = 0.10\ M_s = 0.278w$ = unfrozen w

$\therefore W_u = 0.278$ $\qquad M_s$ = mass of solids

$$\gamma_d = \left[w + \frac{1}{G_s} \right]^{-1} \qquad [B.1]$$

$$= \left[0.36 + \frac{1}{2.65} \right]^{-1}$$

from Kersten, $k_u = .0030$ cal/°C cm s

$k_f = .0053$ cal/°C cm s

$$c_u = \gamma_d\ (0.18 + w)\ \text{cal/°C cm}^3 \qquad [B.2]$$

$$= 1.356(0.18+0.5(.36)) = 0.732\ \text{cal/°C cm}^3$$

$$c_f = \gamma_d\ (0.18+0.5(1+W_u)w) \qquad [B.3]$$

$$= 1.356(0.18+0.5(1+0.278)\times 0.36)$$

$$= 0.556\ \text{cal/°C cm}^3$$

after Nixon & McRoberts (1973),

$$L = \gamma_d\ w(1-W_u)\ L_w \qquad [B.4]$$

$$= 1.356 \times 0.36(1-.278)\ 79.6$$

$$= 28.06\ \text{cal/cm}^3$$

$$Ste = \frac{c_u\ T_s}{L} = \frac{.732 \times 21.1}{28.06} = 0.550 \qquad [B.5]$$

$$\kappa_u = \frac{k_u}{c_u} = \frac{.0030}{.732} = .0041 \qquad [B.6]$$

$$\kappa_f = \frac{k_f}{c_f} = \frac{.0053}{0.556} = .0095 \qquad [B.7]$$

$$\frac{-T_g}{T_s}\frac{k_f}{k_u}\sqrt{\frac{\kappa_u}{\kappa_f}} = \frac{5}{21.1}\ \frac{.0053}{.0030}\ \sqrt{\frac{.0041}{.0095}} = 0.275 \qquad [B.8]$$

using Nixon & McRoberts (1973) graphical solution,

$$\frac{\alpha}{2\sqrt{\kappa_u}} = 0.425$$

$$\therefore\ \alpha = 0.425 \times 2\sqrt{.0041} = 0.0544\ cm/\sqrt{s}$$

$$= 93.5\%\ \alpha_{obs}$$

The reported α value (Nixon & Morgenstern, 1974) of $\alpha_{obs} = 0.0582\ cm/\sqrt{s}$ was based on a thaw-consolidated height of 3.60cm after a root-time of 62 $\sqrt{s}$, as determined from Nixon (1973).

B.2 Example 2: Recalculate α parameter, Test NWU-2 modifying L for volume change

Given $w=0.36$, $W_u = 0.278$

$$\therefore\ \gamma_{d,th} = 1.356\ g/cm^3$$

$$\gamma_{d,f} = \left[w(1-W_u) + \frac{w\,W_u}{G_{ice}} + \frac{1}{G_s}\right]^{-1} \qquad [B.9]$$

$$= \left[0.36(0.722) + \frac{0.36 \times 0.278}{0.917} + \frac{1}{2.65}\right]^{-1}$$

$$= 1.339\ g/cm^3$$

From Example 1,

$k_u = 0.0030$ cal/°C cm s

$c_u = 0.732$ cal/°C cm³

$\kappa_u = 0.0041$ cm²/s

From Kersten,

$k_f = 0.0050$ cal/°C cm s

$c_f = \gamma_{d,f}\,(0.18+0.5(1+W_u)w)$ cal/°C cm³ [B.3]

$= 1.339\,(0.18+0.5(1.278)0.36)$ cal/°C cm³

$= 0.549$

$\kappa_f = 0.0091$ cm²/s

original height H_o= 3.96cm , (Nixon, 1973)

thawed height H= 3.60cm = 91% H_o

$$L = \gamma_{d,th}\, w(1-W_u)\, L_v \qquad [B.4]$$

$$= 1.356\ 0.36(1-0.278)\ 79.6\ cal/cm^3$$

$$= 28.1\ cal/cm^3$$

correcting for thaw strain, $L^*H = LH_o$

$$L^* = L\,\frac{H_o}{H}\ [B.10] = 28.1 \times \frac{1}{0.91} = 30.9\ cal/cm^3$$

$$Ste = \frac{c_u\, T_s}{L^*} \qquad [B.5]$$

$$= \frac{0.549 \times 21}{30.9} = 0.498$$

$$\frac{-T_g\, k_f}{T_s\, k_u}\sqrt{\frac{\kappa_u}{\kappa_f}} = \frac{5}{21.1}\times\frac{.0050}{.0030}\sqrt{\frac{.0041}{.0091}} = 0.265 \qquad [B.8]$$

using Nixon & McRoberts' graphical solution,

$$\frac{\alpha}{2\sqrt{\kappa_u}} = 0.43 \qquad [B.9]$$

$$\therefore\ \alpha = 0.43 \times 2\sqrt{.0041} = 0.0551\ cm/\sqrt{s}$$

$$= 94.7\%\ \alpha_{obs}$$

The unfrozen thermal properties were not adjusted for a change in moisture due to the 1.8mm consolidation from the thawed-undrained conditon. This would reduce the moisture content form w=36% to w=32.5% which would have a negligible effect on the results.

B.3 Example 3: Recalculate α parameter, Test NWU-9, (Nixon & Morgenstern, 1974) after the method of Nixon & McRoberts (1973)

Given $w = 0.50$ $\quad$ w = water content

$\frac{S_t}{S_{max}} = 0.910$

$A_o = 34.5\%$ $\quad$ A_o = thaw strain

$W_u = 0.10 M_s = 0.20w$ = unfrozen water content,

M_s = mass of solids

$$\gamma_{d,f} = \left[wW_u + \frac{w(1-W_u)}{G_{ice}} + \frac{1}{G_s} \right]^{-1} \qquad [B.10]$$

$$= \left[0.50(.20) \frac{0.50(1-0.20)}{0.917} + \frac{1}{2.65} \right]^{-1}$$

$$= 1.0946 \text{ g/cm}^3$$

$V_s = 0.413$ = volume fraction of solids

$V_w = 0.109$ = volume fraction of water

$V_i = 0.478$ = volume fraction of ice

$\Delta V_{i-w} = 0.478 \times (1-0.917) = 0.040$

$\therefore V_w = 0.109 + 0.478 - 0.040 = 0.547$

$A_o = 0.345$

$- \Delta V_{i-w} = \underline{0.040}$

$\Delta V_c = 0.305$

$\frac{S_t}{S_{max}} \Delta V_c = 0.910 \times 0.305 = 0.278$

∴ after thaw consolidation,

$V_w = 0.547 - 0.278 = 0.269$

$w_c = \frac{0.269}{0.413 \times 2.65} = 0.246 = 24.6\%$

$$\therefore \gamma_{d,c} = \left[w_c + \frac{1}{G_s} \right]^{-1} \qquad [B.12]$$

$$= \left[.246 + \frac{1}{2.65} \right]^{-1} = 1.605 \text{ g/cm}^3$$

from Kersten,

$k_u = .0036$ cal/°C cm s

$C_u = \gamma_{d,c} (0.18 + w_c)$

$= 1.605 (0.18+0.246) = 0.684$

$$\kappa_u = \frac{k_u}{c_u} = 0.0052 \text{ cm}^2/\text{s}$$

Total ΔV during thaw consolidation,

$$\Delta V = \Delta V_{i-w} + \Delta V_c \times \frac{S_t}{S_{max}} \qquad [B.11]$$

$$= 0.040 + 0.278 + = 0.318$$

from Latent Heat,

$$L_f = \gamma_{d,f}\, w(1-W_u)\, L_w \qquad [B.4]$$

$$= 1.095 \times 0.50(1-0.20)\ 79.6 = 34.9 \text{ cal/cm}^3$$

equivalent Latent Heat,

$$L^* = \frac{L}{1 - \Delta V} \qquad [B.12]$$

$$= \frac{34.9}{1 - 0.318} = 51.1 \text{ cal/cm}^3$$

$$Ste = \frac{c_u\, T_s}{L^*} = \frac{0.684 \times 21.1}{51.1} = 0.281 \qquad [B.5]$$

from Kersten,

$$k_f = 0.0053 \text{ cal/°C cm s}$$

$$c_f = \gamma_{d,f}\ (0.18+0.5(1+W_u)w) \text{ cal/°C cm}^3 \qquad [B.3]$$

$$= 1.095 \times (0.18+0.5(1+.20).50)$$

$$= 0.526 \text{ cal/°C cm}^3$$

$$\kappa_f = \frac{k_f}{c_f} = \frac{.0053}{.5260} = .0101 \text{ cm}^2/\text{s} \qquad [B.7]$$

$$\frac{-T_g\, k_f}{T_s\, k_u} \sqrt{\frac{\kappa_u}{\kappa_f}} = \frac{5}{21.1}\ \frac{.0053}{.0036} \sqrt{\frac{.0052}{.0101}} = 0.252 \qquad [B.8]$$

using Nixon & McRoberts (1973) graphical solution,

$$\frac{\alpha}{2\sqrt{\kappa_u}} = 0.33 \qquad [B.9]$$

$$\therefore\ \alpha = 0.33 \times 2\sqrt{.0052} = 0.0475 \text{ cm}/\sqrt{\text{s}}$$

$$\doteq 106.3\%\ \alpha_{obs}$$

B.4 Example 4: Recalculate α parameter, Test NWU-9, assuming $W_u=0$

Given $w = 0.50$ $\quad$ w = water content

$$\frac{S_t}{S_{max}} = 0.910$$

$A_o = 34.5\%$ $\quad$ A_o = thaw strain

Assume: $W_u = 0.0$ $\quad$ W_u = unfrozen water content

$$\gamma_{d,f} = \left[\frac{w}{G_{ice}} + \frac{1}{G_s} \right]^{-1} \qquad [B.13]$$

$$= \left[\frac{0.50}{0.917} + \frac{1}{2.65} \right]^{-1} = 1.084 \text{ g/cm}^3$$

$V_s = 0.409$ = volume fraction of solids

$V_i = 0.591$ = volume fraction of ice

V_i melts, $\therefore V_w = 0.591 \times 0.917 = 0.542$

$\Delta V_{i-w} = 0.049$

frozen Latent Heat,

$L_f = 0.542 \times 79.6 = 43.14 \text{ cal/cm}^3$

$A_o = 0.345$

$- \Delta V_{i-w} = \underline{0.049}$

$\Delta V_c = 0.296$

immediately after thaw,

$$\Delta V_w = \Delta V_{i-w} + \Delta V_c \times \frac{S_t}{S_{max}} = .049 + .296 \times .910$$

$$= 0.049 + 0.269 = 0.318$$

$V_{w,c} = 0.542 - 0.269 = 0.273$

$$w_c = \frac{0.273}{0.409 \times 2.65} = 0.252 = 25.2\%$$

$$\therefore \gamma_{d,c} = \left[w_c + \frac{1}{G_s} \right]^{-1} \qquad [B.1]$$

$$= \left[.252 + \frac{1}{2.65} \right]^{-1} = 1.589 \text{ g/cm}^3$$

from Kersten,

$w_c = 25.2\%$

$k_u = .0036$ cal/°C cm s

$$c_u = \gamma_{d,c}\ (0.18+w_c) \qquad [B.2]$$

$= 1.589\ (0.18+0.252) = 0.686$ cal/°C cm³

$$\kappa_u = \frac{k_u}{c_u} = 0.0052 \text{ cm}^2/\text{s} \qquad [B.6]$$

w=50%, $k_f = .0047$ cal/°C cm s

$$c_f = \gamma_{d,c}\ (0.18+0.5(w)) \qquad [B.3]$$

$= 1.084\ (0.18+0.5(0.50)) = 0.466$ cal/°C cm³

$$\kappa_f = \frac{k_f}{c_f} = 0.0101 \text{ cm}^2/\text{s} \qquad [B.7]$$

equivalent Latent Heat,

$$L^* = \frac{L_f}{1 - \Delta V} \qquad [B.14] = \frac{43.14}{1 - 0.318} = 63.25 \text{ cal/cm}^3$$

$$\text{Ste} = \frac{c_u\ T_s}{L^*} \qquad [B.5] = \frac{0.686 \times 21.1}{63.25} = 0.228$$

from Kersten,

$$\frac{-T_g\ k_f}{T_s\ k_u} \sqrt{\frac{\kappa_u}{\kappa_f}} = \frac{.0047}{.0036} \sqrt{\frac{.0052}{.0101}} \times \frac{5}{21.1} = 0.223 \qquad [B.8]$$

using Nixon & McRoberts (1973) graphical solution,

$$\frac{\alpha}{2\sqrt{\kappa_u}} = 0.30 \qquad [B.9]$$

$$\therefore\ \alpha = 0.30 \times 2\sqrt{.0052} = 0.0432 \text{ cm}/\sqrt{\text{s}}$$

$= 96.6\%\ \alpha_{obs}$

The results of this calculation and that of Example 3 bracket the observed value of the thaw penetration rate parameter, α_{obs}.

Appendice C: Normal Distribution of A_o

Thaw settlement data was obtained from Speer, Watson and Rowley (1973) for the Norman Wells, N.W.T. test site. Data points were selected from the plot of the thaw settlement, A_o, versus the frozen bulk density, ρ_b^f. The values of the thaw settlement are presented in Table C.1:

Thaw Strain: Norman Wells Samples

.71	.34	.32	.32	.25	.18	.22	.60	.48	.35	.38	.44
.15	.10	.61	.33	.27	.18	.12	.20	.25	.57	.40	.30
.16	.37	.21	.04	.52	.46	.29	.27	.11	.27	.11	.36
.41	.42	.27	.33	.19	.20	.58	.40	.34	.37	.20	.29
.21	.54	.43	.17	.36	.21	.21	.19	.57	.46	.14	.31
.27	.19	.27	.39	.38	.35	.33	.13	.14	.24	.38	.40
.29	.23	.19	.08	.24	.17	.02	.05	.08	.17	.16	.18
.06	.09	.12	.07	.25	.23	.05	.07	.13	.02	.06	.10
.10	.07	.17	.09	.06	.02	.07	.10	.13	.21	.12	.07
.13	.02	.01	.06	.02	.03	.04	.02				

The pertinent statistical characteristics of these samples are:

Number of Samples, $n = 116$

Cummulative Thaw Settlement, % $\Sigma x = 2716$

Cummulative (Thaw Settlement, %)^2 $\Sigma(x^2)$

$= 91648$

Average Thaw Settlement, $\bar{x} = \frac{\Sigma x}{n} = 23.414$

Standard Deviation, % $s = \sqrt{\frac{\Sigma(x_i - \bar{x})^2}{n-1}}$

$= \sqrt{\frac{\Sigma x^2 - \bar{x}\Sigma x}{n-1}}$

$= 15.619$

Assuming all settlement values are of equal importance, the statistical treatment of the 15 estimated settlements at the Norman Wells, N.W.T. site (Speer, *et al.*, 1973, Figure 1) is :

Number of Samples, $n = 15$

Cummulative Thaw Settlement, % $\Sigma x = 10.69m$

(Cummulative Thaw Settlement, %)^2 $\Sigma x^2 = 9.20m^2$

Average Thaw Settlement, $\bar{x} = \frac{\Sigma x}{n} = 0.713m$

Standard Deviation, % $s = 0.336m$

Reducing these data to a percentage of the estimated 11 m thaw,

$n = 15$

$\Sigma x = 97.18\%$

$\Sigma x^2 = 760.1$

$\bar{x} = 6.48\%$

$s = 3.05\%$

C.1 Extraneous Events

Using a Normal Distribution to represent the laboratory sample population, the occurrence of extraneous events (thaw settlement $\notin [0,1]$ can be determined:

Knowing $\bar{x} = 23.414\%$

$s = 15.619\%$

Assume $\mu = \bar{x}$

$\sigma = s$

For $A_o < 0\%$, $\Delta x = -23.414 = -1.50\sigma$

from a Normal Distribution,

@ $z = -1.50\sigma$

$P(z) = 0.0668$

For A_o > 100%, bc 0.5in> $\Delta x = 75.586 = 4.90\sigma$

from a Normal Distribution, @ $z = 4.90\sigma$

$P(z) \approx 0.9999991$

≈ 1.0

∴ the predicted quantity of samples undergoing heave (A_o < 0%) is 6.68%.

Appendice D: Beta Function Analysis

The distribution of probabilities in a standardized beta (β) function is described by Winkler (1972) as:

$$f(p) = \frac{(n-1)!}{(r-1)!\ (n-r-1)!}\ p^{r-1}\ (1-p)^{n-r-1} \qquad [D.1]$$

$$\text{for } 0 \leq p \leq 1$$

$$= 0 \text{ for other probabilities, } p$$

where r= the number of "successes"

n= the number of trails, $n > r > 0$

However, since a β function is not in terms of a Bernoulli process but is in terms of probabilities of a Bernoulli process, n and r may not be integers. The factorial terms can be replaced by gamma functions:

$$(z-1)! = \Gamma(z) = \int_0^\infty x^{z-1}\ e^{-x}\ dx \qquad \text{for } z > 0 \qquad [D.2]$$

Other writers have expressed the β function in alternative forms (Mann, 1970; Winkler and Hays, 1975; Simon, 1945; Abramowitz and Stegun, 1964).

The distinguishing feature of the β function is that it describes the probability distribution function (PDF) of the fixed *probability* of a Bernoulli process. Using the analogy of a biased coin, the β function provides a PDF of the bias, with the mode being near the mean, as one would expect. In the limit, as the number of trials becomes very large, the PDF becomes more pronounced at the mean value and

essentially is zero elsewhere. The value at the mean would represent the bias of the coin.

In geotechnical materials, there is no single value for the bias, nor does an increase in the number of samples cause the PDF to become more pronounced at the mean value. Instead, the sample population's mean value and variance are equated to the β distribution's definition of mean and variance, from which the values of n and r can be determined. These two parameters should then describe a β function who's PDF is very close to the probability mass function (PMF) of the discrete values of the sample population:

The β function parameters are obtained as follows:

Sample Mean and Variance:

Mean: $\bar{x} = \frac{\Sigma x}{n}$

Variance: $s^2 = \frac{\Sigma x^2 - \bar{x}\Sigma x}{n-1}$

β Mean and Variance:

Mean : $E_\beta = \frac{n}{r} = \bar{x}$

Variance: $V_\beta = \frac{r(n-r)}{n^2(n+1)} = s^2$, then solve for n and r .

Beta Parameters: $P = r$

$Q = n-r$

It is fortuitous that the thaw settlement parameter falls within the range from 0 to 100% and can be expressed as a fraction, so the standardized β distribution function can be applied directly. This is analagous to having an

ideally normally distributed population with a mean of $\bar{x}=0$ and a standard deviation of $s=1$. For populations not fitting this distribution as neatly, change-of-variable equations are available (LaValle, 1970).

Program "SETTLE":

```
C This version created on DATE=10-01-88 TIME=02:09:11
C**********************************************************************
C*                                                                    *
C*  SETTLE - a program to sort Ao values and calculate some           *
C*                          statistical parameters                    *
C*                                                                    *
C**********************************************************************
      REAL AO(120)
C                                          P and Q parameters
      READ(6,601)N
      READ(5,602)(AO(I),I=1,N)
  601 FORMAT(I15)
  602 FORMAT(7F5.2)
C                                          STACK THE A-NDOUGHT VALUES
      L1=N-1
      L2=N
C
      DO 2220 I=1,L1
      SINKER=AO(I)
C
            DO 2221 J=2,L2
            JMINUS=J-1
            IF(AO(J).LT.SINKER)GO TO 333
C                                          AO VALUE HIGHER THAN SINKER
            AO(JMINUS)=SINKER
            SINKER=AO(J)
            GO TO 2221
C                                          SINKER HIGHER THAN AO VALUE
  333       CONTINUE
            AO(JMINUS)=AO(J)
 2221       CONTINUE
C
      AO(J)=SINKER
      L2=L2-1
 2220 CONTINUE
C                                          Headings
      WRITE(6,649)
  649 FORMAT('0X','   N   ',5X,'   Ao   ',5X,'Fractile'
     *     /'0',' ------ ',5X,' ------ ',5X,' ---------- ')
C
      DO 2332 I=1,N
      PCTILE=FLOAT(I)/FLOAT(N)
      WRITE(6,610) I, AO(I), PCTILE
  610 FORMAT(5X, I5, 5X, F6.2, 8X, F6.4)
C                                          TELL-A-GRAPH file
      WRITE(7,710)  AO(I), PCTILE
  710 FORMAT(5X, 2PF6.2,'.', 8X, 2PF6.2)
 2332 CONTINUE
C
      SUM=0.
      SUMSQ=0
      DO 2222 I=1,N
C
      SUM=AO(I)+SUM
      SUMSQ=SUMSQ+AO(I)**2
C
 2222 CONTINUE
C                                          sample mean and variance
      SMEAN=SUM/N
      SVAR=(SUMSQ-(SMEAN*SUM))/(N-1)
      SDEV=SQRT(SVAR)
C                                          Beta dist'n equiv  n & r
      BETAN=(SMEAN*(1.-SMEAN)-SVAR)/SVAR
      BETAR=SMEAN*BETAN
C                                          p=r     / q=(n-r)
      P=BETAR
      Q=BETAN-BETAR
C
      WRITE(6,6000)N,SUM,SUMSQ,SMEAN,SVAR,SDEV,BETAN,BETAR,P,Q
 6000 FORMAT(
     */'0    Number of Samples = ',I10,
     */'     Sum of Samples = ',F10.5,
     */' Sum of (Samples**2) = ',F10.5,
     */'0               Mean = ',F10.5,
     */'           Variance = ',F10.5,
     */'  Standard Deviation = ',F10.5,
     */'0          Beta  n = ',F10.5,
     */'                r = ',F10.5,
     */'0               p = ',F10.5,
     */'                q = ',F10.5)
C
      STOP
      END
```

Program "BETA":

```
      SUM=SUM+AO(I)
C                                                    LIKELIHOOD
      RLIKE=10 /RN10/(AOLAST-AOFRST)
C
      WRITE(6,802)AO(I), FRAC, RLIKE, AOFRST, AOLAST
      WRITE(8,802)AO(I), FRAC, RLIKE, AOFRST, AOLAST
  802 FORMAT(6X,F7 5,3X,F6 2,3X,F7 4,' (',F7 5,'*',F7 5,')')
  802 FORMAT(6X,F7 5,3X,F6 2,3X,F7 4,' (',F7 5,'*',F7 5,')')
      AOFRST=AOLAST
   22 CONTINUE
C
      AVG=SUM/N
      WRITE(6,879)SUM,AVG
  879 FORMAT(/'+                 '/6X,F7 5,' = Sum'
     */6X,F7 5,' = Average'///' Generated Ao Statistics '
     */'  '/'                                 ')
C                                                    Calc Stats
      SUM=0
      SUMSQ=0
           DO 2229 I=1,N
           SUM=SUM+AO(I)
           SUMSQ=SUMSQ+AO(I)**2
 2229      CONTINUE
C
      AVG=SUM/N
      VAR=SUMSQ-AVG*SUM
      VAR=VAR/(N-1)
      SDEV=SQRT(VAR)
      WRITE(6,850)N,SUM,SUMSQ,VAR,SDEV
      WRITE(7,85@)N,SUM,P,SUMSQ,0,VAR,SDEV
  850 FORMAT(/1X,'   N = ',I5,
     */1X,'  SUM = ',F10 5,5X,'      Beta P Variable = ',F10 5,
     */1X,'SUMSQ = ',F10 5,5X,'      Beta Q Variable = ',F10 5,
     */1X,'  VAR = ',F10 5,
     */1X,' SDEV = ',F10 5////)
      WRITE(6,860)
  860 FORMAT(' Soil Parameters (based on the generated Ao values)')
      WRITE(6,810)
  810 FORMAT(//
     *' |    Ao    |    p    |    Vs    |  p-df  |  p-dt  |  Vs-t  |   ps   |   y''   |   Eo   |'/
     *' |   Thaw   |  Bulk   |  Solid   |  Dry   |  Dry   |  Solid |  Satur |  Eff    | Initial |'/
     *' |  Strain  |  Dens.  |  Volum   |  Dens  |  Dens  |  Volum |  Dens  |  Wt     |  Void   |'/
     *' |  Param.  |  Frez   |  Froz    |  Frez  |  Thaw  |  Thaw  |  Thaw  |  Dens   |  Ratio  |')
      WRITE(6,812)
  812 FORMAT(
     *' |          |         |          |        |        |        |        |         |         |')
C
      DO 2222 I=1,N
C                                                    FROZEN BULK DENSITY
      X=(.738-AO(I))/1.018
      DBFR(I)=EXP(X)
C                                                    VOLUME OF SOLIDS, FROZEN
      VS(I)=(DBFR(I)-GICE)/(GS-GICE)
      DDFR(I)=GS*VS(I)
      DDTH(I)=DDFR(I)/(1-AO(I))
C                                                    VOLUME OF SOLIDS, THAWED
      VSTH(I)=DDTH(I)/GS
      VW=1-VSTH(I)
      DSAT(I)=VW*DDTH(I)
      DEFF(I)=DSAT(I)-1.000
      WTEFF(I)=DEFF(I)*8.808
C                                                    FROZEN VOID RATIO
      EO(I)=(AO(I)+E*KPA)/(1-AO(I))
      EREL=EO(I)-EO(1)+0.00001
C
      WRITE(6,811)AO(I),DBFR(I),VS(I),DDFR(I),DDTH(I),VSTH(I), C
     * DSAT(I),WTEFF(I),EO(I)
  811 FORMAT(' ',F6.4,1X,F6.3,
     *1X,F6.4,1X,F6.3,' ',F6.3,' ',F6.4,' ',F6.3,' ',
     *-*F6.2,' ',F6.4)
      WRITE(8,812)
C
 2222 CONTINUE
C                                                    BULK MODULI
      BMOD(1)=10
      BMOD(2)=10
      BMOD(3)=20
      BMOD(4)=75
      BMOD(5)=300
      BMOD(6)=10000
C                                                    FACTOR FOR CALC G
      GFACTR=( 5*(1 +2 *POISSN)/(1 +POISSN)
C                                                    ADINA Input
      WRITE(6,873)
  873 FORMAT(///' |    Ev    |    K    |    G    |    S    |    e    |'/
     */'  |  Volumetric |  Bulk   |  Shear  | Vertical |  Void   |'/
     */'  |   Strain    | Modulus | Modulus |  Stress  |  Ratio  |')
      DO 2270 J=1,N
C
      WRITE(7,799)  DEFF(J),J
  799 FORMAT(43X,'  ',F10 3,'  g/cm**3',20X,'*** Material ',I2,' ***')
      WRITE(8,8666)
 8666 FORMAT(' ')
C
      END7=EO(J)
      DENOM=( 5 8854+(J) *END7)
C
          DO 2271 J=1,6
          SIGMA=BMOD(J)/DENOM
          VOIDR=E*KPA-CSUBC*ALOG10(SIGMA)
          EV(J)=(END7-VOIDR)/(1 +END7)
          GMOD(J)=BMOD(J)*GFACTR
C                                                    SET INITIAL Ev=0
          EV(1)=0 0
          WRITE(8,870)EV(J),BMOD(J),GMOD(J),SIGMA,VOIDR
  870     FORMAT(23X, F7 4, 2X, F7 3, 2X, F7 1,2X, F7 2,2X, F7 4,
     */                  |         |         |         |         |')
 2271     CONTINUE
C
      WRITE(7,700)EV,BMOD,BMOD,GMOD
  700 FORMAT(/8F10 4,2F10 2/8F10 2/8F10 2)
      WRITE(7,8666)
 2270 CONTINUE
C
      STOP
      END
```

Pe 1.88830

Qe 4.88170

Ne 10

Probability Distribution Function

X	PDF(X)
0.02	1.7521
0.04	2.2868
0.06	2.5451
0.08	2.6940
0.10	2.7584
0.12	2.7636
0.14	2.7257
0.16	2.6558
0.18	2.5626
0.20	2.4520
0.22	2.3291
0.24	2.1978
0.26	2.0615
0.28	1.9225
0.30	1.7832
0.32	1.6452
0.34	1.5099
0.36	1.3785
0.38	1.2520
0.40	1.1309
0.42	1.0160
0.44	0.9075
0.46	0.8058
0.48	0.7111
0.50	0.6238
0.52	0.5438
0.54	0.4890
0.56	0.4021
0.58	0.3418
0.60	0.2878
0.62	0.2399
0.64	0.1977
0.66	0.1609
0.68	0.1292
0.70	0.1021
0.72	0.0793
0.74	0.0606
0.76	0.0448
0.78	0.0325
0.80	0.0228
0.82	0.0153
0.84	0.0098
0.86	0.0059
0.88	0.0033
0.90	0.0017
0.92	0.0007
0.94	0.0002
0.96	0.0000
0.98	0.0000

The mode is at
0.11 2.7675

Probability Fractile Pairs for the Generated Beta Curve

variable -->	fractile	fractile	--> variable
0.10	0.22098	0.10	0.05488
0.20	0.48718	0.20	0.09249
0.30	0.69979	0.30	0.12872
0.40	0.84481	0.40	0.16575
0.50	0.93090	0.50	0.20525
0.60	0.97507	0.60	0.24909
0.70	0.99348	0.70	0.30012
0.80	0.99904	0.80	0.36404
0.90	0.99997	0.90	0.45704
1.00	1.00000	1.00	0.97314

Generated Ao Values		Likelihood	Ao Range
0.03180	0.10	1.8284	(0 - 0.05488)
0.07367	0.20	2.8426	(0.05488 - 0.09249)
0.11060	0.30	2.7608	(0.09249 - 0.12872)
0.14709	0.40	2.7003	(0.12872 - 0.16575)
0.18523	0.50	2.5313	(0.16575 - 0.20525)
0.22672	0.60	2.2811	(0.20525 - 0.24909)
0.27384	0.70	1.9588	(0.24909 - 0.30012)
0.33081	0.80	1.5845	(0.30012 - 0.36404)
0.40688	0.90	1.0752	(0.36404 - 0.45704)
0.58030	1.00	0.1938	(0.45704 - 0.97314)

2.34875 = Sum
0.23487 = Average

Generated Ao Statistics

N =	10		
SUM =	2.34875	Beta P Variable =	0.78987
SUMSQ =	0.02855	Beta Q Variable =	0.18294
VAR =			

Solved Parameters (based on the generated Ao values)

Output from "BETA":

Ae	p	Vs	p-df	p-dt	Vs-t	ps	y'	Eo
Thaw Strain Param.	Bulk Dens. Froz	Solid Volum Froz	Dry Dens Froz	Dry Dens. Thaw.	Solid Volum Thaw	Satur Dens Thaw	Eff Wt. Dens.	Initia Void Ratio
0 0218	1.887	.6233	1.852	1.705	.6638	2.082	10.42	1 8389
0.0739	1.916	.5767	1.528	1.850	.6227	2.027	10 07	1.7888
0.1108	1.848	.5378	1.424	1.801	.6043	1.947	9 78	1 8727
0.1471	1.783	.4998	1.325	1.553	.5861	1 867	9.48	1 9956
0 1882	1.718	.4621	1.225	1 503	.5671	1.936	9 18	2 1369
0 2267	1.649	4225	1 120	1 446	.5484	1 901	8 84	2.3041
0 2738	1 575	3794	1 006	1 385	.5225	1 882	8 45	2 5185
0 3306	1 489	.3302	0.875	1 307	.4932	1 814	7 88	2 8189
0 4067	1.382	.2683	0 711	1 198	4522	1 746	7 32	3 2064
0 5603	1 188	1566	0 415	0 944	.3561	1 588	5 76	4 8108

Ev Volum'c Strain	K Bulk Modulus	G Shear Modulus	S Vertical Stress	e Void Ratio
0 0	10.0	3 8	0 67	1 8026
0 0138	10.0	3.8	0 67	1 8028
0.0446	20.0	7.5	1.33	1 5213
0.1032	75.0	28 1	5.00	1.3863
0.1849	300.0	112 5	20.00	1 2037
0 3207	10000 0	3750 0	666.52	0 7928
0.0	10.0	3.8	0 84	1 8078
0.0547	10.0	3.8	0 84	1.8078
0.1842	20.0	7.5	1.28	1 5285
0.1404	75.0	28.1	4.78	1 3715
0.1995	300.0	112.5	19.13	1 2090
0.3683	10000.0	3750.0	637.56	0.7878
0.0	10.0	3 8	0.81	1.8125
0 0906	10 0	3 8	0 81	1 8125
0 1169	20 0	7 5	1 22	1 5312
0 1728	75.0	28 1	4 58	1.3763
0.2294	300 0	112 5	18.37	1.2127
0 3725	10000 0	3750 0	612 27	0 8025
0 0	10 0	3 8	0 59	1.8174
0 1282	10 0	3 8	0 59	1 8174
0 1534	20 0	7 5	1 17	1 5362
0 2051	75 0	28 1	4 40	1.3812
0 2594	300 0	112 5	17 61	1 2186
0 3988	10000 0	3750 0	587 15	0 8074
0 0	10 0	3 8	0.56	1 8228
0 1636	10 0	3 8	0 56	1 8228
0 1895	20 0	7 5	1 12	1 5415
0.2390	75 0	28 1	4 21	1 3865
0.2908	300 0	112 5	16 83	1.2240
0 4219	10000 0	3750 0	560 90	0 8128
0 0	10 0	3 8	0 53	1 8289
0 2043	10 0	3 8	0 53	1 8289
0 2289	20 0	7 5	1 08	1.5477
0 2759	75 0	28 1	3 99	1 3927
0 3251	300 0	112 8	15 97	1.2301
0 4495	10000 0	3750.0	532.33	0 8189
0 0	10 0	3 8	0.50	1.8363
0 2507	10 0	3 8	0.50	1.8363
0 2738	20.0	7 5	1.00	1 5550
0.3178	75 0	28 1	3.75	1 4000
0 3641	300 0	112 5	15.00	1.2375

0.4808	10000.0	3750.0	499.90	0.8283
0.0	10.0	3.8	0.48	1.6458
0.3088	10.0	3.8	0.46	1.6458
0.3281	20.0	7.5	0.82	1.5848
0.3887	75.0	28.1	3.46	1.4098
0.4113	300.0	112.5	13.82	1.2470
0.5190	10000.0	3750.0	460.82	0.8358
0.0	10.0	3.8	0.41	1.6800
0.3823	10.0	3.8	0.41	1.6800
0.4012	20.0	7.5	0.82	1.5787
0.4372	75.0	28.1	3.06	1.4237
0.4749	300.0	112.5	12.25	1.2612
0.5704	10000.0	3750.0	408.44	0.8500
0.0	10.0	3.8	0.30	1.6951
0.5362	10.0	3.8	0.30	1.6951
0.5502	20.0	7.5	0.61	1.6138
0.5788	75.0	28.1	2.27	1.4589
0.6048	300.0	112.5	8.08	1.2983
0.6758	10000.0	3750.0	302.70	0.8851

```
N =      10
SUM =    2.34675          Beta P Variable =     1.48830
SUMSQ =  0.78987          Beta Q Variable =     4.86170
VAR =    0.02855
SDEV =   0.16294
```

1.082 g/cm**3				*** Material 1 ***			
0.0 0.0138	0.0446	0.1033	0.1649	0.2207	10.00	10.00	
20.00 75.00	300.00	10000.00	10.00	10.00	20.00	75.00	
300.00 10000.00	3.75	3.75	7.50	28.13	112.50	3750.00	
1.027 g/cm**3				*** Material 2 ***			
0.0 0.0547	0.0842	0.1404	0.1993	0.2483	10.00	10.00	
20.00 75.00	300.00	10000.00	10.00	10.00	20.00	75.00	
300.00 10000.00	3.75	3.75	7.50	28.13	112.50	3750.00	
0.997 g/cm**3				*** Material 3 ***			
0.0 0.0906	0.1189	0.1728	0.2294	0.2725	10.00	10.00	
20.00 75.00	300.00	10000.00	10.00	10.00	20.00	75.00	
300.00 10000.00	3.75	3.75	7.50	28.13	112.50	3750.00	
0.967 g/cm**3				*** Material 4 ***			
0.0 0.1282	0.1534	0.2051	0.2594	0.2986	10.00	10.00	
20.00 75.00	300.00	10000.00	10.00	10.00	20.00	75.00	
300.00 10000.00	3.75	3.75	7.50	28.13	112.50	3750.00	
0.936 g/cm**3				*** Material 5 ***			
0.0 0.1636	0.1895	0.2390	0.2908	0.3219	10.00	10.00	
20.00 75.00	300.00	10000.00	10.00	10.00	20.00	75.00	
300.00 10000.00	3.75	3.75	7.50	28.13	112.50	3750.00	
0.901 g/cm**3				*** Material 6 ***			
0.0 0.2043	0.2289	0.2759	0.3251	0.4495	10.00	10.00	
20.00 75.00	300.00	10000.00	10.00	10.00	20.00	75.00	
300.00 10000.00	3.75	3.75	7.50	28.13	112.50	3750.00	
0.862 g/cm**3				*** Material 7 ***			
0.0 0.2507	0.2738	0.3179	0.3641	0.4809	10.00	10.00	
20.00 75.00	300.00	10000.00	10.00	10.00	20.00	75.00	
300.00 10000.00	3.75	3.75	7.50	28.13	112.50	3750.00	
0.814 g/cm**3				*** Material 8 ***			
0.0 0.3088	0.3281	0.3887	0.4113	0.5190	10.00	10.00	
20.00 75.00	300.00	10000.00	10.00	10.00	20.00	75.00	
300.00 10000.00	3.75	3.75	7.50	28.13	112.50	3750.00	
0.768 g/cm**3				*** Material 9 ***			
0.0 0.3823	0.4012	0.4372	0.4749	0.5704	10.00	10.00	
20.00 75.00	300.00	10000.00	10.00	10.00	20.00	75.00	
300.00 10000.00	3.75	3.75	7.50	28.13	112.50	3750.00	
0.588 g/cm**3				*** Material 10 ***			
0.0 0.5362	0.5502	0.5788	0.6048	0.6758	10.00	10.00	
20.00 75.00	300.00	10000.00	10.00	10.00	20.00	75.00	
300.00 10000.00	3.75	3.75	7.50	28.13	112.50	3750.00	

```
C THIS version created on DATE=09-27-86 TIME=15:11:31
C ***************************************************************
C * BBBBB   EEEEE  TTTTTT  AA      RRRRRR   EEEEE  SSSS   IIII DDDD   *
C * BBBBBB  EEEEE  TTTTTT  AA      RRRRRRR  EEEEE SS  SS   II  DDDDD  *
C * BB  BB  EE       TT    AAAA    RR   RR  EE    SS  SS   II  DD  DD *
C * BB  BB  EE       TT    AAAA    RR   RR  EE    SS       II  DD  DD *
C * BBBB    EEEE     TT   AA  AA ** RRRRRR   EEEE   SS      II  DD  DD *
C * BBBB    EEEE     TT   AA  AA ** RRRRR    EEEE    SS     II  DD  DD *
C * BB  BB  EE       TT   AAAAAA   RR RR    EE        SS    II  DD  DD *
C * BB  BB  EE       TT   AAAAAA   RR  RR   EE    SS  SS   II  DD  DD *
C * BBBBB   EEEEE    TT   AA  AA   RR   RR  EEEEE SS  SS   II  DDDDD  *
C * BBBBB   EEEEE    TT   AA  AA   RR   RR  EEEEE  SSSS  IIII DDDD   *
C *                                                             *
C * SR BETARESID.C++IMSLLIB where BETARESID.C  * compiled program  *
C *                                                             *
C ***************************************************************
C
      REAL AO(10),DBFR(10),VSFR(10),DDFR(10),DBTH(10),VSTH(10),
     * VWTH(10),DSAT(10),DEFF(10),EO(10),ETH(10),EV(6),RMOD(6),
     * AWTEFF(10),WTEFF(10),GMODI(6),VW(10),VICE(10),
     * RESID(10), EAO(10), RMODD(10), VOIDR(10), STRESS(10)
C                                          $=info / ?=ADINA input
      CALL FTNCMD('ASSIGN  6= -5;')
      CALL FTNCMD('ASSIGN  7= -7;')
      CALL FTNCMD('ASSIGN  8= -8;')
C          <<alter as req'd>>   .. Mean and Variance of Lab samples
C     (Sample mean and variance are 0.23474 and 0.024388)
      SMEAN=0.23414
      SVAR= 0.024398
C                                  ... BETA parameters
      BETAN=(SMEAN*(1.-SMEAN)-SVAR)/SVAR
      BETAR=SMEAN*BETAN
C                                  P = NUMBER OF SUCCESSES    [r]
C                                  O = (NUMBER OF TRIALS - P) [n-r]
      P=BETAR
      O=BETAN-BETAR
C                                  ... ten typical beta values required
      N=10
C                                                ... explicit values
      SS=2.55
      SICE=0.917
C                            **** Material Behaviour ****
C
C          ... slope of the thawed, drained recompression curve Csr
C                                  (Roggensack,PhD '77, Fig 5.15)
      CSR=0.180
C
C                            **** Residual Stress Behaviour ****
C          ...thawed UNdrained void ratio at 1kPa residual stress
C                                  (Roggensack,PhD '77, Fig 5.12)
      ER1KPA=2.15
C                                 ..slope of e:log(residual stress) line
      CRES=0.74
C     [ constituent relations herein are implicitly for nu of 1/3]
      POISSN=1./3.
C
C
C ---------------------------------------------------------------
C     this section generates a set of Ao values using beta's P & O:
      WRITE(6,601)SMEAN,SVAR,BETAN,BETAR,P,O,N
  601 FORMAT(
     */'0Sample Mean= ',F12.5,
     */' Sample  Var= ',F12.5,
     */'0      Beta n= ',F12.5,
     */'       Beta r= ',F12.5,
     */'0      Beta P= ',F12.5,
     */'       Beta O= ',F12.5,
     */'0# generated= ',I10/)
C                                                 GENERATE BETA DISTRIBUTION
      R=P
      RMINUS=R-1
      Z=P+O
      ZMRM1=Z-R-1
C
      WRITE(6,6499)
 6499 FORMAT(///23'Probability Distribution Function '//
     *  10X'   X       PDF(X)  '/'*                                  */)
C
      X=0.01
      F=X**(RMINUS) * (1.-X)**ZMRM1 *GAMMA(Z)/(GAMMA(R)*GAMMA(Z-R))
      WRITE(6,6500)X,F
           DO 2345 I=2,98,2
           X=I/100.
      F=X**(RMINUS) * (1.-X)**ZMRM1 *GAMMA(Z)/(GAMMA(R)*GAMMA(Z-R))
           WRITE(6,6500)X,F
 6500      FORMAT(11X,F4.2,'.      ',F8.6)
 2345      CONTINUE
      WRITE(6,6500)
      RMODE=(R-1)/(Z-2)
      X=RMODE
      IF(P.LE.1.OR.O.LE.1) GO TO 2234
      F=X**(RMINUS) * (1.-X)**ZMRM1 *GAMMA(Z)/(GAMMA(R)*GAMMA(Z-R))
      WRITE(6,6501)X,F
 6501 FORMAT(1X,'The mode is at '/10X,F8.3,'.      ',F8.6)
      GO TO 2235
C
C                DIST'N IS UNIFORM, BI-MODAL @ 0 & 1 or MODAL @ 0 or 1
 2234 CONTINUE
      WRITE(6,6506)X
 6506 FORMAT(1X,'The mode was calculated to be at X=',F12.8,
     *         /' therefore the distibution is modal at 0 or 1,',
     *         /' bi-modal at 0 and 1, or uniform between 0 and 1')
C
 2235 CONTINUE
C
      WRITE(6,666)
  666 FORMAT(//' Probability - Fractile Pairs for the Generated',
     *' Beta Curve',  //1X,' variable  -->  Fractile  ',5X,
     *' Fractile   -->  variable '/)
C
      DO 2331 I=1,10
      XIP=FLOAT(I)/10
      PIP=XIP
C                                        knowing Ao, find its Fractile
      CALL MDBETA(XIP,P,O,POP,IER)
      IF(IER.EQ.129)WRITE(6,6999)IER
      IF(IER.EQ.130)WRITE(6,6999)IER
C                                        KNOWING THE FRACTILE, FIND Ao
      CALL MDBETI(PIP,P,O,XOP,IER)
      IF(IER.EQ.129)WRITE(6,6990)IER
      IF(IER.EQ.130)WRITE(6,6990)IER
      IF(IER.EQ.131)WRITE(6,6990)IER
 6990 FORMAT(/1X,'*** ERROR IN SUBR. MDBETI: IER = ',I3)
 6999 FORMAT(/1X,'*** ERROR IN SUBR. MDBETA: IER = ',I3)
C
      WRITE(6,667)XIP,POP,PIP,XOP
  667 FORMAT('0',4X,F4.2,8X,F7.5,11X,F4.2,8X,F7.5)
 2331 CONTINUE
      WRITE(6,678)
  678 FORMAT(///'0 Generated Ao Values  Likelihood        Ao Range',
     *        /'0                                                  ',
     *                                                  'SUM, AVERAGE')
C
      SUM=0.0
      RN10=FLOAT(N)*10
      AOFRST=0.0
C
         DO 22 I=1,N
         SUMMA=0.
         NBEG1N=(I-1)*10
C                                  ... SUB-DIVIDE FRAC INTO 10 FOR BETTER Ao
```

```
C                                                  (Simpson's Integration used)
            DO 221 J=1,11
            JM1=J-1
            FRAC=FLOAT(NBEGIN+JM1)/RN10
            CALL MDSETI(FRAC,P,0,AOOUT,IER)
            NSMPSN=4
            IF(J/2*2.LT.J) NSMPSN=2
            IF(J.EQ.1.OR.J.EQ.11) NSMPSN=1
          WRITE(6,801)FRAC,AOOUT,NSMPSN
801 FORMAT(1X,'FRAC= ',F6.4,'  Ao= ',F7.5,' NSMPSN= ',I2)
            SUMMA=SUMMA+AOOUT*NSMPSN
221         CONTINUE
          AOLAST=AOOUT
C                                        CALC Ao VALUE FOR THAT FRACTILE RANGE
          AO(I)=SUMMA/30.
          FRAC=I/FLOAT(N)
          SUM=SUM+AO(I)
C                                                  LIKELIHOOD
          RLIKE=10./RN10/(AOLAST-AOFRST)
C
          WRITE(6,602)AO(I), FRAC, RLIKE, AOFRST, AOLAST
          WRITE(8,602)AO(I), FRAC, RLIKE, AOFRST, AOLAST
602       FORMAT(6X,F7.5,3X,F4.2,3X,F7.4,5X,' (',F7.5,',',F7.5,')')
602       FORMAT(6X,F7.5,3X,F4.2,3X,F7.4,5X,' (',F7.5,',',F7.5,')')
          AOFRST=AOLAST
 22       CONTINUE
C
      AVG=SUM/N
      WRITE(6,679)SUM,AVG
679 FORMAT(/'+          '/6X,F7.5,' = Sum',
     */6X,F7.5,' = Average'///' Generated Ao Statistics ',
     */'+                    ')
C                                                  calc stats
      SUM=0.
      SUMSQ=0.
            DO 2228 I=1,N
            SUM=SUM+AO(I)
            SUMSQ=SUMSQ+AO(I)**2
2228        CONTINUE
C
      AVG=SUM/N
      VAR=SUMSQ-AVG*SUM
      VAR=VAR/(N-1)
      SDEV=SQRT(VAR)
      WRITE(8,650)N,SUM,P,SUMSQ,Q,VAR,SDEV
      WRITE(7,650)N,SUM,P,SUMSQ,Q,VAR,SDEV
650 FORMAT(/1X,'O    N = ',I5,
     */1X,'  SUM = ',F10.5,5X,'      Beta P Variable = ',F10.5,
     */1X,'SUMSQ = ',F10.5,5X,'      Beta Q Variable = ',F10.5,
     */1X,'  VAR = ',F10.5,
     */1X,' SDEV = ',F10.5////)
      WRITE(6,690)
690 FORMAT(' Soil Parameters (based on the generated Ao values)')
      WRITE(6,610)
610 FORMAT(
     *' |   Ao   |  P   |   Vs  | p-df| p-dt| Vs-t|  ps  |  y'  |  Eo  |'
     *' |  Eth   |  S'  |  E-Ao |'./'+',57X,'eo'./
     *' |        |      |       |'./
     *' |  Thaw  | Bulk |Solid  |  Dry |  Dry |Solid|Satur| Eff. |Initia|'
     *'Thawed|Resid-| Thaw  |'./
     *' |Strain|Dens. |Volum|Dens. |Dens. |Volum|Dens | Wt.  | Void |'
     *' Undr.|  ual |Strain |'./
     *' |Param.|Freez.|Freez.|Freez.|Thaw. |Thaw.|Thaw.|Dens. |Ratio |'
     *'Void R|Stress|Void R |')
      WRITE(6,612)
612 FORMAT(
     *' |        |      |       |'.)
C
      DO 2222 I=1,N
C                                                  FROZEN BULK DENSITY
      X=(.736-AO(I))/1.018
      DBFR(I)=EXP(X)
C                                                  VOLUME OF SOLIDS, FROZEN
      VSFR(I)=(DBFR(I)-GICE)/(GS-GICE)
C                                                  Volume of Ice
      VICE(I)=1-VSFR(I)
C                                                  Initial Void Ratio
      EO(I)=VICE(I)/VSFR(I)
C                                                  Undrained Volume of Water
      VW(I)=VICE(I)+GICE
C                                                  Thawed Undrained Void Ratio
      ETH(I)=VW(I)/VSFR(I)
C                                                  Calculate Residual Stress=f(e-thaw)
      EXPR=(ER)*(PA-ETH(I))/CRES
      RESID(I)=10**EXPR
C                                                  VOID RATIO AT THAW STRAIN
      EAO(I)=EO(I)-AO(I)*(1.+EO(I))
C                                                  Dry Density, Frozen
      DDFR(I)=GS*VSFR(I)
C                                                  Dry Density, Thaw Strained
      DDTH(I)=DDFR(I)/(1-AO(I))
C                                                  VOLUME OF SOLIDS,THAW Strain
      VSTH(I)=DDTH(I)/GS
C                                                  Volume of Water, Thaw Strain
      VW(I)=1-VSTH(I)
C                                                  Density, saturated, strained
      DSAT(I)=VW(I)*DDTH(I)
      DEFF(I)=DSAT(I)-1.000
      WTEFF(I)=DEFF(I)*9.806
C                                                  Wt. Dens., Corrected for Ao
      AWTEFF(I)=WTEFF(I)*(1.-AO(I))
C
      WRITE(8,611)AO(I),DBFR(I),VSFR(I),DDFR(I),DDTH(I),VSTH(I),
     * DSAT(I),WTEFF(I),EO(I),ETH(I),RESID(I),EAO(I)
611 FORMAT('  ',F8.6,3X,F5.3,
     *1X,F8.4,1X,F5.3,' ',F5.3,' ',F5.3,' ',F8.4,' ',F5.3,' ',
     *F5.2,' ',F6.4,' ',F6.4,' ',F6.2,' ',F6.4)
      WRITE(6,612)
C
2222  CONTINUE
C                                  Calculate Adina Input
C
C                                                  FACTOR FOR CALC, G
      GFACTR=1.5*(1.-2.*POISSN)/(1.+POISSN)
C                                                  ADINA Input
      WRITE(6,673)
673 FORMAT(///' |    Ev    |  K   |   G   |  S   |   e   |'
     */'  |Volum'tic |  Bulk  | Shear  |Vertical| Void  |'
     */'  | Strain |Modulus|Modulus|Stress| Ratio |')
      DO 2270 I=1,N
C
      WRITE(7,799)  DEFF(I),I
799 FORMAT(4X,'1',F10.3,' g/cm**3',20X,'*** Material ',I2,' ***')
      WRITE(8,6666)
6666 FORMAT(' ')
C
      ENOT=EO(I)
C                                  Oedometric RECOMPRESSION FACTOR
      FACTOR=1.535*(1.+ENOT)/CSR
C                                  BULK MOD. AT RESIDUAL STRESS
      RMOD(I)=RESID(I)*FACTOR
C                                  max. stress expected, used in K-e calcs
      STRMAX=6.00
C                                  VOLUMETRIC STRAIN
      EV(I)=0
      STRESS(I)=0.
      VOIDR(I)=ENOT
      IF(AO(I) LT 0.05) GO TO 6666
```

```
C     *-----------------------------------------------------------------
C                        THEREFORE: MAT'L THAW STRAIN > 5%
C                                   arbitrary negligible "K" unit: evsAo
      BMOD(1)=10.
      EV(2)=AO(I)-0.05
      VOIDR(2)=ENOT-EV(2)*(1.+ENOT)
C                                   NEGLIGIBLE STRESS BUILD-UP
      STRESS(2)=EV(2)*BMOD(1)*1.5
C                                   NET STRESS:   (RESID. - NEGL.)
      STR=RESID(I)-STRESS(2)
      BMOD(2)=BMOD(1)
C
      IF(STR.LT.0.) GO TO 5553
C     -----------------------------------------------------------------
C                                   THEREFORE SOME RESIDUAL STRESS
      EV(3)=EV(2)+.0001
      VOIDR(3)=ENOT-EV(3)*(1.+ENOT)
      STRESS(3)=STRESS(2)
      BMOD(3)=2./3.*STR/0.05
      EV(4)=AO(I)
      VOIDR(4)=ENOT-EV(4)*(1.+ENOT)
      BMOD(4)=BMOD(3)
      STRESS(4)=RESID(I)
C                                   BEGIN RECOMPRESSION
      EV(5)=AO(I)+0.0001
      VOIDR(5)=ENOT-EV(5)*(1.+ENOT)
      BMOD(5)=BMOD(1)
      STRESS(5)=RESID(I)
C                                   arbitrary level of 600kPa
      STRESS(6)=600.
C                                   CALC. PARAMETERS FOR P'(=600kPa
      BMOD(6)=600.*FACTOR
C                                   VOID RATIO @ 600 kPa
      E600=EAO(I)-CSR*ALOG10(600./RESID(I))
      EV(6)=(EO(I)-E600)/(1.+EO(I))
      VOIDR(6)=E600
      GO TO 5555
C     -----------------------------------------------------------------
 5551 CONTINUE
C                                   MAT'L STIFF FROM THE VERY START
      BMOD(1)=2./3.*RESID(I)/AO(I)
      EV(2)=AO(I)
      VOIDR(2)=ENOT-EV(2)*(1.+ENOT)
      BMOD(2)=BMOD(1)
      STRESS(2)=EV(2)*BMOD(2)*1.5
C                                   M. BEGIN RECOMPRESSION
      EV(3)=AO(I) + .0001
      VOIDR(3)=ENOT-EV(3)*(1.+ENOT)
      BMOD(3)=RESID(I)*FACTOR
      STRINC=(600.-RESID(I))/3.
      STRESS(3)=RESID(I)
      GO TO 5554
C     -----------------------------------------------------------------
C                                   THERSFORE NEGLIGIBLE RESIDUAL STRES
 5553 CONTINUE
C
      EV(2)=AO(I)
      VOIDR(2)=EAO(I)
      BMOD(2)=BMOD(1)
      STRESS(2)=AO(I)*BMOD(1)*1.5
C
      EV(3)=AO(I) + .0001
      VOIDR(3)=ENOT-EV(3)*(1.+ENOT)
      BMOD(3)=RESID(I)*FACTOR
C                                   ENSURE MINIMAL MODULUS
      IF(BMOD(3).LT.BMOD(1)) BMOD(3)=BMOD(1)
      STRESS(3)=STRESS(2)+0.75*(BMOD(2)+BMOD(3))*(EV(3)-EV(2))
C                                   ENSURE "E"> 0.4
      STRMAX=600.
      E600=EAO(I) - CSR * ALOG10(600./RESID(I))
      IF(E600.GT 0.4) GO TO 5554
C                                   set a minimum "e"
      EMIN=0.4
      EXPM=(EAO(I)-EMIN)/CSR + ALOG10(RESID(I))
      STRMAX=10**EXPM
C
 5554 CONTINUE
      STRINC=(STRMAX-STRESS(3))/3.
      IF(STRINC.LT.0.0) GO TO 5559
C                                   PICK POINTS OFF RECOMPRESSION CURVE
         DO 2629 J=4,6
         JM1=J-1
         STRESS(J)=STRESS(JM1)+STRINC
         BMOD(J)=STRESS(J)*FACTOR
C                                                  arbitrary K minimum
         IF(BMOD(J) LT.10) BMOD(J)=10
         IF(BMOD(J).LT.10) STRESS(J)=10 /FACTOR
         VOIDR(J)=EAO(I) - CSR*ALOG10(STRESS(J)/RESID(I))
         EV(J)=(EO(I)-VOIDR(J))/(1 +EO(I))
 2629    CONTINUE
      GO TO 5555
C     -----------------------------------------------------------------
C                                   MAT'L NEVER PICKS UP LOAD
 5559 CONTINUE
         DO 2321 J=4,6
         JM1=J-1
         BMOD(J)=BMOD(1)
         VOIDR(J)=VOIDR(JM1)=0 SO
         EV(J)=(EO(I) - VOIDR(J))/(1 +EO(I))
         STRESS(J)=EV(J)*BMOD(I))*1.5
 2321    CONTINUE
C
C     -----------------------------------------------------------------
C
 5555 CONTINUE
C
         DO 2271 J=1,6
         GMOD(J)=BMOD(J)*GFACTR
         WRITE(6,670)EV(J),BMOD(J),GMOD(J), STRESS(J), VOIDR(J)
  670    FORMAT(2X, F7.4, 2X, F7.1,2X, F7.1,2X, F7.2,2X, F7.4,
     */                  |          |          |          |          |)
 2271    CONTINUE
C                                   XDINA format
      WRITE(7,700)EV,BMOD,BMOD,GMOD
  700 FORMAT(6F10.4,2F10.2/8F10.2/8F10.2)
 2270 CONTINUE
C
      STOP
      END
```

Output from "BETARESID":

Sample Mean=	0.23414
Sample Var=	0.02440
Beta n=	6.35032
Beta r=	1.48886
Beta P=	1.48888
Beta Q=	4.86346
# generated=	10

Probability Distribution Function

X	PDF(X)
0.01,	1.2993
0.02,	1.7508
0.04,	2.2657
0.06,	2.5446
0.08,	2.6938
0.10,	2.7585
0.12,	2.7838
0.14,	2.7780
0.16,	2.6563
0.18,	2.5830
0.20,	2.4526
0.22,	2.3296
0.24,	2.1883
0.26,	2.0618
0.28,	1.9229
0.30,	1.7835
0.32,	1.6455
0.34,	1.5102
0.36,	1.3787
0.38,	1.2521
0.40,	1.1310
0.42,	1.0160
0.44,	0.9075
0.46,	0.8058
0.48,	0.7111
0.50,	0.6234
0.52,	0.5427
0.54,	0.4689
0.56,	0.4020
0.58,	0.3416
0.60,	0.2877
0.62,	0.2397
0.64,	0.1976
0.66,	0.1608
0.68,	0.1291
0.70,	0.1020
0.72,	0.0792
0.74,	0.0603
0.76,	0.0448
0.78,	0.0325
0.80,	0.0227
0.82,	0.0153
0.84,	0.0098
0.86,	0.0059
0.88,	0.0033
0.90,	0.0017
0.92,	0.0007
0.94,	0.0002
0.96,	0.0000
0.98,	0.0000

The mode is at
0.112, 2.7878

Probability Fractile Pairs for the Generated Beta Curve

variable	-->	fractile	fractile	--> variable
0.10		0.22080	0.10	0.05488
0.20		0.48718	0.20	0.09251
0.30		0.69980	0.30	0.12873
0.40		0.84484	0.40	0.18578
0.50		0.93093	0.50	0.20527
0.60		0.97809	0.60	0.24911
0.70		0.99349	0.70	0.30012
0.80		0.99908	0.80	0.38402
0.90		0.99997	0.90	0.45899
1.00		1.00000	1.00	0.97311

Generated Ao Values		Likelihood	Ao Range
0.03181	0.10	1.8293	(0.0 -0.05488)
0.07388	0.20	2.8428	(0.05488-0.09251)
0.11063	0.30	2.7806	(0.09251-0.12873)
0.14711	0.40	2.7003	(0.12873-0.18578)
0.18525	0.50	2.5313	(0.18578-0.20527)
0.22673	0.60	2.2811	(0.20527-0.24911)
0.27384	0.70	1.9804	(0.24911-0.30012)
0.33060	0.80	1.5848	(0.30012-0.38402)
0.40887	0.90	1.0735	(0.38402-0.45899)
0.55025	1.00	0.1938	(0.45899-0.97311)
2.34678	= Sum		
0.23468	= Average		

Generated Ao Statistics

N =	10		
SUM =	2.34678	Beta P Variable =	1.48588
SUMSQ =	0.78982	Beta Q Variable =	4.86348
VAR =	0.02654		
SDEV =	0.16292		

Soil Parameters (based on the generated Ao values)

Ao Thaw Strain Param.	p Bulk Dens. Froz.	Vs Solid Volum Froz.	p-df Dry Dens. Froz.	p-dt Dry Dens. Thaw.	Vs-t Solid Volum Thaw.	ps Satur Densc Thaw.	y' Eff Wt. Dens.	Eo Initia Void Ratio	Eth Thawed Undr Void R	So Resid- ual Stress	E-Ao Thaw Strain Void R
0.0316	1.997	.8233	1.552	1.705	.8438	2.062	10.42	0.5044	0.5542	143.38	0.5533
0.0739	1.916	.7766	1.528	1.650	.8226	2.027	10.07	0.7342	0.8733	98.99	0.8061
0.1106	1.848	.7374	1.424	1.601	.8043	1.997	9.78	0.8507	0.7852	89.00	0.8548
0.1471	1.783	.6999	1.325	1.553	.7861	1.967	9.48	1.0004	0.9174	46.31	0.7081
0.1852	1.718	.6621	1.224	1.503	.7671	1.936	9.18	1.1642	1.0676	29.02	0.7833
0.2287	1.649	.6225	1.120	1.448	.7464	1.901	8.84	1.3679	1.2535	16.27	0.8303
0.2738	1.575	.5784	1.008	1.385	.7226	1.862	8.45	1.6354	1.4997	7.57	0.9137
0.3308	1.489	.5302	0.875	1.307	.6932	1.814	7.98	2.0287	1.8603	2.86	1.0274
0.4057	1.382	.4683	0.711	1.198	.6522	1.746	7.32	2.7272	2.5008	0.34	1.2114
0.5802	1.188	.3588	0.415	0.944	.5582	1.588	5.76	5.3844	4.9375	0.00	1.8075

Ev Volum'c. Strain	K Bulk Modulus	G Shear Modulus	s Vertical Stress	e Void Ratio
0.0	3004.6	1128.7	0.0	0.5044
0.0316	3004.6	1128.7	143.38	0.5533
0.0319	2206.9	827.6	143.38	0.5532
0.0831	4548.6	1708.1	295.59	0.5031
0.0811	8892.4	2584.6	447.79	0.4742
0.0838	8235.1	3483.2	600.00	0.4539
0.0	10.0	3.8	0.0	0.7342
0.0239	10.0	3.8	0.91	0.6928
0.0240	1315.1	493.2	0.36	0.6926
0.0739	1315.1	493.2	98.99	0.8061
0.0740	9847.0	637.6	98.99	0.8059
0.1481	9952.5	3743.4	600.00	0.4808
0.0	10.0	3.8	0.0	0.8507
0.0806	10.0	3.8	0.91	0.7479
0.0807	907.9	340.5	0.91	0.7477
0.1106	907.9	340.5	89.00	0.8548
0.1107	1231.8	461.9	89.00	0.8546
0.1914	10710.5	4018.4	600.00	0.5045
0.0	10.0	3.8	0.0	1.0004
0.0971	10.0	3.8	1.48	0.8082
0.0972	598.1	224.3	1.48	0.8080
0.1471	598.1	224.3	46.31	0.7081
0.1472	846.8	353.3	46.31	0.7080
0.2381	11514.9	4318.1	600.00	0.5281
0.0	10.0	3.8	0.0	1.1642
0.1352	10.0	3.8	2.03	0.8718
0.1353	388.8	135.0	2.03	0.8713
0.1852	388.8	135.0	29.02	0.7833
0.1853	802.8	228.0	29.02	0.7831
0.2828	12457.8	4671.7	600.00	0.5528
0.0	10.0	3.8	0.0	1.3670
0.1787	10.0	3.8	2.85	0.9487
0.1788	181.8	68.1	2.85	0.9484
0.2287	181.8	68.1	16.27	0.8303
0.2288	388.5	138.8	16.27	0.8301
0.3328	13824.8	5109.4	600.00	0.5798

0.0	10.0	3.8	0.0	1.6354
0.2238	10.0	3.8	3.38	1.0458
0.2238	58.1	21.0	3.38	1.0452
0.2738	58.1	21.0	7.57	0.9137
0.2738	191.3	71.7	7.57	0.9136
0.3892	15170.1	5688.8	600.00	0.6098
0.0	10.0	3.8	0.0	2.0287
0.3306	10.0	3.8	4.96	1.0274
0.3307	71.6	26.8	4.97	1.0271
0.4319	5907.5	2215.3	203.31	0.7207
0.4475	11670.7	4376.5	401.66	0.6734
0.4567	17434.0	6537.7	600.00	0.6455
0.0	10.0	3.8	0.0	2.7272
0.4067	10.0	3.8	6.10	1.2114
0.4068	12.0	4.5	6.10	1.2111
0.5262	7298.9	2736.3	204.07	0.7660
0.5388	14376.7	5390.5	402.03	0.7189
0.5463	21464.4	8045.4	600.00	0.6
0.0	10.0	3.8	0.0	5.
0.5602	10.0	3.8	8.40	1.
0.5603	10.0	3.8	8.41	1.
0.7126	12593.3	4722.5	205.60	0.8348
0.7189	24871.7	9291.9	402.80	0.7880
0.7243	36750.1	13781.3	600.00	0.7603

```
0 N =      10
  SUM =      2.34678          Beta P Variable =      1.48686
SUMSQ =      0.78982          Beta Q Variable =      4.86346
  VAR =      0.02654
 SDEV =      0.16292

    1      1.082 g/cm**3                    *** Material#  1 ***
      0.0          0.0318          0.0318          0.0831          0.0811          0.0938       3004.59       3004.59
   2206.85       4548.81       6892.36       8235.11       3004.59       3004.59       2206.85       4548.81
   6892.36       8235.11       1126.72       1126.72        827.57       1706.10       2584.83       3463.17
    1      1.027 g/cm**3                    *** Material#  2 ***
      0.0          0.0239          0.0240          0.0739          0.0740          0.1481         10.00         10.00
   1315.10       1315.10       1646.95       9982.46         10.00         10.00       1315.10       1315.10
   1646.95       9982.46          3.75          3.75        493.16        493.16        817.81       3743.42
    1      0.997 g/cm**3                    *** Material#  3 ***
      0.0          0.0806          0.0607          0.1108          0.1107          0.1914         10.00         10.00
    907.91        907.91       1231.76      10710.48         10.00         10.00        907.91        907.91
   1231.76      10710.48          3.75          3.75        340.47        340.47        461.91       4016.43
    1      0.967 g/cm**3                    *** Material#  4 ***
      0.0          0.0971          0.0972          0.1471          0.1472          0.2361         10.00         10.00
    598.06        598.06        888.79      11514.93         10.00         10.00        598.06        598.06
    888.79      11514.93          3.75          3.75        224.27        224.27        333.30       4318.10
    1      0.936 g/cm**3                    *** Material#  5 ***
      0.0          0.1352          0.1353          0.1852          0.1853          0.2825         10.00         10.00
    359.91        359.91        802.57      12457.75         10.00         10.00        359.91        359.91
    802.57      12457.75          3.75          3.75        134.96        134.96        225.96       4671.66
    1      0.901 g/cm**3                    *** Material#  6 ***
      0.0          0.1767          0.1768          0.2267          0.2268          0.3326         10.00         10.00
    181.62        181.62        369.52      13624.95         10.00         10.00        181.62        181.62
    369.52      13624.95          3.75          3.75         68.11         68.11        138.57       5109.36
    1      0.862 g/cm**3                    *** Material#  7 ***
      0.0          0.2238          0.2238          0.2738          0.2739          0.3892         10.00         10.00
     56.10         56.10        181.27      15170.11         10.00         10.00         56.10         56.10
    181.27      15170.11          3.75          3.75         21.04         21.04         71.72       5688.79
    1      0.814 g/cm**3                    *** Material#  8 ***
      0.0          0.3306          0.3307          0.4319          0.4475          0.4567         10.00         10.00
     71.57       5907.50      11670.73      17433.85         10.00         10.00         71.57       5907.50
   11670.73      17433.85          3.75          3.75         26.84       2215.31       4376.52       6537.73
    1      0.746 g/cm**3                    *** Material#  9 ***
      0.0          0.4067          0.4068          0.5262          0.5388          0.5463         10.00         10.00
     12.00       7298.93      14376.87      21464.42         10.00         10.00         12.00       7298.93
   14376.87      21464.42          3.75          3.75          4.50       2736.35       5390.88       8045.41
    1      0.588 g/cm**3                    *** Material# 10 ***
      0.0          0.5602          0.5603          0.7126          0.7189          0.7243         10.00         10.00
     10.00      12593.26      24871.69      36750.13         10.00         10.00         10.00      12593.26
   24871.69      36750.13          3.75          3.75          3.75       4722.47       9291.88      13781.30
```

Appendice E: Thermodynamics

E.1 The Thermodynamics of Co-Existing Phases

E.1.1 Energy

The subject of thermodynamics deals with energies and their balances. The "internal energy", u, is a measure of the energy per unit mass of a system under constant volume. Similarly, the "enthalpy", h, is a measure of the energy per unit mass under constant pressure. This differs from the internal energy in that it includes the pressure:volume product, Pv, called "flow work" in a control volume analysis (Reynolds & Perkins, 1977).

Therefore

$$h \equiv u + Pv \qquad [E.1]$$

$$dh \equiv du + Pdv + vdP \qquad [E.2]$$

E.1.2 Entropy

The "entropy", s, is a measure of the level of randomness or disorder per unit mass of a system and can be expressed as a function of its internal energy and its volume. Any change in the system that maintains equilibrium between two co-existing phases requires identical changes in their phase entropies:

$$s = s(u,v)$$

for co-existing ice and water,

$$ds_i = ds_w \qquad [E.3]$$

$$\text{where } ds=\left[\frac{\partial s}{\partial u}\right]_v du + \left[\frac{\partial s}{\partial v}\right]_u dv \qquad [E.4]$$

where $\left[\ \right]_v \equiv$ at constant volume

$\left[\ \right]_u \equiv$ at constant internal energy

Using the thermodynamic definitions of temperature and pressure,

$$\frac{1}{T}\equiv\left[\frac{\partial s}{\partial u}\right]_v \qquad [E.5]$$

$$\frac{P}{T}\equiv\left[\frac{\partial s}{\partial v}\right]_u \qquad [E.6]$$

$$\therefore ds= \frac{du}{T} + \frac{Pdv}{T} \text{ , the "Gibbs Equation"} \qquad [E.7]$$

Enthalpy can now be defined as:

$$h\equiv u + Pv \qquad [E.8]$$

$$dh= du + Pdv + vdP$$

$$= (Tds - Pdv) + Pdv + vdP$$

$$= Tds + vdP \qquad [E.9]$$

E.1.3 Gibbs Free Energy: a statement of balance

A useful function called Gibbs Free Energy is a measure of a system's equilibrium. In every system there is tendency towards lower enthalpy, as would be the case when liquid solidifies. There is also a countering tendency towards increased entropy, as when a solid phase melts. While enthalpy is generally a linear function of the mole fraction of the two co-existing phases, entropy is not. Entropy increases rapidly at the onset of melting and at a decreasing rate thereafter. The Gibbs Free Energy, or the Gibbs function, g, expresses this balance and is defined as:

$$g\equiv h - Ts \qquad [E.10]$$

$$\therefore dg= dh - Tds - sdT$$

$$= vdP - sdT \qquad [E.11]$$

which enables us to find the equilibrium reaction at constant pressure and temperature.

E.1.4 Water Co-Existing with Ice

At the equilibrium point described by Equation [4.11], we know that for a two-phase system of ice and water,

$$dg_i = dg_w \qquad [E.12]$$

$$v_i dP_i - s_i dT_i = v_w dP_w - s_w dT_w \qquad [E.13]$$

under isothermal conditions,

$$dT_w = dT_i = dT$$

$$\therefore v_i dP_i - s_i dT = v_w dP_w - s_w dT \qquad [E.14]$$

If one maintains a constant pressure on the ice, the dP_i term does not enter into the calculation:

$$-s_i dT = v_w dP_w - s_w dT \qquad [E.15]$$

$$dP_w = \frac{(s_w - s_i)}{v_w} dT \qquad [E.16]$$

The change in enthalpy over a phase change is

$$\Delta h = T \Delta s \qquad [E.17]$$

$$\Delta s = \frac{\Delta h}{T} = \frac{L}{T} \qquad \text{where } L \text{ is the latent heat}$$

$$\therefore dP_w = \frac{L}{v_w} \frac{dT}{T} \qquad [E.18]$$

Integrating over the pressure difference between the system at atmospheric and the system under suction, and also over the temperature difference from the freezing temperature, T_0, to T_s^*:

$$(P_w - 0) = \frac{L}{v_w} \ln \frac{T_s^*}{T_0} \qquad [E.19]$$

knowing $\ln(1+x) \approx x - \frac{x^2}{2} \ldots$ for $x \to 0$

$$\approx \chi$$

$$\therefore P_v = \frac{L}{v_w}\left[\frac{T_s^* - T_o}{T_o}\right] \qquad [E.20]$$

the "Kelvin Equation"

If we define $T_s = T_s^* - T_o$; $(T_s<0)$

$$P_v = \frac{L}{v_w\ T_o}\ T_s \qquad [E.21]$$

$$= \frac{334\ J/gm}{1.0002\ cm^3/gm\ 273.15\ K}\ T_s$$

$$= 1.222 T_s\ MJ/m^3K$$

$$= 12.07 T_s\ atm/K\ ,\ T_s<0$$

This provides an expression for the suction in the water due to a freezing point depression of T_s, at the ice/water interface. It assumes no change in the ice pressure and has been verified experimentally (Biermans, *et al.*, 1978). For most practical purposes P_v will be a suction since any pressure in excess of P_i (e.g. atmospheric plus overburden) would not be possible in an open system. It should be emphasized that this equation holds for co-existing phases under different pressures with the unfrozen soil matrix supporting the difference.

In the case where both phases co-exist at the same pressure, $dP_i \neq 0$ and it follows that

$$v_i dP_i - s_i dT = v_v dP_v - s_v dT \qquad [E.22]$$

isobaric $\therefore dP_i = dP_v = dP$

$$(v_i - v_v)dP = (s_i - s_v)\,dT$$

$$\frac{dP}{dT} = \frac{s_i - s_v}{v_i - v_v}$$

$$= \frac{-L}{T\Delta v} \qquad [E.23]$$

the "Clapeyron Equation for fusion"

for water, $\frac{dP}{dT} = \frac{-334 \text{ J/gm}}{273.15 \text{ K } (1.0908 - 1.0002)\text{cm}^3/\text{gm}}$

$= -13.50 \text{ MPa/K} = -133.2 \text{ atm/K}$

This represents a pressure build-up equivalent to 65m of overburden for every Celcius degree of freezing point depression, and its effect can be seen in the frost damage to water mains and lines. It has been experimentally proven by Hoekstra (1969) and by Radd and Oertle (1973). It should be emphasized that the Clapeyron equation predicts a pressure increase with a drop in the freezing temperature, whereas the Kelvin equation predicts a suction.

E.1.5 Pressure in the Ice

Further examination of our simplified Kelvin equation and its derivation shows that a correction is needed when the ice pressure P_i is different from one atmosphere. Changes in the ice pressure, ΔP_i, must be taken into account by using a hybrid between the Kelvin and the Clapeyron equations:

$$v_i dP_i - v_w dP_w = (s_i - s_w)dT \qquad [E.24]$$

$$v_w dP_w = L\frac{dT}{T} + v_i dP_i \qquad [E.25]$$

$$dP_w = \frac{L}{v_w T}dT + \frac{v_i}{v_w}dP_i \qquad [E.26]$$

$$\Delta P_w = 12.07 \text{ atm/K } \Delta T + 1.0906\Delta P_i \qquad [E.27]$$

converting to gauge,

$$P_w = 12.07 \text{ atm/K } \Delta T + 1.0906\Delta P_i \qquad [E.28]$$

In the case where $\Delta P_i = 0$, the Kelvin equation is recovered, and where $P_w = \Delta P_i$, the Clapeyron equation is

recovered. The physics involved are described by Equation [4.28], the "Clausius-Clapeyron" equation. While some authors dispute the appropriateness of the name (Loch, 1978; Daniels and Alberty, 1975), others support it (Adkins, 1983). Never-the-less, the equation does describe the pertinent physics.

```
C This version created on DATE=10-26-86 TIME=21 16 37
C     ********************************************************
C     **                                                    **
C     **          LE SOULEVEMENT UNIDIRECTIONEL DU AU GEL   **
C     **                                  --BY JEAN-MARIE KONRAD **
C     ********************************************************
C     **     THIS PROGRAM HAS BEEN RE-TYPED IN AND COMMENTED BY **
C     **  MYSELF OVER A GREAT LENGTH OF TIME SO GOD HELP ANYONE **
C     **  WHO LOSES IT.                                     **
C     ***                                --- PATRICK COLLINS, MAY 1984 **
C     **                                                    **
C     **     This version differs from the original Konrad, PhD **
C     **  version in that some of the variables are renamed for **
C     **  clarity and that some software changes have been made **
C     **  These are:                                        **
C     **                                                    **
C     **              * inclusion of the pressure effects in **
C     **                subroutine 'SURF'                   **
C     **                                                    **
C     **    . Konrad's use of a modified frozen gradient is dis- **
C     **  putable (Collins, 1987).  However, because the original **
C     **  work uses "DERTF" and the "SURF" subroutine is in terms **
C     **  of this variable, no major changes were made.     **
C     **                                                    **
C     **  The calorie to Joule conversion factor was changed **
C     **  from 4 1855 to the thermochemical value of 4 1840 **
C     **                                                    **
C     ********************************************************
C
C   *  PROGRAM TO SIMULATE ONE-DIMENSIONAL UNSTEADY HEAT FLOW IN
C      A FREEZING SOIL AND TO CALCULATE THE HEAVE WITH
C      TIME AS WELL AS THE ICE CONTENT PROFILE.
C   *  CALCULATES THE THICKNESS OF THE FINAL ICE LENS DURING THE
C      OCCURRENCE OF A RETREATING FROST FRONT FOR FIXED UPPER AND
C      LOWER TEMPERATURE BOUNDARY CONDITIONS.
C   *  THE CRANK-NICHOLSON FINITE DIFFERENCE METHOD IS USED.
C      A FIXED GRID WITH A SUPPLEMENTARY NODE AT THE INTERFACE
C      PERMITS THE MOVING BOUNDARY SITUATION
C   *  FROZEN AND UNFROZEN SOIL THERMAL PROPERTIES ARE CONSIDERED
C      AS INDEPENDENT WITH TEMPERATURE.  WATER REMAINING UNFROZEN
C      BELOW ZERO DEGREES Celsius IS TAKEN INTO ACCOUNT BY THE
C      LUMPED PARAMETER EPS.
C   *  THE PHYSICS OF WATER MIGRATION TO THE SEGREGATION-FREEZING
C      FRONT HAS BEEN ADDED.  THE SEGREGATION POTENTIAL IS DEFINED
C      AS THE RATIO OF THE WATER INTAKE RATE AND THE TEMPERATURE
C      GRADIENT IN THE FROZEN FRINGE AND IS DEPENDENT ON THE RATE
C      OF COOLING OF THE FRINGE AND SUCTION AT THE FROST FRONT.
C   *  THE CHARACTERISTIC FREEZING SURFACE OF A GIVEN SOIL IS
C      OBTAINED FROM EXPERIMENTAL DATA.
C   *  THE PROGRAM CAN INCORPORATE ANY SPECIFIED COLD AND WARM
C      SIDE TEMPERATURE VARIATION.  NO LOAD IS APPLIED TO THE
C      SAMPLE IN THE FOLLOWING MODEL.  HOWEVER, A DIFFERENT
C      CHARACTERISTIC FREEZING SURFACE CORRESPONDING TO THE
C      DESIRED SURCHARGE IS SUFFICIENT FOR PREDICTION OF FROST
C      HEAVE UNDER EXTERNAL LOADS WITH THIS MODEL
C
C   RUN COMMAND: $RUN KONRAD.OBJ 5=1/P 6=0/P1 7=0/P2 7=2SECONDS
C
C  ------------------------------------------------------------
C
C   THE FOLLOWING ARE ASSUMED PURPOSES FOR THE VARIABLES AND
C   MAY NOT BE ENTIRELY CORRECT.  THE ORIGINAL VERSION OF THIS
C   PROGRAM IS APPENDED TO KONRAD'S THESIS.  - P.M. COLLINS
C
C     AREA     CROSS-SECTIONAL AREA                          [ cm**2 ]
C     CAF      "APPARENT" (VOLUMETRIC) HEAT CAPACITY, FROZEN
C     CAU      "APPARENT" (VOLUMETRIC) HEAT CAPACITY, UNFROZEN
C     CF       THERMAL CONDUCTIVITY, FROZEN SOIL          [cal/s/m/C]
C     CFE      THERMAL CONDUCTIVITY, FR SOIL & ICE        [cal/s/m/C]
C     CFR      THERMAL CONDUCTIVITY, FROZEN FRINGE        [cal/s/m/C]
C     CI       THERMAL CONDUCTIVITY, ICE                  [cal/s/m/C]
C     CU       THERMAL CONDUCTIVITY, UNFROZEN SOIL        [cal/s/m/C]
C     CUE      FINAL STEADY-STATE THERMAL COND , UNFROZEN SOIL
C     CUI      INITIAL STEADY-STATE THERMAL COND , UNFROZEN SOIL
C     DH       INCREMENTAL HEAVE                                | mm  |
C     DT       TIME STEP INCREMENT                              | seconds |
C     DX       INCREMENTAL FROST PENETRATION INTO THE SOIL      | mm  |
C     EPS      FRACTION OF IN-SITU WATER THAT FREEZES
C     EPSIL    MIN  COOLING RATE, OTHERWISE CALCS CONTINUE  | C/hr |
C     F        FRACTION UNFROZEN IN THE PARTIALLY FROZEN SEGMENT
C     FA       NOT USED ANYWHERE IN THE PROGRAM
C     FG       STOPS CALCS WHEN STEADY STATE EXISTS IF FG>2
C     GRADT    TEMPERATURE GRADIENT                             | C/mm |
C     HINT     INTAKE HEAVE                                     | mm |
C     HR       TIME                                             | hr |
C     HRC      "DT" IN HOURS INSTEAD OF SECONDS                 | hr |
C     HRF      NOT USED IN THE PROGRAM
C     HRL      A TRIGGER TIME FOR OUTPUT?                       | hr |
C     HRL2     A TIME LIMIT                                     | hr |
C     HR1      TIME THAT TC1 & TW1 EXIST UNTIL                  | hr |
C     HR2      TIME THAT TCF & TWF BEGIN AT                     | hr |
C     HT       TOTAL HEAVE                                      | mm |
C     KEY      TRIGGER TO INTERPOLATE VARYING PLATE TEMPS IF KEY 17 )
C     NJ       NUMBER OF SEGMENTS .
C     NP.      NUMBER OF COMPLETELY UNFROZEN LENGTHS
C     P        SUCTION                                | metres H20 |
C     PARA     PRESSURE CORRECTION FACTOR FOR TSO           | C/MPa |
C     PARB1    PRESSURE CORRECTION FACTOR FOR PERMU1    | mm/s/MPa |
C     PARB2    PRESSURE CORRECTION FACTOR FOR PERMU2    | mm/s/MPa |
C     PARC     PRESSURE CORRECTION FACTOR FOR SPO  |mm**2/(C*s)/MPa|
C     PE       APPLIED STRESS                               | MPa |
C     PERMU1   UNFROZEN PERMEABILITY                        | mm/s |
C     PERMU2   UNFROZEN PERMEABILITY OF SECOND MATERIAL     | mm/s |
C     POR      POROSITY
C     PU1      NOT USED IN THE PROGRAM
C     RC       RATE OF COOLING                              | C/hr |
C     RCC      LIMITTING RATE OF COOLING                    | C/hr |
C     SP       SEGREGATION POTENTIAL                | mm**2/(C*s)|
C     SPFIXD   USER-SPECIFIED SEGREGATION POTENTIAL ? mm**2/(C*s)?
C     TC       APPLIED COLD TEMPERATURE                  | celsius |
C     TCF      FINAL COLD STEP TEMPERATURE               | celsius |
C     TCI      INITIAL COLD STEP TEMPERATURE             | celsius |
C     TD       DELTA TIME                                | seconds |
C     TSO      SEGREGATION FREEZING TEMPERATURE          | celsius |
C     TVOL     TOTAL VOLUME                                 | ML |
C     TW       APPLIED WARM TEMPERATURE                  | celsius |
C     TWF      FINAL COLD STEP TEMPERATURE               | celsius |
C     TWI      INITIAL WARM STEP TEMPERATURE             | celsius |
C     W        HEAT FLOW                            | N))))watts |
C     X        FROZEN THICKNESS                             | mm |
C     XS       FROZEN AND HEAVED HEIGHT                     | mm |
C     V        INFLOW VELOCITY                          | mm/s |
C     Z        UNFROZEN LENGTH                              | mm |
C     ZS       UNFROZEN AND FROZEN FRINGE HEIGHT            | mm |
C     ZU       INITIAL UNFROZEN LENGTH                      | mm |
C     ZU2      LENGTH OF MAT'L WITH PERMU2, IN SERIES WITH PERMU1
C
C
C
C
      REAL A(2000),B(2000),C(2000),D(2000),AA(2000),BT(2000),
     *     DD(2000),DY(200),ZA(200),DWC(200),HI(200),HS(200)
      REAL TWARM(2000),TCOLD(2000),VD(2000),S(200),XP(200),FY(200)
C
      REAL TITLE(20)
C
C                                                  default I/O units
      CALL FTNCMD('DEFAULT  $CARDS=KONRAD )/P,')
      CALL FTNCMD('DEFAULT  $PUNCH=-K8,')
      CALL FTNCMD('DEFAULT  7=-K7,')
```

```
      CALL FTNCMD('DEFAULT  6=-SEGS;')
      CALL FTNCMD('DEFAULT  9=-TOTS;')
      CALL FTNCMD(' EQUATE  5=SCARDS;')
      CALL FTNCMD(' EQUATE  6=SPUNCH;')
C
C ..................ENTER THE PARAMETERS NECESSARY FOR SOLUTION
C
      READ(5,10) TITLE
      READ(5,1) KEY,NI,DT,EPSIL
      READ(5,2) TC,TW,CF,CFR,CU,CAF,CAU
      READ(5,3) ZU,AREA,POR,EPS,HRL
      READ(5,4) ZU2,PERMU1,PERMU2
      READ(5,5) HR1,HR2,TCI,TCF,TWI,TWF
      READ(5,6) HRF,HRL2,FA
C ..................... [ N.B. "TSO" replaces Konrad's "TS" ]
      READ(5,7) FG,TSO,RCC,CUE,CUI,TD
      READ(5,8) PE,PARC
      READ(5,9) SPFIXD
    1 FORMAT(2I5,2F10.8)
    2 FORMAT(2PF 0.5E10.0)
    3 FORMAT(5F10.2)
    4 FORMAT(F10.2,2E10.3)
    5 FORMAT(5F10.2)
    6 FORMAT(3F10.2)
    7 FORMAT(8F10.4)
    8 FORMAT(5F10.2)
    9 FORMAT(E10.3)
   10 FORMAT(20A4)
C                                        SP CORRECTION IN SUBR  "SURF"
C                                                          SI Units
      SICF=CF*4.184
      SICFR=CFR*4.184
      SICU=CU*4.184
      SICAF=CAF*4.184
      SICAU=CAU*4.184
      WRITE(6,100)TITLE
      WRITE(7,100)TITLE
      WRITE(8,100)TITLE
      WRITE(9,100)TITLE
  100 FORMAT('1'/20X,20A4//)
      WRITE(6,55)ZU,POR,EPS,CF,SICF,CFR,SICFR,CU,SICU,
     * CAF,SICAF,CAU,SICAU,PERMU1,NI,EPSIL,AREA,TC,TW
   55 FORMAT(20X,'DATA INPUT'//
     +/9X,'INITIAL UNFROZEN LENGTH IS :',T50,F10.4,' mm'
     +/9X,'POROSITY IS :',T50,F10.4
     +/9X,'PHASE CHANGE FOR :',T50,F10.4,' OF INITIAL WC'
     +/9X,'FROZEN THERMAL CONDUCTIVITY IS :',T50,F10.4,
     +    ' cal/s/m/C'  /T75,F10.4,' W/(m K)'
     +/9X,'FROZEN FRINGE THERMAL CONDUCTIVITY IS :',T50,F10.4,
     +    ' cal/s/m/C'     /T75,F10.4,' W/(m K)'
     +/9X,'UNFROZEN THERMAL CONDUCTIVITY IS :',T50,F10.4,
     +    ' cal/s/m/C'     /T75,F10.4,' W/(m K)'
     +/9X,'Volumetric Heat Capacity, Frozen :',T50,0PF10.4,
     +    ' cal/cc/C',T75,F10.4,' KJ/(m**3 K)'
     +/9X,'Volumetric Heat Capacity, Unfrozen :',T50,0PF10.4,
     +    ' cal/cc/C',T75,F10.4,' KJ/(m**3 K)'
     +/9X,'UNFROZEN PERMEABILITY IS :',T50,1PE10.3,' mm/s'
     +/9X,'NUMBER OF SEGMENTS :',T50,I10
     +/9X,'Minimum Cooling Rate :',T50,0PF10.4,' C/hr'
     +/9X,'Cross-Sectional Area :',T50,0PF10.4,' cm**2'
     +/9X,'COLD SIDE TEMPERATURE :',T50,0PF10.4,' celsius'
     +/9X,'WARM SIDE TEMPERATURE :',T50,F10.4,' celsius')
C
      IF(KEY.LT.1) WRITE(6,559)HR1,HR2,TCI,TCF,TWI,TWF
  559 FORMAT(/ ,9X,'Time at End of Initial Temps :',T50,F10.4,' hr'
     +/9X,'Time at Start of Final Temps :',T50,F10.4,' hr'
     +/9X,'Initial Cold Temperature     :',T50,F10.4,' celsius'
     +/9X,'Final   Cold Temperature     :',T50,F10.4,' celsius'
     +/9X,'Initial Warm Temperature     :',T50,F10.4,' celsius'
     +/9X,'Final   Warm Temperature     :',T50,F10.4,' celsius')
C
      WRITE(6,551)FG,TSO,RCC,CUE,CUI,TD,PE,PARC
  551 FORMAT(/   9X,'FG is                    ',T50,   F10.4,
     +/9X,'TSo Segregation Freezing Temp ',T50,F10.4,' Celsius'
     +/9X,'Limiting Rate of Cooling      ',T50,F10.4,' C/hr'
     +/9X,'Final Steady-State Unf  Therm  Cond.',T51,F8.4,' cal/(m s C)'
     +/9X,'Init. Steady-State Unf  Therm. Cond.',T51,F8.4,' cal/(m s C)'
     +/9X,'Delta Time                    ',T50,F10.4,' seconds'
     +/9X,'Applied Stress                ',T50,F10.4,' MPa'
     +/9X,'Pressure Correction ("c")',T50,F10.4,' mm**2/(s C)/MPa')
C                                                      FIXED SP VALUE
      IF(SPFIXD.LT.1.E-10)GO TO 578
      WRITE(6,577)SPFIXD
  577 FORMAT(/
     +9X,'Fixed value of SP (unloaded) is',T50,E10.3,' mm**2/(s C)')
      GO TO 580
  578 WRITE(6,579)
  579 FORMAT(9X,'SP freely determined within the SPTL subroutine ')
  580 CONTINUE
C                                                 INITIAL NODAL SEPARATION
      DZ=ZU/NI
      WRITE(6,51)DT,DZ
   51 FORMAT(//,10X,'THE TIME STEP IS  ',T50,F10.2,' SECONDS'
     +/10X,'The Initial Node Separation is  ',T50,F10.4,' mm')
C
      WRITE(9,901)
  901 FORMAT('       TIME     TOTAL HEAVE')
      WRITE(8,801)
  801 FORMAT('       TIME    ATTRACTED H ')
C
COMM        BETA= ALPHA*DT/DZ**2   WHERE ALPHA=D2U/DZ**2 = DU/DT
C
      BETA=DT*CU/(DZ*DZ*CAU)
C
C                *** * * INITIALIZE THE UNKNOWNS * * ***
C
C                                  "SP" replaces Konrad's "HP"
      SP=0
      PU1=0
      GRADT=0
      W=0
      H(1)=0
      DF=0
C                                                 THERMAL CONDUCTIVITY OF ICE
      C1=0.9
C                                          ARBITRARY INITIAL RATE OF COOLING
      RC=3
      V=0.000
      HR=0
      TIME=0
      TVOL=0
      DPM=0
      HINT=0.
      HTP=0
      Z=ZU
      X=0
      TPR1=0.5
      TPR2=10
      TPR3=110
      TPR4=2.
      TP4=2.
      TPR8=10
      TP8=10
      KO=1
      KOU=1
      JO=1
      TPRS=HLIM+0.1
      P=0
C                                                 OUTPUT HEADINGS, UNIT 6
      WRITE(6,150)
```

```
  150 FORMAT('1',//,'      TIME UNFROZEN FROZEN COOLING  SUCTION',
     +'     SP      GRAD T    INFLOW    TOTAL    INTAKE    TOTAL  POWER'
     +/11X,' LENGTH  LENGTH    RATE',10X,'  (mm**2)  ',8X,
     +'VELOCITY  VOLUME   HEAVE',
     +'    HEAVE'//'0',T47,'  ____',
     +/'      (hr)    (mm)     (mm)     (C/hr)   (m H2O)   ( s*C )  ',
     +'  (C/mm)    (mm/s)     (m3)     (mm)     (mm)   (m3)(1-W)')
C
C     ***********************************************************
C     **                                                       **
C     **      CALL OUTPUT(HR,Z,X,RC,P,SP,GRADT,V,TVOL,HINT,HT,W)
C     **                                                       **
C     ***********************************************************
      TIME=TIME+DT
      ZM=ZU
      CR=CF-CU
      XO2=ABS((DT*CK+Z*TC)/(EPS*POR+79.6))
      XO=SQRT(XO2)
      DH=0.09*POR*EPS*XO
C                                                 TOTAL UNFROZEN LENGTH
      Z=ZU+DH-XO
C
      HT=DH
C
      K=N1-1
      M=1
      MM=1
C                                    INITIALIZES SOIL TEMP TO TW ...
      DO 13 I=1,K
   13 TWARM(I)=TW
C                                    ...FIRST NODE SET TO 0.5*TC
      TCOLD(1)=TC*0.5
      TCOLD(2)=0
C
C
C     ((((((((((((((((( BEGINNING OF THE TIME LOOP ))))))))))))))))
C
C
 1000 TIME=TIME+DT
      HR=TIME/3600.
C
C       *** * * SOLVE FOR TEMPERATURES IN THE UNFROZEN SOIL * * ***
C                                    NUMBER OF UNFROZEN SEGMENTS
      NP=Z/DZ
C                                    ... ADDITIONAL FRACTION OF A SEGMENT
      F=Z/DZ-NP
      N=NP
C                                    ... SET BOUNDARY NODE TEMP. TO ZERO
      TWARM(N+1)=0.
      NB=N-1
      A(1)=2. +2.*BETA
      B(1)=-BETA
      C(1)=0.
      D(1)=2.*BETA*TW+(2.-2.*BETA)*TWARM(1)+BETA*TWARM(2)
C
         DO 14 I=2,NB
         A(I)=2. +2.*BETA
         B(I)=-BETA
         C(I)=-BETA
   14    D(I)=BETA*TWARM(I-1)+(2.-2.*BETA)*TWARM(I)+BETA*TWARM(I+1)
C
      B(N)=0.
      A(N)=BETA+F
      C(N)=-BETA*F/(1.+F)
      D(N)=BETA*F*TWARM(N-1)/(1.+F)+(F-BETA)*TWARM(N)
C
C     ***********************************************************
C     **                                                       **
C     **                 CALL GAUSEL(A,B,C,D,N)                **
C     **                                                       **
C     ***********************************************************
C
C
C                                                 SET WARM TEMPS TO C(I)
      DO 16 I=1,N
   16 TWARM(I)=C(I)
      IF(HR.GE.10) GO TO 612
C                                    WRITE TEMPS EVERY TP4 HOURS FOR TEN HOURS
      IF(HR.GE.TP4) GO TO 610
      GO TO 600
  610 TP4=TP4+2.
C                                    WRITE WARM TEMPS EVERY TP4 HOURS
  613 WRITE(7,611)HR,TW,(TWARM(I),I=1,N)
  611 FORMAT('///' ELAPSED TIME =',F10.2,' HOURS'//' TEMPERATURES ',
     +10(/8F8.2))
      GO TO 600
  612 IF(HR.LT.TP6) GO TO 600
      TP6=TP6+10
C                                    WRITE TEMPS EVERY TP6 HOURS
      GO TO 613
C                                 UNFROZEN THERMAL GRADIENT OVER )+ SEGMENTS
  600 DERTU=(TWARM(N-1))/((1.+F)*DZ)
      ST=K+ZU/N1
C                 TRANSFER TO 22 IF MORE THAN ONE SEGMENT IS FROZEN
      IF(2.LE.ST) GO TO 22
      IF(M.GT.2) GO TO 29
      IF(M.GT.1) GO TO 23
      H(1)=H(1)+DH
C                                    FROZEN LENGTH OF FIRST SEGMENT
      DY(1)=DZ*H(1)-F*DZ
C                                    FROZEN THERMAL GRADIENT
      DERTF=ABS(TC/DY(1))
C                                    FROZEN FRINGE THERMAL GRADIENT
      GRADT=CF*DERTF/CFR
C                                    TRANSFER TO THE CONTINUITY CALCS.
      GO TO 90
C
C
   22 IF(M.GT.1) GO TO 21
      DY(1)=DZ*H(1)
      GO TO 21
   21 DWC(M)=.9*.74*H(M)/((1.-POR)*DZ*2.7)
      DY(M)=DZ*H(M)
C
C
      K=K-1
      M=M+1
      MM=M-1
   29 HS(MM)=HS(MM-1)+H(MM)
C
   23 HS(1)=H(1)
      H(M)=HT-HS(MM)
      DY(M)=DZ*H(M)-F*DZ
      G=DY(M)/DY(M-1)
      MP=N1-1-NP
      IF(MP.LE.1) GO TO 31
      N=MP
      NK=N-1
C
C.....................SOLVE FOR TEMPERATURES IN THE FROZEN SOIL
C                     (POSSIBLE VARIATION OF COLD STEP TEMPERATURE)
C
C                                    ... SKIP INTERPOLATION IF KEY>1
      IF(KEY.GT.1) GO TO 510
      IF(HR.GE.HR1) GO TO 501
C                                    ... USE INITIAL TEMPERATURES
      TC=TC1
      TW=TW1
      GO TO 510
  501 IF(HR.GE.HR2)GO TO 502
C                                    ... INTERPOLATE TEMPERATURES
```

```
      TC=TCI-(TCI-TCF)*(HR-HR1)/(HR2-HR1)
      TW=TWI-(TWI-TWF)*(HR-HR1)/(HR2-HR1)
      GO TO 510
C                                                  ... USE FINAL TEMPERATURES
  502 TC=TCF
      TW=TWF
  510 TCOLD(N+1)=0.
          DO 26 I=1,NK
          DD(I)=DY(I)+DY(I+1)
          BT(I)=CF*DT/(CAF*DD(I))
          AA(I)=BT(I)*((1./DY(I+1))+(1./DY(I)))
          C(I)=-BT(I)/DY(I)
          B(I)=-BT(I)/DY(I+1)
   26     A(I)=AA(I)+1.
      C(1)=0
      D(1)=(+2.*BT(1)/DY(1))*TC-(AA(1)-1.)*TCOLD(1)-B(1)*TCOLD(2)
      IF(NK.LE.1) GO TO 37
          DO 27 I=2,NK
   27     D(I)=-C(I)*TCOLD(I-1)-(AA(I)-1.)*TCOLD(I)-B(I)*TCOLD(I+1)
   37 B(N)=0.
C                                          BETA FACTOR FOR FROZEN SOIL
C
      BETAF=(CF*DT)/(CAF*DY(N-1)+DY(N-1))
      A(N)=BETAF+G
      C(N)=-BETAF*G/(1.+G)
      D(N)=BETAF*G*TCOLD(N-1)/(1.+G)+(G-BETAF)*TCOLD(N)
C
C     ***************************************************************
C     **                                                           **
C     **                CALL GAUSEL(A,B,C,D,N)                     **
C     **                                                           **
C     ***************************************************************
C
          DO 28 I=1,N
   28     TCOLD(I)=C(I)
      IF(HR.GE.10.) GO TO 712
      IF(HR.GE.TPR4) GO TO 710
      GO TO 700
  710 TPR4=TPR4+2.
C                                                  WRITE COLD TEMPERATURES
  713 NREVRS=N+1
      WRITE(7,711)(TCOLD(NREVRS-I),I=1,N),TC
  711 FORMAT(8F8.2)
      GO TO 700
  712 IF(HR.LT.TPR5) GO TO 700
      TPR5=TPR5+10.
      GO TO 713
C
C
C                                          FROZEN THERMAL GRADIENT
  700 DERTF=ABS(TCOLD(N-1)/(DY(N)+DY(N+1)))
C                                     FROZEN FRINGE THERMAL GRADIENT
      GRADT=CF*DERTF/CPR
C     (NOTE: BILL HORNE IS USING GRADT=(CF*DERTF-V*79.8)/CPR  )
C
      GO TO 50
C                                          FROZEN THERMAL GRADIENT
   31 DERTF=ABS(TC/(DY(1)+DY(2)))
C                                     FROZEN FRINGE THERMAL GRADIENT
      GRADT=CF*DERTF/CPR
C     (NOTE: BILL HORNE IS USING GRADT=(CF*DERTF-V*79.8)/CPR  )
C
C
C.....SOLVE FOR CONTINUITY AT THE INTERFACE AND CALCULATE HEAVE
   50 NRC=DT/3600.
      IF(NR.ST.NRL2) GO TO 388
      IF(NR.GE.NRC) GO TO 389
      GO TO 483
C                                  KONRAD PHD THESIS, (EQ'N  6.14)
  388 RC=(1000./DT)*(DERTF*(2*DX*DFM)-0.1)
      DFM=0.1/DERTF
C                                                  EQUIVALENT PERMEABILITY
  390 IF(Z.LE.ZU2) GO TO 395
      PERMU=Z/((Z-ZU2)/PERMU1)+(ZU2/PERMU2))
      GO TO 398
  395 PERMU=PERMU2
  398 S(1)=0
          DO 470 J1=1,9
C                                                  ... SUCTION   [ M H20 ]
          P=S(J1)
C     ***************************************************************
C     **                                                           **
C     **  CALL SURF(POO,P01,P05,P1,P2,P5,P10,P,SP,RC,PE,PARC,SPF)XD)
C     **                                                           **
C     ***************************************************************
          XP(J1)=SP
          IF(XP(1).LE.0.) GO TO 483
          FY(J1)=(XP(J1)*GRADT-(S(J1))*1000.*(PERMU/Z))*1.E+05
          J1J=J1+1
          S(J1J)=S(J1)+1
  470     CONTINUE
      XP(9)=0
C
          DO 471 J1=1,9
          IF(FY(J1).LT.0.) GO TO 472
  471     CONTINUE
C
  472 P=(FY(J1-1)*S(J1)-FY(J1)*S(J1-1))/(FY(J1-1)-FY(J1))
C     ***************************************************************
C     **                                                           **
C     **  CALL SURF(POO,P01,P05,P1,P2,P5,P10,P,SP,RC,PE,PARC,SPF)XD)
C     **                                                           **
C     ***************************************************************
C
C.....CALCULATE THE WATER FLUX AND FROST FRONT PENETRATION RATE
C
C                    NB  GRADT DERIVED FROM FROZEN THERMAL GRADIENT
  451 V=SP*GRADT
      R=DERTF/DERTU
C
C
      RS=CU/(CF-179.8*SP))
C
C
C                                                  LATENT HEAT POWER GAIN
      W=(CF*DERTF-CU*DERTU)*4.1840
C
C                    GO TO 1500 FOR RETREATING FROST FRONT PHASE
      IF(R.GE.RS) GO TO 1500
      GO TO 450
  483 V=0.
C                                                  LATENT HEAT POWER GAIN
      W=(CF*DERTF-CU*DERTU)*4.1840
      JO=1
C                                     INCREMENTAL FROST PENETRATION
C
  450 DX=DT*(CF*DERTF-CU*DERTU-V*79.8)/(EPS*POR*79.8)
C     DX=TIME*(NET POWER/AREA FOR INSITU)/(INSITU LATENT HEAT/VOL)
      IF(DX.LT.0.)  GO TO 1500
C                                                  INC  INSITU HEAVE
      DHEX=0.09*EPS*POR*DX
C                                                  INC  INTRO  HEAVE
      DHIN=1.09*V*DT
C                                                  TOTAL INC  HEAVE
      DH=DHEX+DHIN
      HT=HT+DH
C                                                  TOTAL INTRO  HEAVE
      HINT=HINT+DHIN
C                                                  INCR  INTRO  WATER
```

```
      DVOL=V*DT*AREA*0.1
C                                                  ... TOTAL INTRO. WATER
      TVOL=TVOL+DVOL
C                                                  .... UNFROZEN HEIGHT
      Z=Z+DX
C                                                  ... HEAVE + FROZEN HEIGHT
      X=ZU+HT-Z
C
      IF(RC.LT.0.) GO TO 35
      IF(RC.LE.RCC) GO TO 341
      GO TO 35
  341 KOU=KOU+1
C     (NB. THE FOLLOWING LINE DIFFERS FROM KONRAD'S ORIGINAL PROGRAM
C          WHICH FAILED TO UPDATE THE VALUES OF "XS" AND "ZS"  )
C
      IF(KOU.LE.2) GO TO 35
C                                          FRINGE + UNFROZEN HEIGHT
C                                                (NB: UNFR  GRADIENT USED)
C                        (NB: KONRAD DOESN'T TAKE THE ABSOLUTE VALUE)
      ZS=Z+ABS(TS/DERTU)
C                                        HEAVE + FROZEN + FRINGE HEIGHT
      XS=X+Z-ZS
C
   35 IF(HR.GE.HRL) GO TO 1500
      IF(HR.GE.110.) GO TO 40
      IF(HR.GE.10.) GO TO 36
      IF(HR.GE.TPR1) GO TO 34
C                                                  ... ANOTHER TIME STEP
      GO TO 1000
   34 TPR1=TPR1+0.5
C                                        PRINT EVERY HALF-HOUR FOR 10 HR
C     ****************************************************************
C     **                                                            **
C          CALL OUTPUT(NR,Z,X,RC,P,SP,GRADT,V,TVOL,HINT,HT,W)
C     **                                                            **
C     ****************************************************************
C
      IF(RC.LE.EPSIL) GO TO 1500
      GO TO 1000
C                                                  ... ANOTHER TIME STEP
   36 IF(HR.GE.TPR2) GO TO 38
      GO TO 1000
C                 (((((((( END OF TIME STEP IF NO PRINTING ))))))))
   38 TPR2=TPR2+1.
C                                        PRINT EVERY HOUR AFTER 10 HR
C     ****************************************************************
C     **                                                            **
C          CALL OUTPUT(NR,Z,X,RC,P,SP,GRADT,V,TVOL,HINT,HT,W)
C     **                                                            **
C     ****************************************************************
      IF(RC.LE.EPSIL) GO TO 1500
C                                                  ... ANOTHER TIME STEP
      GO TO 1000
C
   40 IF(HR.GE.TPR3) GO TO 42
      GO TO 1000
C                                                  ... ANOTHER TIME STEP
C
   42 TPR3=TPR3+10.
C     ****************************************************************
C     **                                                            **
C          CALL OUTPUT(NR,Z,X,RC,P,SP,GRADT,V,TVOL,HINT,HT,W)
C     **                                                            **
C     ****************************************************************
C
      IF(RC.LE.EPSIL) GO TO 1500
C                                                  ... ANOTHER TIME STEP
      GO TO 1000
C       (((((((((( END OF TIME STEP IF PRINTING WAS DONE ))))))))))
C
C
C
C     ****************************************************************
C     **                                                            **
 1500       CALL OUTPUT(NR,Z,X,RC,P,SP,GRADT,V,TVOL,HINT,HT,W)
C     **                                                            **
C     ****************************************************************
C
C
C
C
C
C
C
C                    FROST HEAVE DURING THE RETREATING FROST FRONT PHASE
      IF(FC.GT.2) GO TO 1505
      TIB=HR
      TJF=TJB+TD
      VO=V
      DH=0
      DTIME=0
      WRITE(7,72) DH, VO, DTIME
   72 FORMAT(6X,'DH= ',F10.2,6X,'VO= ',1PE10.4,3X,'DTIME= ',0PF10.1)
C
C              EVENTUAL HEIGHT OF FINAL ICE LENS (KONRAD, EQ'N 5.4 )
      HM=(C1*ABS(TC)+ZS/(CUE*TW))*(C1*XS/CF)
C                                                 ARBITRARY DIVISION INTO 40
      HE=HM/40.
      DFF=(ZS-Z)/40.
C                                                 INCREMENTING THE HEAVE
   70 DH=DH+HE
      Z=Z+DFF
C                                                 PROGRAM STOPS + ***
      IF(Z.GT.ZS) GO TO 32
      DERTF=ABS(TC)/(XS+DH)
      DERTU=TW/Z
C                          EFFECTIVE THERMAL CONDUCTIVITY, FROZEN + ICE
      CFE=(XS+DH)/((XS/CF)+(DH/C1))
      IF(HR.GT.TJF) GO TO 73
C                                  INTERPOLATE ON UNFR  THERMAL K **
      CUE=CU1+((CUE-CU1)*(HR-TIB)/TD)
      GO TO 75
   73 CUE=CUE
C
   75 V=(DERTF*CFE-(DERTU*CUE))/75.6
      IF(V.GT.0) GO TO 71
      V=0.
C                                                 CALC TIME FOR HE TO OCCUR
   71 DTI=2.*HE/(1.09*3600.*(VO+V))
      DTIME=DTIME+DTI
      HR=HR+DTI
      HT=HT+HE
      HINT=HINT+HE
      X=X+HE
C
      DVOL=HE*AREA/10.8
      TVOL=TVOL+DVOL
C
C     ****************************************************************
C     **                                                            **
C          CALL OUTPUT(NR,Z,X,RC,P,SP,GRADT,V,TVOL,HINT,HT,W)
C     **                                                            **
C     ****************************************************************
C
      WRITE(7,772)DH,V,DTIME
  772 FORMAT(6X,'DH= ',F10.2,7X,'V= ',1PE10.4,3X,'DTIME= ',0PF10.1)
C
C                                                 REDEFINE INITIAL VELOCITY
      VO=V
      GO TO 70
 1505 WRITE(6,1501)
```

```
 1501 FORMAT(//,'      STEADY TEMPERATURE STATE HAS BEEN REACHED')
      WRITE(7,599)
  599 FORMAT('1'//18X,'LENGTH OF          INCREASE IN'/
     +18X,          'UNFROZEN SOIL      WATER CONTENT'/
     +18X,          '(MM)               (% DRY WEIGHT)'//)
C
      DR=(1.-P)*DZ
      DWC(M)=81.74*H(M)/((1.-PDR)*DR*2.7)
      ZA(1)=Z+X-DY(1)/2
C
          DO 1502 I=2,M
 1502     ZA(I)=ZA(I-1)-DY(I)
C                 UNFROZEN SOIL LENGTHS AND WATER CONTENT INCREASE
      WRITE(7,501) (ZA(I),DWC(I),I=1,M)
  501 FORMAT(15X,F10.2,10X,F10.2)
   32 STOP
      END
C
C
C
C     ****************************************************************
C     **                                                            **
C     **    SUBROUTINE OUTPUT(HR,Z,X,RC,P,SP,GRADT,V,TVOL,HINT,HT,W)
C     **                                                            **
C     ****************************************************************
C
      WRITE(6,151) HR,Z,X,RC,P,SP,GRADT,V,TVOL,HINT,HT,W
  151 FORMAT(2X,3F8.2,F8.4,F8.2,2X,1PE8.2,0PF8.4,1PE10.2,
     + 0P3F8.3,F8.4)
      WRITE(8,851) HR,HINT
  851 FORMAT(F10.2,',',F14.2)
      WRITE(9,951) HR,HT
  951 FORMAT(F10.2,',',F10.2)
      RETURN
      END
C
C
C
C     ****************************************************************
C     **                                                            **
C     **              SUBROUTINE GAUSEL(A,B,C,D,N)                  **
C     **                                                            **
C     ****************************************************************
C
      REAL A(1),B(1),C(1),D(1)
C
      IF(N.GT.1) GO TO 3
      C(N)=D(N)/A(N)
      GO TO 2
C
    3     DO 1 I=2,N
          A(I)=A(I)-B(I-1)*C(I)/A(I-1)
          D(I)=D(I)-D(I-1)*C(I)/A(I-1)
    1     C(I)=0.
      C(N+1)=0.
      I=N
    4 C(I)=(D(I)-B(I)*C(I+1))/A(I)
      IF(I.LE.1) GO TO 2
      I=I-1
      GO TO 4
C
    2 RETURN
      END
C     ****************************************************************
C     **                                                            **
C     **  SUBROUTINE SURF(P00,P01,P0S,P1,P2,PS,P10,P,SP,RC,PE,PARC,SPFD)
C     **                                                            **
C     **      THIS SUBROUTINE GIVES THE FUNCTIONAL RELATIONSHIP     **
C     **   BETWEEN SP, PU, AND THE RATE OF COOLING OF THE FRINGE    **
C     **   FOR DEVON SILT WITH PE=0.  PE EFFECTS HAVE BEEN ADDED    **
C     **   TO THE SUBROUTINE USING THE "PARC" VALUE.  SPFD TRANSFERS**
C     **   A CONSTANT VALUE OF SP THAT IS MODIFIED BY THE STRESS.   **
C     ****************************************************************
C                                                      Fixed Value of SP
      IF(SPFD.LT.1.E-10) GO TO 359
      SP=SPFD
      GO TO 300
C
  359 CONTINUE
C
      IF(P.LT.0.1) GO TO 302
      SP=0.
      GO TO 300
  302 IF(P.LT.2.) GO TO 532
      P00=(8.-P)**2.2/6.
      P01=(8.-P)**3./6.
      GO TO 534
C
  532 P00=(8.-P)**2.2/6. + .75*(2.-P)**2
      P01=(8.-P)**3./6.+1.2*(2.-P)**2+1.735
  534 P2=6.53-0.36*P+  .1076*P**2   - 0.0306*P**3   + 0.00125*P**4
      P5=3.76+ .0784*P -  .119*P**2   +  .03105*P**3   -  .003087*P**4
      P10=2.19+ .0722*P -  .05986*P**2   +  .015867*P**3 - .0017241*P**4
C
      IF(P.LT.6.) GO TO 520
      P1=(8.-P)**2.2/2.
      P0S=(8.-P)**1.7/2.
      GO TO 304
  520 IF(P.LT.1.5) GO TO 521
      P1=2.2*(8.-P)**7.3/4.5
      P0S=1.7*(8.-P)**8.2/4.5
      GO TO 304
C
  521 P1=(7.35-P)*(10.9/7.35-(0.5*(1.5-P)**1.7)
      P0S=(7.35-P)*(10./7.35-(0.4*(1.5-P)**1.4)
C
  304 IF(RC.LT.2.5) GO TO 409
      SP=0.
      GO TO 300
  409 IF(RC.LT.1.) GO TO 410
      SP=2.E-04*(2.5-RC)*P10/1.5
      GO TO 300
  410 IF(RC.LT.0.5) GO TO 414
      SP=2.E-04*(P10+((1.-RC)*(P5-P10)/0.5))
      GO TO 300
  414 IF(RC.LT.0.2) GO TO 418
      SP=2.E-04*(P5+((0.5-RC)*(P2-P5)/0.3))
      GO TO 300
  418 IF(RC.LT.0.1) GO TO 418
      SP=2.E-04*(P2+((0.2-RC)*(P1-P2)/0.1))
      GO TO 300
  418 IF(RC.LT.0.05) GO TO 420
      SP=2.E-04*(P0S+((RC-0.05)*(P1-P0S)/0.05))
      GO TO 300
  420 IF(RC.LT.0.01) GO TO 422
      SP=2.E-04*(P01+((RC-0.01)*(P0S-P01)/0.04))
      GO TO 300
C                                  (NB: USING 2.3E-04 INSTEAD OF 2.E-04)
  422 SP=2.3E-04*(P00+(RC*(P01-P00)/0.01))
C
  300 CONTINUE
C                                                    ADD IN STRESS EFFECT
      IF(ABS(PE).GT.0.0001)SP=SP/10.**(PARC*PE)
C
      RETURN
      END
```

Sample Input Files:

```
 RS-1 TEST DATA -- SP=92    KONRAD 1.4 //2.00
0    0    28        180.0          0
 -3.4   1.1          .478         .344         .335      .83337      .82017
      104.0            1.         .445         0.80       200.0
00000000.0      1.E-08       1.E-08
       100.0       200.0         -3.4         -3.4         1.1          1.1
         0.0         0.5          0.0
         0.0        -0.1          2.5         0.35         0.35         1.0
         0.0         0.0          0.0          0.0          0.0
(end-of-data)
 23456789 123456789 123456789 123456789 123456789 123456789 12345678

 Alternate conductivities
 -3.4   1.1          .43          .35          .35      .83337      .82017
```

```
 C-10 Test Data -- SP=92.E-08  KONRAD
0    0    28        180.0          0
 -4.7   1.8          .43          .35          .35      .83337      .82017
      101.5            1.         .445         0.80       200.0
00000000.0      1.E-08       1.E-08
       100.0       200.0         -4.7         -4.7         1.8          1.8
         0.0         0.5          0.0
         0.0        -0.1          2.5         0.35         0.35         1.0
         0.1          4.2
 23456789 123456789 123456789 123456789 123456789 123456789 12345678

 Alternate conductivities:
 -3.4   1.1          .43          .35          .35      .83337      .82017
 -3.4   1.1          .478         .344         .335     .83337      .82017
      100.0       200.0         -3.4         -3.4         1.1          1.1
```

Appendicel G: Heave Calculations using "TRANS"

```
C This version created on DATE=10-01-88 TIME=07:02:41
C
C
C
```

```
C                                                  ...no. nodes & elements & time
C
      READ(15,1502)NUMNP,NESL,NEGNL,MODEXT,NPER,TSTART,IPRI,ITPSS,
     * (CHAR(J),J=1,16)
      TMOURS=TSTART/3600.
 1502 FORMAT(615,F10.0,215,35X,16A4)
      IF(NEDS(4).EQ.IDAYS)T=T+24.
      IF(ABS(T-TMOURS).GT.1.E-05) WRITE(7,771) T,TMOURS
  771 FORMAT(1X,8HTIME T,F12.3,10H NE TSTART,F13.3)
C                                                        use precise time
      T=TMOURS
C
C
C     ****************************************
C     **                                    **
C     **      CALL TIME(T,DT,TNEW,DTNEW,SSTEMP)
C     **                                    **
C     ** units are in hours, calculations done in sec.**
C     ****************************************
C
      CHECK=(T+DT)/TNEW
      IF(CHECK.LT.1.01.AND.CHECK.GT.0.99) GO TO 2954
C                                                       ...time error
      WRITE(7,7772)T,DT,TNEW
 7772 FORMAT(/' There''s a problem with the TIME subroutine'/
     *4X,'T=',E12.6,' hr'/'   DT=',E12.5,' hr'/' TNEW=',E12.5,' hr'),
C                                                       ...terminate
      CALL PTNCMD('$EXEC BOMB.TIME.FUNCTION.IN.TRANS. ')
C
 2954 CONTINUE
C
      TSEC=T*3600.
      DTSEC=DT*3600.
      TNSEC=TNEW*3600.
      DTNSEC=DTNEW*3600.
      THED=TNEW
      TNDAYS=TNEW/24.
C                                          ... heading units in "days"
      IF(TNDAYS.LT.3.)GO TO 529
      NEDT(4)=IDAYS
      NEDS(4)=IDAYS
      THED=TNDAYS
  529 CONTINUE
C                                                ... header for next ADINAT run
C
      IF(T.LT.30.)WRITE(14,581)(NEDT(I),I=1,3),THED,(NEDT(J),J=4,16)
      IF(T.GE.30.)WRITE(14,501)(NEDT(I),I=1,3),THED,(NEDT(J),J=4,16)
  581 FORMAT(3A4,F10.1,3X,15A4)
      WRITE(14,1502)NUMNP,NEGL,NEGNL,MODEXT,NPER,TNSEC,
     *   IPRI,ITPSS,(CHAR(J),J=1,16)
C                                                ... header for next SAPIV run
C
      IF(T.LT.30.)WRITE(4, 581)(NEDS(I),I=1,3),THED,(NEDS(J),J=4,16)
      IF(T.GE.30.)WRITE(4, 501)(NEDS(I),I=1,3),THED,(NEDS(J),J=4,16)
C
      READ(5, 502)NUMNP,NELTYP,LL,NF,NDYN,MODEXS,NAD,NEQB,
     *(CHAR(J),J=1,16)
      WRITE(4,502)NUMNP,NELTYP,LL,NF,NDYN,MODEXS,NAD,NEQB,
     * (CHAR(J),J=1,16)
  502 FORMAT(815,40X,16A4)
C
C     ------------------------------------------------...transcribe ADINAT data
      DO 2010 K=1,7
      READ(15,1503)(CHAR(J),J=1,20)
      WRITE(14,1503)(CHAR(J),J=1,20)
 1503 FORMAT(20A4)
 2010 CONTINUE
C     ------------------------------------------------
      READ(15,1503)(CHAR(J),J=1,20)
      WRITE(14,1504)DTNSEC,(CHAR(J),J=4,20)

 1504 FORMAT(F10.0,2X,17A4)
C
C     \                                                  read old time & temps
      READ(55)CLOCK,(OLDTMP(N),N=1,NUMNP)
C                                                        read new time & temps
      READ(55)CLOCK,(TEMP(N),N=1,NUMNP)
C     ------------------------------------------------------------------------
      DO 200 N=1,NUMNP
C                                                  ... xyz coords. from SAP I/P
      READ(5,503)NN,(IX(J),J=1,6),(XYZ(I,N),I=1,3)
      IF(N.NE.NN)WRITE(7,774)N,NN
  774 FORMAT(1X,'BAD SEQUENCE OF NODES WHILE READING IN NODE ',
     *  I5,' IDENTIFIED AS NODE',I5,' IN THE SAP I/P')
C
C                                                  ... xyz coords. from ADINAT I/P
      READ(15,1503)NN,(XYZADT(I,N),I=1,3)
 1503 FORMAT(I5,5X,3F10.6)
      IF(N.NE.NN)WRITE(7,714)N,NN
  714 FORMAT(1X,'BAD SEQUENCE OF NODES WHILE READING IN NODE ',
     *  I5,' IDENTIFIED AS NODE',I5,' IN THE ADINAT I/P')
C
C                          ... trans. new nodal temps to next SAP I/P
C
      WRITE(4,503)N,(IX(J),J=1,6),(XYZ(I,N),I=1,3),TEMP(N)
  503 FORMAT(715, 3F10.4,6X,F10.4)
C                                                  (following command suspended)
CCCCCCCCCC WRITE(10,507)N,(XYZ(I,N),I=1,3),TEMP(N)
  507 FORMAT(1X,'N',I5,'  XYZ:',3(1X,F7.3),'  TEMP ',F7.4)
  200 CONTINUE
C     ------------------------------------------------------------------------
      READ(5,1503)CHAR
      WRITE(4,1503)CHAR
C                                    ....determining global node numbers
C                                                        of local ijkl nodes
C     ********************************
C     **                            **
      CALL RECONN(6,1,2,IELEM)
      CALL RECONN(6,0,3,INUMB)
C     **                            **
C     ********************************
      CALL SKIP(6,1)
C
C     ------------------------------------------------... element global node no.
      DO 2013 L=1,NELE
      READ(6,1502)LL,(NODELE(IJKL,L),IJKL=1,4),NMATL(L)
 1502 FORMAT(2X,615)
C                                                  (following command suspended)
CCCCCCC WRITE(11,1502)L,LL,(NODELE(IJKL,L),IJKL=1,4),NMATL(L)
 1502 FORMAT(1X,'L=',I5,'   LL=',I5,'  IGKL=',4(1X,I5),'  M=',I5)
      IF(LL.NE.L) WRITE(7,770)LL,L
  770 FORMAT(42HINCORRECT "NODELE" SEQUENCING FOR ELEMENT,I6,
     *  ', ITERATION ',I6)
 2013 CONTINUE
C     ------------------------------------------------
C                                                        ...find disp. info
C     ********************************
C     **                            **
      CALL RECONN(6,1,12,ID1)
C     **                            **
C     ********************************
      CALL   SKIP(6,3)
C                                                ...nodal displ., SAP IV o/p
C     ****************************************]
C                                    ... (nb: there is a "/" in format 622)
      DO 2020 N=1,NUMNP
      NREVRS=NUMNP-N+1
      READ(6,622) NODE,(DISPL(I,NODE),I=1,3)
      IF(NODE.NE.NREVRS) WRITE(7,703)NREVRS,NODE
  703 FORMAT(53HINCONSISTENT NODE NUMBERING FOR DISPLACEMENTS AT NODE,
C     *    ***   ********   *********   *** *****   ****    *
```

```
     *    I3, 19H IDENTIFIED AS NODE, I3, '(DISP).')
  822    FORMAT(//17,10X,3(E12.6,2X))
C                                                        displacements
       WRITE(13,800)NODE,(DISPL(I,NODE),I=1,3)
  800  FORMAT(1X,'NODE: ',I3,'  DISPL(I,N):',3(1X,F10.6))
C
 2020  CONTINUE
C     ***************************************
C
C                    S      ement volumes ( double area method )
       IF (T.GE.0.001) GO TO 4638
C
       WRITE(8,8078)
 8078 FORMAT(' ***File 8 *** The Original Volumes of the Elements',
     *  /'  ELE.        VOLSAP(L)')
C     ------------------------------
       DO 4637 L=1,NELE
       VOLSAP(L)=0.0
C        ************************
         DO 4662 NODE=1,8
            N=NODELE(NODE,L)
         NPLUS1=NODELE(JKLI(NODE),L)
         NMINUS=NODELE(LIJK(NODE),L)
         VOLSAP(L)=VOLSAP(L)+XYZ(2,N)*(XYZ(3,NPLUS1)-XYZ(3,NMINUS))
 4662    CONTINUE
C        ************************
       VOLSAP(L)=VOLSAP(L) * 0.5
C
       WRITE(8,8080)L,VOLSAP(L)
 8080 FORMAT(100(1X,I4,6X,E15.8))
 4637 CONTINUE
C     ------------------------------------
       GO TO 4639
C
 4638  CONTINUE
       CALL SKIP(8,2)
       READ(8,8080)(L,VOLSAP(L),L=1,NELE)
 4639  CONTINUE
C
C     ***************************************************************
C     *                                                             *
C     *      THIS SECTION READS THE STRESS MATRICE FROM SAP|V       *
C     *    OUTPUT AND CALCULATES THE PRINCIPAL STRESSES AND         *
C     *    THEIR RESPECTIVE DIRECTION COSINES                       *
C     *                                                             *
C     ***************************************************************
C
C                    ...the following parameters are zero due to 2-d analysis
       SIGXY=0
       SIGXZ=0
C                          searching for the elements' stress o/p info
C      ***************************
C      **                       **
C        **    CALL RECONN(6,0,1,IOELE)
C      **                       **
C      ***************************
C
       BACKSPACE 8
C                                                  read element number
C         ***************************************
          DO 2021 L=1,NELE
C
          READ(8,850)LL
  850     FORMAT(10X,I6)
          IF (LL.NE.L) WRITE(7,772)L,LL
  772     FORMAT(1X,'WRONG SEQUENCE OF ELEMENTS FOR READING',
     *     ' STRESSES, STEP ',I5,' EL EMENT,I6)
C
C                                  centroid stresses from SAP IV o/p
C
          READ(8,851)SIGYY,SIGZZ,SIGXX,SIGYZ
  851     FORMAT(///14X,4(F12.3,2X)/)
C
          SIG(1)=SIGXX
          SIG(2)= SIGXY
          SIG(3)= SIGYY
          SIG(4)= SIGXZ
          SIG(5)= SIGYZ
          SIG(6)= SIGZZ
C                                        ... eigenvalues, eigenvector
          N3=3
          JOB=2
          IZ=3
C
C     ***************************************************************
C     *                                                             *
          CALL EIGRS(SIG,N3,JOB,PRNCPL(1,L),COSSIG(1,1,L),IZ,WORKER,IER)
C     *                                                             *
C     * (REFERENCE:  THE IMSL LIBRARY SUPPORTED BY THE MTS SYSTEM)**
C     ***************************************************************
C
C                .... change of sign convention: from:  tension +ve
C     ------------------------------------------------------ to:  compression +ve
          DO 2024 I=1,3
          PRNCPL(I,L)=(-1.0)*PRNCPL(I,L)
 2024     CONTINUE
C     ------------------------------------------------------
 2021     CONTINUE
C         ***************************
C
C     ***************************************************************
C     **                                                           **
C     ** This section finds the Phase Change info, ADINAT volumes **
C     ** temperature:conductivity info and the insitu volumetric  **
C     ** latent heat.                                             **
C     **                                                           **
C     ***************************************************************
C                                                  find phase change info
C     ********************************
C     **                            **
          CALL RECONN(16,0,2,IPHAS)
C     **                            **
C     ********************************
       CALL SKIP(16,4)
       READ(16,1655)TREF,DTREF,IFLAG
 1655 FORMAT(T39,E13.6,12X,E13.6,24X,I1)
C
       IF(DTREF.GT.1.E-06)WRITE(7,7655)DTREF
 7655 FORMAT(1X,'THE TRANSITION TEMPERATURE INTERVAL FOR THE PHASE',
     *' CHANGE:  ',F10.7,/'IS GREATER THAN ZERO.'/'"TRANS" FORMULAE'
     *,' MUST BE ALTERED ACCORDINGLY.')
       IF(IFLAG.NE.1)WRITE(7,7656)
 7656 FORMAT(1X,'VARIABLE "IFLAG" MUST BE SET EQUAL TO ONE ')
C
C     ***************************************************************
C     *                ELEMENT VOLUME INFORMATION                   *
C     ***************************************************************
C                                                  header for volume file
       WRITE(18,801)(HED7(I),I=1,3),THEW,(HED7(I),I=4,18)
       WRITE(18,1802)
 1802 FORMAT(2X,'ELEMENT  VOLUME(m**3)')
C                          (volumes are written in subroutine shape)
C                                                  skip if time=0.0
       IF(T.LT.1.E-05) GO TO 289
C                                                  read old element volumes
       READ(18,1800)(L,OLDVOL(L),L=1,NELE)
 1800 FORMAT(100(I2,I4,6X,E15.8))
       REWIND 18
       CALL SKIP(18,2)
C                                                  read previous freq. vol  & L's
```

```
      CALL SKIP(19,1)
      READ(19,1901)(L,VFRMAX(L),EPSMAX(L),ICRYO(L),L=1,NELE)
 1901 FORMAT(I5,3X,E12.5,5X,F10.7,5X,I1)
      REWIND 19
      GO TO 290
C
  289 CONTINUE
C     ------------------------------------------------------------
C           DO 2084 L=1,NELE
C                                        assign values to old volumes for t=0.0
C           OLDVOL(L)=VOLSAP(L)
C                                  initializing previous frozen volumes of elements
C           VFRMAX(L)=0.0
C                                  initializing previous %frozen of elements
C           EPSMAX(L)=0.0
C                                                  initialize heave history flag
C           ICRYO(L)=0.0
C
 2084       CONTINUE
C     ------------------------------------------------------------
   290      CONTINUE
C                                          find temp. vs. conductivity info
C     **********************************
C     **                              **
C        CALL RECONN(18,0,47,IPAR18)
C     **                              **
C     **********************************
      BACKSPACE 18
      READ(18,1857)NPAR18,NPAR17
 1857 FORMAT(5X,I5/)
C                                  (NB: only the first mat'l is used)
C           **********************************
C           **                              **
C              CALL RECONN(18,0,11,ICONS)
C           **                              **
C           **********************************
            CALL SKIP(18,8)
C                                                 volumetric latent heat
            READ(18,1858)VLATNT
 1858       FORMAT(T30,E12.5)
            CALL SKIP(18,1)
C                                          number of temp vs. k pairs
            NPAIRS=NPAR17/2
C           ------------------------------------------------------------
               DO 2230 NCON=1,NPAIRS
               READ(18,1859)TEMPK(NCON),CONDUC(NCON)
 1859          FORMAT(10X,E14.7,5X,E14.7)
 2230          CONTINUE
C           ------------------------------------------------------------
C
C                                                 find conductivities
      NK=0
C                                                    frozen: COND(1)
      TEMPKK=TREF-0.001
C
  437 CONTINUE
      NK=NK+1
C     ------------------------------------------------------------
            DO 228 N=1,6
            NPLUS1=N+1
            IF(TEMPKK.GT.TEMPK(NPLUS1))GO TO 228
            COND(NK)=(TEMPKK-TEMPK(N))/(TEMPK(NPLUS1)-TEMPK(N))
     *  *(CONDUC(NPLUS1)-CONDUC(N))  +  CONDUC(N)
C
C                                          frozen fringe:  COND(2)
            TEMPKK=(TREF+0.0)/2
            IF(NK.LT.2)GO TO 437
C                                            unfrozen:  COND(3)
            TEMPKK=0.001
            IF(NK.LT.3)GO TO 437
C
            GO TO 438
  228       CONTINUE
C     ------------------------------------------------------------
  438 CONTINUE
C
C     *  *  *  
```

```
C
C     *  NO ATTRACTED HEAVING OCCURS WHEN THE FROST FRONT
C     *     TRAVERSES AN ELEMENT WITHIN ONE TIME-STEP.
C     *
C     *  A HEAT FLUX CALCULATION IS PERFORMED TO MODERATE THE
C     *     INFLOW RATE.
C     *
C     *  TO ACCOUNT FOR SEASONAL THAWING, HEAVING IS SUSPENDED
C     *     UNTIL THE PREVIOUS MAX. FROZEN VOLUME IS EXCEEDED.
C     *
C     *  NO HEAVING IF AN ELEMENT HAS PREVIOUSLY BEEN FROZEN
C     *     AND WAS BEYOND THE FROST FRONT
C     *
C     ***********************************************************
C
C                    Heaving Criteria:
      IFHEAV(L)=0
C                                                ...on edge of frost front
      IF(NCTREF(L).GE.2.AND.EPS(L).GE.0.001)IFHEAV(L)=1
C                                                ...partially frozen
      IF(EPS(L).GT.0.0.AND.EPS(L).LT.1.0)IFHEAV(L)=1
C                ...frost front has traversed element in one step
      IF(EPS(L).GT.0.99999.AND.NCTREF(L).LT.2)IFHEAV(L)=0
C                ... previously frozen and off the freezing front
      IF(ICRYO(L).EQ.1) IFHEAV(L)=0
C
C     ***********************************************************
C     *                                                         *
C     *  THIS SECTION DETERMINES  THE ELEMENTS'                 *
C     *                                                         *
C     *          -GAUSSIAN  TEMPERATURES                        *
C     *          -THERMAL GRADIENTS                             *
C     *          -JACOBIAN  DETERMINANTS                        *
C     *          -ADINAT VOLUME                                 *
C     *          -THERMAL DIRECTION COSINES                     *
C     *          -HEAT FLUX                                     *
C     *     AND NODAL LATENT HEATS                              *
C     *                                                         *
C     ***********************************************************
C     ... gaussian temps, thermal gradients, jacobian dets, volume
C     ***********************************************************
C
C           CALL SHAPE(L,TEMPG,GRADTG,DJACOB,VOLUME(L))
C     *                                                         *
C     ***********************************************************
C
        GRAD(1,L)=0.
        GRAD(2,L)=0.
        GRAD(3,L)=0.
C                 ------------------------------------------------
        DO 227 NGAUSS=1,4
        GRAD(2,L)=GRAD(2,L)+GRADTG(1,NGAUSS)*DJACOB(NGAUSS)
        GRAD(3,L)=GRAD(3,L)+GRADTG(2,NGAUSS)*DJACOB(NGAUSS)
  227   CONTINUE
C               ------------------------------------------------
C
C                          ... magnitude of avg. element gradient @ fringe
C                                   ( based on frozen gradient)
  337   CONTINUE
        GRAD(2,L)=GRAD(2,L)/VOLUME(L)
        GRAD(3,L)=GRAD(3,L)/VOLUME(L)
        ARG= GRAD(2,L)**2 + GRAD(3,L)**2
        IF(ARG.LE.0.)WRITE(7,7019)L
 7019   FORMAT('*** ERROR *** ATTEMPTING TO TAKE THE ROOT OF
C***nb  1', the element's nodes are at the same temperature,
C       the program may bomb out here. Tightening the convergence
C       tolerance in ADINAT should resolve this problem.
C     *   'NON-POS. NUMBER. ELEMENT(',I2,'). THERMAL GRADIENTS. ')
C                                                  ...thermal gradient
        GRADT(L)=SORT(ARG)
C
C                                                  ... the case of zero thermal gradient
        IF(ABS(GRADT(L)).LT.1.E-06)GO TO 3022
C                                                  ... direction cosines of flux
C                 ------------------------------------------------
        DO 2004 I=1,3
        COSINE(I,L)=GRAD(I,L)/GRADT(L)
 2004   CONTINUE
C               ------------------------------------------------
        GO TO 2128
C
C                                                  ... default to vertical
 3022   CONTINUE
        WRITE(7,7014)L,GRADT(L)
 7014   FORMAT(' ***NEAR-ZERO TEMPERATURE GRADIENT: GRADT(',I3,
     *  ')=',F9.8,' C/m.')
        COSINE(1,L)=0.0
        COSINE(2,L)=0.0
        COSINE(3,L)=1.0
C
 2128   CONTINUE
        HFLUXY=0.
        HFLUXZ=0.
        READ(18,1848) LL
 1848   FORMAT(//3X,I5)
C
        IF(L.NE.LL) WRITE(7,7487) LL,L
 7487 FORMAT(/72,'*** WARNING. NON-SEQUENTIAL ELEMENT DATA',
     *//71X,'ELEMENT(',I3,') FLUX DATA READ DURING ITERATION ',I3)
C
C                                                  ...element average flux
C                 ------------------------------------------------
        DO 2047 NGAUSS=1,4
C
        READ(18,1847) FLUXY, FLUXZ
 1847   FORMAT(T28,F10.4, 5X, F10.4)
        HFLUXY=HFLUXY + FLUXY*DJACOB(NGAUSS)
        HFLUXZ=HFLUXZ + FLUXZ*DJACOB(NGAUSS)
 2047   CONTINUE
C               ------------------------------------------------
C
        HFLUXY=HFLUXY/VOLUME(L)
        HFLUXZ=HFLUXZ/VOLUME(L)
        FLUX(L)=SQRT(HFLUXY**2 + HFLUXZ**2)
 2121   CONTINUE
C
C
C     *  *  *  *  *  *  *  *  *  *  *  *  *  *  *  *  *  *  *  *  *  *  *  *  *  *  *
C     *                                                                              *
C     *        This section reads the latent heat released at                        *
C     *     each node in the ADINAT solution.  This heat is the                      *
C     *     total amount of latent heat released, based on an                        *
C     *     initial liquid phase state.                                              *
C     *                                                                              *
C     *  *  *  *  *  *  *  *  *  *  *  *  *  *  *  *  *  *  *  *  *  *  *  *  *  *  *
C
C                                                  ... find nodal latent heats
C     ********************************
C     **                            **
        CALL RECONN(18,0,24,INHEAT)
C     **                            **
C     ********************************
        CALL SKIP(18,1)
C               ------------------------------------------------
        LIMIT=MINO(NUMNP,50)
        DO 241) J=1,LIMIT
        READ(18,1884)JNLATST(N),N=J,NUMNP,50)
 1884   FORMAT(4(14X,E13.6,3X))
 241)   CONTINUE
```

```
C
C
C     *  *  *  *  *  *  *  *  *  *  *  *  *  *  *  *  *  *  *  *  *  *  *  *  *  *
C     *                                                                           *
C     *          THIS SECTION DETERMINES WHICH ELEMENTS HAVE                      *
C     *     FROZEN COMPLETELY THEN COMPUTES AN AVERAGE THERMAL                    *
C     *     GRADIENT FROM ADJACENT FROZEN ELEMENTS FOR CALCS                      *
C     *                                                                           *
C     *  *  *  *  *  *  *  *  *  *  *  *  *  *  *  *  *  *  *  *  *  *  *  *  *  *
C
C
      DO 2023 L=1,NELE
C
      GRADTK(L)=GRADT(L)
C                                                  ... cold side heat flux
      CFLUX=FLUX(L)
C                                                  default value for vmax
      VMAX(L)=1.E-15
C                                                bypass non-heaving elements
      IF(IPHEAV(L).NE.1)GO TO 2025
C                                                transfer if frozen ---> 2489
      IF(EPS(L).GE.0.99999)GO TO 2489
C
C                 *** Element is Partially Frozen ***
C                                                  find a cold gradient
C                                                  Flux units  Watts/m**2
      GRADTK(L)=0.0
      CFLUX=0.0
      LCOUNT=0
C     ------------------------------------------------------------------A
            DO 2430 NAYBOR=1,NELE
C                                                bypass non-frozen elements
            IF(EPS(NAYBOR).LT 1 bo) GO TO 2430
C           ------------------------------------------------------------B
                  DO 2431 LNODE=1,4
C                                                                  local node
                  LCNODE=NODELE(LNODE,L)
C                 ------------------------------------------------------C
                        DO 2432 MLNODE=1,4
                        IF(LCNODE.NE.NODELE(MLNODE,NAYBOR))GO TO 2432
C
                        GRADTK(L)=GRADTK(L)+GRADT(NAYBOR)
                        CFLUX=CFLUX+FLUX(NAYBOR)
                        LCOUNT=LCOUNT+1
 2432                   CONTINUE
C                 ------------------------------------------------------C
 2431              CONTINUE
C           ------------------------------------------------------------B
 2430       CONTINUE
C     ------------------------------------------------------------------A
      IF(LCOUNT.GT.0)GO TO 4321
C                                                  default flag
        IPOPAL(L)=1
C
        GRADTK(L)=FLUX(L)/COND(1)
        CFLUX=1.0E+10
        LCOUNT=1
        WRITE(7,7321)L,GRADT(L),GRADTK(L)
 7321   FORMAT(/' Default to WARM thermal values:   GRADT(',I3,
     *         ') was ',F10.8,', and is now ',F10.8,' C/m  ')
        GO TO 2489
C
 4321 CONTINUE
      CFLUX=CFLUX/LCOUNT
      GRADTK(L)=GRADTK(L)/LCOUNT
C                                                  used adjacent gradt
      WRITE(7,7223)L,GRADT(L),LCOUNT,GRADTK(L)
 7223 FORMAT(' GRADT(',I3,')=',F10.8,' replaced with avg  of ',
     *I1,' adjacent GRADT''s, now ',F10.8,' C/m')
C
```

```
C                       DETERMINE WARM  FLUX
 2489 CONTINUE
      WFLUX=0.0
      LCOUNT=0
C     ------------------------------------------------------------------1
      DO 2490 NAYBOR=1,NELE
C                                                bypass non-frozen elements
      IF(EPS(NAYBOR).GE.0.00001) GO TO 2490
C     .  ------------------------------------------------  calc  average warm flux
      DO 2491 LNODE=1,4
      LCNODE=NODELE(LNODE,L)
C     .  ------------------------------------------------------------111
            DO 2492 MLNODE=1,4
            IF(LCNODE.NE.NODELE(MLNODE,NAYBOR))GO TO 2492
            WFLUX=WFLUX+FLUX(NAYBOR)
            LCOUNT=LCOUNT+1
 2493       CONTINUE
 2492       CONTINUE
C     .  ------------------------------------------------------------111
 2491       CONTINUE
C     ------------------------------------------------------------------11
 2490 CONTINUE
 2490 CONTINUE
C     ------------------------------------------------------------------1
      IF(LCOUNT.GT.0) GO TO 4322
C                                                  default flag
      IPOPAL(L)=1
      LCOUNT=1
      WRITE(7,7322)L
 7322 FORMAT(/' Default to zero warm thermal flux  ELEMENT ',I3)
C
 4322 CONTINUE
      WFLUX=WFLUX/LCOUNT
      VMAX(L)=CFLUX/334.E+06
C                                  apply Konrad's therm cond  ratio factor
      GRADTK(L)=GRADTK(L) * COND(L)/COND(2)
C
C     .  maximum velocity (m/s)= cflux (W/m**2)/latent heat (J/m**3)
      IF(IPOPAL(L).EQ.0)VMAX(L)=(CFLUX-WFLUX)/334.E+06
      VOP=VMAX(L)*1.E+09
      IF (VMAX(L).LT.0.0)WRITE(7,7327)L,CFLUX,WFLUX,VOP
 7327 FORMAT(/' ***WARNING*** The Fluxes L)',I3,' C/W=',F10.8,'W,
     *,F10.8,')W/m**2, produced a',/'
     *' water velocity of ',F8.2,'E-06 mm/s     velocity now zero ')
C
      VMAX(L)=AMAX1(VMAX(L),0.0)
C     ------------------------------------------------------------------1
            DO 2488 J=1,3
            GRAD(1,L)=GRADTK(L)*COS(NE(1,L))
 2488       CONTINUE
C     ------------------------------------------------------------------1
 2029 CONTINUE
 2023 CONTINUE
C     ------------------------------------------------------------------1
C
C
C
C     *  *  *  *  *  *  *  *  *  *  *  *  *  *  *  *  *  *  *  *  *  *  *  *  *  *
C     *                                                                           *
C     *        THIS SECTION CALCULATES THE COMPONENT VELOCITIES                  *
C     *     OF THE APPROACHING WATER FROM THE SEGREGATION                         *
C     *     POTENTIAL AND THE XYZ COMPONENT THERMAL GRADIENTS                     *
C     *     THEN DETERMINES THE XYZ COEFFICIENTS OF                               *
C     *     THERMAL EXPANSION OF EACH ELEMENT AS A FUNCTION OF                    *
C     *     THE ELEMENTS' VOLUMES.  FROST HEAVE DISTORTION                        *
C     *     AND THE AVERAGE ELEMENT TEMPERATURE                                   *
C     *                                                                           *
C     *  *  *  *  *  *  *  *  *  *  *  *  *  *  *  *  *  *  *  *  *  *  *  *  *  *
C
C                                                                        porosity
```

```
      PGR=1-((RO-RW)/(RS-RW))
C
C     ------------------------------------------------------------------
      DO 2111 L=1,NELE
C     ------------------------------------------------------------------
      VOLFR2=EPS(L)*VOLUME(L)
      OLDVFR=EPSOLD(L)*OLDVOL(L)
      DELVFR=VOLFR2-OLDVFR
      VGAIN=VOLFR2-VFRMAX(L)
C                                  ... negative fraction of vol  gain
      VGFRAC=0.0
      IF(VFRMAX(L).LE.1.E-08)GO TO 2788
      VGFRAC=     VGAIN/VFRMAX(L)
 2788 CONTINUE
      IF(VGFRAC.LT.-0.001 AND.ICRYO(L).EQ.0)
     *                          WRITE(7,7730)L,VGAIN,VOLFR2,VFRMAX(L)
 7730 FORMAT(/' L(',I3,') has Frozen Volume Gain of ',E12.5,' m**3'
     */'   Present Fr Vols',E12.5,' m**3 / Previous Fr Vols',E12.5)
C                                  ... warn of approach of steady-state
      IF(DEPS(L).GE.-1.E-08)GO TO 2435
C                                  !!!!  nb: the "F" scale in format 0079
      DELTAV=VOLUME(L)-OLDVOL(L)
      WRITE(7,0079)L,EPS(L),VOLUME(L),VOLFR2, EPSOLD(L),OLDVOL(L),
     * OLDVFR, DEPS(L),DELTAV,DELVFR
C                                  !!!!  nb: the "F" scale in format 0079
 0079 FORMAT(/1X,131('-')/1X,'|',
     */'  | **** ELEMENT (',I3,') HAS A NEGATIVE CHANGE IN %FROZEN |'
     */'  |                                                       |'
     */'  |Volumes (m**3)  |%Frozen    |  Volume   | Frozen Volume |'
     */'  |----------------|-----------|-----------|---------------|'
     */'  |   Present:     |',2PF10.5,'|',0PF10.4,'|',F10.5,'|'
     */'  |   Previous:    |',2PF10.5,'|',0PF10.4,'|',F10.5,'|'
     */'  |----------------|-----------|-----------|---------------|'
     */'  |   Increments:  |',2PF10.5,'|',0PF10.4,'|',F10.5,'|'
     */'  |-----------------------------------------------------------|')
 2435 CONTINUE
C
C
C ***************************************************************
C **                                        width of frost front **
C **            CALL SPAN(L,EPS(L),NCTREP(L),FPSPAN(L))         **
C **                                                    metres  **
C ***************************************************************
C **
C **                                        segregation potential **
C **         CALL SPTL(L,SPO(L),C,STRPRP(L),SP(L))              **
C **                                                            **
C **                                        Units  kPa, mm**2/s/K **
C ***************************************************************
C
C
C                                       ... heat flow correction
      FACTOR=1.0
      VKONRD=SP(L)*GRADTK(L)/1.0E+06
      IF(VMAX(L).GE.VKONRD) GO TO 2478
      FACTOR=VMAX(L)/VKONRD
         VV=VKONRD*1.0E+09
         VVMAX=VMAX(L)*1.0E+09
         IF(IPHEAV(L).EQ.1)WRITE(7,7384)L,VV,VVMAX
 7384    FORMAT(/T2,'THE WATER VELOCITY FOR ELEMENT (',I3,
     *') HAS BEEN REDUCED'/'  FROM ',F7.1,' TO ',F7.1,' *E-09 mm/s'
     */'  BECAUSE OF LIMITTING HEAT FLUX CAPABILITIES ')
C
 2478 CONTINUE
      TDIF=TAVG(L)-TREF
C                                       approach vel. of water (m/s)
      VEL(L)=VKONRD*FACTOR
      VEL(L)=ABS(VEL(L))
      VEL(L)=AMAX1(VEL(L),1.0E-30)
C                                       skip if not freezing
      IF(IPHEAV(L).EQ.0)VEL(L)=1.0E-30
C                                  ... skip if previous % not  exceeded
      IF(VGFRAC.LE.-0.001)   VEL(L)=1.0E-30
C                                       quantity of water introduced
      QSPM2O=VEL(L)*DTSEC*FPSPAN(L)
C                                  )increments) volume of attracted water
      DVOLSP(L)=QSPM2O*(1.0E+09)
C                                  ... huge increase over previous maximum
      IF(ABS(DEPS(L)).LT.1.E-06)GO TO 2782
      EPSFAC=(EPS(L)-EPSMAX(L))/DEPS(L)
      GO TO 2783
 2782 CONTINUE
      EPSFAC=0
C
 2783 CONTINUE
      IF(EPSFAC.LE.0.)EPSFAC=0
      IF(EPSFAC.GE.1.)EPSFAC=1
C                                       )increments) volume of in situ water
      DVOL1S(L)=VOLSAP(L)*(1.0E+09)*DEPS(L)*PORE*EPSLOB*EPSFAC
C                                  no in-situ heave for non-susceptible soil
      IF(ABS(SPO(L)).LT.0.01) DVOL1S(L)=0.0
      IF(DVOL1S(L).LT.0.0)   DVOL1S(L)=0.0
C
C                                                 incr "z" heave
C                                  !NOT USED AT PRESENT!
      DVSPZ(L)=DVOLSP(L)*COSINE(3,L)
      DV1SZ(L)=DVOL1S(L)*COSINE(3,L)
      DVZ(L)  =DVSPZ(L)+DV1SZ(L)
C
      IF(ABS(TDIF).LT.1.E-08)TDIF=1.E+08
      IF(ABS(TDIF).LT.1.E-05)WRITE(7,7779)S
 7779 FORMAT(/' *** TDIF LT 1.E-05 FOR ELEMENT ',I3)
C
C     ***********************************
C     *                                 *
      CALL COEFF(L,TDIF,ALPHAR,BETA)
C     *                                 *
C     ***********************************
C
C                 elements' heat rate increase from introduced water
      HLRATE(L)=QSPM2O*334.E+06/DTHSEC
C                                  correction for in situ volume
      HLRATE(L)=HLRATE(L) - DEPS(L)*(VOLUME(L)/VOLSAP(L))
     *                    *VLATHP/DTHSEC
C
      READ(5,551)MAT(L),WT, GAMMA, RO, XBETA, (CHAR(I),I=1,10)
      WRITE(6,551)MAT(L),WT, GAMMA, RO, BETA, (CHAR(I),I=1,10)
  551 FORMAT(I2,5,3F10.5,10A4)
C
      IF(WT.EQ.0) WT=1
C                 ------------------------------------------------
      DO 22 K=1,NY
C
C                                       previous soil parameters
      READ(5,552)TIN,EMOD(3),EMOD(2),EMOD(1),STRRAT(3),
     *          STRRAT(2),STRRAT(1),GMOD,OLDALP,OLDALP,OLDALP
  552 FORMAT(F10.4,3F10.0,3F10.5,F10.1/3F10.4)
C
C                                                    soil parameters
      WRITE(6,552)TIN,EMOD(3),EMOD(2),EMOD(1),STRRAT(3),
     *          STRRAT(2),STRRAT(1),GMOD,ALPHAR,ALPHA,ALPHA
   22 CONTINUE
C     ------------------------------------------------------------------
      VFRMAX(L)=AMAX1(VFRMAX(L),VOLFR2)
      EPSMAX(L)=AMAX1(EPSMAX(L),EPS(L))
 2111 CONTINUE
C
C     ------------------------------------------------------------------
C                                       transcribe remaining SAP data
      DO 222 K=1,1000
      READ(5,1503,END=229) CHAR
      WRITE(6,1503)CHAR
      IF(CHAR(1).EQ.ISTOP) GO TO 229
  222 CONTINUE
```

```
C
  229 CONTINUE
C
      IZERO=0
      ICHAR=ICEE
C
            DO 223 N=1,NUMNP
C
                  DO 224  I=1,3                        use displaced mesh
                  COORD(I)=XYZ(I,N)+DISPL(I,N)
  224             CONTINUE
C
C
            WRITE(14,554) N,ICHAR,IZERO,(COORD(I),I=1,3),TEMP(N)
            ICHAR=IBLANK
            WRITE(12,554) N,ICHAR,IZERO,(COORD(I),I=1,3),TEMP(N)
  554       FORMAT(I5,A1,I4,4F10.5)
  223       CONTINUE
C
C                                                  transcribe "icon","ipr"c"
      READ(15,1503)CHAR
      WRITE(14,1503)CHAR
C                                                  use o/p temps as i/p
      READ(15,553)(OLDTMP(N),N=1,NUMNP)
  553 FORMAT(8F12.5)
      WRITE(14,553)(TEMP(N),N=1,NUMNP)
C
C                                    find "ntemp" specified temps
      READ(15,555)NTTF,NPTM,ILCOV,NTEMP,NOCV,NORA,
     *NLOAD,NLOAD2,NLOAD3,NINT,NTOT
C
      NLOLD=NLOAD
C
            DO 2400 N=1,NUMNP
            TDIFFR=TEMP(N)-TREF
            IF(ABS(TDIFFR).GT.1.E-05)NLATNT(N)=0.0
            NLATNT(N)=-1.*NLATNT(N)/DTMSEC
 2400       CONTINUE
C
C                  distribute latent heat from attracted water
C                                                  to the warm nodes
            LOWERT=TREF-1.E-05
C
            DO 2401 L=1,NELE
C
            IF(ABS(NLRATE(L)).LT.1.E-05)GO TO 2408
            UPPERT=9999
C
               DO 2678 IJKL=1,4
               NGLOBL=NODELE(IJKL,L)
               DIFT=TREF-TEMP(NGLOBL)
C                                    preferred distribution to nodes @ tref
               IF(ABS(DIFT).LT.1.E-05) UPPERT=TREF+1.E-05
 2678          CONTINUE
C
C
            NCOUNT=0
C
               DO 2403 IJKL=1,4
               NGLOBL=NODELE(IJKL,L)
C                                    bypass out-of-range nodes
               IF(TEMP(NGLOBL).GT.UPPERT.OR.
                  TEMP(NGLOBL).LT.LOWERT)  GO TO 2408
               NCOUNT=NCOUNT+1
               NCOLD(NCOUNT)=NGLOBL
 2408          CONTINUE
 2403          CONTINUE
C
            IF(NCOUNT.EQ.0)GO TO 2401
C
C                                                  add heat rate to node
               DO 2403 N=1,NCOUNT
               NODE=NCOLD(N)
               NLATNT(NODE)=NLATNT(NODE)+NLRATE(L)/NCOUNT
 2403          CONTINUE
C
 2409          CONTINUE
 2401       CONTINUE
C
C
C                                    determine nodes with heat loading
      NLOAD=0
C
            DO 2404 N=1,NUMNP
            IF(ABS(NLATNT(N)).LT.1.E-05)GO TO 2404
            NLOAD=NLOAD+1
            NODELM(NLOAD)=N
 2404       CONTINUE
C
C
      WRITE(14,555)NTTF,NPTM,ILCOV,NTEMP,NOCV,NORA,
     *NLOAD,NLOAD2,NLOAD3,NINT,NTOT
  555 FORMAT(10I5)
C                                    latent heat and first 5 time functions
C
               DO 225 K=1,14
               READ(15,1503)CHAR
               WRITE(14,1503)CHAR
  225          CONTINUE
C
C                                    insert new soil surface temp
            READ(15,1578) TIME1,SSTMP0,TIME2,SSTMP0,(CHAR(N),N=1,10)
            WRITE(14,1578)TIME1,SSTEMP,TIME2,SSTEMP,(CHAR(N),N=1,10)
 1578       FORMAT(F10.0,F10.3,F10.0,F10.3,40A4)
C                                    transcribe fixed node) temps
C
               DO 2244 NODE=1,NTEMP
               READ(15,1503)CHAR
               WRITE(14,1503)CHAR
 2244          CONTINUE
C
C                                    skip previous node) loads
      IF(NLOLD.GT.0)  CALL SKIP(15,NLOLD)
C                                    no node) thermal) loads
      IF(NLOAD.EQ.0) GO TO 2405
C
C                  thermal) loading at nodes due to phase change
            DO 2405 N=1,NLOAD
            NODE=NODELM(N)
            NTCURV=0
C                                    n.b. "g" format not working correctly
               DO 2412 I=1,6
               IF(ABS(NLATNT(NODE)).GT.999.)GO TO 2414
               WRITE(14,1470)NODE,NTCURV,NLATNT(NODE)
 1470          FORMAT(2I5,F10.5,7X,'0.0     0')
               GO TO 2413
C
 2414          CONTINUE
               NLATNT(NODE)=NLATNT(NODE)*0.001
               NTCURV=NTCURV+1
 2412          CONTINUE
C
 2413       CONTINUE
 2405       CONTINUE
C
C
C                                    transcribe remaining ABINAT info
            DO 2407 N=1,1000
```

```
                    READ(15,1503,END=2408)CHAR
                    WRITE(14,1503)CHAR
 2407               CONTINUE
C
 2408 CONTINUE
C
      WRITE(3,501)(HEDS(I),I=1,3),THED,(HEDS(J),J=4,10)
      WRITE(3,398)
  398 FORMAT(//1X,'ELE| TAVG| %CH | %PR |GRADTK|STRPRP|  SP  |'
     *' VEL |  VOLSAP | DVOLIS| VOLIS |  DVOLSP |  VOLSP')
      WRITE(3,396)
  396      FORMAT(1X,'|   C   |       |     |     |  g/m  | kPa  |  E-5 |'
     *'--mm/s|   cm**3  | cm**3 | cm**3 |  cm**3 |  cm**3 ')
C
      HEAVE=0.
      TDDZS=0.
      TDDZIS=0.
      DO 999 K=1,NELE,3
      WRITE(3,397)
  397      FORMAT('      |       |     |     |       |      |      |'
     *'       |          |       |       |        |        ')
C
      KEND=K+2
      IF(KEND.GT.NELE)KEND=NELE
C     ------------------------------------------------------------------
      DO 994 L=K,KEND,1
        IF(EPSOLD(L).GE.1.0)DZINC(L)= 1.E-20
CCCCCC          TDDZS=TDDZS+DDZS(L)
CCCCCC          TDDZIS=TDDZIS+DDZIS(L)
CCCCCC          DHEAVE=TDDZS+TDDZIS
C
CCCCCC  DZINC(L)=DZINC(L)*1000.
        WRITE(3,399)L,TAVG(L),DEPS(L),EPS(L),GRADTK(L),
     *  STRPRP(L),SP(L), VEL(L),VOLSAP(L),DVOLIS(L),VOLIS(L),
     *  DVOLSP(L),VOLSP(L)
  399 FORMAT(1X,I2,' |',0PF6.2,'|',2PF5.0,'|',2PF6.0,'|',
     *  0PF6.3,'|',0PF6.2,'|',0PF6.2,'|',0PF6.2,'|'
     *  6PF9.0,'|',6PF7.2,'|',6PF7.1,'|',6PF7.1,'  |',6PF8.1)
  998 CONTINUE
C     ------------------------------------------------------------------
C     ------------------------------------------------------------------
  999 CONTINUE
      WRITE(3,391)
  391 FORMAT(  '0_____________________________________________________'
     *'_____________________________________________________')
      WRITE(3,390)
  390 FORMAT(1X,'
     *',3PF8.3,'|',3PF8.3,'|',3PF8.3,'|',3PF8.3)
C
      WRITE(10,1800)
 1800 FORMAT('  ELE',1X,'Max. Frez. Vols.',1X,'Max. %Frozen   Cryo',
     * ' (F)le 10)')
C
      DO 1885 L=1,NELE
C                                          Update Cryo History
C                                             Skip if not frozen
      IF(EPS(L).LT.0.99999)GO TO 2686
C                                    previously frozen and beyond front
      IF(ICRYO(L).EQ.1)GO TO 2686
C                                    presently frozen and beyond front
      IF(NCTREF(L).LE.1)ICRYO(L)=1
 2686 CONTINUE
C                                                 Retain maximum values
      WRITE(10,1901)L,VFRMAX(L),EPSMAX(L),ICRYO(L)
 1885 CONTINUE
C                                    signal successful completion
      CALL PYNCMD('$DESTROY -FILE GR;')
      RETURN
      END
C     ------------------------------------------------------------------
```

```
C
C     ------------------------------------------------------------------
C *****************************************************************
C *                                                               *
C *            SUBROUTINE COEFF(L,TDIF,ALPHA,BETA)                *
C *                                                               *
C *****************************************************************
C
      COMMON/INFO/RUNNP,NELE,T
      COMMON/THERMO/GRAD(3,99),GRADT(99),COSINE(3,99)
      COMMON/VOLS/VOLUME(99),OLDVOL(99),VOLSAP(99),DVOLIS(99),
     *            DVOLSP(99),DVISZ(99),DVSPZ(99),VOLIS(99),VOLSP(99)
C
      REAL COSVOL(3),V(3)
C
      DATA PI/3.14159265E4/, ZERO/0.0/
C                                                  Initial heave = zero
      IF(T.GT.0.000)) GO TO 7190
      WRITE(8,1888)L,VOLSAP(L),(ZERO,I=1,5)
 1888 FORMAT(I5,3E13.8,3F11.7)
      BACKSPACE 8
 7190 CONTINUE
C
      READ(8,1888)LL,VOLSAP(L),VOLIS(L),VOLSP(L),(COSVOL(I),I=1,3)
      IF(L.NE.LL) WRITE(7,7191)L,LL
 7191 FORMAT(/' ***ERROR  ELEMENT',I3,' INCORRECTLY ID''D AS ELE
     * I3,', FILE 18')
C
      VTOT=0.0
C                                          components of total heave
C     ------------------------------------------------------------------
      DO 4560 I=1,3
      V(I)=(VOLIS(L)+VOLSP(L))*COSVOL(I)+(DVOLIS(L)+DVOLSP(L))
     *      *COSINE(I,L)
C                                          scalar of total heave
      VTOT=VTOT+V(I)**2
 4560 CONTINUE
C     ------------------------------------------------------------------
      VTOT=SQRT(VTOT)
C                                     direction cosines of heave
      IF(VTOT.LT.1.E-20) GO TO 4588
C     ------------------
      DO 4581 I=1,3
      COSVOL(I)=V(I)/VTOT
 4581 CONTINUE
C     ------------------
      GO TO 4587
C                                  DEFAULT TO VERTICAL FOR NO HEAVE
 4588 CONTINUE
      COSVOL(1)=0.0
      COSVOL(2)=0.0
      COSVOL(3)=1.0
C                                          increment the heaves
 4587 CONTINUE
      VOLIS(L)=VOLIS(L)+DVOLIS(L)
      VOLSP(L)=VOLSP(L)+DVOLSP(L)
C                                          record heave data
      BACKSPACE 8
      WRITE(8,1888)L,VOLSAP(L),VOLIS(L),VOLSP(L),(COSVOL(I),I=1,3)
C                                    orientation w.r.t. horizontal
      IF(COSVOL(2).LT.1.E-20) GO TO 4582
C
      ARG=COSVOL(3)/COSVOL(2)
C                                                  Beta in radians
      BETA=ATAN(ARG)
      GO TO 4583
C                                    vertical
 4582 BETA= PI / 0.5
 4583 CONTINUE
C                                    coefficient of thermal expansion
```

```
      VOLRAT=(VOLIS(L)+VOLSP(L))/VOLSAP(L)
      ALPHA=VOLRAT/(ABS(COS(BETA))+ABS(SIN(BETA)))/TDIF
C                                                          degrees
      BETA=BETA*180./PI
C
      RETURN
      END
C
C*************************************************************
C *                                                          *
C *          SUBROUTINE RECONN(IOUNIT,ICARRC,KOLUMN,LETTRS)  *
C *                                                          *
C*************************************************************
C
      INTEGER NEWFMT(3)
      DATA NEWFMT/'(I1,','A000',',A4)'/
C
C                              writes column position as integer
      IF(KOLUMN.LT.10)WRITE(99,9901)KOLUMN
 9901 FORMAT(1X,'I',I1)
      IF(KOLUMN.GE.10.AND.KOLUMN.LT.100)WRITE(99,9902)KOLUMN
 9902 FORMAT(1X,'I',I2)
      IF(KOLUMN.GE.100)WRITE(99,9903)KOLUMN
 9903 FORMAT(1X,'I',I3)
C
C                              reads column position as alpha-numeric
      READ(99,9904)NEWFMT(2)
 9904 FORMAT(1X,A4)
C
    1 CONTINUE
      READ(IOUNIT,NEWFMT),ID
      IF(I.NE.ICARRC)GO TO 1
      IF(ID.NE.LETTRS)GO TO 1
C
      RETURN
      END
C
C*************************************************************
C *                                                          *
C *      SUBROUTINE SHAPE(L,TEMPG,GRADTG,DJINV,VOLUME)       *
C *                                                          *
C *                                                          *
C *  THIS SUBROUTINE CALCULATES THE TEMPERATURES AT          *
C *  THE GAUSS POINTS  OF A  FOUR-NODE  ELEMENT  AT          *
C *  FOUR GAUSS POINTS. THE TEMPERATURES ARE STORED          *
C *  IN "TEMPG", ACCORDING TO THE GAUSS POINT LAYOUT         *
C *  IN THE DIAGRAM TO THE RIGHT.                            *
C *                                                          *
C*************************************************************
C
      COMMON/TEMPER/TEMP,TREF
      COMMON/GEOM/XYZ(3,200),XYZADT(3,200),NODELE(4,99),DISP(3,200)
C
      REAL*8  XI(4), ETA(4), TEMPG(4),TEMP(200)
      REAL    GRADTG(2,4), DJINV(4)
      INTEGER ITI(4), IETA(4)
C                                                     gauss co-ord
      DATA  XI/-0.577350269189626,+0.577350269189626,
     *        +0.577350269189626,-0.577350269189626/
      DATA ETA/-0.577350269189626,-0.577350269189626,
     *        +0.577350269189626,+0.577350269189626/
C                                                       node co-ord
      DATA ITI/+1,-1,-1,+1/,IETA/+1,+1,-1,-1/
C
C                                                    element volume
      VOLUME=0.0
C
           DO 22 NGAUSS=1,4
C                                                    matrix elements
           W11=0
           W12=0
           W21=0
           W22=0
C                                                    gaussian temperatures
           TEMPG(NGAUSS)=0.0
C                                                    local gradients
           DTDXI=0.
           DTDETA=0
C
                DO 22 NODE=1,4
                NGLOBE=NODELE(NODE,L)
C
                Y=XYZADT(2,NGLOBE)
                Z=XYZADT(3,NGLOBE)
C                               gauss temps  from shape functions
C
                TEMPG(NGAUSS)=TEMPG(NGAUSS)+0.25*TEMP(NGLOBE)
     *          *(1.+XI(NODE)*XI(NGAUSS))*(1.+ETA(NODE)*ETA(NGAUSS))
C
                PHIXI=XI(NODE)*(1+ETA(NODE)*ETA(NGAUSS))*0.25
                PHIETA=ETA(NODE)*(1.+XI(NODE)*XI(NGAUSS))*0.25
C
CCCCCCCCCC      WRITE(18,181)NGAUSS,PHIXI,PHIETA
C181)          FORMAT('GAUSS',I1,')    PHI/XI=',F8.4,'  PHI/ETA=',
CCCC &          F8.4)
C                                                    creating inverse jacobian
                W11=W11+PHIXI*Z
                W12=W12-PHIXI*Z
                W21=W21-PHIETA*Y
                W22=W22+PHIXI*Y
C                                                    calc the local gradt
                DTDXI=DTDXI+PHIXI*TEMP(NGLOBE)
                DTDETA=DTDETA+PHIETA*TEMP(NGLOBE)
   22      CONTINUE
C                                                    storing local grat.
CCCCCC     WRITE(18,1807)NGAUSS,DTDXI,DTDETA
C1807      FORMAT('G',I1,')     DT/DXI=',F8.4,' DT/DETA=',F8.4)
C
CCCCC WRITE(18,180))L,TEMPG
C180) FORMAT('E',I2,')',4(T15,'TEMPG=',F12.8/))
C
C                    determinant of pre-inverse jacobian(=det jacobian)
      DJINV(NGAUSS)=W11*W22-W12*W21
      IF(DJINV(NGAUSS).LT.0.0)GO TO 7999
C                                                    inverse jacobian
      W11=W11/DJINV(NGAUSS)
      W12=W12/DJINV(NGAUSS)
      W21=W21/DJINV(NGAUSS)
      W22=W22/DJINV(NGAUSS)
C
CCCCC WRITE(18,1809)DJINV(NGAUSS),W11,W12,W21,W22
C1809 FORMAT(5X,'DETERMINANT OF PRE-INVERSE JACOBIAN=',F8.4,//
CCCC & 2(T20,F12.4,T35,F12.4/))
C
C                          convert local gradient to global gradient
      GRADTG(1,NGAUSS)=W11*DTDXI + W12*DTDETA
      GRADTG(2,NGAUSS)=W21*DTDXI + W22*DTDETA
C
CCCCCCCC   WRITE(18,1800)L,NGAUSS,GRADTG(1,NGAUSS),GRADTG(2,NGAUSS)
C1800      FORMAT('E',I2,'G',I1,'GRADTG=',2(3X,F12.4))
C
      VOLUME=VOLUME+DJINV(NGAUSS)
   23  CONTINUE
C                                                    volume (r=1)
      WRITE(18,1800) L, VOLUME
 1800 FORMAT(100(1X,I4,3X,E15.8))
      GO TO 8000
C
 7999 CONTINUE
      WRITE(7,1890)L,NGAUSS,DJINV(NGAUSS)
```

```
 1890 FORMAT(T2,'JACOBIAN DETERMINANT FOR ELEMENT ',I3,', GAUSS P',
     & ,'(',I1,',',I1,') IS ',F12.7)
 8000 CONTINUE
      RETURN
      END
C
C ***********************************************************************
C *                                                                     *
C *                  SUBROUTINE SKIP(IGUNIT,NLINES)                     *
C *                                                                     *
C ***********************************************************************
C
C
      IF(NLINES.EQ.0)GO TO 1
      DO 1 I=1,NLINES
      READ(IGUNIT,88)
   88 FORMAT(1X,'THIS STATEMENT SKIPS A LINE')
    1 CONTINUE
C
      RETURN
      END
C ***********************************************************************
C **                                                                   **
C **              SUBROUTINE SPAN(L,EPS,NCTREF,FFSPAN)                 **
C **                                                                   **
C **       This program finds the length of the TREF isotherm          **
C **    passing through a freezing element.                            **
C **                                                                   **
C ***********************************************************************
      REAL*8 TEMP(200)
      REAL POINT(3,4)
C
      INTEGER JKLI(4),LIJK(4)
      DATA JKLI/2,3,4,1/,LIJK/4,1,2,3/
C
      COMMON/GEOM/XYZ(3,200),XYZADT(3,200),NODELE(4,88),DISP(3,200)
      COMMON/TEMPER/TEMP,TREF
      COMMON/THERMO/GRAD(3,88),GRADT(88),COSINE(3,88)
C
C                                                        no nodes @ TREF
      IF(NCTREF.EQ.0)GO TO 1092
C                                                        some nodes @ TREF
      GO TO (1111,2222,3333,4444),NCTREF
C
C***********************************************************************
C                                                        one node @ TREF
 1111 CONTINUE
      WRITE(7,7850) L
 7850 FORMAT(/' **B: ELEMENT ',I3,' HAS ONLY ONE NODE @ TREF.')
C
      IF(0.0.LT.EPS. AND .EPS.LT.1.0) GO TO 1092
      FFSPAN=1.0E-20
      GO TO 8888
C***********************************************************************
C                                                        two nodes @ TREF
 2222 CONTINUE
      NCOUNT=0
C     ------------------------------------------------------------------
      DO 2850 N=1,4
      NODE=NODELE(N,L)
      TDIF=TEMP(NODE)-TREF
      TDIF=ABS(TDIF)
      IF(TDIF.LT.1.0E-05) NCOUNT=NCOUNT+1
      IF(NCOUNT.EQ.1. AND .TDIF.LT.1.0E-05) NODE1=NODE
      IF(NCOUNT.EQ.NCTREF) GO TO 8888
 2850 CONTINUE
C     ------------------------------------------------------------------
C
 8888 CONTINUE
      NODE2=NODE
      GO TO 8887
C***********************************************************************
 3333 CONTINUE
C                                                        three nodes @ TREF
C     ------------------------------------------------------------------
      DO 2861 N=1,4
      NODE=NODELE(N,L)
      TDIF=TEMP(NODE)-TREF
      TDIF=ABS(TDIF)
      IF(TDIF GT 1 0E-05) GO TO 8888
 2861 CONTINUE
C     ------------------------------------------------------------------
 8888 CONTINUE
C
      NODE1=NODELE(LIJK(N),L)
      NODE2=NODELE(JKLI(N),L)
C***********************************************************************
C                                                        frost front span
 8887 CONTINUE
C
      FFSPAN=0.0
      DO 2862 I=1,3
      FFSPAN=FFSPAN+(XYZADT(I,NODE1)-XYZADT(I,NODE2))**2
 2862 CONTINUE
C
      FFSPAN=SQRT(FFSPAN)
C
      GO TO 8888
C***********************************************************************
C                                                        four nodes @ TREF
 4444 CONTINUE
      WRITE(7,7851) L
 7851 FORMAT(/' **WARNING: ELEMENT ',I3,' HAS FOUR NODES @ TREF '
     */'     SEGREGATION HEAVE SUSPENDED').
      FFSPAN=1.0E+20
      GO TO 8888
C
C***********************************************************************
C**                                                                   **
C**                  no nodes @ TREF                                  **
C**                                                                   **
C***********************************************************************
 1092 CONTINUE
      NPOINT=0
C                                                        interpolation for TREF
      DO 7292 N1=1,4
      N2=N1+1 - N1/4*4
      N1GLOB=NODELE(N1,L)
      N2GLOB=NODELE(N2,L)
      TN1=TEMP(N1GLOB)
      TN2=TEMP(N2GLOB)
      IF(TN1.GE.TREF. AND. TN2.LT.TREF) GO TO 7293
      IF(TN1.LE.TREF. AND. TN2.GT.TREF) GO TO 7293
C
      GO TO 7292
C                                                        determining end points
 7293 CONTINUE
      NPOINT=NPOINT+1
      TR=(TREF-TN1)/(TN2-TN1)
C                                                        TREF co-ordinates
      DO 7295 I=1,3
      POINT(I,NPOINT)=XYZADT(I,N1)+((XYZADT(I,N2)-XYZADT(I,N1)))*TR
 7295 CONTINUE
 7292 CONTINUE
C
C
C***********************************************************************
C                                                        two frost fronts
      IF(NPOINT.NE.4) GO TO 7298
      WRITE(7,794)L
  794 FORMAT(/' **WARNING: ELE ',I3,' HAS 2 FRONTS; NO SP HEAVE')
```

```
      FFSPAN=1.E-20
C
 7288 CONTINUE
C                                                  3 interpolation points
      IF(NPOINT.EQ.3)WRITE(7,795)L
  795 FORMAT(/' ***ERROR: ELE ',I3,' HAS 3 MID-SDRY TREF INTCPTS ')
C
C                                                        frost front span
          DO 7382 I=1,3
          FFSPAN=FFSPAN+(POINT(I,2)-POINT(I,1))**2
 7382     CONTINUE
          FFSPAN=SQRT(FFSPAN)
C
C**********************************************************************
 8869 CONTINUE
      RETURN
      END
C
C_____________________________________________________________________
C     *                                                               *
C     *          SUBROUTINE SPTL(L,SPO,C,STRPRP,SPVALU)               *
C     *                                                               *
C     *    THIS SUBROUTINE FINDS THE SOIL'S SEGREGATION               *
C     *    POTENTIAL AS A FUNCTION OF APPLIED PRESSURE IN             *
C     *    THE DIRECTION OF THE THERMAL GRADIENT                      *
C     *                                                               *
C     *    CALLS: STRESS                                              *
C     *    NEEDS: STRPRP                                              *
C     *    FINDS: SPVALU  IN MM**2/S/K                                *
C     * * * * * * * * * * * * * * * * * * * * * * * * * * * * * * * * *
C
C     ****************************************************************
C     segregation potential=f(pressure)              (Konrad, pg.387+)
C
C     LOG(SP) = LOG(SPO) - C*PE
C
C     ****************************************************************
C
C                    units: spo in mm**2/s/k, c in mm**2/s/k/kPa
C     ****************************************************************
C     *                                                              *
C     *                CALL STRESS( L , STRPRP    )                 *
C     *                                          !strprp in kPa!     *
C     ****************************************************************
C
      SPVALU=10**(ALOG10(SPO)-C*STRPRP)
C                                        Konrad&Morgenstern, CGJ'86
      SPVALU=SPO*EXP(-C*STRPRP)
C
      RETURN
      END
C * * * * * * * * * * * * * * * * * * * * * * * * * * * * * * * * * *
C *                                                                   *
C *          SUBROUTINE STRESS( LMN, STRPRP )                         *
C *                                                                   *
C *    THIS SUBROUTINE FINDS THE MAGNITUDE OF THE STRESS              *
C *    PERPENDICULAR TO THE FROST FRONT FOR EACH ELEMENT              *
C *                                                                   *
C *    CALLED BY: SPTL                                                *
C *        NEEDS: LMN=ELEMENT NUMBER                                  *
C *        FINDS: SIGPRP(3), STRPRP                                   *
C *        UNITS: kPa                                                 *
C * * * * * * * * * * * * * * * * * * * * * * * * * * * * * * * * * *
C
      REAL SIGPRP(3),STRPRP,SUMSIG(3)
C
      COMMON/THERMO/GRAD(3,99),GRADT(99),COSINE(3,99)
      COMMON/FORCES/PRNCPL(3,99),COSSIG(3,3,99)
      COMMON/INPO/NUMNP,NELE,T
C
C                                                  .element & principal stresses
C                                                  (following command suspended)
CCCCCCC  WRITE(17,017)(LMN,I),PRNCPL(I,LMN),I=1,3)
   017   FORMAT(/1X,'L',I3,3(3X,'SIGMA',I1,'=',F10.5))
C                                                thermal gradient direction cosines
C                                                  (following command suspended)
CCCCCCCC WRITE(17,117)(I,COSINE(I,LMN),I=1,3)
   117   FORMAT(/' THERM ',3('COSINE',I1,'=',F10.7,2X))
C
C                                    ensure dir cos are in the gradt dir
      DO 2337 J=1,3
C
      DOT=0.0
      DOT=DOT+COSSIG(1,J,LMN)*COSINE(1,LMN) +COSSIG(2,J,LMN)
     *  *COSINE(2,LMN) + COSSIG(3,J,LMN)*COSINE(3,LMN)
      IF(DOT GT.0.0)GO TO 2337
C
C                                          reverse the direction cosine
        DO 2338 I=1,3
        COSSIG(I,J,LMN)=(-1.0)*  COSSIG(I,J,LMN)
 2338   CONTINUE
 2337 CONTINUE
C                                                  stress direction cosines
C                                                  (following command suspended)
CCCCCCC  DO 2335 I=1,3
CCCCCCC  WRITE(17,019)(COSSIG(I,J,LMN),J=1,3)
C 019    FORMAT(' COSSIG = ',3( 3(F10.7,2X) ) /)
C2335    CONTINUE
C
        STRPRP=0.0
C
        DO 2005 I=1,3
C                                        element's sym2 stress resultants
          SUMSIG(I)=0
C
          DO 2006 J=1,3
          SUMSIG(I)=SUMSIG(I)+COSSIG(I,J,LMN)*PRNCPL(J,LMN)
 2006     CONTINUE
C
C                      dot product with thermal gradient cosines
C                        to get the magnitude of perp'r stress
C
        STRPRP=STRPRP+SUMSIG(I)*COSINE(I,LMN)
C
 2005   CONTINUE
C                                        check for tension || thermal gradient
      IF(STRPRP.GE.0.0)GO TO 795
      WRITE(7,794)STRPRP,LMN
  794 FORMAT(1X,'THE STRESS PERP''R TO FROST FRONT ',
     *,F8.2,'kPa, ELEMENT ',I3,', WAS SET TO ZERO ')
      STRPRP=0.0
C
  795 CONTINUE
      RETURN
      END
C * * * * * * * * * * * * * * * * * * * * * * * * * * * * * * * * * *
C *                                                                   *
C *          SUBROUTINE TIME(T,DT,TNEW,DTNEW,SSTEMP)                  *
C *                                                                   *
C *    THIS SUBROUTINE DETERMINES THE PRESENT TIME INCREMENT,         *
C *    THE FUTURE TIME AND THE FUTURE TIME INCREMENT FOR THE          *
C *    ADINAT INPUT AND FOR TIME CALCULATIONS WITHIN THE              *
C *    ANCILLARY PROGRAM                                              *
C *                                    NEEDS  T                       *
C *                                    FINDS  DT,TNEW,DTNEW           *
C *                                                                   *
C * * * * * * * * * * * * * * * * * * * * * * * * * * * * * * * * * *
```

```
C                                                  (nb: ensure time curves in
C                                                   SAP & ADINAT i/p files are
C                                                   longer than this time curve )
      REAL EPOCH(16)
      INTEGER NDIVS(15),
C
      READ(2,201)(EPOCH(I),I=1,16)
  201 FORMAT(1088.0)
      READ(2,202)(NDIVS(I),I=1,15)
  202 FORMAT(1018)
C                                                        convert days to hours
      DO 501 I=1,16
      EPOCH(I)=EPOCH(I)*24
  501 CONTINUE
C
C                                                                determine dt
      ASSIGN 3998 TO ICNTRL
      TSUBR=T
C                 ------------------------------------------
            DO 2001 J=1,15
            JPLUS1=J+1
            TSUM=EPOCH(J)
            TSPAN=EPOCH(JPLUS1)-EPOCH(J)
            MAX=NDIVS(J)-1
C
            IF(TSUM.GT.(TSUBR+0.995-.00))) GO TO ICNTRL,(3998,3999)
 4000       CONTINUE
C                 ------------------------------------------
                  DO 2002 K=1,MAX
                  TSUM=EPOCH(J)+TSPAN*K/NDIVS(J)
                  IF(TSUM.GT.(TSUBR+0.995)) GO TO ICNTRL,(3998,3999)
 2002             CONTINUE
C                 ------------------------------------------
 2001       CONTINUE
C           ------------------------------------------
C
 3998 T=TSUM
      DT=TSPAN/NDIVS(J)
      TSUBR=T+DT
C                                                  ..... determine tnew, dtnew
      ASSIGN 3999 TO ICNTRL
      GO TO 4000
C
 3999 TNEW=TSUM
      DTNEW=TSPAN/NDIVS(J)+ 1.0E-06
C                                                  CALCS FOR SOIL SURF  TEMP
C                                          (this function is problem-specific)
      TDAYS=TNEW/24.

      TCALC=TDAYS-INT((TDAYS/365.25))*365.25
C                                                        "n" factors- frz/tha
      FACTRN=0.90
      IF(20..LE.TCALC.AND.TCALC.LE.203.)FACTRN=1.03
C                                                  ... Temp. Mean & Amplitude
      AMPL  = 14.5
      TMEAN =  2.5
C                                                        (calcs. in "days")
      SSTEMP=TMEAN + AMPL*FACTRN*SIN(((TCALC-30.7/58.1313))
C
      RETURN
      END

C     *  *  *  *  *  *  *  *  *  *  *  *  *  *  *  *  *  *  *  *  *  *  *  *
C     *                                                                     *
C     *                  V A R I A B L E S                                  *
C     *                                                                     *
C     *    THIS IS A PARTIAL LISTING OF THE VARIABLES USED IN               *
C     *    THE SUBROUTINES AND A SHORT DESCRIPTION OF EACH                  *
C     *                                                                     *
C     *    (NOT UP-TO-DATE)                                                 *
C     *                                                                     *
C     *  *  *  *  *  *  *  *  *  *  *  *  *  *  *  *  *  *  *  *  *  *  *  *
C
C  FLUX(I)          X,Y,Z THERMAL GRADIENTS @ INTEGRATION POINTS
C  GRAD(I)          X,Y,Z COMPONENTS OF AVG. THERMAL GRADIENT
C  NCOUNT           COUNTER OF THE NUMBER OF THE THERMAL GRADIENTS
C  GRADT            MAGNITUDE OF THE THERMAL GRADIENT
C  COS(I)           DIRECTION COSINES OF GRADT
C  SPLOT(I,J)       THE SP=F(PRESSURE) X-Y POINTS
C  SIG(I)           SIGXX SIGXY SIGYY SIGZZ SIGYZ SIGZX
C  PRNCPL           PRINCIPAL STRESSES - SIGMA-1 SIGMA-2 SIGMA-3
C  COSSIG           DIRECTION COSINES OF PRNCPL
C  WORKER           SUBROUTINE EIGEN WORKSPACE
C  STRPRP           STRESS PERPENDICULAR TO FROST FRONT
C  NODELE(L,IJKL)   ELEMENT NUMBER, ELEMENT NODES
C  NXYZ(N,IJK)      NODE NUMBER, X,Y,Z
C  SP               SEGREGATION POTENTIAL, AS A FUNCTION OF PRESSURE
C  TEMP(N)          NODAL TEMPERATURE
C  EPS(L)           FROZEN FRACTION
C  EPSOLD(L)        PREVIOUS FROZEN FRACTION
C  DEPS(L)          CHANGE IN FROZEN FRACTION
C  I                XYZ INDICATOR
C  N                NODE NUMBER INDICATOR
C  L                ELEMENT NUMBER INDICATOR
C  DDS(I)           INCREMENTAL HEAVE DUE TO FREEZING OF ATTRACTED WATER
C  DDIS(I)          INCREMENTAL HEAVE DUE TO FREEZING OF IN SITU WATER
C  D(L,I)           ELEMENTS' TOTAL HEAVE IN THE XYZ DIRECTIONS
C  NEDS(J)          THE SKIP1V HEADING
C  NEDT(J)          THE ADINAT HEADING
C  T                PRESENT TIME
C  CHAR(J)          ALPHANUMERIC DATA
```

Sample Input Files, N.E.S. Site:

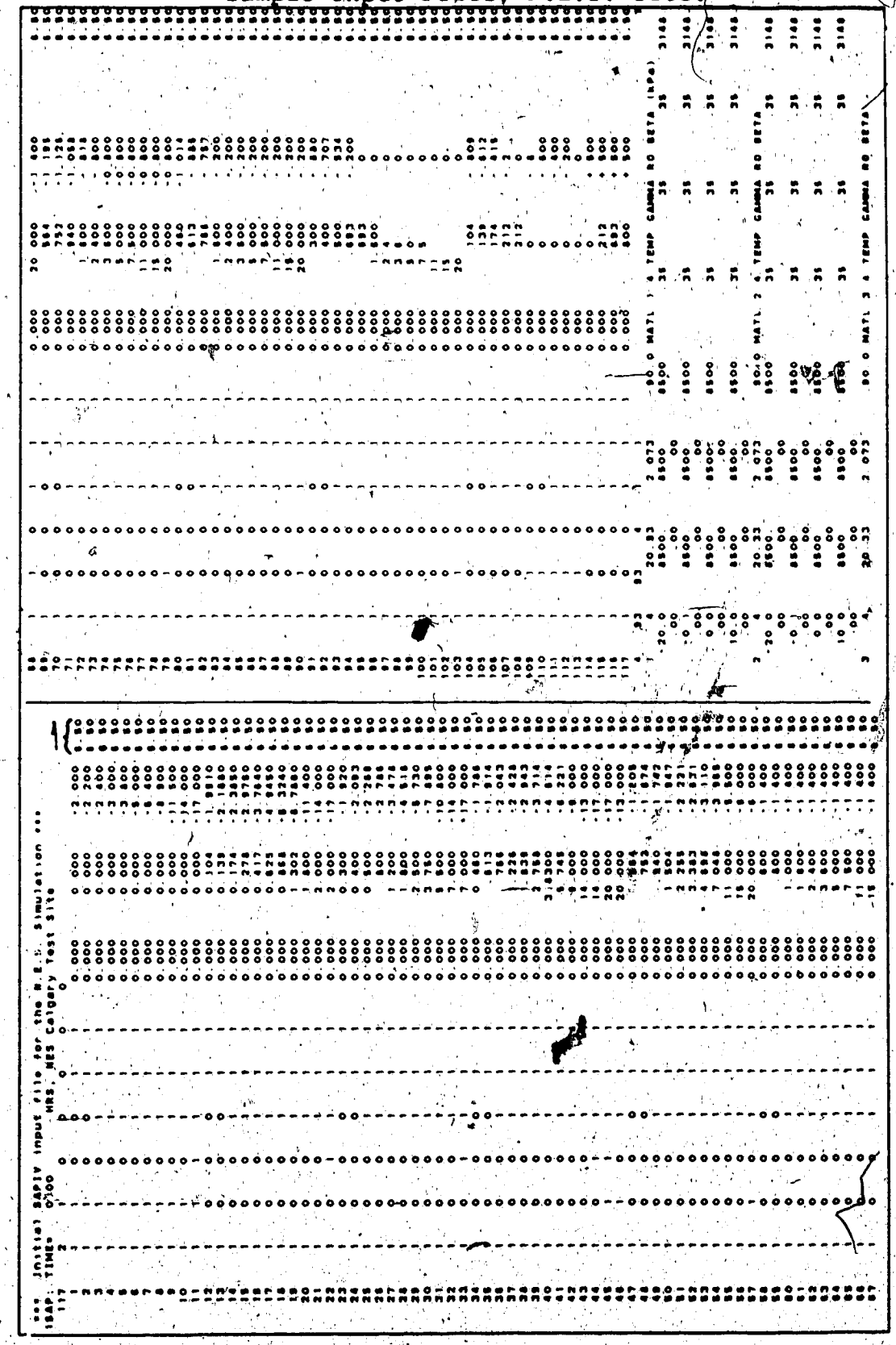

```
 4    4      20.33      2.073      80.0 MATL  4  4 TEMP  GAMMA  RO  BETA
-20.0      8500.      8500.      8500.          .35        .35        .35      3148.
  .00         .00        .00
 -0.1      8500.      8500.      8500.          .35        .35        .35      3148.
  .00         .00        .00
  0.0      8500.      8500.      8500.          .35        .35        .35      3148.
  .00         .00        .00
 10.0      8500.      8500.      8500.          .35        .35        .35      3148.
  .00         .00        .00
 5    4      20.33      2.073      80.0 MATL  5  4 TEMP  GAMMA  RO  BETA
-20.0      8500.      8500.      8500.          .35        .35        .35      3148.
  .00         .00        .00
 -0.1      8500.      8500.      8500.          .35        .35        .35      3148.
  .00         .00        .00
  0.0      8500.      8500.      8500.          .35        .35        .35      3148.
  .00         .00        .00
 10.0      8500.      8500.      8500.          .35        .35        .35      3148.
  .00         .00        .00
 6    4      20.33      2.073      80.0 MATL  6  4 TEMP  GAMMA  RO  BETA
-20.0      8500.      8500.      8500.          .35        .35        .35      3148.
  .00         .00        .00
 -0.1      8500.      8500.      8500.          .35        .35        .35      3148.
  .00         .00        .00
  0.0      8500.      8500.      8500.          .35        .35        .35      3148.
  .00         .00        .00
 10.0      8500.      8500.      8500.          .35        .35        .35      3148.
  .00         .00        .00
 7    4      20.33      2.073      80.0 MATL  7  4 TEMP  GAMMA  RO  BETA
-20.0      8500.      8500.      8500.          .35        .35        .35      3148.
  .00         .00        .00
 -0.1      8500.      8500.      8500.          .35        .35        .35      3148.
  .00         .00        .00
  0.0      8500.      8500.      8500.          .35        .35        .35      3148.
  .00         .00        .00
 10.0      8500.      8500.      8500.          .35        .35        .35      3148.
  .00         .00        .00
 8    4      20.33      2.073      80.0 MATL  8  4 TEMP  GAMMA  RO  BETA
-20.0      8500.      8500.      8500.          .35        .35        .35      3148.
  .00         .00        .00
 -0.1      8500.      8500.      8500.          .35        .35        .35      3148.
  .00         .00        .00
  0.0      8500.      8500.      8500.          .35        .35        .35      3148.
  .00         .00        .00
 10.0      8500.      8500.      8500.          .35        .35        .35      3148.
  .00         .00        .00
 9    4      20.33      2.073      80.0 MATL  9  4 TEMP  GAMMA  RO  BETA
-20.0      8500.      8500.      8500.          .35        .35        .35      3148.
  .00         .00        .00
 -0.1      8500.      8500.      8500.          .35        .35        .35      3148.
  .00         .00        .00
  0.0      8500.      8500.      8500.          .35        .35        .35      3148.
  .00         .00        .00
 10.0      8500.      8500.      8500.          .35        .35        .35      3148.
  .00         .00        .00
10    4      20.33      2.073      80.0 MATL 10  4 TEMP  GAMMA  RO  BETA
-20.0      8500.      8500.      8500.          .35        .35        .35      3148.
  .00         .00        .00
 -0.1      8500.      8500.      8500.          .35        .35        .35      3148.
  .00         .00        .00
  0.0      8500.      8500.      8500.          .35        .35        .35      3148.
  .00         .00        .00
 10.0      8500.      8500.      8500.          .35        .35        .35      3148.
```

```
90    4      20.33      2.073      90.0 MATL      TEMP  GAMMA  RO  BETA (KPA)
-20.0      8500.      8500.      8500.          .35        .35        .35      3148.
  .00         .00        .00
 -0.1      8500.      8500.      8500.          .35        .35        .35      3148.
  .00         .00        .00
  0.0      8500.      8500.      8500.          .35        .35        .35      3148.
  .00         .00        .00
 10.0      8500.      8500.      8500.          .35        .35        .35      3148.
  .00         .00        .00
91    4      20.33      2.073      90.0 MATL      TEMP  GAMMA  RO  BETA (KPA)
-20.0      8500.      8500.      8500.          .35        .35        .35      3148.
  .00         .00        .00
 -0.1      8500.      8500.      8500.          .35        .35        .35      3148.
  .00         .00        .00
  0.0      8500.      8500.      8500.          .35        .35        .35      3148.
  .00         .00        .00
 10.0      8500.      8500.      8500.          .35        .35        .35      3148.
  .00         .00        .00
92    4      20.33      2.073      90.0 MATL      TEMP  GAMMA  RO  BETA (KPA)
-20.0      8500.      8500.      8500.          .35        .35        .35      3148.
  .00         .00        .00
 -0.1      8500.      8500.      8500.          .35        .35        .35      3148.
  .00         .00        .00
  0.0      8500.      8500.      8500.          .35        .35        .35      3148.
  .00         .00        .00
 10.0      8500.      8500.      8500.          .35        .35        .35      3148.
  .00         .00        .00
93    4      20.33      2.073      90.0 MATL      TEMP  GAMMA  RO  BETA (KPA)
-20.0      8500.      8500.      8500.          .35        .35        .35      3148.
  .00         .00        .00
 -0.1      8500.      8500.      8500.          .35        .35        .35      3148.
  .00         .00        .00
  0.0      8500.      8500.      8500.          .35        .35        .35      3148.
  .00         .00        .00
 10.0      8500.      8500.      8500.          .35        .35        .35      3148.
  .00         .00        .00
  1.0        0.0        0.0        0.0        0.0        0.0        A  T P C(XYZ)
  0.0        1.0        0.0        0.0        0.0        0.0        B
  0.0        0.0        0.0        0.0        1.0        0.0        C
  0.0        0.0        0.0        0.0        0.0        0.0        D
  1     2     3    14    13     1    -0.100       0.0        0.0        0.0      1.0000
  2    13    14    25    24     2    -0.100       0.0        0.0        0.0      1.0000
  3    24    25    36    35     3    -0.100       0.0        0.0        0.0      1.0000
  4    35    36    48    48     4    -0.100       0.0        0.0        0.0      1.0000
  5    48    49    60    59     5    -0.100       0.0        0.0        0.0      1.0000
  6    59    60    71    70     6    -0.100       0.0        0.0        0.0      1.0000
  7    70    71    82    81     7    -0.100       0.0        0.0        0.0      1.0000
  8    81    82    93    92     8    -0.100       0.0        0.0        0.0      1.0000
  9    92    93   106   105     9    -0.100       0.0        0.0        0.0      1.0000
 10   105   106   111   110    10    -0.100       0.0        0.0        0.0      1.0000
 11     2     4    15    14    11    -0.100       0.0        0.0        0.0      1.0000
 12    14    15    28    25    12    -0.100       0.0        0.0        0.0      1.0000
 13    25    26    37    36    13    -0.100       0.0        0.0        0.0      1.0000
 14    36    37    50    49    14    -0.100       0.0        0.0        0.0      1.0000
 15    48    50    61    60    15    -0.100       0.0        0.0        0.0      1.0000
 16    60    61    72    71    16    -0.100       0.0        0.0        0.0      1.0000
 17    71    72    83    82    17    -0.100       0.0        0.0        0.0      1.0000
 18    82    83    94    93    18    -0.100       0.0        0.0        0.0      1.0000
```

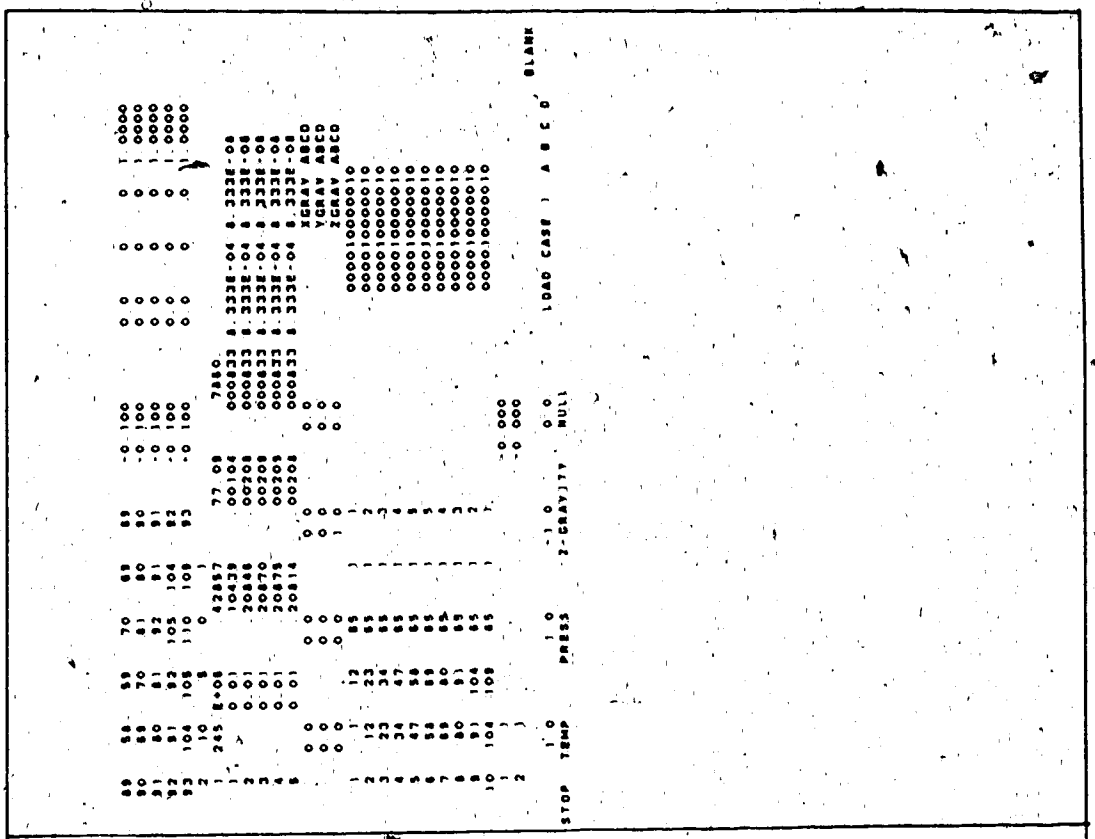
BLANK
LOAD CASE 1 A B C D
2-GRAVITY
PRESS
STOP TEMP

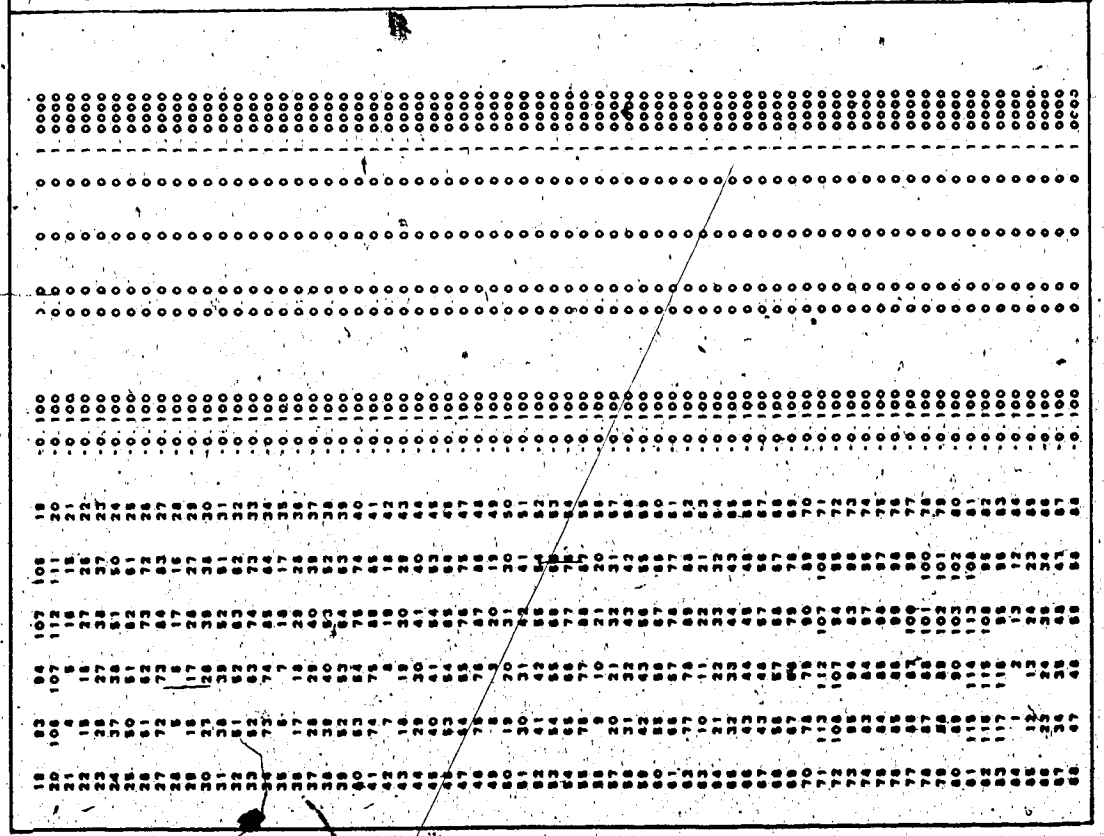

```
*** This is file "1" ("TRANS" input file for the N.S. data) ***

 NELE=  NUMBER OF ELEMENTS IN THE MESH              93
RO=     THE SOIL MASS DENSITY                    2.023   ( G/CC )
GS=     SPECIFIC GRAVITY, SOLIDS                 2.66
EPSLON= FREEZING FRACTION, IN-SITU WATER         0.900     fraction
NSPPRS= NUMBER OF ELEMENT RANGES,SPO,C
    1    93 230.0E-06    9.8E-03          ( MM**2/S/K ) (1/KPA)

 23456789 123456789 123456789 123456789 123456789 123456789 12345678



*** This is file "2" ("TRANS" input for time discretization) ***

     0.      1.      7.     21.     30.    385.    400.
      2       3       6       2      11       1

 23456789 123456789 123456789 123456789 123456789 123456789 12345678
COMMENT: REMEMBER TO CHANGE TIME AND TIME INCR. IN ORIGINAT I/P @t=0.0
 (10 DATA PAIRS ALLOWED)
 data currently in days; modify "TRANS" program to change units
```

```
*** Initial ADINAT file for the "TRANS" analysis of the NES Site

1ADINAT/TIME        0.0     HRS, NES CALGARY-TEST SITE
  117    0    1.    1    1.        0.0    1    1.
    1    0    1                          IHEAT IHEATN NLATHT
    0                                    IEIC  (THERMAL FREQ SOL'N)
    1    1  300    1.E-04                 ISREF IEQUIT ITEMAX RTOL
         1          1.0                  IOPE  ALPHA
    1    1                    NPB    IPRLM  #BLOCKS TEMP O/P, L-VECTOR
    1  117
    1
 43200.
   10    0      0.000      0.000     -2.000
    2    0      0.000      0.000     -2.200
    3    0      0.000      0.000     -2.400
    4    0      0.000      0.000     -3.000
    5    0      0.000      0.000     -3.800
    6    0      0.000      0.000     -5.000
    7    0      0.000      0.000     -6.400
    8    0      0.000      0.000     -8.800
    9    0      0.000      0.000    -11.500
   10    0      0.000      0.000    -16.000
   11    0      0.000      0.000    -17.000
   12    0      0.000      0.104     -1.9910
   13    0      0.000      0.139     -2.1880
   14    0      0.000      0.174     -2.3850
   15    0      0.000      0.278     -2.8780
   16    0      0.000      0.417     -3.7840
   17    0      0.000      0.828     -4.8480
   18    0      0.000      0.868     -6.3240
   19    0      0.000      1.302     -8.7880
   20    0      0.000      1.800    -11.400
   21    0      0.000      2.000    -14.000
   22    0      0.000      2.000    -17.000
   23    0      0.000      0.300     -1.820
   24    0      0.000      0.400     -2.093
   25    0      0.000      0.500     -2.266
   26    0      0.000       .800     -2.788
   27    0      0.000      1.200     -3.478
   28    0      0.000      1.800     -4.518
   29    0      0.000      2.500     -5.730
   30    0      0.000      3.750     -7.885
   31    0      0.000      5.500    -10.800
   32    0      0.000      7.000    -14.000
   33    0      0.000      7.000    -17.000
   34    0      0.000      0.480     -1.788
   35    0      0.000       .613     -1.814
   36    0      0.000       768     -2.043
   37    0      0.000      1.228     -2.428
   38    0      0.000      1.839     -2.943
   39    0      0.000      2.758     -3.714
   40    0      0.000      3.830     -4.614
   41    0      0.000      5.745     -6.221
   42    0      0.000      9.000     -8.000
   43    0      0.000     14.000    -13.000
   44    0      0.000     14.000    -17.000
   45    0      0.000     20.000    -17.000
   46    0      0.000     20.000    -13.000
   47    0      0.000       .584     -1.805
   48    0      0.000       752     -1.874
   49    0      0.000       940     -1.942
   50    0      0.000      1.304     -1.847
   51    0      0.000      2.255     -2.231
   52    0      0.000      3.383     -2.631
   53    0      0.000      4.698     -3.130
   54    0      0.000      7.048     -3.886
   55    0      0.000     11.000     -5.500
   56    0      0.000     15.000     -8.000
   57    0      0.000     20.000     -8.000
   58    0      0.000       .800     -1.400
   59    0      0.000       .800     -1.400
   60    0      0.000      1.000     -1.400
   61    0      0.000      1.800     -1.400
   62    0      0.000      2.400     -1.400
   63    0      0.000      3.800     -1.400
   64    0      0.000      5.000     -1.400
   65    0      0.000      7.500     -1.400
   66    0      0.000     11.000     -1.400
   67    0      0.000     15.000     -1.400
   68    0      0.000     20.000     -1.400
   69    0      0.000       584     -1.185
   70    0      0.000       752     -1.326
   71    0      0.000       940     -1.058
   72    0      0.000      1.800     -.818
   73    0      0.000      2.400     -.800
   74    0      0.000      3.600     -0.800
   75    0      0.000      5.000     -0.800
   76    0      0.000      7.500     -0.800
   77    0      0.000     11.000     -0.800
   78    0      0.000     15.000     -0.800
   79    0      0.000     20.000     -0.800
   80    0      0.000       460     -1.014
   81    0      0.000       613     -.888
   82    0      0.000       768     -.757
   83    0      0.000      1.600     -.200
   84    0      0.000      2.400     -.200
   85    0      0.000      3.800     -.200
   86    0      0.000      5.000     -.200
   87    0      0.000      7.500     -.200
   88    0      0.000     11.000     -.200
   89    0      0.000     15.000     -.200
   90    0      0.000     20.000     -.200
   91    0      0.000       300     -.880
   92    0      0.000       400     -.707
   93    0      0.000       500     -.534
   94    0      0.000       693     -.200
   95    0      0.000       693     0
   96    0      0.000      1.800    0
   97    0      0.000      2.4      0
   98    0      0.000      3.6      0
   99    0      0.000      5.0      0
  100    0      0.000      7.5      0
  101    0      0.000     11        0
  102    0      0.000     15        0
  103    0      0.000     20        0
  104    0      0.000       104     .805
  105    0      0.000       139     .812
  106    0      0.000       174     .435
  107    0      0.000       232     .2
  108    0      0.000       212     .0
  109    0      0.000         0     .8
  110    0      0.000         0     .800
  111    0      0.000         0     .400
  112    0      0.000         0     .200
  113    0      0.000         0     0
  114    0      0.000         0     .500
  115    0      0.000       212     .500
  116    0      0.000       883     .500
  117    0      0.000       800     .500
    1    1                        ICOR JPRIC (init cond free 18yr)
-3.20000000  2.38485885  2.88120832  3.29826412  4.18308328  5.08188648
5.87884443  5.68484185  6.07500875  6.69327838  6.87272762  -3.20000000
2.32809247  2.52232107  3.25174983  4.14725082  5.04588787  5.95864287
5.99252378  6.07474717  6.88970421  6.67302831  -3.20000000  2.03712288
2.21378333  2.88073183  3.70182217  4.73436888  5.39227050  6.87186189
6.87337884  6.87301392  6.87841288  -3.20000000  1.47841834  1.82078880
2.18719381  2.92858306  3.91705886  4.79488280  5.66213242  6.63889320
6.87181773  6.87823812  6.87834280  6.87118305  -3.20000000  0.71184338
0.78491212  1.11992056  1.80233886  2.30327523  3.10471727  4.22270979
5.07084387  5.27089288  6.28075328  -3.20000000  -0.10001000  -0.10001000
```

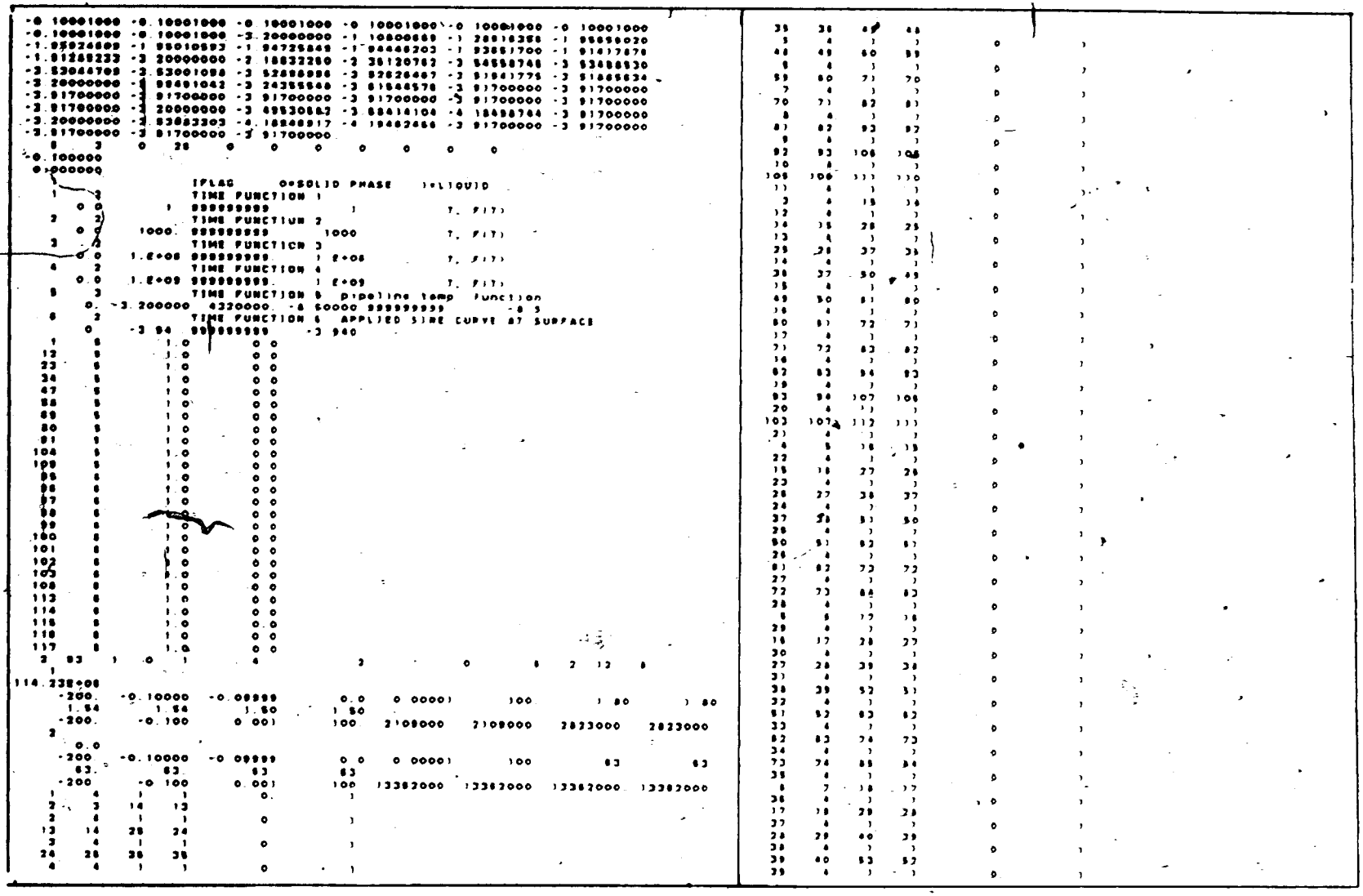

```
-0 10001000 -0.10001000 -0 10001000 -0 10001000 -0 10001000 -0 10001000 -0 10001000
-0.10001000 -0.10001000 -3.20000000 -1 10800688 -1 28818388 -1 99898020
-1.09824888 -1 99010593 -1 94725848 -1 94448203 -1 93881700 -1 91417878
-1.01288232 -3 20000000 -2 18832280 -2 38120782 -3 54558748 -3 53488530
-3.53044708 -2.53001098 -3 52888886 -3 52826467 -3 51841775 -2 51885834
-3 20000000 -1 99491042 -3 24355548 -3 61546578 -3 91700000 -3 91700000
-3.91700000 -3 91700000 -3 91700000 -3 91700000 -3 91700000 -3 91700000
-3.91700000 -3 20000000 -3 49530842 -3 88414104 -4 18488784 -3 91700000
-3.20000000 -3.83883203 -4.18488817 -4 18482466 -3 91700000 -3 91700000
-3.91700000 -3 91700000 -3 91700000
  8    3    0   28    0    0    0    0    0    0    0
-0.100000
 0.000000
     1          IFLAG     0=SOLID PHASE    1=LIQUID
     1    1     TIME FUNCTION 1
     0    0        1  9999999999          1            T, F(T)
     2    2     TIME FUNCTION 2
     0    0     1000. 9999999999       1000            T, F(T)
     3    2     TIME FUNCTION 3
     0    0  1.E+08 9999999999          1 E+08          T, F(T)
     4    2     TIME FUNCTION 4
     0.0  0  1.E+09 9999999999          1 E+09          T, F(T)
     5    3     TIME FUNCTION 5  Pipeline temp  function
     0.  -3.200000    4320000.  -8 60000 9999999999        -8 5
     6    2     TIME FUNCTION 6  APPLIED SINE CURVE AT SURFACE
     0     -3 94  9999999999     -3 940
       1    8          1.0          0 0
      12    8          1.0          0 0
      23    8          1.0          0 0
      34    8          1.0          0 0
      47    8          1.0          0 0
      58    8          1.0          0 0
      69    8          1.0          0 0
      80    8          1.0          0 0
      91    8          1.0          0 0
     104    8          1.0          0 0
     199    8          1.0          0 0
      85    8          1.0          0 0
      86    8          1.0          0 0
      87    8          1.0          0 0
      98    8          1.0          0 0
      99    8          1.0          0 0
     100    8          1.0          0 0
     101    8          1.0          0 0
     102    8          1.0          0 0
     103    8          1.0          0 0
     108    8          1.0          0 0
     113    8          1.0          0 0
     114    8          1.0          0 0
     116    8          1.0          0 0
     118    8          1.0          0 0
     117    8          1.0          0 0
   2  83    1   0    1        4          2          0       8   2  12    8
    1
114.238+08
    -200.   -0.10000   -0.09999      0.0   0 0000)      100        ) 80       ) 80
      1.54       1.54       1.50      1.50
    -200.    -0.100      0 001)      100   2)09000    2)09000    2823000    2823000
   2
     0.0
    -200    -0.10000   -0 09999      0 0   0 0000)      100         83         83
      83.        83         83        83
    -200.      -0 100     0.001)      100   13382000   13382000   13382000   13382000
     1    4     1    1       0.          1
     2    3    14   13                   )
     2    4     1    1       0           )
    13   14    25   24                   )
     3    4     1    1       0           )
    24   25    35   35                   )
     4    4     1    1       0           )
```

```
 35   36   47   48
  5    4    1    1       0           )
 48   49   60   59                   )
  6    4    1    1       0           )
 59   60   71   70                   )
  7    4    1    1       0           )
 70   71   82   81                   )
  8    4    1    1       0           )
 81   82   93   92                   )
  9    4    1    1       0           )
 92   93  106  105                   )
 10    4    1    1       0           )
105  106  111  110                   )
 11    4    1    1       0           )
  3    4   15   14                   )
 12    4    1    1       0           )
 24   25   28   27                   )
 13    4    1    1       0           )
 27   28   37   36                   )
 14    4    1    1       0           )
 36   37   50   49                   )
 15    4    1    1       0           )
 49   50   81   80                   )
 16    4    1    1       0           )
 80   81   72   71                   )
 17    4    1    1       0           )
 71   72   83   82                   )
 18    4    1    1       0           )
 82   83   94   93                   )
 19    4    1    1       0           )
 93   94  107  106                   )
 20    4    1    1       0           )
103  107  112  111                   )
 21    4    1    1       0           )
  4    5   16   15                   )
 22    4    1    1       0           )
 15   16   27   26                   )
 23    4    1    1       0           )
 26   27   38   37                   )
 24    4    1    1       0           )
 37   38   51   50                   )
 25    4    1    1       0           )
 50   51   82   81                   )
 26    4    1    1       0           )
 81   82   73   72                   )
 27    4    1    1       0           )
 72   73   84   83                   )
 28    4    1    1       0           )
  9    5   17   16                   )
 29    4    1    1       0           )
 16   17   28   27                   )
 30    4    1    1       0           )
 27   28   39   38                   )
 31    4    1    1       0           )
 38   39   52   51                   )
 32    4    1    1       0           )
 51   52   83   82                   )
 33    4    1    1       0           )
 82   83   74   73                   )
 34    4    1    1       0           )
 73   74   85   84                   )
 35    4    1    1       0           )
  8    7   18   17                   )
 36    4    1    1       0           )
 17   18   29   28                   )
 37    4    1    1       0           )
 28   29   40   39                   )
 38    4    1    1       0           )
 39   40   53   52                   )
 39    4    1    1       0           )
```

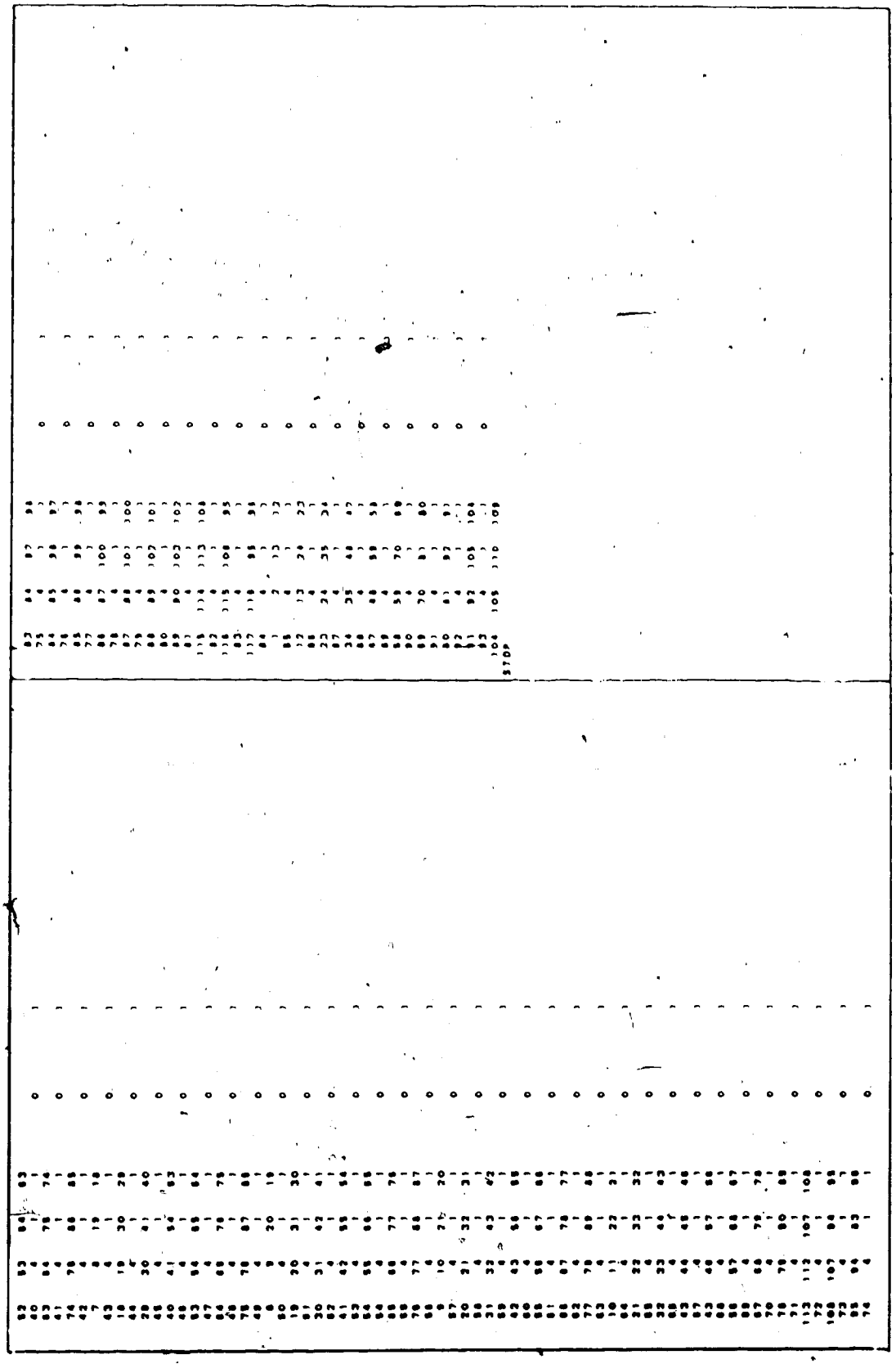

Appendice H: Procedure Files used with the Heave Calculations

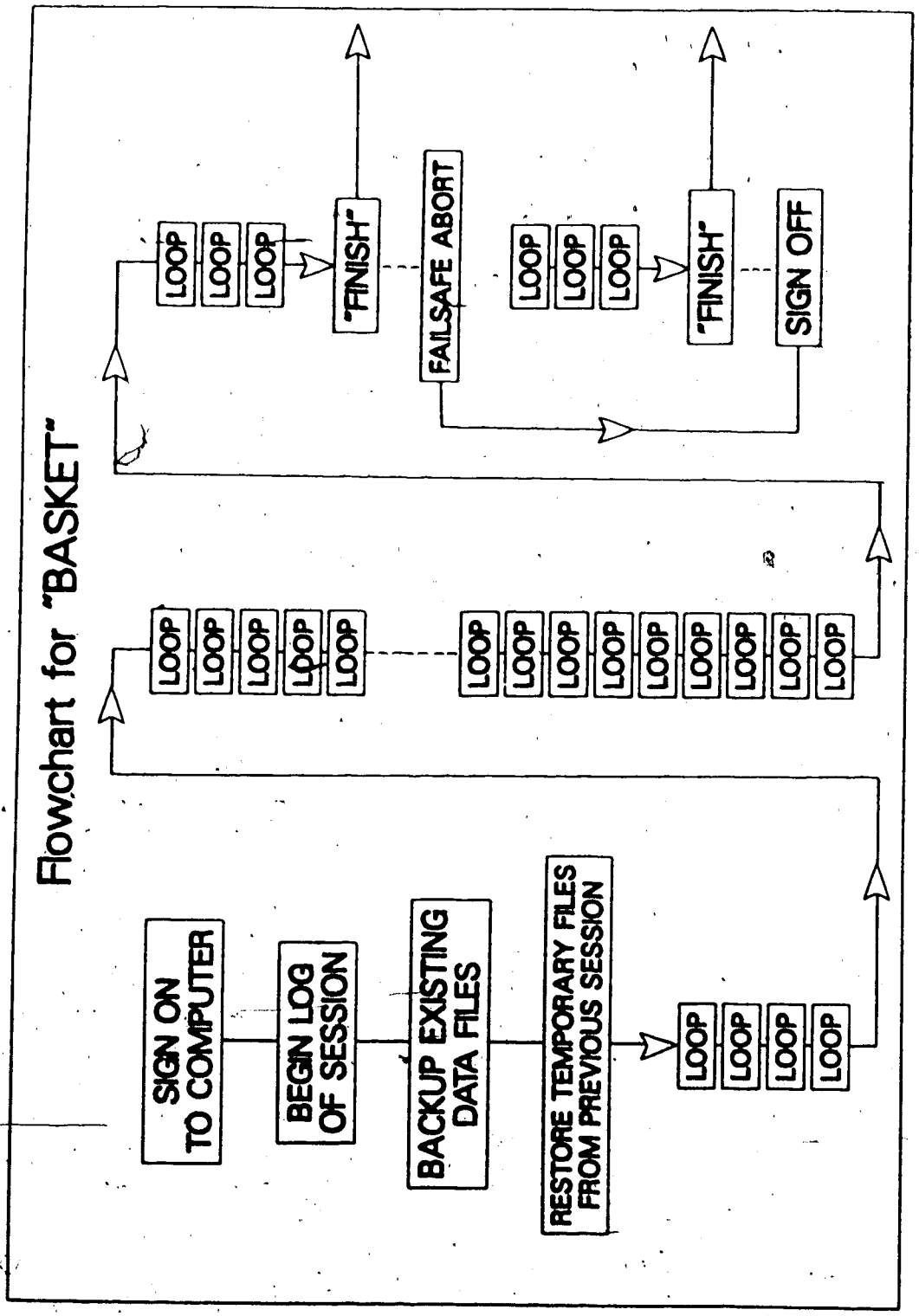

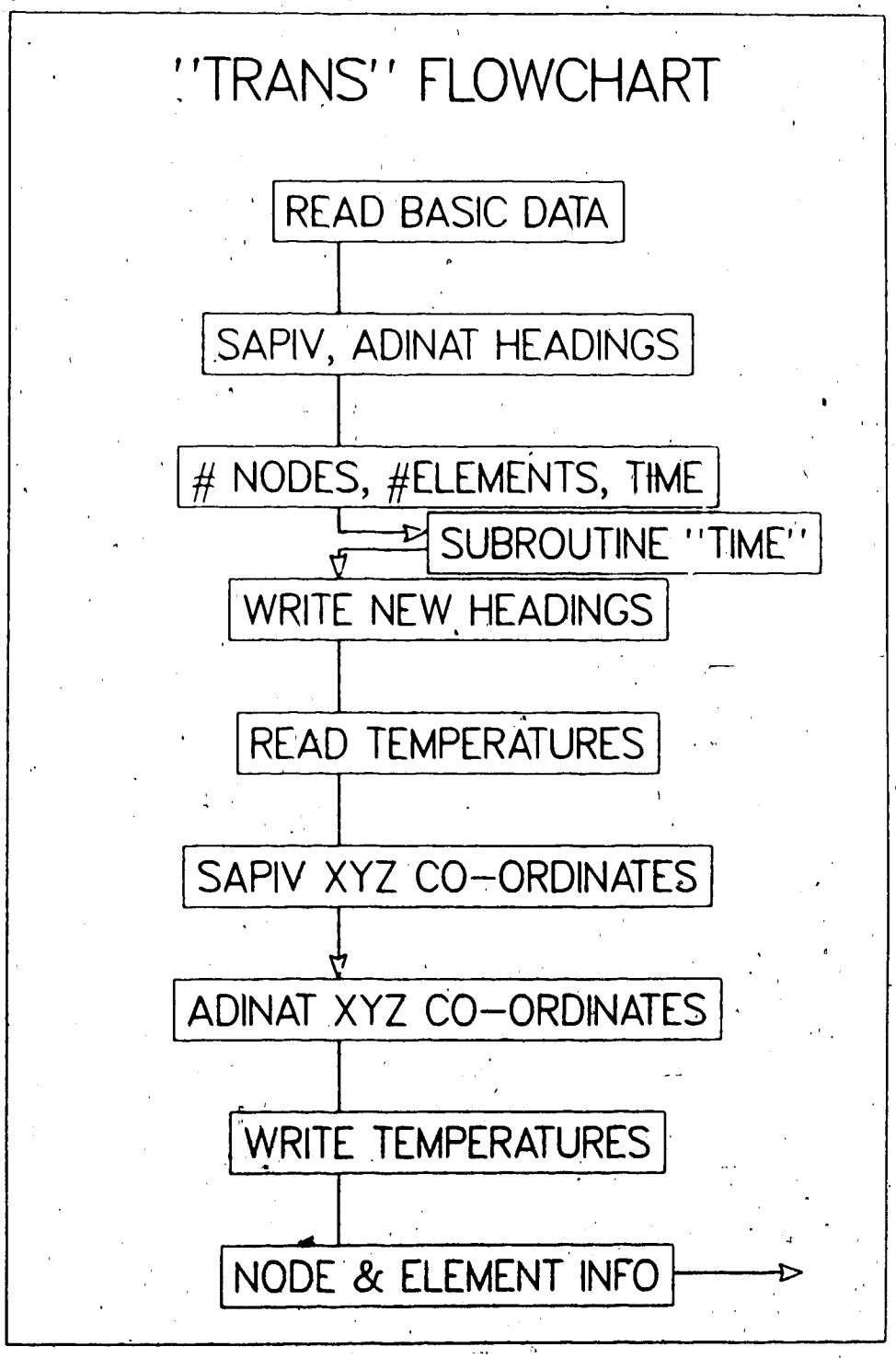
"TRANS" FLOWCHART
READ BASIC DATA
SAPIV, ADINAT HEADINGS
NODES, #ELEMENTS, TIME
SUBROUTINE "TIME"
WRITE NEW HEADINGS
READ TEMPERATURES
SAPIV XYZ CO-ORDINATES
ADINAT XYZ CO-ORDINATES
WRITE TEMPERATURES
NODE & ELEMENT INFO

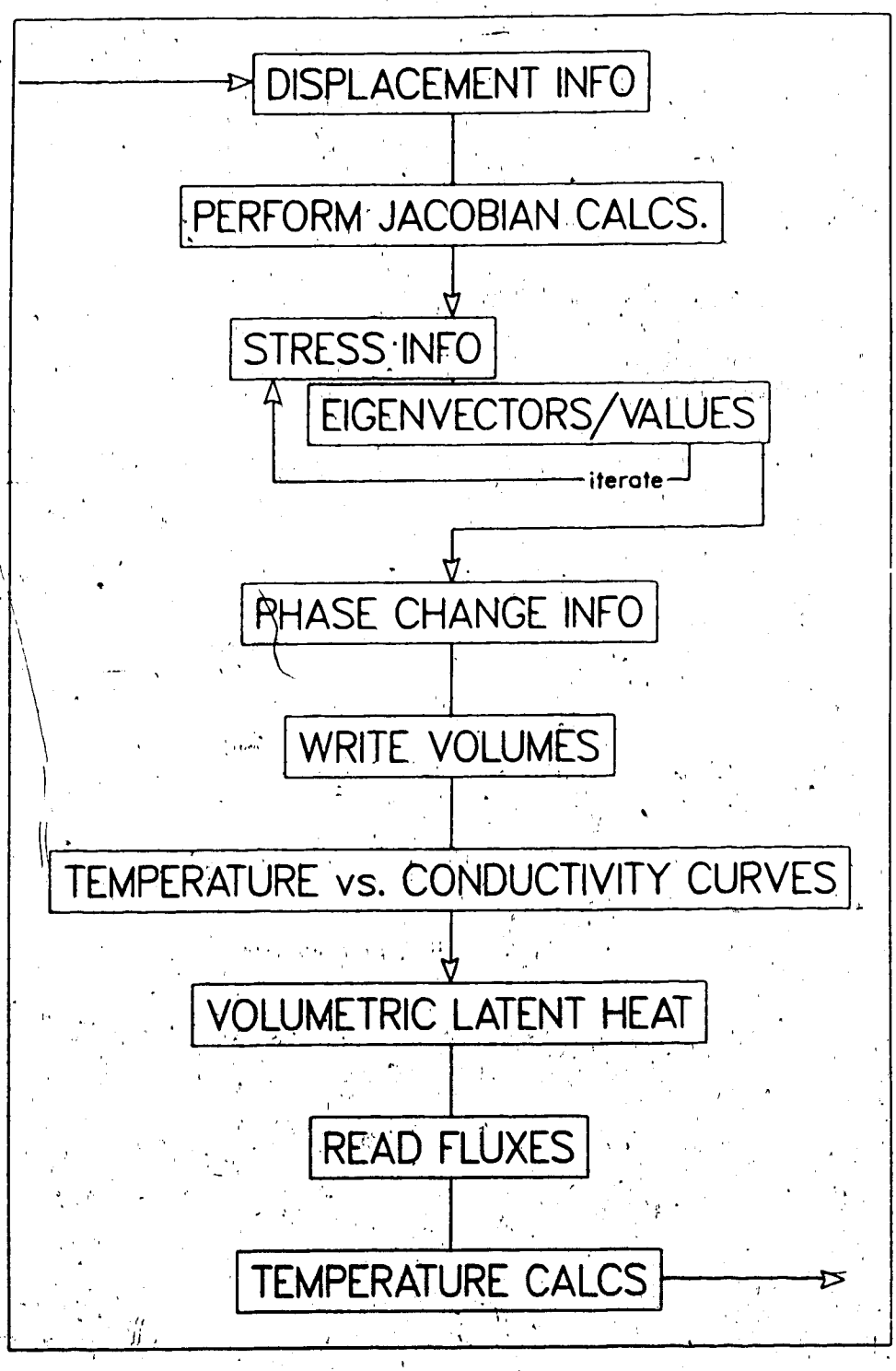
DISPLACEMENT INFO
PERFORM JACOBIAN CALCS.
STRESS INFO
EIGENVECTORS/VALUES
iterate
PHASE CHANGE INFO
WRITE VOLUMES
TEMPERATURE vs. CONDUCTIVITY CURVES
VOLUMETRIC LATENT HEAT
READ FLUXES
TEMPERATURE CALCS

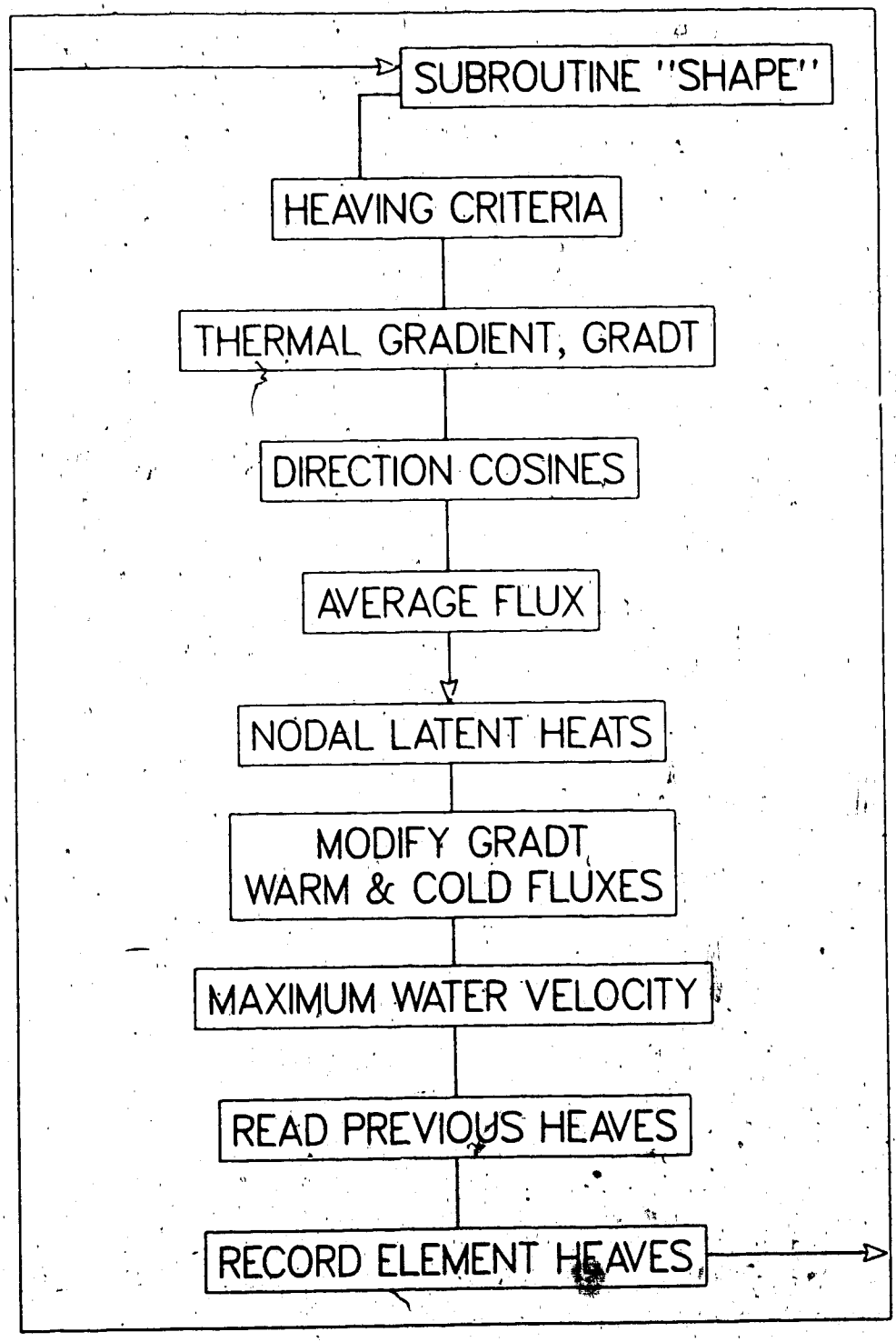
SUBROUTINE "SHAPE"
HEAVING CRITERIA
THERMAL GRADIENT, GRADT
DIRECTION COSINES
AVERAGE FLUX
NODAL LATENT HEATS
MODIFY GRADT
WARM & COLD FLUXES
MAXIMUM WATER VELOCITY
READ PREVIOUS HEAVES
RECORD ELEMENT HEAVES

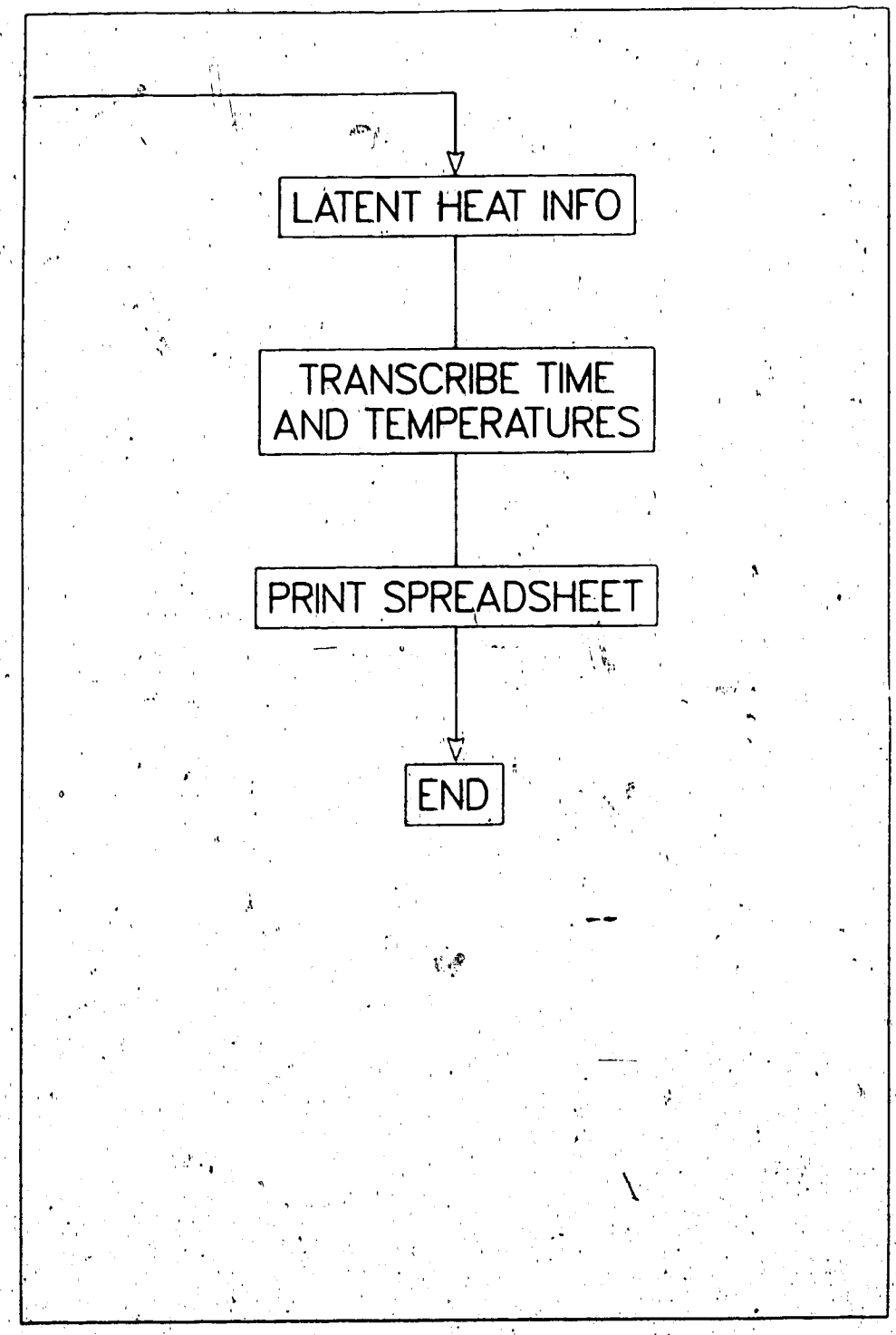
LATENT HEAT INFO
TRANSCRIBE TIME AND TEMPERATURES
PRINT SPREADSHEET
END

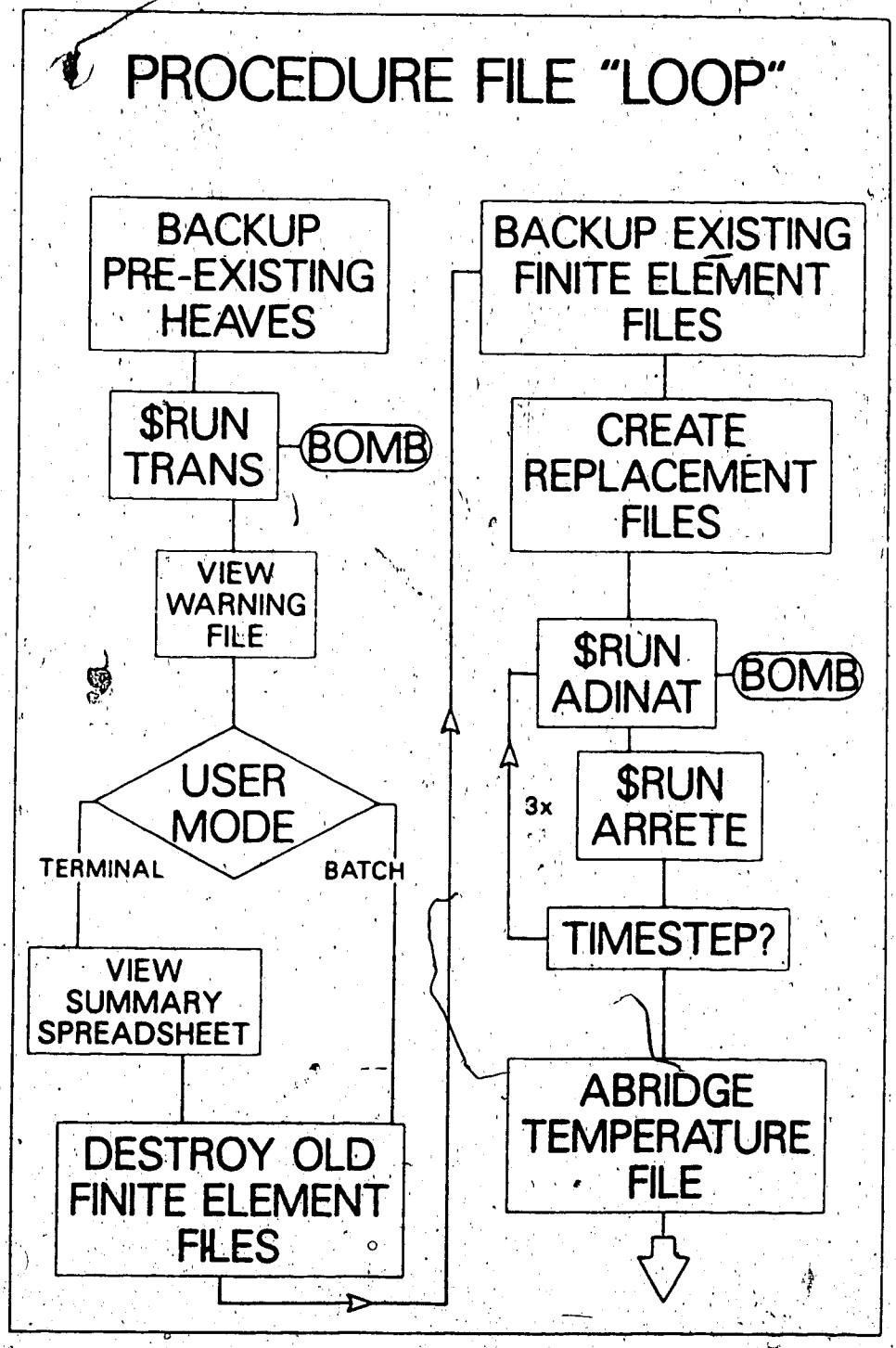
PROCEDURE FILE "LOOP"
BACKUP PRE-EXISTING HEAVES
$RUN TRANS
BOMB
VIEW WARNING FILE
USER MODE
TERMINAL
BATCH
VIEW SUMMARY SPREADSHEET
DESTROY OLD FINITE ELEMENT FILES
BACKUP EXISTING FINITE ELEMENT FILES
CREATE REPLACEMENT FILES
$RUN ADINAT
BOMB
3x
$RUN ARRETE
TIMESTEP?
ABRIDGE TEMPERATURE FILE

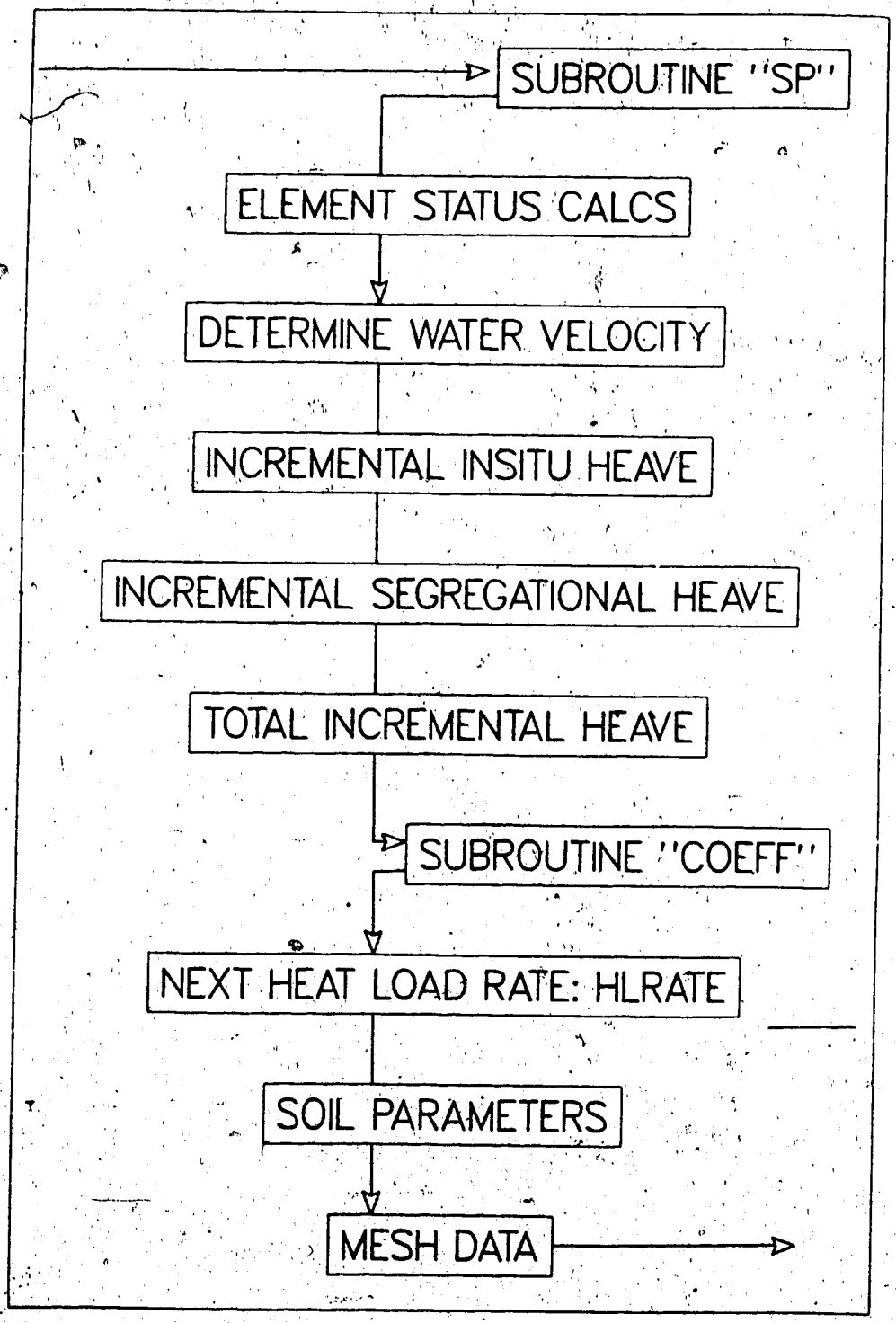
SUBROUTINE "SP"
ELEMENT STATUS CALCS
DETERMINE WATER VELOCITY
INCREMENTAL INSITU HEAVE
INCREMENTAL SEGREGATIONAL HEAVE
TOTAL INCREMENTAL HEAVE
SUBROUTINE "COEFF"
NEXT HEAT LOAD RATE: HLRATE
SOIL PARAMETERS
MESH DATA

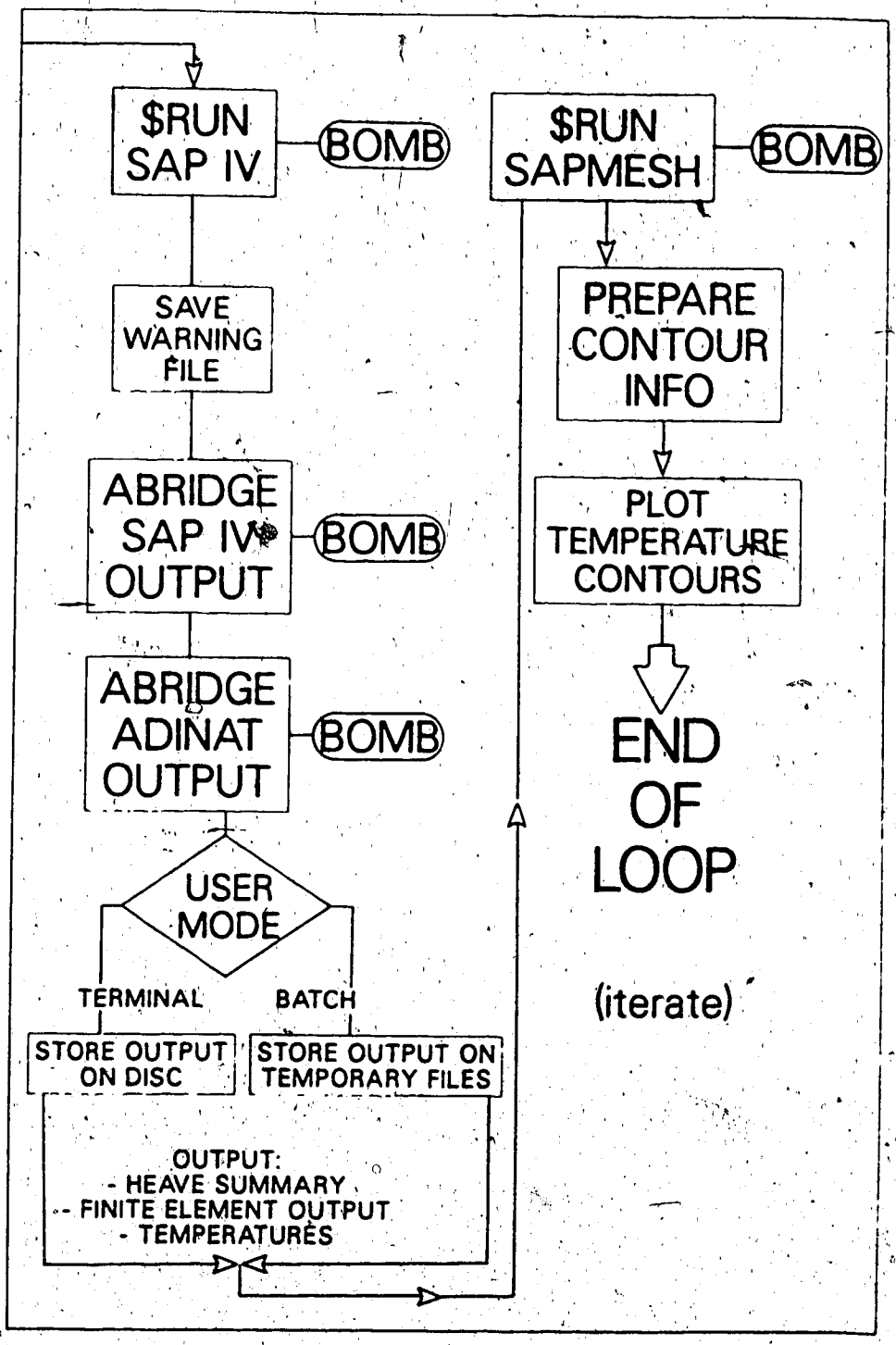
$RUN SAP IV
BOMB
SAVE WARNING FILE
ABRIDGE SAP IV OUTPUT
BOMB
ABRIDGE ADINAT OUTPUT
BOMB
USER MODE
TERMINAL
BATCH
STORE OUTPUT ON DISC
STORE OUTPUT ON TEMPORARY FILES
OUTPUT:
- HEAVE SUMMARY
- FINITE ELEMENT OUTPUT
- TEMPERATURES
$RUN SAPMESH
BOMB
PREPARE CONTOUR INFO
PLOT TEMPERATURE CONTOURS
END OF LOOP
(iterate)

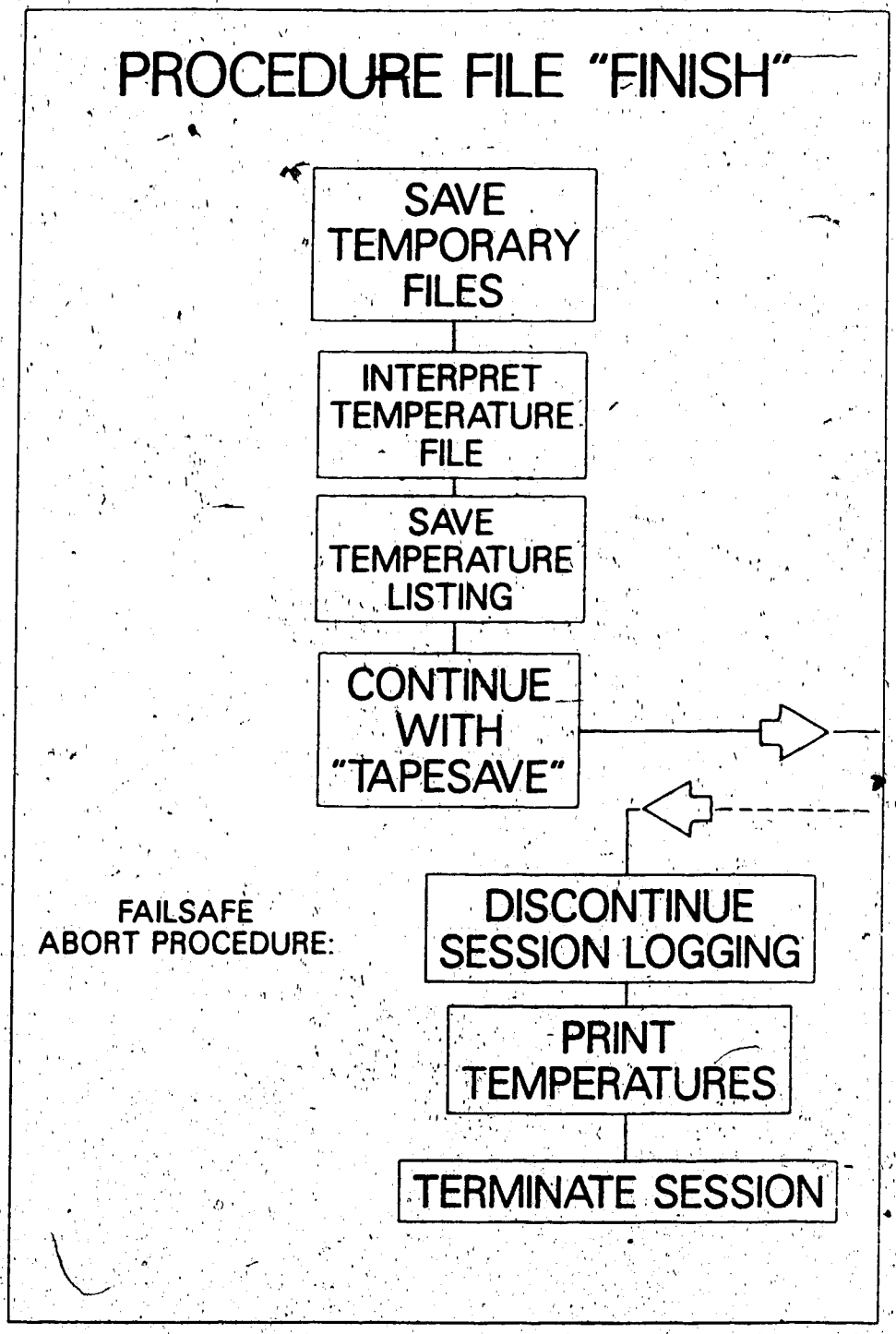
PROCEDURE FILE "FINISH"
SAVE TEMPORARY FILES
INTERPRET TEMPERATURE FILE
SAVE TEMPERATURE LISTING
CONTINUE WITH "TAPESAVE"
FAILSAFE ABORT PROCEDURE:
DISCONTINUE SESSION LOGGING
PRINT TEMPERATURES
TERMINATE SESSION

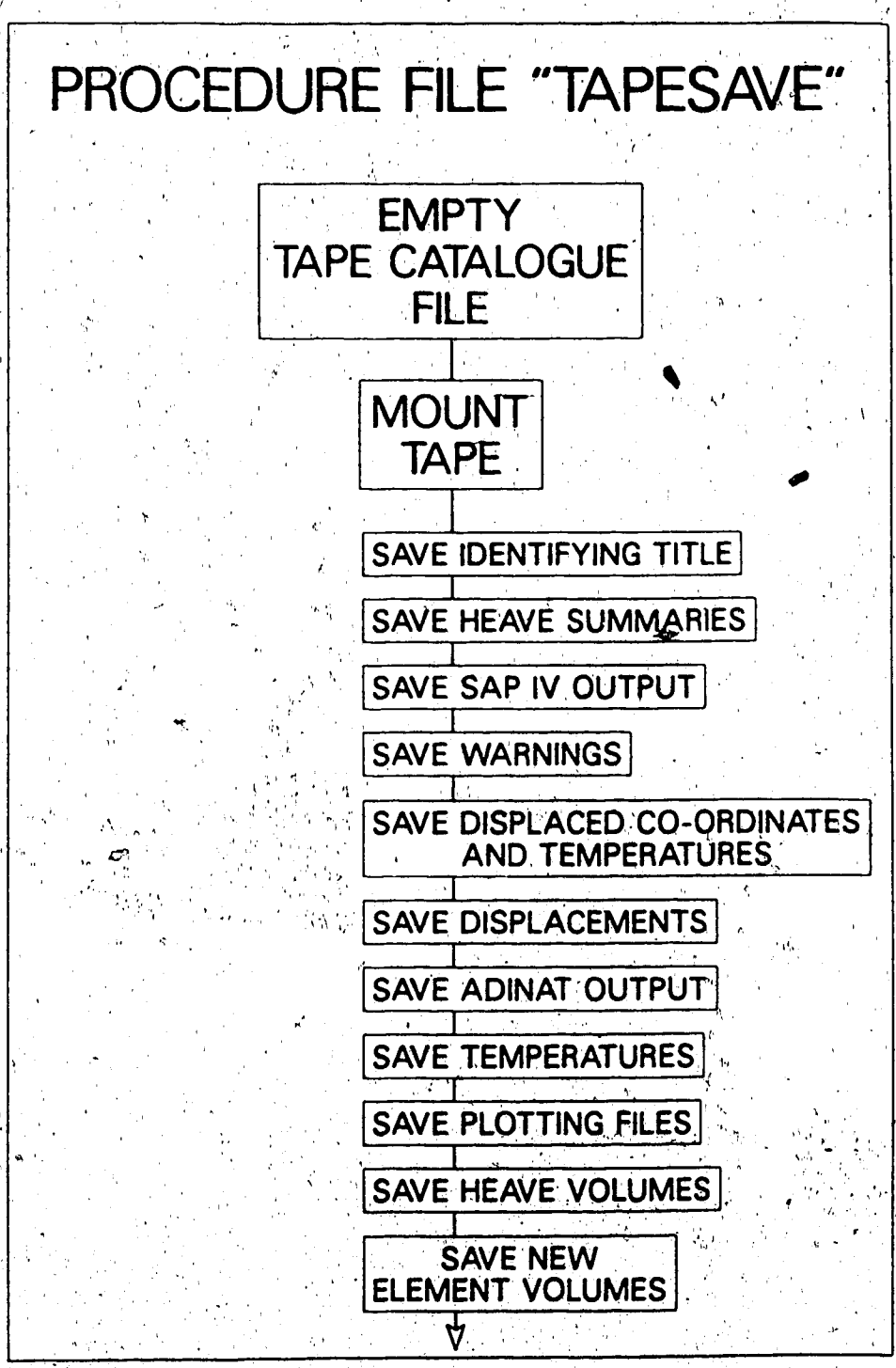
PROCEDURE FILE "TAPESAVE"
EMPTY TAPE CATALOGUE FILE
MOUNT TAPE
SAVE IDENTIFYING TITLE
SAVE HEAVE SUMMARIES
SAVE SAP IV OUTPUT
SAVE WARNINGS
SAVE DISPLACED CO-ORDINATES AND TEMPERATURES
SAVE DISPLACEMENTS
SAVE ADINAT OUTPUT
SAVE TEMPERATURES
SAVE PLOTTING FILES
SAVE HEAVE VOLUMES
SAVE NEW ELEMENT VOLUMES

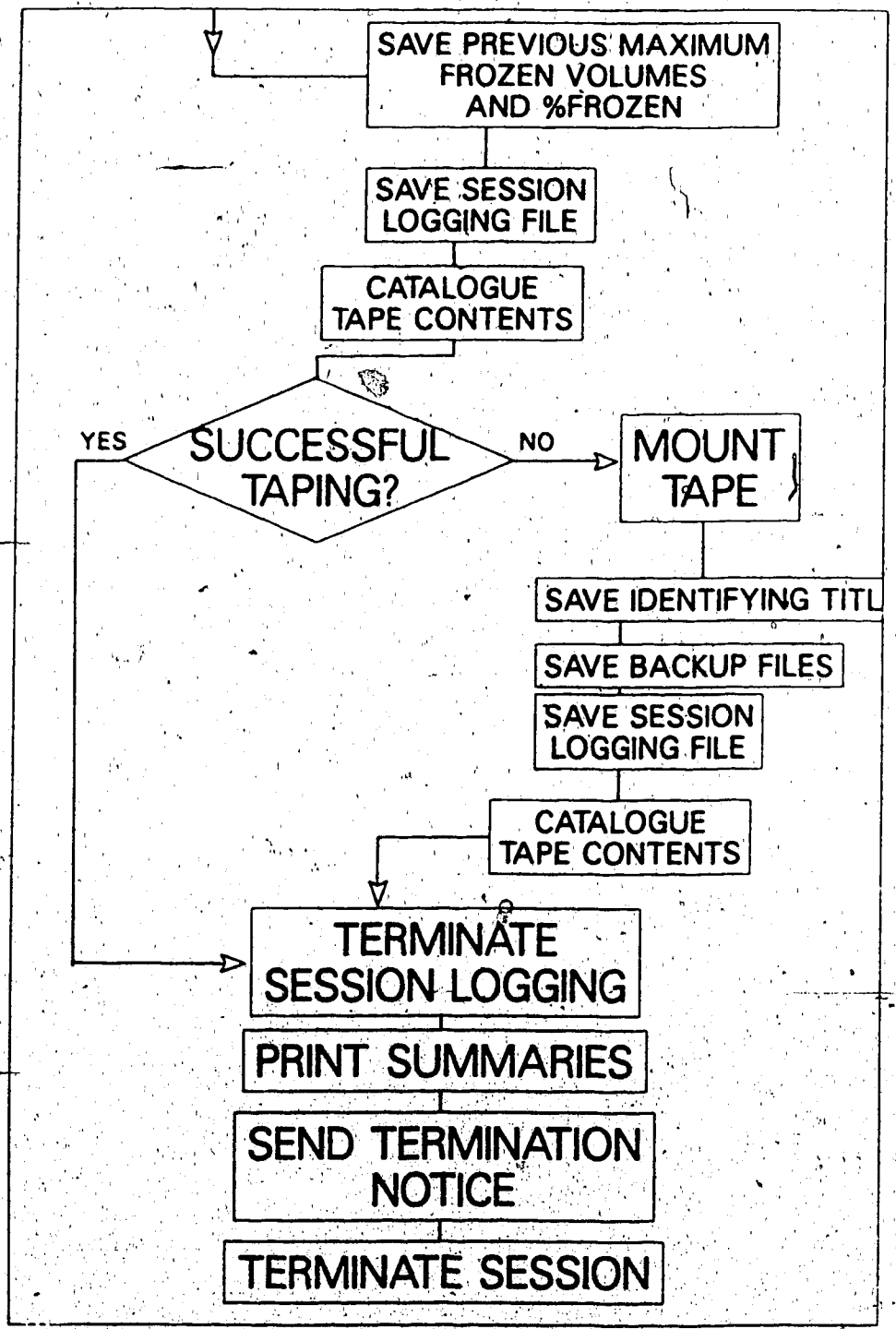
SAVE PREVIOUS MAXIMUM FROZEN VOLUMES AND %FROZEN
SAVE SESSION LOGGING FILE
CATALOGUE TAPE CONTENTS
YES
SUCCESSFUL TAPING?
NO
MOUNT TAPE
SAVE IDENTIFYING TITL
SAVE BACKUP FILES
SAVE SESSION LOGGING FILE
CATALOGUE TAPE CONTENTS
TERMINATE SESSION LOGGING
PRINT SUMMARIES
SEND TERMINATION NOTICE
TERMINATE SESSION

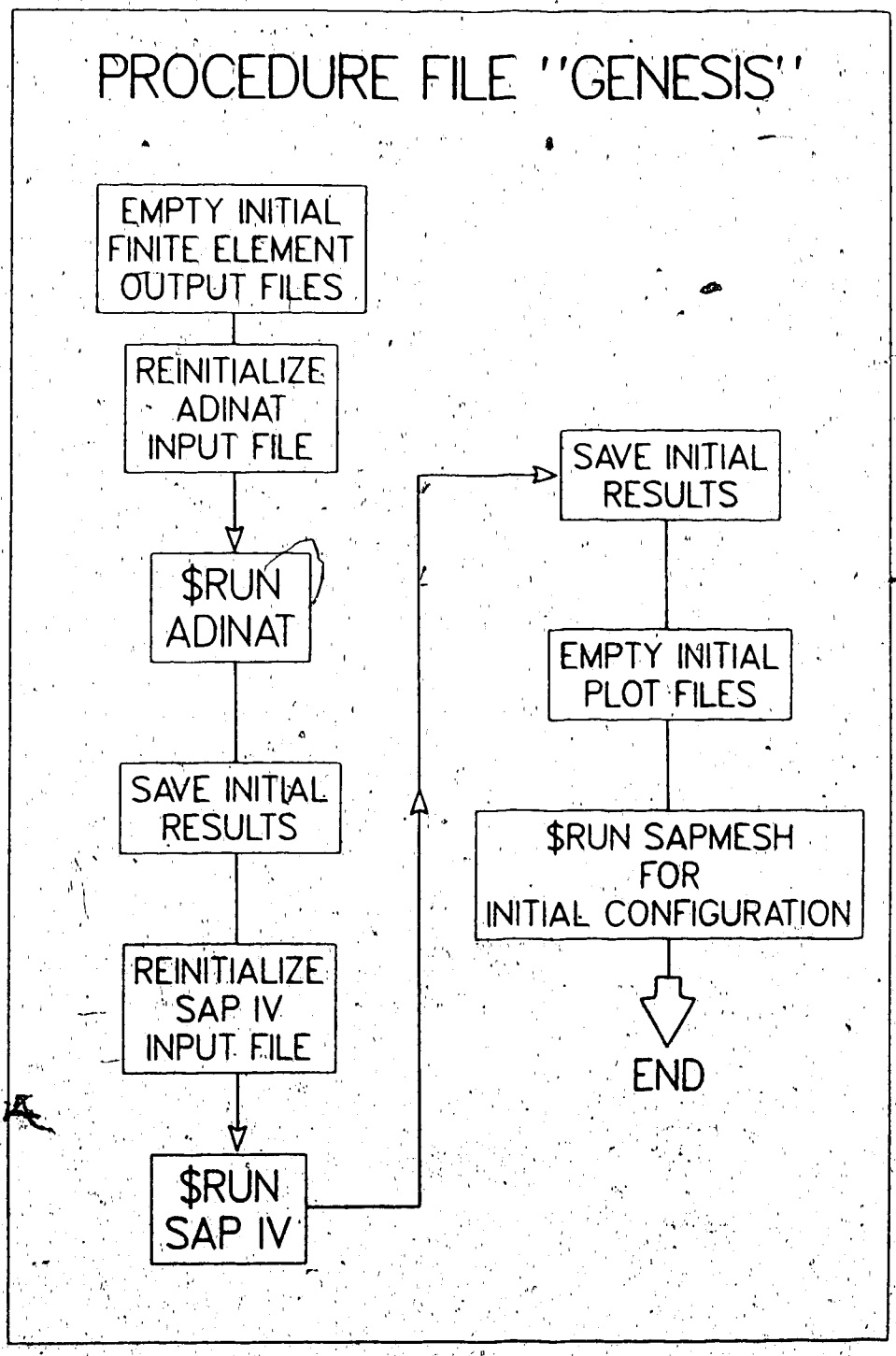
PROCEDURE FILE "GENESIS"
EMPTY INITIAL FINITE ELEMENT OUTPUT FILES
REINITIALIZE ADINAT INPUT FILE
$RUN ADINAT
SAVE INITIAL RESULTS
REINITIALIZE SAP IV INPUT FILE
$RUN SAP IV
SAVE INITIAL RESULTS
EMPTY INITIAL PLOT FILES
$RUN SAPMESH FOR INITIAL CONFIGURATION
END

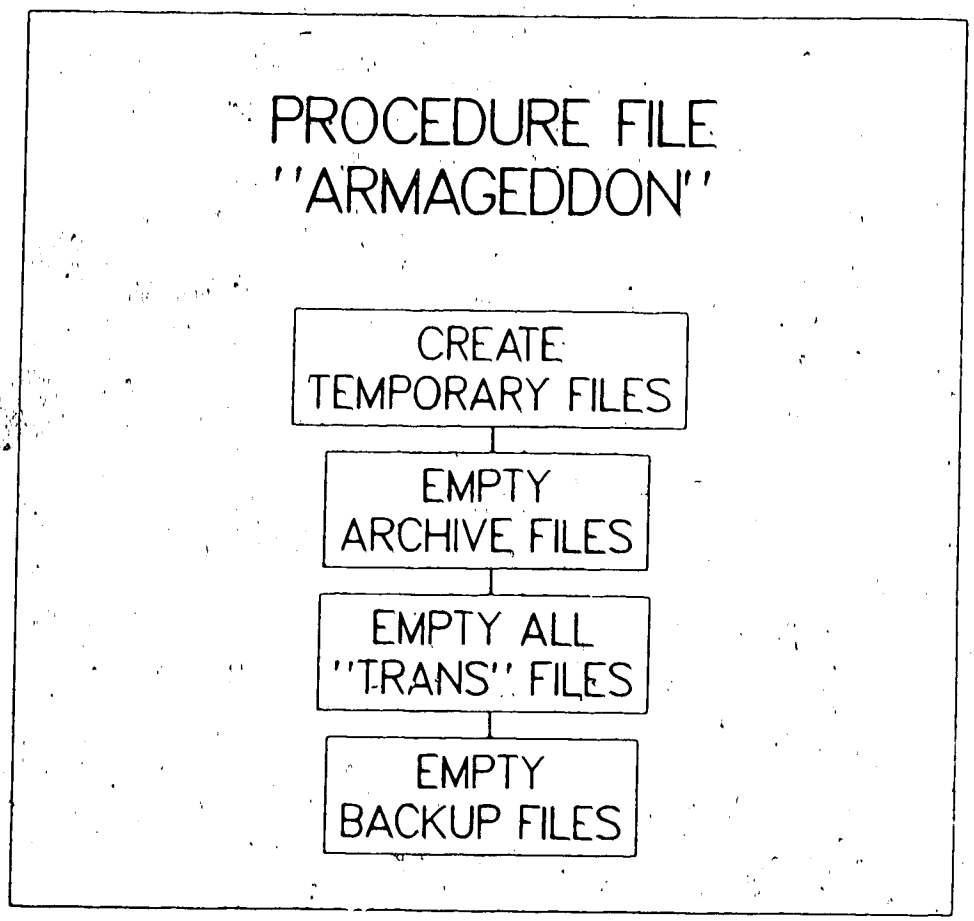
PROCEDURE FILE
"ARMAGEDDON"
CREATE TEMPORARY FILES
EMPTY ARCHIVE FILES
EMPTY ALL "TRANS" FILES
EMPTY BACKUP FILES

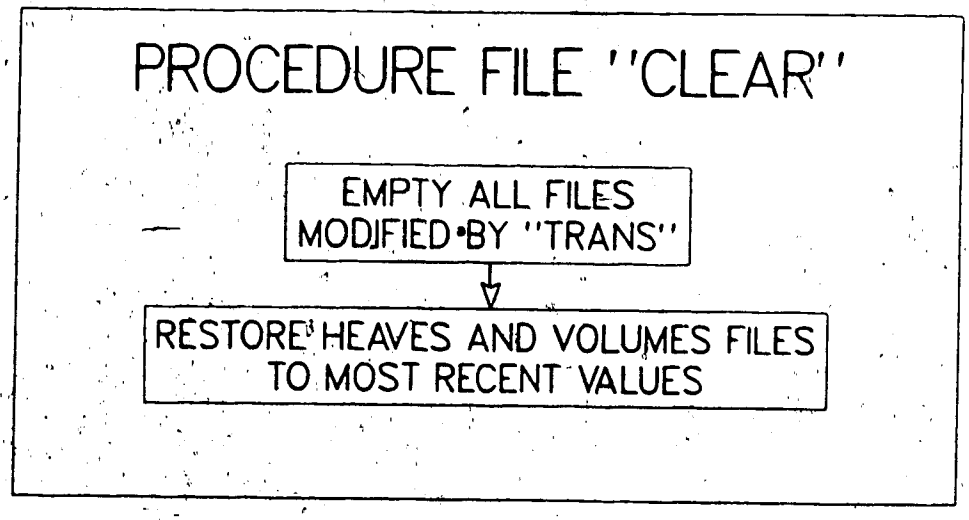
PROCEDURE FILE "CLEAR"
EMPTY ALL FILES MODIFIED BY "TRANS"
RESTORE HEAVES AND VOLUMES FILES TO MOST RECENT VALUES

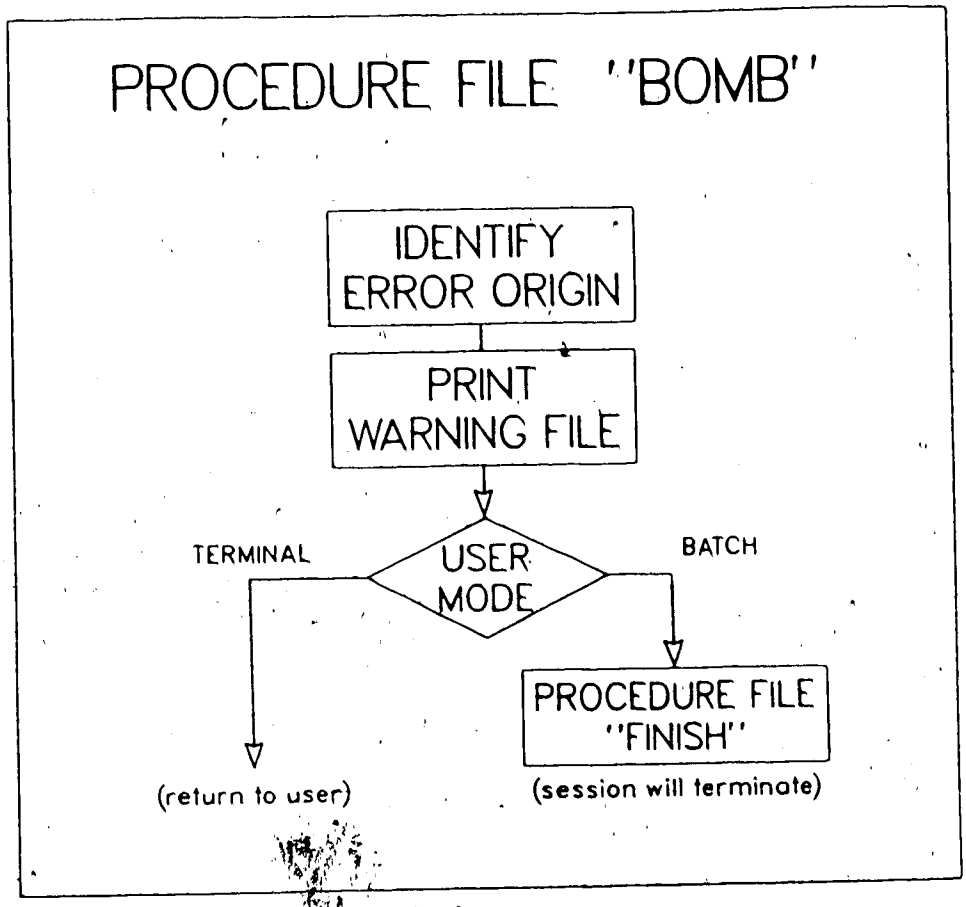
PROCEDURE FILE ''BOMB''
IDENTIFY ERROR ORIGIN
PRINT WARNING FILE
USER MODE
TERMINAL
BATCH
(return to user)
PROCEDURE FILE ''FINISH''
(session will terminate)

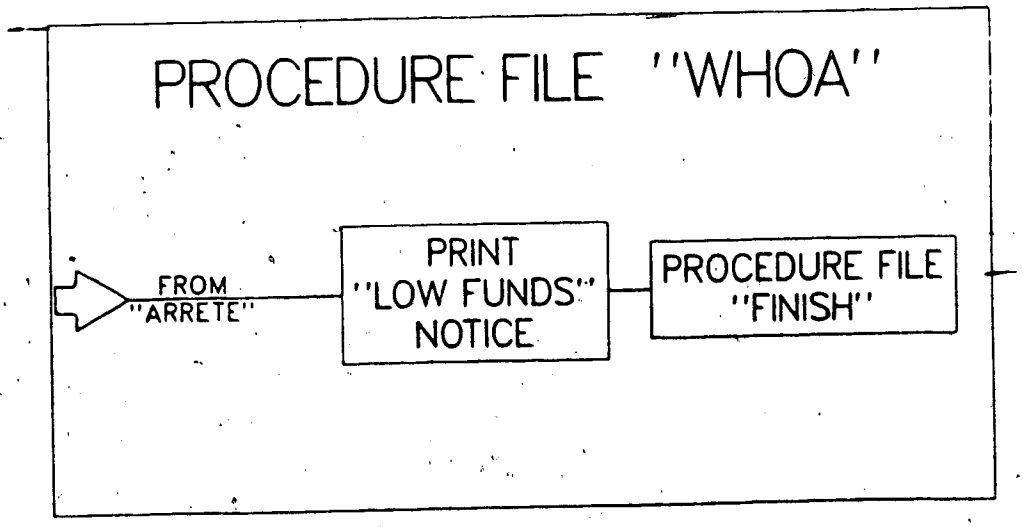
PROCEDURE FILE ''WHOA''
FROM ''ARRETE''
PRINT ''LOW FUNDS'' NOTICE
PROCEDURE FILE ''FINISH''

Appendice I: Summary of C-10 Simulation Results

SAP TIME= 0.100 HRS, ORTHO-THERMO PROPS IN 2D, TEST C-10 V

ELE	TAVG C	%CM	%FR	GRADT C/CM	STRPRP KPA	SP *E-6	VEL -8MM/S	DDZS MM	DDZIS MM	DZINC MM	DZ MM
1	-3.96	1.00	1.00	15.2110	100.010	38.87	0.0	0.000	0.086	0.086	0.086
2	-1.26	1.00	1.00	2.7023	100.120	38.94	106.2	0.041	0.364	0.406	0.406
3	0.21	0.0	0.0	0.6167	100.310	38.87	0.0	0.000	0.0	0.000	0.000
4	0.66	0.0	0.0	0.2722	100.800	38.81	0.0	0.000	0.0	0.000	0.000
5	0.86	0.0	0.0	0.1218	100.890	38.74	0.0	0.000	0.0	0.000	0.000
6	0.94	0.0	0.0	0.0589	100.880	38.68	0.0	0.000	0.0	0.000	0.000
7	0.98	0.0	0.0	0.0290	101.080	38.82	0.0	0.000	0.0	0.000	0.000
8	1.04	0.0	0.0	0.0476	101.250	38.88	0.0	0.000	0.0	0.000	0.000
9	1.10	0.0	0.0	0.0803	101.440	38.80	0.0	0.000	0.0	0.000	0.000
10	1.25	0.0	0.0	0.1868	101.830	38.43	0.0	0.000	0.0	0.000	0.000
11	1.67	0.0	0.0	0.4820	101.820	38.37	0.0	0.000	0.0	0.000	0.000
								0.041	0.418	0.480	0.480

SAP TIME= 0.200 HRS, ORTHO-THERMO PROPS IN 2D, TEST C-10 V

ELE	TAVG C	%CM	%FR	GRADT C/CM	STRPRP KPA	SP *E-6	VEL -8MM/S	DDZS MM	DDZIS MM	DZINC MM	DZ MM
1	-4.37	0.0	1.00	4.3665	100.009	38.97	0.0	0.000	0.0	0.000	0.086
2	-2.07	0.0	1.00	4.6387	100.120	38.94	160.8	0.071	0.0	0.000	0.478
3	0.11	0.0	0.0	0.4322	100.310	38.87	0.0	0.000	0.0	0.000	0.000
4	0.46	0.0	0.0	0.3041	100.800	38.81	0.0	0.000	0.0	0.000	0.000
5	0.72	0.0	0.0	0.1876	100.890	38.74	0.0	0.000	0.0	0.000	0.000
6	0.88	0.0	0.0	0.1176	100.880	38.68	0.0	0.000	0.0	0.000	0.000
7	0.96	0.0	0.0	0.0898	101.080	38.82	0.0	0.000	0.0	0.000	0.000
8	1.07	0.0	0.0	0.0980	101.250	38.88	0.0	0.000	0.0	0.000	0.000
9	1.18	0.0	0.0	0.1421	101.440	38.80	0.0	0.000	0.0	0.000	0.000
10	1.37	0.0	0.0	0.2229	101.830	38.43	0.0	0.000	0.0	0.000	0.000
11	1.84	0.0	0.0	0.2188	101.820	38.37	0.0	0.000	0.0	0.000	0.000
								0.071	0.0	0.071	0.531

SAP TIME= 0.300 HRS, ORTHO-THERMO PROPS IN 2D, TEST C-10 V

ELE	TAVG C	%CM	%FR	GRADT C/CM	STRPRP KPA	SP *E-6	VEL -8MM/S	DDZS MM	DDZIS MM	DZINC MM	DZ MM
1	-4.40	0.0	1.00	3.8577	100.008	38.97	0.0	0.000	0.0	0.000	0.086
2	-2.10	0.0	1.00	4.4809	100.120	38.93	174.5	0.068	0.0	0.000	0.548
3	0.07	0.0	0.0	0.3445	100.310	38.87	0.0	0.000	0.0	0.000	0.000
4	0.38	0.0	0.0	0.2681	100.800	38.81	0.0	0.000	0.0	0.000	0.000
5	0.63	0.0	0.0	0.2138	100.890	38.74	0.0	0.000	0.0	0.000	0.000
6	0.82	0.0	0.0	0.1584	100.880	38.68	0.0	0.000	0.0	0.000	0.000
7	0.98	0.0	0.0	0.1220	101.080	38.82	0.0	0.000	0.0	0.000	0.000
8	1.10	0.0	0.0	0.1358	101.250	38.88	0.0	0.000	0.0	0.000	0.000
9	1.28	0.0	0.0	0.1869	101.440	38.80	0.0	0.000	0.0	0.000	0.000
10	1.64	0.0	0.0	0.2188	101.830	38.43	0.0	0.000	0.0	0.000	0.000
11	1.67	0.0	0.0	0.2982	101.820	38.37	0.0	0.000	0.0	0.000	0.000
								0.068	0.0	0.068	0.599

SAP TIME= 0.400 HRS, ORTHO-THERMO PROPS IN 2D, TEST C-10 V

ELE	TAVG C	%CM	%FR	GRADT C/CM	STRPRP KPA	SP *E-6	VEL -8MM/S	DDZS MM	DDZIS MM	DZINC MM	DZ MM
1	-4.40	0.0	1.00	3.8268	100.007	38.97	0.0	0.000	0.0	0.000	0.086
2	-2.10	0.0	1.00	4.4867	100.120	38.93	173.5	0.068	0.0	0.000	0.813
3	0.08	0.0	0.0	0.2980	100.310	38.87	0.0	0.000	0.0	0.000	0.000
4	0.33	0.0	0.0	0.2897	100.800	38.81	0.0	0.000	0.0	0.000	0.000
5	0.57	0.0	0.0	0.2232	100.890	38.74	0.0	0.000	0.0	0.000	0.000
6	0.78	0.0	0.0	0.1835	100.880	38.68	0.0	0.000	0.0	0.000	0.000
7	0.98	0.0	0.0	0.1615	101.080	38.82	0.0	0.000	0.0	0.000	0.000
8	1.11	0.0	0.0	0.1818	101.250	38.88	0.0	0.000	0.0	0.000	0.000
9	1.28	0.0	0.0	0.1798	101.440	38.80	0.0	0.000	0.0	0.000	0.000
10	1.67	0.0	0.0	0.2074	101.830	38.43	0.0	0.000	0.0	0.000	0.000
11	1.88	0.0	0.0	0.2280	101.820	38.37	0.0	0.000	0.0	0.000	0.000
								0.068	0.0	0.068	0.867

SAP TIME= 0.500 HRS. ORTHO-THERMO PROPS. IN 2D. TEST C-10 V

ELE	TAVG C	%CH	%PR	GRADT C/CM	STRPRP KPA	SP *E-6	VEL -6MM/S	DDZS MM	DDZIS MM	DZINC MM	DZ MM
1	-4.41	0.0	1.00	3.8023	100.006	38.87	0.0	0.000	0.0	0.000	0.088
2	-2.11	0.0	1.00	4.4308	100.121	38.83	172.8	0.088	0.0	0.000	0.681
3	0.03	0.0	0.0	0.2708	100.310	38.87	0.0	0.000	0.0	0.000	0.000
4	0.30	0.0	0.0	0.2586	100.800	38.81	0.0	0.000	0.0	0.000	0.000
5	0.93	0.0	0.0	0.2280	100.890	38.74	0.0	0.000	0.0	0.000	0.000
6	0.78	0.0	0.0	0.1984	100.880	38.88	0.0	0.000	0.0	0.000	0.000
7	0.93	0.0	0.0	0.1814	101.080	38.82	0.0	0.000	0.0	0.000	0.000
8	1.11	0.0	0.0	0.1785	101.250	38.86	0.0	0.000	0.0	0.000	0.000
9	1.29	0.0	0.0	0.1878	101.440	38.80	0.0	0.000	0.0	0.000	0.000
10	1.48	0.0	0.0	0.2024	101.630	38.43	0.0	0.000	0.0	0.000	0.000
11	1.68	0.0	0.0	0.2138	101.820	38.37	0.0	0.000	0.0	0.000	0.000
								0.088	0.0	0.088	0.736

SAP TIME= 0.600 HRS. ORTHO-THERMO PROPS. IN 2D. TEST C-10 V

ELE	TAVG C	%CH	%PR	GRADT C/CM	STRPRP KPA	SP *E-6	VEL -6MM/S	DDZS MM	DDZIS MM	DZINC MM	DZ MM
1	-4.41	0.0	1.00	3.7806	100.006	38.87	0.0	0.000	0.0	0.000	0.088
2	-2.11	0.0	1.00	4.4085	100.121	38.83	171.8	0.087	0.0	0.000	0.748
3	0.03	0.0	0.0	0.2638	100.310	38.87	0.0	0.000	0.0	0.000	0.000
4	0.27	0.0	0.0	0.2486	100.800	38.81	0.0	0.000	0.0	0.000	0.000
5	0.81	0.0	0.0	0.2282	100.890	38.74	0.0	0.000	0.0	0.000	0.000
6	0.72	0.0	0.0	0.2068	100.880	38.88	0.0	0.000	0.0	0.000	0.000
7	0.92	0.0	0.0	0.1937	101.080	38.82	0.0	0.000	0.0	0.000	0.000
8	1.11	0.0	0.0	0.1894	101.250	38.86	0.0	0.000	0.0	0.000	0.000
9	1.30	0.0	0.0	0.1928	101.440	38.80	0.0	0.000	0.0	0.000	0.000
10	1.50	0.0	0.0	0.2031	101.630	38.43	0.0	0.000	0.0	0.000	0.000
11	1.70	0.0	0.0	0.2057	101.820	38.37	0.0	0.000	0.0	0.000	0.000
								0.087	0.0	0.087	0.803

SAP TIME= 0.700 HRS. ORTHO-THERMO PROPS. IN 2D. TEST C-10 V

ELE	TAVG C	%CH	%PR	GRADT C/CM	STRPRP KPA	SP *E-6	VEL -6MM/S	DDZS MM	DDZIS MM	DZINC MM	DZ MM
1	-4.44	0.0	1.00	3.3192	100.004	38.87	0.0	0.000	0.0	0.000	0.088
2	-2.42	0.0	1.00	3.9018	100.121	38.83	0.0	0.000	0.0	0.000	0.748
3	-0.38	1.00	1.00	0.8831	100.310	38.87	25.4	0.010	0.364	0.374	0.374
4	0.08	0.0	0.0	0.3712	100.800	38.81	0.0	0.000	0.0	0.000	0.000
5	0.41	0.0	0.0	0.2868	100.890	38.74	0.0	0.000	0.0	0.000	0.000
6	0.87	0.0	0.0	0.2367	100.880	38.88	0.0	0.000	0.0	0.000	0.000
7	0.90	0.0	0.0	0.2132	101.080	38.82	0.0	0.000	0.0	0.000	0.000
8	1.10	0.0	0.0	0.2017	101.250	38.86	0.0	0.000	0.0	0.000	0.000
9	1.30	0.0	0.0	0.1990	101.440	38.80	0.0	0.000	0.0	0.000	0.000
10	1.50	0.0	0.0	0.2007	101.630	38.43	0.0	0.000	0.0	0.000	0.000
11	1.70	0.0	0.0	0.2028	101.820	38.37	0.0	0.000	0.0	0.000	0.000
								0.010	0.364	0.374	1.177

SAP TIME= 0.800 HRS. ORTHO-THERMO PROPS. IN 2D. TEST C-10 V

ELE	TAVG C	%CH	%PR	GRADT C/CM	STRPRP KPA	SP *E-6	VEL -6MM/S	DDZS MM	DDZIS MM	DZINC MM	DZ MM
1	-4.52	0.0	1.00	2.3388	100.004	38.87	0.0	0.000	0.0	0.000	0.088
2	-3.76	0.0	1.00	2.3894	100.121	38.83	0.0	0.000	0.0	0.000	0.748
3	-0.88	0.0	1.00	2.0718	100.308	38.87	80.5	0.032	0.0	0.000	0.408
4	0.08	0.0	0.0	0.2188	100.800	38.81	0.0	0.000	0.0	0.000	0.000
5	0.38	0.0	0.0	0.2885	100.890	38.74	0.0	0.000	0.0	0.000	0.000
6	0.83	0.0	0.0	0.2830	100.880	38.88	0.0	0.000	0.0	0.000	0.000
7	0.87	0.0	0.0	0.2277	101.080	38.82	0.0	0.000	0.0	0.000	0.000
8	1.08	0.0	0.0	0.2127	101.250	38.86	0.0	0.000	0.0	0.000	0.000
9	1.28	0.0	0.0	0.2057	101.440	38.80	0.0	0.000	0.0	0.000	0.000
10	1.50	0.0	0.0	0.2024	101.630	38.43	0.0	0.000	0.0	0.000	0.000
11	1.70	0.0	0.0	0.2031	101.820	38.37	0.0	0.000	0.0	0.000	0.000
								0.032	0.0	0.032	1.208

SAP, TIME= 0.500 HRS, ORTHO-THERMO PROPS, IN 2D, TEST C-10 V

ELE	TAVG C	%CH	%PR	GRADT C/CM	STRPRP KPA	SP *E-6	VEL -6MM/S	DDZS MM	DDZIS MM	DZINC MM	DZ MM
1	-4.84	0.0	1.00	2.0839	100.004	38.87	0.0	0.000	0.0	0.000	0.085
2	-3.28	0.0	1.00	2.0834	100.122	38.83	0.0	0.000	0.0	0.000	0.748
3	-1.12	0.0	1.00	2.2682	100.308	38.87	88.9	0.035	0.0	0.000	0.441
4	0.05	0.0	0.0	0.2848	100.800	38.81	0.0	0.000	0.0	0.000	0.000
5	0.32	0.0	0.0	0.2808	100.890	38.74	0.0	0.000	0.0	0.000	0.000
6	0.60	0.0	0.0	0.2870	100.880	38.88	0.0	0.000	0.0	0.000	0.000
7	0.84	0.0	0.0	0.2380	101.080	38.82	0.0	0.000	0.0	0.000	0.000
8	1.07	0.0	0.0	0.2210	101.250	38.58	0.0	0.000	0.0	0.000	0.000
9	1.28	0.0	0.0	0.2119	101.440	38.80	0.0	0.000	0.0	0.000	0.000
10	1.49	0.0	0.0	0.2074	101.630	38.43	0.0	0.000	0.0	0.000	0.000
11	1.70	0.0	0.0	0.2058	101.820	38.37	0.0	0.000	0.0	0.000	0.000
								0.035	0.0	0.035	1.243

SAP, TIME= 1.000 HRS, ORTHO-THERMO PROPS, IN 2D, TEST C-10 V

ELE	TAVG C	%CH	%PR	GRADT C/CM	STRPRP KPA	SP *E-6	VEL -6MM/S	DDZS MM	DDZIS MM	DZINC MM	DZ MM
1	-4.84	0.0	1.00	2.0400	100.004	38.87	0.0	0.000	0.0	0.000	0.085
2	-3.28	0.0	1.00	2.0378	100.122	38.83	0.0	0.000	0.0	0.000	0.748
3	-1.15	0.0	1.00	2.2488	100.308	38.87	91.2	0.036	0.0	0.000	0.478
4	0.04	0.0	0.0	0.2788	100.800	38.81	0.0	0.000	0.0	0.000	0.000
5	0.31	0.0	0.0	0.2730	100.890	38.74	0.0	0.000	0.0	0.000	0.000
6	0.58	0.0	0.0	0.2807	100.880	38.88	0.0	0.000	0.0	0.000	0.000
7	0.82	0.0	0.0	0.2402	101.080	38.82	0.0	0.000	0.0	0.000	0.000
8	1.05	0.0	0.0	0.2267	101.250	38.58	0.0	0.000	0.0	0.000	0.000
9	1.27	0.0	0.0	0.2173	101.440	38.80	0.0	0.000	0.0	0.000	0.000
10	1.49	0.0	0.0	0.2117	101.630	38.43	0.0	0.000	0.0	0.000	0.000
11	1.70	0.0	0.0	0.2081	101.820	38.37	0.0	0.000	0.0	0.000	0.000
								0.036	0.0	0.036	1.278

SAP, TIME= 1.250 HRS, ORTHO-THERMO PROPS, IN 2D, TEST C-10 V

ELE	TAVG C	%CH	%PR	GRADT C/CM	STRPRP KPA	SP *E-6	VEL -6MM/S	DDZS MM	DDZIS MM	DZINC MM	DZ MM
1	-4.84	0.0	1.00	2.0242	100.004	38.87	0.0	0.000	0.0	0.000	0.085
2	-3.30	0.0	1.00	2.0242	100.122	38.83	0.0	0.000	0.0	0.000	0.748
3	-1.16	0.0	1.00	2.2658	100.308	38.87	91.6	0.080	0.0	0.000	0.588
4	0.03	0.0	0.0	0.2820	100.800	38.81	0.0	0.000	0.0	0.000	0.000
5	0.29	0.0	0.0	0.2807	100.890	38.74	0.0	0.000	0.0	0.000	0.000
6	0.54	0.0	0.0	0.2821	100.880	38.88	0.0	0.000	0.0	0.000	0.000
7	0.78	0.0	0.0	0.2423	101.080	38.82	0.0	0.000	0.0	0.000	0.000
8	1.03	0.0	0.0	0.2330	101.250	38.58	0.0	0.000	0.0	0.000	0.000
9	1.28	0.0	0.0	0.2258	101.440	38.80	0.0	0.000	0.0	0.000	0.000
10	1.47	0.0	0.0	0.2205	101.630	38.43	0.0	0.000	0.0	0.000	0.000
11	1.69	0.0	0.0	0.2180	101.820	38.37	0.0	0.000	0.0	0.000	0.000
								0.080	0.0	0.080	1.369

SAP, TIME= 1.500 HRS, ORTHO-THERMO PROPS, IN 2D, TEST C-10 V

ELE	TAVG C	%CH	%PR	GRADT C/CM	STRPRP KPA	SP *E-6	VEL -6MM/S	DDZS MM	DDZIS MM	DZINC MM	DZ MM
1	-4.84	0.0	1.00	2.0188	100.003	38.87	0.0	0.000	0.0	0.000	0.085
2	-3.30	0.0	1.00	2.0198	100.121	38.83	0.0	0.000	0.0	0.000	0.748
3	-1.18	0.0	1.00	2.2832	100.308	38.87	91.5	0.080	0.0	0.000	0.658
4	0.03	0.0	0.0	0.2823	100.800	38.81	0.0	0.000	0.0	0.000	0.000
5	0.28	0.0	0.0	0.2821	100.890	38.74	0.0	0.000	0.0	0.000	0.000
6	0.52	0.0	0.0	0.2482	100.880	38.88	0.0	0.000	0.0	0.000	0.000
7	0.77	0.0	0.0	0.2421	101.080	38.82	0.0	0.000	0.0	0.000	0.000
8	1.01	0.0	0.0	0.2360	101.250	38.58	0.0	0.000	0.0	0.000	0.000
9	1.24	0.0	0.0	0.2307	101.440	38.80	0.0	0.000	0.0	0.000	0.000
10	1.45	0.0	0.0	0.2269	101.630	38.43	0.0	0.000	0.0	0.000	0.000
11	1.68	0.0	0.0	0.2248	101.820	38.37	0.0	0.000	0.0	0.000	0.000
								0.080	0.0	0.080	1.469

SAP TIME= 1.750 HRS, ORTHO-THERMO PROPS, IN 2D, TEST C-10 V

ELE	TAVG C	%CH	%FR	GRADT C/CM	STRPRP KPA	SP *E-8	VEL -8MM/S	DDZS MM	DDZIS MM	DZINC MM	DZ MM
1	-4.54	0.0	1.00	2.0122	100.003	38.87	0.0	0.000	0.0	0.000	0.088
2	-3.30	0.0	1.00	2.0121	100.121	38.83	0.0	0.000	0.0	0.000	0.748
3	-1.16	0.0	1.00	2.3434	100.310	38.87	81.1	0.088	0.0	0.000	0.748
4	0.02	0.0	0.0	0.2486	100.500	38.81	0.0	0.000	0.0	0.000	0.000
5	0.27	0.0	0.0	0.2483	100.690	38.74	0.0	0.000	0.0	0.000	0.000
6	0.81	0.0	0.0	0.2483	100.880	38.68	0.0	0.000	0.0	0.000	0.000
7	0.75	0.0	0.0	0.2416	101.060	38.62	0.0	0.000	0.0	0.000	0.000
8	0.89	0.0	0.0	0.2378	101.250	38.56	0.0	0.000	0.0	0.000	0.000
9	1.23	0.0	0.0	0.2338	101.440	38.50	0.0	0.000	0.0	0.000	0.000
10	1.46	0.0	0.0	0.2312	101.630	38.43	0.0	0.000	0.0	0.000	0.000
11	1.69	0.0	0.0	0.2298	101.820	38.37	0.0	0.000	0.0	0.000	0.000
								0.088	0.0	0.088	1.648

SAP TIME= 2.000 HRS, ORTHO-THERMO PROPS IN 2D, TEST C-10 V

ELE	TAVG C	%CH	%FR	GRADT C/CM	STRPRP KPA	SP *E-8	VEL -8MM/S	DDZS MM	DDZIS MM	DZINC MM	DZ MM
1	-4.56	0.0	1.00	1.6131	100.003	38.87	0.0	0.000	0.0	0.000	0.088
2	-3.44	0.0	1.00	1.6100	100.121	38.83	0.0	0.000	0.0	0.000	0.748
3	-1.53	0.0	1.00	1.7855	100.310	38.87	0.0	0.000	0.0	0.000	0.748
4	-0.35	1.00	1.00	0.8765	100.500	38.81	22.4	0.022	0.394	0.388	0.388
5	0.07	0.0	0.0	0.3418	100.690	38.74	0.0	0.000	0.0	0.000	0.000
6	0.39	0.0	0.0	0.3038	100.880	38.68	0.0	0.000	0.0	0.000	0.000
7	0.56	0.0	0.0	0.2767	101.060	38.62	0.0	0.000	0.0	0.000	0.000
8	0.94	0.0	0.0	0.2597	101.250	38.56	0.0	0.000	0.0	0.000	0.000
9	1.20	0.0	0.0	0.2491	101.440	38.50	0.0	0.000	0.0	0.000	0.000
10	1.44	0.0	0.0	0.2428	101.630	38.43	0.0	0.000	0.0	0.000	0.000
11	1.68	0.0	0.0	0.2400	101.820	38.37	0.0	0.000	0.0	0.000	0.000
								0.022	0.394	0.388	1.634

SAP TIME= 2.250 HRS, ORTHO-THERMO PROPS, IN 2D, TEST C-10 V

ELE	TAVG C	%CH	%FR	GRADT C/CM	STRPRP KPA	SP *E-8	VEL -8MM/S	DDZS MM	DDZIS MM	DZINC MM	DZ MM
1	-4.58	0.0	1.00	1.4884	100.003	38.87	0.0	0.000	0.0	0.000	0.088
2	-3.67	0.0	1.00	1.4816	100.121	38.83	0.0	0.000	0.0	0.000	0.748
3	-2.12	0.0	1.00	1.4080	100.311	38.87	0.0	0.000	0.0	0.000	0.748
4	-0.73	0.0	1.00	1.4852	100.499	38.81	57.6	0.057	0.0	0.000	0.443
5	0.05	0.0	0.0	0.3024	100.690	38.74	0.0	0.000	0.0	0.000	0.000
6	0.35	0.0	0.0	0.2955	100.880	38.68	0.0	0.000	0.0	0.000	0.000
7	0.83	0.0	0.0	0.2818	101.060	38.62	0.0	0.000	0.0	0.000	0.000
8	0.91	0.0	0.0	0.2898	101.250	38.56	0.0	0.000	0.0	0.000	0.000
9	1.17	0.0	0.0	0.2802	101.440	38.50	0.0	0.000	0.0	0.000	0.000
10	1.43	0.0	0.0	0.2529	101.630	38.43	0.0	0.000	0.0	0.000	0.000
11	1.68	0.0	0.0	0.2508	101.820	38.37	0.0	0.000	0.0	0.000	0.000
								0.057	0.0	0.057	1.681

SAP TIME= 2.500 HRS, ORTHO-THERMO PROPS, IN 2D, TEST C-10 V

ELE	TAVG C	%CH	%FR	GRADT C/CM	STRPRP KPA	SP *E-8	VEL -8MM/S	DDZS MM	DDZIS MM	DZINC MM	DZ MM
1	-4.58	0.0	1.00	1.3871	100.003	38.87	0.0	0.000	0.0	0.000	0.088
2	-3.73	0.0	1.00	1.3958	100.121	38.83	0.0	0.000	0.0	0.000	0.748
3	-2.24	0.0	1.00	1.3788	100.311	38.87	0.0	0.000	0.0	0.000	0.748
4	-0.80	0.0	1.00	1.5758	100.499	38.81	81.2	0.080	0.0	0.000	0.503
5	0.04	0.0	0.0	0.2872	100.690	38.74	0.0	0.000	0.0	0.000	0.000
6	0.33	0.0	0.0	0.2808	100.880	38.68	0.0	0.000	0.0	0.000	0.000
7	0.81	0.0	0.0	0.2801	101.060	38.62	0.0	0.000	0.0	0.000	0.000
8	0.88	0.0	0.0	0.2728	101.250	38.56	0.0	0.000	0.0	0.000	0.000
9	1.16	0.0	0.0	0.2663	101.440	38.50	0.0	0.000	0.0	0.000	0.000
10	1.41	0.0	0.0	0.2617	101.630	38.43	0.0	0.000	0.0	0.000	0.000
11	1.67	0.0	0.0	0.2592	101.820	38.37	0.0	0.000	0.0	0.000	0.000
								0.080	0.0	0.080	2.087

SAP: TIME= 2.750 HRS, ORTHO-THERMO PROPS, IN 2D, TEST C-10 V

ELE	TAVG C	%CH	%FR	GRADT C/CM	STRPRP KPA	SP *E-6	VEL -6MM/S	DDZS MM	DDZIS MM	DZINC MM	DZ MM
1	-4.69	0.0	1.00	1.3778	100.003	38.97	0.0	0.000	0.0	0.000	0.088
2	-3.78	0.0	1.00	1.3774	100.121	38.93	0.0	0.000	0.0	0.000	0.748
3	-2.27	0.0	1.00	1.3734	100.311	38.87	0.0	0.000	0.0	0.000	0.745
4	-0.81	0.0	1.00	1.5857	100.498	38.81	81.9	0.081	0.0	0.000	0.883
5	0.04	0.0	0.0	0.2788	100.890	38.74	0.0	0.000	0.0	0.000	0.000
6	0.32	0.0	0.0	0.2818	100.880	38.68	0.0	0.000	0.0	0.000	0.000
7	0.60	0.0	0.0	0.2778	101.080	38.62	0.0	0.000	0.0	0.000	0.000
8	0.87	0.0	0.0	0.2737	101.250	38.56	0.0	0.000	0.0	0.000	0.000
9	1.14	0.0	0.0	0.2697	101.440	38.50	0.0	0.000	0.0	0.000	0.000
10	1.40	0.0	0.0	0.2686	101.630	38.43	0.0	0.000	0.0	0.000	0.000
11	1.67	0.0	0.0	0.2660	101.820	38.37	0.0	0.000	0.0	0.000	0.000
								0.081	0.0	0.081	2.111

SAP: TIME= 3.000 HRS, ORTHO-THERMO PROPS, IN 2D, TEST C-10 V

ELE	TAVG C	%CH	%FR	GRADT C/CM	STRPRP KPA	SP *E-6	VEL -6MM/S	DDZS MM	DDZIS MM	DZINC MM	DZ MM
1	-4.58	0.0	1.00	1.3728	100.003	38.97	0.0	0.000	0.0	0.000	0.088
2	-3.78	0.0	1.00	1.3723	100.121	38.93	0.0	0.000	0.0	0.000	0.748
3	-2.28	0.0	1.00	1.3711	100.311	38.87	0.0	0.000	0.0	0.000	0.745
4	-0.82	0.0	1.00	1.5864	100.500	38.81	82.0	0.081	0.0	0.000	0.824
5	0.04	0.0	0.0	0.2768	100.890	38.74	0.0	0.000	0.0	0.000	0.000
6	0.31	0.0	0.0	0.2786	100.880	38.68	0.0	0.000	0.0	0.000	0.000
7	0.59	0.0	0.0	0.2764	101.080	38.62	0.0	0.000	0.0	0.000	0.000
8	0.86	0.0	0.0	0.2738	101.250	38.56	0.0	0.000	0.0	0.000	0.000
9	1.13	0.0	0.0	0.2718	101.440	38.50	0.0	0.000	0.0	0.000	0.000
10	1.40	0.0	0.0	0.2698	101.630	38.43	0.0	0.000	0.0	0.000	0.000
11	1.67	0.0	0.0	0.2686	101.820	38.37	0.0	0.000	0.0	0.000	0.000
								0.081	0.0	0.081	2.172

SAP: TIME= 3.500 HRS, ORTHO-THERMO PROPS, IN 2D, TEST C-10 V

ELE	TAVG C	%CH	%FR	GRADT C/CM	STRPRP KPA	SP *E-6	VEL -6MM/S	DDZS MM	DDZIS MM	DZINC MM	DZ MM
1	-4.59	0.0	1.00	1.3881	100.003	38.97	0.0	0.000	0.0	0.000	0.088
2	-3.78	0.0	1.00	1.3880	100.121	38.93	0.0	0.000	0.0	0.000	0.748
3	-2.28	0.0	1.00	1.3867	100.310	38.87	0.0	0.000	0.0	0.000	0.748
4	-0.82	0.0	1.00	1.5946	100.500	38.81	81.8	0.121	0.0	0.000	0.746
5	0.04	0.0	0.0	0.2725	100.890	38.74	0.0	0.000	0.0	0.000	0.000
6	0.31	0.0	0.0	0.2759	100.880	38.68	0.0	0.000	0.0	0.000	0.000
7	0.58	0.0	0.0	0.2760	101.080	38.62	0.0	0.000	0.0	0.000	0.000
8	0.85	0.0	0.0	0.2740	101.250	38.56	0.0	0.000	0.0	0.000	0.000
9	1.12	0.0	0.0	0.2730	101.440	38.50	0.0	0.000	0.0	0.000	0.000
10	1.40	0.0	0.0	0.2721	101.630	38.43	0.0	0.000	0.0	0.000	0.000
11	1.67	0.0	0.0	0.2717	101.820	38.37	0.0	0.000	0.0	0.000	0.000
								0.121	0.0	0.121	2.234

SAP: TIME= 4.000 HRS, ORTHO-THERMO PROPS, IN 2D, TEST C-10 V

ELE	TAVG C	%CH	%FR	GRADT C/CM	STRPRP KPA	SP *E-6	VEL -6MM/S	DDZS MM	DDZIS MM	DZINC MM	DZ MM
1	-4.60	0.0	1.00	1.3841	100.003	38.97	0.0	0.000	0.0	0.000	0.088
2	-3.81	0.0	1.00	1.3834	100.121	38.93	0.0	0.000	0.0	0.000	0.748
3	-2.44	0.0	1.00	1.3760	100.310	38.87	0.0	0.000	0.0	0.000	0.745
4	-1.08	0.0	1.00	1.3854	100.500	38.81	0.0	0.000	0.0	0.000	0.746
5	-0.28	0.88	0.88	1.4633	100.890	38.74	58.7	0.111	0.367	0.488	0.488
6	0.08	0.0	0.0	0.3583	100.880	38.68	0.0	0.000	0.0	0.000	0.000
7	0.43	0.0	0.0	0.3351	101.080	38.62	0.0	0.000	0.0	0.000	0.000
8	0.78	0.0	0.0	0.3172	101.250	38.56	0.0	0.000	0.0	0.000	0.000
9	1.08	0.0	0.0	0.3054	101.440	38.50	0.0	0.000	0.0	0.000	0.000
10	1.38	0.0	0.0	0.2984	101.630	38.43	0.0	0.000	0.0	0.000	0.000
11	1.68	0.0	0.0	0.2950	101.820	38.37	0.0	0.000	0.0	0.000	0.000
								0.111	0.367	0.488	2.751

SAP: TIME= 4.500 HRS, ORTHO-THERMO PROPS IN 2D, TEST C-10 V

ELE	TAVG C	%CH	%FR	GRADT C/CM	STRPRP KPA	SP *E-6	VEL -6MM/S	DDZS MM	DDZIS MM	DZINC MM	DZ MM
1	-4.61	0.0	1.00	1.0388	100.003	38.87	0.0	0.000	0.0	0.000	0.085
2	-3.94	0.0	1.00	1.0384	100.121	38.83	0.0	0.000	0.0	0.000	0.748
3	-2.77	0.0	1.00	1.0778	100.310	38.87	0.0	0.000	0.0	0.000	0.748
4	-1.83	0.0	1.00	1.0384	100.500	38.81	0.0	0.000	0.0	0.000	0.748
5	-0.89	0.02	1.00	1.1442	100.690	38.75	44.3	0.087	0.008	0.088	0.833
6	0.08	0.0	0.0	0.3280	100.880	38.68	0.0	0.000	0.0	0.000	0.000
7	0.38	0.0	0.0	0.3276	101.080	38.62	0.0	0.000	0.0	0.000	0.000
8	0.71	0.0	0.0	0.3214	101.250	38.56	0.0	0.000	0.0	0.000	0.000
9	1.03	0.0	0.0	0.3188	101.440	38.50	0.0	0.000	0.0	0.000	0.000
10	1.34	0.0	0.0	0.3116	101.630	38.43	0.0	0.000	0.0	0.000	0.000
11	1.65	0.0	0.0	0.3087	101.820	38.37	0.0	0.000	0.0	0.000	0.000
								0.087	0.008	0.088	2.886

SAP: TIME= 5.000 HRS, ORTHO-THERMO PROPS IN 2D, TEST C-10 V

ELE	TAVG C	%CH	%FR	GRADT C/CM	STRPRP KPA	SP *E-6	VEL -6MM/S	DDZS MM	DDZIS MM	DZINC MM	DZ MM
1	-4.62	0.0	1.00	1.0486	100.003	38.87	0.0	0.000	0.0	0.000	0.085
2	-3.97	0.0	1.00	1.0482	100.121	38.83	0.0	0.000	0.0	0.000	0.748
3	-2.85	0.0	1.00	1.0436	100.310	38.87	0.0	0.000	0.0	0.000	0.748
4	-1.73	0.0	1.00	1.0382	100.500	38.81	0.0	0.000	0.0	0.000	0.748
5	-0.84	0.0	1.00	1.1983	100.690	38.75	48.3	0.091	0.0	0.000	0.833
6	0.06	0.0	0.0	0.3184	100.880	38.68	0.0	0.000	0.0	0.000	0.000
7	0.38	0.0	0.0	0.3226	101.080	38.62	0.0	0.000	0.0	0.000	0.000
8	0.70	0.0	0.0	0.3207	101.250	38.56	0.0	0.000	0.0	0.000	0.000
9	1.01	0.0	0.0	0.3188	101.440	38.50	0.0	0.000	0.0	0.000	0.000
10	1.33	0.0	0.0	0.3170	101.630	38.43	0.0	0.000	0.0	0.000	0.000
11	1.64	0.0	0.0	0.3161	101.820	38.37	0.0	0.000	0.0	0.000	0.000
								0.091	0.0	0.091	2.847

SAP: TIME= 5.500 HRS, ORTHO-THERMO PROPS IN 2D, TEST C-10 V

ELE	TAVG C	%CH	%FR	GRADT C/CM	STRPRP KPA	SP *E-6	VEL -6MM/S	DDZS MM	DDZIS MM	DZINC MM	DZ MM
1	-4.62	0.0	1.00	1.0391	100.003	38.87	0.0	0.000	0.0	0.000	0.085
2	-3.88	0.0	1.00	1.0391	100.121	38.83	0.0	0.000	0.0	0.000	0.748
3	-2.86	0.0	1.00	1.0378	100.310	38.87	0.0	0.000	0.0	0.000	0.748
4	-1.75	0.0	1.00	1.0381	100.500	38.81	0.0	0.000	0.0	0.000	0.748
5	-0.85	0.0	1.00	1.2058	100.690	38.75	48.7	0.092	0.0	0.000	0.748
6	0.06	0.0	0.0	0.3188	100.880	38.68	0.0	0.000	0.0	0.000	0.000
7	0.37	0.0	0.0	0.3206	101.080	38.62	0.0	0.000	0.0	0.000	0.000
8	0.69	0.0	0.0	0.3201	101.250	38.56	0.0	0.000	0.0	0.000	0.000
9	1.01	0.0	0.0	0.3194	101.440	38.50	0.0	0.000	0.0	0.000	0.000
10	1.33	0.0	0.0	0.3188	101.630	38.43	0.0	0.000	0.0	0.000	0.000
11	1.64	0.0	0.0	0.3185	101.820	38.37	0.0	0.000	0.0	0.000	0.000
								0.092	0.0	0.092	3.038

SAP: TIME= 6.000 HRS, ORTHO-THERMO PROPS IN 2D, TEST C-10 V

ELE	TAVG C	%CH	%FR	GRADT C/CM	STRPRP KPA	SP *E-6	VEL -6MM/S	DDZS MM	DDZIS MM	DZINC MM	DZ MM
1	-4.62	0.0	1.00	1.0367	100.002	38.87	0.0	0.000	0.0	0.000	0.085
2	-3.88	0.0	1.00	1.0386	100.121	38.83	0.0	0.000	0.0	0.000	0.748
3	-2.87	0.0	1.00	1.0352	100.310	38.87	0.0	0.000	0.0	0.000	0.748
4	-1.78	0.0	1.00	1.0348	100.500	38.81	0.0	0.000	0.0	0.000	0.748
5	-0.85	0.0	1.00	1.2051	100.690	38.74	48.7	0.092	0.0	0.000	0.837
6	0.08	0.0	0.0	0.3188	100.880	38.68	0.0	0.000	0.0	0.000	0.000
7	0.37	0.0	0.0	0.3201	101.080	38.62	0.0	0.000	0.0	0.000	0.000
8	0.68	0.0	0.0	0.3188	101.250	38.56	0.0	0.000	0.0	0.000	0.000
9	1.01	0.0	0.0	0.3197	101.440	38.50	0.0	0.000	0.0	0.000	0.000
10	1.32	0.0	0.0	0.3184	101.630	38.43	0.0	0.000	0.0	0.000	0.000
11	1.64	0.0	0.0	0.3183	101.820	38.37	0.0	0.000	0.0	0.000	0.000
								0.092	0.0	0.092	3.130

SAP: TIME= 7.000 HRS, ORTHO-THERMO PROPS, IN 2D, TEST C-10 V

ELE	TAVG C	%CH	%FR	GRADT C/CM	STRPRP KPA	SP *E-5	VEL -6MM/S	DDZS MM	DDZIS MM	DZINC MM	DZ MM
1	-4.82	0.0	1.00	1.0010	100.002	38.97	0.0	0.000	0.0	0.000	0.058
2	-4.01	0.0	1.00	1.0006	100.121	38.93	0.0	0.000	0.0	0.000	0.748
3	-3.93	0.0	1.00	0.9988	100.310	38.87	0.0	0.000	0.0	0.000	0.745
4	-1.68	0.0	1.00	0.9882	100.500	38.81	0.0	0.000	0.0	0.000	0.746
5	-0.78	0.0	1.00	0.9857	100.690	38.74	0.0	0.000	0.0	0.000	0.837
6	-0.10	0.48	0.48	1.1638	100.880	38.68	44.8	0.178	0.178	0.354	0.354
7	0.25	0.0	0.0	0.3602	101.080	38.62	0.0	0.000	0.0	0.000	0.000
8	0.60	0.0	0.0	0.3525	101.250	38.56	0.0	0.000	0.0	0.000	0.000
9	0.95	0.0	0.0	0.3471	101.440	38.50	0.0	0.000	0.0	0.000	0.000
10	1.29	0.0	0.0	0.3436	101.630	38.43	0.0	0.000	0.0	0.000	0.000
11	1.63	0.0	0.0	0.3421	101.820	38.37	0.0	0.000	0.0	0.000	0.000
								0.178	0.178	0.354	3.486

SAP: TIME= 8.000 HRS, ORTHO-THERMO PROPS, IN 2D, TEST C-10 V

ELE	TAVG C	%CH	%FR	GRADT C/CM	STRPRP KPA	SP *E-5	VEL -6MM/S	DDZS MM	DDZIS MM	DZINC MM	DZ MM
1	-4.63	0.0	1.00	0.8704	100.002	38.97	0.0	0.000	0.0	0.000	0.058
2	-4.10	0.0	1.00	0.8698	100.121	38.93	0.0	0.000	0.0	0.000	0.748
3	-3.17	0.0	1.00	0.8826	100.310	38.87	0.0	0.000	0.0	0.000	0.745
4	-2.25	0.0	1.00	0.8487	100.500	38.81	0.0	0.000	0.0	0.000	0.746
5	-1.34	0.0	1.00	0.8277	100.690	38.74	0.0	0.000	0.0	0.000	0.837
6	-0.50	0.61	1.00	0.9329	100.880	38.68	56.1	0.142	0.185	0.328	0.681
7	0.05	0.0	0.0	0.3827	101.080	38.62	0.0	0.000	0.0	0.000	0.000
8	0.48	0.0	0.0	0.3868	101.250	38.56	0.0	0.000	0.0	0.000	0.000
9	0.88	0.0	0.0	0.3815	101.440	38.50	0.0	0.000	0.0	0.000	0.000
10	1.24	0.0	0.0	0.3788	101.630	38.43	0.0	0.000	0.0	0.000	0.000
11	1.61	0.0	0.0	0.3745	101.820	38.37	0.0	0.000	0.0	0.000	0.000
								0.142	0.185	0.328	3.611

SAP: TIME= 9.000 HRS, ORTHO-THERMO PROPS, IN 2D, TEST C-10 V

ELE	TAVG C	%CH	%FR	GRADT C/CM	STRPRP KPA	SP *E-5	VEL -6MM/S	DDZS MM	DDZIS MM	DZINC MM	DZ MM
1	-4.63	0.0	1.00	0.8414	100.002	38.97	0.0	0.000	0.0	0.000	0.058
2	-4.12	0.0	1.00	0.8413	100.121	38.93	0.0	0.000	0.0	0.000	0.748
3	-3.21	0.0	1.00	0.8387	100.310	38.87	0.0	0.000	0.0	0.000	0.745
4	-2.31	0.0	1.00	0.8270	100.500	38.81	0.0	0.000	0.0	0.000	0.746
5	-1.41	0.0	1.00	0.8237	100.690	38.74	0.0	0.000	0.0	0.000	0.837
6	-0.52	0.0	1.00	0.9884	100.880	38.68	37.5	0.147	0.0	0.000	0.828
7	0.09	0.0	0.0	0.3805	101.080	38.62	0.0	0.000	0.0	0.000	0.000
8	0.47	0.0	0.0	0.3848	101.250	38.56	0.0	0.000	0.0	0.000	0.000
9	0.85	0.0	0.0	0.3836	101.440	38.50	0.0	0.000	0.0	0.000	0.000
10	1.23	0.0	0.0	0.3826	101.630	38.43	0.0	0.000	0.0	0.000	0.000
11	1.61	0.0	0.0	0.3822	101.820	38.37	0.0	0.000	0.0	0.000	0.000
								0.147	0.0	0.147	3.958

SAP: TIME= 10.000 HRS, ORTHO-THERMO PROPS, IN 2D, TEST C-10 V

ELE	TAVG C	%CH	%FR	GRADT C/CM	STRPRP KPA	SP *E-5	VEL -6MM/S	DDZS MM	DDZIS MM	DZINC MM	DZ MM
1	-4.64	0.0	1.00	0.8331	100.002	38.97	0.0	0.000	0.0	0.000	0.058
2	-4.12	0.0	1.00	0.8330	100.121	38.93	0.0	0.000	0.0	0.000	0.748
3	-3.23	0.0	1.00	0.8328	100.310	38.87	0.0	0.000	0.0	0.000	0.745
4	-2.33	0.0	1.00	0.8319	100.500	38.81	0.0	0.000	0.0	0.000	0.746
5	-1.44	0.0	1.00	0.8308	100.690	38.74	0.0	0.000	0.0	0.000	0.837
6	-0.54	0.0	1.00	0.9871	100.880	38.68	37.4	0.147	0.0	0.000	0.828
7	0.09	0.0	0.0	0.3798	101.080	38.62	0.0	0.000	0.0	0.000	0.000
8	0.47	0.0	0.0	0.3840	101.250	38.56	0.0	0.000	0.0	0.000	0.000
9	0.85	0.0	0.0	0.3829	101.440	38.50	0.0	0.000	0.0	0.000	0.000
10	1.23	0.0	0.0	0.3827	101.630	38.43	0.0	0.000	0.0	0.000	0.000
11	1.61	0.0	0.0	0.3826	101.820	38.37	0.0	0.000	0.0	0.000	0.000
								0.147	0.0	0.147	4.105

SAP: TIME= 11.000 HRS. ORTHO-THERMO PROPS. IN 2D. TEST C-10 V

ELE	TAVG C	%CM		%PR	GRADT C/CM	STRPRP KPA	SP *E-6	VEL -6MM/S	DDZS MM	DDZIS MM	DZINC MM	DZ MM
1	-4.84	0.0		1.00	0.8302	100.002	38.87	0.0	0.000	0.0	0.000	0.088
2	-4.13	0.0		1.00	0.8302	100.121	38.83	0.0	0.000	0.0	0.000	0.748
3	-3.23	0.0		1.00	0.8300	100.310	38.87	0.0	0.000	0.0	0.000	0.748
4	-2.34	0.0		1.00	0.8297	100.500	38.81	0.0	0.000	0.0	0.000	0.748
5	-1.45	0.0		1.00	0.8292	100.690	38.74	0.0	0.000	0.0	0.000	0.837
6	-0.55	0.0		1.00	0.9880	100.880	38.68	37.4	0.147	0.0	0.000	1.121
7	0.09	0.0		0.0	0.3787	101.080	38.62	0.0	0.000	0.0	0.000	0.000
8	0.47	0.0		0.0	0.3838	101.250	38.56	0.0	0.000	0.0	0.000	0.000
9	0.85	0.0		0.0	0.3838	101.440	38.50	0.0	0.000	0.0	0.000	0.000
10	1.23	0.0		0.0	0.3838	101.630	38.43	0.0	0.000	0.0	0.000	0.000
11	1.61	0.0		0.0	0.3838	101.820	38.37	0.0	0.000	0.0	0.000	0.000
									0.147	0.0	0.147	4.262

SAP: TIME= 12.000 HRS. ORTHO-THERMO PROPS. IN 2D. TEST C-10 V

ELE	TAVG C	%CM		%PR	GRADT C/CM	STRPRP KPA	SP *E-6	VEL -6MM/S	DDZS MM	DDZIS MM	DZINC MM	DZ MM
1	-4.84	0.0		1.00	0.7702	100.002	38.87	0.0	0.000	0.0	0.000	0.088
2	-4.17	0.0		1.00	0.7700	100.121	38.83	0.0	0.000	0.0	0.000	0.748
3	-3.34	0.0		1.00	0.7686	100.310	38.87	0.0	0.000	0.0	0.000	0.748
4	-2.52	0.0		1.00	0.7803	100.500	38.81	0.0	0.000	0.0	0.000	0.748
5	-1.71	0.0		1.00	0.7505	100.690	38.74	0.0	0.000	0.0	0.000	0.837
6	-0.88	0.0		1.00	0.7368	100.881	38.68	0.0	0.000	0.0	0.000	1.121
7	-0.28	0.82		0.92	0.8588	101.080	38.62	33.2	0.130	0.338	0.486	0.486
8	0.18	0.0		0.0	0.4686	101.250	38.56	0.0	0.000	0.0	0.000	0.000
9	0.85	0.0		0.0	0.4727	101.440	38.50	0.0	0.000	0.0	0.000	0.000
10	1.12	0.0		0.0	0.4819	101.630	38.43	0.0	0.000	0.0	0.000	0.000
11	1.87	0.0		0.0	0.4867	101.820	38.37	0.0	0.000	0.0	0.000	0.000
									0.130	0.338	0.486	4.718

SAP: TIME= 13.000 HRS. ORTHO-THERMO PROPS. IN 2D. TEST C-10 V

ELE	TAVG C	%CM		%PR	GRADT C/CM	STRPRP KPA	SP *E-6	VEL -6MM/S	DDZS MM	DDZIS MM	DZINC MM	DZ MM
1	-4.84	0.0		1.00	0.7160	100.002	38.87	0.0	0.000	0.0	0.000	0.088
2	-4.20	0.0		1.00	0.7158	100.121	38.83	0.0	0.000	0.0	0.000	0.748
3	-3.44	0.0		1.00	0.7128	100.310	38.87	0.0	0.000	0.0	0.000	0.748
4	-2.67	0.0		1.00	0.7011	100.500	38.81	0.0	0.000	0.0	0.000	0.748
5	-1.81	0.0		1.00	0.6990	100.690	38.74	0.0	0.000	0.0	0.000	0.837
6	-1.16	0.0		1.00	0.6881	100.881	38.68	0.0	0.000	0.0	0.000	1.121
7	-0.44	0.08		1.00	0.7877	101.088	38.62	30.4	0.119	0.028	0.148	0.814
8	0.14	0.0		0.0	0.4822	101.250	38.56	0.0	0.000	0.0	0.000	0.000
9	0.82	0.0		0.0	0.4785	101.440	38.50	0.0	0.000	0.0	0.000	0.000
10	1.09	0.0		0.0	0.4770	101.630	38.43	0.0	0.000	0.0	0.000	0.000
11	1.86	0.0		0.0	0.4758	101.820	38.37	0.0	0.000	0.0	0.000	0.000
									0.119	0.028	0.148	4.866

SAP: TIME= 14.000 HRS. ORTHO-THERMO PROPS. IN 2D. TEST C-10 V

ELE	TAVG C	%CM		%PR	GRADT C/CM	STRPRP KPA	SP *E-6	VEL -6MM/S	DDZS MM	DDZIS MM	DZINC MM	DZ MM
1	-4.85	0.0		1.00	0.8988	100.002	38.87	0.0	0.000	0.0	0.000	0.088
2	-4.22	0.0		1.00	0.8987	100.121	38.83	0.0	0.000	0.0	0.000	0.748
3	-3.47	0.0		1.00	0.8978	100.310	38.87	0.0	0.000	0.0	0.000	0.748
4	-2.72	0.0		1.00	0.8981	100.500	38.81	0.0	0.000	0.0	0.000	0.748
5	-1.87	0.0		1.00	0.8939	100.690	38.74	0.0	0.000	0.0	0.000	0.837
6	-1.21	0.0		1.00	0.8914	100.881	38.68	0.0	0.000	0.0	0.000	1.121
7	-0.48	0.0		1.00	0.8033	101.088	38.62	31.0	0.122	0.0	0.000	0.738
8	0.14	0.0		0.0	0.4744	101.250	38.56	0.0	0.000	0.0	0.000	0.000
9	0.81	0.0		0.0	0.4804	101.440	38.50	0.0	0.000	0.0	0.000	0.000
10	1.09	0.0		0.0	0.4788	101.630	38.43	0.0	0.000	0.0	0.000	0.000
11	1.86	0.0		0.0	0.4788	101.820	38.37	0.0	0.000	0.0	0.000	0.000
									0.122	0.0	0.122	4.887

SAP: TIME= 15.000 HRS, ORTHO-THERMO PROPS IN 2D, TEST C-10 V

ELE	TAVG C	%CH	%FR	GRADT C/CM	STRPRP KPA	SP *E-6	VEL -6MM/S	DDZS MM	DDZIS MM	DZINC MM	DZ MM
1	-4.88	0.0	1.00	0.8843	100.002	38.97	0.0	0.000	0.0	0.000	0.055
2	-4.22	0.0	1.00	0.8843	100.121	38.93	0.0	0.000	0.0	0.000	0.748
3	-3.47	0.0	1.00	0.8940	100.310	38.87	0.0	0.000	0.0	0.000	0.748
4	-2.73	0.0	1.00	0.8936	100.498	38.81	0.0	0.000	0.0	0.000	0.748
5	-1.98	0.0	1.00	0.8830	100.690	38.74	0.0	0.000	0.0	0.000	0.837
6	-1.22	0.0	1.00	0.8923	100.881	38.68	0.0	0.000	0.0	0.000	1.121
7	-0.47	0.0	1.00	0.8083	101.080	38.62	31.1	0.122	0.0	0.000	0.858
8	0.13	0.0	0.0	0.4738	101.250	38.56	0.0	0.000	0.0	0.000	0.000
9	0.81	0.0	0.0	0.4802	101.440	38.50	0.0	0.000	0.0	0.000	0.000
10	1.08	0.0	0.0	0.4802	101.630	38.43	0.0	0.000	0.0	0.000	0.000
11	1.56	0.0	0.0	0.4802	101.820	38.37	0.0	0.000	0.0	0.000	0.000
								0.122	0.0	0.122	5.110

SAP: TIME= 16.000 HRS, ORTHO-THERMO PROPS, IN 2D, TEST C-10 V

ELE	TAVG C	%CH	%FR	GRADT C/CM	STRPRP KPA	SP *E-6	VEL -6MM/S	DDZS MM	DDZIS MM	DZINC MM	DZ MM
1	-4.88	0.0	1.00	0.8923	100.002	38.97	0.0	0.000	0.0	0.000	0.055
2	-4.22	0.0	1.00	0.8923	100.121	38.93	0.0	0.000	0.0	0.000	0.748
3	-3.48	0.0	1.00	0.8922	100.310	38.87	0.0	0.000	0.0	0.000	0.748
4	-2.73	0.0	1.00	0.8920	100.498	38.81	0.0	0.000	0.0	0.000	0.748
5	-1.98	0.0	1.00	0.8918	100.690	38.75	0.0	0.000	0.0	0.000	0.837
6	-1.23	0.0	1.00	0.8918	100.881	38.68	0.0	0.000	0.0	0.000	1.121
7	-0.47	0.0	1.00	0.8058	101.080	38.62	31.1	0.122	0.0	0.000	0.980
8	0.13	0.0	0.0	0.4737	101.250	38.56	0.0	0.000	0.0	0.000	0.000
9	0.81	0.0	0.0	0.4802	101.440	38.50	0.0	0.000	0.0	0.000	0.000
10	1.08	0.0	0.0	0.4802	101.630	38.43	0.0	0.000	0.0	0.000	0.000
11	1.56	0.0	0.0	0.4802	101.820	38.37	0.0	0.000	0.0	0.000	0.000
								0.122	0.0	0.122	5.232

SAP: TIME= 17.000 HRS, ORTHO-THERMO PROPS, IN 2D, TEST C-10 V

ELE	TAVG C	%CH	%FR	GRADT C/CM	STRPRP KPA	SP *E-6	VEL -6MM/S	DDZS MM	DDZIS MM	DZINC MM	DZ MM
1	-4.88	0.0	1.00	0.8910	100.002	38.97	0.0	0.000	0.0	0.000	0.055
2	-4.22	0.0	1.00	0.8910	100.121	38.93	0.0	0.000	0.0	0.000	0.748
3	-3.48	0.0	1.00	0.8909	100.310	38.87	0.0	0.000	0.0	0.000	0.748
4	-2.74	0.0	1.00	0.8908	100.498	38.81	0.0	0.000	0.0	0.000	0.748
5	-1.98	0.0	1.00	0.8906	100.690	38.75	0.0	0.000	0.0	0.000	0.837
6	-1.23	0.0	1.00	0.8903	100.881	38.68	0.0	0.000	0.0	0.000	1.121
7	-0.47	0.0	1.00	0.8043	101.080	38.62	31.1	0.122	0.0	0.000	1.102
8	0.13	0.0	0.0	0.4737	101.250	38.56	0.0	0.000	0.0	0.000	0.000
9	0.81	0.0	0.0	0.4802	101.440	38.50	0.0	0.000	0.0	0.000	0.000
10	1.08	0.0	0.0	0.4802	101.630	38.43	0.0	0.000	0.0	0.000	0.000
11	1.56	0.0	0.0	0.4802	101.820	38.37	0.0	0.000	0.0	0.000	0.000
								0.122	0.0	0.122	5.353

SAP: TIME= 18.000 HRS, ORTHO-THERMO PROPS, IN 2D, TEST C-10 V

ELE	TAVG C	%CH	%FR	GRADT C/CM	STRPRP KPA	SP *E-6	VEL -6MM/S	DDZS MM	DDZIS MM	DZINC MM	DZ MM
1	-4.88	0.0	1.00	0.8897	100.002	38.97	0.0	0.000	0.0	0.000	0.055
2	-4.22	0.0	1.00	0.8897	100.121	38.93	0.0	0.000	0.0	0.000	0.748
3	-3.48	0.0	1.00	0.8898	100.310	38.87	0.0	0.000	0.0	0.000	0.748
4	-2.74	0.0	1.00	0.8895	100.498	38.81	0.0	0.000	0.0	0.000	0.748
5	-2.00	0.0	1.00	0.8893	100.690	38.75	0.0	0.000	0.0	0.000	0.837
6	-1.24	0.0	1.00	0.8891	100.881	38.68	0.0	0.000	0.0	0.000	1.121
7	-0.48	0.0	1.00	0.8029	101.080	38.62	31.0	0.122	0.0	0.000	1.223
8	0.13	0.0	0.0	0.4737	101.250	38.56	0.0	0.000	0.0	0.000	0.000
9	0.81	0.0	0.0	0.4802	101.440	38.50	0.0	0.000	0.0	0.000	0.000
10	1.08	0.0	0.0	0.4802	101.630	38.43	0.0	0.000	0.0	0.000	0.000
11	1.56	0.0	0.0	0.4802	101.820	38.37	0.0	0.000	0.0	0.000	0.000
								0.122	0.0	0.122	5.476

SAP, TIME= 20.000 HRS. ORTHO-THERMO PROPS. IN 2D, TEST C-10 V

ELE	TAVG C	%CM	%PR	GRADT C/CM	STRPRP KPA	SP *E-6	VEL -6MM/S	DDZS MM	DDZIS MM	DZINC MM	DZ MM
1	-4.85	0.0	1.00	0.8762	100.002	38.87	0.0	0.000	0.0	0.000	0.088
2	-4.23	0.0	1.00	0.8782	100.121	38.83	0.0	0.000	0.0	0.000	0.748
3	-3.51	0.0	1.00	0.8788	100.310	38.87	0.0	0.000	0.0	0.000	0.748
4	-2.78	0.0	1.00	0.8781	100.498	38.81	0.0	0.000	0.0	0.000	0.748
5	-2.08	0.0	1.00	0.8741	100.890	38.78	0.0	0.000	0.0	0.000	0.837
6	-1.31	0.0	1.00	0.8728	100.881	38.88	0.0	0.000	0.0	0.000	1.121
7	-0.87	0.0	1.00	0.8707	101.080	38.82	0.0	0.000	0.0	0.000	1.223
8	0.09	0.18	0.18	0.7817	101.290	38.86	30.1	0.237	0.069	0.308	0.306
9	0.88	0.0	0.0	0.9043	101.440	38.80	0.0	0.000	0.0	0.000	0.000
10	1.05	0.0	0.0	0.8027	101.830	38.43	0.0	0.000	0.0	0.000	0.000
11	1.86	0.0	0.0	0.9018	101.820	38.37	0.0	0.000	0.0	0.000	0.000
								0.237	0.069	0.308	6.781

SAP, TIME= 22.000 HRS. ORTHO-THERMO PROPS. IN 2D, TEST C-10 V

ELE	TAVG C	%CM	%PR	GRADT C/CM	STRPRP KPA	SP *E-6	VEL -6MM/S	DDZS MM	DDZIS MM	DZINC MM	DZ MM
1	-4.85	0.0	1.00	0.8188	100.002	38.87	0.0	0.000	0.0	0.000	0.088
2	-4.27	0.0	1.00	0.8187	100.121	38.83	0.0	0.000	0.0	0.000	0.748
3	-3.61	0.0	1.00	0.8171	100.310	38.87	0.0	0.000	0.0	0.000	0.748
4	-2.85	0.0	1.00	0.8141	100.498	38.81	0.0	0.000	0.0	0.000	0.748
5	-2.29	0.0	1.00	0.8098	100.890	38.78	0.0	0.000	0.0	0.000	0.837
6	-1.62	0.0	1.00	0.8034	100.881	38.88	0.0	0.000	0.0	0.000	1.121
7	-0.95	0.0	1.00	0.8953	101.080	38.82	0.0	0.000	0.0	0.000	1.223
8	-0.33	0.70	0.88	0.8838	101.290	38.86	4.8	0.038	0.285	0.283	0.899
9	0.27	0.0	0.0	0.8228	101.440	38.80	0.0	0.000	0.0	0.000	0.000
10	0.89	0.0	0.0	0.8149	101.830	38.43	0.0	0.000	0.0	0.000	0.000
11	1.60	0.0	0.0	0.8110	101.820	38.37	0.0	0.000	0.0	0.000	0.000
								0.038	0.285	0.283	6.074

SAP, TIME= 24.000 HRS. ORTHO-THERMO PROPS. IN 2D, TEST C-10 V

ELE	TAVG C	%CM	%PR	GRADT C/CM	STRPRP KPA	SP *E-6	VEL -6MM/S	DDZS MM	DDZIS MM	DZINC MM	DZ MM
1	-4.85	0.0	1.00	0.8883	100.002	38.87	0.0	0.000	0.0	0.000	0.088
2	-4.28	0.0	1.00	0.8883	100.121	38.83	0.0	0.000	0.0	0.000	0.748
3	-3.64	0.0	1.00	0.8887	100.310	38.87	0.0	0.000	0.0	0.000	0.748
4	-3.00	0.0	1.00	0.8878	100.498	38.81	0.0	0.000	0.0	0.000	0.748
5	-2.36	0.0	1.00	0.8864	100.890	38.78	0.0	0.000	0.0	0.000	0.837
6	-1.70	0.0	1.00	0.8847	100.881	38.88	0.0	0.000	0.0	0.000	1.121
7	-1.04	0.0	1.00	0.8827	101.080	38.82	0.0	0.000	0.0	0.000	1.223
8	-0.40	0.11	1.00	0.8887	101.248	38.86	25.8	0.208	0.041	0.248	0.848
9	0.22	0.0	0.0	0.8384	101.440	38.80	0.0	0.000	0.0	0.000	0.000
10	0.85	0.0	0.0	0.8378	101.830	38.43	0.0	0.000	0.0	0.000	0.000
11	1.48	0.0	0.0	0.8368	101.820	38.37	0.0	0.000	0.0	0.000	0.000
								0.208	0.041	0.248	6.323

SAP, TIME= 26.000 HRS. ORTHO-THERMO PROPS. IN 2D, TEST C-10 V

ELE	TAVG C	%CM	%PR	GRADT C/CM	STRPRP KPA	SP *E-6	VEL -6MM/S	DDZS MM	DDZIS MM	DZINC MM	DZ MM
1	-4.85	0.0	1.00	0.8938	100.002	38.87	0.0	0.000	0.0	0.000	0.088
2	-4.28	0.0	1.00	0.8938	100.121	38.83	0.0	0.000	0.0	0.000	0.748
3	-3.65	0.0	1.00	0.8938	100.310	38.87	0.0	0.000	0.0	0.000	0.748
4	-3.01	0.0	1.00	0.8935	100.498	38.81	0.0	0.000	0.0	0.000	0.748
5	-2.37	0.0	1.00	0.8931	100.889	38.78	0.0	0.000	0.0	0.000	0.837
6	-1.72	0.0	1.00	0.8927	100.881	38.88	0.0	0.000	0.0	0.000	1.121
7	-1.08	0.0	1.00	0.8922	101.081	38.82	0.0	0.000	0.0	0.000	1.223
8	-0.41	0.0	1.00	0.8898	101.250	38.86	25.8	0.208	0.0	0.000	1.087
9	0.22	0.0	0.0	0.8380	101.440	38.80	0.0	0.000	0.0	0.000	0.000
10	0.85	0.0	0.0	0.8381	101.830	38.43	0.0	0.000	0.0	0.000	0.000
11	1.48	0.0	0.0	0.8380	101.820	38.37	0.0	0.000	0.0	0.000	0.000
								0.208	0.0	0.208	6.532

SAP; TIME= 28.000 HRS, ORTHO-THERMO PROPS, IN 2D, TEST C-10 V

ELE	TAVG C	%CH	%FR	GRADT C/CM	STRPRP KPA	SP *E-6	VEL -6MM/S	DDZS MM	DDZIS MM	DZINC MM	DZ MM
1	-4.85	0.0	1.00	0.8816	100.002	38.87	0.0	0.000	0.0	0.000	0.055
2	-4.29	0.0	1.00	0.8815	100.121	38.83	0.0	0.000	0.0	0.000	0.748
3	-3.88	0.0	1.00	0.8815	100.310	38.87	0.0	0.000	0.0	0.000	0.745
4	-3.02	0.0	1.00	0.8814	100.498	38.81	0.0	0.000	0.0	0.000	0.748
5	-2.38	0.0	1.00	0.8812	100.688	38.75	0.0	0.000	0.0	0.000	0.837
6	-1.73	0.0	1.00	0.8810	100.881	38.68	0.0	0.000	0.0	0.000	1.121
7	-1.07	0.0	1.00	0.8807	101.081	38.62	0.0	0.000	0.0	0.000	1.223
8	-0.42	0.0	1.00	0.8863	101.280	38.66	28.8	0.208	0.0	0.000	1.288
9	0.22	0.0	0.0	0.8378	101.440	38.80	0.0	0.000	0.0	0.000	0.000
10	0.85	0.0	0.0	0.8381	101.630	38.43	0.0	0.000	0.0	0.000	0.000
11	1.48	0.0	0.0	0.8381	101.820	38.37	0.0	0.000	0.0	0.000	0.000
								0.208	0.0	0.208	8.740

SAP; TIME= 30.000 HRS, ORTHO-THERMO PROPS, IN 2D, TEST C-10 V

ELE	TAVG C	%CH	%FR	GRADT C/CM	STRPRP KPA	SP *E-6	VEL -6MM/S	DDZS MM	DDZIS MM	DZINC MM	DZ MM
1	-4.85	0.0	1.00	0.8896	100.002	38.87	0.0	0.000	0.0	0.000	0.055
2	-4.28	0.0	1.00	0.8896	100.121	38.83	0.0	0.000	0.0	0.000	0.748
3	-3.88	0.0	1.00	0.8896	100.310	38.87	0.0	0.000	0.0	0.000	0.745
4	-3.02	0.0	1.00	0.8897	100.498	38.81	0.0	0.000	0.0	0.000	0.748
5	-2.38	0.0	1.00	0.8896	100.688	38.75	0.0	0.000	0.0	0.000	0.837
6	-1.74	0.0	1.00	0.8894	100.881	38.68	0.0	0.000	0.0	0.000	1.121
7	-1.08	0.0	1.00	0.8892	101.081	38.62	0.0	0.000	0.0	0.000	1.223
8	-0.43	0.0	1.00	0.8866	101.280	38.66	28.8	0.208	0.0	0.000	1.472
9	0.22	0.0	0.0	0.8379	101.440	38.80	0.0	0.000	0.0	0.000	0.000
10	0.85	0.0	0.0	0.8381	101.630	38.43	0.0	0.000	0.0	0.000	0.000
11	1.48	0.0	0.0	0.8381	101.820	38.37	0.0	0.000	0.0	0.000	0.000
								0.208	0.0	0.208	8.948

SAP; TIME= 32.000 HRS, ORTHO-THERMO PROPS, IN 2D, TEST C-10 V

ELE	TAVG C	%CH	%FR	GRADT C/CM	STRPRP KPA	SP *E-6	VEL -6MM/S	DDZS MM	DDZIS MM	DZINC MM	DZ MM
1	-4.85	0.0	1.00	0.8863	100.002	38.87	0.0	0.000	0.0	0.000	0.055
2	-4.29	0.0	1.00	0.8863	100.121	38.83	0.0	0.000	0.0	0.000	0.748
3	-3.88	0.0	1.00	0.8863	100.310	38.87	0.0	0.000	0.0	0.000	0.745
4	-3.03	0.0	1.00	0.8862	100.499	38.81	0.0	0.000	0.0	0.000	0.748
5	-2.39	0.0	1.00	0.8861	100.688	38.75	0.0	0.000	0.0	0.000	0.837
6	-1.75	0.0	1.00	0.8879	100.881	38.68	0.0	0.000	0.0	0.000	1.121
7	-1.08	0.0	1.00	0.8877	101.080	38.62	0.0	0.000	0.0	0.000	1.223
8	-0.43	0.0	1.00	0.8848	101.251	38.66	28.4	0.207	0.0	0.000	1.880
9	0.22	0.0	0.0	0.8378	101.440	38.80	0.0	0.000	0.0	0.000	0.000
10	0.85	0.0	0.0	0.8381	101.630	38.43	0.0	0.000	0.0	0.000	0.000
11	1.48	0.0	0.0	0.8381	101.820	38.37	0.0	0.000	0.0	0.000	0.000
								0.207	0.0	0.207	7.155

SAP; TIME= 34.000 HRS, ORTHO-THERMO PROPS, IN 2D, TEST C-10 V

ELE	TAVG C	%CH	%FR	GRADT C/CM	STRPRP KPA	SP *E-6	VEL -6MM/S	DDZS MM	DDZIS MM	DZINC MM	DZ MM
1	-4.85	0.0	1.00	0.8868	100.002	38.87	0.0	0.000	0.0	0.000	0.055
2	-4.29	0.0	1.00	0.8867	100.121	38.83	0.0	0.000	0.0	0.000	0.748
3	-3.88	0.0	1.00	0.8867	100.310	38.87	0.0	0.000	0.0	0.000	0.745
4	-3.03	0.0	1.00	0.8866	100.499	38.81	0.0	0.000	0.0	0.000	0.748
5	-2.40	0.0	1.00	0.8865	100.688	38.75	0.0	0.000	0.0	0.000	0.837
6	-1.75	0.0	1.00	0.8883	100.881	38.68	0.0	0.000	0.0	0.000	1.121
7	-1.10	0.0	1.00	0.8881	101.080	38.62	0.0	0.000	0.0	0.000	1.223
8	-0.44	0.0	1.00	0.8830	101.251	38.66	28.3	0.207	0.0	0.000	1.888
9	0.22	0.0	0.0	0.8378	101.440	38.80	0.0	0.000	0.0	0.000	0.000
10	0.85	0.0	0.0	0.8381	101.630	38.43	0.0	0.000	0.0	0.000	0.000
11	1.48	0.0	0.0	0.8381	101.820	38.37	0.0	0.000	0.0	0.000	0.000
								0.207	0.0	0.207	7.382

SAP, TIME= 38.000 HRS, ORTHO-THERMO PROPS, IN 2D, TEST C-10 V

ELE	TAVG C	%CH	%FR	GRADT C/CM	STRPRP KPA	SP *E-6	VEL -6MM/S	DDZS MM	DDZIS MM	DZINC MM	DZ MM
1	-4.85	0.0	1.00	0.8852	100.002	38.87	0.0	0.000	0.0	0.000	0.085
2	-4.28	0.0	1.00	0.8852	100.121	38.83	0.0	0.000	0.0	0.000	0.748
3	-3.67	0.0	1.00	0.8851	100.310	38.87	0.0	0.000	0.0	0.000	0.748
4	-3.04	0.0	1.00	0.8851	100.498	38.81	0.0	0.000	0.0	0.000	0.748
5	-2.41	0.0	1.00	0.8849	100.688	38.78	0.0	0.000	0.0	0.000	0.837
6	-1.78	0.0	1.00	0.8848	100.881	38.88	0.0	0.000	0.0	0.000	1.121
7	-1.11	0.0	1.00	0.8848	101.080	38.82	0.0	0.000	0.0	0.000	1.223
8	-0.44	0.0	1.00	0.8812	101.281	38.86	28.3	0.206	0.0	0.000	2.093
9	0.22	0.0	0.0	0.8378	101.440	38.80	0.0	0.000	0.0	0.000	0.000
10	0.85	0.0	0.0	0.8381	101.630	38.43	0.0	0.000	0.0	0.000	0.000
11	1.48	0.0	0.0	0.8381	101.820	38.37	0.0	0.000	0.0	0.000	0.000
								0.206	0.0	0.206	7.888

SAP, TIME= 38.000 HRS, ORTHO-THERMO PROPS, IN 2D, TEST C-10 V

ELE	TAVG C	%CH	%FR	GRADT C/CM	STRPRP KPA	SP *E-6	VEL -6MM/S	DDZS MM	DDZIS MM	DZINC MM	DZ MM
1	-4.85	0.0	1.00	0.8837	100.002	38.87	0.0	0.000	0.0	0.000	0.085
2	-4.30	0.0	1.00	0.8837	100.121	38.83	0.0	0.000	0.0	0.000	0.748
3	-3.67	0.0	1.00	0.8837	100.310	38.87	0.0	0.000	0.0	0.000	0.748
4	-3.04	0.0	1.00	0.8836	100.498	38.81	0.0	0.000	0.0	0.000	0.748
5	-2.41	0.0	1.00	0.8835	100.688	38.78	0.0	0.000	0.0	0.000	0.837
6	-1.77	0.0	1.00	0.8833	100.881	38.88	0.0	0.000	0.0	0.000	1.121
7	-1.12	0.0	1.00	0.8831	101.080	38.82	0.0	0.000	0.0	0.000	1.223
8	-0.45	0.0	1.00	0.8795	101.282	38.86	28.2	0.208	0.0	0.000	2.284
9	0.22	0.0	0.0	0.8378	101.440	38.80	0.0	0.000	0.0	0.000	0.000
10	0.85	0.0	0.0	0.8381	101.630	38.43	0.0	0.000	0.0	0.000	0.000
11	1.48	0.0	0.0	0.8381	101.820	38.37	0.0	0.000	0.0	0.000	0.000
								0.208	0.0	0.208	7.773

SAP, TIME= 40.000 HRS, ORTHO-THERMO PROPS, IN 2D, TEST C-10 V

ELE	TAVG C	%CH	%FR	GRADT C/CM	STRPRP KPA	SP *E-6	VEL -6MM/S	DDZS MM	DDZIS MM	DZINC MM	DZ MM
1	-4.85	0.0	1.00	0.8822	100.002	38.87	0.0	0.000	0.0	0.000	0.085
2	-4.30	0.0	1.00	0.8821	100.121	38.83	0.0	0.000	0.0	0.000	0.748
3	-3.67	0.0	1.00	0.8821	100.310	38.87	0.0	0.000	0.0	0.000	0.748
4	-3.05	0.0	1.00	0.8820	100.498	38.81	0.0	0.000	0.0	0.000	0.748
5	-2.42	0.0	1.00	0.8819	100.688	38.78	0.0	0.000	0.0	0.000	0.837
6	-1.78	0.0	1.00	0.8818	100.881	38.88	0.0	0.000	0.0	0.000	1.121
7	-1.13	0.0	1.00	0.8818	101.080	38.82	0.0	0.000	0.0	0.000	1.223
8	-0.45	0.0	1.00	0.8777	101.282	38.86	28.9	0.201	0.0	0.000	2.498
9	0.22	0.0	0.0	0.8378	101.440	38.80	0.0	0.000	0.0	0.000	0.000
10	0.85	0.0	0.0	0.8381	101.630	38.43	0.0	0.000	0.0	0.000	0.000
11	1.48	0.0	0.0	0.8381	101.820	38.37	0.0	0.000	0.0	0.000	0.000
								0.201	0.0	0.201	7.874

SAP, TIME= 42.000 HRS, ORTHO-THERMO PROPS, IN 2D, TEST C-10 V

ELE	TAVG C	%CH	%FR	GRADT C/CM	STRPRP KPA	SP *E-6	VEL -6MM/S	DDZS MM	DDZIS MM	DZINC MM	DZ MM
1	-4.85	0.0	1.00	0.8808	100.002	38.87	0.0	0.000	0.0	0.000	0.085
2	-4.30	0.0	1.00	0.8806	100.121	38.83	0.0	0.000	0.0	0.000	0.748
3	-3.67	0.0	1.00	0.8808	100.310	38.87	0.0	0.000	0.0	0.000	0.748
4	-3.05	0.0	1.00	0.8805	100.498	38.81	0.0	0.000	0.0	0.000	0.748
5	-2.42	0.0	1.00	0.8804	100.688	38.78	0.0	0.000	0.0	0.000	0.837
6	-1.78	0.0	1.00	0.8802	100.880	38.88	0.0	0.000	0.0	0.000	1.121
7	-1.14	0.0	1.00	0.8800	101.080	38.82	0.0	0.000	0.0	0.000	1.223
8	-0.46	0.0	1.00	0.8758	101.282	38.86	26.8	0.188	0.0	0.000	2.894
9	0.22	0.0	0.0	0.8378	101.440	38.80	0.0	0.000	0.0	0.000	0.000
10	0.85	0.0	0.0	0.8381	101.630	38.43	0.0	0.000	0.0	0.000	0.000
11	1.48	0.0	0.0	0.8381	101.820	38.37	0.0	0.000	0.0	0.000	0.000
								0.188	0.0	0.188	6.188

SAP TIME= 44.000 HRS, ORTHO-THERMO PROPS IN 2D, TEST C-10 V

ELE	TAVG C	%CM	%PR	GRADT C/CM	STRPRP KPA	SP *E-5	VEL -6MM/S	DDZS MM	DDZIS MM	DZINC MM	DZ MM
1	-4.88	0.0	1.00	0.8781	100.002	38.87	0.0	0.000	0.0	0.000	0.086
2	-4.30	0.0	1.00	0.8781	100.121	38.83	0.0	0.000	0.0	0.000	0.748
3	-3.68	0.0	1.00	0.8781	100.310	38.87	0.0	0.000	0.0	0.000	0.748
4	-3.06	0.0	1.00	0.8780	100.498	38.81	0.0	0.000	0.0	0.000	0.748
5	-2.43	0.0	1.00	0.8788	100.688	38.78	0.0	0.000	0.0	0.000	0.837
6	-1.79	0.0	1.00	0.8787	100.880	38.88	0.0	0.000	0.0	0.000	1.121
7	-1.16	0.0	1.00	0.8786	101.088	38.82	0.0	0.000	0.0	0.000	1.223
8	-0.46	0.0	1.00	0.8742	101.283	38.86	24.0	0.188	0.0	0.000	2.883
9	0.22	0.0	0.0	0.8378	101.440	38.80	0.0	0.000	0.0	0.000	0.000
10	0.85	0.0	0.0	0.8361	101.630	38.43	0.0	0.000	0.0	0.000	0.000
11	1.48	0.0	0.0	0.8361	101.820	38.37	0.0	0.000	0.0	0.000	0.000
								0.188	0.0	0.188	8.356

SAP TIME= 46.000 HRS, ORTHO-THERMO PROPS IN 2D, TEST C-10 V

ELE	TAVG C	%CM	%PR	GRADT C/CM	STRPRP KPA	SP *E-5	VEL -6MM/S	DDZS MM	DDZIS MM	DZINC MM	DZ MM
1	-4.88	0.0	1.00	0.8777	100.002	38.87	0.0	0.000	0.0	0.000	0.086
2	-4.30	0.0	1.00	0.8777	100.121	38.83	0.0	0.000	0.0	0.000	0.748
3	-3.68	0.0	1.00	0.8777	100.310	38.87	0.0	0.000	0.0	0.000	0.748
4	-3.06	0.0	1.00	0.8776	100.498	38.81	0.0	0.000	0.0	0.000	0.748
5	-2.43	0.0	1.00	0.8776	100.688	38.78	0.0	0.000	0.0	0.000	0.837
6	-1.80	0.0	1.00	0.8774	100.880	38.88	0.0	0.000	0.0	0.000	1.121
7	-1.16	0.0	1.00	0.8772	101.088	38.82	0.0	0.000	0.0	0.000	1.223
8	-0.47	0.0	1.00	0.8726	101.283	38.86	23.3	0.183	0.0	0.000	3.066
9	0.22	0.0	0.0	0.8378	101.440	38.80	0.0	0.000	0.0	0.000	0.000
10	0.85	0.0	0.0	0.8361	101.630	38.43	0.0	0.000	0.0	0.000	0.000
11	1.48	0.0	0.0	0.8361	101.820	38.37	0.0	0.000	0.0	0.000	0.000
								0.183	0.0	0.183	8.541

SAP TIME= 48.000 HRS, ORTHO-THERMO PROPS IN 2D, TEST C-10 V

ELE	TAVG C	%CM	%PR	GRADT C/CM	STRPRP KPA	SP *E-5	VEL -6MM/S	DDZS MM	DDZIS MM	DZINC MM	DZ MM
1	-4.88	0.0	1.00	0.8784	100.002	38.87	0.0	0.000	0.0	0.000	0.086
2	-4.30	0.0	1.00	0.8784	100.121	38.83	0.0	0.000	0.0	0.000	0.748
3	-3.68	0.0	1.00	0.8783	100.310	38.87	0.0	0.000	0.0	0.000	0.748
4	-3.06	0.0	1.00	0.8783	100.498	38.81	0.0	0.000	0.0	0.000	0.748
5	-2.44	0.0	1.00	0.8781	100.688	38.78	0.0	0.000	0.0	0.000	0.837
6	-1.81	0.0	1.00	0.8780	100.880	38.88	0.0	0.000	0.0	0.000	1.121
7	-1.16	0.0	1.00	0.8786	101.088	38.82	0.0	0.000	0.0	0.000	1.223
8	-0.47	0.0	1.00	0.8710	101.283	38.86	22.8	0.177	0.0	0.000	3.243
9	0.22	0.0	0.0	0.8378	101.440	38.80	0.0	0.000	0.0	0.000	0.000
10	0.85	0.0	0.0	0.8361	101.630	38.43	0.0	0.000	0.0	0.000	0.000
11	1.48	0.0	0.0	0.8361	101.820	38.37	0.0	0.000	0.0	0.000	0.000
								0.177	0.0	0.177	8.718

SAP TIME= 50.000 HRS, ORTHO-THERMO PROPS IN 2D, TEST C-10 V

ELE	TAVG C	%CM	%PR	GRADT C/CM	STRPRP KPA	SP *E-5	VEL -6MM/S	DDZS MM	DDZIS MM	DZINC MM	DZ MM
1	-4.88	0.0	1.00	0.8781	100.002	38.87	0.0	0.000	0.0	0.000	0.086
2	-4.30	0.0	1.00	0.8781	100.121	38.83	0.0	0.000	0.0	0.000	0.748
3	-3.68	0.0	1.00	0.8780	100.310	38.87	0.0	0.000	0.0	0.000	0.748
4	-3.07	0.0	1.00	0.8748	100.498	38.81	0.0	0.000	0.0	0.000	0.748
5	-2.46	0.0	1.00	0.8748	100.688	38.78	0.0	0.000	0.0	0.000	0.837
6	-1.81	0.0	1.00	0.8747	100.880	38.88	0.0	0.000	0.0	0.000	1.121
7	-1.17	0.0	1.00	0.8745	101.088	38.82	0.0	0.000	0.0	0.000	1.223
8	-0.48	0.0	1.00	0.8695	101.256	38.58	21.9	0.172	0.0	0.000	3.418
9	0.22	0.0	0.0	0.8378	101.440	38.80	0.0	0.000	0.0	0.000	0.000
10	0.85	0.0	0.0	0.8361	101.630	38.43	0.0	0.000	0.0	0.000	0.000
11	1.48	0.0	0.0	0.8361	101.820	38.37	0.0	0.000	0.0	0.000	0.000
								0.172	0.0	0.172	8.880

SAP, TIME= 55 000 HRS, ORTHO-THERMO PROPS IN 2D, TEST C-10 V

ELE	TAVG C	XCM	XPR	GRADT C/CM	STRPRP KPA	SP +E-6	VEL -6MM/S	DDZS MM	DDZIS MM	DZINC MM	DZ MM
1	-4.86	0.0	1.00	0.8726	100.002	38.87	0.0	0.000	0.0	0.000	0.088
2	-4.30	0.0	1.00	0.8726	100.121	38.83	0.0	0.000	0.0	0.000	0.748
3	-3.88	0.0	1.00	0.8726	100.310	38.87	0.0	0.000	0.0	0.000	0.748
4	-3.07	0.0	1.00	0.8726	100.498	38.81	0.0	0.000	0.0	0.000	0.748
5	-2.46	0.0	1.00	0.8726	100.688	38.75	0.0	0.000	0.0	0.000	0.837
6	-1.82	0.0	1.00	0.8724	100.880	38.68	0.0	0.000	0.0	0.000	1.121
7	-1.18	0.0	1.00	0.8724	101.086	38.62	0.0	0.000	0.0	0.000	1.223
8	-0.48	0.0	1.00	0.8684	101.284	38.56	21.9	0.422	0.0	0.000	3.837
9	0.22	0.0	0.0	0.8378	101.440	38.50	0.0	0.000	0.0	0.000	0.000
10	0.85	0.0	0.0	0.8361	101.630	38.43	0.0	0.000	0.0	0.000	0.000
11	1.48	0.0	0.0	0.8361	101.820	38.37	0.0	0.000	0.0	0.000	0.000
								0.422	0.0	0.422	9.312

SAP, TIME= 60 000 HRS, ORTHO-THERMO PROPS IN 2D, TEST C-10 V

ELE	TAVG C	XCM	XPR	GRADT C/CM	STRPRP KPA	SP +E-6	VEL -6MM/S	DDZS MM	DDZIS MM	DZINC MM	DZ MM
1	-4.86	0.0	1.00	0.8723	100.002	38.87	0.0	0.000	0.0	0.000	0.088
2	-4.30	0.0	1.00	0.8724	100.121	38.83	0.0	0.000	0.0	0.000	0.748
3	-3.88	0.0	1.00	0.8723	100.310	38.87	0.0	0.000	0.0	0.000	0.748
4	-3.07	0.0	1.00	0.8723	100.498	38.81	0.0	0.000	0.0	0.000	0.748
5	-2.46	0.0	1.00	0.8723	100.688	38.75	0.0	0.000	0.0	0.000	0.837
6	-1.83	0.0	1.00	0.8722	100.880	38.68	0.0	0.000	0.0	0.000	1.121
7	-1.18	0.0	1.00	0.8722	101.086	38.62	0.0	0.000	0.0	0.000	1.223
8	-0.48	0.0	1.00	0.8670	101.285	38.56	20.9	0.403	0.0	0.000	4.248
9	0.22	0.0	0.0	0.8378	101.440	38.50	0.0	0.000	0.0	0.000	0.000
10	0.85	0.0	0.0	0.8361	101.630	38.43	0.0	0.000	0.0	0.000	0.000
11	1.48	0.0	0.0	0.8361	101.820	38.37	0.0	0.000	0.0	0.000	0.000
								0.403	0.0	0.403	9.721

SAP, TIME= 65 000 HRS, ORTHO-THERMO PROPS, IN 2D, TEST C-10 V

ELE	TAVG C	XCM	XPR	GRADT C/CM	STRPRP KPA	SP +E-6	VEL -6MM/S	DDZS MM	DDZIS MM	DZINC MM	DZ MM
1	-4.86	0.0	1.00	0.8695	100.002	38.87	0.0	0.000	0.0	0.000	0.088
2	-4.31	0.0	1.00	0.8694	100.121	38.83	0.0	0.000	0.0	0.000	0.748
3	-3.89	0.0	1.00	0.8694	100.310	38.87	0.0	0.000	0.0	0.000	0.748
4	-3.08	0.0	1.00	0.8694	100.498	38.81	0.0	0.000	0.0	0.000	0.748
5	-2.47	0.0	1.00	0.8693	100.688	38.75	0.0	0.000	0.0	0.000	0.837
6	-1.84	0.0	1.00	0.8692	100.880	38.68	0.0	0.000	0.0	0.000	1.121
7	-1.21	0.0	1.00	0.8690	101.087	38.62	0.0	0.000	0.0	0.000	1.223
8	-0.49	0.0	1.00	0.8632	101.286	38.56	19.1	0.378	0.0	0.000	4.821
9	0.22	0.0	0.0	0.8378	101.440	38.50	0.0	0.000	0.0	0.000	0.000
10	0.85	0.0	0.0	0.8361	101.630	38.43	0.0	0.000	0.0	0.000	0.000
11	1.48	0.0	0.0	0.8361	101.820	38.37	0.0	0.000	0.0	0.000	0.000
								0.378	0.0	0.378	10.098

SAP, TIME= 70 000 HRS, ORTHO-THERMO PROPS, IN 2D, TEST C-10 V

ELE	TAVG C	XCM	XPR	GRADT C/CM	STRPRP KPA	SP +E-6	VEL -6MM/S	DDZS MM	DDZIS MM	DZINC MM	DZ M
1	-4.86	0.0	1.00	0.8688	100.002	38.87	0.0	0.000	0.0	0.000	0.088
2	-4.31	0.0	1.00	0.8688	100.121	38.83	0.0	0.000	0.0	0.000	0.748
3	-3.70	0.0	1.00	0.8685	100.310	38.87	0.0	0.000	0.0	0.000	0.748
4	-3.08	0.0	1.00	0.8685	100.498	38.81	0.0	0.000	0.0	0.000	0.748
5	-2.46	0.0	1.00	0.8684	100.688	38.75	0.0	0.000	0.0	0.000	0.837
6	-1.86	0.0	1.00	0.8683	100.880	38.68	0.0	0.000	0.0	0.000	1.121
7	-1.22	0.0	1.00	0.8681	101.087	38.62	0.0	0.000	0.0	0.000	1.223
8	-0.50	0.0	1.00	0.8599	101.286	38.56	17.8	0.348	0.0	0.000	4.857
9	0.22	0.0	0.0	0.8378	101.440	38.50	0.0	0.000	0.0	0.000	0.000
10	0.85	0.0	0.0	0.8361	101.630	38.43	0.0	0.000	0.0	0.000	0.000
11	1.48	0.0	0.0	0.8361	101.820	38.37	0.0	0.000	0.0	0.000	0.000
								0.348	0.0	0.348	10.442

SAP; TIME= 75 000 HRS, ORTHO-THERMO PROPS IN 2D, TEST C-10 V

ELE	TAVG C	%CM	%PR	GRADT C/CM	STRPRP KPA	SP *E-6	VEL -6MM/S	DDZS MM	DDZIS MM	DZINC MM	DZ MM
1	-4.88	0.0	1.00	0.8840	100.002	38.87	0.0	0.000	0.0	0.000	0.088
2	-4.31	0.0	1.00	0.8840	100.121	38.83	0.0	0.000	0.0	0.000	0.748
3	-3.70	0.0	1.00	0.8840	100.310	38.87	0.0	0.000	0.0	0.000	0.748
4	-3.10	0.0	1.00	0.8839	100.498	38.81	0.0	0.000	0.0	0.000	0.748
5	-2.49	0.0	1.00	0.8838	100.688	38.75	0.0	0.000	0.0	0.000	0.837
6	-1.87	0.0	1.00	0.8837	100.879	38.68	0.0	0.000	0.0	0.000	1.121
7	-1.24	0.0	1.00	0.8838	101.088	38.62	0.0	0.000	0.0	0.000	1.223
8	-0.61	0.0	1.00	0.8588	101.287	38.56	15.3	0.318	0.0	0.000	8.285
9	0.22	0.0	0.0	0.8378	101.440	38.50	0.0	0.000	0.0	0.000	0.000
10	0.85	0.0	0.0	0.8381	101.630	38.43	0.0	0.000	0.0	0.000	0.000
11	1.48	0.0	0.0	0.8381	101.820	38.37	0.0	0.000	0.0	0.000	0.000
								0.318	0.0	0.318	10.761

SAP TIME= 80 000 HRS, ORTHO-THERMO PROPS IN 2D, TEST C-10 V

ELE	TAVG C	%CM	%PR	GRADT C/CM	STRPRP KPA	SP *E-6	VEL -6MM/S	DDZS MM	DDZIS MM	DZINC MM	DZ MM
1	-4.88	0.0	1.00	0.8818	100.002	38.87	0.0	0.000	0.0	0.000	0.088
2	-4.31	0.0	1.00	0.8818	100.121	38.83	0.0	0.000	0.0	0.000	0.748
3	-3.71	0.0	1.00	0.8818	100.310	38.87	0.0	0.000	0.0	0.000	0.748
4	-3.10	0.0	1.00	0.8818	100.498	38.81	0.0	0.000	0.0	0.000	0.748
5	-2.50	0.0	1.00	0.8815	100.688	38.75	0.0	0.000	0.0	0.000	0.837
6	-1.88	0.0	1.00	0.8814	100.878	38.68	0.0	0.000	0.0	0.000	1.121
7	-1.25	0.0	1.00	0.8813	101.088	38.62	0.0	0.000	0.0	0.000	1.223
8	-0.62	0.0	1.00	0.8942	101.288	38.56	15.0	0.285	0.0	0.000	8.561
9	0.22	0.0	0.0	0.8378	101.440	38.50	0.0	0.000	0.0	0.000	0.000
10	0.85	0.0	0.0	0.8381	101.630	38.43	0.0	0.000	0.0	0.000	0.000
11	1.48	0.0	0.0	0.8381	101.820	38.37	0.0	0.000	0.0	0.000	0.000
								0.285	0.0	0.285	11.066

SAP TIME= 85 000 HRS, ORTHO-THERMO PROPS IN 2D, TEST C-10 V

ELE	TAVG C	%CM	%PR	GRADT C/CM	STRPRP KPA	SP *E-6	VEL -6MM/S	DDZS MM	DDZIS MM	DZINC MM	DZ MM
1	-4.88	0.0	1.00	0.8886	100.002	38.87	0.0	0.000	0.0	0.000	0.088
2	-4.31	0.0	1.00	0.8886	100.121	38.83	0.0	0.000	0.0	0.000	0.748
3	-3.71	0.0	1.00	0.8893	100.310	38.87	0.0	0.000	0.0	0.000	0.748
4	-3.11	0.0	1.00	0.8893	100.498	38.81	0.0	0.000	0.0	0.000	0.748
5	-2.51	0.0	1.00	0.8892	100.688	38.75	0.0	0.000	0.0	0.000	0.837
6	-1.89	0.0	1.00	0.8891	100.879	38.68	0.0	0.000	0.0	0.000	1.121
7	-1.27	0.0	1.00	0.8890	101.088	38.62	0.0	0.000	0.0	0.000	1.223
8	-0.63	0.0	1.00	0.8516	101.288	38.56	13.9	0.272	0.0	0.000	8.663
9	0.22	0.0	0.0	0.8378	101.440	38.50	0.0	0.000	0.0	0.000	0.000
10	0.85	0.0	0.0	0.8381	101.630	38.43	0.0	0.000	0.0	0.000	0.000
11	1.48	0.0	0.0	0.8381	101.820	38.37	0.0	0.000	0.0	0.000	0.000
								0.272	0.0	0.272	11.326

SAP; TIME= 90.000 HRS, ORTHO-THERMO PROPS, IN 2D, TEST C-10 V

ELE	TAVG C	%CM	%PR	GRADT C/CM	STRPRP KPA	SP *E-6	VEL -6MM/S	DDZS MM	DDZIS MM	DZINC MM	DZ MM
1	-4.88	0.0	1.00	0.8888	100.002	38.87	0.0	0.000	0.0	0.000	0.088
2	-4.31	0.0	1.00	0.8888	100.121	38.83	0.0	0.000	0.0	0.000	0.748
3	-3.72	0.0	1.00	0.8888	100.310	38.87	0.0	0.000	0.0	0.000	0.748
4	-3.12	0.0	1.00	0.8888	100.498	38.81	0.0	0.000	0.0	0.000	0.748
5	-2.52	0.0	1.00	0.8888	100.688	38.75	0.0	0.000	0.0	0.000	0.837
6	-1.91	0.0	1.00	0.8883	100.878	38.68	0.0	0.000	0.0	0.000	1.121
7	-1.29	0.0	1.00	0.8882	101.088	38.62	0.0	0.000	0.0	0.000	1.223
8	-0.64	0.0	1.00	0.8880	101.288	38.56	0.0	0.000	0.0	0.000	8.663
9	0.21	0.01	0.01	0.8480	101.440	38.50	11.1	0.218	0.004	0.222	0.222
10	0.85	0.0	0.0	0.8406	101.630	38.43	0.0	0.000	0.0	0.000	0.000
11	1.48	0.0	0.0	0.8403	101.820	38.37	0.0	0.000	0.0	0.000	0.000
								0.218	0.004	0.222	11.550

SAP TIME= 95.000 HRS, ORTHO-THERMO PROPS IN 2D, TEST C-10 V

ELE	TAVG C	%CH	%PR	GRADT C/CM	STRPRP KPA	SP *E-6	VEL -6MM/S	DDZS MM	DDZIS MM	DZINC MM	DZ MM
1	-4.66	0.0	1.00	0.8533	100.002	38.97	0.0	0.000	0.0	0.000	0.055
2	-4.32	0.0	1.00	0.8533	100.121	38.93	0.0	0.000	0.0	0.000	0.748
3	-3.72	0.0	1.00	0.8532	100.310	38.87	0.0	0.000	0.0	0.000	0.748
4	-3.13	0.0	1.00	0.8532	100.498	38.81	0.0	0.000	0.0	0.000	0.748
5	-2.83	0.0	1.00	0.8531	100.588	38.78	0.0	0.000	0.0	0.000	0.837
6	-1.82	0.0	1.00	0.8529	100.878	38.68	0.0	0.000	0.0	0.000	1.121
7	-1.21	0.0	1.00	0.8528	101.068	38.62	0.0	0.000	0.0	0.000	1.223
8	-0.86	0.0	1.00	0.8525	101.258	38.56	0.0	0.000	0.0	0.000	0.853
9	0.21	0.02	0.03	0.8440	101.440	38.50	0.1	0.002	0.007	0.008	0.230
10	0.86	0.0	0.0	0.8382	101.630	38.43	0.0	0.000	0.0	0.000	0.000
11	1.46	0.0	0.0	0.8383	101.820	38.37	0.0	0.000	0.0	0.000	0.000
								0.002	0.007	0.008	11.559

SAP TIME= 100.000 HRS, ORTHO-THERMO PROPS IN 2D, TEST C-10 V

ELE	TAVG C	%CH	%PR	GRADT C/CM	STRPRP KPA	SP *E-6	VEL -6MM/S	DDZS MM	DDZIS MM	DZINC MM	DZ MM
1	-4.88	0.0	1.00	0.8490	100.002	38.97	0.0	0.000	0.0	0.000	0.055
2	-4.32	0.0	1.00	0.8491	100.121	38.93	0.0	0.000	0.0	0.000	0.748
3	-3.73	0.0	1.00	0.8490	100.310	38.87	0.0	0.000	0.0	0.000	0.748
4	-3.14	0.0	1.00	0.8489	100.498	38.81	0.0	0.000	0.0	0.000	0.748
5	-2.85	0.0	1.00	0.8488	100.588	38.78	0.0	0.000	0.0	0.000	0.837
6	-1.85	0.0	1.00	0.8488	100.878	38.68	0.0	0.000	0.0	0.000	1.121
7	-1.33	0.0	1.00	0.8484	101.068	38.62	0.0	0.000	0.0	0.000	1.223
8	-0.88	0.0	1.00	0.8480	101.258	38.56	0.0	0.000	0.0	0.000	0.853
9	0.17	0.08	0.08	0.8388	101.440	38.50	0.2	0.008	0.020	0.028	0.258
10	0.83	0.0	0.0	0.8349	101.630	38.43	0.0	0.000	0.0	0.000	0.000
11	1.47	0.0	0.0	0.8348	101.820	38.37	0.0	0.000	0.0	0.000	0.000
								0.008	0.020	0.028	11.584

SAP TIME= 105.000 HRS, ORTHO-THERMO PROPS IN 2D, TEST C-10 V

ELE	TAVG C	%CH	%PR	GRADT C/CM	STRPRP KPA	SP *E-6	VEL -6MM/S	DDZS MM	DDZIS MM	DZINC MM	DZ MM
1	-4.88	0.0	1.00	0.8483	100.002	38.97	0.0	0.000	0.0	0.000	0.055
2	-4.32	0.0	1.00	0.8483	100.121	38.93	0.0	0.000	0.0	0.000	0.748
3	-3.73	0.0	1.00	0.8483	100.310	38.87	0.0	0.000	0.0	0.000	0.748
4	-3.14	0.0	1.00	0.8483	100.498	38.81	0.0	0.000	0.0	0.000	0.748
5	-2.85	0.0	1.00	0.8483	100.588	38.78	0.0	0.000	0.0	0.000	0.837
6	-1.85	0.0	1.00	0.8482	100.879	38.68	0.0	0.000	0.0	0.000	1.121
7	-1.34	0.0	1.00	0.8482	101.068	38.62	0.0	0.000	0.0	0.000	1.223
8	-0.89	0.0	1.00	0.8482	101.258	38.56	0.0	0.000	0.0	0.000	0.853
9	0.17	0.00	0.08	0.8388	101.440	38.50	0.0	0.000	0.002	0.002	0.257
10	0.82	0.0	0.0	0.8557	101.630	38.43	0.0	0.000	0.0	0.000	0.000
11	1.47	0.0	0.0	0.8557	101.820	38.37	0.0	0.000	0.0	0.000	0.000
								0.000	0.002	0.002	11.586

SAP TIME= 110.000 HRS, ORTHO-THERMO PROPS IN 2D, TEST C-10 V

ELE	TAVG C	%CH	%PR	GRADT C/CM	STRPRP KPA	SP *E-6	VEL -6MM/S	DDZS MM	DDZIS MM	DZINC MM	DZ MM
1	-4.88	0.0	1.00	0.8480	100.002	38.97	0.0	0.000	0.0	0.000	0.055
2	-4.32	0.0	1.00	0.8480	100.121	38.93	0.0	0.000	0.0	0.000	0.748
3	-3.73	0.0	1.00	0.8480	100.310	38.87	0.0	0.000	0.0	0.000	0.748
4	-3.14	0.0	1.00	0.8480	100.498	38.81	0.0	0.000	0.0	0.000	0.748
5	-2.85	0.0	1.00	0.8480	100.588	38.78	0.0	0.000	0.0	0.000	0.837
6	-1.85	0.0	1.00	0.8480	100.878	38.68	0.0	0.000	0.0	0.000	1.121
7	-1.34	0.0	1.00	0.8480	101.068	38.62	0.0	0.000	0.0	0.000	1.223
8	-0.89	0.0	1.00	0.8480	101.258	38.56	0.0	0.000	0.0	0.000	0.853
9	0.17	0.00	0.08	0.8387	101.440	38.50	0.0	0.000	0.001	0.001	0.258
10	0.82	0.0	0.0	0.8580	101.630	38.43	0.0	0.000	0.0	0.000	0.000
11	1.47	0.0	0.0	0.8580	101.820	38.37	0.0	0.000	0.0	0.000	0.000
								0.000	0.001	0.001	11.587

SAP TIME= 118.000 HRS, ORTHO-THERMO PROPS, IN 2D, TEST C-10 V

ELE	TAVG C	%CH	%PR	GRADT C/CM	STRPRP KPA	SP *E-6	VEL -6MM/S	DDZS MM	DDZIS MM	DZINC MM	DZ MM
1	-4.86	0.0	1.00	0.8480	100.002	38.87	0.0	0.000	0.0	0.000	0.055
2	-4.32	0.0	1.00	0.8480	100.121	38.83	0.0	0.000	0.0	0.000	0.748
3	-3.73	0.0	1.00	0.8480	100.310	38.87	0.0	0.000	0.0	0.000	0.745
4	-3.14	0.0	1.00	0.8480	100.499	38.81	0.0	0.000	0.0	0.000	0.748
5	-2.55	0.0	1.00	0.8480	100.688	38.75	0.0	0.000	0.0	0.000	0.837
6	-1.95	0.0	1.00	0.8480	100.878	38.68	0.0	0.000	0.0	0.000	1.121
7	-1.34	0.0	1.00	0.8480	101.084	38.62	0.0	0.000	0.0	0.000	1.223
8	-0.80	0.0	1.00	0.8480	101.280	38.56	0.0	0.000	0.0	0.000	8.853
9	0.17	0.00	0.08	0.8387	101.440	38.50	0.0	0.000	0.000	0.000	0.259
10	0.82	0.0	0.0	0.8580	101.630	38.43	0.0	0.000	0.0	0.000	0.000
11	1.47	0.0	0.0	0.8580	101.820	38.37	0.0	0.000	0.0	0.000	0.000
								0.000	0.000	0.000	11.587

SAP TIME= 120.000 HRS, ORTHO-THERMO PROPS, IN 2D, TEST C-10 V

ELE	TAVG C	%CH	%PR	GRADT C/CM	STRPRP KPA	SP *E-6	VEL -6MM/S	DDZS MM	DDZIS MM	DZINC MM	DZ MM
1	-4.86	0.0	1.00	0.8480	100.002	38.87	0.0	0.000	0.0	0.000	0.055
2	-4.32	0.0	1.00	0.8480	100.121	38.83	0.0	0.000	0.0	0.000	0.748
3	-3.73	0.0	1.00	0.8480	100.310	38.87	0.0	0.000	0.0	0.000	0.745
4	-3.14	0.0	1.00	0.8480	100.499	38.81	0.0	0.000	0.0	0.000	0.748
5	-2.55	0.0	1.00	0.8480	100.688	38.75	0.0	0.000	0.0	0.000	0.837
6	-1.95	0.0	1.00	0.8480	100.878	38.68	0.0	0.000	0.0	0.000	1.121
7	-1.34	0.0	1.00	0.8480	101.084	38.62	0.0	0.000	0.0	0.000	1.223
8	-0.80	0.0	1.00	0.8480	101.280	38.56	0.0	0.000	0.0	0.000	8.853
9	0.17	0.00	0.08	0.8387	101.440	38.50	0.0	0.000	0.000	0.000	0.259
10	0.82	0.0	0.0	0.8580	101.630	38.43	0.0	0.000	0.0	0.000	0.000
11	1.47	0.0	0.0	0.8580	101.820	38.37	0.0	0.000	0.0	0.000	0.000
								0.000	0.000	0.000	11.587

SAP TIME= 130.000 HRS, ORTHO-THERMO PROPS, IN 2D, TEST C-10 V

ELE	TAVG C	%CH	%PR	GRADT C/CM	STRPRP KPA	SP *E-6	VEL -6MM/S	DDZS MM	DDZIS MM	DZINC MM	DZ MM
1	-4.86	0.0	1.00	0.8479	100.002	38.87	0.0	0.000	0.0	0.000	0.055
2	-4.32	0.0	1.00	0.8480	100.121	38.83	0.0	0.000	0.0	0.000	0.748
3	-3.73	0.0	1.00	0.8480	100.310	38.87	0.0	0.000	0.0	0.000	0.745
4	-3.14	0.0	1.00	0.8480	100.499	38.81	0.0	0.000	0.0	0.000	0.748
5	-2.55	0.0	1.00	0.8480	100.688	38.75	0.0	0.000	0.0	0.000	0.837
6	-1.95	0.0	1.00	0.8480	100.878	38.68	0.0	0.000	0.0	0.000	1.121
7	-1.34	0.0	1.00	0.8480	101.084	38.62	0.0	0.000	0.0	0.000	1.223
8	-0.80	0.0	1.00	0.8480	101.280	38.56	0.0	0.000	0.0	0.000	8.853
9	0.17	0.00	0.08	0.8387	101.440	38.50	0.0	0.000	0.000	0.000	0.259
10	0.82	0.0	0.0	0.8580	101.630	38.43	0.0	0.000	0.0	0.000	0.000
11	1.47	0.0	0.0	0.8580	101.820	38.37	0.0	0.000	0.0	0.000	0.000
								0.000	0.000	0.000	11.588

.... (ABRIDGED) ....

SAP TIME= 400.000 HRS, ORTHO-THERMO PROPS, IN 2D, TEST C-10 V

ELE	TAVG C	%CH	%PR	GRADT C/CM	STRPRP KPA	SP *E-6	VEL -6MM/S	DDZS MM	DDZIS MM	DZINC MM	DZ MM
1	-4.86	0.0	1.00	0.8479	100.002	38.87	0.0	0.000	0.0	0.000	0.055
2	-4.32	0.0	1.00	0.8480	100.121	38.83	0.0	0.000	0.0	0.000	0.748
3	-3.73	0.0	1.00	0.8480	100.310	38.87	0.0	0.000	0.0	0.000	0.745
4	-3.14	0.0	1.00	0.8480	100.499	38.81	0.0	0.000	0.0	0.000	0.748
5	-2.55	0.0	1.00	0.8480	100.688	38.75	0.0	0.000	0.0	0.000	0.837
6	-1.95	0.0	1.00	0.8480	100.878	38.68	0.0	0.000	0.0	0.000	1.121
7	-1.34	0.0	1.00	0.8480	101.084	38.62	0.0	0.000	0.0	0.000	1.223
8	-0.80	0.0	1.00	0.8480	101.280	38.56	0.0	0.000	0.0	0.000	8.853
9	0.17	0.0	0.08	0.8387	101.440	38.50	0.0	0.000	0.0	0.000	0.259
10	0.82	0.0	0.0	0.8581	101.630	38.43	0.0	0.000	0.0	0.000	0.000
11	1.47	0.0	0.0	0.8581	101.820	38.37	0.0	0.000	0.0	0.000	0.000
								0.000	0.0	0.000	11.588

Appendice J: Experience with *ADINAT*

The *ADINAT 81* finite element program used in this analysis was a powerful general purpose program that allowed a flexible approach to solving problems. Unfortunately the program also had peculiarities that were not immediately obvious to informed users. The problems that arose were traced back to errors in the program or to under emphasized conditions stated within the user manual or its reference.

Problems arising out of this analysis were necessarily examined and their causes identified. This appendice, then, is a brief compilation of these findings. The evidence and conclusions presented may be specific to this analysis and may not be directly applicable to other problems, however the general behaviour of the *ADINAT* program can be discerned.

J.1 Comparison of ADINAT with Closed Form Methods

As with all numerical procedures, it is prudent to compare the numerical results with known closed-form solutions. While a close fit with the exact solution does not ensure similitude for all cases, it does provide a benchwork for comparision and extrapolation. Conversely, a poor fit with the closed form should alert the user to programming, numerical or data entry errors. The importance of performing these closed-form comparisons cannot be over-emphasized.

The initial mesh for test *NS-1* was used for the simulation of frost penetration into a semi-infinite medium. While the mesh was of finite length *(104mm)* this would have no effect for the early stages of frost progression. Under similar conditions, Gupta (1971) found close agreement with the semi-infinite closed form up to a frost penetratiton of *75%*.

Eight rectangular elements comprised the mesh. Each element had four nodes. Element widths were identical but the element heights were arbitrarily increased with depth (Figure 5.2). This was done in order to more finely discretize the mesh near the surface in order to trace the rapid frost front penetration at the onset of freezing.

The results were less than satisfactory. When compared with the Neumann or Stefan solution (Figure J.1) for this material, it was found that the frost front did not advance as smoothly. This was not unexpected, given the implicit approximations of a numerical analysis, however the deviation from the closed form was concentrated at the boundaries between elements. (Figure J.2). This was because

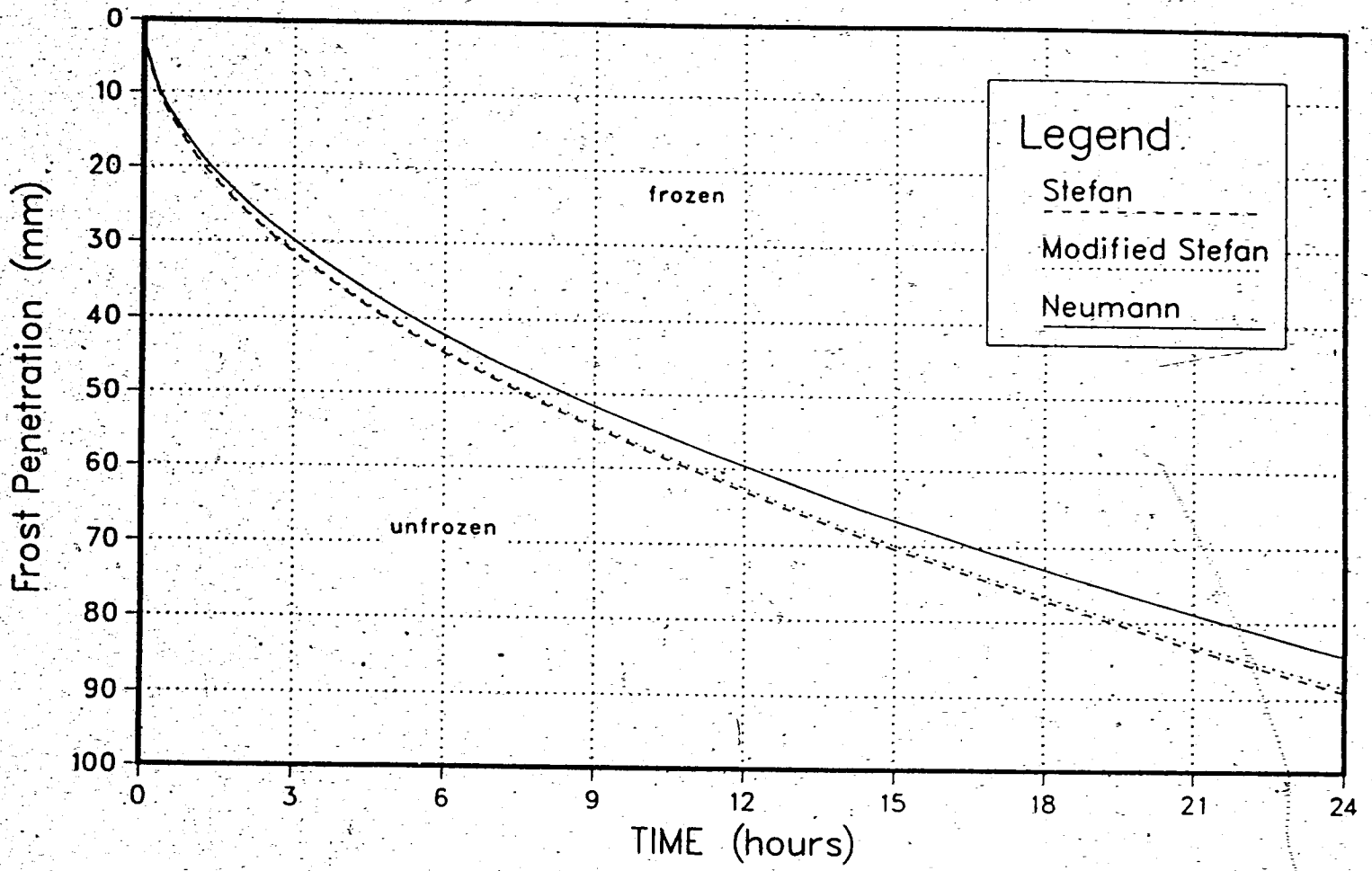

Closed Form Solutions for Frost Front Advance in a Semi-Infinite Medium

Figure J.1

FROST FRONT PROGRESSION

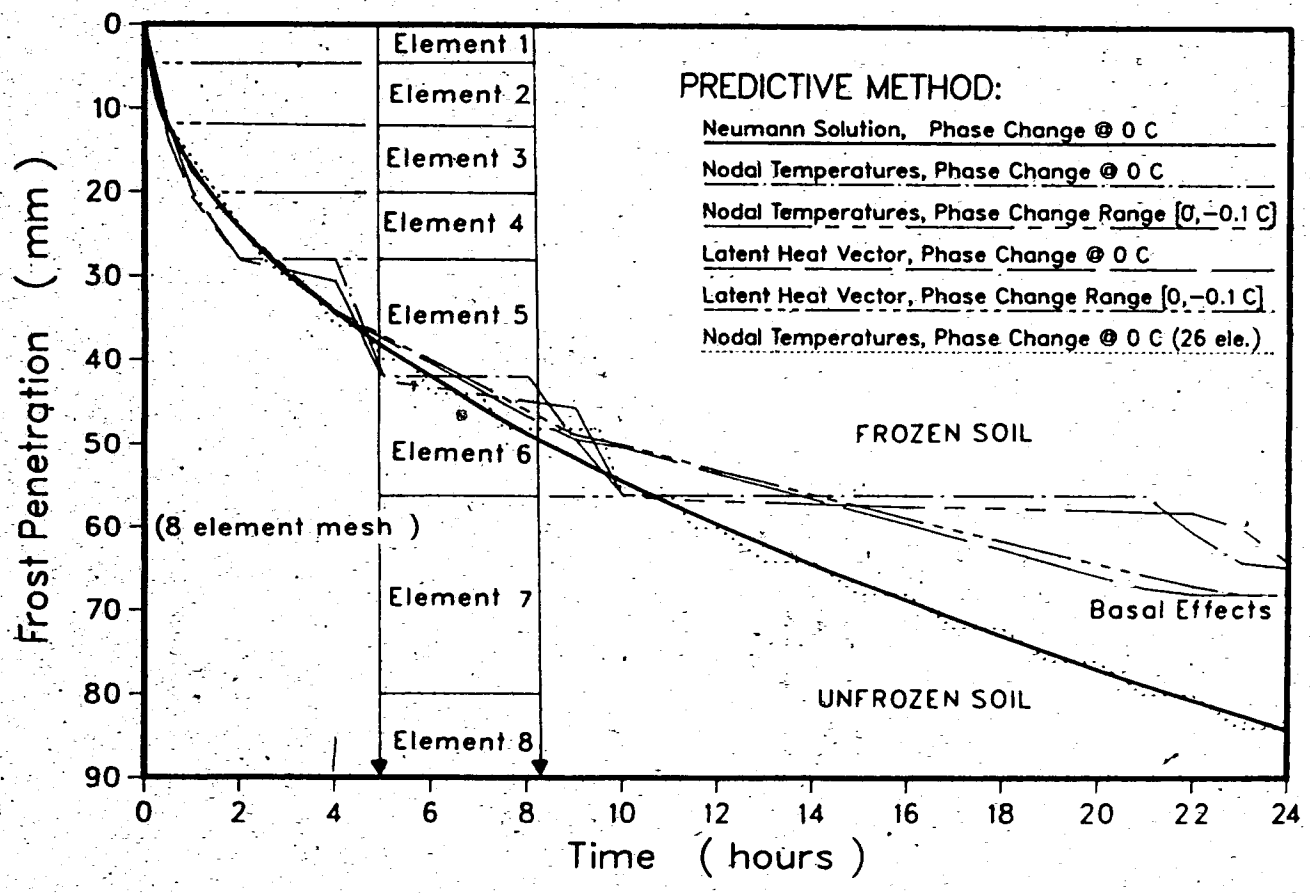

Figure J.2 Comparison of ADINAT Results with the Neumann Solution

both the specific heat capacity and the latent heat were lumped at the nodes, resulting in a concentrated latent heat source at each node. When this source was exhausted, the frost front rapidly advanced until the next set of nodes was encountered, resulting in a step-wise frost front advance. To smoothen this curve, a melting temperature range of [-0.1°C, 0.0°C] was used instead of the discrete melting temperature of 0.0°C. Marginal improvements were obtained, in that the frost front advanced slightly during freezing as it passed through a pair of nodes.

The previous two frost front progressions represent interpolations between nodal temperatures to obtain the depth of freezing. The lumped latent heats were blamed for the distortion from the closed form, and as a check on this, the frost front advance was calculated based on latent heat. This was done by summing the latent heat released during the analysis at any given time and dividing by the volumetric latent heat to obtain the volume of frozen material at that time. The plotted results provide a smooth progression of frost into the soil. The curve for the latent heat range analysis slightly underpredicts the advance because it is of the range's midpoint isotherm (-0.05°C) rather than the 0°C isotherm.

The deviation of the frost front from the closed form was greatest at the nodal points and increased with depth. This increase was due to the lumping procedure, in which the latent heat capacity of an element is distributed to its nodes. As the element size increased with depth, the amount of latent heat lumped at the nodes also increased, resulting in prolonged freezing at deeper nodes. This disparate distribution of latent heat resulted in a discontinuous progression of the frozen thermal gradient with time. As a direct result of this, any application of *SP* theory would result in rapidly changing values of incremental heave. This was objectionable because it departed from observed behaviour and could introduce unrealistically high freezing stresses in a restrained soil.

As the analysis was inextricabaly dependent upon the latent heat effects, a more homogeneous dispersion of latent heat throughout the mesh would result in improved performance. A new mesh was designed for test *NS-1* in which 26 elements, each 4mm in height, were stacked into a column. Although this resulted in a high aspect ratio (length *vs.* width) the heat flow was vertical which eliminated any numerical difficulties arising from extreme geometries of the elements.

For the simulation of the progressing frost front, the bottom element was grossly elongated to remove the effect of the warm basal platen from the analysis. The resultant frost front progression (Figure J.2) shows a highly controlled,

even advance of the 0° isotherm, straddling the Neumann solution. With this excellent corroboration of the closed-form, the simulation of test *NS-1* was continued, using the revised mesh.

J.2 Mesh Optimization

Before the simulations of the frost heave tests were begun, the behavior of the finite elements was looked at to optimize the solution characteristics of the finite element approach. The *ADINAT* program offer a convenient mean of varying the number of nodes and level of Gaussian integration of the elements to study the sensitivity of the analysis to these parameters.

The 26-element mesh for test *NS-1* was used as the test mesh. Since the problem was one of longitudinal heat flow it was essentially a one-dimensional problem examined in two dimensions. This greatly simplified the hand calculation checks on the numerical solution. The mesh itself consisted of 26 4-node elements at an initial temperature of +1.0°C. For the 6-node elements, pairs of 4-node elements were combined by eliminating the common side. This reduced the number of elements from 26 to 13. Alternatively, for the 8-node elements the 4-node elements were supplemented by adding mid-size nodes. This increased the number of nodes from 54 to 133. At the start of the analysis, a special nodal temperature of -3.4°C was applied at the top of the column of elements and +1.1°C was applied at the base. The transient analysis was stopped after one time step of 360 seconds.

For comparison, the 4-, 6-, and 8-node element meshes were solved using 2×2 and 3×3 Gaussian integration, for a total of 6 analyses. The number of equilibrium iterations was used as a measure of effectiveness since the iterations were responsible for most of the computational costs, with the other costs being fairly insensitive to the particular mesh being used. The analyses were run with an arbitrary convergence tolerance of RTOL=10^{-5} (Table J.1).

The 4-node 2×2 analysis produced acceptable results, with a distinct phase change front at the pair of nodes next to the surface. The 6-node 2×2 and 3×3 analyses also produced good results and used far fewer iterations. This was expected as fewer, more complex, elements generally behave better than more numbers simple elements (Zienkiewicz, 1977). The 6-node element mesh advanced the frost front by 8 mm, compared to 4 mm for the 4-node mesh. This is a function of the lumping of the latent heat and the nearby boundary condition. The difference would be minimal in the longer term.

Table J.1

ADINAT OPTIMIZATION RESULTS

($RTOL = 10^{-5}$)

Number of Nodes per Element	Gaussian Integration	Number of Equilibrium Iterations	Phase Change Front
4 (Mesh A)	2 x 2	150	good
	3 x 3	40	smeared
6 (Mesh B)	2 x 2	91	good
	3 x 3	96	good
8 (Mesh C)	2 x 2	169	smeared
	3 x 3	180	smeared

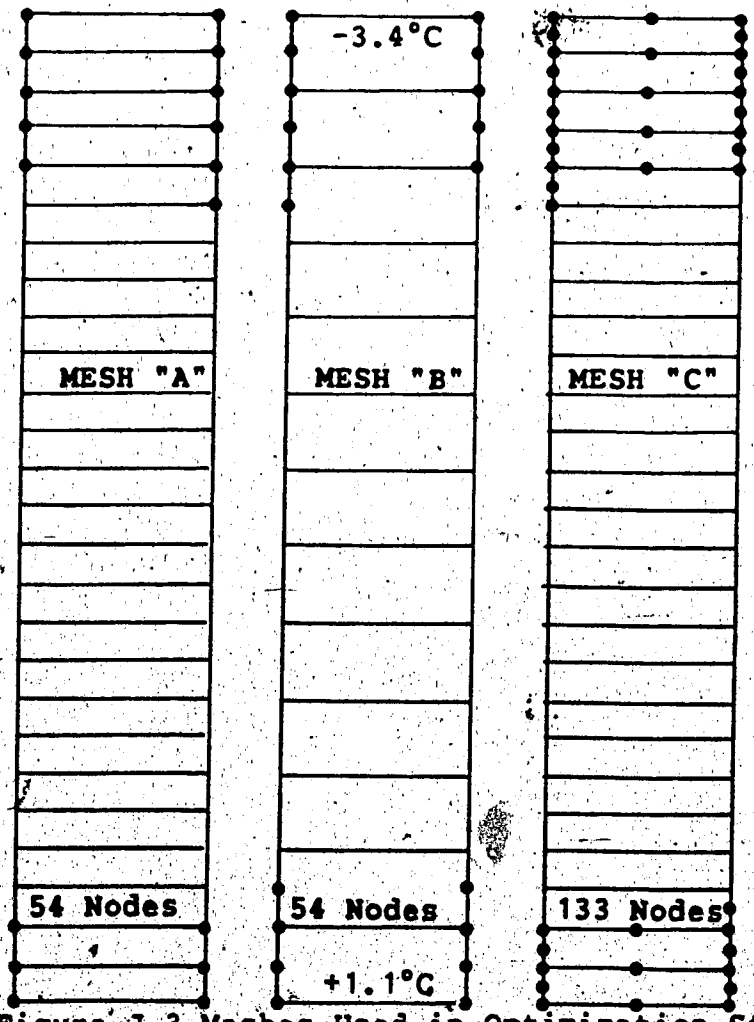

Figure J.3 Meshes Used in Optimization Study

The results of the three other tests were unacceptable as they produced a smearing of the phase change front over the second element from the applied cold source. This occurs when several nodes, at different distances from the cold source, are at the phase change temperature but at different degrees of phase conversion. These analyses are unacceptable for adaptation to Konrad's theory of frost heaving because the numerically-determined thermal gradients within these elements are zero.

The results of these analyses are instructive in ~~that~~ they demonstrate the deviation of mesh performance from the expected performance. In changing from 2×2 to 3×3 Gaussian integration, an improvement in the convergence performance was expected. This was not the case, with the exception of the 4-node elements results which are disregarded due to the phase smearing. The use of higher levels of Gaussian integration in a purely conductive heat flow problem is still expected to improve performance but in this instance the latent heat component was the overriding feature of the problem.

The 8-node element mesh converged with unacceptable results due to phase smearing. This mesh is identical to the 4-node mesh except for the additional mid-side nodes which would define the temperature regime more precisely and further refine the latent heat discretization. The more precise result was expected, although at a higher cost due to the larger number of nodes, yet this was not the case. Since the Gaussian conductivities and the spatial distribution of latent heat would be roughly the same in the 4-node and 8-node case, it was reasoned that the 8-node analysis failed to converge to acceptable results simply because the higher number of nodes resulted in a larger Euclidean norm of the temperature vector (Equation J.1). Assuming miniscule changes in the temperatures between iterations, the convergence criterion would be met simply because of the larger number of nodes. To test this hypothesis, the convergence tolerance RTOL could have been tightened by an amount equal to the increase in the Euclidean norm but this was not done as it was incidental to the purpose of these analyses.

The 6-node element mesh produced the best results by far. The single difficulty with elements of this type was that an analogous element with desirable material properties was unavailable in the *SAP IV* stress-displacement finite element program. Moreover, the modification of the directional coefficients of thermal expansion for the larger 6-node elements would result in a smoothening of the heave-dependent incremental pressure effect at the frost front.

On the basis of these results, the Konrad simulation was developed for 4-node quadrilateral elements. At this stage of the program development, however, the significant effect of stipulating a boundary temperature of a different phase than the initial temperature was not known. This would affect the comparison of the 4-, 6-, and 8-node elements bacause the nodal lumping of latent heat and heat capacity would differ. The study of the variation in convergence characteristics with an increased level of Gaussian integration would be unaffected.

J.3 The Choice of Units Affects Convergence

The convergence characteristics of *ADINAT* are significantly affected by the choice of temperature units.

In a permafrost analysis most temperatures are clustered around the solid/liquid phase change temperature. In the Celsius, Kelvin, Fahrenheit and Rankine scales this is at 0°C, 273.15 K, 32°F and 491.67 R respectively (omitting secondary effects). Ideally, identical finite element results would be expected regardless of the choice of units, however, a close examination of the convergence criterion reveals an easier convergence compliance when the magnitude of the temperatures are larger:

Convergence declared iff:

$$\frac{\| {}^{t+\Delta t}\underline{\theta}^{(i-1)} - {}^{t+\Delta t}\underline{\theta}^{(i)} \|_2}{\| {}^{t}\underline{\theta} \|_2} \leq \text{RTOL} \qquad [J.1]$$

where "$\| \quad \|_2$" represents the Euclidean norm of the enclosed vector (Bathe, 1982).

∴ If $\underline{\theta}$ is in degrees Kelvin, $\underline{\theta} = \theta + \underline{K}$, where $\underline{K}=\{273.15\}$ then

$$\frac{\| ({}^{t+\Delta t}\underline{\theta}^{(i-1)} + \underline{K}) - ({}^{t+\Delta t}\underline{\theta}^{i} + \underline{K}) \|_2}{\| {}^{t}\underline{\theta} + \underline{K} \|_2} \leq \text{RTOL} \qquad [J.2]$$

$$\frac{\| {}^{t+\Delta t}\underline{\theta}^{(i-1)} - {}^{t+\Delta t}\underline{\theta}^{(i)} \|_2}{\| {}^{t}\underline{\theta} + \underline{K} \|_2} \leq \text{RTOL} \qquad [J.3]$$

$$\text{but } \| {}^{t}\underline{\theta} + \underline{K} \|_2 = \sqrt{({}^{t}\underline{\theta})^2 + 2({}^{t}\underline{\theta}\,\underline{K}) + \underline{K}^2} \qquad [J.4]$$

$$>> \| {}^{t}\underline{\theta} \|_2$$

For a temperature vector of $\underline{\theta} \cong \{ 5°C \} = \{ 278.15 \text{ K} \}$
∴ the denominator is, in Celcius $\| {}^{t}\underline{5} \|_2 = 5\sqrt{n}$

in Kelvin $\| {}^{t}\underline{5} + \underline{273.15} \|_2 = 278.15\sqrt{n}$

where "*n*" is the number of nodes in the mesh. This gives a

ratio of denominators of:

$$\frac{\text{Kelvin}}{\text{Celsius}} = 56$$

Note that the magnitude of the denominator is loosely a function of the square root of the number of nodes, $\sqrt{n}$. If the magnitude of the nodal temperature differences between iterations is roughly constant, the numerator is also roughly a function of $\sqrt{n}$, and the size of the mesh has no bearing on convergence. However, where the temperature changes are largely limited to a small percentage of the nodes, which is particularly the situation when the latent heat option is used, the convergence performance of the problem will be different. In such a case, the numerator is a function of a number smaller than $\sqrt{n}$. Convergence will then become a function of the mesh size and refinement, with larger meshes allowing faster convergence for a given tolerance without a comparable increase in the precision of temperatures.

Latent heat is affected by the convergence tolerance because the latent heat vector can vary significantly with no accompanying change in the nodal temperature vector, which is the sole measure of convergence. By imposing a tight convergence tolerance on the program, *ADINAT 81* is constrained so it iterates, resetting the specified nodal temperatures within each iteration, thus providing a heat source or sink for the latent heat from the specific heat vector. Figure J.4 shows the effect of varying the convergence tolerance on the amount of latent heat introduced into the affected nodes.

J.4 *ADINAT* and Phase Change

A problem developed during the simulation of test *NS-1*: the mesh was cooling too rapidly, allowing the freezing front to advance to the steady state position prematurely. The cause of the problem was not obvious, but it appeared to be linked to the phase specification for nodes at the phase change temperature. This specification meant that all nodes at this temperature, "TREF", were to be of one phase (in this case, frozen).

The solution appeared to be to use a temperature interval for the phase change, as opposed to a pure-substance phase change at a single temperature. This would uniquely define the extent of nodal freezing as an initial condition of each run by specifying nodal temperatures existing within the transition temperature range.

Convergence Rate vs. Latent Heat

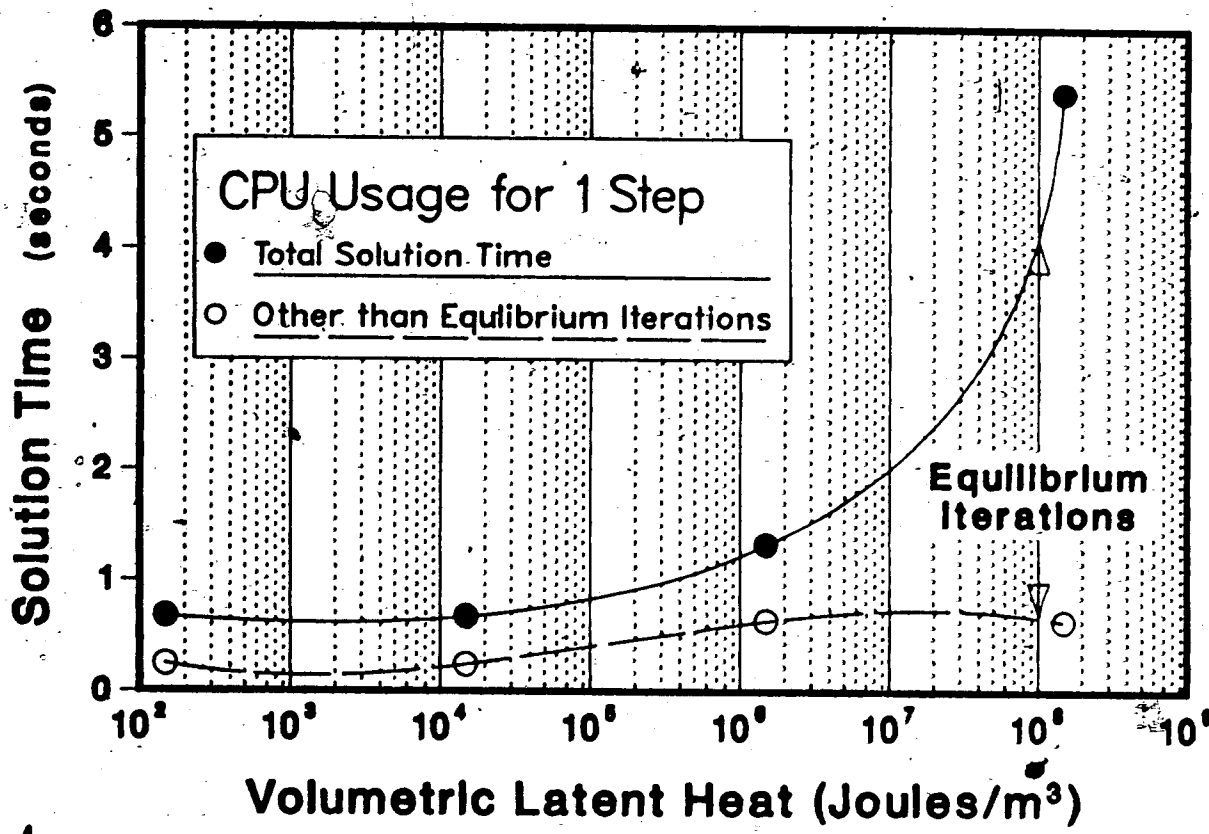

Figure J.4

A series of computer simulations were run to pinpoint the proper approach to restarting the ADINAT problem using output temperatures form the previous run as input for the subsequent run. (The *ADINAT* restart facility was not used since nodal co-ordinates would have to be continually modified to account for heaving distortion.)

As a measure, the Neumann solution was simulated using multiple time steps within one *ADINAT* run. This model, Case "A", consisted of a semi-infinite column with a pure-substance phase change at -0.1°C, simulated for 1 hour in five time steps of 0.2 hours. Case "B" was a complete simulation of test *NS-1* for 5.5 hours using 25 time steps of increasing size. Although this test was of a column 10.4 cm high with a basal temperature of +1.1°C, the Neumann solution was a good control for the initial stages of freezing when the lower boundary effects does not affect the thermal regime of the elements undergoing phase change. The phase change began at -0.100001°C and ended at -0.100000°C, for a transition temperature interval of 10^{-6}°C. The transcription of nodal temperatures from the results of one loop to the initial conditions of the next were accurate to 10^{-8} °C, with no allowance made for truncation. This would make the initial conditions of the latent heat at the nodes accurate to within 1% of the latent heat released at that node as calculated by the previous run.

At the end of the 5.5 hour simulation, it was obvious that latent heat was being lost at the nodes between runs.

Case "C" took an intermediate result of Case B at time *t=0.3 hr* and ran the thermal analysis for 1 second. A simple heat flow calculation predicted a latent heat change of 16 Joules while the computer simulation produced an answer of 2600 J . Even after allowing for minor changes in nodal locations due to heaving, updated thermal conductivities and specific heats, the simulation grossly overpredicted the thermal balance when temperatures within the phase change interval were used as initial conditions. In contrast, similar hand calculations of heat flow showed good agreement with *ADINAT* results obtained using multiple time steps which produced intermediate results.

Case "D" was another simulation of test *NS-1*, but using a transition temperature interval of 10^{-4}°C. With an accuracy of 10^{-8}°C in the temperature information, the latent heat should have been accurate to 0.01%. This simulation was run for 0.5 hours using 5 uniform time steps. Again, the frost front prematurely penetrated the soil due to a lack of continuity of nodal latent heats between runs.

Case "E" repeated the Case B simulation of frost penetration of test *NS-1* but used 3×3 Gaussian integration instead of 2×2 integration. No significant improvement in

performance was found.

Case "F" repeated the Neumann solution of Case A for 1 hour but used a phase transition temperature interval of 10^{-6}°C. The excellent correlation with the Neumann solution of a pure substance, combined with the poor results of Case D showed that the source of error lay in the inability of *ADINAT* to correctly accept an initial nodal temperature within the phase transition temperature interval. Case "G" began from Case F at *t=0.4hr*, with poor correlation with the results of "F", thus confirming this finding. The next approach was to somehow implement the nodal latent heat vector into the input for the next *ADINAT* run. This should only have been necessary for the nodes undergoing phase change as all other nodes are implicitly defined as either solid or liquid.

Case "H" was a successful attempt at restarting Case F using nodal temperatures at the phase change. The material was redefined as a pure substance, with a phase change at -0.1°C. At the end of 0.4 hours, the nodal temperature and the latent heats at the nodes were compared, and any node at the phase change had its latent heat input into the next run as a concentrated heat flow. This was done by setting the default phase at the phase change temperature to "liquid" for the next run, and dividing the latent heat previously absorbed at those nodes by the time increment for the next step. This value was then applied as a negative concentrated heat flow, thereby restoring the affected nodes to their respective degrees of phase change. Excellent correlation with the continuous case was found. The "TRANS" program was altered to incorporate this calculation into its preparation of the pending *ADINAT* input file. Researchers using a range of temperatures for the phase change should be aware of *ADINAT*'s idiosyncracy in this regard.

J.5 The Effect of Timestep Size on Convergence Characteristics

Another problem presented itself during the running of *ADINAT* within the iterating command structure of file "LOOP".

As the solution progressed from the simulation of T=120 hours to T=168 hours, the input file for *ADINAT* at time T=168 hours was automatically prepared by program "TRANS" implementing the time increment as specified by file "2". When this input was run on ADINAT with a local time estimate of 20 seconds, the limit was exceeded even though the previous *ADINAT* run used less than 5 seconds of CPU time. Unfortunately, with this type of program abort, the MTS operating system fails to generate a positive return code, so the test for a greater than zero return code passes.

The next check on *ADINAT*'S success comes within program ARRETE. This program was designed to prevent further computations if the *ADINAT* program failed to converge or if the user's computer account fell below an explicit amount. Without such safeguards the command file would continue with the calculations until another program failed, due to the lack of a solution from the ADINA output, or all computer funds were exhausted causing a loss of all temporary files. What ARRETE was not explicitly designed for was an end-of-file on *ADINAT's* output, as was the case. Instead, the ARRETE program was allowed to fail, thereby generating a non-positive return code for it, which would be detected by the system test. This resulted in a bomb from the command iterations with a controlled salvaging of all pertinent files for documentation and subsequent restarting of the run.

The *ADINAT* problem was examined to determine the cause of the high CPU usage in order to prevent further occurrances of program abort. The program had been allowed 800 iterations to achieve a convergence tolerance of RTOL=10^{-4}, with a local time limit of 20 seconds. The same data file was re-run with a local limit of 100 seconds in order to force a solution to provide some information for analysis. After a normal completion of *ADINAT*, the program failed to converge after 91.2 seconds and 800 iterations. Increasing the allowable number of iterations was not a viable solution, given the exorbitant number already allowed, the high CPU usage associated with a large number of iterations and the lack of any output from *ADINAT* that would indicate how the soution was converging, if at all.

The alternate approach was to increase the convergence tolerance to RTOL=10^{-3} and re-run the problem. The program converged and provided a solution after only 14 equilibrium iterations and 2.65 seconds (1.60 seconds of which was for iterating). However, on closer examination the solution was found to be imprecise with a smearing of the phase change over the first and second nodes away from the pipeline in the freezing region below the pipeline. As there nodes enclose elements 1 through 4, the gradients in these elements were zero, rendering the thermal solution useless for an application of Konrad's frost heave theory.

Obviously a method was required that would result in a precise definition of the frost front without using copious amounts of CPU time. The previous two runs and the formulation for the implementation of latent heat in *ADINAT* were examined. It because obvious that the numerical difficulty was caused by the program's back-correcting for latent heat (Rolphe and Bathe, 1982) without being able to restrict the phase change to the nodes next to the old freezing front, within the given constraints. It was reasoned that by restricting the conductive advance of heat

at the beginning of each time step, the number of nodes requiring latent heat correction would be reduced, thereby simplifying the problem. This was tested by again re-running the problem with the tighter tolerance of RTOL=10^{-4} but breaking the analysis down into 10 time steps of one-tenth the original time increment of 675000 seconds.

The results were a significant improvement over the two previous attempts. The nodes at phase change at the onset of the solution remained there for 5 time steps, after which the frost front advanced through the elements establishing the phase change temperature at a new set of nodes. The frost front advance was so gradual that the number of nodes at the phase change fluctuated as the freezing isotherm progressed between adjacent frozen and unfrozen nodes. The analysis required up to 14 equilibrium iterations for each time step for a total of 127. The total solution required 19.46 seconds of CPU time.

A numerically efficient solution would optimize the CPU usage by adjusting the number of time steps to minimize the total number of equilibrium iterations, since these are responsible for most of the computing cost. This could be done by roughly calculating the maximum time step allowable to advance the phase change isotherm up to but not including, the next group of unfrozen nodes before latent heat was correlated for. This would maximize the amount of heat capacity available for conversion to latent heat at each phase change node. A savings in the number of iterations and time stops would be realized.

An efficient system is not necessarily effective. The calculations necessary for optimizing the *ADINAT* solution one, in themselves, tedious and not easiliy implemented in a self-regulating command system. The alternative is to pre-set a realistically sufficient local time limit or number of iterations for the *ADINAT* problem and a method for arbitrarily increasing the number of time steps should the program fail to converge or require excessive compatatioal time.

A modified ARRETE program provided such an opportunity to examine ADINAT'S results and, if necessary, re-run the program using time steps. A flag was also generated to by pass abridging of the results by program ABRAT, and the machine language temparature output, file 56, was reduced to its initial and final temperatures to make it compatible with ancillary programs. The need for breaking the problem into steps was only anticipated to be required at the onset of a heave analysis because of the high heat flux gradients and close nodal spacing around the frost front. The alternative solution would be to further discretize the driving time file, (file "2"), so that the whole heave analysis would be done using smaller time steps. While some

more thermal precision would result, the present heave analysis is designed to simulate the heave behaviour as the analysis approaches steady state, where most of the heaving will occur. Any refinements in the thermal analysis during the early stages of heaving would be non-productive without commensurate refinement in the application of Konrad's concept of segregation potential and in the numerical approximations used throughout the analysis.

J.6 The Initialization of Temperatures for N.E.S. Simulation

The initial temperatures for the *ADINAT* simulation are the output temperatures at the soil surface and the interior of the pipeline. Rather than correct for partially frozen nodes, all nodes initially at the phase change temperature were set to -0.10001°C, thereby predetermining them to be frozen. This accelerated the advance of the frost front for the beginning of the analysis however this does not greatly affect the long-term thermal balance between the applied surface temperatures and the soil, nor does it control the behaviour in the area of interest around the pipeline.

One idiosyncracy of the *ADINAT* program is its inability to accept a specified nodal temperature in which the node in question is to bypass the phase change temperature. Those nodes initially above freezing but specified to be below freezing were hung up at the phase change temperature. Decreasing the program's convergence tolerance from a tight 10^{-4} to 10^{-5} and then to 10^{-7} effectively changed nothing.

Within *ADINAT*, the program accounts for temperature boundary conditions by doing two things (viz. *ADINAT* manual pg. A.21, Bathe 1981b). First, a specified zero temperature at a node is implemented by ignoring that nodes' heat flow equilibrium equation. Secondly, non-zero temperatures are implemented in the program by adding a high thermal conductivity associated with that node to the heat flow equilibrium equations, as specified by the convection boundary option by the program.

Latent heat is introduced into the program as a latent heat flow vector using the enthalpy of the system (Rolphe & Bathe, 1982). This requires the volumetric latent heat of the material, the contributing area associated with a node and the phase change temperature or temperature range. Using a vector that accumulates the net nodal latent heats, the latent heat flow vector is constructed by dividing the available nodal latent heat vector by the time step, Δt.

At the beginning of a time step, the heat flow due to phase change is assumed to be zero. If the temperature at a node transgresses the phase change temperature in an iteration, the nodal temperature is brought back to the

phase change temperature. The commensurate change in the node's heat capacity flow is expressed as change in the latent heat flow, until the latent heat capacity of the node is exhausted or the convergence criterion is met. Because of this, when a specified cold temperature is assigned to an existing warm node, the program iterates. It is accepting the initial temperatures, imposing the specified non-zero nodal temperatures by adding to the heat flow equilibrium equations, then back-correcting those same specified nodal temperatures for latent heat.

The effect of specifying a nodal temperature that should result in a phase change can be seen in Figures J.5 and J.6. The former shows the effect of tightening the convergence tolerance on the number of equilibrium iterations required for a solution. The strong correlation between the number of iterations and the degree to which the node had changed phase is a physical expression of *ADINAT's* algorithm for latent heat. Figure J.6 presents a set of temperature profiles through the soil showing their monthly fluctuation within the trumpet curve. The numerical error, shown as a 4°C underprediction of surface temperature, would result in a marginal reduction in cooling for that time step.

Fortunately, this error was not seen at depth due to the thermal inertia of using a lumped analysis. Equally re-assuring was the identical mapping of tautochrones from three consecutive years, as this indicated that no cummulative error was being accrued.

The effect of tightening the convergence tolerance on the number of equilibrium iterations necessary for convergence over a number of time steps is shown in Figure J.7. The number of iterations required for convergence was plotted against the respective time step for the analysis of the initialization of ground temperatures in response to a seasonally varying applied temperature loading at the surface. The *ADINAT* program simulated the temperature distributions from the 15th through the 18th years. The ground temperatures were cyclic by the 15th year, and the three year analysis, conducted in 36 monthly time steps, provided a manageable output of freeze/thaw cycles.

The analysis was run twice using RTOLs of 10^{-3} and 10^{-4}. Some important observations can be made in comparing the two curves in Figure J.7. The most obvious observation is that it takes more iterations to reach convergence with a tighter tolerance. Secondly, the two curves vary over time in a similar manner, which is expected because the data files are identical except for the convergence tolerances. Thirdly, the iteration curve for the looser tolerance is attenuated with fewer abrupt changes in the number of iterations. This is reasonable, given the gradual change in the applied

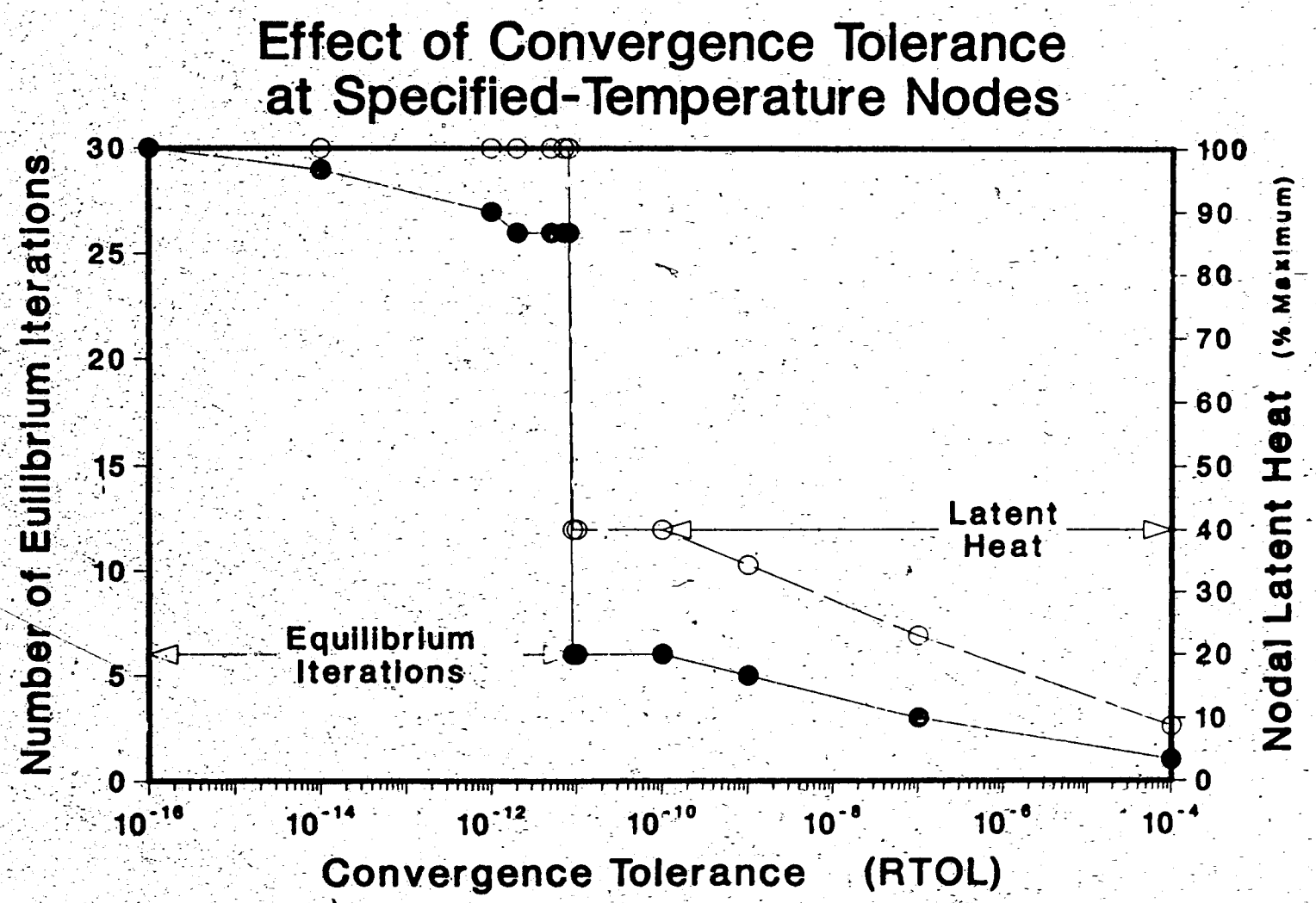

Figure J.5 Effect of Convergence Tolerance at Specified-Temperature Nodes

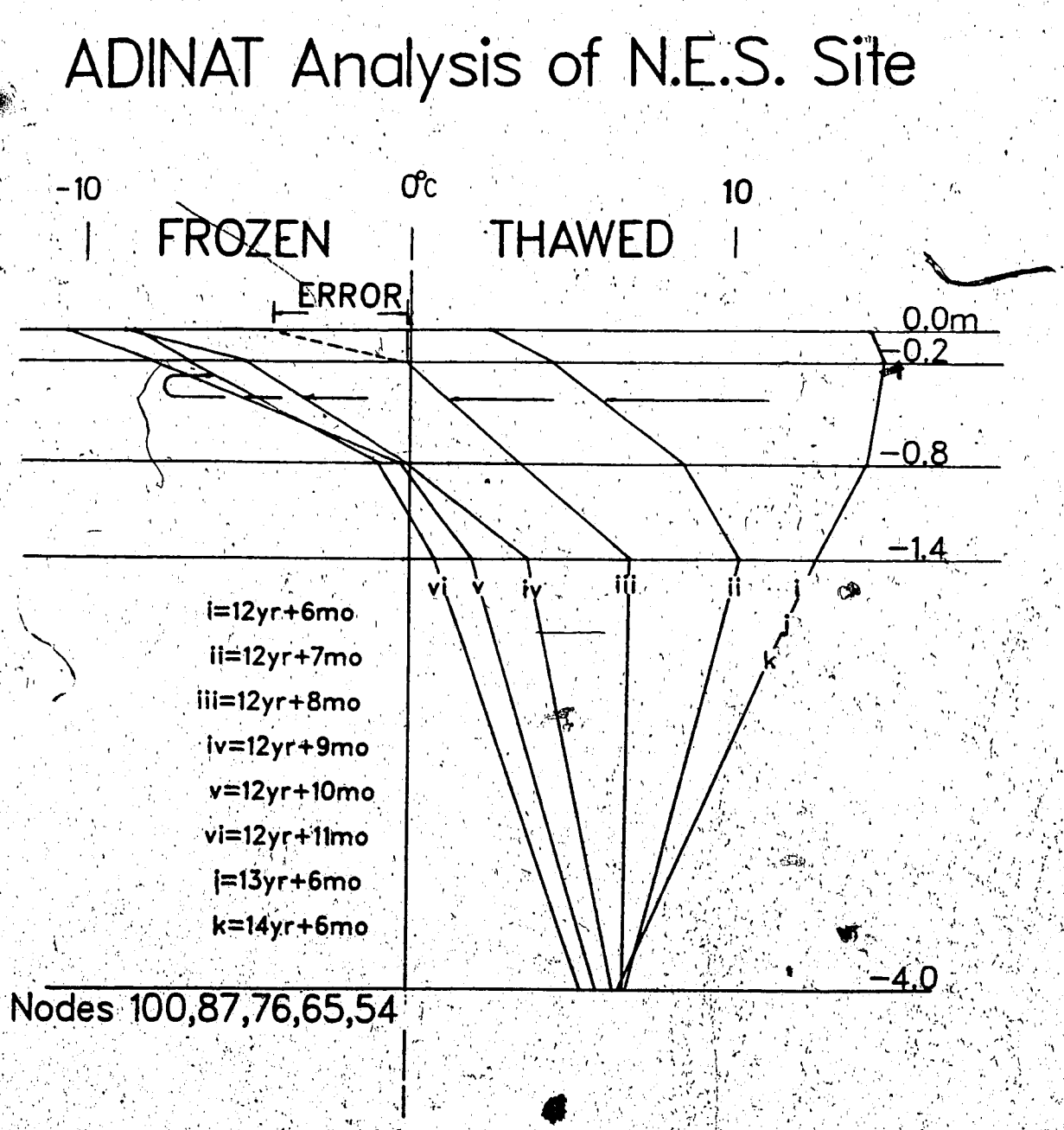

Figure J.6 Monthly Fluctuation of Temperature Profiles

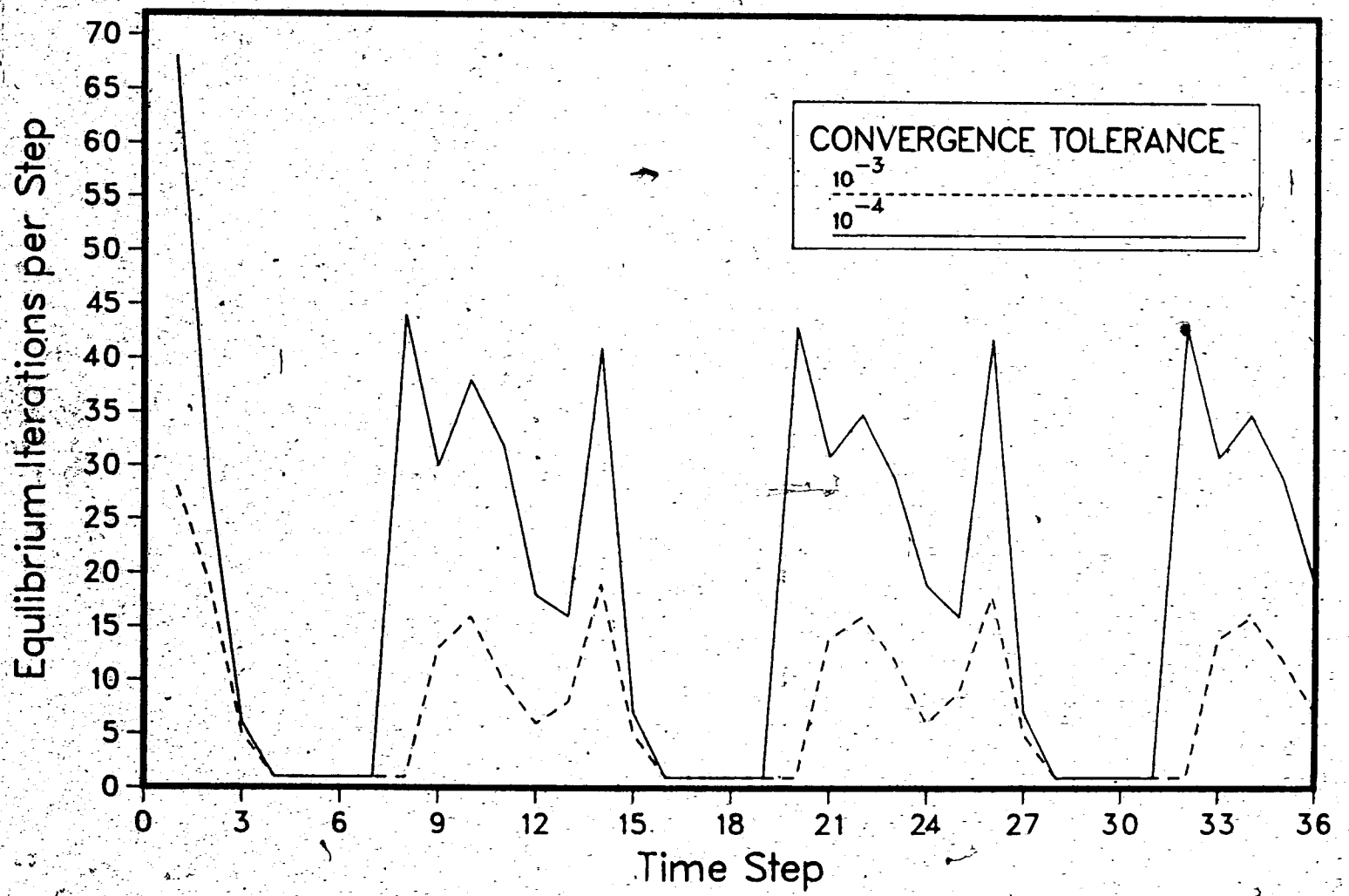

Figure J.7 Equilibrium Iterations for Solution

temperature loading. Fourthly, the iterations required for convergence in the first time step are significantly higher than for any other time step. This is due to the initialization of nodal temperatures using the temperature output of a previous run from 12 to 15 years, in which some of the nodes are at the phase change. In using the output temperatures as input, without specifying heat loadings to the nodes undergoing phase change, the previous latent heat vector is essentially lost and replaced, in this case, with a vector in which all phase-change nodes are totally thawed. This perturbs the transient heat flux for the first few time steps, requiring more iterations for convergence.

The last, and the key observation, is that as the program begins to apply freezing temperatures to the surface to simulate the onset of winter, the two analyses differ markedly. During the eighth step with an RTOL of 10^{-4} the specified nodal temperatures progressed from +2.397°C to -4.114°C as expected, but requiring 44 equilibrium iterations to do so. For the looser tolerance of 10^{-3}, only 1 iteration was required, however, the "specified nodal temperature" at the surface remained at the phase change temperature, -0.1°C. Only in the next time step do the specified nodal temperatures follow the applied temperature loading curve.

Fortunately, this error was not seen at depth due to the thermal inertia of a lumped analysis. Equallly re-assuring was the identical mapping of tautochrones from three consecutive years, as this indicated that no cummulative error was being accrued.

This being the case, one would expect similar behavior as the surface temperatures change from freezing to thawing. On the contrary, time step 13 is without an increase in the number of equilibrium iterations or a loss of syncronicity of the two curves. On closer examination, both analyses fail to comply with the applied temperature curve and instead the surface temperatures remain at -0.1°C. As expected, the next time step in both instance requires far more iterations for convergence. Rather than correct for this, the program was allowed to proceed with this idiosyncracy. This remained a subtle error within the analysis, and researchers should be aware of *ADINAT's* limitations in this regard.

Appendice K: Elimination of the Tension Field within the N.E.S. Mesh

The second version of the N.E.S. mesh was run on the SAP IV program under gravity loading and no thermal effects in order to examine the suitability of the mesh and its accompanying assumptions to the problem of hand (Figure 5.34). Figure K.1 shows a blow-up of the mirrored mesh in the vicinity of the pipe. Stresses in the thin ring of elements adjacent the void have not been plotted, for clarity. Note that the principal stresses nearest the void rotated into an almost radial/tangential stress pattern, with the distortion from circular being due to boundary effects and gravity. The surface elements exhibited some undesirable rotations of principal stresses due to soil arching above the pipe. The centre of the berm was under low stress due to its position at the surface and because the node at the top of the berm on the centreline (node 89) was not fixed. This node was freed to allow movement in the berm to prevent it from becoming a controlling structural feature in the heaving mesh.

It should be emphasized that the stress path followed by the soil is for a soil with a pipe placed in it under no gravity and subsequently subjected to gravity. This is different than placing a pipe into a soil that has already undergone gravity loading. In the physical model, the excavation of a pipeline trench would result in stress relief at the boundary of the excavation, and accompanying principal stress rotation in the contiguous soil mass. Pipeline placement and back filling would partially reload the trench surface, but not significantly unless compactive force was used. More subtly, the finite element stress field is affected by placing a stiff pipe into a flexible medium which, when subjected to loading, would tend to shed load onto the more rigid pipe. This can be seen in Figure K.1 where soil stresses near the springline are slightly higher than those at a similar depth elsewhere. The net result of this dissimilarity is that the finite element analysis results in soil arching above the pipe and higher stresses below it.

K.1 Tension Anomaly within the Mesh

On closer examination of the mesh's stress field an anomaly was found in the upper right-hand corner of the mesh, far removed from the area of interest near the pipe (Fig. K.2). The elements near the surface had small components of tension parallel to the free surface. This finding was of concern because the basic premise in creating

such a deep and broad mesh was to distance the pipe from the boundaries. This was done so that any stress changes near the pipe could be attenuated before reaching any boundary of non-symmetry. This ensures that the boundary will have minimal effect on the pipe. The tension implied a surficial stretching resulting, perhaps, from residual effects of soil arching above the pipe.

K.2 Restraining the Berm Horizontally

To examine if the freedom of the top-centre node was affecting the stresses, the node (node 89) was fixed horizontally which should have buttressed the berm, preventing any horizontal movement. Fixing the degree of freedom in this manner was effective in restricting the berm as evidence in the slightly higher berm stresses in Figure K.3 . Unfortunately, this did little to alter the tension field on the far side of the mesh.

K.3 Reduced Void Radius

The berm was made weightless to remove its loading effect from the analysis. Still working on the premise that deformations due to soil arching were responsible for the tension, the mesh was altered by reducing the pipe void radius from 0.6m to 0.1m. This should have increased the amount of soil above the now smaller void thereby reducing strains due to soil arching stresses. The analysis of this change found this to be true but the tension field remained. (Figures K.4 , K.5). The cause of the tension field was as yet unknown and believed to be due to some feature of the mesh near the pipe, however a simple check on the effect of the far boundary was attempted. To further remove the boundary from the pipe, all the nodes on the right hand side were moved from x=18.6m to x=25m. This increased the existing high aspect ratios of the elements at the right boundary, but as they all were orthogonal to the principal loading (gravity) this was not a major concern (Figure K.6). Even with the reduced pipe radius, this modification changed the tension field negligibly. Efforts were redirected to the vicinity of the pipe.

K.4 Altered Berm Geometry and Materials Infilled Void

To totally discount the effect of the berm on the analysis, another berm element geometry was tested to examine its affect on the tension field. As seen in Figure K.7 , the berm and the first layer of elements below the berm are now regular right elements with the exception of the trapezoidal element at the berm slope. This alteration, particularly the replacement of the collapsed quadrilateral

element with a trapezoidal one, was intended to soften any effect the density of Gauss points might have had on the analysis. As can be seen in Figure K.8 no appreciable difference was noted.

By creating another material that was weightless and with an extremely low Young's modulus, the contribution of the berm could be effectively reduced to zero. This was done by assigning this new material to the berm. In addition, the pipe void was filled by using a common node at the centre of the void. This node was chosen to minimize the range of node numbers for the elements in order to minimize the band width. Renumbering was seen as a tedious alternative that was unnecessary given the insignificant solution time for the original problem (<2 seconds). The analysis was run (Fig K.9) with no better results since the top-right tension field prevailed.

The possibility existed that the general configuration of the elements near the pipe was causing the difficulty. In general, however, a higher density of elements should overly restrict the strains, resulting in a stiffer region. The question was moot when the altered infilling of the hole did not mitigate the tension (Figure K.10). Even altering the junction of the berm toe with the concentric elements had no effect (Figure K.11, K.12).

K.5 Degrees-of-Freedom of the Top-Right Node

At this point, neither the berm, nor the pipe void nor the mesh in the vicinity of the pipe had any effect on the horizontal tension in the top right corner of the mesh. It appeared that the undesirable tension field was due to some factor from outside the area of the pipe. The top-right corner was examined directly to try and discover the reasons for the tension field.

The top right node of the mesh was freed in the horizontal direction as well as the vertical direction. Although the aspect ratio of the top right element is of the order of 40:1 this additional freedom was expected to relax the top right element and reduce the stress to an acceptable level. Had this happenned, the most practical solution would have been to allow this node the additional freedom, the resulting stress field would have been more true-to-life. Instead, the tension persisted (Figure K.13) As the study of the stress field was not very fruitful, attention was directed towards the displacement field. If the mode of movement inducing the tension could be identified, the problem would be better defined. To aid in this, the facilities of the SAPMESH plotting program, developed specifically for this analysis, were used.

The stress field for the previous analysis was re-draughted using a deformation exaggeration of 50. This produced the grossly distorted mesh shown in Figure K.14. Note that the bottom left elements appear inverted because their factored nodal displacements exceeded the elements' vertical dimensions while the basal nodes remained fixed and stationary.

What is obvious is that the left side of the mesh has compressed more than the right side of the mesh, resulting in uneven surface settlements. The surface is not an inclined plane either, but more of an "S"-shape with the sagbend on the left and the overbend on the right which would help explain both the compression stresses above the pipe and the tension stresses in the top right corner. A plot of the surface settlement versus the anticipated settlement based on oedometric conditions showed that the settlements were of the correct magnitude (Figure K.15).

K.6 Conceptual Simplification of the Mesh

The problem was becoming clouded because of the complexity of the mesh and the subtlety of the factor controlling the tension field. A level of objectivity, unobtainable with the present mesh, was required to re-examine the problem. The "conceptual simplification" of the N.E.S. Calgary test site was created to fill this need.

This new mesh (Fig. K.16) was almost entirely composed of rectangular elements arranged in 8 layers of 6 elements each, This thickness of each layer varied to reflect the element layering in the original mesh and the need for small elements in the vicinity of the pipe. Berm elements existed but were effectively inactive. The principal stresses in each layer were constant with K_o conditions existing everywhere. Exaggerating the deformations (Fig K.17) verified the stresses' uniformity. The surface deformation was identical to that predicted using an oedometric modulus.

To simulate the effect of the pipe void, one element was made inactive at the approximate position of the pipe (Fig K.18). As expected, the stresses in the adjacent elements indicate soil arching, although the true effect of a void is not evident because of the coarse discretization of the mesh. Significantly, no differential surface settlements or tension fields arose.

The element representing the pipe void was re-activated and the berm was activated. The stress field in Figure K.19 shows the small effect of the berm on the nearby stresses with the resulting deformations also being commensurately higher. No tension developed in the top right corner of the mesh.

K.7 Corroboration using the ADINA Program

The possibility of an internal numerical "bug" was also considered. The original "cobweb" version of the mesh (Fig K.9) was re-coded for the ADINA program and run. The results were plotted, with a deformation exaggeration of 50, using the ADMESH program (Figure K.20). The bottom of the mesh below the lower boundary was not plotted.

The deformation pattern is identical to that of the SAP IV program (Figure K.14). This indicated that the tension problem was particular to the specified numerical model and not the analytical total used to solve it. The problem was also insensitive to minor adjustments in the mesh, material properties, and boundary conditions. The only difference so far was the total absence of the tension field when the mesh was simplified into a gridwork.

K.8 The Effect of Lumped Mass

The grid stiffness and the lumped gravity load are both affected by the mesh geometry. (A "lumped" gravity analysis was uses some numerical method to distribute the body force to the nodes as equivalent concentrated loads). In order to separate the two effects the following test was run: using the original *SAP IV* mesh, the gravity load was replaced with a surficial pressure of 100 kPa. If the large elements in the bottom right of the mesh were "hanging up" the top right elements, this would still be apparent with a surficial load. Alternatively, if the lumping of the gravity forces were responsible for inducing the tension field in the analysis, a uniform displacement should be seen. The pipe void was filled and the berm de-activated to ensure a uniform base.

As can be seen in Figure K.21, the surficial load resulted in uniform displacements across the mesh, indicating that the lumped gravity loading was responsible for the tension field. To examine the effect of lumping, a simple calculation was performed on a unit width through the mesh of the conceptual simplification. The results are presented in Table K.1 and show that the finite element method can obtain excellent agreement with the closed-form solution (Figure K.15). Due to the nodal lumping, however, the stresses in the elements increase with depth in a step-wise manner, alternatively over-estimating and under-estimating the actual vertical stress corresponding to any particular depth.

In a regular grid mesh as in Figure K.16, this discretization balances out because the average strain throughout each element is identical to the average strain of the physical model in the same location. However, in an

irregular grid, the nodal lumping of gravity loads can have a varying effect, dependent upon the particular mesh configuration. In the more complex mesh with the "cobweb" pattern (Fig K.22) the approximate contributary areas for nodal lumping to the base are shown. Essentially, the gravity associated with the shaded area is not felt within the analysis because it is distributed to the basal nodes which have no vertical degree of freedom. As the contributary area is highly skewed, the gravity forces are unevenly distributed so the mesh experiences a torsional moment which is resisted by internal straining of the material. The tension field is one expression of this resistance.

To mitigate the tension problem, the mesh was re-designed to ensure a more equitable nodal lumping of gravity to the base (*viz.* Chapter 5).

TABLE K.1 Lumped-Mass Analysis along the Right Side of the Mesh

Layer	Depth (m)	Thickness (m)	Lumped Thickness (m)	Stress (kPa)	Cum. Stress (kPa)	Displ (m)	Cum. Displ (m)
I	0.0	0.2	0.1	2.033	2.033	-	.2154
II	-0.2	0.6	0.1+0.3 = 0.4	8.132	10.165	.0004	.2154
III	-0.8	0.6	0.3+0.3 = 0.6	12.198	22.363	.0010	.2149
IV	-1.4	0.6	0.3+0.3 = 0.6	12.198	34.561	.0015	.2139
V	-2.0	1.0	0.3+0.5 = 0.8	16.264	50.825	.0037	.2124
VI	-3.0	2.0	0.5+1.0 = 1.5	30.495	81.320	.0119	.2086
VII	-5.0	4.0	1.0+2.0 = 3.0	60.990	142.310	.0417	.1960
VIII	-9.0	8.0	2.0+4.0 = 6.0	121.98	264.290	.1550	.1550
	-17.		4.0 = 4.0	81.32	345.610		
		17.0	17.0 x 20.33 = 345.61			d = .2154m	

Young's Modulus = 8500. kPa
Poisson's Ratio = 0.35
Oedometric Modulus = 13642. kPa
Weight Density = 20.33 kN/m**3

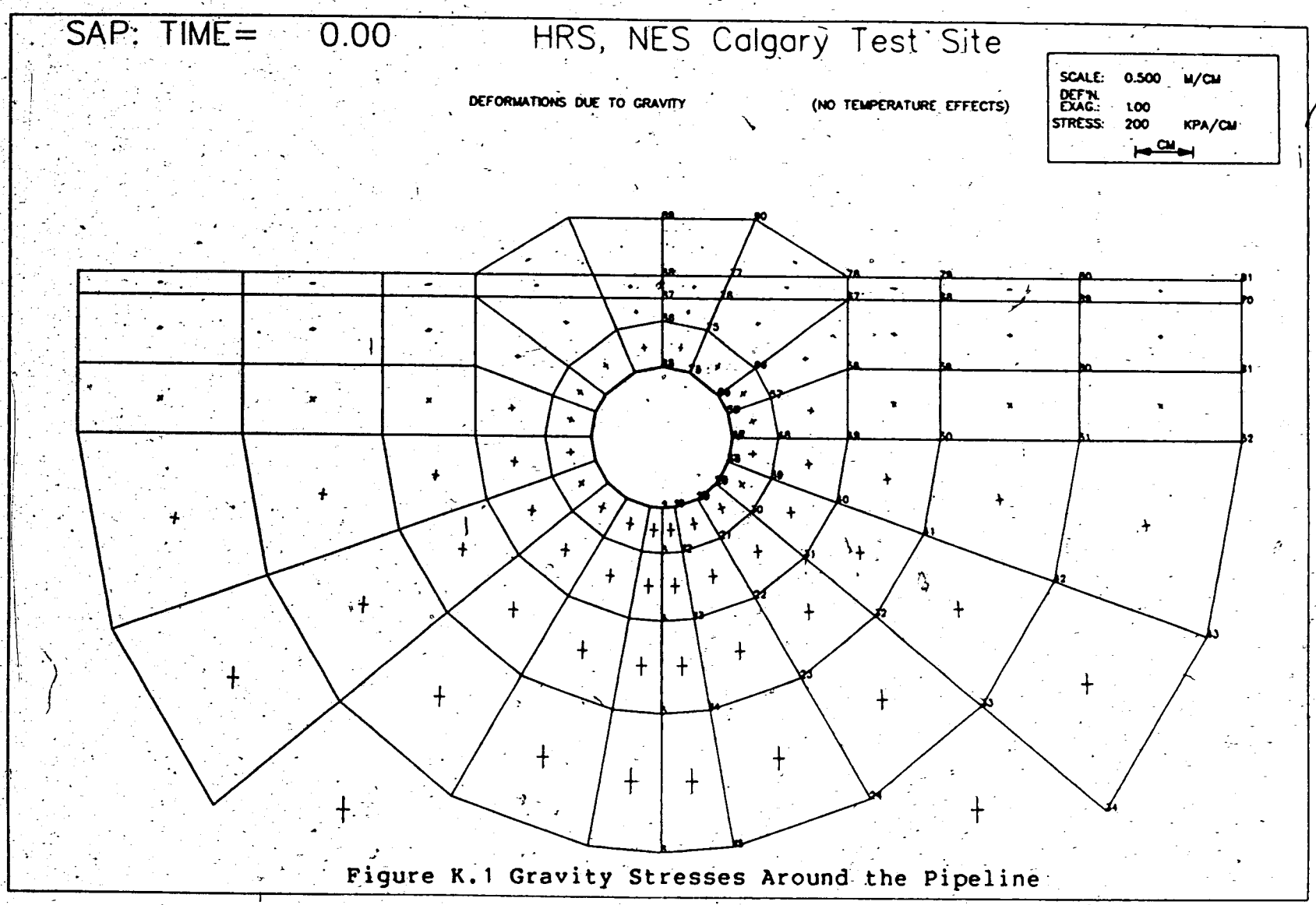

Figure K.1 Gravity Stresses Around the Pipeline

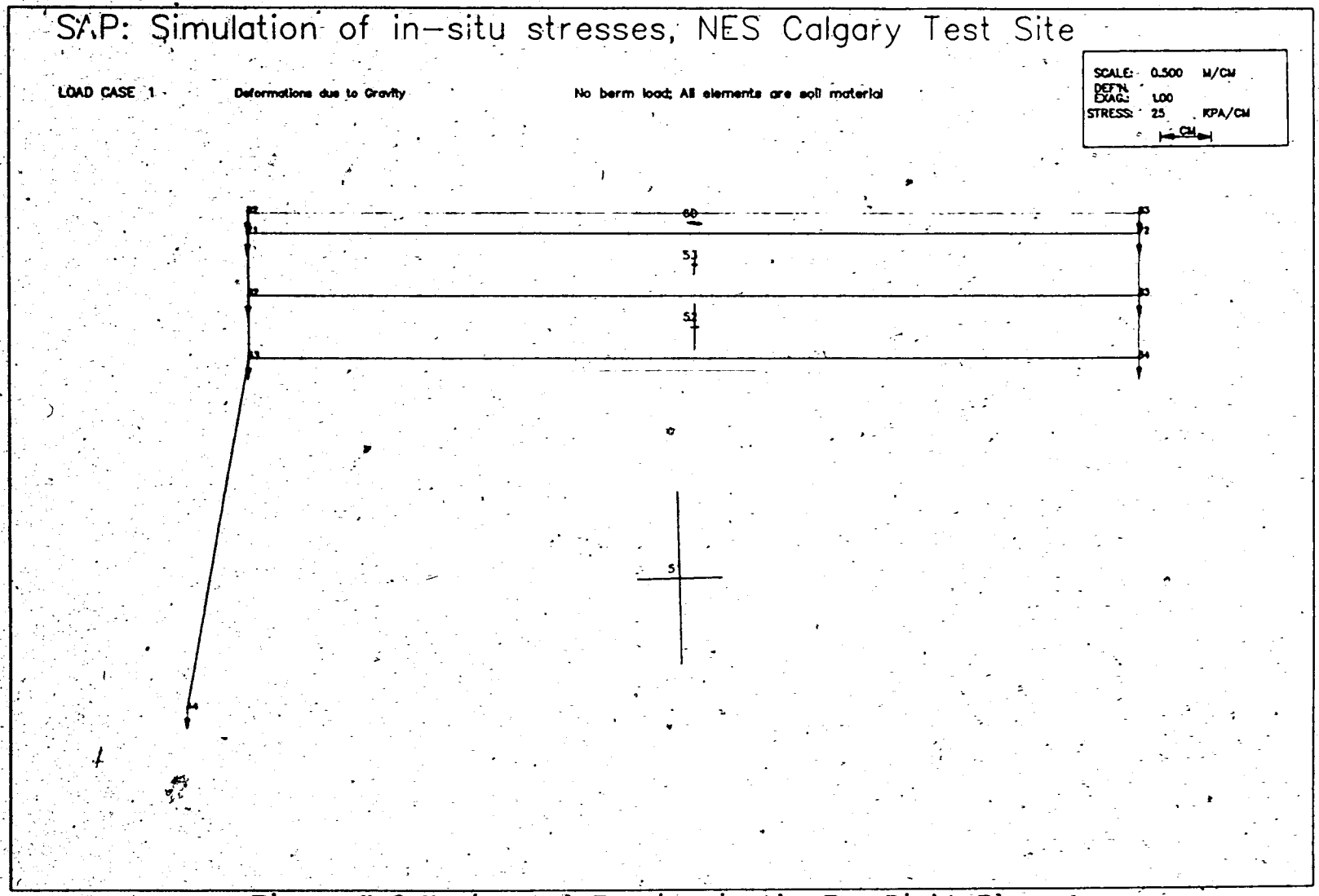

Figure K.2 Horizontal Tension in the Top-Right Elements

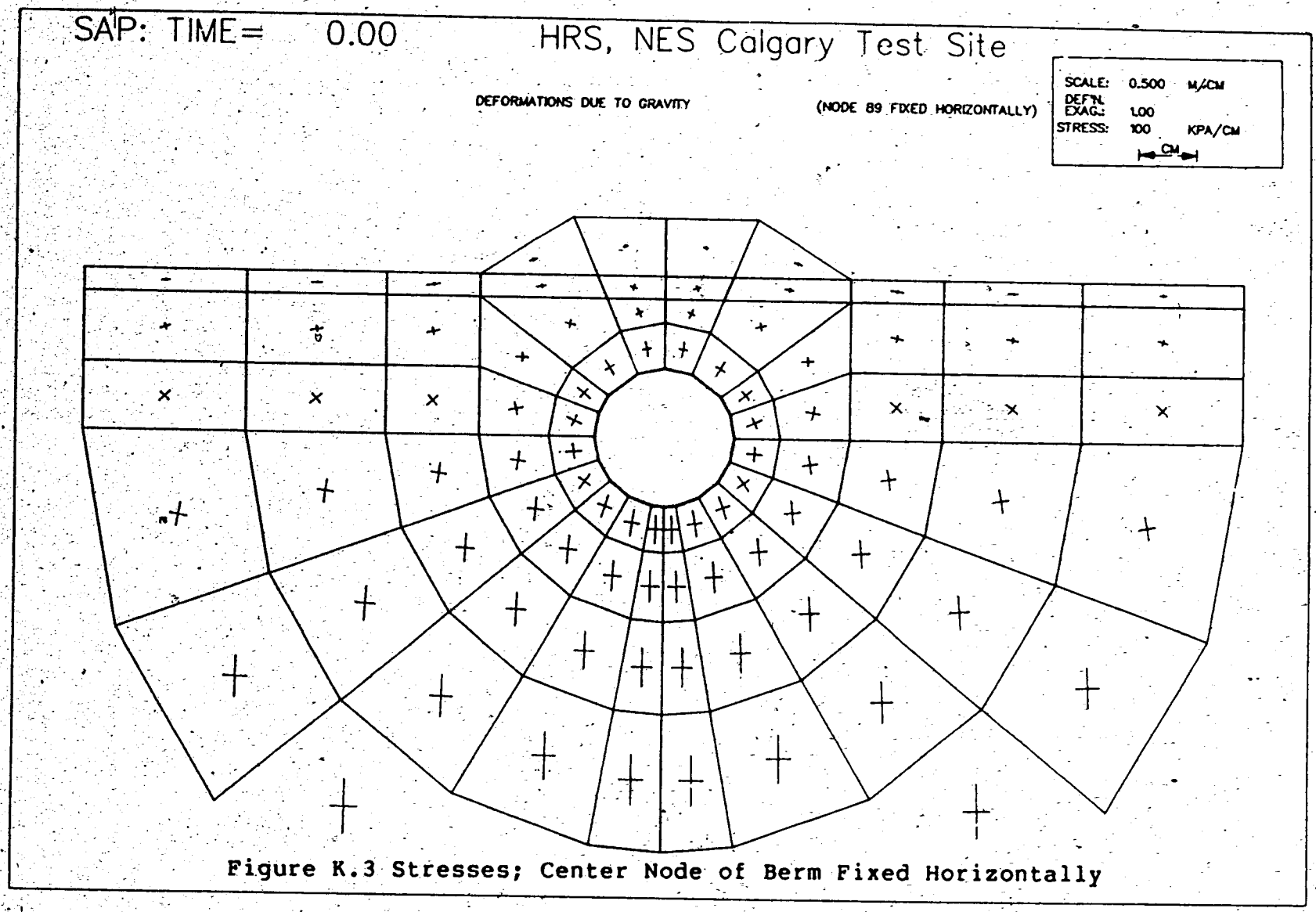

Figure K.3 Stresses; Center Node of Berm Fixed Horizontally

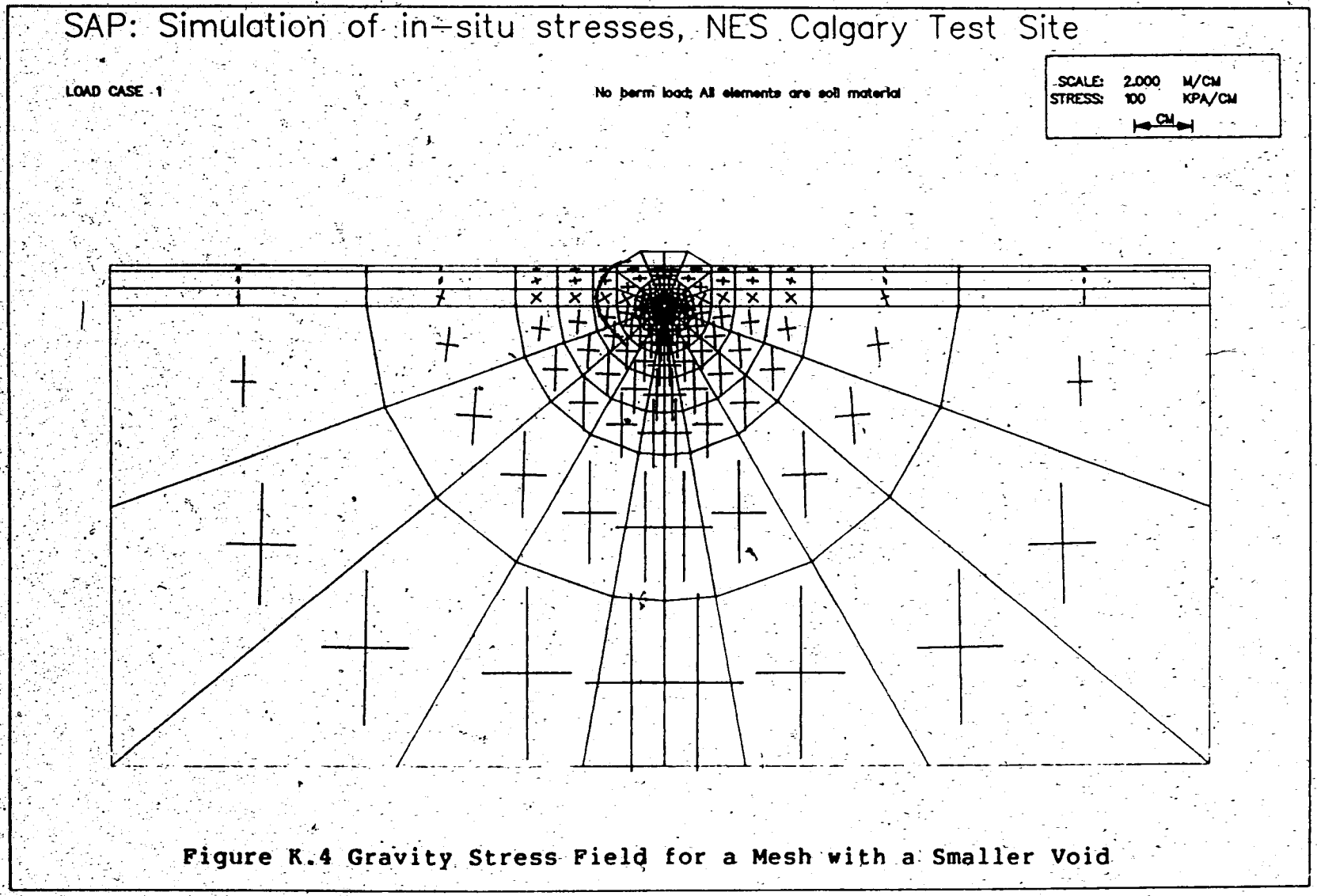

Figure K.4 Gravity Stress Field for a Mesh with a Smaller Void

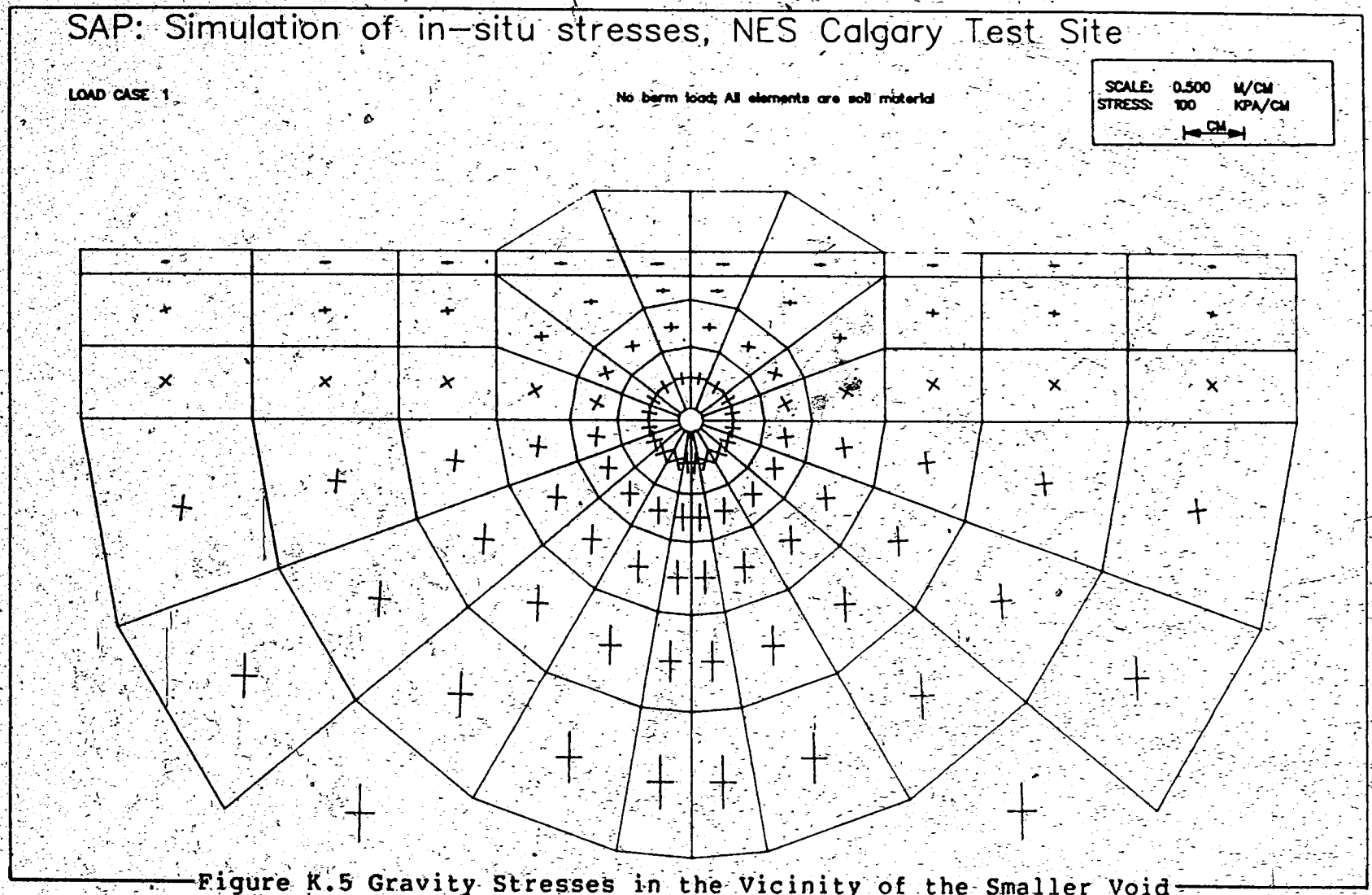

Figure K.5 Gravity Stresses in the Vicinity of the Smaller Void

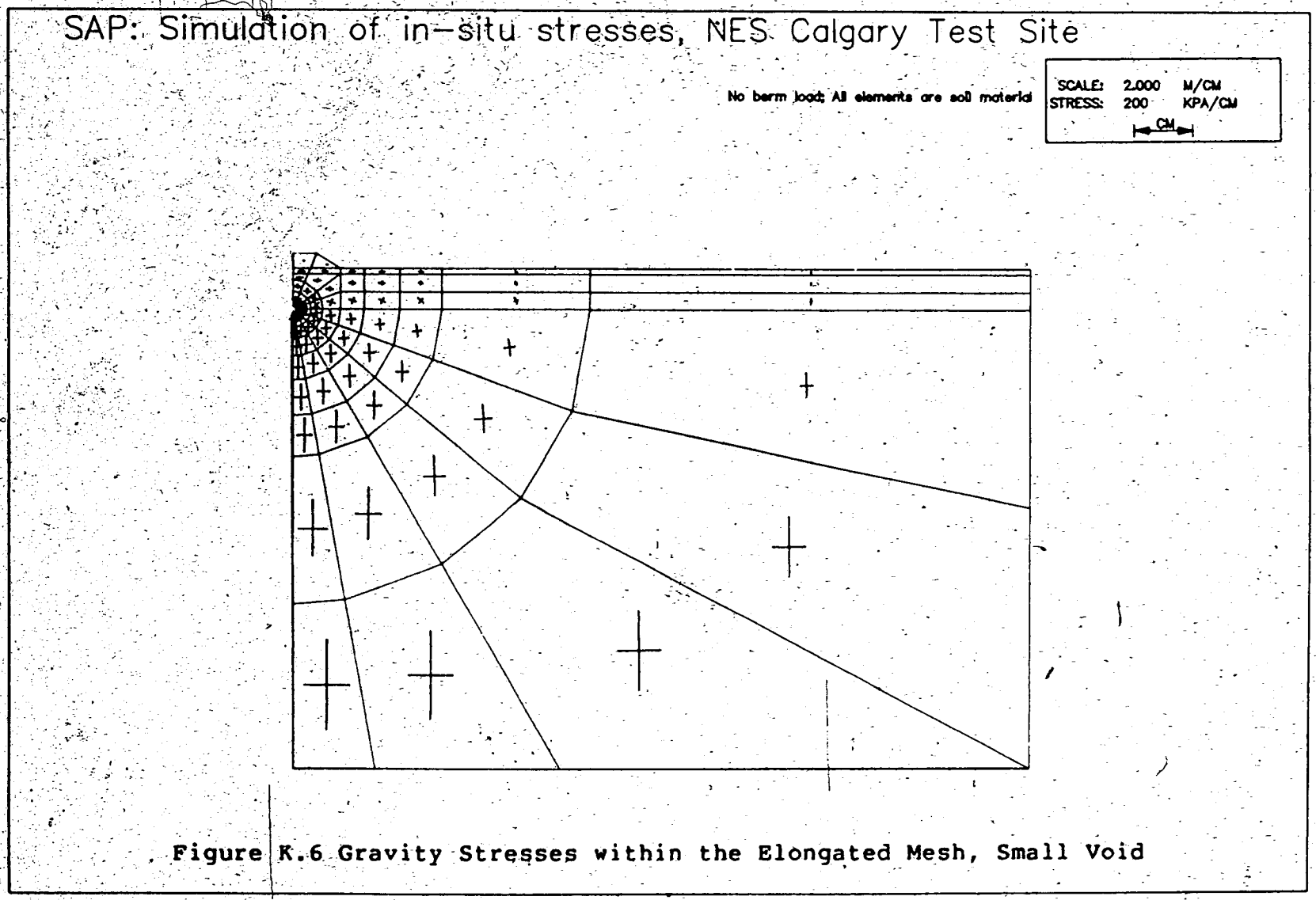

Figure K.6 Gravity Stresses within the Elongated Mesh, Small Void

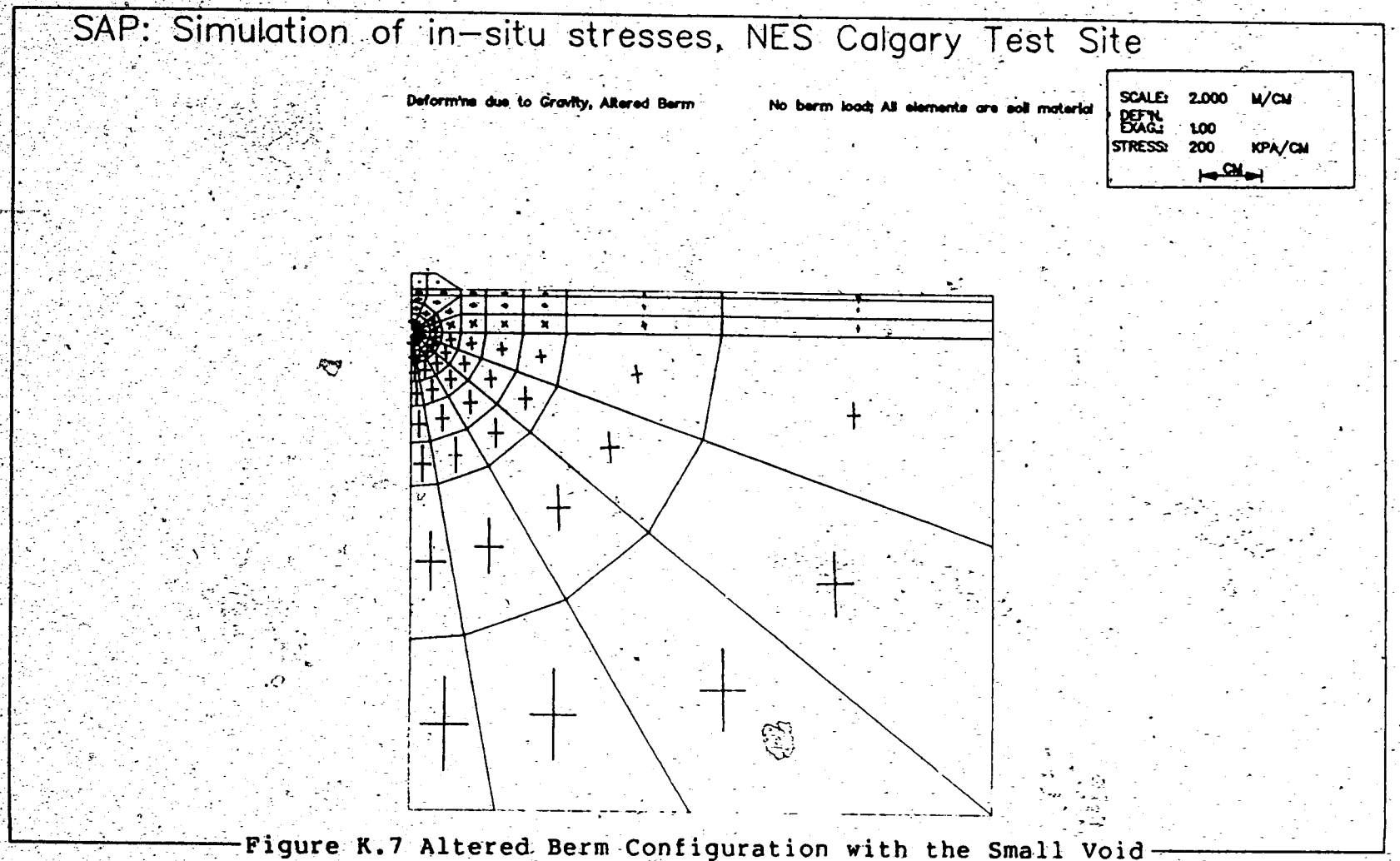

Figure K.7 Altered Berm Configuration with the Small Void

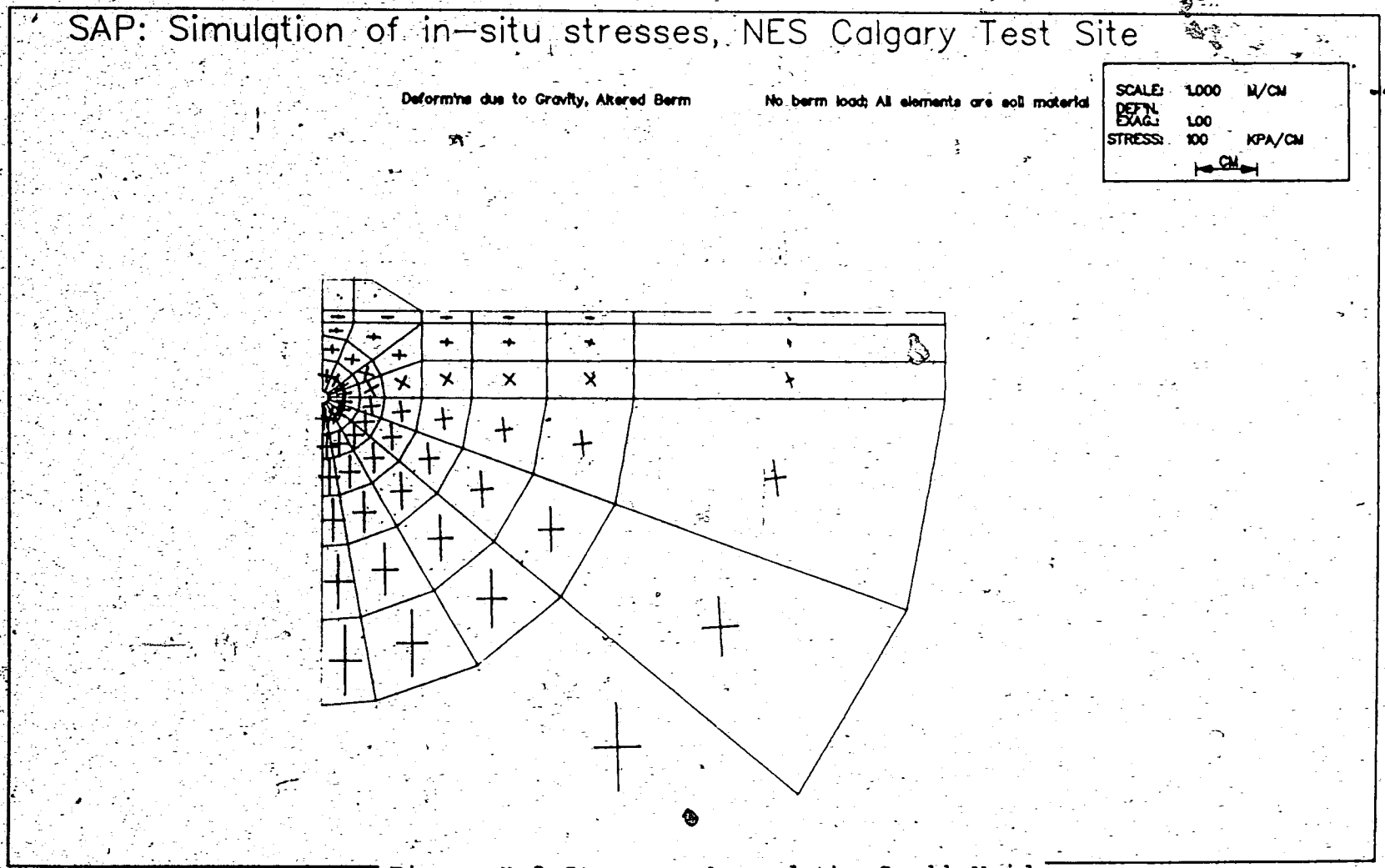

Figure K.8 Stresses Around the Small Void

SAP: Simulation of In-Situ Stresses, NES Calgary Test Site, 2 Matls

Gravity Deformations, No Hole, No Berm

All elements are soil material

SCALE: 2.059 M/CM
DEFN. EXAG.: 1.00
STRESS: 200 KPA/CM
CM

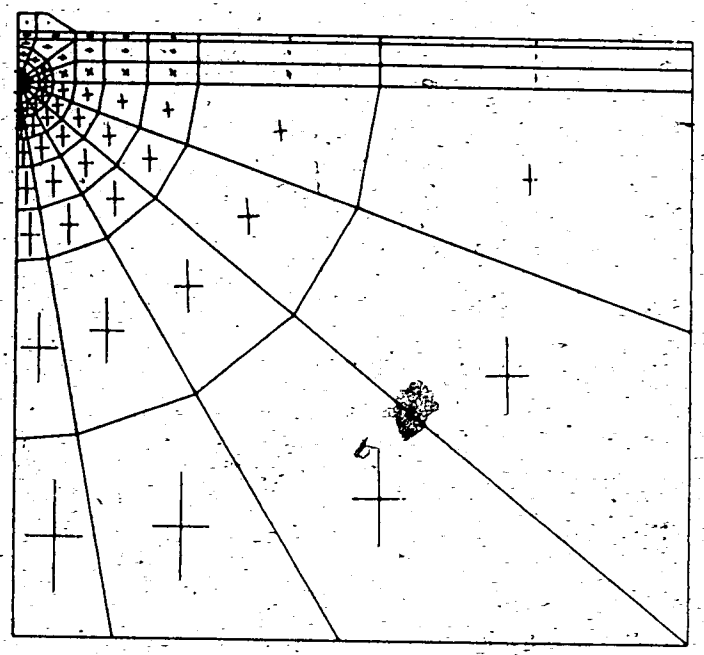

Figure K.9 Gravity Stresses with No Void

SAP: Simulation of in-situ stresses, NES Calgary Test Site

Deform'ns due to Gravity, Hole Filled No berm load; All elements are soil material

SCALE: 2.000 M/CM
DEFN. EXAG.: 1.00
STRESS: 200 KPA/CM
CM

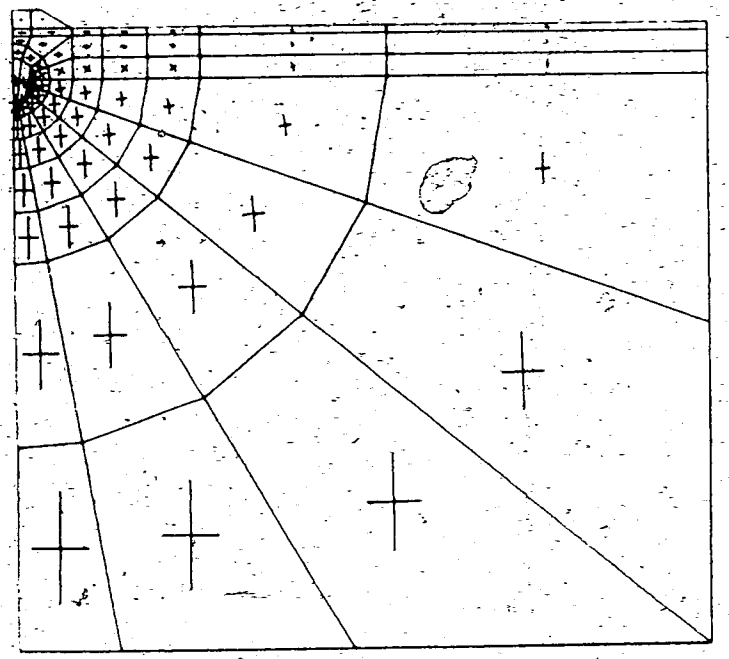

Figure K.10 Vertical Infilling of Hole

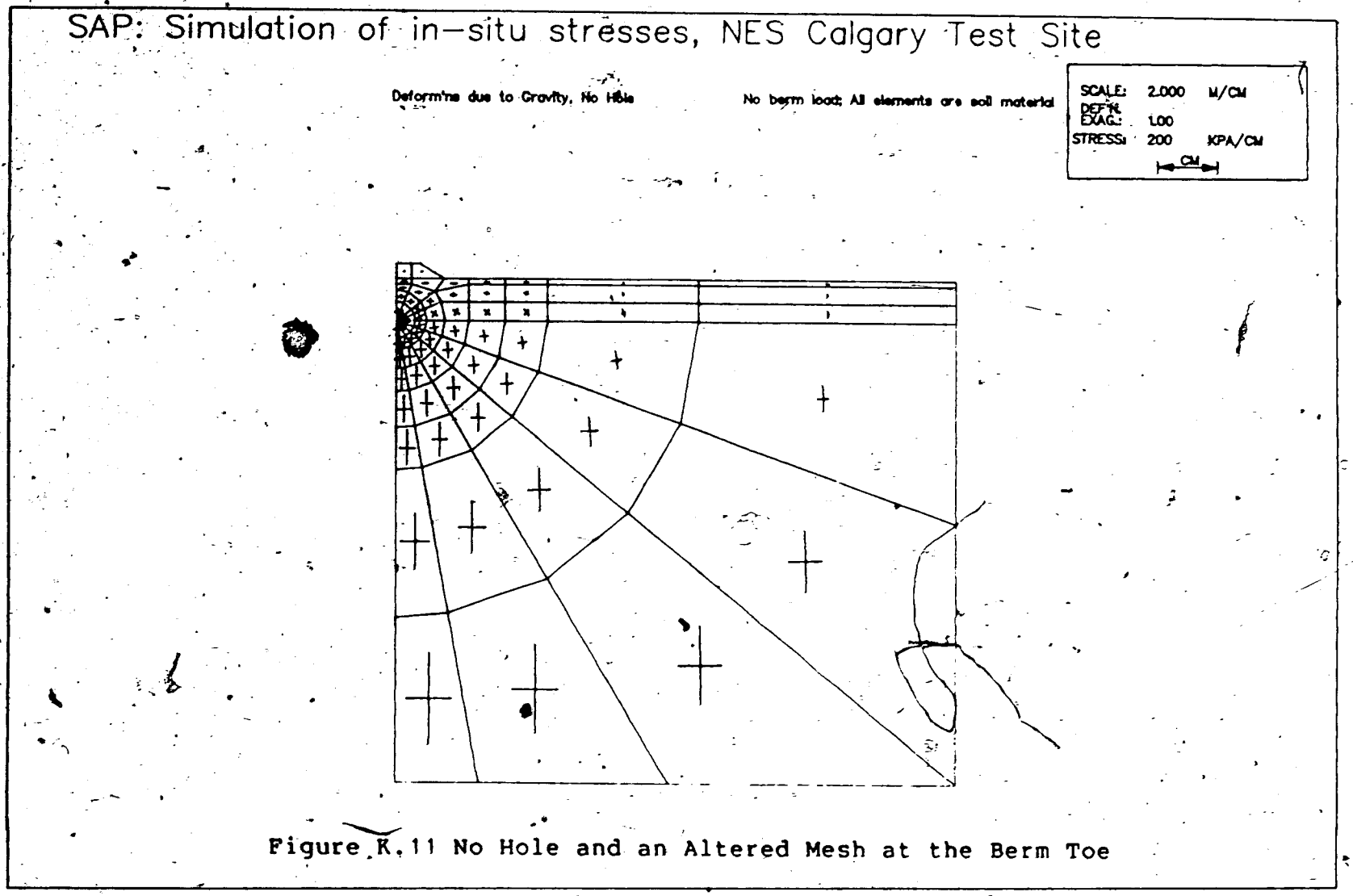

Figure K.11 No Hole and an Altered Mesh at the Berm Toe

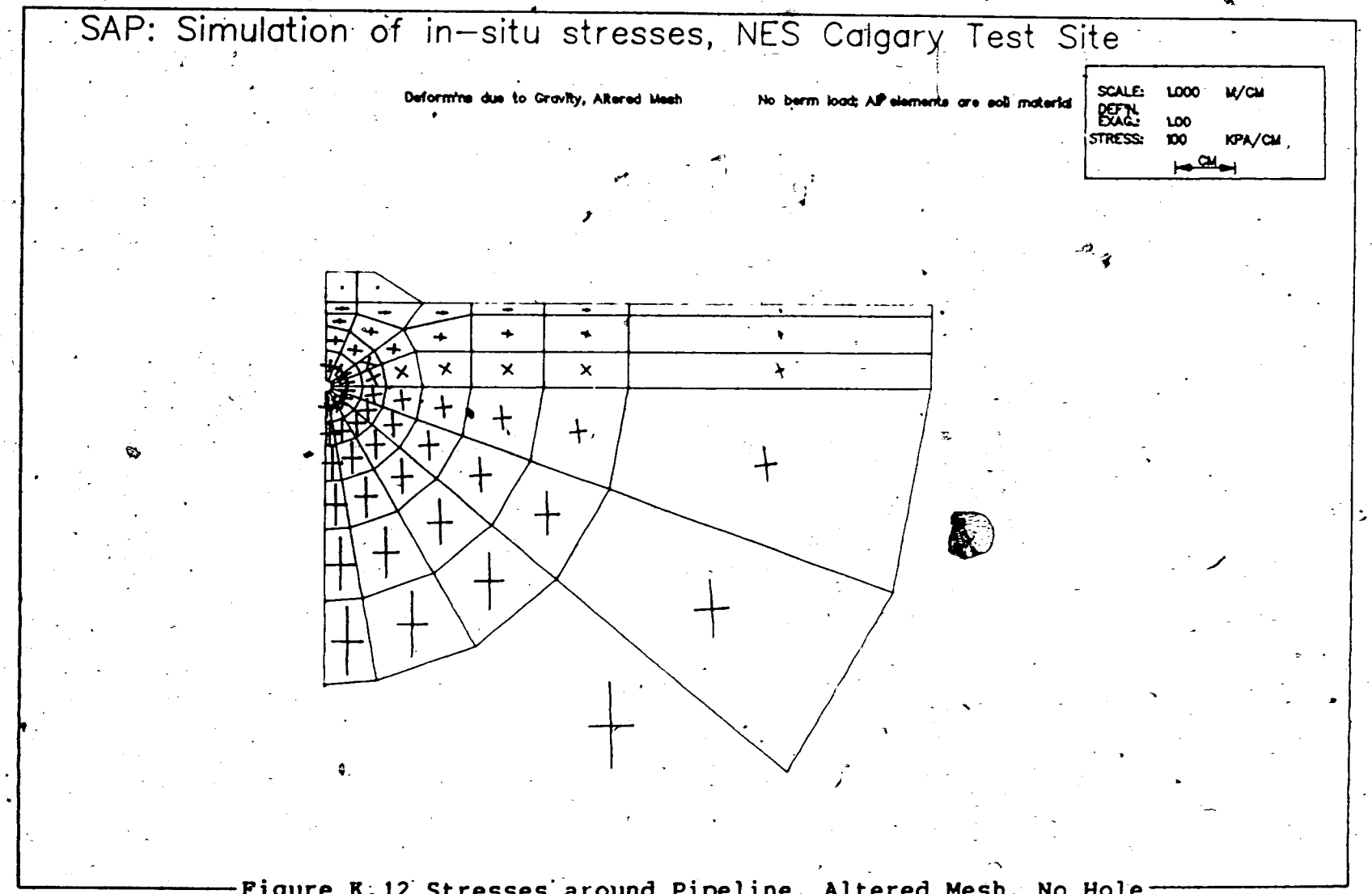

Figure R.12 Stresses around Pipeline, Altered Mesh, No Hole

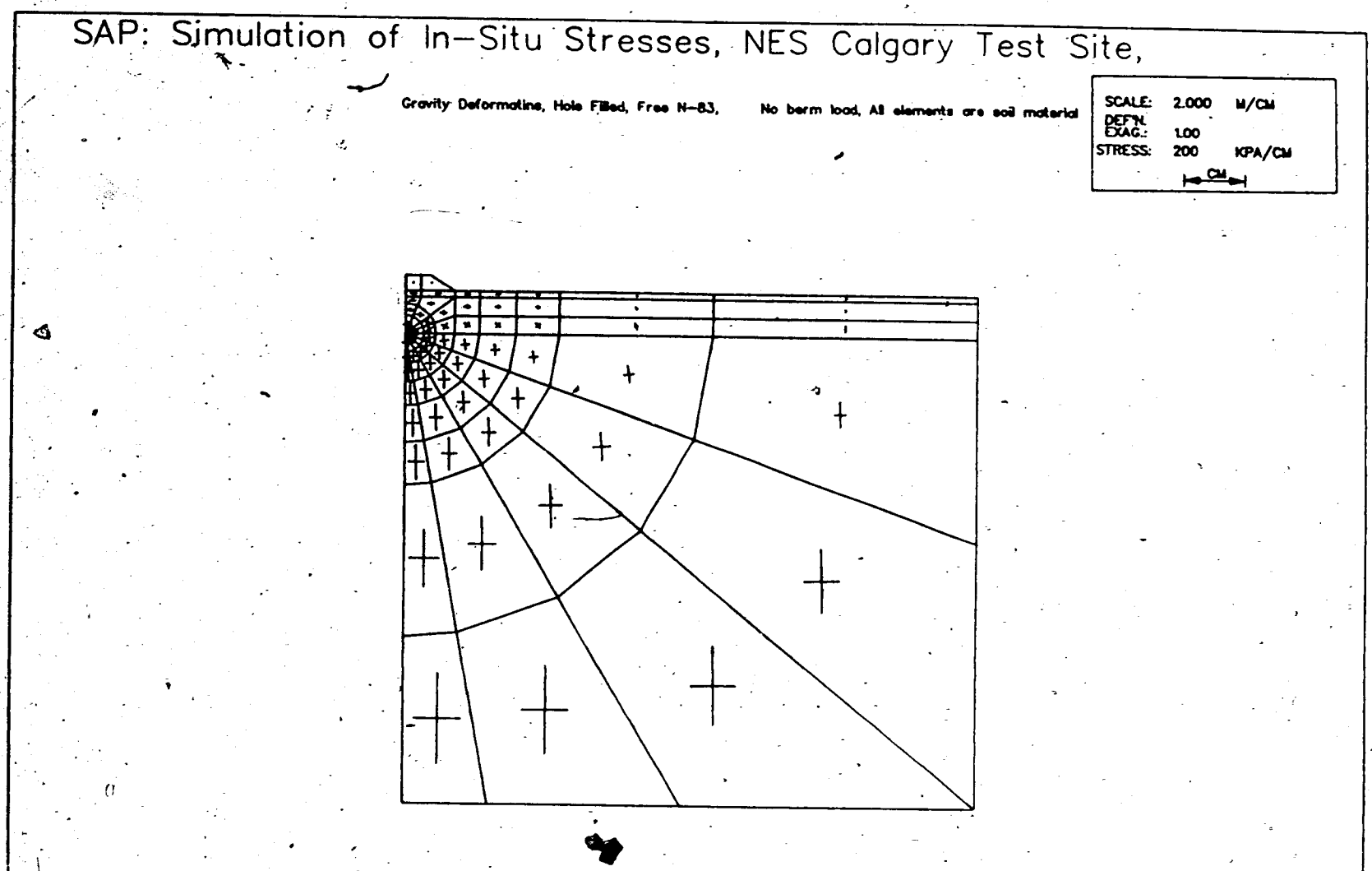

Figure R.13 Top-Right Corner Freed and No Hole

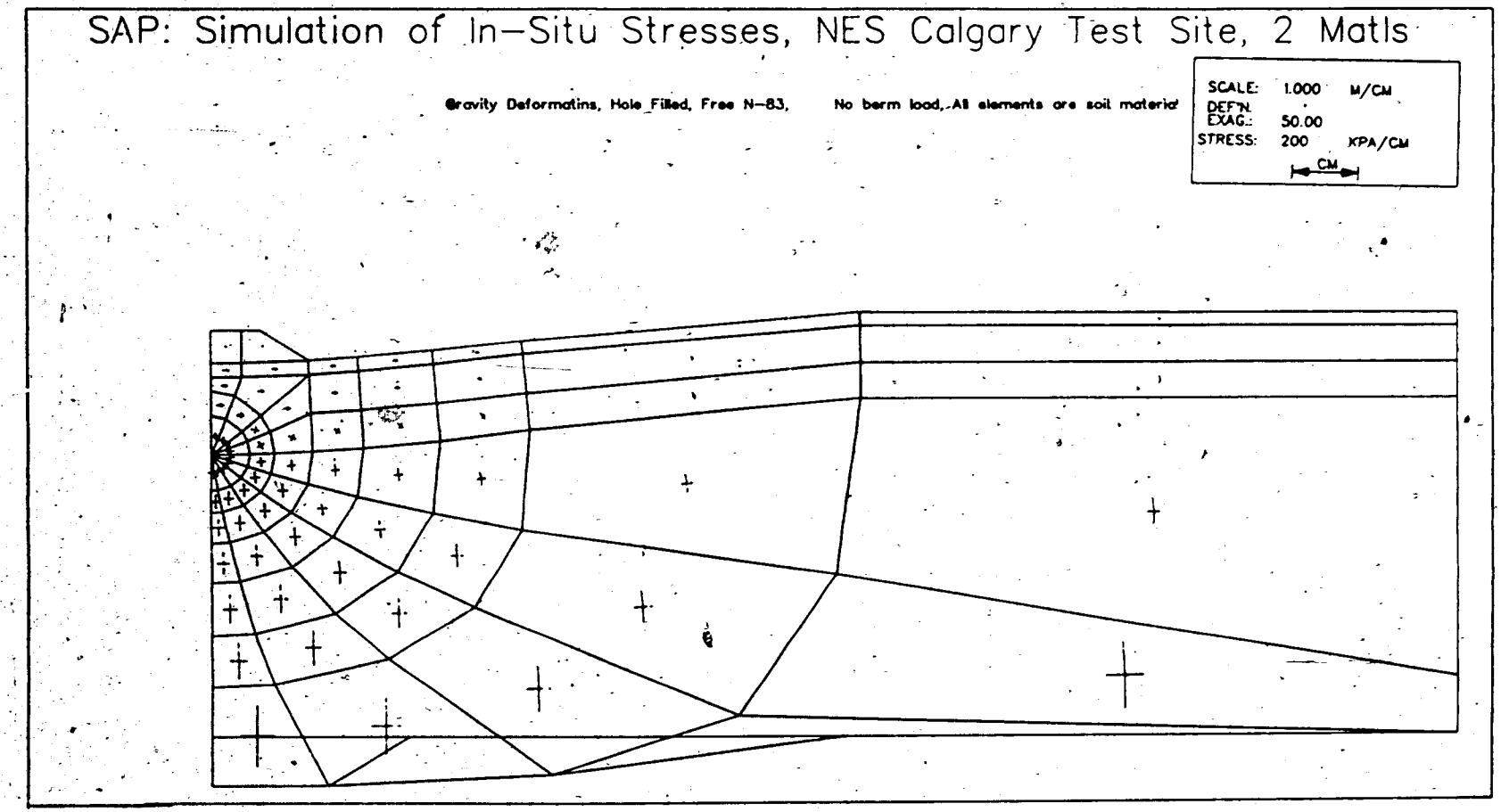

Figure K.14 Grossly Exaggerated Displacements (50×), No Hole

SURFACE SETTLEMENT PROFILE

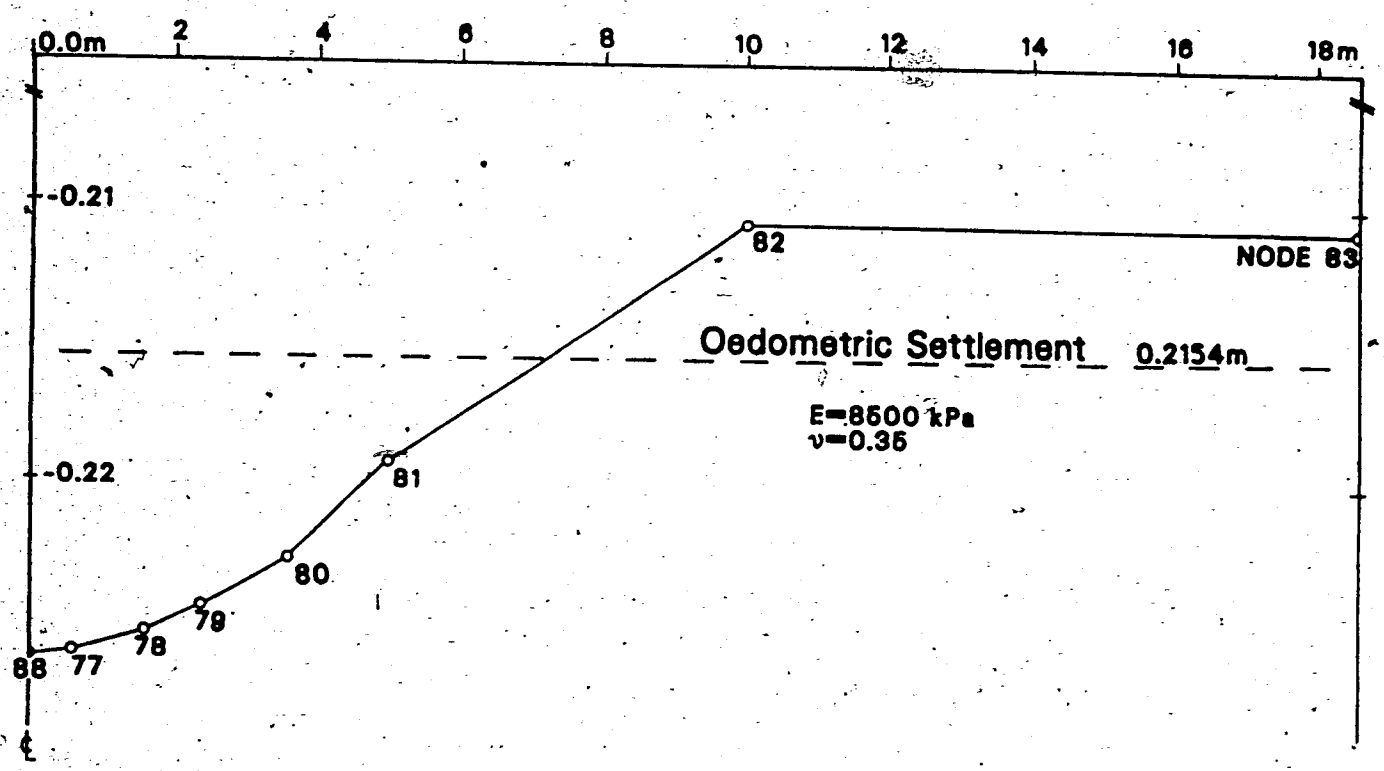

Figure K.15 Surface Settlement Profile

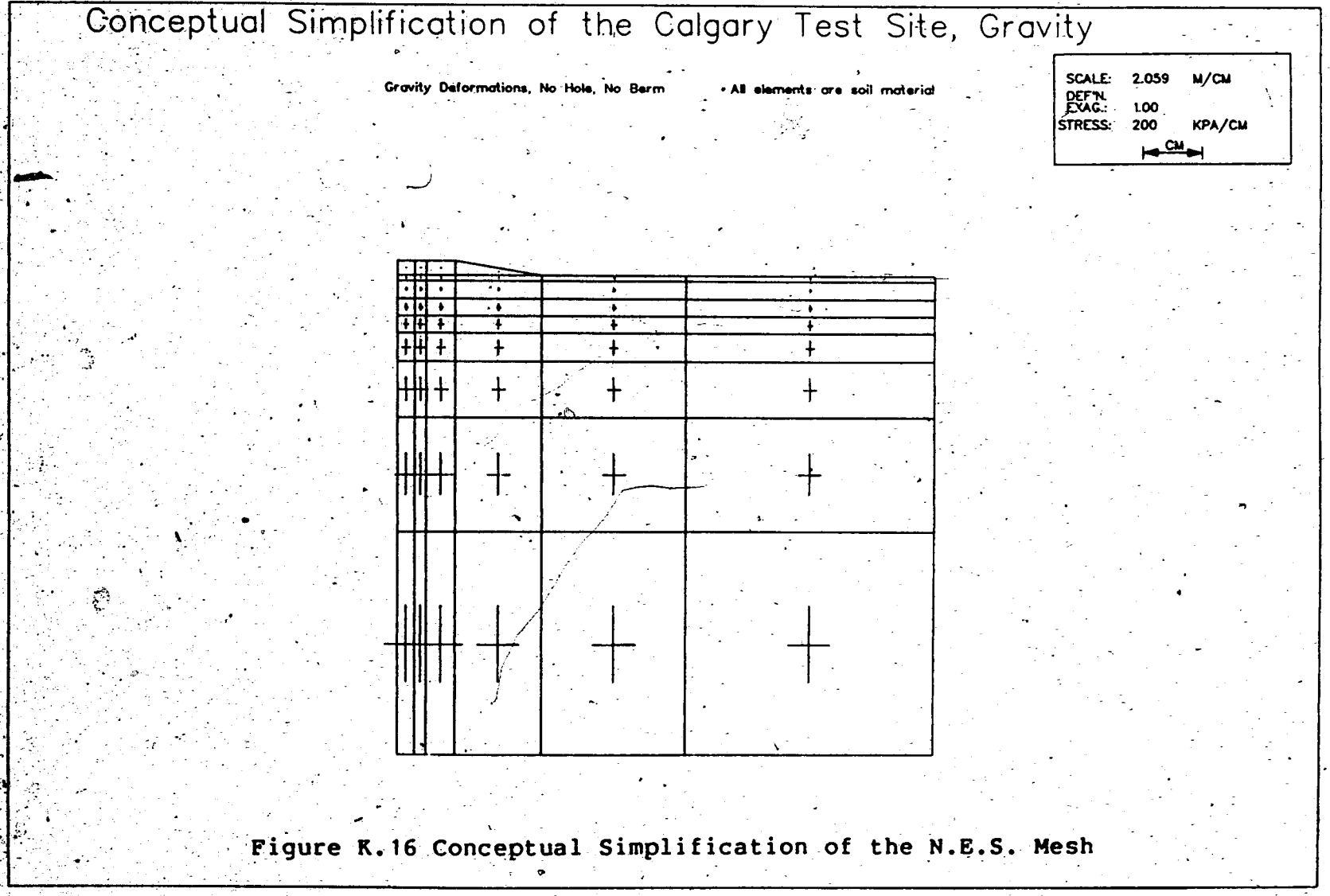

Figure K.16 Conceptual Simplification of the N.E.S. Mesh

Conceptual Simplification of the Calgary Test Site, Gravity

Gravity Deformations, No Hole, No Berm All elements are soil material

SCALE: 2.059 M/CM
DEFN. EXAG.: 25.00
STRESS: 200 KPA/CM
1 CM

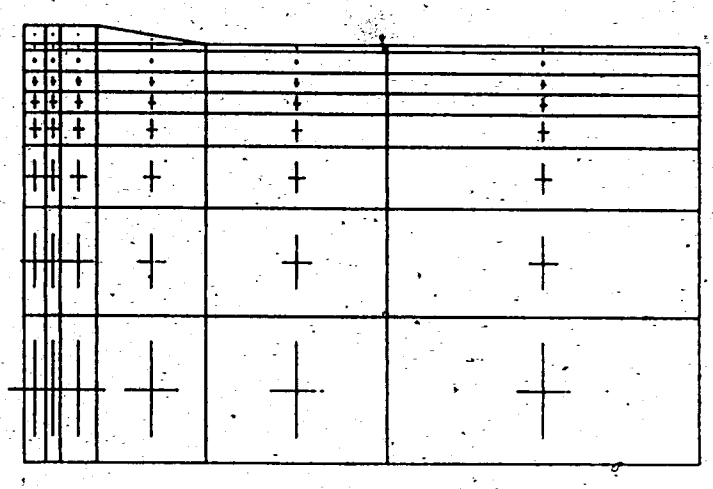

Figure K.17 Simplified Mesh under Gravity Loading, No Hole, No Berm

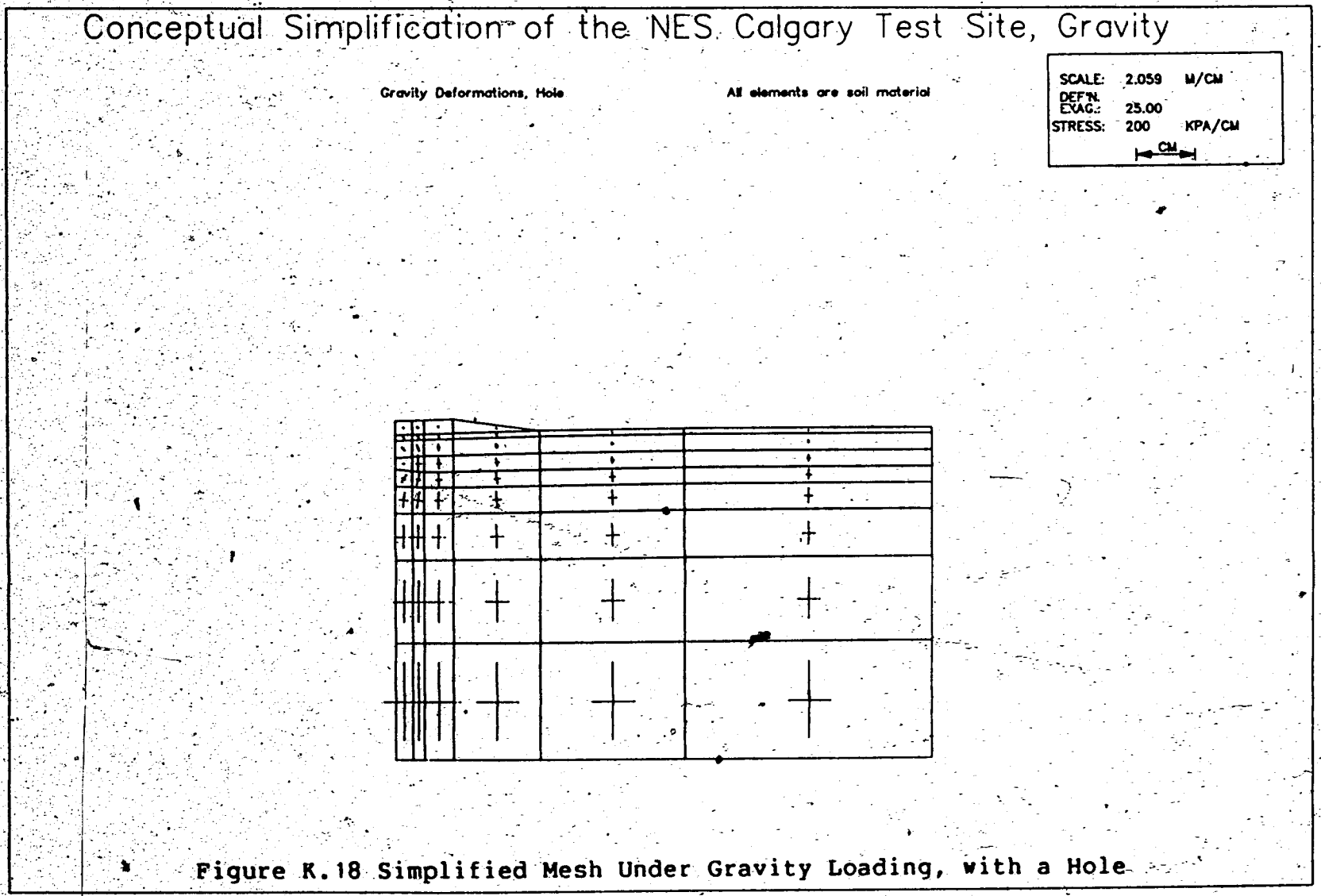

Figure K.18 Simplified Mesh Under Gravity Loading, with a Hole

Conceptual Simplification of the Calgary Test Site, Gravity

Gravity Deformations No Hole All elements are soil material

SCALE: 2.059 M/CM
DEFN. EXAG.: 25.00
STRESS: 200 KPA/CM
CM

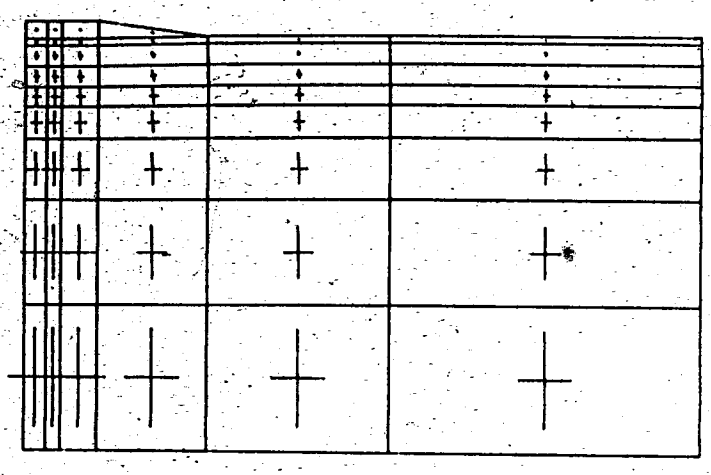

Figure K.19 Simplified Mesh Under Gravity Loading (including Berm)

NES CALGARY TEST SITE GRAVITY TURN-ON

THE FIRST TEST RUN OF ADINA'S CHECK ON SAP

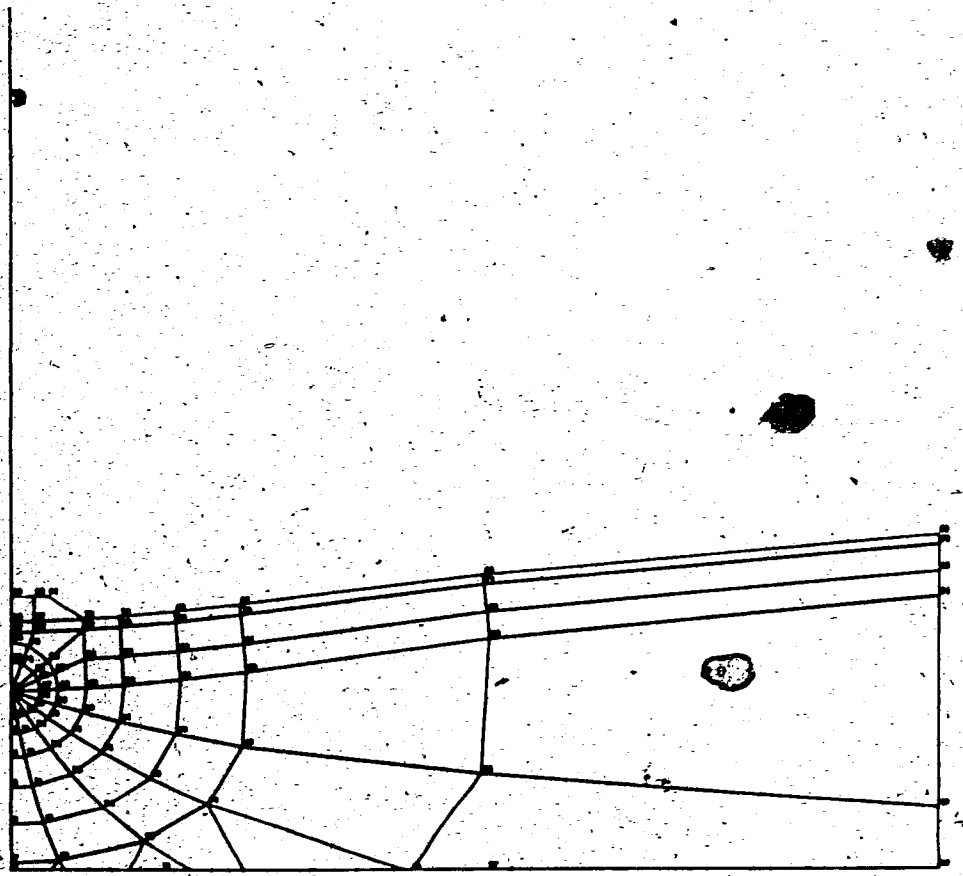

Figure K.20 Check on the Original Mesh using ADINA (δ×50)

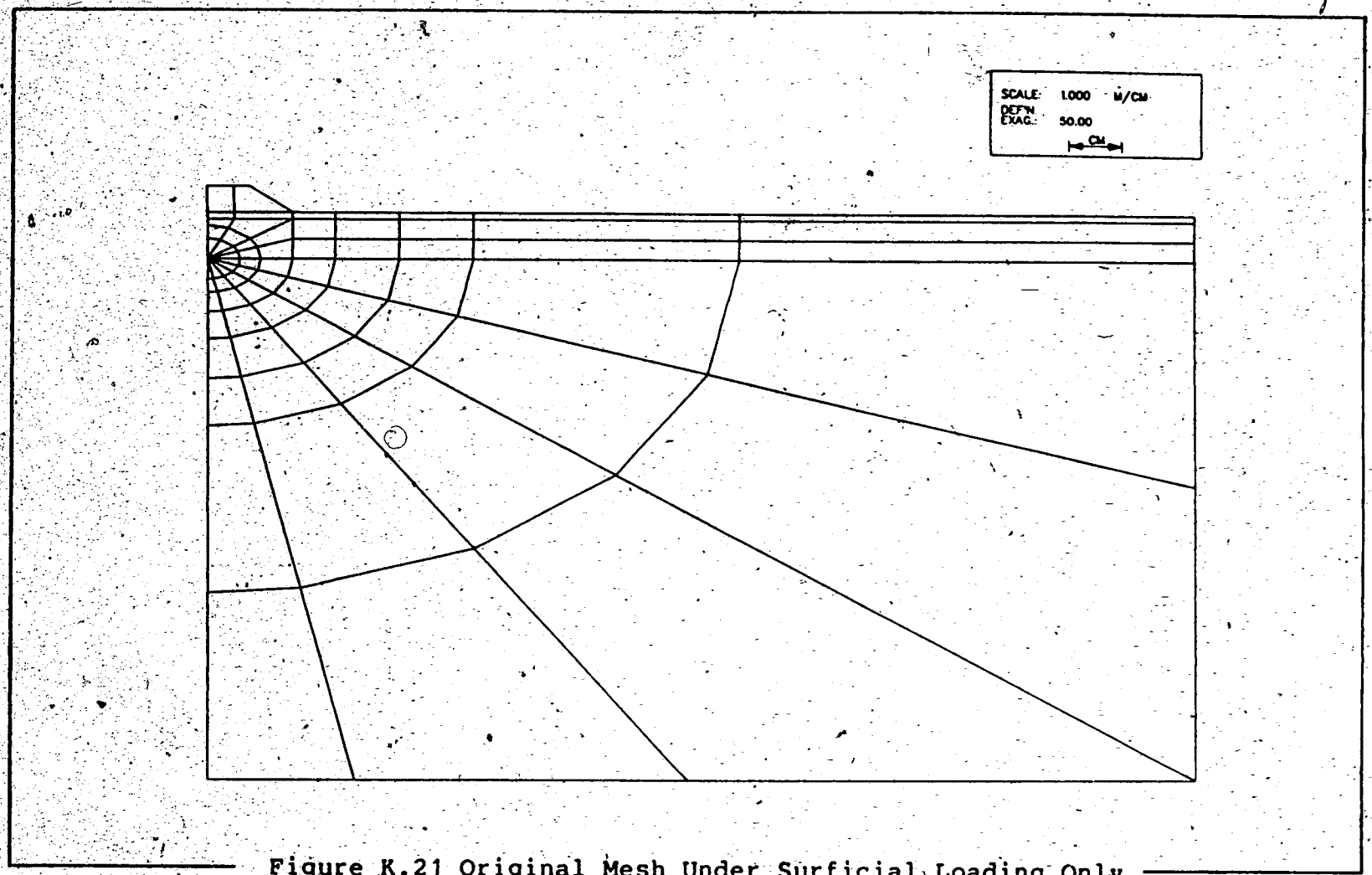

Figure K.21 Original Mesh Under Surficial Loading Only

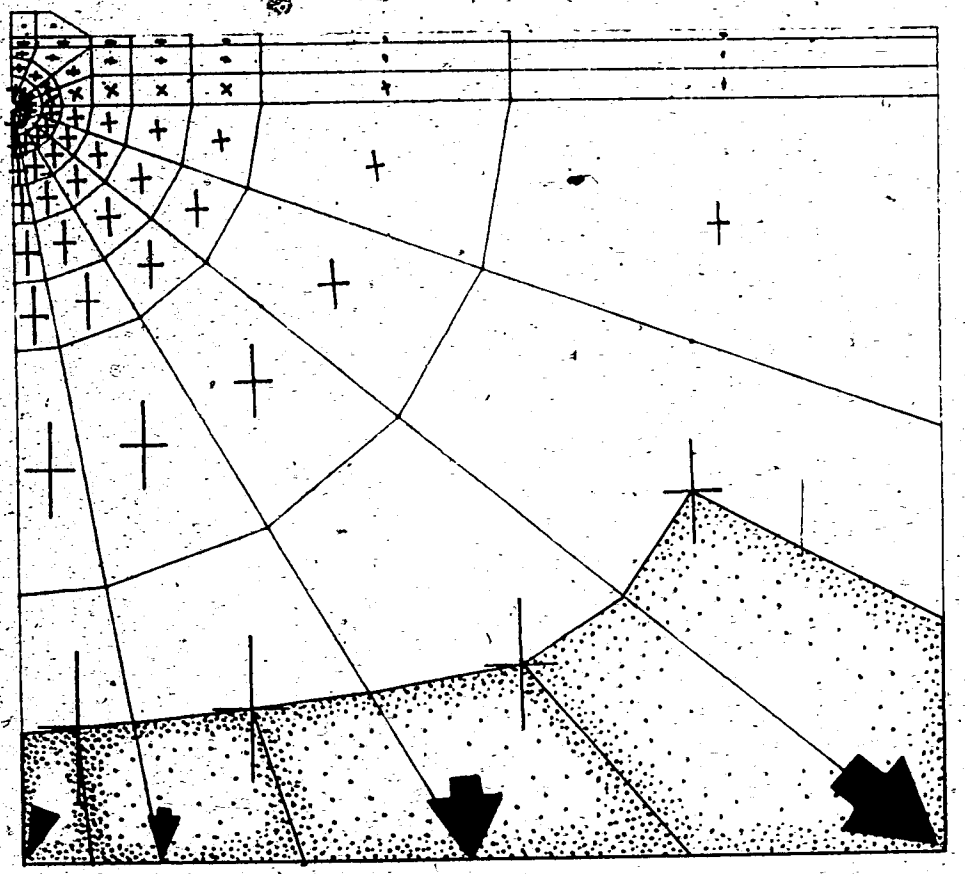

Figure K.22 Disparate Contributary Areas for Lumped Gravity Analysis

Appendice L: Sample Input Files

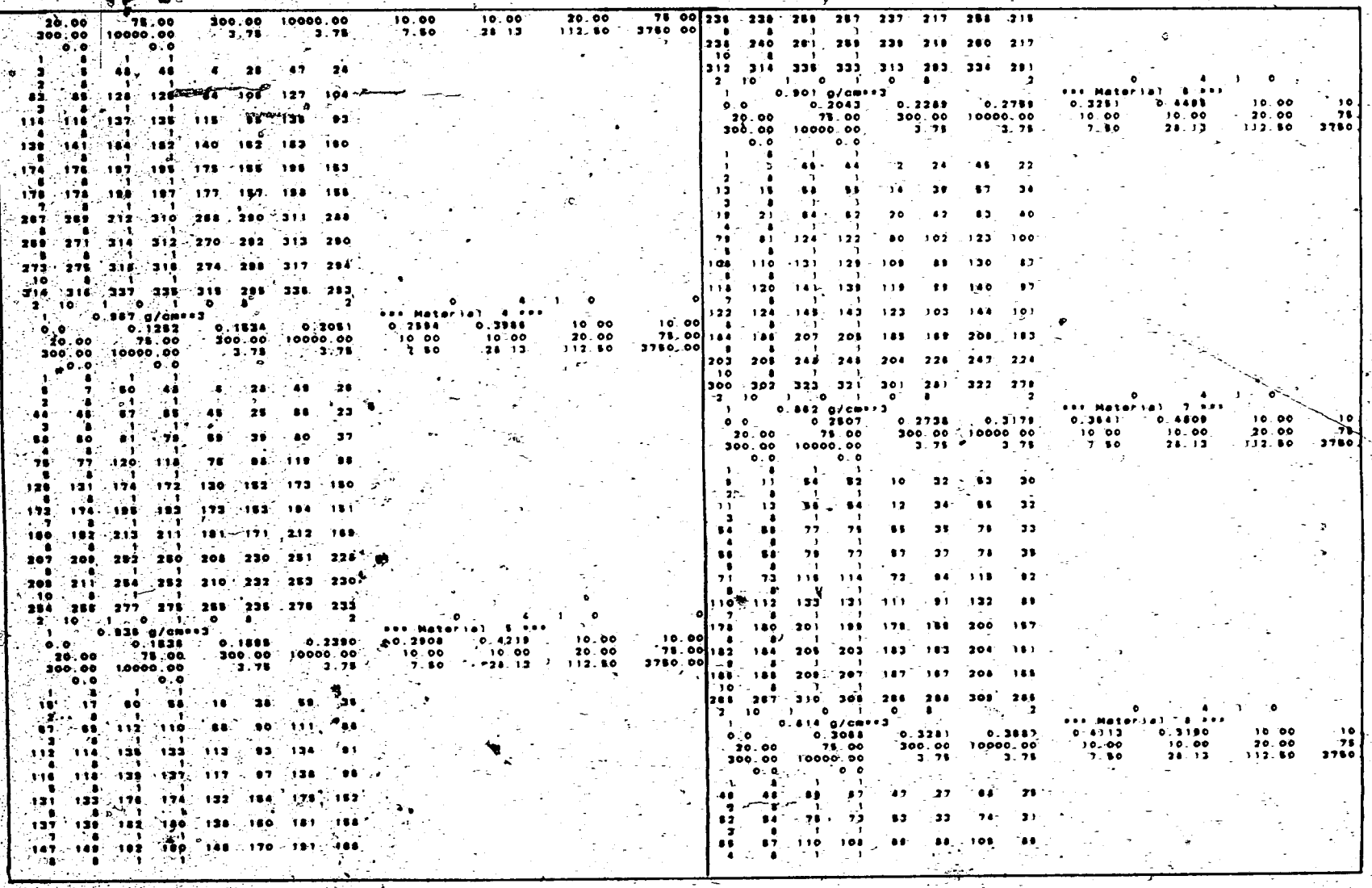

```
  77   79  122  120   78  100  121   98
   8    8    1    1
 120  122  143  141  121  101  142   99
   8    8    1    1
 123  125  170  170  124  188  177  184
   7    8    1    1
 143  145  188  186  144  186  187  184
   8    8    1    1
 188  190  211  209  189  189  210  187
   9    8    1    1
 240  242  263  261  241  221  262  219
  10    8    1    1
 302  304  325  323  303  283  324  281
   2   10    1    0    1    0    8    2                0    4    1    0    0
   1      0.748 g/cm**3                  *** Material  9 ***
   0.0          0.3823       0.4012       0.4372      0.4749       0.5704      10.00      10.00
    20.00         75.00       300.00     10000.00      10.00        10.00       20.00      75.00
   300.00     10000.00         3.75         3.75       7.50        28.13      112.50    3750.00
     0.0          0.0
   1    8    1    1
  17   19   62   60   18   40   81   38
   2    8    1    1
  62   64   85   83   83   43   84   41
   3    8    1    1
  68   71  114  112   70   82  113   80
   4    8    1    1
 124  126  147  145  125  105  146  103
   5    8    1    1
 145  147  190  188  146  188  189  186
   6    8    1    1
 180  182  203  201  181  181  202  199
   7    8    1    1
 197  199  242  240  198  220  241  218
   8    8    1    1
 242  244  265  263  243  223  264  221
   9    8    1    1
 283  285  308  306  284  288  307  284
  10    8    1    1
 308  310  331  329  309  289  330  287
   2   10    1    0    1    0    8    2                0    4    1    0    0
   1      0.888 g/cm**3                  *** Material 10 ***
   0.0          0.5382       0.5502       0.5788      0.6068       0.6758      10.00      10.00
    20.00         75.00       300.00     10000.00      10.00        10.00       20.00      75.00
   300.00     10000.00         3.75         3.75       7.50        28.13      112.50    3750.00
     0.0          0.0
   1    8    1    1
  80   82   83   81   81   41   82   39
   2    8    1    1
  81   83  128  126   82  104  125  102
   3    8    1    1
 138  137  180  178  136  158  179  156
   4    8    1    1
 193  195  238  236  194  216  237  214
   5    8    1    1
 201  203  246  244  202  224  245  222
   6    8    1    1
 211  213  256  254  212  234  255  232
   7    8    1    1
 258  261  304  302  260  262  303  280
   8    8    1    1
 271  273  316  314  272  294  315  292
   8    8    1    1
 310  312  333  331  311  291  332  289
  10    8    1    1
 316  318  338  337  317  297  338  295
   1    1    0      20.0         20.0          0        0.0          3
  44    1   22
   1    1    0      20.0         20.0          0        0.0          3
  85   44   23
   1    1    0      20.0         20.0          0        0.0          3
```

```
 108   88   88
   1    1    0      20.0         20.0          0        0.0          3
 129  108   87
   1    1    0      20.0         20.0          0        0.0          3
 172  129  150
   1    1    0      20.0         20.0          0        0.0          3
 193  172  193
   1    1    0      20.0         20.0          0        0.0          3
 236  193  214
   1    1    0      20.0         20.0          0        0.0          3
 257  238  215
   1    1    0      20.0         20.0          0        0.0          3
 300  257  278
   1    1    0      20.0         20.0          0        0.0          3
 321  300  279
   2    0.0          0.0          1.0       -3.80E
STOP
```

Appendice M: Ignoring the Different Thermal Conductivity of Ice Lenses

The principal effect of this conductivity difference is that ice has a thermal conductivity of 2.22 W/m·K while this frozen soil has a thermal conductivity of 1.76 W/m·K therefore the ice provides 26% more resistance to heat flow. This has the effect of lessening the heat flux through the frozen portion which should, in turn, mitigate the effect of attracted water flow to the frost front, as the system cannot thermodynamically allow all the to change phase. The net result would be a slower rate of freezing and a reduced heave.

The equivalent thermal resistivity of a frozen soil, with ice lenses, perpendicular to the heat flow is the same as the sum of the resistivities of the component materials:

$$\bar{R}_s = \sum_{i=1}^{n} R_i \text{ where } R = \frac{l}{kA} \qquad [M.1]$$

To examine the effect of differentiating between the thermal conductivities of frozen soil and ice, rather than using the frozen conductivity of frozen soil alone, the numerical results from Test C-10 are used.

Using the frozen gradient of 0.5530°C/m and the temperature difference of 4.6°C (-4.7 - -0.1) there is a frozen length of 8.318cm. Knowing the *in situ* heave to be 0.303cm, The segregational heave is then 1.053-0.303=0.750cm, and the length of frozen soil, (excluding segregation heave) is 8.318-0.750=7.568cm. With a constant cross-sectional area,

$$\bar{R} = \frac{I}{\bar{k}} = \frac{l_{ice}}{k_{ice}} + \frac{l_f}{k_f} \qquad [M.2]$$

$$= \frac{0.793 \times l_{ice} + l_f}{k_f}$$

$$= \frac{0.793 \times 0.750\text{cm} + 7.568\text{cm}}{1.76\text{W/m·K}} = .04638 \text{ W/m}^2\text{·K}$$

Ignoring ice, $R_i = \frac{l_f}{k_f} = \frac{8.318\text{cm}}{1.76\text{W/m·K}} = .04726 \text{ W/m}^2\text{·K}$

$= 98\%$ of $\bar{R}$

This shows that by ignoring the contribution of the ice the thermal resistivity underestimated by 2%. Obviously, as the total thickness of the lenses increases a larger effect will be seen however this is mitigated by the relatively

close conductances of frozen soil and ice and by the fact that the largest effect occurs when the system is nearing steady state and no further heave. It can well be argued that the frozen soil and ice lens material cannot be treated as a homogeneous material because the ice lenses are more prevalent closest to the frost front at steady state. It would require a continuous non-linear conductivity distribution to exactly simulate the thermodynamics of the heat flux through the frozen soil. Such a distribution, with more of an ice effect closest to the frost front, would result in a non-linear temperature distribution with lower thermal gradients in regions of high ice content. Again, this would reduce the amount of segregational heave. In all respects, the assumption of using k_f for the thermal and heave analyses is slightly conservative and an acceptable simplification of the physical problem.

Appendice N: Glossary of Files, Programs and Procedures

ABRAT	complied version of program "abridge.at". Abridges *ADINAT* output
ABRSAP	complied version of program "abridge.sap". Abridges *SAP IV* output
ARCH	procedure file for archiving *TRANS* output
ARCH3	data file of cummulative heave summaries from *TRANS*
ARMAGEDDON	procedure file for destroying all *TRANS* files
ARRETE	program for stopping *LOOP* procedure due to an *ADINAT* error or low funds in the computer account
B.TAPE	*BATCH* procedure file for using a tape
BASKET	*BATCH* procedure file for the heave calculations, from which the *LOOP* procedure is called
BATCH	procedure file for queing *BATCH* jobs
BATCHNO	data file cataloguing *BATCH* requests
BETA	program for calculating beta distributions and *ADINA* material model input assuming normal consolidation
BETAGEN	program for calculating beta distributions
BETARESID	program for calculating beta distributions and *ADINA* material model input assuming some residual stress in the soil
BOMB	procedure file for terminating the *LOOP* procedure for frost heave calculations due to a program error
CALCOMPQ	*EXEC* procedure file for queuing plotfiles for plotting
CAPTAINS.LOG	data file used by the *BASKET* procedure to record the commands and responses issued during the remote computer session
CLEAR	procedure file to restore *TRANS* I/O files to their initial status prior to the last *TRANS*

	run
CONT	program for plotting temperature contours (by David H. Chan)
CONT.I/P	input file for *CONT*, used by *CONTPREP*
CONT.INFO	input file for *CONT*, used by *CONTPREP*
CONTPREP	program to process *ADINAT* output for *CONT* input
CONTROL	data file for *SAPMESH* with plotting commands
D.TRANS	procedure file for debugging *TRANS*
DEARCH	program to prepare a time:SP+GRADT curve input using *ARCH3* as input
FINISH	procedure file for a controlled termination of the heaving calcs using *BASKET*
FORT	*EXEC* procedure file for compiling programs
GENESIS	procedure file for initializing files for heave calculations
GEO.:EXISTS	program generates a non-zero return code if the specified file doesn't exist
GEO.:TIME	program to print the current time and date
GSB	*EXEC* procedure file for obtaining printed output
HEAVE.2D	data file for *SAP IV* for the simulation of Test C-10
*IMSLLIB	system-supported subroutines
INITCONTROL	data file for *SAPMESH*, controlling the plotting commands for the initial mesh configuration
INITPLOT	plotfile of the initial mesh, using *SAPMESH*
INITREPLOT	data file in machine language for storing *SAPMESH* results for future plotting.
INITTEMPS	program to interpret *ADINAT's* machine language temperature file into readable format for *ADINAT* input
INIT16	data file of *ADINAT* output for the initial

	run
INIT56	data file of *ADINAT* machine language temperature output for the initial run
INIT6	data file of *SAP IV* output for the initial run
ISSCOQ	*EXEC* procedure file for queuing files for plotting
K.C10.I/P	data input for Konrad's finite difference program, Test C-10
K.NS1.I/P	data input for Konrad's finite difference program, Test NS-1
KONRAD	program listing of Konrad's finite difference program, with modifications
KONRAD.I/P	data input for Konrad's finite difference program
LOOP	procedure file containing all programs and file manipulation commands for one iteration of frost heave calculations
MESH	procedure file for plotting (included in *LOOP*)
MOUNT	*EXEC* procedure file for mounting tapes
NES.GRAV	data file of gravity deformations of the N.E.S. *SAP IV* mesh, to be subtracted from subsequent deformations before plotting
NODE	program to prepare a time:displacement curve input from the displacements in *ARCH13*
PHOENIX	procedure file for reinitializing *TRANS* I/O files for the beginning of heave calculations. Similar to *GENESIS* except that the original finite element output files are used.
PLOT	plotfile written on by *SAPMESH*
*PLOTLIB	plotting package subroutines
PLOTT	plotfile output from *CONT*
Q	data file containing the carriage control command for skipping to the front of a new sheet

READBINARY	program for interpretting the accumulated machine language temperatures from *ADINAT*'s unit 56
REPLOT	rendata file in machine language for storing *SAPMESH* results for future plotting
REVERSE	procedure file for undoing one iteration of *LOOP*
SAFE8	secure data file of existing *in situ* and segregational heaves and volumes, used when re-starting an iteration of *LOOP*
SAFE9	secure data file of original element volumes
SAFE18	secure data file of existing heaved element volumes, used when re-starting an iteration of *LOOP*
SAFE19	secure data file of heave history information, used when re-starting an iteration of *LOOP*
SAPMESH	plotting program written as a post-processor of *SAP IV* output
SAP3D	three-dimensional version of *SAPMESH*
SAVE	procedure file for renaming temporary files, used in the *LOOP* procedure, as permanent files (see *UNSAVE*)
SETTLE	program for processing random data for beta distribution analysis
SHOW:TERMINAL	program generates a zero return code (*RC*) if the command was issued from a computer terminal and *RC* > 0 if the computer session is in *BATCH* mode
SKIPVIEW	a flag within *LOOP* for branching of operations
STEP	procedure file for running *ADINAT* and *SAP IV* (included in procedure file *LOOP*)
SUM3	program to summarize heaves by reading the *ARCH3* file generated by the one-dimensional version of *TRANS*
SWITCH	procedure file for manipulating input and output files (included in procedure file

	LOOP)
T.NAME	data file cataloguing contents of tape "NAME"
TAGPF	plotfile for the *TELL-A-GRAF* plotting package
TAPESAVE	procedure file for storing the results of the heave calculations generated using *BASKET*
TEMP	data file for *ADINAT* for the initial N.E.S. run
TRANS	program for combining the thermal output from *ADINAT* and the stress output from *SAP IV* with Konrad's segregation potential theory to generate new input files for both finite element programs
TRANSIODUMP	*EXEC* procedure file for listing all *TRANS* output files
TRIP	procedure file for running *TRANS* (included in procedure file *LOOP*)
TSYM	plotting subroutine for accessing improved character sets (Tom Casey, U of A)
UNSAVE	procedure file for restoring some data files, used in *LOOP*, to their original temporary status
USEDDISC	a flag within *LOOP* for branching of operations
WHOA	procedure file, used within *LOOP*, for terminating the session for lack of computer funds
XLIMIT.C	dummy subroutine
X9700	*EXEC BATCH* procedure file for plotting
1	data file for *TRANS* containing data for *SP* calculations
2	data file for *TRANS* containing the time function used for calculating time increments between heave intervals
3	data file from *TRANS* containing the heave summary for that iteration of *TRANS*

4	input file for *SAP IV* generated by *TRANS*
5	input file for *SAP IV*
6	output file for *SAP IV*
7	output file for *TRANS*, containing warnings and flags
8	data file for *TRANS*, *in situ* and segregational heaves and volumes
9	data file for *TRANS* containing elements' original volumes
10	data file for *TRANS* containing node numbers and their coordinates and temperatures
11	data file for *TRANS* containing the node numbers for each element
12	data file for *TRANS* containing displaced coordinates and temperatures
13	data file for *TRANS* containing nodal displacements
14	input file for *ADINAT* generated by *TRANS*
15	input file for *ADINAT*
16	output file from *ADINAT*
17	data file from *TRANS* containing principal stresses, thermal flux cosines
18	data file for *TRANS* containing heaved element volumes
19	data file for *TRANS* containing heave history information
56	output file from *ADINAT* containing machine language temperatures
57	restart file for *ADINAT*